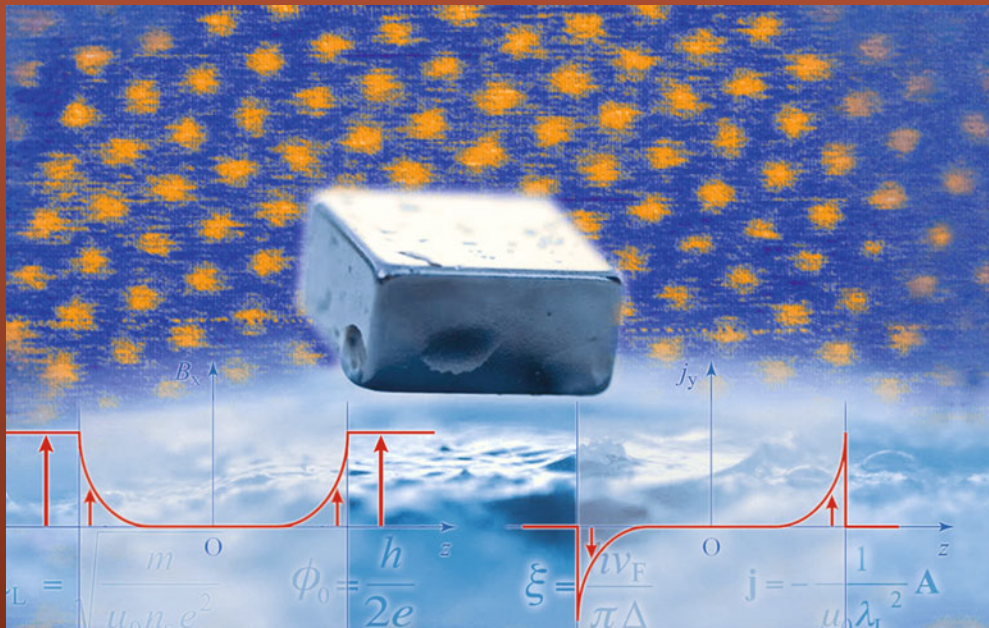


# Superconductivity

## An introduction



*Philippe Mangin - Rémi Kahn*

# Superconductivity

## Grenoble Sciences

The aim of Grenoble Sciences is twofold:

- ▶ to produce works corresponding to a clearly defined project, without the constraints of trends nor curriculum,
- ▶ to ensure the utmost scientific and pedagogic quality of the selected works: each project is selected by Grenoble Sciences with the help of anonymous referees. In order to optimize the work, the authors interact for a year (on average) with the members of a reading committee, whose names figure in the front pages of the work, which is then co-published with the most suitable publishing partner.

### Contact

Tel.: (33) 4 76 51 46 95

E-mail: [grenoble.sciences@ujf-grenoble.fr](mailto:grenoble.sciences@ujf-grenoble.fr)

Website: <https://grenoble-sciences.ujf-grenoble.fr>

### Scientific Director of Grenoble Sciences

Jean BORNAREL, Emeritus Professor at the Grenoble Alpes University, France

**Grenoble Sciences** is a department of the Grenoble Alpes University supported by the *Ministère de l'Education nationale, de l'Enseignement supérieur et de la Recherche* and the *Région Auvergne-Rhône-Alpes*.

**Mines Nancy** is one of the French top ranked Graduate School of Science, Engineering and Management. The *Fondation Mines Nancy* aims to enhance the international development of Mines Nancy by supporting its actions and projects abroad.

*Superconductivity, an introduction* is an improved version of the original book *Supraconductivité - Introduction* by P. MANGIN (Mines Nancy) & R. KAHN (CEA-Saclay), EDP Sciences, Grenoble Sciences Series, 2013, ISBN 978 2 7598 0657 7

The reading committee of the French version included the following members:

- ▶ Jean-Pascal BRISON, Researcher at the CEA (French Alternative Energies and Atomic Energy Commission), Statistical Physics, Magnetism and Superconductivity Department - CEA Grenoble
- ▶ Hervé COURTOIS, Professor at the Grenoble Alpes University, *Institut Néel* - Grenoble
- ▶ Thierry KLEIN, Professor at the Grenoble Alpes University, *Institut Néel* - Grenoble
- ▶ Jérôme LESUEUR, Professor at the *Ecole supérieure de physique et de chimie industrielles, Paris Tech*
- ▶ Stéphane PAILHÈS, Researcher at the CNRS (National Center for Scientific Research), *Institut Lumière Matière* - Lyon
- ▶ José TEIXEIRA, Senior researcher at the CNRS, Léon BRILLOUIN Laboratory - CEA Saclay
- ▶ Pierre VEDRINE, engineer at the CEA, Institute of Research into the Fundamental Laws of the Universe - Saclay
- ▶ Georges WAYSAND, Director of research at the CNRS, Low Noise Inter Disciplinary Underground Science and Technology - Rustrel

Translation from original French version performed by Timothy ZIMAN, Senior researcher at the CNRS, *Institut Laue Langevin* (ILL) - Theory Group member

Editorial coordination: Laura CAPOLO; typesetting: Sylvie BORDAGE and Anne-Laure PASSAVANT; cover illustration: Alice GIRAUD, from: image of the vortex lattices obtained by Scanning Tunneling Spectroscopy, team of D. RODITCHEV, Paris Institute of Nanosciences - UMR 75-88 at the CNRS, Pierre and Marie CURIE University, Paris 6; magnet levitating above a superconductor, J. BOBROFF, J. QUILLIAM, F. BOUQUET, Laboratory of Solid State Physics (LPS), Orsay.

Philippe Mangin · Rémi Kahn

# Superconductivity

An introduction

Translation by Timothy Ziman



Springer

Philippe Mangin  
Jean Lamour Institute  
University of Lorraine  
Nancy  
France

Rémi Kahn  
Léon Brillouin Laboratory  
CEA Saclay  
Gif sur Yvette  
France

*Translator*  
Dr. Timothy Ziman  
Institut Laue-Langevin (ILL)  
Grenoble  
France

Co-published by Springer International Publishing AG, Gewerbestrasse 11, 3330 Cham, Switzerland, and Grenoble Sciences, Université Grenoble Alpes, 230 rue de la physique, CS 40700, 38058 Grenoble Cedex 9, France.

ISBN 978-3-319-50525-1  
DOI 10.1007/978-3-319-50527-5

ISBN 978-3-319-50527-5 (eBook)

Library of Congress Control Number: 2016959752

© Springer International Publishing AG 2017

This work is subject to copyright. All rights are reserved by the Publisher, whether the whole or part of the material is concerned, specifically the rights of translation, reprinting, reuse of illustrations, recitation, broadcasting, reproduction on microfilms or in any other physical way, and transmission or information storage and retrieval, electronic adaptation, computer software, or by similar or dissimilar methodology now known or hereafter developed.

The use of general descriptive names, registered names, trademarks, service marks, etc. in this publication does not imply, even in the absence of a specific statement, that such names are exempt from the relevant protective laws and regulations and therefore free for general use.

The publisher, the authors and the editors are safe to assume that the advice and information in this book are believed to be true and accurate at the date of publication. Neither the publisher nor the authors or the editors give a warranty, express or implied, with respect to the material contained herein or for any errors or omissions that may have been made.

Printed on acid-free paper

This Springer imprint is published by Springer Nature  
The registered company is Springer International Publishing AG  
The registered company address is: Gewerbestrasse 11, 6330 Cham, Switzerland

## PREFACE

This book was written based on original material from Master's level courses for scientists and engineers. Given the lack of elementary texts on the subject, especially in the French language of the original edition, it was intended as an introduction to superconductivity accessible to beginning graduate students or advanced undergraduates. We wished to make a textbook where simple approaches were preferred, assumptions clearly stated, and calculations given in sufficient detail to be followed with ease. A number of the applications of electromagnetism, thermodynamics or quantum physics can make for stimulating exercises for science and engineering students.

In view of the vast state of knowledge of the subject nowadays, this volume can only be an introduction. Other titles in preparation: *Supraconductivité - Matériaux et applications* and *Supraconductivité conventionnelle et non-conventionnelle*<sup>1</sup> should bring both a broader and a more specialized view of the current state of superconductivity.

The contents of this book have benefitted from the expert advice of our many colleagues in the *Jean Lamour Institute* in Nancy, of the *Léon Brillouin Laboratory* in Saclay and the the French Center for Atomic and Alternative Energies (CEA). The review panel: Jean-Pascal BRISON, Hervé COURTOIS, Thierry KLEIN, Jérôme LESUEUR, Stephane PAILHÈS, Pierre VEDRINE and Georges WAYSAND, brought crucial insight to the content of several chapters. The great pedagogue, José TEIXEIRA, re-read the work in great detail and greatly improved the explanation of several delicate issues.

H. COURTOIS, P. DUBOS, C. GOURDON, V. JEUDY, T. KLEIN, B. PANNETIER, A. PAUTRAT, D. RODITCHEV and J.C. VILLEGIER generously gave us much appreciated advice and were kind enough to allow us to use illustrations from their original publications.

The staff of **Grenoble Sciences** directed by Jean BORNAREL encouraged and stimulated us and did much to create an environment favoring a work of high quality. Laura CAPOLO, Sylvie BORDAGE and Anne-Laure PASSAVANT have, with much patience and good humour produced a remarkably elegant manuscript with careful attention to type-setting and to the thousand details that are so important for a beginning reader.

---

<sup>1</sup> *Materials and Application and Conventional and Unconventional Superconductivity*

The *Fondation Mines Nancy* generously funded this translation of the original french edition.

We extend our heartfelt thanks to all of the above.

We would also like to express our warmest thanks to Dr Timothy ZIMAN of the Institut Laue-Langevin, Grenoble, who kindly accepted to translate the French version into English. Being an eminent theoretical physicist himself, Tim went far beyond providing a simple translation, making precious comments resulting in an optimal presentation of the work. It was indeed a real pleasure to work with Tim during the period of the translation.

Finally, we would like to make a special mention of the students who followed our courses which lead to this book. Their enthusiasm, the many questions they asked, and the comments they made, were the primary motivation to complete this work.

Philippe MANGIN

Emeritus Professor at the Mines Nancy Graduate School - Lorraine University  
Nanomagnetism and Spintronics research group - Jean Lamour Institute

Rémi KAHN

Retired senior research scientist at the CEA-Saclay  
Quasi-elastic neutron scattering group - Léon Brillouin Laboratory

# CONTENTS

<b>1 - Introduction .....</b>	1
1.1 - A history of women and men .....	1
1.2 - Experimental signs of superconductivity .....	1
1.2.1 - The discovery of superconductivity: the critical temperature .....	1
1.2.2 - The magnetic behavior of superconductors.....	3
The MEISSNER-OCHSENFELD effect.....	3
Critical fields and superconductors of types I and II.....	3
1.2.3 - Critical current .....	3
1.2.4 - The isotope effect .....	4
1.2.5 - JOSEPHSON currents and flux quantification.....	4
1.3 - Phenomenological models.....	5
1.3.1 - LONDON theory .....	5
1.3.2 - The thermodynamic approach .....	6
1.3.3 - GINZBURG-LANDAU theory.....	6
1.3.4 - Vortices.....	7
1.4 - The microscopic BCS theory.....	8
1.5 - Tunnelling effects .....	9
1.6 - A great diversity of superconducting materials .....	9
1.7 - “Unconventional” superconductors.....	10
1.8 - Numerous spectacular applications .....	11
1.9 - Superconductivity in the history of mankind .....	12
<b>2 - LONDON theory.....</b>	13
2.1 - MAXWELL’s equations.....	13
2.2 - The behavior expected for a perfect conductor .....	14
2.2.1 - Electrical conduction in a normal conductor .....	14
2.2.2 - Electrical conduction in a perfect conductor .....	15
2.2.3 - Magnetic fields in a perfect conductor .....	16
Application to a perfectly conducting slab .....	17
2.3 - Superconductor <i>versus</i> perfect conductor.....	19
2.3.1 - Cooling in zero field followed by application of a field.....	19
2.3.2 - Application of the magnetic field when $T > T_c$ followed by cooling in the field.....	20
2.4 - The LONDON equations.....	22
2.4.1 - “Superconducting electrons” .....	22
2.4.2 - First LONDON equation .....	22
2.4.3 - Second LONDON equation.....	23

2.4.4 - Superconducting slab in an applied magnetic field .....	23
Thick slab ( $d \gg \lambda_L$ ).....	23
Thin slab ( $d \leq \lambda_L$ ).....	24
2.5 - The LONDON penetration depth .....	25
2.5.1 - Experimental measurement of $\lambda_L$ .....	25
2.5.2 - Temperature dependence of the LONDON penetration depth.....	26
2.6 - Applications to superconducting wires.....	26
2.6.1 - A wire in magnetic field .....	26
2.6.2 - A current-carrying wire .....	29
2.6.3 - Thin current-carrying wire.....	30
2.6.4 - Generalized response of the wire.....	30
2.7 - The OCHSENFELD experiment.....	31
2.8 - Non-simply-connected superconductor.....	32
2.8.1 - Sequence 1: cooling in zero field.....	33
2.8.2 - Sequence 2: field cooling.....	33
2.8.3 - Conclusion .....	34
2.9 - Analysis from the point of view of energy .....	34
2.9.1 - Energetic interpretation of the LONDON penetration depth .....	34
Magnetic energy .....	35
Kinetic energy of the superconducting electrons .....	35
2.9.2 - The second LONDON equation by a variational method .....	35
2.10 - Description of superconductivity in fluid-mechanical terms .....	37
Two remarks.....	38
2.11 - The LONDON moment .....	38
2.11.1 - Intuitive approach .....	38
2.11.2 - Calculating the LONDON moment.....	39
2.12 - The LONDON equation in the LONDON gauge.....	41
2.12.1 - Concept of gauge .....	41
2.12.2 - LONDON gauge .....	42
2.12.3 - Second LONDON equation in the LONDON gauge .....	43
2.12.4 - Momentum $p$ and the LONDON equation .....	43
2.12.5 - Non-simply-connected superconductors .....	44
<b>Appendix 2A - Total and partial derivatives with respect to time .....</b>	<b>45</b>
<b>Appendix 2B - Property of a harmonic function for which the component to the surface normal of the gradient vanishes .....</b>	<b>46</b>
<b>Appendix 2C - Modified BESSEL functions .....</b>	<b>47</b>
In the neighborhood of the origin ( $x \rightarrow 0$ ) .....	47
Asymptotic behavior at infinity ( $x \rightarrow \infty$ ) .....	48
<b>3 - The non-local PIPPARD equations.....</b>	<b>49</b>
3.1 - Origin of the non-local equations .....	49
3.2 - Non-locality in pure superconductors.....	50
3.3 - Penetration depth of the magnetic field .....	51
3.4 - FOURIER analysis of the PIPPARD equations .....	52
3.5 - “Dirty” superconductors .....	55

<b>4 - Thermodynamics of type I superconductors.....</b>	59
4.1 - Thermodynamic description .....	60
4.2 - The thermodynamic variables of superconductivity .....	61
4.2.1 - The relation between LONDON currents and magnetization .....	61
Magnetic material .....	61
Superconducting material .....	61
4.2.2 - Thermodynamic systems .....	62
System of solenoid + matter .....	62
Superconducting matter as a closed system .....	63
4.2.3 - Interpreting the levitation of type I superconductors.....	64
4.3 - Thermodynamic functions of superconductivity .....	65
4.4 - Thermodynamic data .....	66
4.4.1 - Equations of state.....	67
Normal phase .....	67
Superconducting phase .....	67
4.4.2 - Specific heat.....	67
Lattice specific heat $C^{\text{vib}}$ .....	67
Electronic specific heat $C_n^{\text{el}}$ in the normal phase.....	68
Electronic specific heat $C_s^{\text{el}}$ in the superconducting phase .....	68
4.4.3 - Phase diagram - The critical field line.....	69
4.5 - The transition between superconducting and normal states .....	70
4.5.1 - Free enthalpy of condensation.....	70
4.5.2 - Relation between the specific heat and the slope of the transition line .....	72
4.5.3 - Latent heat of transformation.....	74
4.5.4 - Order of the phase transitions .....	75
First order transitions .....	75
Second order transitions .....	75
Appendix 4 - <b>Magnetic media .....</b>	77
A4.1 - Fields in magnetized materials	
The equivalence magnetization - distribution of AMPÈRE currents .....	77
AMPÈRE currents in a uniformly magnetized cylinder.....	78
Magnetic field <b>B</b> .....	78
Field <b>H</b> .....	78
<b>B</b> and <b>H</b> fields in a uniformly magnetized cylinder.....	79
<b>B</b> and <b>H</b> fields in an infinite cylinder placed in a solenoid.....	80
A uniformly magnetized ellipsoid .....	81
The general case.....	83
A4.2 - Work performed in the magnetization of matter .....	84
The work to establish a field in an empty solenoid .....	84
Work to establish a field in a solenoid containing a solid cylinder of material .....	84
Work performed on the magnetized material alone.....	85
<b>5 - The intermediate state of type I superconductors .....</b>	87
5.1 - Criteria for the occurrence of a S/N transition .....	87
5.2 - S/N transition of an infinite cylinder .....	88
5.3 - Transition in small samples .....	89

5.3.1 - Thin slab .....	89
5.3.2 - Thin wire.....	90
5.4 - Effects of sample shape .....	91
5.4.1 - Reminder of relevant results in magnetism .....	91
5.4.2 - Application to superconductors .....	91
LONDON currents squeezed on the surface .....	91
Decompressing the LONDON currents.....	92
5.5 - Intermediate state for a sphere .....	93
5.5.1 - First approach .....	93
5.5.2 - More realistic structures .....	95
5.6 - Intermediate state of a thin plate.....	97
5.6.1 - Laminar model.....	97
5.6.2 - Energy balance.....	98
Energy of interface formation.....	99
Energy due to perturbation of the magnetic field outside the plate.....	99
Energy due to perturbation of the magnetic field in the plate .....	100
5.6.3 - Structure of the intermediate state of the plate .....	100
5.7 - Avoiding confusion .....	101
5.8 - Wire carrying a current (model of the intermediate state).....	102
5.8.1 - Formulation of the problem .....	102
5.8.2 - Model for the intermediate state .....	104
5.8.3 - A thin wire .....	106
5.9 - Critical current of a wire in a magnetic field.....	106
5.9.1 - General case.....	106
5.9.2 - Magnetic field applied parallel to the axis of the wire .....	107
5.9.3 - Magnetic field applied perpendicular to the axis of the wire .....	108
<b>6 - Type II superconductors .....</b>	<b>111</b>
6.1 - Two types of magnetic behavior .....	111
6.1.1 - The emergence of type II superconductors.....	111
6.1.2 - Magnetic behavior of type II superconductors .....	112
Type I superconductors .....	112
Type II superconductors .....	112
6.1.3 - Classification of superconducting materials.....	113
6.2 - Surface magnetic free enthalpy .....	114
6.2.1 - Surface magnetic free enthalpy density .....	114
6.2.2 - A first step toward vortices.....	116
6.3 - Surface free enthalpy of condensation.....	118
6.3.1 - Coherence length .....	118
6.3.2 - Geometric interpretation of the coherence length .....	118
6.3.3 - Surface free enthalpy of condensation.....	120
6.4 - Total surface free enthalpy .....	120
6.5 - Vortices and type II superconductors .....	121
6.5.1 - Description of a vortex .....	121
6.5.2 - Stability of vortices.....	123
Stability condition.....	123
Temperature dependence .....	124

Impurity effects.....	125
6.5.3 - Quantization of the flux carried by a vortex .....	125
6.5.4 - Results of “GLAG” theory .....	126
6.6 - Vortex lattice .....	127
6.6.1 - ABRIKOSOV lattice .....	127
6.6.2 - Imaging vortex lattices .....	129
6.7 - Critical field $H_{c2}$ .....	131
6.8 - Elements of the structure and dynamics of vortices .....	132
6.8.1 - Penetration of vortices .....	133
6.8.2 - Phase diagrams of vortices .....	134
Vortex crystals.....	134
BRAGG glass.....	135
Vortex glass .....	135
Vortex liquid.....	135
Phase diagram.....	135
6.9 - Electric transport in type II superconductors.....	136
6.9.1 - The problem of type II superconductors.....	136
6.9.2 - Distribution of the current density .....	136
6.9.3 - Critical current density .....	137
6.10 - Levitation in the presence of vortices.....	138
6.11 - A few illustrations of the diverse behavior of vortices.....	139
6.11.1 - Effect of the demagnetizing field .....	140
6.11.2 - Crystal growth by transported current .....	140
6.11.3 - Repulsion by surfaces .....	141
6.11.4 - Trapping vortex lines by depressions in thin films.....	142
6.11.5 - Effects of confinement.....	142
<b>7 - Fields and currents in type II superconductors</b>	
<b>Models of the critical state.....</b>	<b>147</b>
7.1 - Forces acting on vortices .....	147
7.1.1 - Force exerted on a vortex by a transported current .....	148
7.1.2 - Interaction forces between vortices .....	148
Force between two vortices .....	148
Force on a vortex within a group of vortices.....	149
Force density.....	149
7.2 - Energy dissipation by vortex displacement .....	150
7.2.1 - Model of vortex flow .....	150
7.2.2 - Induced electric field .....	151
7.2.3 - The BARDEEN-STEPHEN model .....	152
7.3 - Critical current density in type II superconductors .....	152
7.3.1 - Pinning force.....	152
7.3.2 - Critical current density .....	153
7.3.3 - Return to the flux-flow resistivity .....	153
7.3.4 - Vortex jumps .....	155
7.3.5 - Vortex flux creep .....	155
7.3.6 - Other behavior .....	156
7.4 - Models of the critical state.....	156

7.4.1 - Critical state .....	156
7.4.2 - Laws of behavior .....	157
7.5 - The BEAN model .....	158
7.5.1 - Increasing field: vortex penetration .....	158
7.5.2 - Decreasing field: field profile and the vortex distribution .....	160
7.5.3 - Rules for the profile of magnetic field and current density (in planar geometry) .....	161
7.6 - Magnetization of a type II superconducting plate .....	162
7.6.1 - Geometry and magnetization .....	162
7.6.2 - Initial magnetization curve (BEAN model) .....	163
7.6.3 - Hysteresis loop in the BEAN model .....	165
7.6.4 - Hysteresis loop in the KIM-JI model .....	166
7.7 - Magnetization in cylindrical geometry (BEAN model) .....	168
7.7.1 - Magnetization of a solid cylinder .....	168
7.7.2 - Magnetization of a thick-walled tube .....	170
7.8 - Experimental evidence for critical states .....	171
7.9 - Current transport in the SCHUBNIKOV phase .....	173
7.9.1 - Current transport in the absence of applied magnetic field .....	173
7.9.2 - Current transport in an applied magnetic field .....	176
<b>Appendix 7A - Differents aspects of the "LORENTZ force" .....</b>	<b>178</b>
A7A.1 - Introduction .....	178
A7A.2 - LORENTZ force .....	179
A7A.3 - LONDON force .....	179
Field and kinetic energies .....	179
Evaluation of the energy of an isolated vortex .....	180
Interaction energy between vortices .....	180
Force between vortices .....	181
Force acting on a vortex immersed in a uniform current density .....	181
A7A.4 - MAGNUS force .....	182
Fixed cylinder in a moving fluid .....	182
Velocity of the electrons around the core of an isolated vortex .....	182
MAGNUS force .....	183
A7A.5 - Conclusions .....	184
<b>Appendix 7B - Energy dissipated by a moving vortex - The BARDEEN-STEPHEN model .....</b>	<b>185</b>
A7B.1 - Construction of the argument .....	185
A7B.2 - Current density .....	185
A7B.3 - Exterior electric field .....	185
A7B.4 - Charge density at the core surface .....	186
A7B.5 - Internal field .....	187
A7B.6 - Dissipated power and flux-flow resistivity .....	187
<b>8 - COOPER pairs - Principal results of BCS theory .....</b>	<b>189</b>
8.1 - Free electron gas .....	189
8.1.1 - Free electron gas at 0 K .....	189
Density of states .....	190
FERMI level .....	191
Effects of temperature .....	192

8.2 - Interacting electron gas.....	193
8.2.1 - Wave functions of two independent particles.....	193
8.2.2 - Interaction potential.....	194
8.2.3 - Interaction mediated by phonons.....	195
8.3 - The reference system .....	197
8.3.1 - One particle system.....	197
System of degenerate states .....	197
Generalization to $N$ degenerate states.....	198
System with non-degenerate states.....	199
Generalization to $N$ non-degenerate states .....	200
8.3.2 - Systems of pairs.....	201
8.4 - COOPER pairs .....	203
8.4.1 - The accessible pair states.....	203
8.4.2 - Redefinition of the zero of energy .....	204
8.4.3 - Bound state of the COOPER pair at 0 K .....	204
8.4.4 - Wave function, occupation probability.....	206
8.4.5 - Spatial extent of a COOPER pair.....	207
8.5 - Elements of BCS theory .....	207
8.5.1 - Collection of COOPER pairs .....	207
8.5.2 - Ground state.....	208
8.5.3 - Quasiparticles .....	210
8.6 - Consequences of the energy structure .....	212
8.6.1 - Critical temperature .....	212
8.6.2 - Nature of the superconducting gap .....	215
8.6.3 - Coherence length .....	215
8.6.4 - Critical field - Free enthalpy of condensation .....	216
8.6.5 - Electronic specific heat.....	217
8.6.6 - Critical current density .....	218
Normal metal .....	218
Metal in the superconducting phase .....	220
Energy balance .....	221
8.7 - Superconducting electrons and the LONDON penetration depth .....	222
<i>Appendix 8 - Matrix elements for the interaction potential between particles</i> .....	224
<b>9 - Coherence and the flux quantum .....</b>	<b>225</b>
9.1 - Current density and the LONDON equation .....	225
9.2 - Phase of the wave function .....	226
9.3 - Flux quantization .....	227
9.3.1 - The fluxon.....	227
9.3.2 - Simply connected superconductor.....	228
9.3.3 - Multiply connected superconductor .....	229
9.3.4 - Experimental proof of the existence of COOPER pairs.....	229
9.4 - Back to gauges.....	231
9.4.1 - The seconde LONDON equation .....	231
9.4.2 - Simply connected superconductor .....	231
9.4.3 - Multiply connected superconductor .....	232
9.5 - Flux quantization: application to vortices .....	232

9.5.1 - Fluxon carried by a single vortex .....	232
9.5.2 - Fluxon in the ABRIKOSOV lattice .....	233
9.5.3 - A confined vortex .....	234
9.5.4 - Current density around a vortex core.....	235
9.6 - Generalized LONDON equation in the presence of vortices .....	236
9.7 - Return to the LONDON moment .....	236
<b>Appendix 9 - Generalised momentum</b> .....	238
A9.1 - Lagrangian and Hamiltonian mechanics.....	238
Notation .....	238
The Lagrangian and the LAGRANGE equations.....	238
Lagrangian of a charged particle .....	238
Momentum of a charged particle.....	238
The HAMILTON function.....	239
A9.2 - The passage to quantum mechanics.....	239
A few principles.....	239
Momentum and wave vector .....	239
Hamiltonian of a particle in an electromagnetic field .....	240
Current density .....	240
A9.3 - Gauges .....	240
<b>10 - The JOSEPHSON effect</b> .....	243
10.1 - JOSEPHSON equations in an SIS junction .....	243
10.1.1 - The ionized hydrogen molecule.....	244
10.1.2 - Transfer between superconducting blocks.....	244
10.2 - The d.c. JOSEPHSON effect .....	245
10.2.1 - The JOSEPHSON current.....	245
10.2.2 - Critical intensity of the JOSEPHSON current.....	247
The AMBEGAOKAR and BARATOFF relation (SIS junction).....	247
10.3 - The a.c. JOSEPHSON effect .....	248
10.3.1 - The JOSEPHSON frequency .....	248
10.3.2 - Application: definition of the standard volt.....	248
10.4 - “Current-voltage” characteristics of an SIS JOSEPHSON junction .....	249
10.4.1 - Voltage-biased JOSEPHSON junction.....	249
10.4.2 - The RCSJ model .....	250
10.4.3 - Equations for the current-biased RCSJ system.....	251
10.4.4 - Mechanical analogy to the RCSJ model.....	252
10.4.5 - Characteristic frequencies.....	254
Of oscillation of the free pendulum.....	254
Of oscillation of the phase difference between the leads of a junction .....	254
10.4.6 - Comparison of the response of the mechanical systems and RCSJ “biased” by a torque $\Gamma$ or an intensity $I$ .....	254
Initial state .....	255
JOSEPHSON regime .....	255
Critical threshold .....	255
Beyond the critical threshold.....	255
Return to below the critical threshold - Hysteresis.....	256
10.4.7 - Over-damped regime .....	256
10.4.8 - Graphical representations .....	258

10.4.9 - Weak and intermediate damping .....	260
10.4.10 - Some examples of SIS junctions .....	261
10.5 - Energy stocked in a JOSEPHSON junction (SIS).....	262
10.6 - JOSEPHSON junction subject to an electromagnetic wave.....	263
10.6.1 - Resonance effects .....	263
10.6.2 - SHAPIRO steps .....	264
10.7 - SNS junctions .....	266
10.7.1 - Proximity effect, the ASLAMAZOV-LARKIN model.....	266
10.7.2 - JOSEPHSON current <i>via</i> the ANDREEV levels.....	267
Quasiparticles .....	267
ANDREEV-SAINT JAMES reflections .....	268
ANDREEV levels .....	269
JOSEPHSON current.....	270
10.7.3 - Examples of SNS junctions .....	271
10.7.4 - Signature of the JOSEPHSON effect.....	273
10.8 - $\pi$ type JOSEPHSON junctions.....	273
10.8.1 - Definition and energy .....	273
10.8.2 - Families of JOSEPHSON $\pi$ junctions .....	275
10.8.3 - SFS junctions: mechanisms of $\pi$ junctions .....	276
10.9 - JOSEPHSON junction: a system with many states .....	279
10.9.1 - Electron on a chain of atoms .....	279
10.9.2 - Generalization.....	281
10.9.3 - Application to the JOSEPHSON effect .....	281
First JOSEPHSON equation .....	283
Stored energy in a junction .....	283
Second JOSEPHSON equation.....	283
10.9.4 - A general property of BOSE-EINSTEIN condensats .....	284
<i>Appendix 10A - Solution of the coupling equations</i> .....	285
<i>Appendix 10B - JOSEPHSON junction in the over-damped regime</i> .....	286
Initial equations.....	286
Average voltage $\langle V \rangle$ and the period $T$ .....	286
Average voltage $\langle V \rangle$ as a function of injected current $I$ .....	286
<i>Appendix 10C - JOSEPHSON junction subject to an alternating voltage</i> .....	288
<b>11 - Superconducting QUantum Interference Device "SQUID"</b> .....	289
11.1 - Nature of the SQUID current.....	289
11.2 - rf-SQUID with vanishing inductance .....	292
11.2.1 - Single junction non-inductive rf-SQUID .....	292
11.2.2 - Non-inductive rf-SQUID with two junctions .....	293
11.3 - Inductive rf-SQUID .....	295
11.3.1 - Magnetic phase change and the external field flux .....	295
11.3.2 - Operation of the inductive rf-SQUID .....	297
11.4 - rf-SQUID with $\pi$ junction.....	299
11.5 - Inductive single junction SQUID: energetic approach.....	300
11.6 - rf-SQUID with two JOSEPHSON junctions of different types.....	303
11.6.1 - 0- $\pi$ rf-SQUID with zero inductance .....	303

11.6.2 - 0- $\pi$ rf-SQUID of significant inductance .....	304
11.7 - Reading an rf-SQUID .....	306
11.8 - DC-SQUID (SQUID polarized by Direct Current) .....	306
11.8.1 - Principle of the DC-SQUID .....	306
DC-SQUID with zero inductance ( $\beta_L = 0$ ) .....	307
Inductive DC-SQUID ( $\beta_L \neq 0$ ) .....	308
11.8.2 - DC-SQUID in the over-damped regime .....	309
11.8.3 - Reading a DC-SQUID .....	309
11.8.4 - 0- $\pi$ DC-SQUID .....	310
<b>12 - JOSEPHSON junctions in a magnetic field</b> .....	313
12.1 - Magnetic field on a short JOSEPHSON junction .....	314
12.2 - Current in a short JOSEPHSON junction under a magnetic field .....	315
12.3 - Short 0- $\pi$ junction in a magnetic field .....	321
12.4 - Introduction to the JOSEPHSON penetration depth .....	324
12.4.1 - General equations .....	324
12.4.2 - Behavior in very weak fields .....	325
Case of a long junction .....	326
Critical magnetic field .....	327
Limiting case of a short junction .....	328
12.5 - Long JOSEPHSON junction in a high magnetic field .....	328
12.5.1 - Mechanical analogy .....	328
12.5.2 - Special movements of the pendulum .....	330
First scenario .....	330
Second scenario .....	332
12.5.3 - Long JOSEPHSON junction in the MEISSNER regime .....	333
12.5.4 - Long junction in the vortex regime .....	335
12.5.5 - Isolated JOSEPHSON vortex .....	337
12.6 - Current transport in a long JOSEPHSON junction .....	339
12.6.1 - Long junction carrying a current .....	339
12.6.2 - Long JOSEPHSON current subject to a magnetic field and carrying a current .....	341
MEISSNER regime .....	341
Vortex regime .....	342
12.7 - Half fluxon at the 0- $\pi$ connection of a hybrid JOSEPHSON junction .....	343
<b>Appendix 12 - Phase slip between the superconducting blocks</b>	
<b>within an infinite 0-<math>\pi</math> junction</b> .....	346
A12.1 - The equations governing the junction .....	346
A12.2 - Boundary conditions .....	346
A12.3 - Profile of the phase difference .....	347
<b>Notation</b> .....	349
<b>Some works of reference</b> .....	355
<b>Index</b> .....	357

# Chapter 1

## INTRODUCTION

### 1.1 - A history of women and men

Since its discovery in 1911, the history of superconductivity is perhaps one of the most exciting adventures in physics. It was directly responsible for no fewer than five NOBEL prizes:

Heike Kamerlingh ONNES, for the discovery of the phenomenon (1913), John BARDEEN, Leon COOPER and Robert SCHRIEFFER, who provided a microscopic theory (1972), Brian JOSEPHSON and Ivar GIAEVER, whose theoretical and experimental contributions showed effects of quantum coherence and tunnelling (1973), Alex MÜLLER and Johannes Georg BEDNORZ, for the discovery of high temperature superconductors (1987), and Alexei ABRIKOSOV and Vitaly GINZBURG for their extensive work on type II superconductors and the physics of vortices (2003).

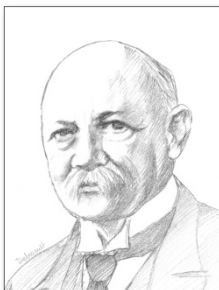
Less directly, we can note other winners of this prestigious award who made major contributions to the subject, such as Lev LANDAU (1962), Philip Warren ANDERSON (1967), Pierre-Gilles DE GENNES (1991) and John Michael KOSTERLITZ (2016) and David THOULESS (2016). Besides them, many famous physicists and chemists left their trace in the story. We can cite Walther MEISSNER and Robert OCHSENFELD, the brothers Fritz and Heinz LONDON, Brian PIPPARD, Bern MATTHIAS, Herbert FRÖHLICH, Paul CHU, all of whose names which will come back to us in this book. Finally, numerous women and men have devoted time and enthusiasm to the subject in the past, and continue to do so to this day.

As for the future, it is more than probable that the list of winners will be joined by whoever explains convincingly the mechanisms of what is termed “high-temperature” (High-T<sub>c</sub>) superconductivity, or who may discover new materials with critical temperature close to, or even higher than, room temperature.

### 1.2 - Experimental signs of superconductivity

#### 1.2.1 - *The discovery of superconductivity: the critical temperature*

The story begins in Leiden in Holland in the first decade of the 20th century. The research group of H.K. ONNES was unique in having both an almost industrial level of the apparatus needed for the liquefaction of oxygen and, subsequently, of hydrogen,



Heike Kamerlingh ONNES

and to have sufficient quantities of helium<sup>1</sup> to be able to liquify that as well. He succeeded on July 10th, 1908 and was then able to make experiments down to a temperature of 1 K. H.K. ONNES chose to attack one of the great problems that interested the physics community of that age: what is the behavior of the electrical resistance of metals when we approach absolute zero? Does it tend to vanish because of the disappearance of thermal noise? Does it increase because of the localization of free electrons? Does it approach some limiting value determined by impurities, as Augustus MATTHIESSEN had already predicted?

In this project, Gilles HOLST, a student of Heike Kamerlingh ONNES, was given the job of measuring the electrical resistivity of mercury, which can easily be purified by distillation. The measurements were communicated on April 28, 1911 in a short note to the Royal Academy of the Netherlands. It announced “with all reservations” that *“the resistivity of mercury apparently disappears just above 4 K.* Superconductivity had just been discovered in its most spectacular form: the total disappearance of electrical resistivity. The resistivity of the metal does not become weak or even very weak, it becomes strictly zero.



Gilles HOLST

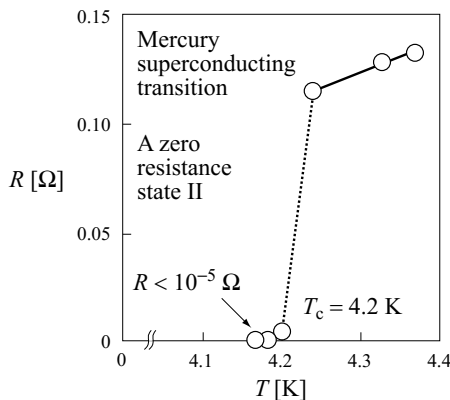


**Figure 1.1**  
**The historical evidence showing superconductivity**  
The original figure showing that mercury loses its resistivity at a temperature just below 4.2 K was published by H. K. ONNES<sup>2</sup>

In this new state of matter, it is possible to make a current flow in a closed circuit, without any generator (other than briefly to set the electrons in motion). Once started, the electrons flow indefinitely with constant speed. At this stage, the first quantity characterizing a superconducting material is the transition temperature  $T_c$  (the critical temperature) between the normal and superconducting states.

<sup>1</sup> He brought it from North Carolina in the United States, where the bulk of the world's supplies were to be found at that time.

### 1.2.2 - The magnetic behavior of superconductors

If the drop to zero of the electrical resistivity of superconductors is the most spectacular phenomenon, their response to a magnetic field was just as unexpected and has turned out to be particularly rich in consequences.

#### *The MEISSNER-OCHSENFELD effect*



Robert OCHSENFELD

In 1933, in Berlin, Walther MEISSNER and Robert OCHSENFELD showed that magnetic field  $\mathbf{B}$  is “expelled” from superconductors, that is to say that when subjected to an external magnetic field, they divert the field lines so that the magnetic field vanishes inside<sup>2</sup>. The superconducting material behaves as a perfect diamagnet.<sup>3</sup>



Walther MEISSNER

#### *Critical fields and superconductors of types I and II*

Very early on, magnetization measurements showed that the superconducting phase existed in a limited range, not only of temperature but also of magnetic field. After much confusion and conflicting experimental results it was finally the theoretical analysis of A. ABRIKOSOV<sup>4</sup> in 1957 that showed that superconductivity can disappear via two distinct scenarios, thus leading to the classification of superconducting materials into those of type I and of type II.

In a superconductor of type I, the superconductivity vanishes abruptly at a critical value  $H_c$  of the field.  $H_c$  is always small, with  $\mu_0 H_c$  no more than 0.1 tesla. Only pure elemental superconductors (with a few exceptions, such as Niobium), are of type I.

In a type II superconductor, there is no discontinuity to be seen, but rather a gradual weakening of the magnetic response starting from a lower critical magnetic field  $H_{c1}$ . Complete suppression of superconductivity occurs only when the field reaches an upper critical value  $H_{c2}$  which can be very high ( $\mu_0 H_{c2}$  may be several tens of, or even a hundred, teslas). Superconducting compounds and alloys are all of type II.

### 1.2.3 - Critical current

As well as the temperature and magnetic field, a finite density of electrical current also destroys superconductivity when it exceeds some critical value. We shall see

2 W. MEISSNER, R. OCHSENFELD (1933) *Naturwissenschaften* **21**, 787.

3 W. MEISSNER and R. OCHSENFELD interpreted their result as seeing “a possible analogy to ferromagnetism”; this will be taken up by the LONDON brothers. It is true that W. HEISENBERG had just provided a “microscopic” quantum theory based on interactions between the spins of closely neighbouring electrons.

4 A.A. ABRIKOSOV (1957) *Sov. Phys. JETP* **5**, 1974.

that in type I superconductors, the critical current density is intrinsically related to the field  $H_c$ , while in type II superconductors the critical current depends strongly on the metallurgy and, more generally, on the microstructure of the material. The mechanisms determining the critical currents are very different in the two types of superconductor. We note that wires of Nb-Ti (the type II superconducting alloy most used in the manufacture of magnets) can survive current densities of 1000, even 5000 A mm<sup>-2</sup>, without generating any heat.

#### 1.2.4 - The isotope effect<sup>5</sup>

This is a more discrete effect, which could have passed unnoticed, but fundamental to the understanding of superconductivity: for a given material it was noticed that the transition temperature  $T_c$  is linear in the inverse of the square root of the atomic mass. This observation shows that it is not only the electronic structure that is to be considered, but that atomic vibrations, whose frequency is inversely proportional to the square root of the atomic mass, are actively involved.

#### 1.2.5 - JOSEPHSON currents and flux quantization

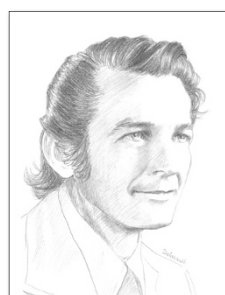


Brian JOSEPHSON

The very specific nature of the superconducting state appeared without question in 1962 in a paper by Brian JOSEPHSON which shocked the scientific community;<sup>6</sup> according to this brilliant young thesis student, an electrical current may flow between two bulk superconductors separated by a thin insulating layer, *even when there is no potential difference between the two*. Even more surprising, his theory predicted that applying a constant potential leads to the appearance of an alternating current between the two superconductors.

These predictions, based on a kind of BOSE condensation of the superconducting charges and on the fixing of the phases of the associated wave-functions, were immediately confirmed by experiment. Formation of a macroscopic quantum state, which implies quantification of the magnetic field flux, is the basis of the development of an ultra-sensitive technique for measuring magnetic fields (SQUID) as well as a multitude of other subtle effects.

Ivar GIAEVER demonstrated the existence of a tunnelling effect between a superconductor and a normal metal separated by a thin insulating barrier.



Ivar GIAEVER

<sup>5</sup> Isotope Effect: The transition temperature  $T_c$  depends on the isotope, *i.e.* on the atomic mass. Now the mass determines the vibrational frequency of the atomic lattice.

<sup>6</sup> B.D. JOSEPHSON (1962) *Phys. Lett.* **1**, 251.

## 1.3 - Phenomenological models

Despite its spectacular features, superconductivity proved to be one of the most difficult problems that the physicists of the first half of the 20th century had to deal with. The community had to wait 44 years (1911-1955) before finally a satisfactory theory (BCS) was published by John BARDEEN, Leon COOPER and Robert SCHRIEFFER.

The initial attempts to explain this “super-conductivity” were all trying to consider the perfect conductivity as a limiting case of metallic conductivity. As only classical models of electrical conduction were available (BOHR’s model of the atom dates from 1913) such efforts were in vain. In 1922 Albert EINSTEIN, whose assistance H.K. ONNES had called for in clarifying the question, admitted:

*...With our considerable ignorance of complicated quantum mechanic systems, we are far from being able to formulate these ideas in a comprehensive theory. We can only attack the problem experimentally...*

With no more success, the most brilliant minds of this era, from EINSTEIN to FEYNMAN, including SCHRÖDINGER and many others, agonized over this phenomenon with the aim of finding an acceptable microscopic theory.

During all this time, however, experiments and results were accumulating. While lacking a credible microscopic model, physicists made several phenomenological models based on *ad hoc* equations with varying degrees of intuitive appeal or success, each describing a set of experimental results.

### 1.3.1 - LONDON theory

LONDON theory is one of the most noteworthy phenomenological theories. Following the work of W. MEISSNER and R. OCHSENFELD, Fritz LONDON and his younger brother Heinz recognized the condition  $\mathbf{B} = \mathbf{0}$  as the fundamental property of the superconducting state. The challenge was no longer to explain the perfect conductivity

but the perfect diamagnetism, *i.e.* the state where the system responds to an external magnetic field by developing a super-current which generates a field in response that is equal, but opposite to, the applied field. In face of this challenge, the LONDON brothers invented the radically new concept of the existence of a macroscopic quantum state. Proceeding by analogy with LANGEVIN’s model for the magnetic susceptibility of atoms, they made the hypothesis that *the bulk superconductor can be considered as a single, enormous, diamagnetic atom*<sup>7</sup>.



Fritz LONDON

7 F. LONDON (1960) *Superfluids: Vol I Macroscopic Theory of Superconductivity* 2<sup>nd</sup> edition, Dover, New York; (2005) *Une conception nouvelle de la supra-conductibilité*, re-edition Hermann.



Heinz LONDON

With the equations that bear his name, Fritz LONDON presented the first satisfactory electromagnetic model in 1933,<sup>8</sup> which described in a precise way the MEISSNER effect of the expulsion of magnetic fields **B**. It also showed that if the magnetic field really vanishes at the heart of the superconductor it does not do so near the surface, but penetrates a distance  $\lambda_L$  called the LONDON penetration depth. This was the first characteristic length scale that emerged for the superconducting state.

In the wake of this result, and in order to obtain numerical values for the

penetration depth closer to the experimental results, Brian PIPPARD generalized LONDON's equations to include non-local effects, thereby introducing the coherence length, which was to become the second characteristic length of superconductivity. Inherent to superconductivity and reduced by the impurities, the coherence length leads also to a renormalisation of the LONDON penetration depth, renamed simply penetration depth  $\lambda$ .



Brian PIPPARD

### 1.3.2 - *The thermodynamic approach*

In parallel with LONDON's work, Cornelius Jacobus GORTER and Hendrik CASIMIR developed a thermodynamic approach to superconductivity in which they considered the normal-superconducting transition as a proper phase transition. They constructed a phenomenological model of two fluids, one superconducting and the other normal, with both intensive and extensive variables, an internal energy, thermodynamic functions and potentials; in short all the tools of thermodynamics. The success was all the greater as it described the superconducting/normal phase transition and, by integrating the negative surface energy associated with the penetration depth, it opened up the path towards an understanding of type II superconductivity.

### 1.3.3 - *GINZBURG-LANDAU Theory*

We have to wait until 1950, however, to see an approach associating electromagnetism and thermodynamics as was proposed by Vitaly GINZBURG and Lev LANDAU<sup>9</sup>. By generalizing the LANDAU model of phase transitions, they proposed a set of equations (the GINZBURG-LANDAU equations) to describe the behavior of the order parameter of the transition, vanishing in the normal phase and non-vanishing in the superconducting phase. With Alexei ABRIKOSOV



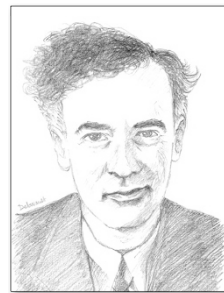
Vitaly GINZBURG

<sup>8</sup> F. LONDON (1934) *Phys. Rev.* **45**, 379.

<sup>9</sup> V. GINZBURG & L. LANDAU (1950) *Zh. Eksp. Teor. Fiz.* **20**, 1064.

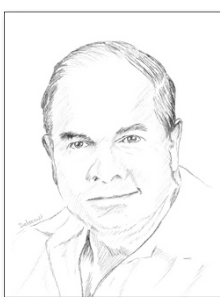
and Lev GORKOV, they assisted in the birth of the GLAG (GINZBURG-LANDAU-ABRIKOSOV-GORKOV) theory.

This formulation, essentially derived from pure intuition, proved to be very powerful in practice. The equations imply not only the MEISSNER effect and the penetration depth of the magnetic field, but also lead to the appearance of the second characteristic length. This coherence length,  $\xi$ , can be interpreted as the minimal distance required for any variation in the density of superconducting carriers.



Lev LANDAU

### 1.3.4 - Vortices



Alexei ABRIKOSOV



Lev GORKOV

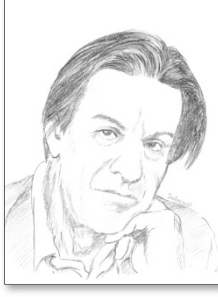
By solving, towards the middle of the 1950's, the GINZBURG-LANDAU equations, A. ABRIKOSOV showed that the sign of the surface energy for a normal-superconducting interface depends on the ratio between the characteristic lengths for penetration of a magnetic field  $\lambda$  (the penetration depth) and for coherence  $\xi$ :

- » in materials where  $\xi < \lambda$  the interface surface energy turns negative when the material is subject to a field exceeding  $H_{c1}$ , which leads the system to develop internal "lines of normal phase" (or vortices), thus explaining the decrease in magnetization density of type II superconductors above this field  $H_{c1}$ ;
- » in materials where  $\xi > \lambda$  the interface surface energy is always positive and the material remains uniformly superconducting until the transition to the normal state. When the field reaches the critical value  $H_c$  the transition occurs simultaneously throughout the material.

The nature, type I or II, of the superconductor thus depends on the relative values of these two lengths.



Daniel CRIBIER



Pierre-Gilles DE GENNES

Daniel CRIBIER was the first experimentalist to show explicitly the existence of a vortex lattice, following the suggestion of Pierre-Gilles DE GENNES, the most prominent leader of the *Orsay "School" of Physics*.

## 1.4 - The microscopic BCS theory

Despite the advances facilitated by the GINZBURG-LANDAU theory, at the beginning of the 1950's superconductivity remained as mysterious as ever with respect to its microscopic origins. Things started to move faster, however, with the arrival of two fundamental results: the proof of the rôle of phonons and the appearance of COOPER pairs.

While the involvement of lattice vibrations (phonons), seen via the isotope effect, was well known, it was only in 1953 and the calculations of Herbert FRÖHLICH<sup>10</sup> that the idea emerged of an attractive interaction, *via* the phonons, between two electrons of opposite velocities and spins (*phonon drag*).

The following year, Leon COOPER<sup>11</sup> showed that if two electrons of opposite wave-vector and spin on the FERMI surface feel an attractive interaction, they will form a bound pair whose energy is less than the sum of the kinetic energy of the individual particles. Such a pair is called a “COOPER pair”.

Starting from these results, John BARDEEN, Leon COOPER and Robert SCHRIEFFER developed the BCS theory, for which they were to receive the NOBEL prize in 1972.<sup>12</sup> They described the collective behavior of COOPER pairs by exploiting many-body techniques of calculation. With a very limited number of parameters they reproduced, explained and quantified most experimental results: the MEISSNER effect, the electrodynamic behavior, the coherence length, the critical field, the critical temperature, specific heat, thermodynamic properties... They showed that the charge carriers are definitely not individual electrons but COOPER pairs, and that a minimal energy  $\Delta$  must be applied to the system in order to create the first excited states in the form of single electrons (quasi-particles). This energy  $\Delta$ , called the superconducting gap, plays a central role in superconductivity.



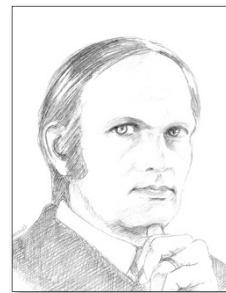
Herbert FRÖHLICH



John BARDEEN



Leon COOPER



Robert SCHRIEFFER

<sup>10</sup> H. FROHLICH (1950) *Phys. Rev.* **79**, 845; (1952) *Proc. Roy. Soc. A* **215**, 291; (1954) *Adv. Phys.* **3**, 325.

<sup>11</sup> L.N. COOPER (1956) *Phys. Rev.* **104**, 1189.

<sup>12</sup> J. BARDEEN, L.N. COOPER & J.R. SCHRIEFFER (1957) *Phys. Rev.* **108**, 1175.

## 1.5 - Tunnelling effects

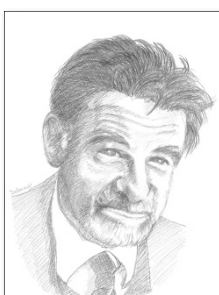
Coming shortly after BCS, studies of tunnelling effects between two bulk superconductors separated by an insulating barrier shed light on two processes:

- » the JOSEPHSON effect, which corresponds to the transport of “whole” COOPER pairs from one bulk superconductor to the other. This transfer is controlled by the phase difference between the coherent condensates formed by the COOPER pairs of each superconductor;
- » tunnelling across the insulating barrier by individual electrons (or more exactly by quasi-particles) formed by the unbinding of COOPER pairs.<sup>13</sup> This gives rise to many spectacular effects, including ANDREEV-SAINT-JAMES reflections<sup>14</sup> predicted independently by Alexander ANDREEV in Moscow and Daniel SAINT-JAMES in Paris, and provides vital information on the gaps, densities of state, the intensities of electron-phonon coupling and so on...

## 1.6 - A great diversity of superconducting materials

For a long time, the only known superconductors were metals or metal alloys. As their critical temperatures did not exceed 9.2 K for Niobium (the pure element with the highest  $T_c$ ) or 23.2 K for the metallic compound  $\text{Nb}_3\text{Ge}$  discovered in 1973, there was a certain waning of interest in superconductors. Nonetheless some activity continued. It was rewarded by an initial success constituted by the discovery, in 1980 by Denis JÉRÔME and his group, of purely organic superconductors<sup>15</sup> whose critical temperatures were not very high, but this proved that superconductivity was not just restricted to metals and metal alloys.

Then came the real revolution at the hands of Alex MÜLLER and Georg BEDNORZ. Convinced that the most promising candidates for high critical temperatures would



Alex MÜLLER



Georg BEDNORZ

be found more in the direction of oxides, they managed to synthesize a material with Lanthanum (La), Barium (Ba), Copper (Cu) and Oxygen (O). On January 27th 1986 they observed a rapid decrease in the resistivity at around 30 K which they interpreted as signalling the presence of a superconducting phase.

13 I. GIAEVER (1960) *Phys. Rev. Lett.* **5**, 147.

14 A. ANDREEV (1964) *Zh. Ekspерим. i. Teор. Fiz.* **46**, 1823 (*Soviet Physics JETP* **19**, 1228)  
D. SAINT-JAMES (1964) *J. de Physique* **25**, 899.

15 D. JÉRÔME *et al.* (1980) *J. Phys. Lett. (Paris)* **41**, L45.

Just like H. K. ONNES and G. HOLST in an earlier age, they made sure that the results were reproducible and with the caution of their predecessors, submitted to the journal *Zeitschrift für Physik*<sup>16</sup> an article with the title *Possibility of a high temperature superconductor in the system Ba-La-Cu-O*. This started a race to find similar compounds with a transition temperature that would be even higher. This was how shortly after, the compound Y-Ba-Cu-O, whose critical temperature  $T_c$  of 93 K is therefore above that of liquid nitrogen, was discovered by Paul CHU.<sup>17</sup> It was then the turn of more complex compounds with  $T_c = 110$  K (1988), 128 K (1991), 138 K (1993)! All have in common the existence of CuO<sub>2</sub> planes carrying the superconductivity, whence their generic name of “cuprates”.



Paul CHU

More recently a multitude of new superconducting materials have been discovered: in 1991 the family of doped fullerenes doped with alkaline elements ( $T_c \leq 40$  K),<sup>18</sup> in 2001 the metallic compound MgB<sub>2</sub> ( $T_c = 39$  K),<sup>19</sup> in 2008 the iron-based family (pnictides) ( $T_c \leq 55$  K)<sup>20</sup> and in 2015 the compound SH<sub>3</sub>, the critical temperature of which reached 203K under a pressure of 155GPa.<sup>21</sup>

## 1.7 - “Unconventional” superconductors

As a good number of the new compounds possess electronic structures which are very different from those of metals and alloys, many researchers have questioned the very nature of the new superconductors and whether the model of BCS is appropriate for them.

From an experimental point of view, the zero resistivity, the MEISSNER effect, the penetration depth, the critical fields  $H_{c1}$  and  $H_{c2}$ , the flux quantum, the JOSEPHSON effects are all similar. In contrast, for some cases the gap is either anisotropic or multiple; in others, such as the cuprates, heavy fermions and certain organic compounds, the conducting phases coexists with magnetic fluctuations,<sup>22</sup> or even coexists with a magnetically ordered phase, two properties considered hitherto as being incompatible.

From the point of view of theory, the COOPER pair remains the fundamental component even if in some cases it seems to be constituted by two electrons of the same

16 A. MÜLLER & G. BEDNORZ (1986) *Zeitschrift für Physik* **4**, 189.

17 M.K. WU *et al.* (1987) *Phys. Rev. Lett.* **58**, 908.

18 A.F. HEBARD *et al.* (1991) *Nature* **350**, 600;  
M.J. ROSSEINSKY *et al.* (1991) *Phys. Rev. Lett.* **66**, 2830.

19 J. NAGAMATSU *et al.* (2001) *Nature* **410**, 63.

20 Y. KAMIHARA *et al.* (2008) *J. Am. Chem. Soc.* **130**, 3296.

21 A.P. DROZDOV *et al.* (2015) *Nature* **525**, 73.

22 See for example D. MANSKE (2004) *Theory of unconventional superconductors*, Springer.

spin (triplet superconductivity) in contrast to BCS where they are of opposite spin (singlet superconductivity). Perhaps more importantly, the pairing mechanism mediated by phonons is called into question; several theoretical models have been proposed with pairing mechanisms including magnetic fluctuations<sup>22</sup> as numerous experimental results<sup>23</sup> in cuprates and other systems would seem to suggest.



Jean ROSSAT-MIGNOT

In any case, a large number of the new superconductors differ, in one way or another, from the BCS model and intensive research is in progress to clarify the situation.

Jean ROSSAT-MIGNOT showed, by the inelastic scattering of neutrons, the occurrence of anti-ferromagnetic fluctuations in the superconductivity state of the cuprates. He showed in particular that the intensity of the antiferromagnetic resonance peak decreases with temperature, vanishing at  $T_c$ .

## 1.8 - Numerous spectacular applications

Thanks to their extraordinary properties, superconductors have never ceased to inspire. Many applications, linked to their perfect electrical conductivity, the expulsion of magnetic fields and to coherence effects have been dreamed up, and for a good number of them, implemented.

Thus the immense majority of the apparatus for Magnetic Resonance Imaging (MRI) are equipped with superconducting coils. Electromagnets with superconducting windings are familiar to scientific laboratories and are crucial to the operation of large instruments, such as the enormous hadron collider LHC of CERN or the future *tokamak* of the ITER project. On a more experimental level, motors, transformers and transmission lines and current limiters with superconducting wires have been designed and tested. A number of magnetically levitated trains function with superconducting coils and superconducting bearings are being developed.

Relying on the properties of JOSEPHSON junctions, the SQUID is an extremely sensitive probe of magnetic fields. Already the instrument of choice for ultra-sensitive measurements of magnetization, its use in medicine is under development in order to detect the electromagnetic activity of several different organs of the human body.

In a host of other contexts, superconductivity is also used in astrophysics (as ultra-sensitive particle detectors) in the engineering large particle detectors (for intense magnetic fields in very large volumes), in the resonant cavities of particle accelerators... Computers based on JOSEPHSON junctions using the flux quantum to store information have been tested with the idea of making ultra-rapid machines with low energy consumption.

---

23 J. ROSSAT-MIGNOD *et al.* (1991) *Physica C* **86**, 91.

The search for materials combining both extreme superconducting parameters (high transition temperatures, critical currents and critical fields) and satisfactory physico-chemical and mechanical properties of ductility and resistance, is currently very active in university laboratories as well as in industry. Advances in this will certainly lead to even more applications and extension of existing one on a greater scale.

### 1.9 - Superconductivity in the history of mankind

We should not forget that superconductivity is also a history of people. Several of the protagonists were directly involved in the drama and dark moments of the 20th century: the LONDON brothers, as German Jews, had to flee to live as exiles in England; Lev SHUBNIKOV was executed on the basis of falsified documents during the great Stalinist purges; the issue of the Soviet physics Journal *Zh. Eksperim. i. Teor. Fiz.*, published during the worst period of McCarthyism and the communist witch-hunt, and which included the famous article by GINZBURG and LANDAU, was thrown into the sea by the New York dock workers when it arrived by boat, and their work remained unknown until years later.

Following the “rediscovery” of superconductivity with the materials with high superconducting temperatures, several historical and popular works have been published. Amongst them, we note *The Cold Wars: A History of Superconductivity*<sup>24</sup> which follows the scientific paths pursued, the successes and the blind alleys, but also relates the story of the people who took part in the advancement of our scientific knowledge.

As specialist in low temperature physics, SHUBNIKOV worked on type II superconductors in particular. The intermediate phase between the completely MEISSNER phase and the normal state of type II superconductors now bears his name.



Lev SHUBNIKOV

<sup>24</sup> J. MATRICON & G. WAYSAND (1994) *The Cold Wars: A History of Superconductivity*, Rutgers University Press, translated from the French edition (1994) of *La guerre du froid : une histoire de la supraconductivité*, Seuil.

## Chapter 2

### LONDON THEORY

The first phenomenological approach to the electromagnetic behavior of superconductors was published in 1935 by the brothers Fritz and Heinz LONDON.<sup>1</sup> Fascinated by the results of MEISSNER and OCHSENFELD,<sup>2</sup> who had shown that within the superconductor the magnetic field  $\mathbf{B}$  vanishes irrespective of the thermal and magnetic history of the sample, they understood that the key feature of superconductivity is not the disappearance of the electrical resistance but rather the expulsion of the magnetic flux.

Now MAXWELL's equations, that govern electromagnetism, turn out to be incapable of including this effect. The most they can show is that, in a perfect conductor, the magnetic field cannot *vary* with time; to include the *exclusion* of the magnetic field, we must add some additional ingredient. This is precisely what was done by F. and H. LONDON, with the equations now bearing their name.

#### 2.1 - MAXWELL's equations

The theory of electromagnetism is based on the equations of MAXWELL in their bulk form:<sup>3</sup>

$$\nabla \times \mathbf{E} = -\frac{\partial \mathbf{B}}{\partial t} \quad (\text{M1}) \quad \nabla \cdot \mathbf{E} = \frac{\rho}{\epsilon_0} \quad (\text{M2}) \quad (2.1a)$$

$$\nabla \cdot \mathbf{B} = 0 \quad (\text{M3}) \quad \nabla \times \mathbf{B} = \mu_0 \mathbf{j} + \epsilon_0 \mu_0 \frac{\partial \mathbf{E}}{\partial t} \quad (\text{M4})$$

where  $\rho$  and  $\mathbf{j}$  represent respectively, the total charge and total current densities of the system, including polarization charges, displacement currents and AMPÈRE currents.

---

1 F. LONDON & H. LONDON (1935) *Proc. Roy. Soc. (London) A* **155**, 71.

2 W. MEISSNER & R. OCHSENFELD (1933) *Naturwissenschaften* **21**, 787.

3 In this book we will use the symbol  $\nabla$  for the gradient operator. Alternative notations that are common in the literature are:

$\nabla U = \mathbf{grad} U$ ;  $\nabla \cdot \mathbf{A} = \operatorname{div} \mathbf{A}$ ;  $\nabla \times \mathbf{A} = \mathbf{curl} \mathbf{A} = \mathbf{rot} \mathbf{A}$ ;  $\nabla \cdot \nabla U \equiv \nabla^2 U = \Delta U$ ;  $\nabla^2 \mathbf{A} = \Delta \mathbf{A}$  (vector with components  $\Delta A_x, \Delta A_y, \Delta A_z$ ).

At the surface, they imply the boundary conditions:

$$\begin{aligned}\mathbf{E}_{t1} &= \mathbf{E}_{t2} & (\mathbf{E}_2 - \mathbf{E}_1) \cdot \mathbf{n}_{12} &= \frac{\sigma_{\text{surf}}}{\epsilon_0} \\ (\mathbf{B}_{t2} - \mathbf{B}_{t1}) \times \mathbf{n}_{12} &= \mu_0 \mathbf{j}_{\text{surf}} & (\mathbf{B}_2 - \mathbf{B}_1) \cdot \mathbf{n}_{12} &= 0\end{aligned}\quad (2.1b)$$

where  $\sigma_{\text{surf}}$  and  $\mathbf{j}_{\text{surf}}$  represent the surface charge and current densities,  $\mathbf{n}_{12}$  is the unit vector normal to the surface, and the suffix “t” indicates that it is the tangential components of the variables that is concerned. These equations remain valid under all circumstances.

We must add the condition of charge conservation,

$$\nabla \cdot (\rho \mathbf{v}) + \frac{\partial \rho}{\partial t} = 0 \quad (2.1c)$$

where  $\mathbf{v}$  is the velocity of the electric charges.

In normal conductors we derive a constitutive relation between the current and electrical field: OHM’s law.

**Notation** - to avoid any confusion in signs, throughout this book the charge of the electron is defined as  $q_e = -e$  where  $e = 1.602 \cdot 10^{-19} \text{ C}$ .

## 2.2 - The behavior expected for a perfect conductor

Since from the point of view of electricity, the superconductor appears as a conductor offering no resistance (once it has been established in a superconducting ring, the current does not decay), it seems to be logical to first examine the effect of an electric field, and then of a magnetic field, on a perfect conductor.

### 2.2.1 - Electrical conduction in a normal conductor

Suppose that the ends of a normal metal wire are subject to a constant difference in potential. Within the metal a permanent electric field  $\mathbf{E}$  appears. Each electron experiences a force due to this field  $\mathbf{F} = q_e \mathbf{E}$ , to which is added a damping force  $\mathbf{f}$  which, to a first approximation, is proportional, and opposite, to its mean velocity of motion

$$\mathbf{f} = -\eta \langle \mathbf{v} \rangle. \quad (2.2)$$

The fundamental equation of motion is then written as ( $m$  is the electron mass)

$$q_e \mathbf{E} - \eta \langle \mathbf{v} \rangle = m \frac{d \langle \mathbf{v} \rangle}{dt}. \quad (2.3)$$

By integrating,

$$\langle \mathbf{v} \rangle = \frac{q_e}{\eta} \mathbf{E} \left( 1 - e^{-\frac{t}{\tau}} \right) \quad (2.4a)$$

where  $\tau = m/\eta$  is the characteristic time for reaching a steady velocity. From this result (Fig. 2.1), the speed increases linearly at short times ( $t \ll \tau$ ) and reaches a limiting value for long times ( $t \gg \tau$ )

$$\langle \mathbf{v}_\infty \rangle = \frac{q_e}{\eta} \mathbf{E}. \quad (2.4b)$$

In the steady state, the current density is proportional to the electronic density  $n$  and to the electric field  $\mathbf{E}$ ,

$$\mathbf{j} = n q_e \langle \mathbf{v}_\infty \rangle = \frac{n e^2}{\eta} \mathbf{E} \quad (2.5)$$

which is none other than the usual OHM's law  $\mathbf{j} = \sigma \mathbf{E}$ . The coefficient of proportionality  $\sigma$  is the *electrical conductivity* of the material and the resistivity is  $\rho = 1/\sigma$ .

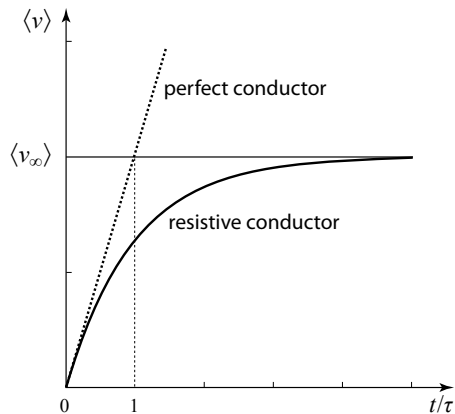


**Figure 2.1 - Variation in the mean velocity of electrons in a conductor subject to an electric field  $\mathbf{E}$**

For short times ( $t \ll \tau$ ), the velocity increases linearly to reach the steady state value  $\langle v_\infty \rangle$ , leading to OHM's law.

For copper with resistivity  $\rho = 1.7 \mu\Omega \text{ cm}$  at room temperature and electronic density  $n = 1.1 \cdot 10^{29} \text{ electrons m}^{-3}$ ,  $\tau = 2.5 \cdot 10^{-14} \text{ s}$ . Transient effects are therefore extremely short-lived and are only felt if the electrical field is carried by an electromagnetic wave of frequency at least  $10^{14} \text{ Hz}$ .

### 2.2.2 - Electrical conduction in a perfect conductor

A perfect conductor is defined as having a resistivity zero, *i.e.* with a damping coefficient  $\eta = 0$ . The equation of motion of an electron is simply

$$m \frac{d\mathbf{v}}{dt} = q_e \mathbf{E}. \quad (2.6a)$$

On the other hand, as the current density is determined by the velocity of electrons that at time  $t$  are to be found at the point  $\mathbf{r}$

$$\mathbf{j}(\mathbf{r}, t) = n q_e \mathbf{v}(\mathbf{r}, t) \quad (2.6b)$$

we have

$$\frac{\partial \mathbf{j}}{\partial t} = nq_e \frac{\partial \mathbf{v}}{\partial t} \quad (2.6c)$$

with (see App. 2A)

$$\frac{\partial \mathbf{v}}{\partial t} = \frac{d\mathbf{v}}{dt} - (\mathbf{v} \cdot \nabla) \mathbf{v}. \quad (2.7)$$

The difference between the total derivative and the partial derivative leads to the appearance of a non-linear term  $(\mathbf{v} \cdot \nabla) \mathbf{v}$  which vanishes if we have sufficient symmetry. If we restrict ourselves to such cases,

$$\frac{\partial \mathbf{j}}{\partial t} = \frac{ne^2}{m} \mathbf{E}. \quad (2.8)$$

It will be enough to consider such special cases in order to explain the fundamental difference between a perfect conductor and a superconductor.

### 2.2.3 - Magnetic fields in a perfect conductor

By taking the vector **curl** ( $\nabla$ ) of the equation (2.8) and taking into account the first equation of MAXWELL (2.1a-M1), we obtain the first relation between the *partial time derivatives* of  $\mathbf{B}$  and  $\mathbf{j}$

$$\mu_0 \nabla \times \left( \frac{\partial \mathbf{j}}{\partial t} \right) = -\frac{1}{\lambda_L^2} \left( \frac{\partial \mathbf{B}}{\partial t} \right) \quad (2.9)$$

where the characteristic length  $\lambda_L$  is defined by

$$\lambda_L^2 = \frac{m}{\mu_0 ne^2}. \quad (2.10)$$

Provided  $\mathbf{E}$  does not change too quickly, *i.e.* within the Quasi-Static Approximation (QSA),<sup>4</sup> the fourth MAXWELL equation (2.1a-M4) reduces to

$$\nabla \times \mathbf{B} = \mu_0 \mathbf{j} \quad (2.11)$$

and with this, we obtain a second relation between the same partial derivatives<sup>5</sup>

$$\nabla \times \left( \frac{\partial \mathbf{B}}{\partial t} \right) = \mu_0 \left( \frac{\partial \mathbf{j}}{\partial t} \right). \quad (2.12)$$

By taking the vector **curl** of expressions (2.9) and (2.12) and using:

» the vector relation  $\nabla \times (\nabla \times \mathbf{B}) = \nabla (\nabla \cdot \mathbf{B}) - \nabla^2 \mathbf{B}$ ,

» the third MAXWELL equation (2.1a-M3),  $\nabla \cdot \mathbf{B} = 0$ ,

<sup>4</sup> In a normal conductor, this approximation amounts to the neglect of  $(\epsilon_0 \mu_0 \partial \mathbf{E} / \partial t)$  which, at a frequency  $\omega$ , is  $\epsilon_0 \mu_0 \omega \mathbf{E}$ , to be compared to  $\mu_0 \mathbf{j} = \mu_0 \sigma \mathbf{E}$ . We can check that the two terms become of the same order of magnitude when  $\omega \approx 10^{12}$  Hz.

<sup>5</sup> The approximation consists of neglecting, within the expression (2.12), a term  $(\epsilon_0 \mu_0 \partial^2 \mathbf{E} / \partial t^2)$ , of order  $\epsilon_0 \mu_0 \omega^2 \mathbf{E}$ , with respect to  $(\mu_0 \partial \mathbf{j} / \partial t)$ , that by Equation (2.8) equals  $(\mathbf{E} / \lambda_L^2)$ . This means that  $\omega$  must be of order  $10^{15}$  Hz for the two terms to be comparable.

» and the condition of charge conservation in the steady state,  $\nabla \cdot \mathbf{j} = 0$ , we find the equations

$$\nabla^2 \left[ \frac{\partial \mathbf{B}(\mathbf{r}, t)}{\partial t} \right] = \frac{1}{\lambda_L^2} \left[ \frac{\partial \mathbf{B}(\mathbf{r}, t)}{\partial t} \right] \quad (2.13a)$$

$$\nabla^2 \left[ \frac{\partial \mathbf{j}(\mathbf{r}, t)}{\partial t} \right] = \frac{1}{\lambda_L^2} \left[ \frac{\partial \mathbf{j}(\mathbf{r}, t)}{\partial t} \right] \quad (2.13b)$$

which determine the *spatial variation of time derivatives* of the magnetic field  $\mathbf{B}$  and of the current density  $\mathbf{j}$  within a perfect conductor.

#### **Application to a perfectly conducting slab**

Consider a perfectly conducting slab, infinite in the  $y$  and  $z$  directions, and bounded by the surfaces  $x = \pm d/2$  (*i.e.* of thickness  $d$ ) (Fig. 2.2).

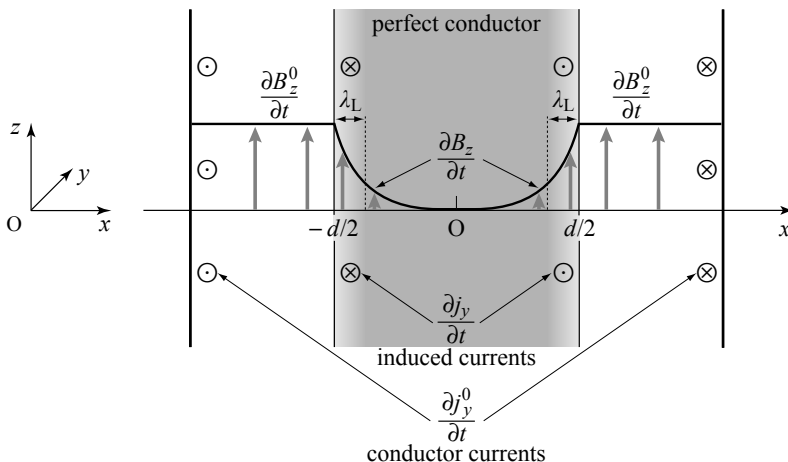


**Figure 2.2 - Variation of the current density  $\partial j_y / \partial t$  and magnetic field  $\partial B_z / \partial t$  inside a perfectly conducting slab that is subject to a time-varying magnetic field  $\partial B^0 / \partial t$**

A change in the current density  $j^0$  on the external layers creates a change in the field  $\mathbf{B}^0$ . The variation of the current densities  $j$  near the surface of the perfect conductor is that induced by the variation of  $\mathbf{B}^0$ . It is such that  $\mathbf{B}$  stays constant ( $\partial B_z / \partial t = 0$ ) inside the slab except for a transitional region of thickness  $\lambda_L$ .

When current densities  $\mathbf{j}^0(t)$  are applied by an experimentalist to metallic layers outside and parallel to the  $yz$  plane, they generate in the space around the perfect conductor, and inside it, a magnetic field  $\mathbf{B}^0(t)$  in the  $z$ -direction (the “field” of the conductor). How does the magnetic field  $\mathbf{B}(t)$  then develop within the slab of perfect conductor?

Because of the symmetries of the system,  $\mathbf{B}$  has a single component  $B_z(x)$  in the  $z$  direction that depends only the variable  $x$ .

Equation (2.13a) simplifies to

$$\frac{\partial^2}{\partial x^2} \left[ \frac{\partial B_z(x)}{\partial t} \right] - \frac{1}{\lambda_L^2} \left[ \frac{\partial B_z(x)}{\partial t} \right] = 0 \quad (2.14)$$

with solution

$$\frac{\partial B_z(x)}{\partial t} = \alpha e^{\frac{x}{\lambda_L}} + \beta e^{-\frac{x}{\lambda_L}} \quad (2.15)$$

where the constants of integration  $\alpha$  and  $\beta$  are determined by the conditions of continuity of the magnetic field, that is,

$$B_z \left( x = \frac{d}{2} \right) = B_z \left( x = -\frac{d}{2} \right) = B^0 \quad (2.16a)$$

and also

$$\frac{\partial B_z(x)}{\partial t} \left( x = \frac{d}{2} \right) = \frac{\partial B_z(x)}{\partial t} \left( x = -\frac{d}{2} \right) = \frac{\partial B^0}{\partial t}. \quad (2.16b)$$

This leads to the equation for the variation of the magnetic field in the perfect conductor

$$\frac{\partial B_z(x)}{\partial t} = \frac{\partial B^0}{\partial t} \frac{\cosh\left(\frac{x}{\lambda_L}\right)}{\cosh\left(\frac{d}{2\lambda_L}\right)} \quad (2.17)$$

whose form as a function of  $x$  is shown in Figure 2.2.

When  $d \gg \lambda_L$ , the expression (2.17) is close to being exponentially decreasing<sup>6</sup> from each surface of the perfect conductor

$$\frac{\partial B_z}{\partial t} \approx \frac{\partial B^0}{\partial t} e^{-\frac{u}{\lambda_L}} \quad (2.18)$$

where the variable  $u$  is the distance separating a given point in the material from its closest surface ( $u = d/2 - x$  for  $x > 0$  and  $u = d/2 + x$  for  $x < 0$ ).

To give a feeling for the scales, in copper this characteristic length  $\lambda_L$  is about 16 nm.

*Therefore, beyond a few times  $\lambda_L$ , a change in the external field  $\mathbf{B}^0(t)$  has no effect on the magnetic field inside a perfect conductor which remains unchanged.*

Qualitatively, the origin of this behavior is the appearance, near the surfaces of the slab of induced current densities  $\mathbf{j}(t)$  creating a field  $\mathbf{B}^a(t)$  equal and opposite to  $\mathbf{B}^0(t)$  beyond  $\lambda_L$ : this is the phenomenon of induction. According to the expression (2.12),  $\partial \mathbf{j}/\partial t$  has only one component  $\partial j_y(x)/\partial t$  in the  $y$ -direction and it depends only on the coordinate  $x$ ,

---

6 For  $x$  close to  $+d/2$  and putting  $x = d/2 - u$ , we have for  $x$  and  $d \gg \lambda_L$ ,  $\cosh(x/\lambda_L) \approx e^{x/\lambda_L}/2$  and  $\cosh(d/2 \lambda_L) \approx e^{d/2\lambda_L}/2$ .

$$\frac{\partial j_y(x)}{\partial t} = -\frac{1}{\mu_0} \frac{\partial}{\partial x} \left( \frac{\partial B_z}{\partial t} \right) \quad (2.19)$$

which gives, by differentiating (2.17) with respect to  $x$ ,

$$\frac{\partial j_y(x)}{\partial t} = \frac{-1}{\mu_0 \lambda_L} \frac{\partial B^0}{\partial t} \frac{\sinh\left(\frac{x}{\lambda_L}\right)}{\cosh\left(\frac{d}{2\lambda_L}\right)}. \quad (2.20)$$

Just as for  $\partial B_z / \partial t$ , this term decreases exponentially from the surface when  $d \gg \lambda_L$ ,

$$\frac{\partial j_y}{\partial t} \approx -\frac{1}{\mu_0 \lambda_L} \frac{\partial B^0}{\partial t} e^{-\frac{u}{\lambda_L}} \quad \text{for } x > 0 \quad (2.21)$$

confirming that in order to neutralize the *change* in magnetic field within the slab, there arises a *change* in the current density  $\partial j_y(x)/\partial t$  near its surface. This is of opposite sign to the *change* in current density in the external layers  $\partial j^0/\partial t$ .

This inductive mechanism is seen in all metals. In a normal metal, however, the induced current is damped by the resistivity in a time of order  $\tau$  ( $10^{-14}$  s in copper). After this time  $\mathbf{B}^a$  vanish and the magnetic field  $\mathbf{B}^0$  can “penetrate” the sample.

We have shown, therefore, that the perfect conductor reacts, in agreement with LENZ’s law, in opposing any change in the magnetic field in its interior (beyond a distance of  $\lambda_L$ ).

## 2.3 - Superconductor *versus* perfect conductor

In fact it is seen experimentally that the magnetic behavior of a superconductor is not what we would expect of a perfect conductor. To illustrate this difference, let us imagine two metallic conductors undergoing, at a temperature  $T_c$ , a normal/perfect conductor transition for the first, and a normal/superconductor transition for the second.

### 2.3.1 - Cooling in zero field followed by application of a field

We first consider an experiment in which, starting from a temperature  $T > T_c$  (Fig. 2.3, column 1), the samples are cooled in zero magnetic field (Figs 2.3a and 2.3c) to a temperature below  $T_c$ . Then, at this low temperature, a magnetic field  $\mathbf{B}^0$  is applied (Figs. 2.3b and 2.3d). Following this procedure, no difference in behavior appears between the “perfect conductor” and the superconductor: application of the magnetic field below the transition temperature leads in each case to the appearance very close to the surface of screening currents, which oppose the penetration of magnetic fields into the bulk of the samples.

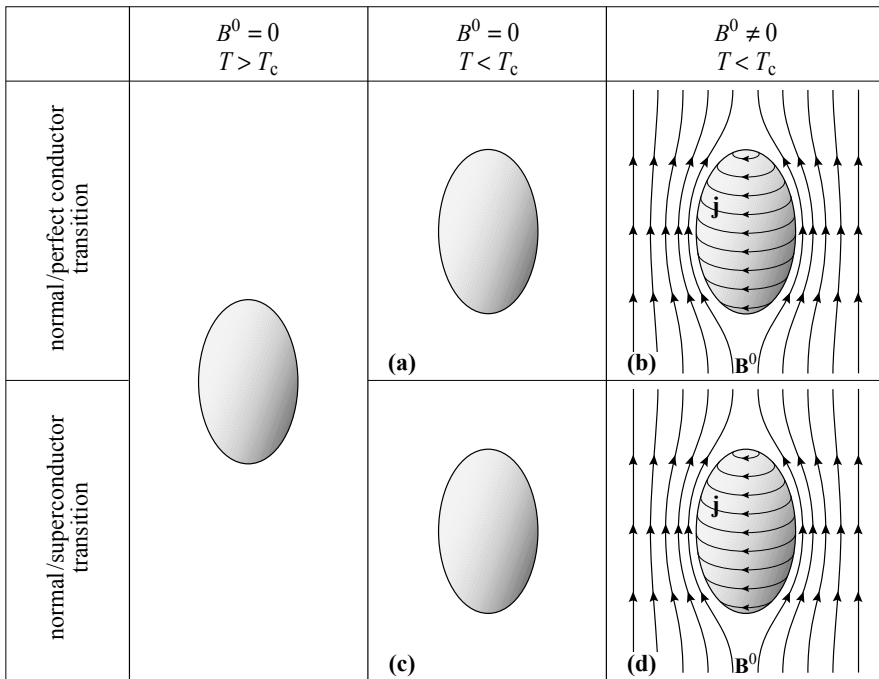


**Figure 2.3 - Magnetic behavior of a perfect conductor and of a superconductor cooled in zero field, and then subjected to a field  $B^0$  below the transition temperature**

No difference in the behavior can be seen. Despite the application of an external field, the magnetic field  $\mathbf{B}$  inside the sample remains zero.

### 2.3.2 - Application of the magnetic field when $T > T_c$ followed by cooling in the field

In the second experiment, we first apply the magnetic field  $\mathbf{B}^0$  on the samples when they are in the normal state at temperature  $T > T_c$  and then since they are conductors, as we emphasized at the end of section 2.2.3, the screening current are immediately damped and the magnetic field penetrates both samples (Fig. 2.4, column 1). We then cool both samples in the field, and it is here that very different behavior will be seen.

In the perfect conductor, the magnetic field stays the same and continues to cross the sample. As the external field has not varied below the transition temperature no induced current has been generated (Fig. 2.4a).

In contrast, in the superconductor, starting from  $T_c$  spontaneous screening currents, also known as LONDON currents, appear and expel the magnetic field from the sample (Fig. 2.4c). *The magnetic field is “expelled” from the superconductor by screening without induction.* This is the MEISSNER effect.

If we then turn off the magnetic field  $\mathbf{B}^0$ , the screening currents of the superconductor disappear just as spontaneously as they appeared (Fig. 2.4d) and the magnetic field remains at zero in the sample.

In contrast in the “perfect conductor”, which obeys LENZ’s law, turning off the magnetic field below  $T_c$  induces screening currents which oppose the *changes* in magnetic field in the sample, with the effect of trapping the magnetic field (Fig. 2.4b) applied above the transition temperature.

	$B^0 \neq 0$ $T > T_c$	$B^0 \neq 0$ $T < T_c$	$B^0 = 0$ $T < T_c$
normal/perfect conductor transition			
normal/superconductor transition			

Figure 2.4 - Comparison of the magnetic behavior of a perfect conductor and a superconductor cooled under a non-zero field  $\mathbf{B}^0$ , before (a and c) and after the field is turned off (b and d)

The magnetic field is *always* expelled from the superconductor (c and d)

while only its *changes* vanish in the perfect conductor (a and b).

The fundamental difference between the perfect conductor and the superconductor is therefore clearly seen: the perfect conductor obeys LENZ’s law with  $\partial\mathbf{B}/\partial t = \mathbf{0}$  while the superconductor maintains  $\mathbf{B} = \mathbf{0}$  inside. While the magnetic state of the “perfect conductor” depends on its history (compare Fig. 2.3a with 2.4b or 2.3b with 2.4a), the magnetic state of the superconductor does not (compare Fig. 2.3c with 2.4d or 2.3d with 2.4c).

## 2.4 - The LONDON equations

As experimental results showed that MAXWELL's equations were insufficient to describe the magnetic state of the superconductor, additional equations had to be added. These were originally written on intuitive grounds and are known as the LONDON equations.

### 2.4.1 - "Superconducting electrons"

Up to now the electrons that we have considered are implicitly the mobile electrons of the metal, that is to say all its free electrons. One of the first questions we may ask is, which of the electrons are "superconducting"?

The answer is that at 0 K all the free electrons can be considered as superconducting, but at non-zero temperatures a certain fraction of them behave as normal electrons, thereby reducing, by the same fraction, those that are superconducting. To take this into account, GORTER and CASIMIR<sup>7</sup> introduced a two-fluid model in which they divided the free electrons of density  $n$  into a sum of superconducting electrons of density  $n_s$  and normal electrons of density  $n_n$ ,

$$n = n_n + n_s. \quad (2.22)$$

The two, artificially separated, groups of electrons react in parallel to external stimuli, each according to its own nature. The non-resistive superconducting electrons "short-circuit" the resistive normal electrons. The qualitative justification and interpretation of this two-fluid model will be discussed in Chapter 8.

In the following discussion, only the superconducting electrons will be considered.

### 2.4.2 - First LONDON equation

The first LONDON equation is none other than the generalization of equation (2.8) with the symmetry constraint lifted. As only the superconducting electrons are involved, it can be written

$$\frac{\partial \mathbf{j}}{\partial t} = \frac{n_s e^2}{m} \mathbf{E} = \frac{1}{\mu_0 \lambda_L^2} \mathbf{E}. \quad (2.23)$$

This is an equation for the evolution of the current density; *i.e.* the acceleration of the charge density. The length

$$\lambda_L = \sqrt{\frac{m}{\mu_0 n_s e^2}} \quad (2.24)$$

is called the "LONDON penetration depth".

---

<sup>7</sup> C.J. GORTER & H.B.G. CASIMIR (1934) *Physica C* **153-155**, 1405.

### 2.4.3 - Second LONDON equation

The second LONDON equation is written by simply transposing equation (2.9). To include the fact that in the superconductor it is not the time derivative  $\partial\mathbf{B}/\partial t$  that is zero but  $\mathbf{B}$  itself. In the equations for the perfect conductor we then replace the time derivatives of  $\mathbf{j}$  and of  $\mathbf{B}$  simply by  $\mathbf{j}$  and  $\mathbf{B}$  themselves. In other words we substitute

$$\left( \frac{\partial \mathbf{B}}{\partial t} \right) \Rightarrow \mathbf{B} ; \quad \left( \frac{\partial \mathbf{j}}{\partial t} \right) \Rightarrow \mathbf{j} \quad (2.25)$$

which leads to LONDON's second equation

$$\mu_0 \nabla \times \mathbf{j} = - \frac{1}{\lambda_L^2} \mathbf{B} \quad (2.26)$$

and therefore, to the equations that determine the spatial variations of the magnetic field  $\mathbf{B}$  and the current density  $\mathbf{j}$  in the superconductor (see eq. 2.13a and 2.13b):

$$\nabla^2 \mathbf{B} - \frac{\mathbf{B}}{\lambda_L^2} = \mathbf{0} \quad (2.27a)$$

$$\nabla^2 \mathbf{j} - \frac{\mathbf{j}}{\lambda_L^2} = \mathbf{0}. \quad (2.27b)$$

We should not forget that here we have a phenomenological description whose microscopic justification will be seen only with the appearance of the microscopic BCS theory of superconductivity.

### 2.4.4 - Superconducting slab in an applied magnetic field

For the experimental set-up of Figure 2.2, by making the substitutions (2.25) into the results of section 2.2.3 (equations 2.17 and 2.20) we can obtain the distributions in space of the magnetic field and the current density in a superconducting slab of thickness  $d$ :

$$B_z(x) = B^0 \frac{\cosh\left(\frac{x}{\lambda_L}\right)}{\cosh\left(\frac{d}{2\lambda_L}\right)} \quad (2.28a)$$

$$j_y(x) = - \frac{B^0}{\mu_0 \lambda_L} \frac{\sinh\left(\frac{x}{\lambda_L}\right)}{\cosh\left(\frac{d}{2\lambda_L}\right)}. \quad (2.28b)$$

#### **Thick slab ( $d \gg \lambda_L$ )**

If the thickness of slab is large compared to the characteristic length  $\lambda_L$ , the approximations (2.18) and (2.21) remain valid, with both the magnetic field and current

density decreasing exponentially (Fig. 2.5) from each surface ( $u$  is the distance from the surface)

$$B_z \approx B^0 e^{-\frac{u}{\lambda_L}} ; \quad j_y \approx \pm \frac{B^0}{\mu_0 \lambda_L} e^{-\frac{u}{\lambda_L}}. \quad (2.29)$$

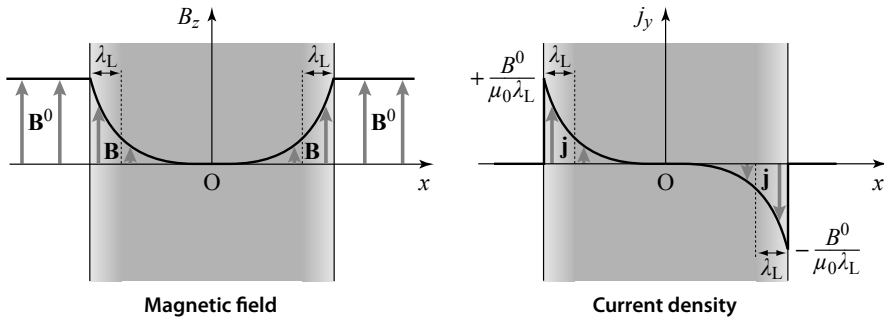


Figure 2.5 - Profiles of the magnetic field and current density in a thick superconducting slab ( $d \gg \lambda_L$ ) placed in a magnetic field  $B^0$  parallel to its surface

The magnetic field decreases exponentially from the surface over a distance of order the LONDON penetration depth and goes to zero deep within the sample. The current density, which decreases exponentially with the same length-scale, screens the external magnetic field.

#### *Thin slab ( $d \leq \lambda_L$ )*

If the slab thickness is comparable or smaller than the length  $\lambda_L$ , the approximation to decreasing exponentials is no longer justified. The magnetic field never approaches zero and the current density varies quasi-linearly from one surface of the sample to the other (Fig. 2.6) with a maximum value smaller than  $B_0/\mu_0 \lambda_L$ .

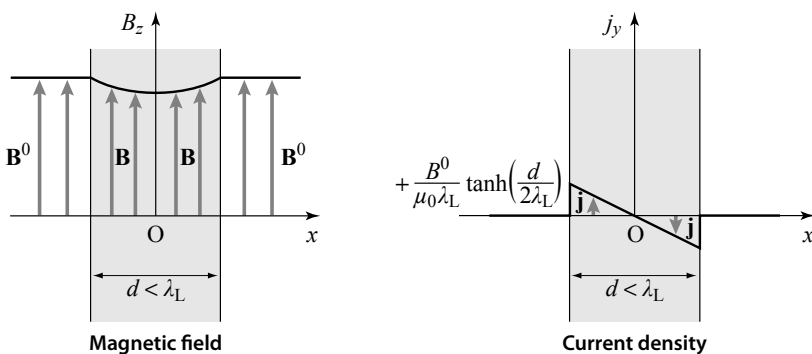


Figure 2.6 - Profiles of magnetic field and current density for a thin superconducting slab ( $d < \lambda_L$ ) placed in a magnetic field  $B^0$  parallel to its surface

The magnetic field does not have "sufficient space" to go to zero and therefore does not vanish. The current density at the surface is reduced.

Qualitatively, the superconducting currents do not have sufficient space to flow in order to completely screen the magnetic field.

The MEISSNER effect which requires exclusion of the magnetic field from the superconductor is therefore only complete after a few times the length  $\lambda_L$ .

## 2.5 - The LONDON penetration depth

### 2.5.1 - Experimental measurement of $\lambda_L$

We shall see later that the magnetic moment  $\mathcal{M}$  carried by a slab of thickness  $d$  subject to a magnetic field  $\mathbf{B}^0$  parallel to its largest surface is along  $\mathbf{B}^0$  and equals<sup>8</sup>

$$\mathcal{M} = \frac{\mathcal{V}}{\mu_0} \left[ \frac{1}{d} \int_{-d/2}^{d/2} \mathbf{B}(x) dx - \mathbf{B}^0 \right] \quad (2.30a)$$

i.e. it is the product of the sample volume  $\mathcal{V}$  and the difference between the mean magnetic field in the sample and the field  $\mathbf{B}^0$  generated by the external current. By integrating (2.30a) we find

$$\mathcal{M} = -\mathbf{B}^0 \frac{\mathcal{V}}{\mu_0} \left[ 1 - \frac{2\lambda_L}{d} \tanh\left(\frac{d}{2\lambda_L}\right) \right] \quad (2.30b)$$

with limiting behavior:<sup>9</sup>

$$\text{» for } d \gg \lambda_L \quad \mathcal{M} \approx -\mathbf{B}^0 \frac{\mathcal{V}}{\mu_0} \left[ 1 - \frac{2\lambda_L}{d} \right] \approx -\mathbf{B}^0 \frac{\mathcal{V}}{\mu_0} \quad (2.30c)$$

the magnetic moment is proportional to the sample volume.

$$\text{» for } d \leq \lambda_L \quad \mathcal{M} \approx -\frac{1}{3} \mathbf{B}^0 \frac{\mathcal{V}}{\mu_0} \left( \frac{d}{2\lambda_L} \right)^2 \quad (2.30d)$$

The magnetic moment depends explicitly on the ratio  $d/2\lambda_L$ , thus allowing for the determination of  $\lambda_L$  by making measurements on samples of varying thicknesses.

Other methods exist, using thin films or via inductive methods. In any case they are always subtle and relatively imprecise. In Table 2.1 we give a few values measured at 0 K, to be compared with those calculated from the relation (2.24).

For reasons that we will return to in the next chapter the measured values of the effective magnetic penetration depth, or simply penetration depth, denoted  $\lambda$ , are systematically greater than the LONDON penetration depth expressed by the relation (2.10).

<sup>8</sup> See the proof of this formula in the appendix to Chapter 4.

<sup>9</sup>  $\tanh(x) \approx 1$  for  $x \gg 1$  and  $[\tanh(x) \sim x - (x^3/3)]$  for  $x \ll 1$ .

**Table 2.1 - Values for the LONDON penetration depths as calculated and measured for a few metals**

Element	Al	Sn	Pb	Cd	Nb
Theoretical $\lambda_L$ [nm]	10	34	37	110	39
Measured $\lambda$ [nm] extrapolated to 0 K	50	51	39	130	44

### 2.5.2 - Temperature dependence of the LONDON penetration depth

Experiments show that the LONDON penetration depth  $\lambda_L(T)$  increases slowly at low temperatures and diverges approaching the transition temperature  $T_c$  (Fig. 2.7). The empirical law quoted most often to represent its behavior is

$$\lambda_L(T) = \lambda_L(0) \left[ 1 - \left( \frac{T}{T_c} \right)^4 \right]^{-\frac{1}{2}} \quad (2.31)$$

with near  $T_c$

$$\lambda_L(T) \approx (T_c - T)^{-\frac{1}{2}} \quad (2.32)$$

implying, from relations (2.24) and (2.32),

$$n_s(T) \approx (T_c - T) \text{ near } T_c. \quad (2.33)$$

This also indicates that the superconductivity disappears with the “conversion” of the superconducting electrons to normal electrons.

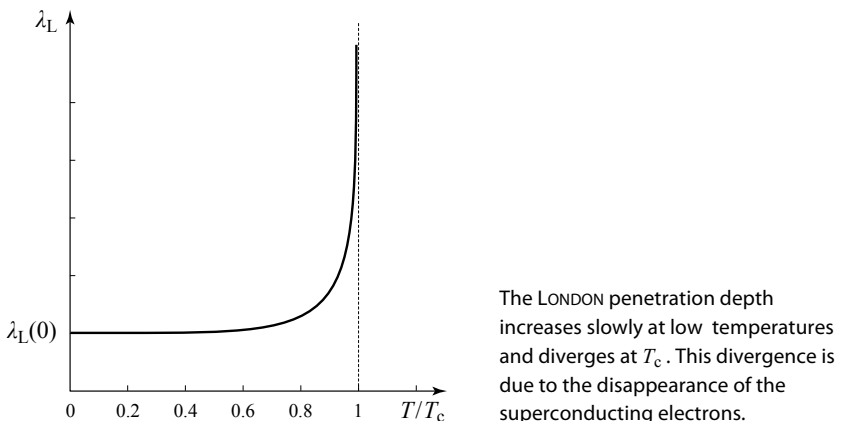


**Figure 2.7 - Thermal dependence of the LONDON penetration depth**

## 2.6 - Applications to superconducting wires

### 2.6.1 - A wire in magnetic field

The behavior of a cylindrical superconductor of radius  $R$ , placed in a magnetic field  $\mathbf{B}^0$  parallel to its axis (Fig. 2.8) is not fundamentally different from that of a slab.

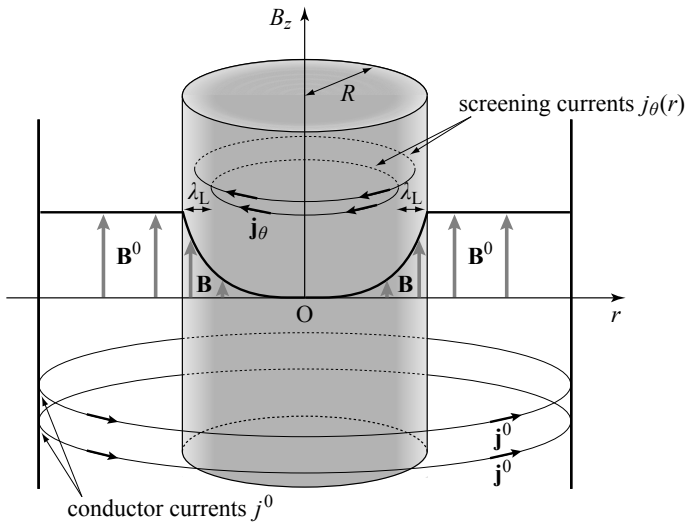


**Figure 2.8 - Superconducting wire subject to an applied field  $\mathbf{B}^0$  generated by the current density  $\mathbf{j}^0$  flowing in an external solenoid**

The axial magnetic field  $\mathbf{B}$  decreases exponentially under the influence of the screening current density  $\mathbf{j}$  normal to the radial direction. The large circles carrying  $\mathbf{j}^0$  represent the solenoid generating the field  $\mathbf{B}^0$  inside which the (solid) cylinder of radius  $R$  is placed.

The distribution of magnetic fields  $\mathbf{B}$  inside the cylinder is the solution of equation (2.27a) where, in cylindrical coordinates  $(r, \theta, z)$ ,  $\mathbf{B}$  has a single component along  $z$  and  $B_z$  depends only on  $r$ , leading to

$$\frac{d^2 B_z(r)}{dr^2} + \frac{1}{r} \frac{dB_z(r)}{dr} - \frac{1}{\lambda_L^2} B_z(r) = 0 \quad (2.34a)$$

or, changing to the variable  $\tilde{r} = r/\lambda_L$

$$\frac{d^2 B_z(\tilde{r})}{d\tilde{r}^2} + \frac{1}{\tilde{r}} \frac{dB_z(\tilde{r})}{d\tilde{r}} - B_z(\tilde{r}) = 0 \quad (2.34b)$$

which is the modified BESSEL equation of order zero<sup>10</sup> whose solutions are

$$B_z(\tilde{r}) = \alpha \mathcal{I}_0(\tilde{r}) + \beta \mathcal{K}_0(\tilde{r}) \quad (2.35)$$

where  $\mathcal{I}_0$  and  $\mathcal{K}_0$  are the modified BESSEL functions of first and second kind, respectively, of order zero.<sup>11</sup>

10 M. ABRAMOWITZ, I. STEGUN (1972) *Handbook of mathematical functions*, Wiley, 1972.

11 We can find in Appendix 2C, at the end of this chapter, the relevant properties of these special functions.

$\alpha$  and  $\beta$  are constants determined by the boundary conditions:

- » at the origin ( $r = 0$ ),  $B_z$  must be finite while the function  $\mathcal{K}_0$  diverges, implying that  $\beta = 0$ ;
- » at the surface ( $r = R$ ), the component  $B_z$  tangent to the surface must be continuous, or

$$B_z \left( \tilde{r} = \frac{R}{\lambda_L} \right) = B^0 \quad (2.36)$$

which leads to the expression for the magnetic field in the wire,

$$B_z(r) = B^0 \frac{\mathcal{I}_0\left(\frac{r}{\lambda_L}\right)}{\mathcal{I}_0\left(\frac{R}{\lambda_L}\right)}. \quad (2.37)$$

The current density  $\mathbf{j}$  can be found from  $\mathbf{B}$  by the fourth MAXWELL equation, using the symmetries and the formula for the derivatives of BESSEL functions (2.120)

$$j_\theta(r) = -\frac{1}{\mu_0} \frac{\partial B_z(r)}{\partial r} = -\frac{B^0}{\mu_0 \lambda_L} \frac{\mathcal{I}_1\left(\frac{r}{\lambda_L}\right)}{\mathcal{I}_0\left(\frac{R}{\lambda_L}\right)} \quad (2.38)$$

where  $\mathcal{I}_1$  is the modified BESSEL function of the first kind of order 1 (see App. 2C, Fig. 2.13).

If the wire's radius is large compared to the LONDON penetration depth ( $R \gg \lambda_L$ ), near the surface  $\tilde{r} \gg 1$ , we can replace the BESSEL functions by their asymptotic behavior (2.118 and 2.119) and using the fact that  $r$  is very close  $R$ , we find

$$B_z(r) \approx B^0 \frac{e^{-\frac{R-r}{\lambda_L}}}{\sqrt{\frac{r}{R}}} \approx B^0 e^{-\frac{u}{\lambda_L}} \quad ; \quad u = R - r \quad (2.39)$$

$$\text{and} \quad j_\theta(r) \approx -\frac{B^0}{\mu_0 \lambda_L} e^{-\frac{u}{\lambda_L}}. \quad (2.40)$$

Once again,  $B_z(r)$  and  $j_\theta(r)$  decrease exponentially below the surface. Within a layer of thickness a few times the LONDON penetration depth, there appears a circular current density that screens the magnetic field inside the cylinder. This is the equivalent, in cylindrical symmetry, of the thick slab shown in Figure 2.5. If the radius of the cylinder is small compared to  $\lambda_L$ , we find the equivalent of Figure 2.6.

### 2.6.2 - A current-carrying wire

When connected to the terminals of a current generator, the superconducting wire (a cylinder of radius  $R$ ) carries a total current of intensity  $I$  distributed according the current density  $\mathbf{j}(\mathbf{r})$ , which is the solution to equation (2.27b). In cylindrical coordinates with the  $z$  axis along the wire,  $\mathbf{j}$  has a single component  $j_z$  depending only on  $r$  and, as in the previous paragraph, it follows that

$$\frac{d^2 j_z(r)}{dr^2} + \frac{1}{r} \frac{d j_z(r)}{dr} - \frac{1}{\lambda_L^2} j_z(r) = 0 \quad (2.41)$$

whose solution is, after removing the divergent term at the origin,

$$j_z(r) = \alpha \mathcal{I}_0 \left( \frac{r}{\lambda_L} \right) \quad (2.42)$$

where the constant  $\alpha$  must be such that the flux of  $\mathbf{j}$  across the cross-section of the wire equals the injected current  $I$

$$I = \int_0^R j_z(r) 2\pi r dr = 2\pi \alpha \lambda_L^2 \int_0^{R/\lambda_L} \left( \frac{r}{\lambda_L} \right) \mathcal{I}_0 \left( \frac{r}{\lambda_L} \right) d \left( \frac{r}{\lambda_L} \right) \quad (2.43)$$

which gives by integration (relation 2.121),

$$j_z(r) = \frac{I}{2\pi R \lambda_L} \frac{\mathcal{I}_0 \left( \frac{r}{\lambda_L} \right)}{\mathcal{I}_1 \left( \frac{R}{\lambda_L} \right)}. \quad (2.44)$$

Once again, the current density is concentrated in a layer near the surface of thickness a few times the LONDON penetration depth, in which it decreases exponentially

$$j_z(u) \approx \frac{I}{2\pi R \lambda_L} e^{-\frac{u}{\lambda_L}} \quad ; \quad u = R - r. \quad (2.45a)$$

The profile of the magnetic field  $\mathbf{B}$  produced inside the wire by the current can be deduced from that of  $\mathbf{j}$  via LONDON's second equation (2.26). By the symmetries of the problem, it is purely tangential and decreases near the surface with the form

$$B_\theta(u) \approx \frac{\mu_0 I}{2\pi R} e^{-\frac{u}{\lambda_L}}. \quad (2.45b)$$

We see, then, that the localization of the current density close to the surface leads to the vanishing of the magnetic field  $\mathbf{B}$  in the bulk, which is a new example of the MEISSNER effect (Fig. 2.9).

Outside the wire, the magnetic field decreases as  $1/r$  as can easily be calculated using AMPÈRE's law.

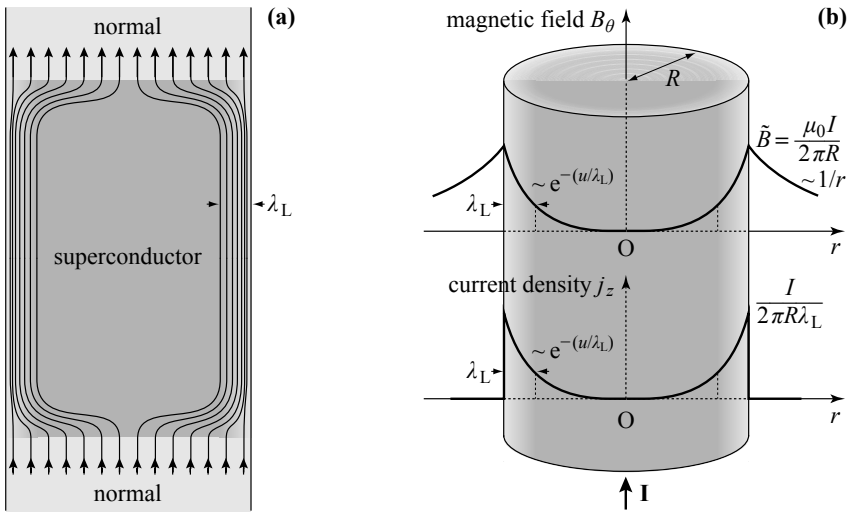


**Figure 2.9 - Profile of the current density  $I$  flowing in a superconducting wire**  
The axial current is distributed in close proximity to the surface, within a LONDON penetration depth. It is such that the magnetic field generated, which is tangential to radial vectors, is also localized within the LONDON penetration depth and vanishes at the core. The magnetic field falls off as  $1/r$  outside the wire.

### 2.6.3 - Thin current-carrying wire

By exactly same logic as that of section 2.4.4, we show that if the wire has a diameter equal to or less than the LONDON penetration depth, the current density does not have enough space to fall to zero. At most it will be slightly smaller in the center than near the surface. If  $R \ll \lambda_L$ ,  $j_z$  is almost uniform within the sample and then takes the value

$$j_z(r) \approx \frac{I}{\pi R^2} \quad (2.46a)$$

and the magnetic field is obtained from AMPÈRE's law:

$$\begin{aligned} \text{for } r < R \quad B_\theta(r) &\approx \frac{I}{\pi R^2} r \\ \text{for } r > R \quad B_\theta(r) &\approx \frac{I}{2\pi r}. \end{aligned} \quad (2.46b)$$

### 2.6.4 - Generalized response of the wire

These laws for the variation of the magnetic field and the current density in a superconducting wire whose diameter is much greater than  $\lambda_L$ , can be generalized, by defining  $\tilde{B}$  as the value of the magnetic field on the surface of the sample, to

$$B(u) = \tilde{B} e^{-\frac{u}{\lambda_L}} \quad (2.47a)$$

$$j(u) = \frac{\tilde{B}}{\mu_0 \lambda_L} e^{-\frac{u}{\lambda_L}} \quad (2.47b)$$

where:

- »  $\tilde{B} = B^0$  if the wire is placed in a field produced by external currents (relations 2.39 and 2.40);
- »  $\tilde{B} = \frac{\mu_0 I}{2\pi R}$  if the wire carries an injected current  $I$  (relations 2.45);
- »  $\tilde{B}$  is a combination of two components when the wire simultaneously carries a current and is subject to an external magnetic field  $\mathbf{B}^0$ .

**Remark** - When the superconductor is not infinite in the field direction, as can be the case of an actual wire or slab,  $\tilde{B}$  is the superposition of the applied field  $B^0$  and a contribution from the demagnetizing field (see Chap. 5).

## 2.7 - The OCHSENFELD experiment

We have now seen that, if it is placed in a magnetic field, the superconductor creates screening currents in a layer with characteristic thickness  $\lambda_L$ . These currents generate a magnetic field inside the material that we shall call  $\mathbf{B}^a$  (in reference to AMPÈRE currents in magnetism), which exactly compensates the applied field  $\mathbf{B}^0$ .

If the superconducting object is of finite size, the screening currents also strengthen the magnetic field outside the sample by the return of the field lines  $\mathbf{B}^a$  (Fig. 2.10b). We then have the classic image of magnetic field lines that go around the sample (Fig. 2.10c).

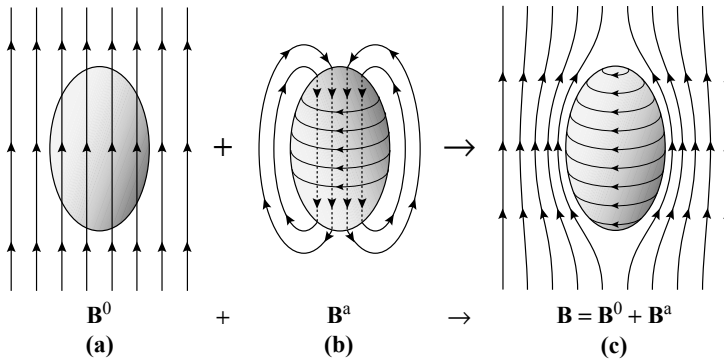
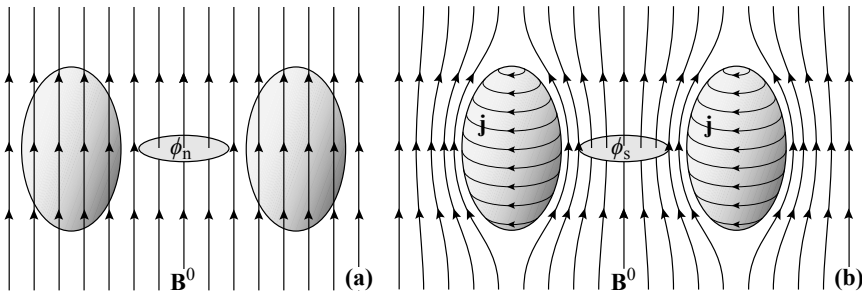


Figure 2.10 - Exclusion of the magnetic field

(a) The field  $B^0$  arising from external conductors. (b) The field  $B^a$  generated by the screening currents. (c) The total magnetic field: inside the superconductor, the fields  $B^0$  and  $B^a$  compensate, while outside they reinforce each other, thus the field lines near the surface are squeezed together.

Such an increase in the field near the surface was proved by OCHSENFELD by inserting a magnetic flux-meter between two superconducting samples separated by a small gap and subject to a uniform  $\mathbf{B}^0$  (Fig. 2.11).

- » When  $T > T_c$ : the metal is normal and the magnetic field uniform everywhere: the measured flux equals  $\phi_n = B^0 S$ .
- » When  $T < T_c$ : the metal becomes superconducting, the field lines “avoid” the samples and the magnetic field strengthens in the gap between them. The measured flux  $\phi_s$  becomes larger than  $\phi_n$ .



**Figure 2.11 - The OCHSENFELD experiment**

Made out of a material with a superconducting transition at temperature  $T_c$ , two identical ellipsoids, separated by a distance  $D$ , are placed in a uniform magnetic field  $\mathbf{B}^0$ . Using a coil with cross-section  $S$ , we measure the magnetic flux across the space separating the ellipsoids. **(a)**  $T > T_c$ : the metal is in its normal state and the magnetic field is uniform: the measured flux equals  $\phi_n = B^0 S$ . **(b)**  $T < T_c$ : the metal is superconducting. Part of the excluded magnetic field comes out and strengthens the field between the two ellipsoids. The flux through the coil increases.

In their original experiment,<sup>2</sup> MEISSNER and OCHSENFELD used two tin cylinders with parallel axes orientated perpendicular to the magnetic field. With their apparatus, they found a ratio  $\phi_s/\phi_n = 1.70$ , in remarkable agreement with the predicted value from calculations of 1.77.

## 2.8 - Non-simply-connected superconductor

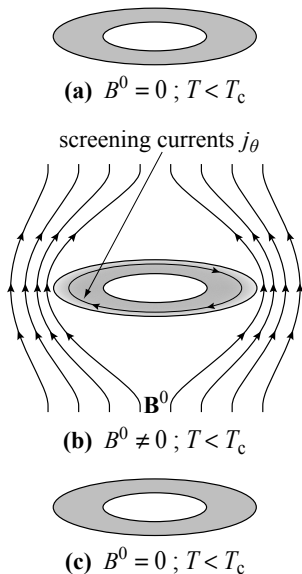
In section 2.3 we saw that a superconductor excludes the magnetic field in its bulk and, in particular, never traps a flux inside itself. Let us now see what happens to a superconductor that is not “simply connected”,<sup>12</sup> for example a punctured disc, and the possibility of trapping a magnetic field *in a hole* surrounded by superconducting material. To do this we will repeat the two procedures of turning on and then off the magnetic field, as in section 2.3.

<sup>12</sup> A solid is simply connected if any loop can be transformed to a point by continuous deformation. We also say that any loop is then homotopic to a point. A hollow sphere is simply connected, whereas a sphere with a hole drilled from one side to the other, or a torus, is not.

- » Sequence 1 - after cooling in zero field, a magnetic field is applied and then turned off while staying in the superconducting phase.
- » Sequence 2 - the field is applied in the normal phase, and then is turned off in the superconducting state after cooling in the field.

We follow the behavior of the magnetic field in each case.

### 2.8.1 - Sequence 1: cooling in zero field

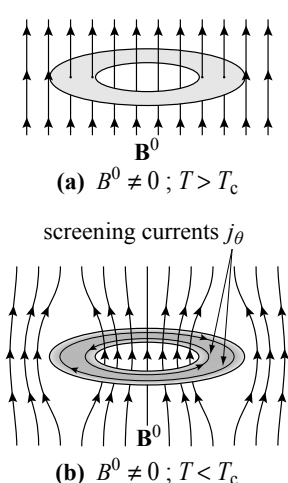


A disc with a hole is cooled in zero field below the critical temperature  $T_c$  of the superconducting transition of the material.

A magnetic field  $\mathbf{B}^0$  is applied parallel to the axis of the disc. The field lines go around the superconductor, with the appearance of screening currents at the outer edge of the disc.

The field  $\mathbf{B}^0$  is cut, the screening currents disappear, and we recover the initial state.

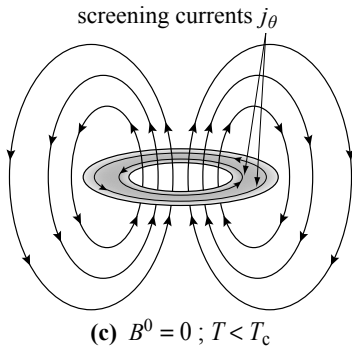
### 2.8.2 - Sequence 2: field cooling



The magnetic field is applied at high temperatures. It is uniform in the material and in the hole.

As we pass the transition under applied field, superconducting currents appear near the inner and outer surfaces in order to “expell” the magnetic field from the superconductor.

We note that they turn in opposite directions. The field lines are pushed towards the exterior and interior spaces.



When the field  $\mathbf{B}^0$  is turned off, the flux through the hole stays trapped. There remain both an interior screening current which preserves the magnetic field in the hole and an exterior current (which has reversed its direction) which prevents the returning flux lines from penetrating the sample.

### 2.8.3 - Conclusion

As we saw in the two sequences, at no moment, even temporarily, does the magnetic field cross the superconductor: neither after cooling in zero field, in order to transport the flux in the hole as the field is applied, nor after cooling in the field, then reducing this field to zero, in order to expel the flux initially in the hole.

## 2.9 - Analysis from the point of view of energy

### 2.9.1 - Energetic interpretation of the LONDON penetration depth

To go beyond electromagnetic and phenomenological arguments, it is now urgent to reconsider the LONDON penetration depth and see whether there is a stronger reason why both the magnetic field and the current density should decrease on the length scale  $\lambda_L$ , and not on some other scale.

To examine this question, we make the hypothesis that in a semi-infinite superconductor the magnetic field does decrease from the surface exponentially, but that it does so on a length-scale  $\Lambda$  that is *a priori* unknown,

$$B(u) = \tilde{B} e^{-\frac{u}{\Lambda}}. \quad (2.48)$$

Then by MAXWELL's fourth equation the current density decreases with the same length,

$$j(u) = \frac{\tilde{B}}{\mu_0 \Lambda} e^{-\frac{u}{\Lambda}} = \frac{B(u)}{\mu_0 \Lambda}. \quad (2.49)$$

We will show that minimizing the energy of the system implies

$$\Lambda = \sqrt{\frac{m}{\mu_0 n_s e^2}} = \lambda_L. \quad (2.50)$$

To do this, we consider the two relevant energies.

### Magnetic energy

The magnetic energy density equals  $B^2/2\mu_0$  which, by integration in the direction normal to the surface, leads to a surface magnetic energy per unit area

$$E_{\text{mag}} = \frac{\tilde{B}^2}{2\mu_0} \int_0^\infty e^{-\frac{2u}{\Lambda}} du = \frac{\Lambda \tilde{B}^2}{4\mu_0}. \quad (2.51)$$

### Kinetic energy of the superconducting electrons

By virtue of their velocity  $\mathbf{v}$ , the superconducting electrons possess a kinetic energy density,

$$n_s \left( \frac{1}{2} m v^2 \right) = \frac{1}{2} \left( \frac{m}{n_s e^2} \right) \mathbf{j}^2(\mathbf{r}) \quad (2.52)$$

which, after integrating as previously, leads to a kinetic energy per unit surface area

$$E_{\text{kin}} = \frac{1}{2} \frac{m}{n_s e^2} \frac{\tilde{B}^2}{\Lambda^2 \mu_0^2} \int_0^\infty e^{-\frac{2u}{\Lambda}} du = \frac{1}{4} \frac{m}{n_s e^2} \frac{\tilde{B}^2}{\Lambda \mu_0^2}. \quad (2.53)$$

The total energy is therefore

$$E_{\text{tot}} = E_{\text{kin}} + E_{\text{mag}} = \frac{1}{4} \frac{m}{n_s e^2} \frac{\tilde{B}^2}{\Lambda \mu_0^2} + \frac{\Lambda \tilde{B}^2}{4\mu_0} \quad (2.54)$$

and its minimization  $\frac{dE_{\text{tot}}}{d\Lambda} = 0$  leads to the equilibrium value  $\Lambda$  that is none other than the LONDON penetration depth

$$\Lambda^2 = \frac{m}{\mu_0 n_s e^2} = \lambda_L^2. \quad (2.55)$$

*The LONDON penetration depth  $\lambda_L$  appears as the value of  $\Lambda$  which minimizes the sum of the magnetic field energy and the kinetic energy of the superconducting charges inside the superconductor.*

#### 2.9.2 - The second LONDON equation by a variational method

Armed with this result found from a sample that is assumed semi-infinite, let us now demonstrate that the second LONDON equation can be obtained by minimizing the sum of the magnetic and electron kinetic energies over the whole volume of a superconductor of any shape.

The magnetic energy stored in the whole sample volume  $\mathcal{V}$  is

$$E_{\text{mag}} = \iiint_{\mathcal{V}} \frac{\mathbf{B}^2(\mathbf{r})}{2\mu_0} d^3r. \quad (2.56)$$

The total kinetic energy of the superconducting electrons is written as

$$E_{\text{kin}} = \frac{1}{2} \iiint_V m n_s \mathbf{v}^2(\mathbf{r}) d^3 r. \quad (2.57)$$

Knowing that the current density is linked to the velocity of the electrons by  $\mathbf{j}(\mathbf{r}) = n_s q_e \mathbf{v}(\mathbf{r})$  and taking into account MAXWELL's fourth equation that connects  $\mathbf{B}$  to  $\mathbf{j}$ , the kinetic energy of the superconducting electrons becomes

$$E_{\text{kin}} = \frac{1}{2\mu_0} \lambda_L^2 \iiint_V (\nabla \times \mathbf{B})^2 d^3 r \quad (2.58)$$

giving the total energy

$$E_{\text{tot}} = \frac{1}{2\mu_0} \iiint_V [\mathbf{B}^2 + \lambda_L^2 (\nabla \times \mathbf{B})^2] d^3 r. \quad (2.59)$$

As required by variational methods with fixed boundary conditions,<sup>13</sup> the profile of the actual magnetic fields  $\mathbf{B}(\mathbf{r})$  is that which is "stationary" with respect to the total energy  $E_{\text{tot}}$ , the surface magnetic field being fixed. In other words,  $\mathbf{B}$  adopts a profile such that to first order,  $\delta E_{\text{tot}}$  vanishes for any variation  $\delta \mathbf{B}(\mathbf{r})$  of the magnetic fields.

Let us consider then, a small variation of the magnetic field  $\delta \mathbf{B}(\mathbf{r})$ . The energy variation which results is written

$$\delta E_{\text{tot}} = \frac{1}{2\mu_0} \iiint_V [2\mathbf{B} \cdot \delta(\mathbf{B}) + 2\lambda_L^2 (\nabla \times \mathbf{B}) \cdot \delta(\nabla \times \mathbf{B})] d^3 r \quad (2.60)$$

which, using the vector identity,

$$\nabla \cdot (\mathbf{u} \times \mathbf{w}) = \mathbf{w} \cdot (\nabla \times \mathbf{u}) - \mathbf{u} \cdot (\nabla \times \mathbf{w})$$

with  $\mathbf{w} = \delta \mathbf{B}$  and  $\mathbf{u} = \nabla \times \mathbf{B}$  and STOKES' law

$$\iint (\mathbf{u} \times \mathbf{w}) d\mathbf{S} = \iiint \nabla \cdot (\mathbf{u} \times \mathbf{w}) d^3 r$$

can be written as a sum of bulk and surface terms

$$\begin{aligned} \delta E_{\text{tot}} &= \frac{1}{\mu_0} \iiint_V \delta \mathbf{B}(\mathbf{r}) \cdot [\mathbf{B}(\mathbf{r}) + \lambda_L^2 \nabla \times (\nabla \times \mathbf{B}(\mathbf{r}))] d^3 r \\ &\quad + \frac{1}{\mu_0} \iint_S [\delta \mathbf{B}(\mathbf{r}_{\text{surf}}) \times (\nabla \times \mathbf{B}(\mathbf{r}_{\text{surf}}))] d\mathbf{S}. \end{aligned} \quad (2.61)$$

---

<sup>13</sup> The variational method with fixed boundary conditions is the same used when we deduce the equations of LAGRANGE from the principle of least action: C. COHEN-TANNOUDJI, B. DIU & F. LALOE (1977) *Quantum Mechanics - Volume II*, 1481-1497, Hermann, Paris, 2<sup>nd</sup> revised edition.

The surface integral always vanishes as, by hypothesis,  $\mathbf{B}$  is fixed on the surface ( $\delta\mathbf{B}(\mathbf{r}_{\text{surf}}) = \mathbf{0}$ ). Looking for stationary values of the energy therefore implies that the volume integral must vanish for any  $\delta\mathbf{B}(\mathbf{r})$ , which requires

$$\left[ \mathbf{B} + \lambda_L^2 \nabla \times (\nabla \times \mathbf{B}) \right] = \mathbf{0}. \quad (2.62)$$

By use of the fourth equation of MAXWELL,  $\nabla \times \mathbf{B} = \mu_0 \mathbf{j}$ , this relation leads to the second LONDON equation (relation 2.26).

*Thus LONDON's equation has a deep meaning in terms of energy, as it follows from a principle of the stationary value of the sum of magnetic energy in the sample and the kinetic energy of the superconducting electrons.*

## 2.10 - Description of superconductivity in fluid-mechanical terms

Rather than starting with a perfect conductor, an alternative approach to deriving LONDON's equations is by reference to the equations of fluid mechanics.<sup>14</sup>

For this purpose we consider a non-viscous fluid consisting of particles of mass  $m$ , density  $n_s$  each bearing a charge  $q_e$ . If subject to electric  $\mathbf{E}$  and magnetic  $\mathbf{B}$  fields and in the absence of viscosity, each particle has dynamics governed by the equation

$$m \frac{d\mathbf{v}}{dt} = q_e (\mathbf{E} + \mathbf{v} \times \mathbf{B}) \quad (2.63)$$

which using the relation (appendix 2A, relation 2.105),

$$\frac{d\mathbf{v}}{dt} = \frac{\partial \mathbf{v}}{\partial t} + \frac{1}{2} \nabla \mathbf{v}^2 - \mathbf{v} \times (\nabla \times \mathbf{v}) \quad (2.64)$$

leads to the equation

$$\frac{\partial \mathbf{v}}{\partial t} - \frac{q_e}{m} \mathbf{E} + \frac{1}{2} \nabla \mathbf{v}^2 = \mathbf{v} \times \left( \nabla \times \mathbf{v} + \frac{q_e}{m} \mathbf{B} \right). \quad (2.65)$$

Taking the **curl** of the two sides of the equation (*i.e.* applying  $\nabla \times$ ), using the MAXWELL equation  $\nabla \times \mathbf{E} = -\frac{\partial \mathbf{B}}{\partial t}$  and defining,

$$\mathbf{w} = \nabla \times \mathbf{v} + \frac{q_e}{m} \mathbf{B} \quad (2.66)$$

we have, in addition,

$$\frac{\partial \mathbf{w}}{\partial t} = \nabla \times (\mathbf{v} \times \mathbf{w}). \quad (2.67)$$

This relation is known in hydrodynamics as the HELMHOLTZ equation, and is a first order linear differential equation. With the specific boundary condition  $\mathbf{w} = \mathbf{0}$  at

---

<sup>14</sup> For the complete derivation, see F. LONDON (1960) *Superfluids - Macroscopic theory of superconductivity - Volume 1*, Dover, New York, 27-95.

$t = 0$ ,  $\mathbf{w}$  stays zero for all times. The “fluid mechanical” approach to the LONDON equations consists, then, in proposing that the superconductor behaves as a non-viscous liquid satisfying the HELMHOLTZ equation in which we require that in all circumstances

$$\mathbf{w} = \mathbf{0}. \quad (2.68)$$

Substituted in equation (2.65), with the definition (2.66) of  $\mathbf{w}$ , leads to the equations

$$\frac{\partial \mathbf{v}}{\partial t} + \frac{1}{2} \nabla \mathbf{v}^2 = \frac{q_e}{m} \mathbf{E} \quad (2.69)$$

$$\nabla \times \mathbf{v} = -\frac{q_e}{m} \mathbf{B}. \quad (2.70)$$

Equation (2.69) is none other than the first LONDON equation (2.23) with the addition of the non-linear term  $\frac{1}{2} \nabla \mathbf{v}^2$  that LONDON<sup>13</sup> showed to be very small. In fact, in the literature, depending on the author, we find both forms of the first LONDON equation, with and without the non-linear terms.

The relation (2.70) leads, using  $\mathbf{j} = n_s q_e \mathbf{v}$ , to the second LONDON equation (2.26).

### Two remarks

- » This approach suggests, and in fact this is true, that the equation (2.70) is more general than LONDON’s second equation and that we should return to it if, for some reason the relation  $\mathbf{j} = n_s q_e \mathbf{v}$  is not satisfied (see, for example, the problem of the LONDON moment of a rotating superconducting sphere to be discussed in the following paragraph). For this reason, the relation (2.70) will be called the “root” of the second LONDON equation.
- » The “fluid-mechanic” approach is similar to the “inductive” approach developed in section 2.4.3, in the sense that we impose specific conditions on general equations. To propose  $\mathbf{w} = \mathbf{0}$  and its corollary  $\partial \mathbf{w} / \partial t = \mathbf{0}$  is the parallel of the replacement of  $\partial \mathbf{B} / \partial t = \mathbf{0}$  by  $\mathbf{B} = \mathbf{0}$ .

## 2.11 - The LONDON moment

### 2.11.1 - Intuitive approach

By adopting the “fluid mechanics” view of the previous section, BECKER and co-workers<sup>15</sup> analysed the effect of the rotation of a superconducting sphere on one of its axes.

The scenario is as follows:

- » initially the sphere is at rest,  $\mathbf{B} = \mathbf{0}$ ,  $\mathbf{v} = \mathbf{0}$ ,  $\mathbf{w} = \mathbf{0}$ ;

---

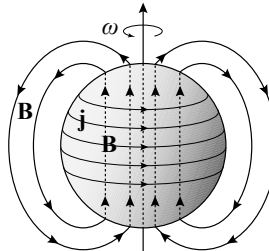
<sup>15</sup> R. BECKER, F. SAUTER & G. HELLER (1933) *Z. Physik* **85**, 772.

- » the sphere and the positive charges, the “ions”, that are rigidly tied to it, are sent into rotation. But owing to the lack of viscosity the superconducting electrons stay at rest, leading to an increasing “ionic” current inside the sphere;
- » the “ionic” current generates a magnetic field  $\mathbf{B}$  within the sphere;
- » this increasing field induces currents which oppose its cause. This means they tend to cancel the initial currents, something they can do only by imparting a velocity  $\mathbf{v} \neq \mathbf{0}$  to the superconducting electrons which then start to move;
- » in the limit where the rotational speed of the electrons catches up to that of the ions, the current density goes to zero everywhere in the sample and the internal magnetic field completely disappears. This leads to a contradiction since we would have a state where  $\mathbf{B} = \mathbf{0}$  and  $\mathbf{v} \neq \mathbf{0}$  with  $\nabla \times \mathbf{v} \neq \mathbf{0}$ , and therefore  $\mathbf{w} \neq \mathbf{0}$ , which contradicts the originally assumed (2.68);
- » intuition, and our calculations will back this up, tells us that the electrons towards the outside, those within a penetration depth, will turn less quickly than the ions, and create a current loop generating a magnetic field  $\mathbf{B}$  inside the sphere such that at every point in the sphere  $\mathbf{w} = \mathbf{0}$ ;
- » the magnetization associated with this field  $\mathbf{B}$  constitutes the LONDON moment.

**Figure 2.12 - A rotating superconducting sphere**

A superconducting sphere in rotation generates in its interior (below  $\lambda_L$ ) a uniform magnetic field  $\mathbf{B}$ .

This field is caused by currents concentrated within a LONDON penetration depth, resulting from the difference in velocities of the electrons and the ions fixed to the sphere.



### 2.11.2 - Calculating the LONDON moment

Let  $\mathbf{v}$  be the speed of the superconducting electrons,  $\mathbf{v}_0$  the velocity of the ions and  $\boldsymbol{\omega}$  the angular velocity of the sphere. By definition,

$$\mathbf{v}_0 = \boldsymbol{\omega} \times \mathbf{r}. \quad (2.71)$$

The relations between the electron velocity  $\mathbf{v}$ , the current density  $\mathbf{j}$  and the magnetic field  $\mathbf{B}$  are rather unusual since the current density is written

$$\mathbf{j} = n_s q_e (\mathbf{v} - \mathbf{v}_0) \quad (2.72)$$

which, substituted into the fourth MAXWELL equation, gives

$$\nabla \times \mathbf{B} = \mu_0 \mathbf{j} = \mu_0 n_s q_e (\mathbf{v} - \mathbf{v}_0). \quad (2.73)$$

In this atypical case, the “root” LONDON equation (2.70)

$$\nabla \times \mathbf{v} = -\frac{q_e}{m} \mathbf{B} \quad (2.74)$$

cannot be transformed into the second LONDON equation because  $\mathbf{j}$  and  $\mathbf{v}$  are connected by (2.72) and not (2.6b).

In addition, noticing that  $\nabla \times \mathbf{v}_0 = 2 \boldsymbol{\omega}$  and therefore

$$\nabla \times (\nabla \times \mathbf{v}_0) = \mathbf{0} \quad (2.75)$$

we can verify that the relations (2.73), (2.74) and (2.75) lead to

$$\nabla \times [\nabla \times (\mathbf{v} - \mathbf{v}_0)] = -\frac{1}{\lambda_L^2} (\mathbf{v} - \mathbf{v}_0) \quad (2.76a)$$

and that, in so far as we are looking for a stationary state, we have,

$$\nabla \cdot \mathbf{j} = n_s q_e \nabla \cdot (\mathbf{v} - \mathbf{v}_0) = 0. \quad (2.76b)$$

As a consequence the equation (2.76a) can be written in the form <sup>16</sup>

$$\nabla^2 (\mathbf{v} - \mathbf{v}_0) = \frac{1}{\lambda_L^2} (\mathbf{v} - \mathbf{v}_0). \quad (2.77)$$

On the other hand, using the relations (2.71) and (2.74) and the fact that, as  $\mathbf{w}$  is constant, its curl vanishes, we see that the fourth MAXWELL equation leads to the relation

$$\nabla \times \left[ \nabla \times \left( \mathbf{B} + \frac{2m}{q_e} \boldsymbol{\omega} \right) \right] = -\frac{1}{\lambda_L^2} \left( \mathbf{B} + \frac{2m}{q_e} \boldsymbol{\omega} \right) \quad (2.78)$$

and since  $\nabla \cdot \mathbf{B} = 0$  by the third MAXWELL equation and  $\nabla \cdot \boldsymbol{\omega} = 0$  as we are in a steady state, we can also write

$$\nabla \cdot \left( \mathbf{B} + \frac{2m}{q_e} \boldsymbol{\omega} \right) = 0 \quad (2.79)$$

which leads finally to, just as in (2.77),

$$\nabla^2 \left( \mathbf{B} + \frac{2m}{q_e} \boldsymbol{\omega} \right) = \frac{1}{\lambda_L^2} \left( \mathbf{B} + \frac{2m}{q_e} \boldsymbol{\omega} \right). \quad (2.80)$$

Equations of the type of (2.77) and (2.80) have been solved in sections 2.2 and 2.4. Their solutions are functions that vanish in the bulk except for a layer of thickness of order  $\lambda_L$  near the surface, which appears as a transitional zone. Below a thickness  $\lambda_L$ , therefore

$$\mathbf{v} = \mathbf{v}_0 \quad \text{and} \quad \mathbf{B} = -\frac{2m}{q_e} \boldsymbol{\omega} \quad (2.81)$$

---

<sup>16</sup>  $\nabla^2 \mathbf{A} = \nabla(\nabla \cdot \mathbf{A}) - \nabla \times (\nabla \times \mathbf{A})$

which signifies that the speed of the electrons inside the sphere has caught up with that of the ions and that the magnetic field there is uniform (and not zero!).

In the Appendix to Chapter 4 (section A4.1) we recall that to establish a uniform magnetic field  $\mathbf{B}$  inside a sphere, it is necessary to form a distribution of circular surface currents, with axes parallel to the direction of the field, and whose intensity is (see Fig. 4.15)

$$j_{\text{surf}} = \frac{3}{2\mu_0} B \sin \theta \quad (2.82)$$

where  $\theta$  is the azimuthal angle measured from the axis of magnetization of the sphere. These are currents that develop over a layer of thickness  $\lambda_L$  and are caused by the superconducting electrons rotating more slowly than the ions.

The magnetization below  $\lambda_L$  is then (see App. 4, section 4.1, Tables 4.6 and 4.7;  $N = \frac{1}{3}$  for a sphere)

$$\mathbf{M} = \frac{3}{2\mu_0} \mathbf{B} = \frac{3m}{\mu_0 e} \boldsymbol{\omega} \quad (2.83)$$

and the total moment of the rotating sphere of radius  $R \gg \lambda_L$ , to be called the “LONDON moment” equals

$$\mathcal{M} = \frac{4\pi R^3 m}{\mu_0 e} \boldsymbol{\omega}. \quad (2.84)$$

Predicted by BECKER *et al.* in 1933,<sup>15</sup> worked out in detail by LONDON,<sup>14</sup> the LONDON moment was measured for the first time by HILDEBRANDT en 1964.<sup>17</sup> It was recently used in an extremely precise experiment aiming to measure the curvature of space-time near the Earth (The *Gravity Probe B Experiment*).<sup>18</sup>

## 2.12 - The LONDON equation in the LONDON gauge

### 2.12.1 - The concept of gauge

In electromagnetism, the electric  $\mathbf{E}$  and magnetic  $\mathbf{B}$  fields,

$$\mathbf{E} = -\nabla V - \frac{\partial \mathbf{A}}{\partial t} \quad ; \quad \mathbf{B} = \nabla \times \mathbf{A} \quad (2.85)$$

are derived from a pair of scalar and vector potentials ( $V, \mathbf{A}$ ) which are not unique since the same electromagnetic field ( $\mathbf{E}, \mathbf{B}$ ) can stem also from a pair ( $V', \mathbf{A}'$ ) related to the pair ( $V, \mathbf{A}$ ) by the transformation

$$V' = V - \frac{\partial \chi(\mathbf{r}, t)}{\partial t} \quad \text{and} \quad \mathbf{A}' = \mathbf{A} + \nabla \chi(\mathbf{r}, t) \quad (2.86)$$

<sup>17</sup> A.F. HILDEBRANDT (1964) *Phys. Rev. Lett.* **12**, 190.

<sup>18</sup> See the site: <http://einstein.stanford.edu/>

where  $\chi(\mathbf{r}, t)$  is a **scalar** function of space and time.

Such a change of potentials is called a “gauge transformation” and the choice of the pair  $(V, \mathbf{A})$  is called a “gauge fixing”.

For each problem one can chose the most practical gauge that leads to the simplest equations most directly. For example, for the propagation of electromagnetic waves the LORENTZ gauge is usually used,

$$\nabla \cdot \mathbf{A} + \epsilon_0 \mu_0 \frac{\partial V}{\partial t} = 0 \quad (2.87)$$

as it has the advantage of symmetrizing the space-time equations of potentials  $\mathbf{A}$  and  $V$  and to have them appear as wave equations.

### 2.12.2 - The LONDON gauge

By replacing  $\mathbf{B}$  by  $\nabla \times \mathbf{A}$  in the second LONDON equation (2.26) it becomes

$$\nabla \times \left( \mathbf{j} + \frac{1}{\mu_0 \lambda_L^2} \mathbf{A} \right) = \mathbf{0} \quad (2.88)$$

which can be integrated by noting that the curl of a gradient is zero, so that

$$\mathbf{j} + \frac{1}{\mu_0 \lambda_L^2} \mathbf{A} = \nabla \chi(\mathbf{r}, t) \quad \text{or, equivalently, } \mathbf{j} = \frac{n_s q_e}{m} [\nabla \chi(\mathbf{r}, t) - q_e \mathbf{A}] \quad (2.89)$$

where the integration constant  $\chi(\mathbf{r}, t)$  is any scalar function of space and time.

As the current density  $\mathbf{j}$  is a measurable quantity, and hence a physical quantity that must be invariant under gauge transformations, it follows that the gradient of the integration constant  $\nabla \chi(\mathbf{r}, t)$  and the vector potential  $\mathbf{A}$  cannot be independent: to choose one is to determine the other. The choice of the LONDON gauge has the effect of making the equations for  $\mathbf{A}$  and  $\mathbf{j}$  resemble each other.

Now  $\mathbf{j}$  is subject to two physical constraints:

» conservation of charge, which in a stationary state is written

$$\nabla \cdot \mathbf{j} = 0 \quad (2.90)$$

» the impossibility of the current to leave the superconductor, which forces the component of the current density  $\mathbf{j}$  along the normal  $\mathbf{n}$  to the surface to vanish

$$\mathbf{j} \cdot \mathbf{n}|_{\text{surf}} = 0. \quad (2.91)$$

The LONDON gauge consists of imposing the same constraints on the vector potential  $\mathbf{A}$  as on  $\mathbf{j}$

$$\begin{aligned} \nabla \cdot \mathbf{A} &= 0 && \text{in the bulk} \\ \mathbf{A} \cdot \mathbf{n}|_{\text{surf}} &= 0 && \text{at the surface.} \end{aligned} \quad (2.92)$$

Applying the divergence and the scalar product with the normal to the two lines of equation (2.89) gives, using the vector relation  $\nabla \cdot \nabla \chi = \nabla^2 \chi$ , the two relations

$$\nabla^2 \chi = 0 \quad \text{and} \quad \mathbf{n} \cdot \nabla \chi = 0 \quad \text{at the surface. (2.93)}$$

### 2.12.3 - The second LONDON equation in the LONDON gauge

The relation  $\nabla^2 \chi = 0$  associated with the continuity of  $\chi$  makes this function a harmonic function with the property of being constant in a simply connected<sup>11</sup> volume if the component of its gradient normal to the surface is zero.<sup>19</sup>

With this property of  $\chi$ , the relation (2.89) becomes

$$\mathbf{j}(\mathbf{r}) = -\frac{n_s e^2}{m} \mathbf{A}(\mathbf{r}) = -\frac{1}{\mu_0 \lambda_L^2} \mathbf{A}(\mathbf{r}) \quad \text{in the LONDON gauge. (2.94)}$$

Thus, in the LONDON gauge, where we impose the choice  $\nabla \cdot \mathbf{A} = 0$  and  $\mathbf{n} \cdot \mathbf{A} = 0$ ,  $\mathbf{A}$  and  $\mathbf{j}$  are proportional. As a corollary, the vector potential satisfies the same equation as  $\mathbf{j}$  and  $\mathbf{B}$  (relations 2.27) or

$$\nabla^2 \mathbf{A} - \frac{\mathbf{A}}{\lambda_L^2} = \mathbf{0}. \quad (2.95)$$

### 2.12.4 - Momentum $\mathbf{p}$ and the LONDON equation

The momentum  $\mathbf{p}$  of a particle of charge  $q_e$ , placed in the magnetic field of vector potential  $\mathbf{A}$  is (see App. 9.1)<sup>20</sup>

$$\mathbf{p} = m\mathbf{v} + q_e \mathbf{A}. \quad (2.96)$$

The LONDON equation can also be obtained with the postulate that its **curl** be zero. Indeed, using  $\mathbf{B} = \nabla \times \mathbf{A}$ , we have

$$\frac{1}{m} \nabla \times \mathbf{p} = \nabla \times \mathbf{v} + \frac{q_e}{m} \mathbf{B} = \mathbf{0} \quad (2.97)$$

which is none other than the equation (2.74), that is to say the “root” second LONDON equation that again appears to be the more fundamental. The usual second LONDON equation is found by writing  $\mathbf{j} = n_s q_e \mathbf{v}$ .

If, in addition, we require  $\mathbf{p} = \mathbf{0}$ , we obtain, in the LONDON gauge

$$\mathbf{p} = \left[ \frac{m}{n_s q_e} \mathbf{j} + q_e \mathbf{A} \right] = \mathbf{0} \quad (2.98)$$

which is the LONDON equation in the LONDON gauge!

<sup>19</sup> See Appendix 2B.

<sup>20</sup> C. COHEN-TANNOUDJI, B. DIU & F. LALOE (1977) *Quantum Mechanics - Volume II*, 1481-1497, Hermann, Paris, 2<sup>nd</sup> revised edition.

The LONDON gauge in a simply connected superconductor is that for which the momentum  $\mathbf{p}$  of the superconducting electrons is set to zero.

**Note** - in contrast to the “quantity of movement”  $mv$ , which is measurable and should be gauge-independent, the “conjugate” momentum  $\mathbf{p}$  is a non-physical quantity dependent on the choice of gauge. In quantum mechanics the wave-vector  $\mathbf{k}$  of the wave associated with a particle is related to this momentum  $\mathbf{p}$ , via the relation  $\mathbf{p} = \hbar\mathbf{k}$ .

### 2.12.5 - Non-simply-connected superconductors

If a superconductor is not simply connected, the relations  $\nabla \cdot \mathbf{A} = 0$  and  $\mathbf{n} \cdot \mathbf{A} = 0$  turn out to be insufficient on their own to define a gauge. We must add to them a relation giving the circulation of  $\mathbf{A}$  on each closed loop  $\Gamma$  around a given hole (which opens out in two different places of the surface).

$$\int_{\Gamma} \mathbf{A} \cdot d\mathbf{l} = \phi. \quad (2.99)$$

We shall come back in length to this point in Chapter 9, which will be devoted to the effects of coherence.

## Appendix 2A

### Total and partial derivatives with respect to time

Let us consider the movement of a fluid such as water where each elementary particle moves with a velocity  $\mathbf{v}(\mathbf{r}, t)$  that depends on its position and the time.

Let  $\mathbf{r}_0$  be the position of a particle at time  $t_0$  and  $(\mathbf{r}_0 + d\mathbf{r})$  its position at time  $(t_0 + dt)$ . Clearly we have  $d\mathbf{r} = \mathbf{v}(\mathbf{r}_0, t_0) dt$ .

If  $\mathbf{F}$  represents the net result of the various forces acting on this particle, during the time interval  $dt$  the change in its velocity is given by the fundamental law of mechanics

$$\mathbf{F} = m \frac{d\mathbf{v}}{dt}. \quad (2.100)$$

This change in velocity  $d\mathbf{v}$  can be divided into two terms:

- » as the fluid changes in time, the velocity of particles located at  $\mathbf{r}_0$  at time  $t_0 + dt$  exceeds by  $\left\{ \frac{\partial \mathbf{v}}{\partial t} \Big|_{\mathbf{r}_0} dt \right\}$  that of particles located at  $\mathbf{r}_0$  at time  $t_0$ .  $\left. \frac{\partial \mathbf{v}}{\partial t} \right|_{\mathbf{r}_0}$  is the local acceleration at the point  $\mathbf{r}_0$ ;
- » at time  $t_0$  the velocity of particles located at  $\mathbf{r}_0 + d\mathbf{r}$  exceeds by  $\left. \frac{\partial \mathbf{v}}{\partial \mathbf{r}} \right|_{t_0} d\mathbf{r}$  that of particles found at  $\mathbf{r}_0$ .

Combining these two contributions gives

$$d\mathbf{v} = \left. \frac{\partial \mathbf{v}}{\partial t} \right|_{\mathbf{r}_0} dt + \left. \frac{\partial \mathbf{v}}{\partial \mathbf{r}} \right|_{t_0} d\mathbf{r} \quad (2.101)$$

which is written, for example for the  $v_x$  component

$$dv_x = \frac{\partial v_x}{\partial t} dt + \frac{\partial v_x}{\partial x} dr_x + \frac{\partial v_x}{\partial y} dr_y + \frac{\partial v_x}{\partial z} dr_z \quad (2.102)$$

or, dividing by  $dt$

$$\frac{dv_x}{dt} = \frac{\partial v_x}{\partial t} + \frac{\partial v_x}{\partial x} v_x + \frac{\partial v_x}{\partial y} v_y + \frac{\partial v_x}{\partial z} v_z. \quad (2.103)$$

For each component  $v_i$  we then have

$$\frac{dv_i}{dt} = \frac{\partial v_i}{\partial t} + \sum_j \frac{\partial v_i}{\partial r_j} \frac{dr_j}{dt} = \frac{\partial v_i}{\partial t} + \sum_j \left( v_j \frac{\partial}{\partial r_j} \right) v_i = \frac{\partial v_i}{\partial t} + \sum_j (v_j \nabla_j) v_i \quad (2.104)$$

which is written in vector form as,

$$\frac{d\mathbf{v}}{dt} = \frac{\partial \mathbf{v}}{\partial t} + (\mathbf{v} \cdot \nabla) \mathbf{v} = \frac{\partial \mathbf{v}}{\partial t} + \frac{1}{2} \nabla \mathbf{v}^2 - \mathbf{v} \times (\nabla \times \mathbf{v}). \quad (2.105)$$

## Appendix 2B

### Property of a harmonic function for which the component to the surface normal of the gradient vanishes

By hypothesis,  $\chi$  is a function of  $\mathbf{r}$  such that

$$\nabla^2 \chi = 0 \quad \text{and} \quad \nabla \chi \cdot \mathbf{n} = 0 \quad \text{at the surface} \quad (2.106a)$$

Consider the vector  $\chi \nabla \chi$ . Like any vector, it obeys STOKES' law

$$\iint_S \chi \nabla \chi \cdot d\mathbf{S} = \iiint_V \nabla \cdot [\chi \nabla \chi] d^3r \quad (2.106b)$$

where  $S$  is a closed surface and  $V$  the volume bounded by this surface. With the vector relation

$$\nabla \cdot [\chi \nabla \chi] = \chi \nabla \cdot \nabla \chi + \nabla \chi \cdot \nabla \chi \quad (2.107)$$

this leads to  $\iint_S \chi \nabla \chi \cdot d\mathbf{S} = \iiint_V \chi \nabla \cdot \nabla \chi d^3r + \iiint_V [\nabla \chi]^2 d^3r$ .  $(2.108)$

As  $d\mathbf{S}$  is oriented in the sense of a normal  $\mathbf{n}$  pointing outwards, we have

$$\iint_S \chi \nabla \chi \cdot d\mathbf{S} = \iint_S \chi [\nabla \chi \cdot \mathbf{n}] dS = 0. \quad (2.109)$$

Since  $\nabla^2 \chi$  is zero,  $\iiint_V \chi \nabla \cdot \nabla \chi d^3r = \iiint_V \chi \nabla^2 \chi d^3r = 0$   $(2.110)$

leading to

$$\iiint_V [\nabla \chi]^2 d^3r = 0 \quad (2.111)$$

and as the integral of a never negative function can vanish only if the function is everywhere zero,

$$\nabla \chi = \mathbf{0} \quad i.e. \quad \chi \text{ is a constant.}$$

## Appendix 2C

### Modified BESSEL functions

The “modified BESSEL functions of order  $v$ ” of the first kind  $\mathcal{I}_v(x)$  and of the second kind  $\mathcal{K}_v(x)$  are the particular solutions of the following differential equation,

$$\frac{d^2y}{dx^2} + \frac{1}{x} \frac{dy}{dx} - \left[ 1 + \left( \frac{v}{x} \right)^2 \right] y = 0. \quad (2.112)$$

The general solution is then written

$$y(x) = A \mathcal{I}_v(x) + B \mathcal{K}_v(x). \quad (2.113)$$

These are, in two dimensions, the equivalent of the increasing and decreasing exponentials that we are familiar with in one dimension.

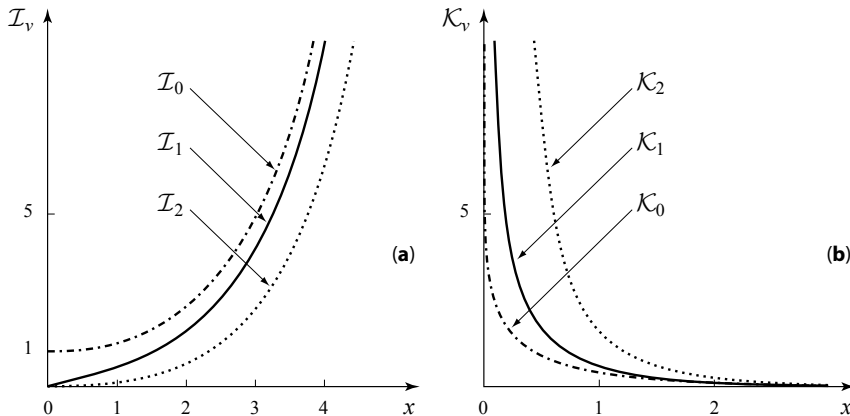


**Figure 2.13 - Graphical representation of the modified BESSEL functions of order 0, 1 and 2**  
**(a)** Modified function of the first kind  $\mathcal{I}_v(x)$  - **(b)** Modified function of the second kind  $\mathcal{K}_v(x)$

#### In the neighborhood of the origin ( $x \rightarrow 0$ )

For values of  $x$  close to 0, the functions  $\mathcal{I}_v(x)$  have the expansions

$$\mathcal{I}_0(x) \rightarrow 1 + \frac{x^2}{2^2} + \frac{x^4}{2^2 4^2} + \frac{x^6}{2^2 4^2 6^2} + \dots \quad (2.114)$$

$$\mathcal{I}_1(x) \rightarrow \frac{x}{2} + \frac{x^3}{2^2 4} + \frac{x^5}{2^2 4^2 6} + \dots \quad (2.115)$$

while the functions  $\mathcal{K}_v(x)$  diverge,

$$\mathcal{K}_0(x) \rightarrow -\ln x \quad (2.116)$$

$$\mathcal{K}_1(x) \rightarrow \frac{1}{x}. \quad (2.117)$$

### ***Asymptotic behavior at infinity ( $x \rightarrow \infty$ )***

When  $x$  is very large,  $\mathcal{I}_v(x)$  and  $\mathcal{K}_v(x)$  are dominated by increasing and decreasing exponentials respectively

$$\mathcal{I}_v(x) \rightarrow \frac{1}{\sqrt{2\pi x}} e^x \quad (2.118)$$

$$\mathcal{K}_v(x) \rightarrow \frac{1}{\sqrt{2\pi x}} e^{-x}. \quad (2.119)$$

The modified BESSEL functions are related to one another by many relations such as

$$\frac{d\mathcal{I}_0(x)}{dx} = \mathcal{I}_1(x) \quad (2.120)$$

$$\int x\mathcal{I}_0(x)dx = x\mathcal{I}_1(x). \quad (2.121)$$

# Chapter 3

## THE NON-LOCAL PIPPARD EQUATIONS

While LONDON theory is actually rather simple, there are in fact non-local phenomena inherent to superconductivity that enter the picture and modify the relations between the current density and the magnetic field. This brief chapter will extend the description of LONDON theory, and allow us to become familiar with the non-local character of superconductivity. This concept can be a little disturbing at first sight.

### 3.1 - Origin of the non-local equations

By increasing the concentration of impurities of indium in superconducting tin, and thereby reducing the mean free path of the electrons in the normal phase, PIPPARD<sup>1</sup> observed that the penetration depth of the magnetic field increased while the thermodynamic properties of the superconducting phase were unchanged ( $T_c$  was not modified). Inspired by the non-local relation proposed between the current density  $\mathbf{j}(\mathbf{r})$  and the electric field  $\mathbf{E}(\mathbf{r})$  to explain the anomalous skin effect by REUTER and SONDHEIMER and, later, CHAMBERS<sup>2</sup>,

$$\mathbf{j}(\mathbf{r}) = \frac{3\sigma}{4\pi\ell} \iiint \frac{[(\mathbf{r} - \mathbf{r}') \cdot \mathbf{E}(\mathbf{r}')] }{|\mathbf{r} - \mathbf{r}'|^4} (\mathbf{r} - \mathbf{r}') e^{-\frac{|\mathbf{r}-\mathbf{r}'|}{\ell}} d^3 r' \quad (3.1)$$

where  $\sigma$  is the electrical conductivity and  $\ell$  the mean free path of the electrons, PIPPARD proposed the relation (3.25) between the current density  $\mathbf{j}$  and the vector potential  $\mathbf{A}$  which will figure at the end of this chapter.

In fact later work showed that the magnetic penetration depth, named now  $\lambda$ , differs from the theoretical LONDON penetration depth  $\lambda_L$  because of two very different mechanisms: one intrinsic, due to the nature of the COOPER pairs, the other extrinsic, that adds to the previous one when the superconductor has a high concentration of impurities reducing the mean free path (*i.e.* is a “dirty” superconductor).

---

<sup>1</sup> A.B. PIPPARD (1953) *Proc. Roy. Soc. A* **216**, 547.

<sup>2</sup> G.E.H. REUTER & E.H. SONDHEIMER (1948) *Proc. Roy. Soc. A* **195**, 336.  
R.G. CHAMBERS (1952) *Proc. Phys. Soc. (London) A* **65**, 458.

This was a distinction that PIPPARD could not have made at the time. With the benefit of hindsight, and in order to clearly separate these two contributions, we will discuss first the case of the pure superconductor, and afterwards the dirty superconductor that PIPPARD had addressed directly with his formula (3.25).

### 3.2 - Non-locality in pure superconductors

The intrinsic non-locality originates in the fact that superconductivity is carried by COOPER pairs formed by two electrons that can be very far apart (up to several hundreds of nanometers), while intuitively the current density  $\mathbf{j}(\mathbf{r})$  may be better identified with the displacement of their centers of gravity. With such a description, we might well question the local form of the proportionality between  $\mathbf{j}(\mathbf{r})$  and  $\mathbf{A}(\mathbf{r})$  (eq. 2.94) since, if they are far apart, the two electrons of the same COOPER pair can “feel” very different values of the vector potential (Fig. 3.1).

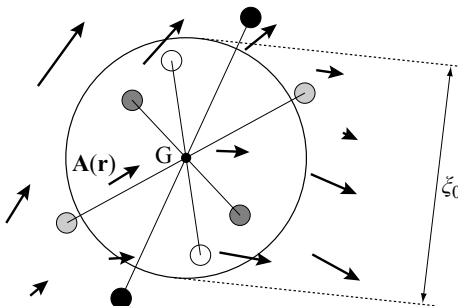


**Figure 3.1 - COOPER pairs in a non-uniform vector potential**

The figure represents COOPER pairs with the same centre of gravity in a non-uniform vector potential  $\mathbf{A}$ . As they are separated by an average distance  $\xi_0$ , two electrons in the same pair “feel” different values of  $\mathbf{A}$ .

Should we retain LONDON’s equation (2.94) by taking for  $\mathbf{A}$  its value at the center of gravity of the COOPER pair, or should we instead use some averaging, taking into account the values of  $\mathbf{A}$  where the electrons actually are? The experimental results show that the second solution should be retained. In the *LONDON gauge*, this leads us to write, by analogy with the anomalous skin effect which has similar origins,

$$\mathbf{j}(\mathbf{r}) = -\frac{n_s e^2}{m} K \iiint \left[ \frac{[(\mathbf{r} - \mathbf{r}') \cdot \mathbf{A}(\mathbf{r}')] (\mathbf{r} - \mathbf{r}')} {|\mathbf{r} - \mathbf{r}'|^4} \right] e^{-\frac{|\mathbf{r} - \mathbf{r}'|}{\xi_0}} d^3 r' \quad (3.2)$$

where  $\xi_0$  is (at 0 K) the average value of the distance between two electrons in the same COOPER pair.

For a more thorough analysis, this expression can be put in the form

$$\mathbf{j}(\mathbf{r}) = -\frac{n_s e^2}{m} \left\{ \frac{3}{4\pi\xi_0} \iiint \left[ \frac{(\mathbf{r} - \mathbf{r}') \cdot \mathbf{A}(\mathbf{r}')}{|\mathbf{r} - \mathbf{r}'|} \frac{(\mathbf{r} - \mathbf{r}')}{|\mathbf{r} - \mathbf{r}'|} \right] \left[ \frac{1}{|\mathbf{r} - \mathbf{r}'|^2} e^{-\frac{|\mathbf{r} - \mathbf{r}'|}{\xi_0}} \right] d^3 r' \right\} \quad (3.3)$$

where:

- » the first (square) bracket expresses the projection of the vector  $\mathbf{A}(\mathbf{r}')$  on the direction  $(\mathbf{r}' - \mathbf{r})$ ;
- » the second (square) bracket represents the weighting of  $\mathbf{A}(\mathbf{r}')$  in the integral. This weight decreases exponentially with the distance between  $\mathbf{r}$  and  $\mathbf{r}'$ , with characteristic length  $\xi_0$ ;
- » the value  $3/4\pi\xi_0$  taken for the normalisation  $K$  is chosen so that if the action of the vector potential on the charge carriers becomes purely local, or if  $\mathbf{A}(\mathbf{r})$  is uniform over distances greater than  $\xi_0$ , we recover the LONDON equation (2.94).

To summarize, we can also write

$$\mathbf{j}(\mathbf{r}) = -\frac{n_s e^2}{m} \bar{\mathbf{A}}_{\xi_0}(\mathbf{r}) = -\frac{1}{\mu_0 \lambda_L^2} \bar{\mathbf{A}}_{\xi_0}(\mathbf{r}) \quad (3.4)$$

where  $\bar{\mathbf{A}}_{\xi_0}(\mathbf{r})$  is a vector potential averaged, as in (3.3), over a volume of characteristic dimension  $\xi_0$ .

**Note** - the length  $\xi_0$  can be identified with the BCS coherence length at 0 K  
 $\xi_0 \equiv \xi_{\text{BCS}}(T=0)$ . (3.5)

At finite temperatures it is still  $\xi_0$ , as defined by (3.5), that we must introduce into the relation (3.2).  $\mathbf{j}(\mathbf{r})$  depends on the temperature only via the penetration depth  $\lambda_L$ .

### 3.3 - Penetration depth of the magnetic field

We saw in the previous chapter (section 2.5) that in a sufficiently thick superconducting sample, the magnetic field  $\mathbf{B}$  and the current density  $\mathbf{j}$  decrease exponentially from the surfaces with a characteristic length  $\lambda_L$ . Without altering the evanescent nature of the magnetic field and the screening currents associated, the non-local PIPPARD relation will modify the laws governing the decrease of these variables within the sample.

Experience shows that, to a first approximation, we can still keep the exponentially decreasing form of the magnetic field and the current density by writing the relation (3.4) as a local equation,

$$\mathbf{j}(\mathbf{r}) = -\frac{1}{\mu_0 \lambda_L^2} \bar{\mathbf{A}}_{\xi_0}(\mathbf{r}) \approx -\frac{1}{\mu_0 \lambda^2} \mathbf{A}(\mathbf{r}) \quad (3.6)$$

provided the LONDON penetration depth scale  $\lambda_L$  is replaced by an effective magnetic penetration depth  $\lambda$ .

*A priori*, this length  $\lambda$  is a function of the characteristic lengths  $\lambda_L$  and  $\xi_0$  and we can find different approximations for it in the literature. Close to a plane surface

from which  $\mathbf{j}$  and  $\mathbf{A}$  decrease in the perpendicular direction  $\mathbf{n}$ , two limiting cases can be imagined:

»  $\xi_0 \ll \lambda_L \Rightarrow \mathbf{A}(\mathbf{r})$  varies little in a sphere of diameter  $\xi_0$  over which the average (3.3) is taken:

$$\bar{\mathbf{A}}_{\xi_0}(\mathbf{r}) \approx \mathbf{A}(\mathbf{r}), \quad \mathbf{j}(\mathbf{r}) \approx -\frac{n_s e^2}{m} \mathbf{A}(\mathbf{r}) \text{ and } \lambda \approx \lambda_L \quad (\xi_0 \ll \lambda_L). \quad (3.7)$$

»  $\xi_0 \gg \lambda_L \Rightarrow \mathbf{A}(\mathbf{r})$  takes a non-zero value only on a distance  $\lambda$  small compared to  $\xi_0$ . Integration of (3.3) shows that,

$$\bar{\mathbf{A}}_{\xi_0}(\mathbf{r}) \approx \frac{\lambda}{\xi_0} \mathbf{A}(\mathbf{r}) \quad (3.8)$$

leading to  $\mathbf{j}(\mathbf{r}) \approx -\frac{1}{\mu_0 \lambda_L^2} \left( \frac{\lambda}{\xi_0} \right) \mathbf{A}(\mathbf{r}) = -\frac{1}{\mu_0 \lambda^2} \mathbf{A}(\mathbf{r}) \quad (3.9)$

with  $\lambda = \left( \lambda_L^2 \xi_0 \right)^{1/3} = \lambda_L \left( \frac{\xi_0}{\lambda_L} \right)^{1/3} = \xi_0 \left( \frac{\lambda_L}{\xi_0} \right)^{2/3} \quad (\xi_0 \gg \lambda_L). \quad (3.10)$

As shown in Table 3.1, the penetration depth  $\lambda$  derived from the relation (3.9) is always greater than the LONDON penetration depth  $\lambda_L$ ; the more  $\xi_0$  exceeds  $\lambda_L$ , the greater is this difference.

**Table 3.1 - Effect of the coherence length on the effective LONDON penetration depth predicted by the relation (3.9)**

$\xi_0/\lambda_L$	3	4	5	6
$\lambda/\lambda_L$	1.442	1.587	1.710	1.817

### 3.4 - FOURIER analysis of the PIPPARD equations

The non-local expression (3.3) for the relation between the current density  $\mathbf{j}$  and the vector potential  $\mathbf{A}$  can in fact be written in a more general form

$$\mathbf{j}(\mathbf{r}) = -\frac{K}{\mu_0 \lambda_L^2} \iiint \{ [\mathbf{A}(\mathbf{r}') \cdot \mathbf{u}_R] \mathbf{u}_R \} \frac{F(R)}{R^2} d^3 r' \quad (3.11)$$

where:

- ›  $\mathbf{u}_R$  is the unit vector in the direction  $\mathbf{R} = \mathbf{r}' - \mathbf{r}$ ;
- ›  $[\mathbf{A}(\mathbf{r}') \cdot \mathbf{u}_R] \mathbf{u}_R$  is the projection of  $\mathbf{A}(\mathbf{r}')$  along  $\mathbf{R}$ ;
- ›  $F(R)$  is a weighting function which, in the special case of expression (3.2), equals  $e^{-R/\xi_0}$ ;
- ›  $K$  is a normalizing factor [ $3/4\pi\xi_0$  for the special case of (3.2)] allowing the relation (3.11) to reduce to the LONDON equation (2.94) when  $\mathbf{A}$  tends to the limit where it is uniform on the scale of a correlation length.

To go further, consider a vector potential  $\mathbf{A}(\mathbf{r})$  restricted to a single FOURIER component,

$$\mathbf{A}(\mathbf{r}) = \mathbf{A}(\mathbf{q}) e^{i\mathbf{q} \cdot \mathbf{r}} \quad (3.12)$$

which in the LONDON gauge ( $\nabla \cdot \mathbf{A}(\mathbf{r}) = 0$ ), satisfies

$$\mathbf{q} \cdot \mathbf{A}(\mathbf{q}) = 0. \quad (3.13)$$

By choosing the wave vector  $\mathbf{q}$  in the  $z$ -direction,  $\mathbf{A}$  along the  $x$ -axis, and writing  $\mathbf{R}$  in spherical coordinates (Fig. 3.2),

$$\mathbf{q} = \begin{vmatrix} 0 \\ 0 \\ q \end{vmatrix}, \quad \mathbf{A} = \begin{vmatrix} A \\ 0 \\ 0 \end{vmatrix}, \quad \mathbf{R} = \begin{vmatrix} R \sin \theta \cos \varphi \\ R \sin \theta \sin \varphi \\ R \cos \theta \end{vmatrix}, \quad \mathbf{u}_R = \begin{vmatrix} \sin \theta \cos \varphi \\ \sin \theta \sin \varphi \\ \cos \theta \end{vmatrix}.$$

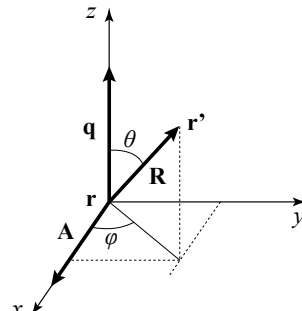


Figure 3.2  
Spatial configuration of the vector potential and of the wave vector of its FOURIER component

As  $\mathbf{r}$  is fixed, the element of volume of integration is

$$d^3r' = R^2 \sin \theta d\theta d\phi dr \quad (3.14)$$

and rewriting  $\mathbf{A}(\mathbf{r}') = \mathbf{A}(\mathbf{q}) e^{i\mathbf{q} \cdot \mathbf{r}} e^{i\mathbf{q} \cdot (\mathbf{r}' - \mathbf{r})}$

$$\mathbf{u}_R \cdot \mathbf{A}(\mathbf{r}') = A e^{i\mathbf{q} \cdot \mathbf{r}} \sin \theta \cos \varphi e^{iqR \cos \theta} \quad (3.15)$$

the only non-zero component of  $\mathbf{j}$  is

$$j_x(\mathbf{q}) = -\frac{n_s e^2}{m} K A(\mathbf{q}) e^{i\mathbf{q} \cdot \mathbf{r}} \int_0^{2\pi} \cos^2 \phi d\phi \int_0^\infty \left[ \int_0^{2\pi} \sin^3 \theta e^{iqR \cos \theta} d\theta \right] F(R) dR \quad (3.16)$$

which, since  $\mathbf{j}$  and  $\mathbf{A}$  are collinear, allows us to write a vector equation

$$\mathbf{j}(\mathbf{r}) = -\frac{1}{\mu_0 \lambda_L^2} \mathbf{A}(\mathbf{q}) \gamma(q) e^{i\mathbf{q} \cdot \mathbf{r}} = \mathbf{j}(\mathbf{q}) e^{i\mathbf{q} \cdot \mathbf{r}} \quad (3.17)$$

with

$$\mathbf{j}(\mathbf{q}) = -\frac{1}{\mu_0 \lambda_L^2} \gamma(q) \mathbf{A}(\mathbf{q}) \quad (3.18)$$

and

$$\gamma(q) = 4\pi K \int_0^\infty \frac{j_1(qR)}{qR} F(R) dR \quad (3.19)$$

where

$$j_1(x) = \frac{\sin x}{x^2} - \frac{\cos x}{x} \quad (3.20)$$

is the spherical BESSEL function<sup>3</sup> of order 1. As the function  $j_1(x)/x$  is oscillating,  $\gamma(q)$  resembles somewhat the FOURIER transform of  $F(R)$ ; in fact it is a variant of the HANKEL transform.

The equation (3.11), which was non-local in real space, has now become “local” in the space of wave-vectors, since the vector  $\mathbf{j}(\mathbf{q})$ , the FOURIER component of  $\mathbf{j}(\mathbf{r})$ , is equal to a simple product of the scalar  $\gamma(q)$  and the FOURIER component  $\mathbf{A}(\mathbf{q})$ .  $\gamma(q)$  is a “response function”.

This analysis calls for several remarks:

- » If the field  $\mathbf{A}(\mathbf{r})$  is uniform over a distance greater than  $\xi_0$ , only the components  $\mathbf{A}(\mathbf{q} = \mathbf{0})$  and  $\mathbf{j}(\mathbf{q} = \mathbf{0})$  are non-zero. The current density  $\mathbf{j}$  is uniform and proportional to  $\mathbf{A}$  and we must have  $\gamma(q = 0) = 1$  in (3.18), in order to recover the LONDON equation (2.94). By replacing in (3.20)  $j_1(qR)/qR$  by  $\frac{1}{3}$ , the limiting value for  $j_1(x)/x$  when  $x \rightarrow 0$ , this normalization requires

$$K = \frac{3}{4\pi} \frac{1}{\int_0^\infty F(R) dR}. \quad (3.21)$$

For  $F(R) = e^{-R/\xi_0}$ , we find  $K = 3/4\pi\xi_0$ , which we recognize as the normalization coefficient of formula (3.2).

- » By using (3.21), the expression (3.19) can also be written

$$\gamma(q) = 3 \frac{\int_0^\infty \frac{j_1(qR)}{qR} F(R) dR}{\int_0^\infty F(R) dR}. \quad (3.22)$$

- » As  $F(R)$  is a decreasing function of  $R$ ,

$$\xi_0 = \frac{1}{F(0)} \int_0^\infty F(R) dR \quad (3.23)$$

is a measure of its spatial extension, as is clearly seen for the special case of  $F(R) = e^{-R/\xi_0}$ .

<sup>3</sup> As well as having other properties,  $j_1(x)/x$  is an oscillating function which behaves at the origin as  $\frac{1}{3} \left( 1 - \frac{2x^2}{5} \right)$  and decreases asymptotically for large  $x$  as  $1/x^2$ ; in addition we have  $\int_0^\infty \frac{j_1(x)}{x} dx = \frac{\pi}{4}$ .

For large  $q$ ,  $\gamma(q) \rightarrow 4\pi F(0)K \int_0^\infty \frac{j_1(qR)}{qR} d(R) \approx \frac{3\pi}{4q\xi_0}$ , which means that the

larger the value of  $\xi_0$  the faster  $\gamma(q)$  decreases. Therefore, if  $F(R)$  extends over  $\xi_0$ ,  $\gamma(q)$  is of order  $1/\xi_0$  (Fig. 3.3).  $F(R)$  and its transform  $\gamma(q)$  share the property of conjugacy with FOURIER transforms, namely that their widths  $\delta R$  and  $\delta q$  satisfy the “uncertainty principle” (Fig. 3.3),

$$\delta R \delta q \approx 1. \quad (3.24)$$

» When  $\xi_0$  tends to 0,  $\frac{F(R)}{\int_0^\infty F(R) dR}$  becomes the DIRAC distribution  $\delta(R)$ , and  $\gamma(q)$

tends to 1 (relation 3.19). We then have  $\mathbf{j}(\mathbf{q}) = -\frac{1}{\mu_0 \lambda_L^2} \mathbf{A}(\mathbf{q})$  for any wave vector  $\mathbf{q}$ , which leads once again to the local LONDON equation (2.94).

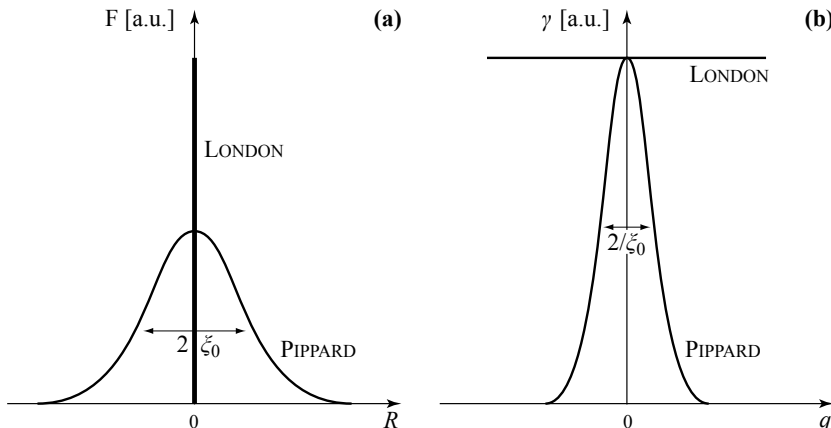


**Figure 3.3 - Local (LONDON) or non-local (PIPPARD) characters of the response function of superconducting electrons**

**(a) Real space ( $r$ )** - In the LONDON model, the current density is locally proportional to the vector potential and the weighting function  $F(R)$  is a DIRAC delta function at  $R = 0$ . In the PIPPARD model, the current density is proportional to a weighted average of the vector potential. The weight factor  $F(R)$  extends over a distance  $\xi_0$ . **(b) The space of wave-vectors (reciprocal space) ( $q$ )** - The response function  $\gamma(q)$  takes the constant value 1 in the LONDON model while it decreases over a range  $1/\xi_0$  in that of PIPPARD.

### 3.5 - “Dirty” superconductors

We can now come back to the measurements on samples of tin containing a variable concentration of indium atoms, which showed that the effective penetration depth of the magnetic field increases when there is a decrease in the mean free path of the electrons as measured in the normal phase (Fig. 3.4).

These observations lead PIPPARD to write

$$\mathbf{j}(\mathbf{r}) = -\frac{n_s e^2}{m} \left\{ \frac{3}{4\pi\xi_0} \iiint \left[ \frac{(\mathbf{r} - \mathbf{r}') \cdot \mathbf{A}(\mathbf{r}')}{|\mathbf{r} - \mathbf{r}'|} \frac{(\mathbf{r} - \mathbf{r}')}{|\mathbf{r} - \mathbf{r}'|} \right] \left[ \frac{1}{|\mathbf{r} - \mathbf{r}'|^2} e^{-\frac{|\mathbf{r} - \mathbf{r}'|}{\xi_p}} \right] d^3 r' \right\} \quad (3.25)$$

which is rather different from (3.3), since even if the coefficient  $K = 3/4\pi\xi_0$  is identical, the weight of the contribution of  $\mathbf{A}(\mathbf{r}')$  is significantly reduced. The distance over which the exponential is reduced is no longer  $\xi_0$  but a length  $\xi_p$ , called the “PIPPARD length”, which was later shown to be connected to the intrinsic coherence length  $\xi_0$  and the mean free path of the electrons  $\ell$  by

$$\frac{1}{\xi_p} = \frac{1}{\xi_0} + \frac{1}{\ell} \quad (3.26)$$

suggesting that the mean free path of the electrons now limits the natural extent of COOPER pairs.

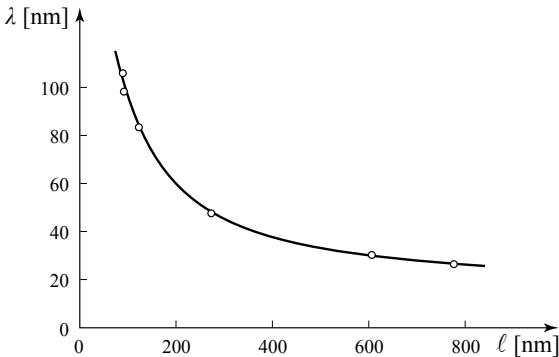


**Figure 3.4 - Effect of impurities on the penetration depth**  
Variation of the penetration depth  $\lambda$  as a function of the mean free path  $\ell$  of electrons in the normal state.  
[From PIPPARD, 1953, Fig. 1, p. 551, © The Royal Society]<sup>1</sup>

Qualitatively, this substitution of  $\xi_0$  by  $\xi_p$  in the exponential without changing the expression of  $K$ , in which  $\xi_0$  still enters, lessens the weight of  $\mathbf{A}(\mathbf{r}')$  and reduces  $\mathbf{j}(\mathbf{r})$ , which consequently increases the distance  $\lambda$  needed to screen an external magnetic field.

An extreme case is that of a superconductor in which the mean free path  $\ell$  is very small compared to  $\xi_0$  and  $\lambda_L$  and where therefore  $\xi_p \approx \ell$ . With the same arguments that lead to equation (3.6), the response is found to be local, but the weight of the contribution of  $\mathbf{A}$  is found to be reduced by a factor  $\xi_p/\xi_0$ . We have, therefore,

$$\mathbf{j}(\mathbf{r}) = -\frac{n_s e^2}{m} \frac{\xi_p}{\xi_0} \mathbf{A}(\mathbf{r}) \approx -\frac{1}{\mu_0} \left( \frac{\ell}{\lambda_L^2 \xi_0} \right) \mathbf{A}(\mathbf{r}) = -\frac{1}{\mu_0 \lambda^2} \mathbf{A}(\mathbf{r}) \quad (3.27)$$

which leads to

$$\lambda = \lambda_L \sqrt{\frac{\xi_0}{\ell}} \quad (3.28)$$

( $\ell \ll \lambda_L$ ,  $\ell \ll \xi_0$ ,  $\xi_p \approx \ell$ ).

Table 3.2 summarizes the different limiting behavior that we may find. In the literature we find other approximations corresponding to intermediate situations.<sup>4</sup>

**Table 3.2 - Different forms of dependence of the magnetic penetration depth according to the relative values of  $\lambda_L$ ,  $\xi_0$  and  $\ell$**

Pure superconductor		Dirty Superconductor
Type II	Type I	Always Type II
$\xi_0 < \lambda_L$	$\xi_0 > \lambda_L$	$\ell \ll \lambda_L$
$\ell \gg \xi_0$	$\ell \gg \lambda_L$	$\ell \ll \xi_0$
$\xi_p \approx \xi_0 < \lambda_L$	$\xi_p \approx \xi_0 > \lambda_L$	$\xi_p \approx \ell$
$\lambda \approx \lambda_L$	$\lambda \approx (\lambda_L^2 \xi_0)^{1/3}$	$\lambda \approx \lambda_L \sqrt{\xi_0 / \ell}$

<sup>4</sup> See, for example, J. WALDRAM (1996) *Superconductivity of metal and cuprates*, Institute of Physics Publishing, Bristol and Philadelphia, Chap. 7.

### THERMODYNAMICS OF TYPE I SUPERCONDUCTORS

A decisive step in the history of superconductivity was the recognition that there was a true phase to be reckoned with, and the aim of this chapter is to bring a thermodynamic description of that phase. We will restrict ourselves here to the case of type I superconductors whose superconducting and normal phases are separated in the  $(H, T)$  plane by a single line<sup>1</sup> defining the critical field  $H_c(T)$  (Fig. 4.1a). Type II superconductors, where a mixed state appears, will be treated in Chapter 6.

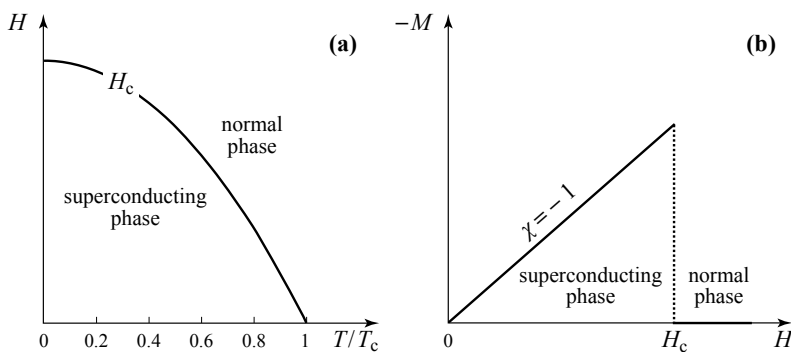


**Figure 4.1 - Type I superconductor**

**(a)** The superconducting and normal states are separated by a single line  $H_c(T)$ . **(b)** In the superconducting state the magnetization  $M$  is equal and opposite to the field  $H$ ,<sup>2</sup> which makes it a perfect diamagnet. In the normal state, the magnetization vanishes, but in fact the normal state is very weakly diamagnetic.  $\chi$  is the magnetic susceptibility defined by  $M = \chi H$ .

- 1 Type I superconductors are, without exception, pure metals of a single element. A few pure metals of a single element, such as niobium and vanadium, are of type II, as are all alloys and compounds.
- 2 In this book we will encounter  $\mathbf{H}$  and  $\mathbf{B}$  on numerous occasions. The notation in the literature follows (at least) three different conventions. The first is to call  $\mathbf{H}$  “the magnetizing field” and  $\mathbf{B}$  the “magnetic field.” The second has  $\mathbf{H}$  the “magnetic field” and  $\mathbf{B}$  the “magnetic induction.” The third denotes  $\mathbf{B}$  the “magnetic field” and  $\mathbf{H}$  the “ $\mathbf{H}$  field.” We have taken the third option.

## 4.1 - Thermodynamic description

Thermodynamics provides a description for the exchanges between a system and its environment in terms of a restricted number of parameters which mask extremely complex microscopic situations. It relies essentially on two principles whose application is described in great detail in textbooks. In practice a thermodynamic analysis must proceed in several stages.

» The first consists of defining the system and its boundary with the environment. Heat and work that the system receives from the environment are defined to be positive.

» The second step is to introduce the thermodynamic variables:

- › the two universal variables, temperature  $T$  and entropy  $S$ . From these variables, we can write the quantity of heat exchanged during an infinitesimal reversible transformation as  $\delta Q = T dS$ ;

- › variables specific to each problem that allow us to express exchanges of work. These last variables always appear in conjugate pairs  $(X_i, Y_i)$  where  $X_i$  and  $Y_i$  are intensive and extensive variables, respectively. The exchange of work during an infinitesimal reversible transformation can be expressed as

$$\delta W = \sum_i X_i dY_i. \quad (4.1)$$

It can be expressed as  $\delta W = -P dV$  for a system for which the work is exchanged by variation of the volume  $V$  under the effect of pressure  $P$ ,  $\delta W = \mathbf{H} \cdot d\mathbf{B}$  for a magnetic system, or  $\delta W = -P dV + \mathbf{H} \cdot d\mathbf{B}$  when both types of work are included.

» The third step aims to express the differential forms of thermodynamic functions, or their densities<sup>3</sup> when the system is suitable, as is the case here: densities of internal energy  $u$ , of enthalpy  $h$ , of free energy  $f$  (the HELMHOLTZ function) and of free enthalpy  $g$  (the GIBBS function). The equilibrium state generally corresponds to an extremum in one of these functions, which then appears as a thermodynamic potential. For the case of the system  $(P, V)$ , at fixed  $P$  and  $T$ , the equilibrium state minimizes the free enthalpy, while if  $V$  and  $T$  are constrained, it is the free energy that is lowest.

» Finally, going beyond the very general relations that the principles imply, each physical system has its own specific properties. These are equations of state that connect thermodynamic variables to one another, laws of behavior and numerical values of the specific heat, the coefficient of thermal expansion and the coefficient of compressibility (which, incidentally, may be related). All of these properties, including the equation of state, are either taken from macroscopic measurements or deduced from microscopic models.

---

<sup>3</sup> The densities of thermodynamic quantities are denoted by lower-case letters.

## 4.2 - The thermodynamic variables of superconductivity

### 4.2.1 - The relation between LONDON currents and magnetization

#### *Magnetic material*

Let us consider “magnetizable” matter placed in an infinitely long solenoid. The experimentalist energizes the solenoid by injecting a current  $\mathbf{j}^0$ . The material reacts and becomes magnetized, in some cases by forming microscopic magnetic moments or in others by orienting pre-existing ones. The total magnetic field is then the superposition of the magnetic field  $\mathbf{B}^0$  generated by the current flowing in the solenoid and of the field  $\mathbf{B}^a$  generated by the magnetization  $\mathbf{M}$  that the material has acquired. Now from the point of view of the magnetic fields produced and the energies involved there is a strict equivalence between a distribution of magnetization  $\mathbf{M}$  and a distribution of surface  $\mathbf{j}_{\text{surf}}^a$  and volume  $\mathbf{j}_{\text{vol}}^a$  current densities. These AMPÈRE currents are determined as (see App. 4 for definitions and examples of  $\mathbf{n}$ ,  $\mathbf{j}_{\text{surf}}^a$  and  $\mathbf{j}_{\text{vol}}^a$ )

$$\mathbf{j}_{\text{vol}}^a = \nabla \times \mathbf{M} \quad \text{and} \quad \mathbf{j}_{\text{surf}}^a = \mathbf{M} \times \mathbf{n}. \quad (4.2)$$

We can therefore consider the system (solenoid + magnetized material) as two paired electrical circuits through which flow an injected conductor current density  $\mathbf{j}^0$ , for the first, and in reaction an AMPÈRE current density  $\mathbf{j}^a$  associated with the induced magnetization, for the second.

#### *Superconducting material*

We now replace the “magnetizable” material by a superconductor. When the experimentalist ramps up the solenoid by injecting a current density  $\mathbf{j}^0$  to create the magnetic field  $\mathbf{B}^0$ , the material reacts by forming screening super-currents (LONDON currents) localized at its surface (more precisely within the penetration depth). By following the inverse procedure to that just described (Fig. 4.2), we can then consider that the material reacts by magnetizing with a magnetization  $\mathbf{M}$  linked to the LONDON currents by the relation (4.2).

Macroscopically, a superconductor appear as “magnetizable” matter, even though its magnetization does not consist microscopically of magnetic dipoles. We can then apply the results of the thermodynamics of magnetized materials, both to treat exchange between the material and the environment, and to determine the equilibrium state.

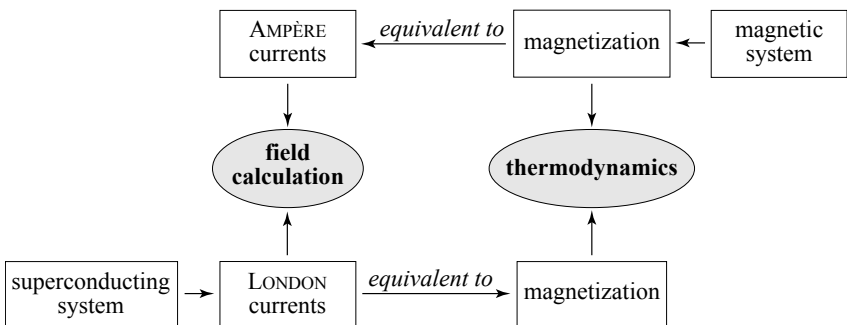


**Figure 4.2 - Magnetism-Superconductivity Equivalence**

A magnetic system magnetizes by creating, or orienting existing, magnetic moments. The magnetization creates a magnetic field  $\mathbf{B}^a$  that can be calculated from the equivalent AMPÈRE currents. The superconducting system develops screening LONDON currents which can be identified with AMPÈRE currents. Because of the equivalence between AMPÈRE currents and magnetization, the superconductor can be considered as a magnetized material.

#### 4.2.2 - Thermodynamic systems

##### System of solenoid + matter

In magnetism, the work performed on a system comprising the exciting electrical circuit (the external solenoid) and the magnetized material is written (see App. 4.2)

$$\delta W_{\text{tot}} = \iiint_{\text{all space}} \mathbf{H}(\mathbf{r}) \cdot d\mathbf{B}(\mathbf{r}) d^3 r. \quad (4.3)$$

- »  $\mathbf{B} = \mathbf{B}^0 + \mathbf{B}^a$  is the total magnetic field, the sum of the field  $\mathbf{B}^0$  created by the currents  $\mathbf{j}^0$  of the exciting circuit, and the field  $\mathbf{B}^a$  associated with the AMPÈRE currents  $\mathbf{j}^a$ .
- » The field  $\mathbf{H}$  is defined by

$$\mathbf{H} = \frac{\mathbf{B}}{\mu_0} - \mathbf{M} \quad (4.4)$$

but can also be calculated by the use of magnetic poles (fictional in magnetism and all the more so in superconductivity) which produce a demagnetizing field  $\mathbf{H}^m$  depending on the shape of the sample. We then have (see App. 4.1),

$$\mathbf{H} = \mathbf{H}^0 + \mathbf{H}^m \quad (4.5)$$

$$\text{with } \mathbf{H}^0 = \frac{\mathbf{B}^0}{\mu_0}.$$

As a consequence, inside a superconductor where  $\mathbf{B}_{\text{int}} = \mathbf{0}$  (except over the penetration depth), we have the relation,

$$\mathbf{M} = -\mathbf{H} \quad (4.6)$$

that makes the superconductor a perfect diamagnet, with magnetic susceptibility  $\chi = -1$  ( $\mathbf{M} = \chi \mathbf{H}$ ).

In the case of an infinitely long sample (a cylinder or a plate), subject to a magnetic field  $\mathbf{B}^0$  parallel to the large dimension, the demagnetizing field  $\mathbf{H}^m$  is zero and therefore  $\mathbf{H}$  is uniform, with the same value  $\mathbf{H} = \mathbf{H}^0$  inside and outside the magnetized material. The magnetic field  $\mathbf{B}$  takes the value  $\mathbf{B}_{\text{ext}} = \mathbf{B}^0$  outside the material and  $\mathbf{B}_{\text{int}} = \mu_0(\mathbf{H} + \mathbf{M})$  inside. The field configuration is shown in Figure 4.3. We can compare it with Figure 4.14 for an ordinary magnetic system, where the AMPÈRE currents replace the LONDON currents. The currents are similar, because in both cases they are created as a response to an external magnetic field.

Note that in this, and in any of the following figures, even though  $\mathbf{H}$  and  $\mathbf{B}$  are not in the same units, they are represented by identical arrows whenever they are related by  $\mathbf{B} = \mu_0\mathbf{H}$ . In other words, in units of the magnetic field (tesla), what is marked as  $\mathbf{H}$  or  $\mathbf{M}$  is in fact  $\mu_0\mathbf{H}$  or  $\mu_0\mathbf{M}$ .

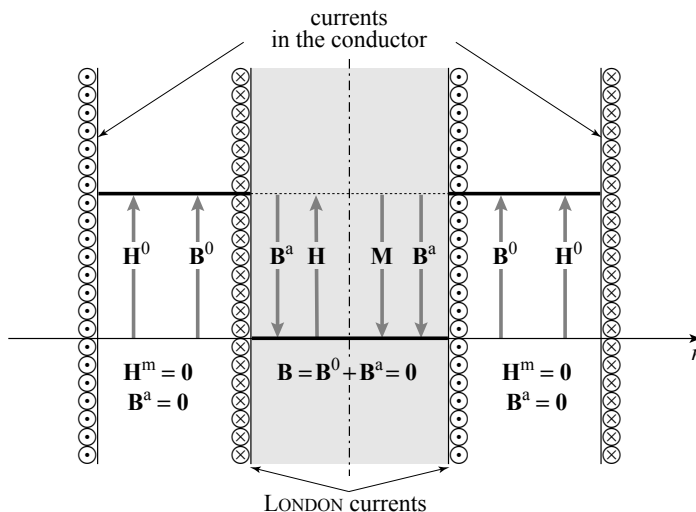


**Figure 4.3 - Field  $\mathbf{H}$  and magnetic field  $\mathbf{B}$  in a cylindrical superconductor placed in an external solenoid**

The current  $\mathbf{j}^0$  flowing in a solenoid creates a magnetic field  $\mathbf{B}^0$  and a field  $\mathbf{H}^0 = \mathbf{B}^0/\mu_0$ . Because of the absence of a demagnetizing field ( $\mathbf{H}^m = 0$ ), the field  $\mathbf{H}$  is uniformly equal to  $\mathbf{H}^0$ , inside as well as outside the material. Its magnetization is  $\mathbf{M} = -\mathbf{H}$ . Inside the material, the magnetic field  $\mathbf{B}^a$  created by the LONDON currents (equivalent to AMPÈRE currents) is equal and opposite to  $\mathbf{B}^0$ , which is what gives a vanishing total  $\mathbf{B}$ . Outside the material, where  $\mathbf{B}^a = 0$  because of the infinite geometry, the total magnetic field is everywhere equal to  $\mathbf{B}^0$ .

#### *Superconducting matter as a closed system*

As is usual in magnetism, we can reduce the system to the superconducting material alone by subtracting from the work  $\delta W_{\text{tot}}$  the work  $\delta W_{\text{vac}}$ , calculated by relation (4.3), which we would have had to provide to the solenoid to inject the current  $\mathbf{j}^0$  in the absence of superconducting material (see App. 4.2),

$$\delta W_{\text{vac}} = \iiint_{\text{all space}} [\mathbf{H}^0(\mathbf{r}) \cdot d\mathbf{B}^0(\mathbf{r})] d^3r. \quad (4.7)$$

The work provided to the closed system of “superconducting material only” is then,

$$\delta W = \delta W_{\text{tot}} - \delta W_{\text{vac}} = \iiint_{\text{all space}} [\mathbf{H}(\mathbf{r}) \cdot d\mathbf{B}(\mathbf{r}) - \mathbf{H}^0(\mathbf{r}) \cdot d\mathbf{B}^0(\mathbf{r})] d^3r \quad (4.8)$$

or, in the absence of a demagnetizing field,

$$\delta W = \iiint_V [\mathbf{H}(\mathbf{r}) \cdot d\mathbf{M}(\mathbf{r})] d^3r = \mu_0 \mathcal{V} \mathbf{H} \cdot d\mathbf{M}. \quad (4.9)$$

As long as the volume is fixed, we can take the work per unit volume of material and write,

$$\delta w = \mu_0 \mathbf{H} \cdot d\mathbf{M}. \quad (4.10)$$

In the terms of paragraph (4.1),  $\mu_0 \mathbf{M}$  is the extensive variable of the thermodynamic system restricted to the superconducting material and  $\mathbf{H}$  the conjugate intensive variable.

#### 4.2.3 - Interpreting the levitation of type I superconductors

In general, the energy of interaction between a sample of magnetic moment  $\mathbf{M}$  and an applied magnetic field  $\mathbf{B}^0$  is written

$$E_{\text{interaction}} = - \mathbf{M} \cdot \mathbf{B}^0. \quad (4.11)$$

Taking into account that the magnetization of a type I superconductor (ignoring effects of demagnetizing fields) is <sup>4</sup>

$$\mathbf{M} = - \mathbf{H}^0 \quad (4.12)$$

this energy becomes

$$E_{\text{interaction}} = - \mathcal{V} \mathbf{M} \cdot \mathbf{B}^0 = \frac{1}{\mu_0} (\mathbf{B}^0)^2 \mathcal{V} \quad (4.13)$$

which leads to a force,

$$\mathbf{F} = - \mathcal{V} \frac{1}{\mu_0} \nabla (\mathbf{B}^0)^2 \quad (4.14)$$

that tends to displace the sample towards the regions of lower field.

A superconducting block placed above a magnet therefore feels a repulsive force that leads it to levitate to a height where the force of repulsion balances its weight. The phenomenon of levitation constitutes a proof that the superconductor behaves as a magnetic material, whose magnetization develops in the direction opposite to the field of the magnet (diamagnetism).

4 For a sample with demagnetizing factor N, the magnetization and the final force are reduced by the factor  $(1 - N)$ ; this in no way modifies the explanation of levitation phenomena.

However, without special care, the sample will “slide” so as to move out of the magnetic field. It will be stabilized laterally only if, by positioning magnets appropriately, the magnetic field creates a reactive force towards a central axis. If, in the mirror-symmetric situation, a magnet is placed above a fixed superconductor, the magnet can also levitate.

We note that the explanation given here is for levitation of type I superconductors (and type II in the MEISSNER state).

For obvious practical reasons, demonstrations of levitation (such as is seen on the cover of this book) are usually presented with high critical temperature superconductors (YBaCuO, for example), which are superconductors of type II. The mechanisms maintaining levitation and lateral stabilization (see section 6.10) are, however, rather different because of the presence of vortices. They both modify and pin the moment  $\mathcal{M}$  carried by the superconductor. We will even see that in this case, the superconductor can not only levitate, but it can also stay suspended *under* a magnet, a phenomenon that would be inconceivable for a type I superconductor.

### 4.3 - Thermodynamic functions of superconductivity<sup>5</sup>

With this new system and its intensive and extensive variables, we can reconstruct all the thermodynamic functions. The simplest way to proceed is to start from the system  $(P, \mathcal{V})$  that is well known, with  $\delta W = -Pd\mathcal{V}$ , and substitute

$$-P \Rightarrow H \quad \text{and} \quad \mathcal{V} \Rightarrow \mu_0 M. \quad (4.15)$$

The definitions, the differential forms and the MAXWELL's relations which follow are given in Table 4.1.

**Table 4.1 - Thermodynamic functions and MAXWELL's relations (per unit volume)**

The thermodynamic functions of the magnetic material, and by equivalence, of a superconducting medium can be obtained from the system  $(P, \mathcal{V})$  by simply substituting  $-P$  by  $H$  and  $\mathcal{V}$  by  $\mu_0 M$ .

Internal energy density	$u$	$du = Tds + \mu_0 HdM$	$\left(\frac{\partial T}{\partial M}\right)_s = \mu_0 \left(\frac{\partial H}{\partial s}\right)_M$
Enthalpy density	$h = u - \mu_0 MH$	$dh = Tds - \mu_0 MdH$	$\left(\frac{\partial T}{\partial H}\right)_s = -\mu_0 \left(\frac{\partial M}{\partial s}\right)_H$
Free energy density (HELMHOLTZ)	$f = u - Ts$	$df = -sdT + \mu_0 HdM$	$-\left(\frac{\partial s}{\partial M}\right)_T = \mu_0 \left(\frac{\partial H}{\partial T}\right)_M$
Free enthalpy density (GIBBS)	$g = u - Ts - \mu_0 MH$	$dg = -sdT - \mu_0 MdH$	$\left(\frac{\partial s}{\partial H}\right)_T = \mu_0 \left(\frac{\partial M}{\partial T}\right)_H$

5 See M.W. ZEMANSKY (1957) *Heat and Thermodynamics*, McGraw-Hill Book company Inc., New York, 382.

Useful relations and the equilibrium conditions at constant temperature and magnetization or at fixed temperature and field  $H$  are summarized in Table 4.2. If we take the approximation of constant superconducting volume, the extensive variables can be defined per unit volume and denoted by lower-case letters.

**Table 4.2 - Free energy and free enthalpy densities:  
thermodynamic properties and associated relations**

Fixed Independent Variables			
Temperature $T$	Magnetization $M$	Temperature $T$	Field $H$
Characteristic functions			
$f = u - Ts$	$s = -\left(\frac{\partial f}{\partial T}\right)_M$	$g = u - Ts - \mu_0 MH$	$s = -\left(\frac{\partial g}{\partial T}\right)_H$
Total differentials			
$Tds = T\left(\frac{\partial s}{\partial T}\right)_M dT + T\left(\frac{\partial s}{\partial M}\right)_T dM$		$Tds = T\left(\frac{\partial s}{\partial T}\right)_H dT + T\left(\frac{\partial s}{\partial H}\right)_T dH$	
Definitions of Specific Heat			
$C_M = T\left(\frac{\partial s}{\partial T}\right)_M = -T\left(\frac{\partial^2 f}{\partial T^2}\right)_M$		$C_H = T\left(\frac{\partial s}{\partial T}\right)_H = -T\left(\frac{\partial^2 g}{\partial T^2}\right)_H$	
Equations for $Tds$			
$Tds = C_M dT - \mu_0 T\left(\frac{\partial H}{\partial T}\right)_M dM$		$Tds = C_H dT + \mu_0 T\left(\frac{\partial M}{\partial T}\right)_H dH$	
Differentials of $u$ and $h$			
$du = C_M dT + \mu_0 \left[ H - T\left(\frac{\partial H}{\partial T}\right)_M \right] dM$		$dh = C_H dT - \mu_0 \left[ M - T\left(\frac{\partial M}{\partial T}\right)_H \right] dH$	
Specific Heat			
$C_M = \left(\frac{\partial u}{\partial T}\right)_M$		$C_H = \left(\frac{\partial h}{\partial T}\right)_H$	
Equilibrium state			
Minimum of the <b>free energy density <math>f</math></b> <b>(HELMHOLTZ function)</b>		Minimum of the <b>free enthalpy density <math>g</math></b> <b>(GIBBS function)</b>	

#### 4.4 - Thermodynamic data

Beyond these general equations, we still have to introduce the specific thermodynamic data of the “magnetic system” coming from both its superconducting and its normal phases: equations of state, specific heat, equations for the line of phase transitions.

#### 4.4.1 - Equations of state

Each phase has its own equation of state:

##### *Normal phase*

In the normal phase, the magnetization is zero (in reality the system is very weakly diamagnetic). The equation of state is,

$$\mathbf{M} = \mathbf{0}. \quad (4.16)$$

##### *Superconducting phase*

In the superconducting phase, the magnetic field  $\mathbf{B}$  is zero within the sample. Through the relation linking  $\mathbf{B}$ ,  $\mathbf{H}$  and  $\mathbf{M}$ , the equation of state reduces to (see eq. 4.6),

$$\mathbf{M} = -\mathbf{H}. \quad (4.17)$$

#### 4.4.2 - Specific heat

In each phase there are two contributions to the specific heat: the lattice specific heat and the electronic specific heat.

##### *Lattice specific heat $C^{\text{vib}}$*

The lattice specific heat  $C^{\text{vib}}$  is practically the same in the different phases. It arises from the vibrations of atoms around their equilibrium positions, the “amplitude” of which increases with temperature.  $C^{\text{vib}}$  grows slowly at low temperatures with, in the DEBYE model,<sup>6</sup>

$$C^{\text{vib}} = \frac{12\pi^4}{5} N_A k_B \left( \frac{T}{\theta_D} \right)^3 \quad T \ll \theta_D \quad (4.18a)$$

where  $N_A$  = the atomic density;  $\theta_D$  = the DEBYE temperature;  $k_B$  = the BOLTZMANN constant, and then increases rapidly up to the DEBYE temperature, saturating at high temperatures where it reaches a limiting value (the law of DULONG and PETIT),

$$C^{\text{vib}} = 3N_A k_B \quad T \geq \theta_D. \quad (4.18b)$$

Examples of DEBYE temperatures for a few superconducting elements are given in Table 4.3.

Table 4.3 - DEBYE temperatures for a few superconducting elements

Element	Hg	Sn	Nb	Al
DEBYE temperature $\theta_D$ [K]*	72	200	276	433

\* [http://www.knowledgedoor.com/2/elements\\_handbook/debye\\_temperature.html](http://www.knowledgedoor.com/2/elements_handbook/debye_temperature.html)

6 L.D. LANDAU & E.M. LIFSHITZ (1959) *Statistical Physics*, Pergamon Press, 180.

### **Electronic specific heat $C_n^{el}$ in the normal phase**

Superimposed on the lattice specific heat is the electronic specific heat  $C_n^{el}$ , which represents the energy gained by the electron gas when the temperature increases by 1 kelvin. In a model of free electrons, this specific heat is linear in  $T$  (see Chap. 8),

$$C_n^{el} = \gamma T \quad (4.19)$$

where  $\gamma$  is SOMMERFELD's constant.

In most metals,  $C_n^{el}$  and  $C^{vib}$  are equal at around 2 to 3 K, with  $C^{vib} \ll C_n^{el}$  for very low temperatures and  $C^{vib} \gg C_n^{el}$  for high temperatures (Fig. 4.4).

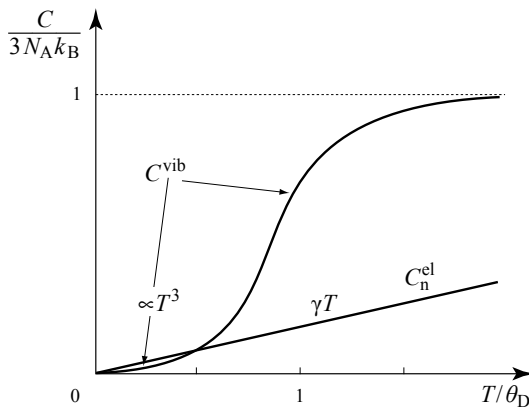


**Figure 4.4**

#### **Specific heat of a normal metal**

The specific heat of a normal metal is the sum of two contributions:

- ›  $C^{vib}$ , the vibrational specific heat of the lattice (phonons) that greatly dominates at high temperatures and increases as  $T^3$  at low temperatures;
- ›  $C_n^{el}$ , electronic specific heat, linear in  $T$ , dominant at very low temperatures.

### **Electronic specific heat $C_s^{el}$ in the superconducting phase**

Measurements (Fig. 4.5) of the electronic specific heat (obtained by subtraction of  $C^{vib}$  from the total specific heat) performed on the same material in its normal  $C_n^{el}$  and superconducting  $C_s^{el}$  phases<sup>7</sup> revealed three outstanding features:

- » at very low temperatures,  $C_s^{el}$  increases exponentially with temperature remaining less than  $C_n^{el}$ , which increases linearly;
- » near  $T \sim 0.6 T_c$  the electronic specific heat of the superconducting phase  $C_s^{el}$  crosses that of the normal phase  $C_n^{el}$  and exceeds it at higher temperatures;
- » across the superconductor/normal transition, a strong discontinuity of the electronic specific heat occurs. At temperature  $T_c$  and at zero field, this discontinuity is close to

$$\frac{C_s^{el} - C_n^{el}}{C_n^{el}} \approx 1.43. \quad (4.20)$$

<sup>7</sup> Below  $T_c$ ,  $C_n^{el}$  is measured by applying a magnetic field exceeding the critical field  $H_c(T)$ .

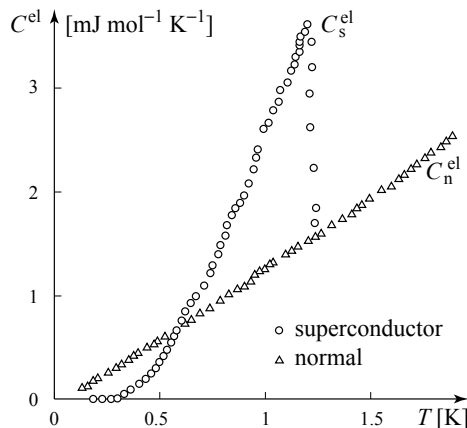


**Figure 4.5 - Electronic specific heat of aluminum in the normal and superconducting states**  
 [from N.E. PHILLIPS, 1959, © The American Physical Society, with permission]<sup>8</sup>

- › the electronic specific heat of the normal state  $C_n^{\text{el}}$  varies linearly with temperature;
- › the electronic specific heat of the superconducting state varies exponentially at very low temperatures;
- › the S/N transition shows a discontinuity in electronic specific heat.

#### 4.4.3 - Phase diagram - The critical field line

Based on experimental results, several empirical expressions for the critical field line separating the superconducting phase from the normal phase have been proposed. The simplest and most popular is TUYN's law,

$$H_c(T) = H_c(0) \left[ 1 - \left( \frac{T}{T_c} \right)^2 \right] \quad (4.21)$$

where  $T_c$ , implicitly  $T_c(H=0)$ , is the critical temperature in zero field and  $H_c(0)$  the critical field extrapolated to zero temperature.

Other empirical laws, including higher powers of temperature, have also been suggested, justified by better fits to the experimental curves (Fig. 4.6), and they include higher powers of temperature with for example for tin<sup>5</sup>

$$H_c(T) = H_c(0) \left[ 1 - 1.211 \left( \frac{T}{T_c} \right)^2 + 0.211 \left( \frac{T}{T_c} \right)^3 \right]. \quad (4.22)$$

It is important to note that all these laws have in common that the slope  $\frac{dH_c(T)}{dT}$  vanishes at 0 K but remains finite at  $T_c$ .

---

8 N.E. PHILLIPS (1959) *Phys. Rev.* **114**, 676.

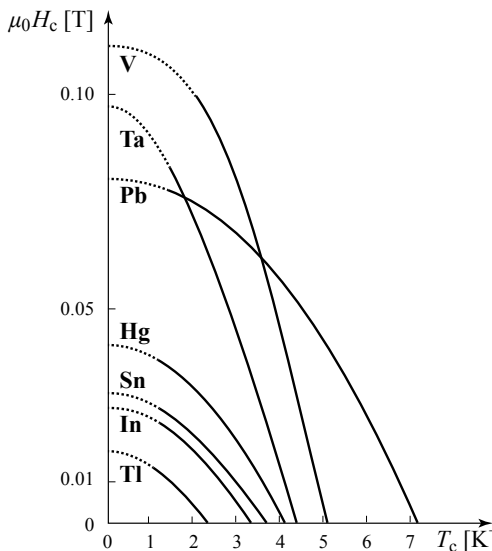


**Figure 4.6**  
**Critical field lines of**  
**common metallic**  
**superconductors of type I**  
 [from D. SHOENBERG, 1952,  
 © Cambridge University Press]<sup>9</sup>

**Table 4.4 - Critical temperatures  $T_c$  at zero field, critical fields  $H_c(0)$  at zero temperature and slopes of the critical field as a function of temperature, seen in some pure metals**<sup>5</sup>

Element	Al	Cd	Ga	La	Nb*	Pb	Sn	Ta	V*
$T_c$ [K]**	1.175	0.517	1.083	4.880	8.250	7.196	3.720	4.470	5.400
$\mu_0 H_c(0)$ [mT]	10.6	2.88	5.03	103	196	81.2	30.7	86	134
$-\mu_0 \frac{dH_c}{dT} \Big _{T_c}$ [mT K <sup>-1</sup> ]	16.3	8.6	9.3	—	—	22.6	14.7	33.4	48.2

\* Niobium and vanadium are type II superconductors.

\*\* <http://www.superconductors.org/type1.htm>

## 4.5 - The transition between superconducting and normal states

### 4.5.1 - Free enthalpy of condensation

As indicated in Table 4.2, the equilibrium state of a system, maintained at temperature  $T$  and subject to a field  $H$ , is that which minimizes the free enthalpy density  $g(T, H)$ . When at fixed  $H$  and  $T$ , there is competition between two phases, as here between normal and superconducting phases, the stable phase is the one for which the free enthalpy density is lower. Co-existence of two phases occurs when their free enthalpy densities are equal. We will now examine the free enthalpy densities for the normal and superconducting phases.

9 D. SHOENBERG (1952) *Superconductivity*, Cambridge University Press.

Starting from the general differential relation  $dg = -sdT - \mu_0 M(H') dH'$ , which expresses the variation of  $g$  as a function of variations  $dT$  of the temperature and  $dH'$  of the magnetic field, we have at a given temperature  $T$  and, independently of the phase, after integration of the field from  $H' = 0$  to  $H' = H$

$$g(T, H) = g(T, 0) - \mu_0 \int_0^H M(H') dH'. \quad (4.23)$$

So that in the normal state, with equation of state  $M(H) = 0$ ,

$$g_n(T, H) = g_n(T, 0) \quad (4.24)$$

and in the superconducting state, with equation of state  $M(H) = -H$ ,

$$g_s(T, H) = g_s(T, 0) + \mu_0 \frac{H^2}{2}. \quad (4.25)$$

Since there is coexistence of the two phases when the field  $H = H_c(T)$ ,

$$g_s[T, H_c(T)] = g_n[T, H_c(T)] \quad (4.26)$$

we have, using relations (4.24) and (4.25),

$$g_s(T, H) = g_n(T, 0) - \mu_0 \left[ \frac{H_c^2(T)}{2} - \frac{H^2}{2} \right] \quad (4.27)$$

where the difference in the free enthalpy density between the superconducting and normal states includes two terms:

» the free enthalpy density of condensation,

$$g_s^{\text{cond}} = -\mu_0 \frac{H_c^2(T)}{2} \quad (4.28)$$

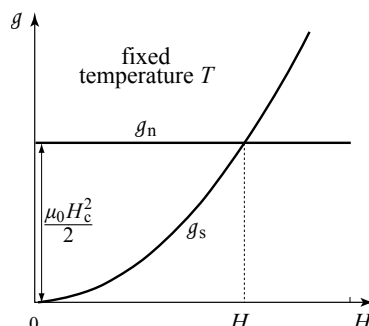
which is interpreted as the free enthalpy of the formation of COOPER pairs per unit volume at temperature  $T$ . The field for which the difference between the free enthalpies of the superconducting and normal phases are equal is called  $H_c$ , the “thermodynamic critical field.”

» the free magnetic enthalpy density,

$$g_s^{\text{mag}} = \mu_0 \frac{H^2}{2} \quad (4.29)$$

which reflects the increase in free enthalpy density that the superconductor experiences when it is inserted into the field  $\mathbf{H}$  (Fig. 4.7).

**Figure 4.7**  
Free enthalpy densities of the superconducting state and the normal state  
Variation of the free enthalpy densities of the normal phase and superconducting phase as a function of field  $\mathbf{H}$  at constant temperature  $T$ . When  $H = H_c$  the free enthalpy densities are equal and there is coexistence of the two phases.



#### 4.5.2 - Relation between the specific heat and the slope of the transition line

At constant field  $H$ , the specific heat of a magnetic system is given in Table 4.2 as

$$C_H = -T \left( \frac{\partial^2 g}{\partial T^2} \right)_H. \quad (4.30)$$

This leads to the expression for the difference between the electronic specific heat of the two phases,

$$C_s^{\text{el}} - C_n^{\text{el}} = -T \left( \frac{\partial^2 (g_s - g_n)}{\partial T^2} \right)_H \quad (4.31)$$

which, using the relation (4.27), becomes

$$C_s^{\text{el}} - C_n^{\text{el}} = \mu_0 T \left[ \left( \frac{\partial H_c(T)}{\partial T} \right)^2 + H_c \left( \frac{\partial^2 H_c(T)}{\partial T^2} \right) \right] \quad (4.32)$$

with, at the transition temperature  $T_c$  for which  $H_c = 0$ ,

$$(C_s^{\text{el}} - C_n^{\text{el}})_{T=T_c} = \mu_0 T_c \left( \frac{\partial H_c(T)}{\partial T} \right)_{T=T_c}^2. \quad (4.33)$$

This relation, between the amplitude of the discontinuity of the specific heat at  $T_c$  (Figs. 4.5 and 4.8) and the slope of the transition line  $H_c(T)$  at  $T_c$ , is called the “RUTGERS’ law.”

At a temperature  $T$ , TUYN’s law (4.21), combined with the relation (4.32), leads to an expression for the difference between the specific heat of the superconducting and normal phases

$$C_s^{\text{el}} - C_n^{\text{el}} = 2\mu_0 [H_c(0)]^2 \frac{T}{T_c^2} \left[ 3 \left( \frac{T}{T_c} \right)^2 - 1 \right]. \quad (4.34)$$

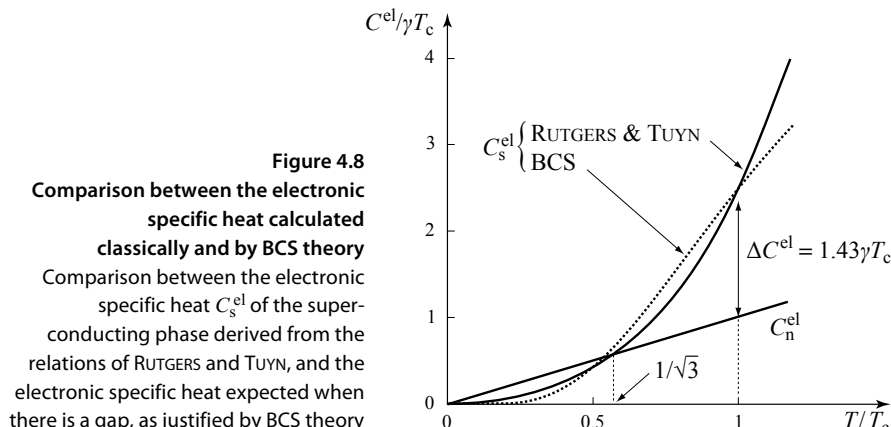
The temperature dependence in this law can be compared to that of BCS theory, which predicts exponential variation of the electronic specific heat at low temperatures,

$$C_s^{\text{el}} \approx a e^{-\frac{\Delta(0)}{2k_B T}} \quad T \ll T_c \quad (4.35)$$

( $\Delta(T)$  is the gap to be discussed in Chapter 8) and a discontinuity equal to  $1.43 \gamma T_c$  at the superconducting/normal transition for zero field. The comparison between  $C_s^{\text{el}}$  deduced from (4.34) and the behavior expected from BCS is shown in Figure 4.8, where the parameters have been adjusted so that the specific heat discontinuity at  $T_c$  derived from (4.34) is identical to the BCS predictions, *i.e.* with

$$(C_s^{\text{el}} - C_n^{\text{el}})_{T=T_c} = 4 \frac{\mu_0 [H_c(0)]^2}{T_c} = 1.43 \gamma T_c. \quad (4.36)$$

Although the agreement is satisfactory overall, the principal weakness of the TUYN-RUTGERS' laws is to predict at very low temperatures a variation of  $C_s^{\text{el}}$  that would be a power law, whereas experimentally (see Fig. 4.5), and according to BCS, it varies exponentially.



Their validity can also be tested by the consistency between the results of calorimetric measurements of the jump in specific heat at the critical temperature and the values calculated via the relation (4.34) from the measurements of  $H_c(0)$ . The comparison between the values obtained (Table 4.5) generally shows a very satisfactory agreement.

**Table 4.5 - Specific heat jump at the superconducting transition in zero field**<sup>5</sup>

Direct measurement (by calorimetry) and indirect determination by measurement of  $H_c(T)$  (magnetometry) and application of equation (4.32)

Material	Sn	In	Tl	Ta	Pb
$T_c$ [K]*	3.72	3.41	2.38	4.47	7.2
$C_s^{\text{el}} - C_n^{\text{el}}$ [ $10^{-3}$ J mol $^{-1}$ K $^{-1}$ ]	10.6	9.75	6.2	41.5	52.6
Calorimetric measurement					
$C_s^{\text{el}} - C_n^{\text{el}}$ [ $10^{-3}$ J mol $^{-1}$ K $^{-1}$ ]	10.6	9.62	6.15	41.6	41.8
Magnetic measurement					

\* <http://www.superconductors.org/type1.htm>

As the differences between the specific heat do not depend on the field (see relation 4.34), they are identical in zero and finite applied fields. This implies that the amplitudes of specific heat jumps at the transition in a field  $H$ , which occurs at the temperature  $T_c(H)$  remains as in the relation (4.34), with  $T$  replaced by  $T_c(H)$  and the  $T_c$  of (4.34) kept at its value in a zero field.

#### 4.5.3 - Latent heat of transformation

Since at any point on the coexistence line the free enthalpy densities of the normal and superconducting phases are equal, for any displacement along the equilibrium line where  $T = T_c(H)$ , we have (Fig. 4.9)

$$dg_n = dg_s|_{\text{eq}}. \quad (4.37)$$

|<sub>eq</sub> means the equation is valid if we move along the line of equilibrium.

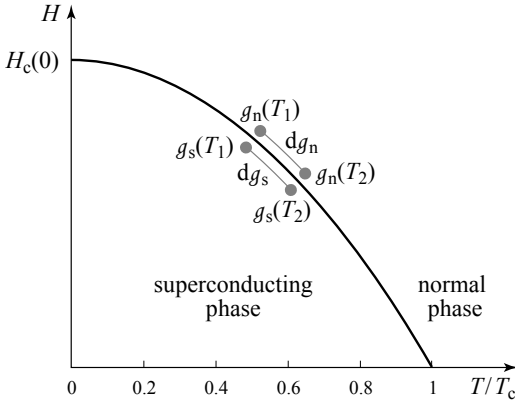


**Figure 4.9**  
**Phase diagram of the normal/superconductor transition**  
When we move along the coexistence curve, the variation of the free enthalpy density in one phase is equal to that in the other phase.

By writing the differentials of the free enthalpy densities of each phase,

$$dg_n = -s_n dT \quad \text{and} \quad dg_s = -s_s dT - \mu_0 M dH \quad (4.38)$$

this leads to

$$(s_n - s_s)dT = \mu_0 M dH_c|_{\text{eq}} \quad (4.39)$$

where  $s_n - s_s$  is the difference of specific entropy between two points located on either side of the critical line, and since in the superconductor,  $M = -H$ ,

$$s_n - s_s = -\mu_0 H_c \frac{dH_c}{dT}|_{\text{eq}}. \quad (4.40)$$

The latent heat of transformation  $\mathcal{L}$  is then written as

$$\mathcal{L} = T(s_n - s_s) = -\mu_0 T H_c \frac{dH_c}{dT}|_{\text{eq}} \quad (4.41)$$

which is the *CLAPEYRON equation* of the phase transition.  $\mathcal{L}$  represents the quantity of heat that the system receives when it passes from the superconducting state to the normal state. If  $H_c(T)$  varies according to TUYN's law (4.21),

$$\frac{dH_c}{dT}|_{\text{eq}} = -2H_c(0) \frac{T}{T_c^2} \quad (4.42)$$

and so

$$\mathcal{L}(T) = 2\mu_0 H_c(0) \left( \frac{T}{T_c} \right)^2 H_c(T). \quad (4.43)$$

The latent heat (Fig. 4.10) is zero at  $T = 0$  as well as at  $T = T_c$  (since  $H_c(T_c) = 0$ ). It shows a maximum at  $T/T_c = 1/\sqrt{2}$ .

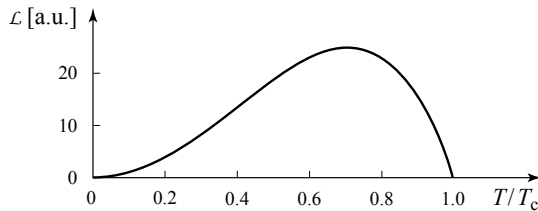


**Figure 4.10 - Latent heat of transformation at the superconductor/normal transition**

In zero field, the latent heat of transformation vanishes at  $T_c$ , which shows that the transition **is not** of first order. In finite field, [ $T_c(H) < T_c$ ] the latent heat is non-zero, which shows that in this case the transition **is** of first order.

#### 4.5.4 - Order of the phase transitions

Starting from considerations about the continuity of a system's extensive variables and their derivatives (the classification of EHRENFEST), the very great majority of phase transitions can be classified into two broad categories.

##### **First order transitions**

These are phase transitions which are accompanied by a discontinuity in the first derivatives of the free enthalpy (extensive variables) and therefore of the entropy and of the magnetization of the system. According to CLAPEYRON's formula, such transitions have a non-zero latent heat of transformation.

They are, furthermore, characterized by a coexistence of two phases, as there is during the melting of ice in water. The order parameter is discontinuous.

##### **Second order transitions**

At a second order phase transition the extensive variables, such as entropy, are continuous and the discontinuities are only in second derivatives of the free enthalpy (specific heat...). With the entropy now continuous, the latent heat vanishes.

There is no coexistence of phases in this case. The transition is described by an order parameter which is zero above the critical temperature and which grows continuously from zero when the temperature descends below  $T_c$ .

##### **Superconducting/Normal transitions**

As we have just shown, the latent heat of a transition under a finite magnetic field is non-zero; *the superconducting/normal transition in a magnetic field is a first order transition.*

On the other hand, in zero field, there is no entropy discontinuity at  $T_c$ . The latent heat is zero whereas the first derivatives of extensive variables (for example the specific heat) are discontinuous. *The superconducting/normal transition at  $T_c$  in zero magnetic field is a second order transition.*

We have yet to determine the order parameter, which could be, for example, the density of superconducting electrons  $n_s$ , zero above  $T_c$  and increasing from zero below  $T_c$  (see Eq. 2.33). We shall see, however, that the order parameter of the superconducting phase is a much more subtle quantity.

## Appendix 4

### Magnetic media

#### A4.1 - Fields in magnetized materials

##### The equivalence magnetization - distribution of AMPÈRE currents

As we know from reference books on magnetism:<sup>10</sup>

- » a current loop of intensity  $i$  and oriented surface  $S$ , behaves as a magnetic dipole with moment  $\mu = iS$  (Fig. 4.11). Placed at the origin, it creates at a point  $r$ , lying at a large distance, a magnetic field

$$\mathbf{b}(\mathbf{r}) = \frac{\mu_0}{4\pi r^5} [3(\mu \cdot \mathbf{r})\mathbf{r} - r^2\mu]; \quad (4.44)$$

- » by the principle of superposition, the magnetic field  $\mathbf{B}(\mathbf{r})$  created at each point in space by a distribution of elementary magnetic moments is the sum of the fields  $\mathbf{b}(\mathbf{r})$  created by each of them;
- » to each distribution of magnetic moments which leads to a magnetization  $\mathbf{M}(\mathbf{r})$  (the average, per unit volume, of the elementary moments around a point  $\mathbf{r}$ ), corresponds an equivalent distribution of bulk  $\mathbf{j}_{vol}^a$  and surface  $\mathbf{j}_{surf}^a$  currents that generate a magnetic field  $\mathbf{B}^a(\mathbf{r}) \equiv \mathbf{B}(\mathbf{r})$  at all points in space.

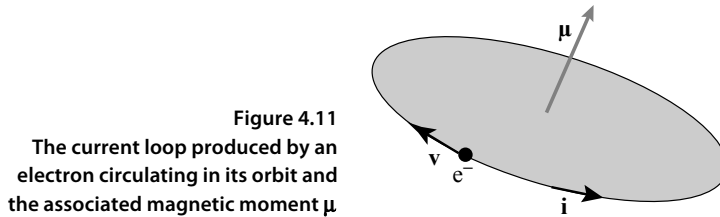


**Figure 4.11**  
The current loop produced by an electron circulating in its orbit and the associated magnetic moment  $\mu$

The current densities (“AMPÈRE currents”) and the magnetization which produce, at each point in space, the same magnetic field  $\mathbf{B}^a$  are connected by the relations

$$\mathbf{j}_{vol}^a = \nabla \times \mathbf{M} \quad \text{and} \quad \mathbf{j}_{surf}^a = \mathbf{M} \times \mathbf{n} \quad (4.45)$$

where  $\mathbf{n}$  is the unit vector locally perpendicular to the surface of the sample, and pointing outwards.

---

<sup>10</sup> See *Magnetism I and II* (2004) D. GIGNOUX, E. DU TRÉMOLET DE LACHEISSE, M. SCHLENKER, Grenoble Sciences, EDP Sciences.

### **AMPÈRE currents in a uniformly magnetized cylinder**

We now consider an infinite cylinder with uniform magnetization  $\mathbf{M}$  parallel to its axis. By applying the relations (4.45), this magnetization is equivalent to a surface AMPÈRE current density only of magnitude  $j_{\text{surf}}^{\text{a}} = M$  flowing around the cylinder (see Fig. 4.13).

This result can be very clearly interpreted by considering the orbital currents associated with dipole moments uniformly distributed in the cylinder and oriented along its axis. In a normal cross-section of this cylinder the current loops are tangent and, by superposition of currents flowing locally in opposite directions, the bulk current density is zero. Only the current loops tangential to the external surface are uncompensated, which leads to the surface current density already mentioned. *A uniformly magnetized cylinder of magnetization  $\mathbf{M}$  along its axis is, as far as the magnetic field it generates is concerned, equivalent to a cylindrical surface carrying a surface current of density  $j_{\text{surf}}^{\text{a}}$*  (Fig. 4.12).

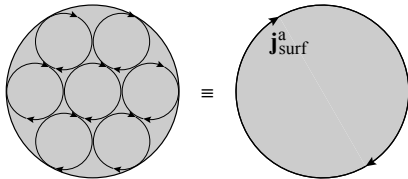


**Figure 4.12**  
**Equivalence between a uniform assembly of current loops and a surface AMPÈRE current**  
In the bulk, the currents of the different loops cancel out.

### **Magnetic field $\mathbf{B}$**

Very generally, a “magnetic system” includes both an external electrical circuit and the material. The experimentalist injects into the electrical circuit, by means of a generator, a current distribution  $\mathbf{j}^0$  (called the “conductor currents”) creating magnetic fields  $\mathbf{B}^0(\mathbf{r})$ . The material develops a magnetization  $\mathbf{M}$ , equivalent to a distribution of AMPÈRE currents  $\mathbf{j}_{\text{vol}}^{\text{a}}$  and  $\mathbf{j}_{\text{surf}}^{\text{a}}$ , which create magnetic fields  $\mathbf{B}^{\text{a}}(\mathbf{r})$ .

As a result, the total magnetic field  $\mathbf{B}(\mathbf{r})$  at each point in space is the superposition of the two contributions

$$\mathbf{B}(\mathbf{r}) = \mathbf{B}^0(\mathbf{r}) + \mathbf{B}^{\text{a}}(\mathbf{r}) \quad (4.46)$$

with locally  $\nabla \times \mathbf{B}^0 = \mu_0 \mathbf{j}^0 \quad ; \quad \nabla \times \mathbf{B}^{\text{a}} = \mu_0 \mathbf{j}^{\text{a}}$  (4.47)

$$\nabla \times \mathbf{B}(\mathbf{r}) = \mu_0 [\mathbf{j}^0(\mathbf{r}) + \mathbf{j}^{\text{a}}(\mathbf{r})].$$

### **Field $\mathbf{H}$**

By definition, we call the field  $\mathbf{H}$  the difference between the magnetic field  $\mathbf{B}$  divided by  $\mu_0$  and the magnetization  $\mathbf{M}$

$$\mathbf{H} = \frac{\mathbf{B}}{\mu_0} - \mathbf{M} \Leftrightarrow \mathbf{B} = \mu_0(\mathbf{H} + \mathbf{M}). \quad (4.48)$$

Although the field  $\mathbf{H}$  can be determined directly from its definition, it is often easier to calculate it by introducing the *fictitious bulk*  $\rho_{\text{vol}}^{\text{m}}$  and *surface*  $\sigma_{\text{surf}}^{\text{m}}$  *magnetic charges*, modelled on polarization charges and defined by:

$$\rho_{\text{vol}}^{\text{m}} = -\nabla \cdot \mathbf{M} \quad (4.49\text{a})$$

$$\sigma_{\text{surf}}^{\text{m}} = \mathbf{M} \cdot \mathbf{n}. \quad (4.49\text{b})$$

$\mathbf{H}$  is then the sum of two contributions,

$$\mathbf{H} = \mathbf{H}^0 + \mathbf{H}^{\text{m}} \quad (4.50)$$

where  $\mathbf{H}^0 = \mathbf{B}^0/\mu_0$  is the field created by the conductor currents  $\mathbf{j}^0$ , and  $\mathbf{H}^{\text{m}}$  can be derived from the distribution of magnetic charges.  $\mathbf{H}^{\text{m}}$  is calculated just like the field  $\mathbf{E}$  in electrostatics. Indeed it suffices to rewrite the laws of electrostatics (COULOMB, GAUSS, continuity equations) to determine it by replacing  $\mathbf{E}$  by  $\mathbf{H}^{\text{m}}$ , electric charges by magnetic charges, and to suppressing  $\epsilon_0$  in each formula.

Like the electric field  $\mathbf{E}$ , the **curl** of  $\mathbf{H}^{\text{m}}$  is zero and by combining the relations (4.47), (4.48) and (4.50) and AMPÈRE's theorem,  $\mathbf{H}$  reduces to

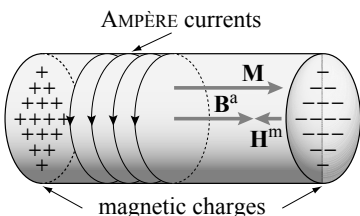
$$\nabla \times \mathbf{H} = \mathbf{j}^0 \quad (4.51)$$

which means that the **curl** of  $\mathbf{H}$  comes only from the conductor currents injected by the experimentalist, whereas the curl of  $\mathbf{B}$  is connected to all the currents, those of the conductor as well as the AMPÈRE currents which appear in response.

### B and H fields in a uniformly magnetized cylinder

When we apply the relations (4.49), it appears that in a uniformly magnetized cylinder the density of magnetic charges in the bulk is zero ( $\nabla \cdot \mathbf{M} = 0$ ) and the magnetic surface charges are localized on the two circular disks defining the ends of the cylinder.

They are positive on the perpendicular circular disk with outgoing normal vector parallel to  $\mathbf{M}$  and negative on the opposite disk (Fig. 4.13). This makes the cylinder a “magnetic condenser” formed by two finite dimensional plates, carrying a charge density  $\sigma_{\text{surf}}^{\text{m}} = \pm M$ . The field  $\mathbf{H}^{\text{m}}$  is in the opposite sense to the magnetization  $\mathbf{M}$  (see relation 4.48), and for this reason it is called the “demagnetizing field.”



The AMPÈRE currents flow on the surface of the cylinder and the magnetic charges are localized on the discs that close the cylinder at its two ends. The demagnetizing field  $\mathbf{H}^{\text{m}}$  created by the magnetic charges fades away when the cylinder becomes very long and the magnetic charges are pushed to infinity.

Figure 4.13 - The AMPÈRE currents and surface magnetic charges associated with a uniformly magnetized material

### B and H fields in an infinite cylinder placed in a solenoid

**Note** - In the figure below (Fig. 4.14), as in the others following, the fields  $\mathbf{H}$  and  $\mathbf{B}$ , which are not expressed in the same physical units, are nonetheless represented by arrows of identical length when they satisfy  $\mathbf{B} = \mu_0 \mathbf{H}$ . In other words, what we label  $\mathbf{H}$  and  $\mathbf{M}$  are in fact  $\mu_0 \mathbf{H}$  and  $\mu_0 \mathbf{M}$ .

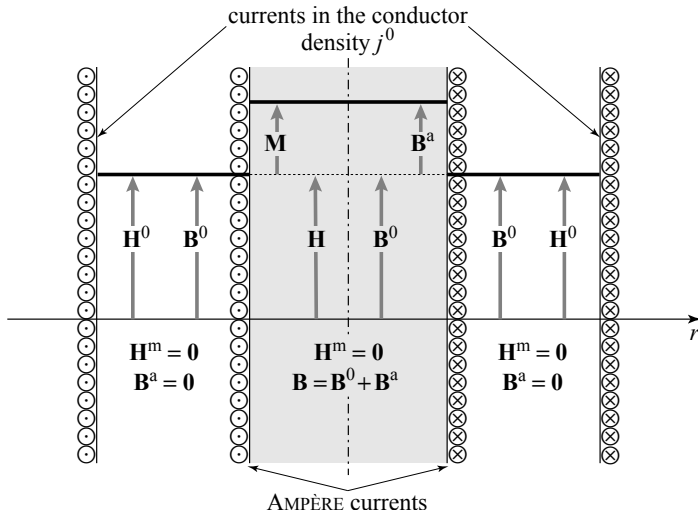


Figure 4.14 -  $\mathbf{H}$  and  $\mathbf{B}$  fields in the interior and the exterior of an infinite cylinder (demagnetizing factor  $N = 0$ ) of uniform magnetization density  $\mathbf{M}$  placed in a uniform field  $\mathbf{B}^0$

$\mathbf{B}^0$  is the magnetic field created by the currents  $j^0$  flowing in the external solenoid.

$\mathbf{H}^0$  is the contribution of the currents  $j^0$  to the field  $\mathbf{H}$ . In fact it is the only contribution for both the exterior and the interior of the cylinder since in this geometry of an infinite cylinder, the demagnetizing field  $\mathbf{H}^m$  is zero.  $\mathbf{B}^a$  is the magnetic field created by the AMPÈRE currents. It is uniform within the cylinder and zero outside.  $\mathbf{M}$  is the magnetization equivalent to the AMPÈRE currents. The total field  $\mathbf{H}$  is everywhere equal to  $\mathbf{H}^0$  and the total field  $\mathbf{B}$  is the sum of the applied field  $\mathbf{B}^0$  and the field  $\mathbf{B}^a$ .

In an infinite cylinder with uniform magnetization  $\mathbf{M}$  inserted in a magnetic field  $\mathbf{B}^0$ :

- » the magnetization is equivalent to surface AMPÈRE currents of density  $j_{\text{surf}}^a = M$  that create a uniform magnetic field  $\mathbf{B}^a = \mu_0 \mathbf{M}$  within the cylinder only, and a vanishing magnetic field outside. The total magnetic field is therefore  $\mathbf{B} = \mathbf{B}^0$  outside the cylinder and  $\mathbf{B} = \mathbf{B}^0 + \mu_0 \mathbf{M}$  inside;
- » as the surface magnetic charges have been sent infinitely far away, the demagnetizing field  $\mathbf{H}^m$  is constant and zero. The total field  $\mathbf{H}$  is reduced to  $\mathbf{H} = \mathbf{H}^0 = \frac{\mathbf{B}^0}{\mu_0}$  both inside and outside the magnetized material.

### A uniformly magnetized ellipsoid

The axially symmetric ellipsoid is a particularly interesting system for two reasons:

- » it can be used in a broad variety of situations, since by varying the ratio of its axes, it becomes a flat plate, a sphere or a cylinder, as well as all of the intermediate forms;
- » when the magnetization  $\mathbf{M}$  is uniform in the bulk, so too are the magnetic field  $\mathbf{B}^a$  of AMPÈRE currents and the field  $\mathbf{H}^m$  of magnetic charges. They depend only on  $\mathbf{M}$  and a factor for the ellipsoid  $N$ , called the “demagnetizing field factor” (Table 4.6).

**Table 4.6**

a - Examples of demagnetizing field factor  $N$  for an ellipsoid with the magnetic field applied along the axis of revolution  $c$

$c/a$	0 (plate)	1 (sphere)	2	4	$\infty$ (infinite cylinder)
$N(\mathbf{B}/c)$	1	$\frac{1}{3}$	$\sim 0.25$	$\sim 0.1$	0

b - Demagnetizing factor  $N$  of a cylinder with magnetic field applied perpendicular to its axis

$c/a$	$\infty$ (infinite cylinder)
	$\frac{1}{2}$

In addition, when the response is linear, applying a constant magnetic field  $\mathbf{B}^0$  creates a magnetization  $\mathbf{M}$ , a magnetic field  $\mathbf{B}$  and a field  $\mathbf{H}$ , all three of which are uniform inside the ellipsoid. The three quantities are related to one another by the expressions of Table 4.7.

**Table 4.7 - Summary of the magnitudes of the different fields  $H$  and  $B$  within and on the surface of an ellipsoid placed in a uniform field  $B^0$  with demagnetizing field factor  $N$ , uniform magnetization  $M$**

Uniform applied magnetic field $\mathbf{B}^0 = \mu_0 \mathbf{H}^0$ $\mathbf{M}$ uniform in the sample
At any point, inside or outside the ellipsoid $\mathbf{B} = \mathbf{B}^0 + \mathbf{B}^a \quad ; \quad \mathbf{H} = \mathbf{H}^0 + \mathbf{H}^m$
Inside the ellipsoid $\mathbf{B}_{\text{int}}^a$ and $\mathbf{H}_{\text{int}}^m$ are uniform. $\mathbf{B}_{\text{int}}^a = (1 - N) \mu_0 \mathbf{M} \quad ; \quad \mathbf{H}_{\text{int}}^m = - N \mathbf{M}$
Outside the ellipsoid $\mathbf{B}_{\text{ext}}^a$ and $\mathbf{H}_{\text{ext}}^m$ are not uniform. At each point $\mathbf{B}_{\text{ext}}^a = \mu_0 \mathbf{H}_{\text{ext}}^m$
Tangentially to the surface of the ellipsoid, at the equator $\tilde{\mathbf{B}} = \mathbf{B}^0 - N \mu_0 \mathbf{M} \quad ; \quad \tilde{\mathbf{H}} = \mathbf{H}^0 - N \mathbf{M} \quad ; \quad \tilde{\mathbf{B}} = \mu_0 \tilde{\mathbf{H}}$

The Figures 4.15, 4.16 and 4.17 represent successively:

- » the distribution of the densities of AMPÈRE currents  $j_{\text{surf}}^{\text{a}}$  and surface magnetic charges  $\sigma_{\text{surf}}^{\text{m}}$ . As the magnetization is uniform, the bulk current densities and bulk magnetic charges are zero.  $j_{\text{surf}}^{\text{a}}$  has a maximum at the equator where it takes the value  $M$  and decreases towards the poles where it vanishes. Conversely,  $\sigma_{\text{surf}}^{\text{m}}$  equals  $\pm M$  at the poles, and zero at the equator. For the special case of a sphere we have:

$$j_{\text{surf}}^{\text{a}} = M \sin \theta \quad ; \quad \sigma_{\text{surf}}^{\text{m}} = M \cos \theta \quad (\text{spherical case})$$

where  $\theta$  is the angle between the direction of magnetization and the point considered (Fig. 4.15);

- » the magnetization and the (uniform) fields within the solenoid (Fig. 4.16);
- » the profiles of fields  $\mathbf{B}$  and  $\mathbf{H}$  in a cross-section passing by the equatorial plane of the ellipsoid (Fig. 4.17).

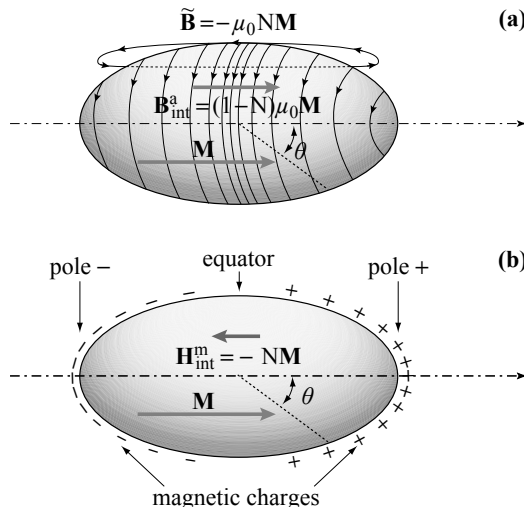


**Figure 4.15 - AMPÈRE currents and magnetic charges at the surface of a uniformly magnetized ellipsoid**

- (a)** There are only surface AMPÈRE currents. Their intensity is zero at the poles and maximal at the equator where they take the value  $j_{\text{surf}}^{\text{a}} = M$ . The magnetic field is uniform in the ellipsoid with value  $\mathbf{B}_{\text{int}}^{\text{a}} = (1 - N) \mu_0 \mathbf{M}$ . **(b)** There are only surface magnetic charges. Their density is maximal at the poles with value  $\sigma^{\text{m}} = \pm M$ ; it vanishes at the equator. The demagnetizing field inside the ellipsoid is uniform and equals  $\mathbf{H}_{\text{int}}^{\text{m}} = -N \mathbf{M}$ . We recall the note preceding Figure 4.14 concerning representations of the vectors of  $\mathbf{H}$  and  $\mathbf{M}$ .

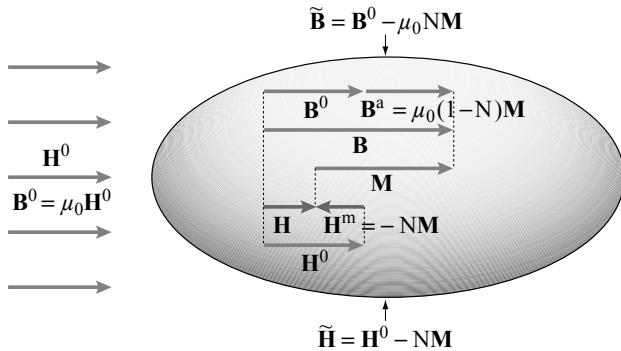


**Figure 4.16 - Fields within an ellipsoid of magnetic form factor  $N$ , and uniform magnetization  $M$ , placed in a uniform field  $B^0 = \mu_0 H^0$**

The total magnetic field  $\mathbf{B}$  is the sum of  $\mathbf{B}^0$  created by the conductor currents and of  $\mathbf{B}^a$  created by the AMPÈRE currents. The total field  $\mathbf{H}$  is the sum of  $\mathbf{B}^0/\mu_0$  and  $\mathbf{H}^m$  created by the magnetic charges.  $\tilde{\mathbf{H}}$  and  $\tilde{\mathbf{B}}$  are fields at the equator. See the note preceding Figure 4.14 concerning representations of the vectors  $\mathbf{H}$  and  $\mathbf{M}$ .

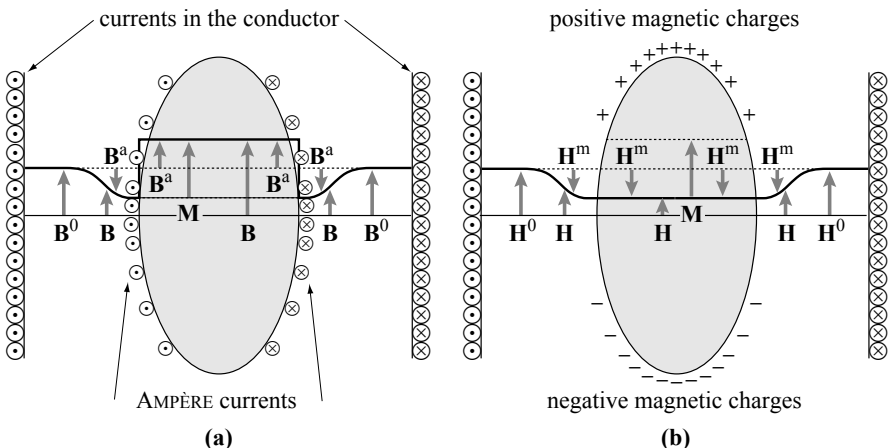


**Figure 4.17 - Profiles across the equator of fields  $\mathbf{H}$  and  $\mathbf{B}$  in the interior and exterior of an ellipsoid of uniform magnetization  $M$  placed in a uniform field  $B^0 = \mu_0 H^0$**

The total  $\mathbf{B}$  is the sum of  $\mathbf{B}^0$  and  $\mathbf{B}^a$  created by the AMPÈRE currents.

The total  $\mathbf{H}$  is the sum of  $\mathbf{H}^0$  and  $\mathbf{H}^m$  created by the magnetic charges.

### The general case

In the general case of a sample of arbitrary shape, there is a complex distribution of the AMPÈRE currents, the magnetic charges, of the fields  $\mathbf{B}$  and  $\mathbf{H}$  and of the magnetization  $\mathbf{M}$ . The magnetic moment carried by the whole sample is written

$$\mathcal{M} = \iiint_{\text{sample}} \mathbf{M}(\mathbf{r}) d^3r = \iiint_{\text{sample}} \left[ \frac{\mathbf{B}(\mathbf{r})}{\mu_0} - \mathbf{H}(\mathbf{r}) \right] d^3r. \quad (4.52)$$

#### A4.2 - Work performed in the magnetization of matter

##### The work to establish a field in an empty solenoid

We consider a solenoid of length  $L$ , formed by a winding of  $n_1 L$  turns of cross-sectional area  $S$ , connected to a generator ( $n_1$  is the number of turns per unit length). In order to generate the magnetic field, the experimentalist gradually increases the current intensity  $i^0$  in the winding.

Suppose  $i^0(t)$  is the value of the current intensity at the instant  $t$ , the magnetic field  $\mathbf{B}^0(t)$  created inside the solenoid is of magnitude

$$B^0(t) = \mu_0 H^0(t) = \mu_0 n_1 i^0(t) \quad (4.53a)$$

and its flux through the  $n_1 L$  turns of the solenoid is

$$\phi(t) = n_1 L B^0(t) S. \quad (4.53b)$$

In order to increase the magnetic field by an amount  $dB^0$  during a time interval  $dt$ , the experimentalist must, through the generator, overcome the opposing induced electromotive force  $v(t) = -d\phi/dt$ . The work  $\delta W$  received by the system is equal and opposite to the work performed by this force, or

$$\delta W = -v(t)i^0(t)dt = i^0(t)d\phi. \quad (4.54)$$

By replacing  $i^0$  and  $\phi$  by their expressions (4.53) as a function of  $B^0$ , we find

$$\delta W = \left( \frac{B^0}{\mu_0 n_1} \right) (n_1 L S dB^0) = \mathcal{V} \left( \frac{B^0}{\mu_0} \right) dB^0 = \mathcal{V}(H^0 dB^0) \quad (4.55)$$

where  $\mathcal{V}$  is the volume inside the solenoid.

##### Work to establish a field in a solenoid containing a solid cylinder of material

When there is material completely filling the solenoid volume, the magnet fields  $\mathbf{B}^0$  and  $\mathbf{B}^a$  are superimposed and the opposing electromotive force resisting the increase of flux through the turns can be written

$$v(t) = -\frac{d\phi}{dt} = -\frac{d}{dt} [n_1 L B(t) S] = -\frac{d}{dt} n_1 L [B^0(t) + B^a(t)] S. \quad (4.56)$$

The work that the experimentalist must provide becomes

$$\delta W = i^0 \delta\phi = \left( \frac{H^0}{n_1} \right) (n_1 dBS) = \mathcal{V} H^0 dB = \mathcal{V} H dB. \quad (4.57)$$

To establish the intensity  $i^0$  in the solenoid necessary for creation of the field  $B^0$ , the experimentalist must counter simultaneously the variation of fluxes of both the magnetic field  $B^0$  produced by the variation of current  $i^0$ , and the magnetic field  $B^a$  produced by the AMPÈRE currents. The AMPÈRE currents and the current  $i^0$  appear in the expression for the work in inequivalent ways, since the AMPÈRE currents are created in response and unlike  $i^0$ , the experimentalist does not control them directly.

The expression for the exchange of work between the experimentalist and the system can be generalized to any geometry of the conducting circuit and magnetic material as

$$\delta W = \iiint_{\text{all space}} [\mathbf{H}(\mathbf{r}) \cdot d\mathbf{B}(\mathbf{r})] d^3 r \quad (4.58)$$

with  $\mathbf{B}(\mathbf{r}) = \mathbf{B}^0(\mathbf{r}) + \mathbf{B}^a(\mathbf{r}) \quad (4.59)$

and  $\mathbf{H}(\mathbf{r}) = \mathbf{H}^0(\mathbf{r}) + \mathbf{H}^m(\mathbf{r}). \quad (4.60)$

In this expression for the work performed, the presence of  $d\mathbf{B}(\mathbf{r})$  reminds us that the variation of flux is due to both contributions of the magnetic field, while the field  $\mathbf{H}$  depends, via its **curl**, only on the current density  $\mathbf{j}^0$  of the conductors, on which the experimentalist acts directly (relation 4.51).

#### **Work performed on the magnetized material alone**

Up to now, we have considered the work stored by the whole system (solenoid + magnetized material), but sometimes it is preferable to consider the material alone.

In this case, the work provided to the system “material alone” is equal to the work on the system “solenoid + material”, reduced by the work on the solenoid without the material, or

$$\delta W = \iiint_{\text{all space}} [\mathbf{H}(\mathbf{r}) \cdot d\mathbf{B}(\mathbf{r}) - \mathbf{H}^0(\mathbf{r}) \cdot d\mathbf{B}^0(\mathbf{r})] d^3 r \quad (4.61)$$

which can also be written as <sup>11</sup>

$$\delta W = \iiint_{\text{material}} \mu_0 [\mathbf{H}^0(\mathbf{r}) \cdot d\mathbf{M}(\mathbf{r})] d^3 r \quad (4.62)$$

where  $\mathbf{M}(\mathbf{r})$  is the magnetization of the material and  $\mathbf{H}^0(\mathbf{r})$  the field produced by the currents of the conductor alone. This relation is obvious when  $\mathbf{H} = \mathbf{H}^0$ , but in fact is completely general.

---

11 L.D. LANDAU & E.M. LIFSHITZ (1969) *Electrodynamics of Continuous Media*, Pergamon Press, Oxford.

# Chapter 5

## THE INTERMEDIATE STATE OF TYPE I SUPERCONDUCTORS

The aim of this chapter is to examine the way in which Superconductor to Normal (S/N) phase transitions occur in type I superconducting samples of finite size and varying shapes. In addition to the temperature, the transitions can be just as well provoked by magnetic fields or by currents flowing in the samples.

### 5.1 - Criteria for the occurrence of a S/N transition

We first consider the simple case of an infinite cylinder placed in a current-carrying solenoid. The three quantities we shall consider are the magnetic field  $\mathbf{B}$ , the field  $\mathbf{H}$  and the current density  $\mathbf{j}$  in the sample.

Outside the cylinder, the magnetic field is that which is created by the solenoid, denoted  $\mathbf{B}^0$ . Within the sample, it decreases exponentially from the surface according to

$$B(u) = B^0 e^{-\frac{u}{\lambda}} \quad (5.1)$$

where  $u$  is the distance to the surface and  $\lambda$  is the magnetic field penetration depth or simply the penetration depth (see section 3.3).

Because of the absence of any demagnetizing field for the infinite cylinder, the field  $\mathbf{H}$  is uniform in all the space, inside or outside the sample,

$$H = \frac{B^0}{\mu_0} = H^0. \quad (5.2)$$

The superconducting current density decreases from the surface of the sample, where it takes its largest value, according to the expression<sup>1</sup>

$$j(u) = \frac{B^0}{\lambda \mu_0} e^{-\frac{u}{\lambda}}. \quad (5.3)$$

---

<sup>1</sup> In a rigorous treatment of the PIPPARD model, the decrease of the field is not strictly exponential and the maximum in the superconducting current is not exactly localized at the surface, but is slightly displaced. Use of the local equation with a renormalization of  $\lambda$  gives us these simple laws again.

Furthermore, when the field  $H$  reaches the critical field  $H_c$ , the magnetic field and the current density at the surface, where they are strongest, take values

$$B(u=0) \equiv \tilde{B} = B_c = \mu_0 H_c \quad \text{and} \quad j(u=0) = \frac{B_c}{\lambda \mu_0} = \frac{H_c}{\lambda} = j_c \quad (5.4)$$

where  $B_c$  is the critical magnetic field and  $j_c$  the critical current density. Seeing these correlations, it would appear to be equivalent to say that the material enters into a transition from the superconducting state to the normal state if:

- › the field  $H_{\text{int}}$  *inside* the sample reaches  $H_c$ ;
- › the magnetic field  $\tilde{B}$  *at the surface* of the sample attains  $B_c$ ;
- › the current density reaches  $j_c$  *somewhere* in the sample (in fact, at the surface).

These considerations lead, in 1916, to the formulation of the *SILSBEE criterion*:<sup>2</sup>  
*A superconductor loses its vanishing resistance when at any point of its surface the total magnetic field  $\tilde{B}$  attains the critical value  $B_c$ .*

Later the *generalized SILSBEE criterion*<sup>3</sup> was formulated:

*If the current density  $j$  somewhere attains the critical current density  $j_c$ , the part of the sample where it does so transforms into the normal state.*

In actual fact the two formulations are only equivalent if the dimensions of the sample are large compared to the penetration depth  $\lambda$ . When they are inequivalent for geometrical reasons, we should retain the generalized version, and thus the criterion of critical current density. This criterion was shown to be valid by the microscopic theory of COOPER pairs (see section 8.6.6). Beyond a critical velocity (related to the critical current density  $j_c$ ) the kinetic energy of the electrons in a COOPER pair exceeds the sum of the condensation energy and the kinetic energy of the unpaired electrons, and this leads to pair-breaking.

## 5.2 - S/N transition of an infinite cylinder

Following the argument of the generalized SILSBEE criterion, we shall see first how the transition should proceed towards the normal state in a cylindrical superconductor subject to an increasing magnetic field  $B^0$ .

- »  $B^0 < B_c$ : the cylinder is entirely superconducting. The LONDON region extends from the external surface. The highest current density  $j_{\text{high}}$  is located at the sample surface and is lower than  $j_c$ :  $j_{\text{high}} = B_0 / (\lambda \mu_0) < j_c$  (Fig. 5.1a).
- »  $B^0 = B_c = \mu_0 H_c = \lambda \mu_0 j_c$ : the current density reaches  $j_c$  at the surface and, according to the generalized SILSBEE criterion, the “surface” makes a transition to the normal state. A normal skin (Fig. 5.1b) appears with a corresponding reduction of

2 F.B. SILSBEE (1916) *J. Wash. Acad. Sci.* **6**, 597.

3 A.C. ROSE-INNES & E.H. RHODERICK (1977) *Introduction to Superconductivity*, Pergamon Press, Oxford, Chapter 7.

the radius of the part of the cylinder that remains superconducting. The LONDON region is then shifted further inside the sample.

» As the superconducting current density flowing at the surface of the new LONDON region is still equal to  $B_c / (\lambda \mu_0)$ , the radius of the superconducting region diminishes still further (Fig. 5.1c) and, little by little, the superconductivity disappears.

Analyzed in this way, we see a sort of “melting” of the superconductivity starting from the outside surface of the sample.

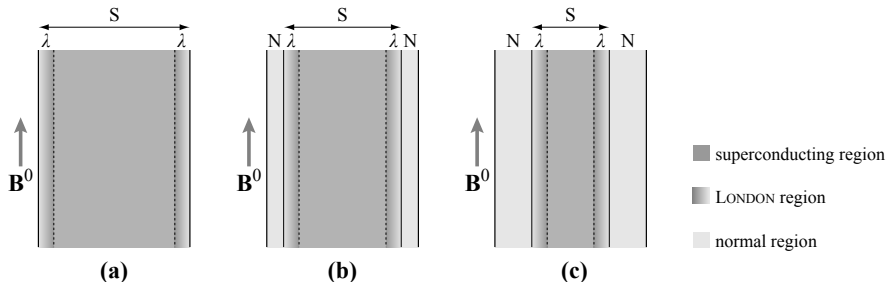


**Figure 5.1 - Superconducting-normal transition  
of an infinite cylinder inserted in a uniform magnetic field**

**(a)** As long as  $B^0 < B_c$ , the cylinder is entirely superconducting. Screening of the magnetic field is due to current flowing in the LONDON region. **(b)** When  $B^0$  reaches  $B_c$ , the transition begins at the surface, with the formation of a normal sheath which reduces the radius of the superconducting phase and moves the LONDON region towards the center of the sample. **(c)** The radius of the superconducting region decreases spontaneously until it completely disappears.

## 5.3 - Transition in small samples

### 5.3.1 - Thin slab

We saw in Chapter 2 (section 2.4.4) that small samples behave in a special way, in particular those that are slabs whose thickness  $d$  is of the order of, or smaller than, the penetration depth. In that case the magnetic field  $B$  decreases from the surface but does not reach zero at the heart of the sample.

Following the relation (2.28b), the highest current density is

$$j_{\text{high}} = \frac{B^0}{\mu_0 \lambda} \tanh \frac{d}{2\lambda}. \quad (5.5)$$

According to the generalized SILSBEY criterion, the transition only begins locally when this current density reaches  $j_c$ , and therefore the highest magnetic field  $B^0$  (and field  $H^0 = B^0 / \mu_0$ ) that this film can bear while staying in the superconducting state is determined by the condition,

$$\frac{B^0}{\mu_0 \lambda} \tanh \frac{d}{2\lambda} = j_c = \frac{B_c}{\mu_0 \lambda} \quad (5.6)$$

where:

- » if  $d \gg \lambda$ ,  $\tanh \frac{d}{2\lambda} \approx 1$ . The case of large samples is recovered, so that the transition begins when  $H^0 = H_{\text{int}} = H_c$  or  $B^0 = \tilde{B}$  reaches the critical magnetic field  $B_c$ ;
- » if  $d$  is of the same order as, or less than  $\lambda$ ,  $\tanh \frac{d}{2\lambda} < 1$ . The transition starts when

$$B^0 = \tilde{B} = \frac{B_c}{\tanh \frac{d}{2\lambda}} > B_c \quad \text{and} \quad H^0 = H_{\text{int}} = \frac{H_c}{\tanh \frac{d}{2\lambda}} > H_c; \quad (5.7)$$

- » in the extreme case when  $d \ll \lambda$

$$j_{\text{high}} \approx \frac{B^0}{\mu_0 \lambda} \frac{d}{2\lambda}. \quad (5.8)$$

The superconducting slab of thickness  $d$  can bear any field up to the critical value  $H_c(d)$  defined by

$$H_c(d) = \frac{2\lambda}{d} H_c \gg H_c. \quad (5.9)$$

$H_c$  without any precision is taken implicitly to mean  $H_c(d = \infty)$ .

### 5.3.2 - Thin wire

In a wire of radius  $R \ll \lambda$  subject to a magnetic field  $B^0$ , the current density  $j_{\text{high}}$  derived from the relation (2.38) can be written using the expansion of the modified BESSEL functions,

$$j_{\text{high}} \approx \frac{B^0}{\mu_0 \lambda} \frac{R}{2\lambda} \quad (5.10)$$

leading to

$$H_c(R) \approx \frac{2\lambda}{R} H_c. \quad (5.11)$$

These expressions indicate that in general a thin wire can endure a field  $H$  which is higher than the critical field  $H_c$  of the bulk material without undergoing a transition.

**Remark** - There is a slight qualification that we should make to such arguments, to include the effects of a finite coherence length. The expression found in GINZBURG-LANDAU theory for the critical field of a thin slab is

$$H_c(d) \approx 2\sqrt{6} \frac{\lambda}{d} H_c. \quad d \ll \lambda \quad (5.12)$$

But beware, while this closely resembles the expression (5.9), the mechanism invoked is quite different and is based on the very long coherence length of type I superconductors (a concept to be made precise in Chap. 6).

## 5.4 - Effects of sample shape

### 5.4.1 - Reminder of relevant results in magnetism

Up to now, we have avoided effects due to the shape of samples by restricting ourselves to plates or infinitely long cylinders with applied fields in the longest direction. In magnetism these geometries possess the advantage of having no demagnetizing fields and of producing a magnetic field  $\mathbf{B}^a$  due to AMPÈRE currents (or their equivalents, LONDON currents) that is uniform inside the material and vanishes outside.

If the sample is not infinite, things are no longer so simple because of the appearance of a demagnetizing field and the return of the lines of magnetic field  $\mathbf{B}^a$  outside the sample (see Fig. 2.10b). For the particular case of an ellipsoidal sample, however, when it is placed in a uniform field  $\mathbf{B}^0$  along one of its axes, the magnetic field  $\mathbf{B}$ , the field  $\mathbf{H}$  and the magnetization  $\mathbf{M}$  remain uniform inside the material, but not outside. For a given magnetizing field factor  $N$ , these three quantities are related by the relations given in Appendix 4, section A4.1 and summarized in Table 5.1.

**Table 5.1 -  $\mathbf{H}$  and  $\mathbf{B}$  fields inside an ellipsoid of demagnetizing field factor  $N$  and magnetization  $\mathbf{M}$ , inserted in a magnetic field  $\mathbf{B}^0$**

$\mathbf{H}$  and  $\mathbf{B}$  are uniform inside the ellipsoid, but not outside. Their values on the outside surface are found from the continuity conditions of  $\mathbf{H}$  and  $\mathbf{B}$ .

	Magnetic field $\mathbf{B}$	Field $\mathbf{H}$
In the bulk	$\mathbf{B}_{\text{int}} = \mathbf{B}^0 + (1 - N)\mu_0\mathbf{M}$	$\mathbf{H}_{\text{int}} = \mathbf{H}^0 - N\mathbf{M}$
On the surface, at the equator	$\tilde{\mathbf{B}} = \mathbf{B}^0 - N\mu_0\mathbf{M}$	$\tilde{\mathbf{H}} = \mathbf{H}^0 - N\mathbf{M}$

### 5.4.2 - Application to superconductors

#### LONDON currents squeezed on the surface

In the following discussion, all dimensions of the ellipsoid will be supposed to be large compared to the penetration length of the magnetic field. As a first step, the superconducting currents of the LONDON region may be considered as being squeezed onto the surface.

For the magnetic field  $\mathbf{B}$  to be zero inside the superconducting ellipsoid we must have, according to Table 5.1,

$$\mathbf{B}_{\text{int}} = \mathbf{B}^0 + \mu_0(1 - N)\mathbf{M} = \mathbf{0} \quad (5.13)$$

implying a magnetization

$$\mathbf{M} = -\frac{\mathbf{B}^0}{\mu_0(1 - N)}. \quad (5.14)$$

It then follows that the field  $\mathbf{H}$ , related to the magnetization by  $\mathbf{H} = -\mathbf{M}$  inside the ellipsoid (Figs 5.2 and 5.3) equals

$$\mathbf{H}_{\text{int}} = \frac{\mathbf{B}^0}{\mu_0(1-N)}. \quad (5.15)$$

By continuity of  $\mathbf{H}$  at the equator, where there are no magnetic charges, we find on the equatorial circle, where detailed calculation show that the magnetic field is the greatest,

$$\tilde{H} = H_{\text{int}} \quad \text{and} \quad \tilde{B} = \frac{B^0}{1-N} \quad (5.16)$$

with  $\tilde{B}$  greater than  $B^0$ , since  $N$  is always between 0 and 1.

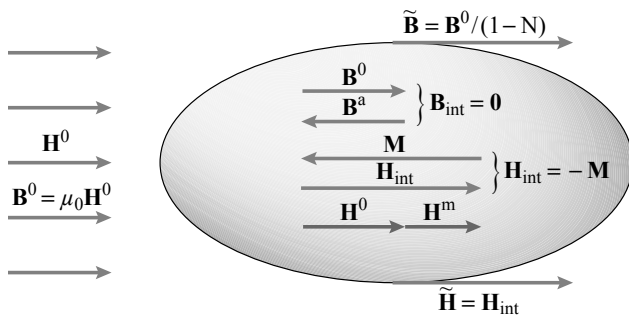


**Figure 5.2 - Magnetization  $\mathbf{M}$ , field  $\mathbf{H}$  and magnetic field  $\mathbf{B}$  in a superconducting ellipsoid inserted in a uniform magnetic field  $\mathbf{B}^0$**

The total  $\mathbf{B}$  is the sum of  $\mathbf{B}^0$  and the  $\mathbf{B}^a$  created by the LONDON currents. The total  $\mathbf{H}$  is the sum of  $\mathbf{H}^0$  and the  $\mathbf{H}^m$  created by the magnetic charges. In this schematic figure, the LONDON region is supposed to be very small and is not shown. See the note preceding Figure 4.3 concerning representations of the vectors  $\mathbf{H}$  and  $\mathbf{M}$ .

#### Decompressing the LONDON currents

“Decompressing” the LONDON currents does not change the equatorial field  $\tilde{B}$  tangential to the sample surface. It simply replaces the discontinuity of the magnetic field by an exponential decay as we move into the sample interior

$$B_{\text{int}}(u) \approx \tilde{B} e^{-\frac{u}{\lambda}}, \quad (5.17)$$

a dependence associated with the superconducting current density (see section 2.6),

$$j(u) = \frac{\tilde{B}}{\lambda \mu_0} e^{-\frac{u}{\lambda}} \quad (5.18)$$

with maximum value

$$j_{\text{high}} = \frac{\tilde{B}}{\mu_0 \lambda} = \frac{B^0}{\mu_0 \lambda (1-N)}. \quad (5.19)$$

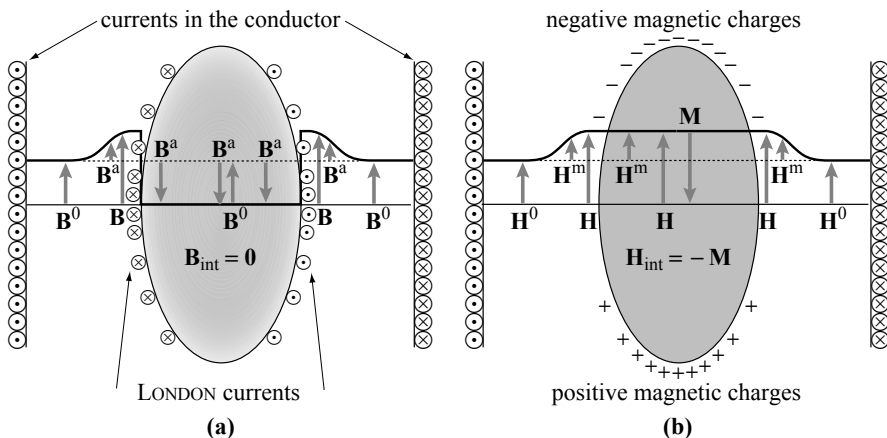


**Figure 5.3 - Magnetization  $\mathbf{M}$ , field  $\mathbf{H}$  and magnetic field  $\mathbf{B}$  inside and outside a superconducting ellipsoid inserted in an infinite solenoid**

(a)  $\mathbf{B}^0$  is the magnetic field created by the currents  $j^0$  flowing in the external solenoid.  $\mathbf{B}^a$  is the magnetic field created by the LONDON currents flowing around the ellipsoid and which are greatest at the level of the equator. (b)  $\mathbf{H}^0$  is the contribution of the currents  $j^0$  to the field  $\mathbf{H}$ .  $\mathbf{H}^m$  is the demagnetizing field created by the magnetic charges, whose density is highest near the poles.  $\mathbf{M}$  is the magnetization. The total field  $\mathbf{H}$  is the sum of  $\mathbf{H}^0$  and  $\mathbf{H}^m$ . The total magnetic field  $\mathbf{B}$  is the sum of the applied field  $\mathbf{B}^0$  and the field  $\mathbf{B}^a$ . It vanishes inside the ellipsoid (see Fig. 5.2).

## 5.5 - Intermediate state for a sphere

### 5.5.1 - First approach

Suppose we place a superconducting sphere in the magnetic field  $\mathbf{B}^0$  (Fig. 5.4a). As its demagnetizing field factor  $N$  is  $1/3$ , the surface magnetic field at the equator, where it is highest, takes the value (see the expression 5.16)

$$\tilde{B} = \frac{3}{2} B^0 \quad (5.20)$$

and the highest current density, which is situated at the surface of the equator, is given by

$$j_{high} = \frac{3}{2} \frac{B^0}{\lambda \mu_0}. \quad (5.21)$$

By virtue of the generalized SILSSEE criterion, the transition begins locally when  $j_{high} = j_c$ , i.e. when

$$B^0 = \frac{2}{3} \mu_0 H_c = \frac{2}{3} B_c. \quad (5.22)$$

It is therefore the part of the sphere near the equator that first makes a transition to the normal state, when the magnetic field  $B^0$  reaches  $\frac{2}{3} B_c$  (Fig. 5.4a).

Now a curious phenomenon appears, since with the transition at the equatorial zone, the superconducting region is no longer spherical in shape. It turns into an ellipse with a ratio  $(c/a)$  greater than 1 (Fig. 5.4b) and with a new demagnetizing field factor  $N' < N$  (see App. 4, Table 4.6a). By applying the relation (5.16), the tangential magnetic field at the new equator becomes

$$\tilde{B}' = \frac{B^0}{1 - N'} < \tilde{B} \quad (5.23)$$

which reduces the superconducting current density at the surface to

$$j'_{\text{high}} = \frac{1}{1 - N'} \frac{B^0}{\lambda \mu_0} < j_c \quad (5.24)$$

and makes the field  $B^0 = \frac{2}{3}B_c$  insufficient for the new equatorial zone to make the transition. We have therefore to increase  $B^0$  to  $(1 - N')B_c$  before the transition continues within the new equatorial surface (Fig. 5.4c) which makes the superconducting material even more elliptic... which will require an even higher value of the field  $B^0$  for the transition to continue.

Little by little, with the increase of  $B^0$ , the volume of material staying superconducting is reduced and it becomes more and more elongated. At the end of this process, all that is left is an almost cylindrical superconducting needle with a demagnetizing field factor  $N \approx 0$ . The transition is complete when  $B^0$  reaches  $B_c$  (Fig. 5.4d).

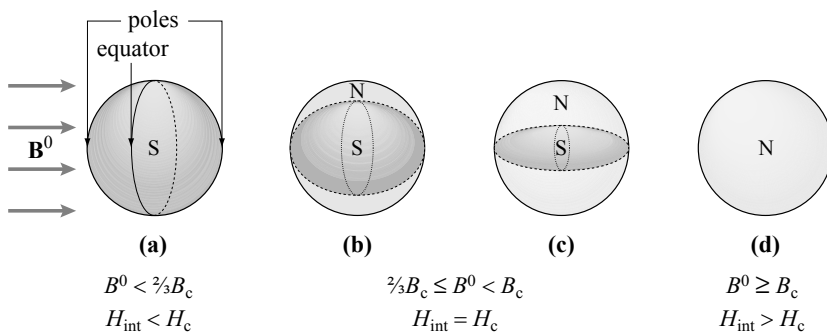


**Figure 5.4 - The transitional process of a sphere from superconducting to normal states under the influence of an applied magnetic field  $B^0$**

- (a) As long as  $B^0 < \frac{2}{3}B_c \Rightarrow H_{\text{int}} < H_c$ , the sphere stays completely superconducting.
- (b) When  $B^0$  reaches  $\frac{2}{3}B_c$ , the current density at the equator attains the critical current density  $j_c$ ; The S/N transition begins, making the superconducting material lose its spherical form.
- (c) Because of the reduced demagnetizing field factor  $N$ , the transition can only continue if  $B^0$  is increased further.
- (d) The transition is complete when  $B^0$  reaches  $B_c = \mu_0 H_c$ .

To summarize, from the time the transition begins at  $B^0 = \frac{2}{3}B_c$  until it finishes at  $B^0 = B_c$ , the magnetic field  $\tilde{B}$  at the circumference of the equator of the

superconducting part stays at the value  $B_c$  and the field  $H_{\text{int}}$  inside the superconducting volume<sup>4</sup> stays constant and uniform at  $H_c$ .

*The transition therefore occurs at constant  $H_c$  and is reminiscent of the solid-liquid phase transition with changing pressure. Like the pressure, the field  $H_{\text{int}}$  is an intensive parameter that stays constant in the regime of co-existence of the two phases.*

### 5.5.2 - More realistic structures

We have seen that when superconducting and normal phases are at equilibrium in a sufficiently large sample, the system can arrange itself so that at each point  $H_{\text{int}} = H_c$ .

Even so, in order to define the structure and topology of the mixture of phases, we need to consider, in addition to this condition of thermodynamic equilibrium, other relevant energies. These include in particular the interfacial energies between the normal and superconducting phases and the magnetic energy resulting from deformation of the field lines inside and outside the sample. As in a ferromagnet, where the domains arrange themselves so as to reduce these two energies, the sample will “split up” into superconducting and normal regions maintaining  $H_{\text{int}} = H_c$ . The morphology of the phases<sup>5</sup> is then determined by the following parameters:

- » *topological aspects*: the field penetrating into the sample must leave it somewhere ( $\nabla \cdot \mathbf{B} = 0$ ), which implies that there are channels of normal phase;
- » *surface energy*: as we are discussing a type I superconductor, the interface energy between a normal and a superconducting region is positive. This tends to reduce the number of interfaces (*i.e.* the domains are large) and make them as flat as possible;
- » *magnetic field energy*: as the average density of magnetic energy is  $\langle B^2 \rangle / 2\mu_0$ , the magnetic field must stay as homogeneous as possible since any spatial distortion of  $\mathbf{B}$  increases the average of  $B^2$ .

Thus for a given relative volume of normal and superconducting regions, it proves less costly in magnetic energy to distribute the normal fraction in parallel bands allowing a moderate magnetic field to pass (Fig. 5.5b), rather than keeping the superconducting part as a compact block that the magnetic field would have to turn around, making it stronger at the equator (Fig. 5.5a).

---

4 These conclusions are only valid if the dimensions of the sample are greater than the penetration depth  $\lambda$  of the magnetic field.

5 C.G. KUPPER (1968) *An Introduction to the Theory of Superconductivity*, Clarendon Press, Oxford, 83.

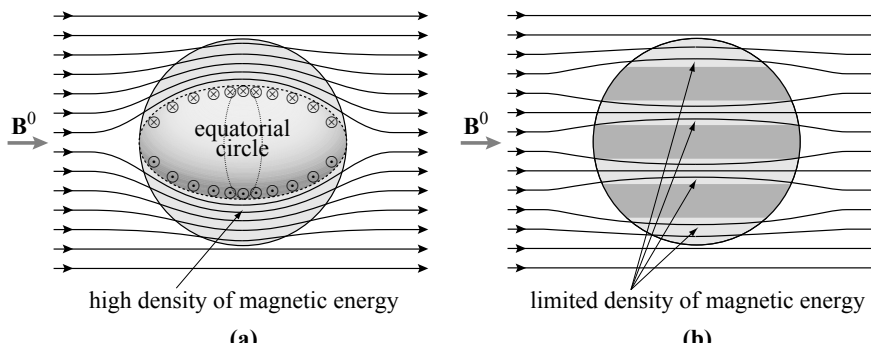


**Figure 5.5 - Sphere in the intermediate state**

To pass around a compact superconducting phase, the field lines must be strongly compressed, leading to high magnetic energy densities. The emergence of multiple normal canals reduces the distortions of the magnetic field and its regions of high intensity, which contributes to the lowering of the magnetic energy. The resulting increase in interface energy tends to limit splitting up the sphere into too many different regions.

For the same reason, seeking to gain magnetic energy, it is favorable to reduce the demagnetizing field and therefore the density of magnetic charges  $\sigma_{\text{surf}}^m = \mathbf{n} \cdot \mathbf{M}$ . To do this, the system takes form so as to minimize the surface of the superconducting phase that comes out near the poles by bifurcation of the phases and curving the final N/S interfaces. An example of a model structure that includes the different energy terms is shown in Figure 5.6.

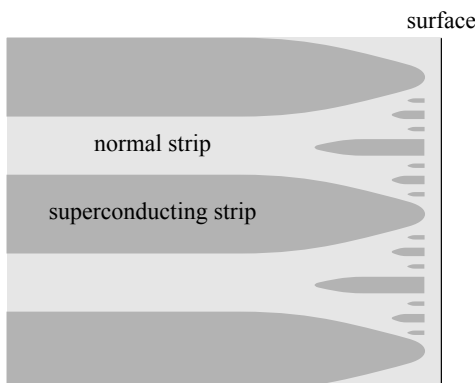


**Figure 5.6**  
**Reduction of the demagnetizing field**  
A model with alternately normal and superconducting layers constitutes a first approximation to the intermediate phase. A more detailed analysis of the various terms in the energy predicts branching near the surfaces.<sup>6</sup>

We can summarize in the following way the “magnetic” state of an ellipsoid of demagnetizing field factor  $N$ :

»  $B^0 < (1 - N) B_c$  : the sample is completely superconducting

6 L. LANDAU L.P. PITAEVSKII, E.M. LIFSHITZ (1969) *Electrodynamics of Continuous Media* 2<sup>nd</sup> Edition, Pergamon Press, Oxford.

$$H_{\text{int}} = \frac{B^0}{\mu_0(1-N)} ; M = -H_{\text{int}} ; \langle M \rangle = -\frac{B^0}{\mu_0(1-N)} ; \langle B \rangle = 0; \quad (5.25)$$

»  $(1-N)B_c < B^0 < B_c$ : the sample is in the intermediate state. Its bulk is a *coarse* mixture of normal phase of proportion  $\beta$ , and of superconducting phase of proportion  $1 - \beta$ . The field  $H$  is everywhere equal to  $H_c$ , in the superconducting as well as in the normal regions. The magnetic field  $B$  is zero in the superconductor and equals  $\mu_0 H_c$  in the normal channels. The average magnetization  $\langle M \rangle$  is related to the field  $H$  and the average  $\langle B \rangle$  of the magnetic field  $B$  over the whole sample by

$$\langle M \rangle = \frac{\langle B \rangle}{\mu_0} - H_{\text{int}} \quad (5.26a)$$

with  $H_{\text{int}} = H^0 - N\langle M \rangle$ .

$$\text{Thus } H_{\text{int}} = H_c ; 1 - \beta = \frac{H^0 - H_c}{NH_c} ; \langle B \rangle = \mu_0 \beta H_c ; \langle M \rangle = (\beta - 1)H_c ; \quad (5.26b)$$

»  $B^0 > B_c$ : the sample is normal everywhere

$$H_{\text{int}} = H^0 ; \langle B \rangle = B^0 ; M = 0. \quad (5.27)$$

The variations of the mean magnetic field  $\langle B \rangle$ , the field  $H$  and the mean magnetization  $\langle M \rangle$ , for a sphere of demagnetizing field factor  $N = \frac{1}{3}$ , are shown in the three graphs of Figure 5.7.

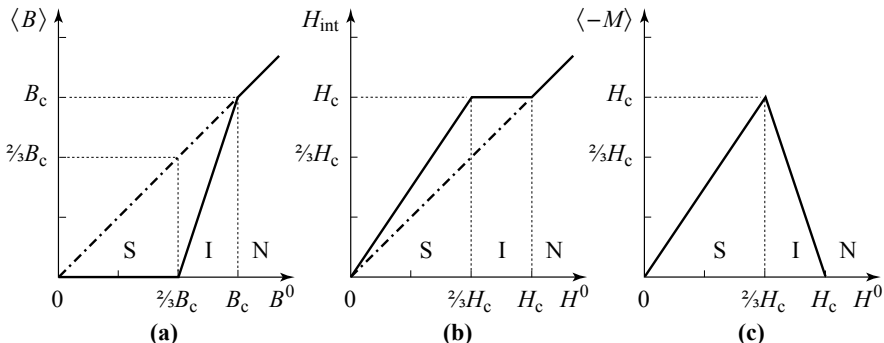


**Figure 5.7 - Magnetic properties of a superconducting sphere inserted in a uniform external field  $B^0$  ( $N = \frac{1}{3}$ )**

(a) Mean magnetic field over the whole sample  $\langle B \rangle$ . (b) Internal field to the sample  $H_{\text{int}}$ . (c) Mean magnetization  $\langle -M \rangle$  in the superconducting (S), intermediate (I) and normal (N) states

## 5.6 - Intermediate state of a thin plate

### 5.6.1 - Laminar model

We now turn to the case of a rectangular plate, with a large area and thickness  $d$ , placed in a uniform magnetic field  $\mathbf{B}^0$  perpendicular to its plane.

Intuitively we can imagine that as soon as  $B^0 \neq 0$ , normal regions will be formed in order to allow the magnetic flux to cross the sample without forcing the field lines to pass around the plate. Within the framework we have just discussed, it is an ellipsoid of demagnetizing field factor  $N$  close to 1 and with an “equatorial” magnetic field  $\tilde{B} = B^0/(1 - N)$  much greater than  $B^0$ . The plate transforms into the intermediate state for very small values of  $B^0$ .

According to the previous section, in the intermediate state, the sample must satisfy the thermodynamic condition  $H_{\text{int}} = H_c$  and have a structure that is as fine and regular as possible, in order to minimize the inhomogeneities of  $\mathbf{B}$ , but coarse enough to limit the S/N interfaces.

A simple model we can consider (Fig. 5.8) is the formation of stripes of normal phase (of width  $D_n$ ), inside which is a magnetic field  $B = \mu_0 H_c$ , and stripes of superconducting phase (of width  $D_s$ ), in which the magnetic field is zero. The stripes alternate in the  $x$  direction with period  $D = D_n + D_s$ .

The flux of the magnetic field  $B^0$  over a period  $D$  is concentrated in the normal stripe of width  $D_n$ , so flux conservation requires that

$$DB^0 = D_n \mu_0 H_c. \quad (5.28)$$

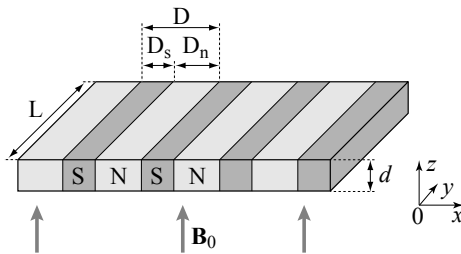


**Figure 5.8**  
**Stripe model of the intermediate state for a plate of thickness  $d$**   
The model alternates in the  $x$  direction normal stripes of width  $D_n$  and superconducting stripes of width  $D_s$ .

### 5.6.2 - Energy balance

It is generally agreed in magnetism that the field lines squeezed in strips of width  $D_n$ , separated by intervals of width  $D_s$  need a distance of the order of  $D_p$  to redistribute homogeneously with, (Fig. 5.9a)

$$\frac{1}{D_p} = \frac{1}{D_n} + \frac{1}{D_s}. \quad (5.29)$$

To simplify the discussion, we assume that the perturbed region reduces to a layer of thickness  $D_p$  on each side of the plate, within which the field  $B$  alternates between the values 0 over the width  $D_s$  and the value  $\mu_0 H_c$  over the width  $D_n$  (Fig. 5.9b).

We shall now evaluate the surface and magnetic energies that enter into the model.

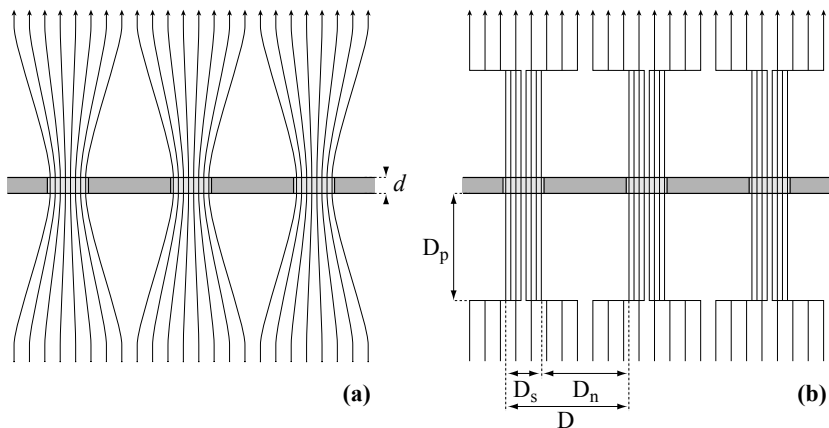


**Figure 5.9 - Model magnetic profile of a thin plate in its intermediate state**

(a) The flux of the applied magnetic field  $B^0$  "crosses" the plate via the normal stripes in which, as a consequence, the field lines must be squeezed and the magnetic field is enhanced. (b) Rectangular model for the constriction of the field lines.

#### *Energy of interface formation*

For each period  $D$  in the  $x$  direction, there are two interfaces N/S of length  $L$  (Fig. 5.8) in the  $y$  direction. Since each unit length in the  $x$  direction can accommodate  $1/D$  of a period, the interface energy per unit length in this direction is

$$\varepsilon_{\text{interface}} = \frac{2Ld\gamma}{D} \quad (\text{per unit length in the } x \text{ direction}) \quad (5.30)$$

where  $\gamma$  is the interfacial energy per unit of surface. As we will see in Chapter 6, this energy is positive for type I superconductors.

#### *Energy due to perturbation of the magnetic field outside the plate*

In the absence of constriction, the magnetic field in the stripes of the neighboring layer of thickness  $D_p$  is uniform. Its energy, per unit of length in the  $x$  direction is

$$\varepsilon_{\text{mag 1}} = \frac{(B^0)^2}{2\mu_0} \frac{D(2D_p)}{D} L. \quad (5.31)$$

With constriction, the magnetic field is concentrated in the stripes of width  $D_n$  where it is  $B_c$ ; the energy per unit of length (in the  $x$  direction) becomes

$$\varepsilon_{\text{mag 2}} = \frac{(B_c)^2}{2\mu_0} \frac{D_n(2D_p)}{D} L \quad (5.32)$$

giving an energy difference of

$$\varepsilon_{\text{mag}} = \varepsilon_{\text{mag 2}} - \varepsilon_{\text{mag 1}} = 2L \frac{(B_c)^2}{2\mu_0} \frac{D_n D_p}{D} \left[ 1 - \frac{D}{D_n} \left( \frac{B^0}{B_c} \right)^2 \right]. \quad (5.33)$$

### **Energy due to perturbation of the magnetic field in the plate**

In the plate, the field  $H$  is constant and equals  $H_c$  ( $H_{\text{int}} = H_c$ ). Flux conservation requires a fraction  $\beta$  of normal phase, so that

$$B^0 = \beta \mu_0 H_c \quad (5.34)$$

independent of the model.

The magnetic energy stored in the plate  $\frac{1}{2} \beta \mu_0 H_c^2$  is therefore constant, independent of the model and, *a fortiori*, of the periodicity. This energy does not then enter into the calculation of D.

#### **5.6.3 - Structure of the intermediate state of the plate**

The difference (up to a multiplicative constant)  $\varepsilon_{\text{total}}$  between the reference state without constriction and the state with constriction (the intermediate state) is then

$$\varepsilon_{\text{total}} = \varepsilon_{\text{interface}} + \varepsilon_{\text{mag}}. \quad (5.35)$$

Making use of (5.34) and the fact that

$$D_n = \beta D \quad (5.36)$$

that leads to

$$D_n D_p = \beta^2 (1 - \beta) D^2 \quad (5.37)$$

giving

$$\varepsilon_{\text{total}} = 2L \left[ \frac{d\gamma}{D} + D \beta^2 (1 - \beta)^2 \frac{\mu_0 H_c^2}{2} \right]. \quad (5.38)$$

Minimizing  $\varepsilon_{\text{total}}$  by putting its derivative with respect to D is zero, gives

$$D = \frac{1}{\beta(1 - \beta)} \sqrt{\frac{d\gamma}{(\mu_0 H_c^2)/2}}. \quad (5.39)$$

The interface energy between normal and superconducting phases in a material of type I is (see Chap. 6)

$$\gamma \approx \frac{B_c^2}{2\mu_0} \xi \quad (5.40)$$

where  $\xi$  is the coherence length, which can be identified with the width of the “wall” between the two phases. As a result, the periodicity can be written

$$D = \frac{1}{\beta(1 - \beta)} \sqrt{d\xi}. \quad (5.41)$$

For a lead plate ( $\xi \approx 550$  nm) of 2 mm thickness, inserted into an external field  $B^0 = B_c/2$  ( $\beta = \frac{1}{2}$ ) the period D is found to be of order 0.1 mm and values  $D_n \approx D_s$  of order 0.05 mm.

Naturally this whole discussion makes sense only if the width of the N/S interface, (the coherence length  $\xi$ ), is much smaller than the plate thickness.

While simplified, this treatment of the lamellar model brings out the essential elements that characterize the intermediate state of a plate in a perpendicular field: the alternating normal and superconducting lamellae, the regularity of the structure and the millimetric scale of the period. The real structures obtained are often more complex but we can recognize the features mentioned above, at least providing one of the phases is not extremely dominated by the other (Fig. 5.10).

Some unsolved questions remain, however, concerning the self-organization of these domains that results from the competition between interactions of short range (associated with a surface tension) and of long range (magnetic, electrostatic or elastic). Problems such as the initial growth of bubble, the transition bubble-lamellae, the role of defects, the nucleation and annihilation of superconducting domains... continue to be studied both for the statics and for the dynamics of domain formation.

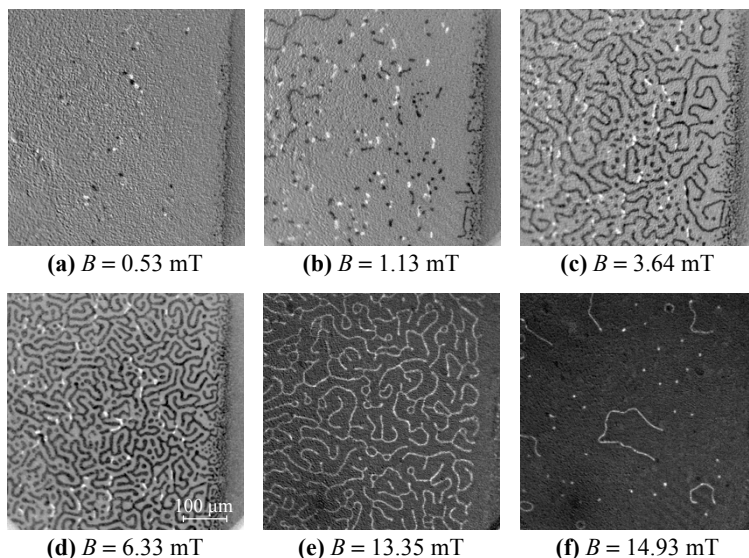


**Figure 5.10 - Intermediate states of a slab of indium under increasing field at  $T = 1.9\text{ K}$**

The superconducting zones (lightly colored) and normal (darkly colored) are tangled in the form of "curved" lamellae whose width is regular on a scale of micrometers. We see clearly the normal regions invade the sample with increasing external magnetic field. The white traces have been left by regions carrying flux that were trapped at zero field, and that move when the external field increases. Images kindly provided by C. GOURDON (Institute for Nanophysics, Pierre and Marie CURIE University, Paris) and V. JEUDY (Laboratory of the Physics of Solids, Paris-Sud University, Orsay).

## 5.7 - Avoiding confusion

We must insist on the fact that the stripes, which may become tubes, of the normal phase that enter the superconducting phase have nothing to do with the vortices that

will be introduced in Chapter 6. Here we are dealing with a state, said to be “intermediate” and which is characterized by a *phase separation on the scale of millimeters*. It is caused by the geometric form of the samples and the demagnetizing field that they carry. This precipitation occurs despite the *positive* N/S interface energy of type I superconductors. By contrast, the appearance of vortices that are, roughly speaking, “normal threads” crossing the superconductor, is due to the *negative* sign of the interface energy characteristic of type II superconductors. They appear independently of any demagnetizing field and their scales are very much smaller than the structures seen in the intermediate state we have here.

We must therefore distinguish clearly the intermediate state of type I superconductors, which is a phase separation, from the thermodynamic SHUBNIKOV mixed phase of type II superconductors where the vortices infiltrate the sample.<sup>7</sup>

## 5.8 - Wire carrying a current (model of the intermediate state)

### 5.8.1 - Formulation of the problem

We will now reconsider the wire of radius  $R$  in which the experimentalist drives a current of intensity  $I$ . As we saw in section 2.6.2, the current density is not distributed uniformly in a cross-section of the superconducting wire, but is concentrated near the surface on the scale of a penetration depth  $\lambda$ . To be more precise, the current density  $j_z$  decreases following the relation (2.45a),

$$j_z(u) \approx j_{\text{high}} e^{-\frac{u}{\lambda}} \quad (5.42)$$

where  $u$  is the distance separating a point in the material from the closest surface. The highest value of the current density, situated immediately below the surface is

$$j_{\text{high}} = \frac{I}{2\pi R \lambda}. \quad (5.43)$$

By applying the generalized SILSBEY criterion, the wire remains completely superconducting as long as the current density is everywhere less than the critical current  $j_c$ .

Like the infinite cylinder subject to a magnetic field, a skin of normal metal appears when the current density at the surface  $j_{\text{high}}$  reaches  $j_c$ , and the radius of the superconducting part is reduced. The current density is still given by (5.42), but with a new radius  $R' < R$ , which leads to a value  $j'_{\text{high}} > j_{\text{high}}$  and therefore a rapid “melting” of the superconducting phase into a normal sheath that rapidly invades the whole sample.

---

<sup>7</sup> In many texts, at least those written in English, the SHUBNIKOV phase is called the “mixed state.”

If we follow this logic, the wire should pass abruptly and totally into the normal state when the current intensity  $I$  reaches a critical intensity  $I_c$  such that

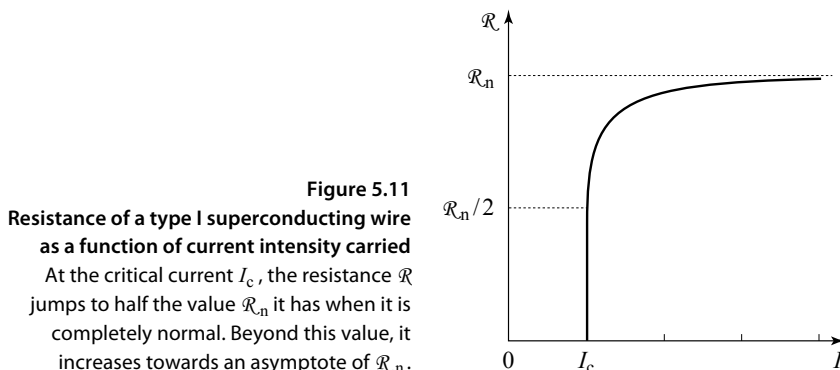
$$j_{\text{high}} = j_c = \frac{I_c}{2\pi R \lambda} \quad \text{or} \quad I_c = 2\pi R H_c \quad (5.44a)$$

with a jump in the electrical resistance which should pass from zero to

$$\mathcal{R}_n = \rho_n \frac{L}{\pi R^2} \quad (5.44b)$$

where  $\rho_n$  and  $\mathcal{R}_n$  are, respectively, the resistivity of the material and the resistance of the wire of radius  $R$  and length  $L$  in the normal state.

In fact, if we have written “should” in the previous paragraph, it was because the experimental results are rather different. The wire’s resistivity  $\rho$  is indeed zero when the intensity is less than the critical value  $I_c$ , and there *is* a discontinuity in the resistance  $\mathcal{R}$  when  $I_c = 2\pi R \lambda j_c$ , but the discontinuity has an amplitude of only  $\mathcal{R}_n/2$ . As Figure 5.11 shows, the resistance  $\mathcal{R}_n$  of the normal state is reached only asymptotically for current intensities much greater than  $I_c$ .



To understand this result, we must remember that, in the normal state, the current density is distributed uniformly in the wire. Therefore when  $I$  reaches  $I_c$  and the wire becomes normal, the current density is redistributed uniformly with a density  $j = I_c / \pi R^2$ , much less than the critical current density... and so this allows the wire to return to the superconducting state. But in the superconducting state, the current density localizes again into the LONDON region, and once again its value  $j_{\text{high}}$  exceeds  $j_c$ . This sequence of “melting” of the superconducting state starting from the exterior surface begins again: the wire goes normal, the current density becomes uniform again, which brings the wire back to its superconducting state...

*Thus when the current driven reaches the critical value  $I_c$ , neither the normal state nor the superconducting state is stable. Some intermediate state must appear that can stabilize the system.*

### 5.8.2 - Model for the intermediate state

Many models have been proposed to explain the experimental results. The simplest, represented in Figure 5.12, separates the wire into two different concentric regions:

- » the first (variables with index 1) is a completely normal sheath with cylindrical core of radius core  $a$  and an external surface of radius  $R$ ;
- » the second (variables with index 2) occupies the cylindrical core of radius  $a$ . In this region, within which  $H = H_c$ , the material passes into an intermediate state composed of a “coarse” mixture of normal and superconducting phases.

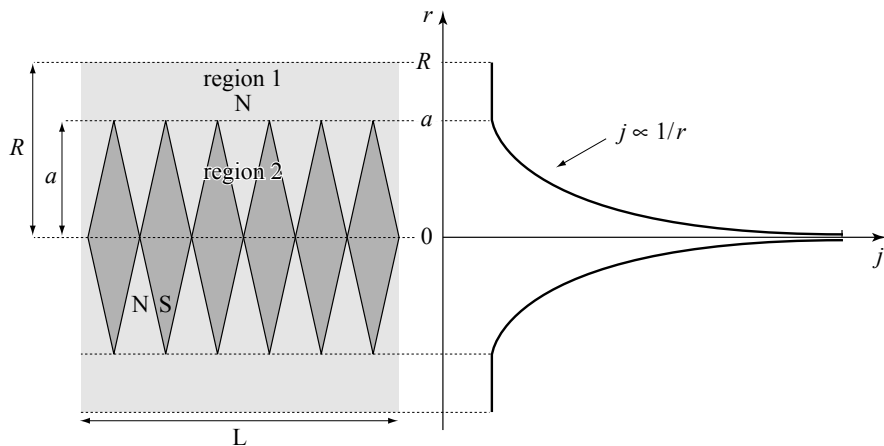


**Figure 5.12 - Model of the intermediate state in a current-carrying wire**

- (a) The wire divides into a normal sheath and a core of radius  $a$  in an intermediate state, within which the field takes the value  $H = H_c$ . (b) The current density is uniform in the normal sheath and varies as  $1/r$  in the central region, with continuity at the interface between the two regions.

The total intensity of the current  $I$  can then be divided into the two components  $I_1$  and  $I_2$  transported by each of the two regions.

- » In the completely normal exterior sheath of conductivity  $\sigma_n = 1/\rho_n$ , the current density  $j_1$  is related to the electric field resulting from the applied voltage between the extremities of the wire as

$$j_1 = \sigma_n E \quad (5.45)$$

and the current intensity carried is

$$I_1 = j_1 \pi(R^2 - a^2). \quad (5.46)$$

- » Within the internal cylinder, which is in an intermediate state, the field  $H$  is everywhere equal to  $H_c$ . The current density  $\mathbf{j}$ , because it is injected by the experimentalist, is a conductor current and therefore related to the field  $H$  by  $\nabla \times \mathbf{H} = \mathbf{j}$ .

It is not an induced current as are the AMPÈRE currents. In this geometry this gives

$$j_2(r) = \frac{H_\theta}{r} = \frac{H_c}{r}, \quad (5.47)$$

and

$$I_2 = \iint_S j_2(r) 2\pi r dr = \int_o^a \frac{H_c}{r} 2\pi r dr = 2\pi a H_c. \quad (5.48)$$

Adding in the continuity condition of the current density  $j_1(a) = j_2(a)$ , which requires<sup>8</sup>

$$\sigma_n E = H_c / a, \quad (5.49)$$

expressions (5.46) and (5.48) lead to

$$I = I_1 + I_2 = \pi H_c \left( \frac{R^2 - a^2}{a} + 2a \right) = \pi R H_c \left( \frac{R}{a} + \frac{a}{R} \right), \quad (5.50)$$

that relates the intensity of the current  $I$  to the radius  $a$  of the central core. Consistent with relation (5.44), the transition to the normal state begins when  $I = 2\pi R H_c = I_c$ , corresponding to  $a = R$ , and is only complete when  $a$  goes to zero, *i.e.* for infinite current.

Using expressions (5.44) and (5.49), the total intensity (5.50) can be expressed as a function of the electric field  $E$  and of the critical current,

$$I = \frac{I_c}{2} \left[ \frac{\alpha E}{I_c} + \frac{I_c}{\alpha E} \right] = \frac{1}{2} \left[ \frac{(\alpha E)^2 + I_c^2}{\alpha E} \right] \text{ where } \alpha = 2\pi R^2 \sigma_n. \quad (5.51)$$

When the experimentalist injects a current of intensity  $I$  by means of an applied voltage, the electric field  $E$  in the normal sheath and, by continuity, in the central core obeys the quadratic equation

$$\alpha^2 E^2 - 2I\alpha E + I_c^2 = 0 \quad (5.52)$$

whose positive solution is  $E = \frac{I}{\alpha} \left[ 1 + \sqrt{1 - \left( \frac{I_c}{I} \right)^2} \right]$ . (5.53)

This leads to a wire resistance  $\mathcal{R} = EL/I$ , which can be expressed in terms of its normal state resistance  $\mathcal{R}_n = \rho_n L / \pi R^2$  as

$$\begin{aligned} I < I_c \quad & \mathcal{R}(I) = 0 \\ I > I_c \quad & \mathcal{R}(I) = \frac{\mathcal{R}_n}{2} \left[ 1 + \sqrt{1 - \left( \frac{I_c}{I} \right)^2} \right] \end{aligned} \quad (5.54)$$

<sup>8</sup> A discontinuity in the current density would give rise to a DIRAC delta function singularity in the magnetic field at the interface.

producing a discontinuity in resistance of  $\mathcal{R}_n/2$  when the intensity  $I$  passes  $I_c$  and an asymptotic value of  $\mathcal{R}_n$  beyond. Experimentally, the jump in resistance is to a value between 0.7 and 0.8  $\mathcal{R}_n$ .

**Remark** - The “diamond” shape in superconducting grains in the central cylinder is rather arbitrary. More complex shapes have been considered. For example, there is a dynamic model where the interfaces between normal and superconducting phases are mobile, which would increase the resistance jump at the critical value  $I_c$  of the injected current.<sup>9</sup>

### 5.8.3 - A thin wire

In a wire whose diameter is equal to or less than the penetration depth of the field, the current density – which decreases below the surface – does not have enough space to go to zero at the center. In the limit  $R \ll \lambda$ , it even tends to become uniform, the critical intensity then being

$$I_c = \pi R^2 j_c. \quad R \ll \lambda \quad (5.55)$$

Since when  $R \gg \lambda$ , the critical intensity is reached for  $I_c = 2\pi R \lambda j_c$ , we see that we can, without provoking a transition towards the normal state, pass a higher net intensity of current in  $N$  wires of diameter  $d$  in parallel than in a single wire of total equivalent cross-section, *i.e.* one of diameter  $D = \sqrt{N}d$ .

**Remark** - Once again this result is only valid for type I superconductors. It is true that superconducting wires designed to transport electric currents are made up of micrometer-diameter filaments, but they are type II superconductors (see Chap. 6) and the reason for their multi-filament structure is very different from what we discuss here.

## 5.9 - Critical current of a wire in a magnetic field

### 5.9.1 - General case

When a superconducting wire carrying a current  $I^{\text{trans}}$  injected by a generator is, in addition, subject to a magnetic field  $\mathbf{B}^0$ , the total current density  $\mathbf{j}^{\text{tot}}$  in the wire is the vector sum of the density  $\mathbf{j}^{\text{trans}}$  of the current transported and the screening current density  $\mathbf{j}^{\text{screen}}$  from the LONDON currents associated with  $\mathbf{B}^0$ ,

$$\mathbf{j}^{\text{tot}} = \mathbf{j}^{\text{trans}} + \mathbf{j}^{\text{screen}}. \quad (5.56)$$

According to the principle of superposition, each current density is distributed as it was without the other:  $\mathbf{j}^{\text{trans}}$  as it was without  $\mathbf{B}^0$  and  $\mathbf{j}^{\text{screen}}$  without the transported current. According to the generalized SILSBEE criterion, the transition begins when

---

<sup>9</sup> A.F ANDREEV (1968) *Proc. 11<sup>th</sup> Intl. Conf. On Low Temp. Phys.*, Univ. of St. Andrews, 831.

the modulus of the total current density somewhere reaches the critical current density of the material.

### 5.9.2 - Magnetic field applied parallel to the axis of the wire

The LONDON currents are normal to the radial vectors (Fig. 5.13a), and are thus perpendicular to the current carried. The total current density is then

$$j^{\text{tot}} = \sqrt{(j^{\text{trans}})^2 + (j^{\text{screen}})^2}. \quad (5.57)$$

Since each of the densities taking its highest value at the surface,

$$j_{\text{high}}^{\text{trans}} = \frac{I_c(B^0)}{2\pi R\lambda} \quad \text{and} \quad j_{\text{high}}^{\text{screen}} = \frac{B^0}{\mu_0\lambda} \quad (5.58)$$

the critical intensity  $I_c(B^0)$  now depends on  $B^0$ . Since the transition towards the normal state begins when  $j^{\text{tot}}$  reaches  $j_c$ , we have

$$j_c^2 = \left( \frac{I_c(B^0)}{2\pi R\lambda} \right)^2 + \left( \frac{B^0}{\mu_0\lambda} \right)^2 \quad (5.59)$$

which means that, in an axial field  $\mathbf{B}^0$ , the maximum current intensity that can pass in a type I superconducting wire of radius  $R$  is

$$I_c(B^0) = \sqrt{I_c^2(B^0=0) - \left( \frac{2\pi R}{\mu_0} \right)^2 (B^0)^2}. \quad (5.60)$$

The dependence of this critical intensity as a function of  $B^0$  is shown in Figure 5.13b. This intensity vanishes for  $B^0 = B_c$ , beyond which field the wire no longer transports current without energy dissipation.

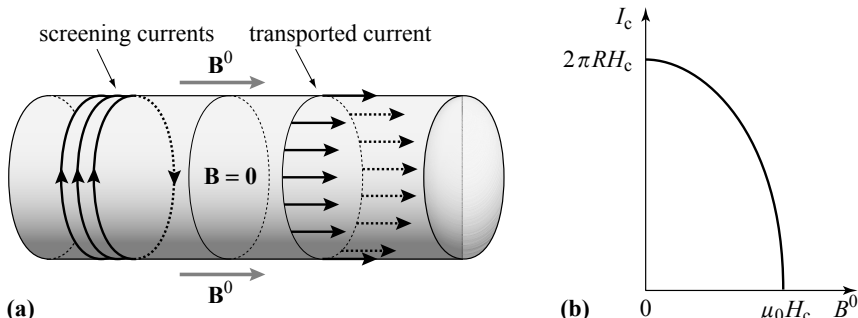


**Figure 5.13 - Critical current of a wire in a magnetic field parallel to its axis**

**(a)** Distribution of the transported currents  $j^{\text{trans}}$  and the screening currents  $j^{\text{screen}}$  in a superconducting wire carrying a current  $I^{\text{trans}}$  and subject to an applied field  $\mathbf{B}^0$  parallel to the wire. The two distributions of current are orthogonal. **(b)** Variation of the critical current intensity as a function of  $B^0$ .

### 5.9.3 - Magnetic field applied perpendicular to the axis of the wire

As the wire can be considered as a very elongated ellipsoid, any direction perpendicular to the cylinder axis constitutes a principal axis with associated demagnetizing factor  $N = \frac{1}{2}$ . The screening currents flow around the direction of the wire's axis with density

$$j^{\text{screen}} = j_{\text{high}}^{\text{screen}} \sin \theta \quad \text{with } j_{\text{high}}^{\text{screen}} = \frac{B^0}{\lambda \mu_0 (1-N)} = \frac{2 B^0}{\lambda \mu_0} \quad (5.61)$$

where  $\theta$  is the angle between  $\mathbf{B}^0$  and the radial vector passing through the point considered (Fig. 5.14). The screening current therefore flows in *opposite directions* on the different sides of the wire and the highest screening current densities occur at two positions on the surface directly opposite each other.

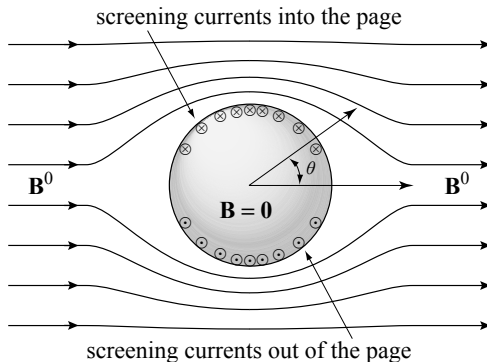


**Figure 5.14**

Screening currents in a wire placed in a magnetic field perpendicular to its axis (cross-section perpendicular to the axis of a cylindrical wire)

The screening currents flow in the direction of the wire's axis, which is a special case of an ellipsoid of demagnetizing factor  $N = \frac{1}{2}$ . The surface current density varies as  $\sin \theta$ .

The density of transported current is distributed, as always, within the penetration depth, in a *single direction* and it is highest at the surface of the sample where it equals

$$j_{\text{high}}^{\text{trans}} = \frac{I_{\text{trans}}}{2\pi R \lambda}. \quad (5.62)$$

As a consequence, the highest total current density is on the surface of the wire, at the position where the densities of transported and screening currents are simultaneously greatest, and where they flow in the same sense.

In this geometry, the relation between the critical current density and the external field is then

$$\frac{2B^0}{\lambda \mu_0} + \frac{I_{\text{c}}(B^0)}{2\pi R \lambda} = j_{\text{c}}. \quad (5.63)$$

Thus in a transverse field  $B^0$  the maximum current intensity that a type I superconducting wire of radius  $R$  can transport without loss is

$$I_c(B^0) = I_c(B^0 = 0) - \frac{4\pi RB^0}{\mu_0}. \quad (5.64)$$

This critical intensity decreases linearly as the field increases until it vanishes when  $B^0$  reaches  $B_c/2$  (Fig. 5.15b).

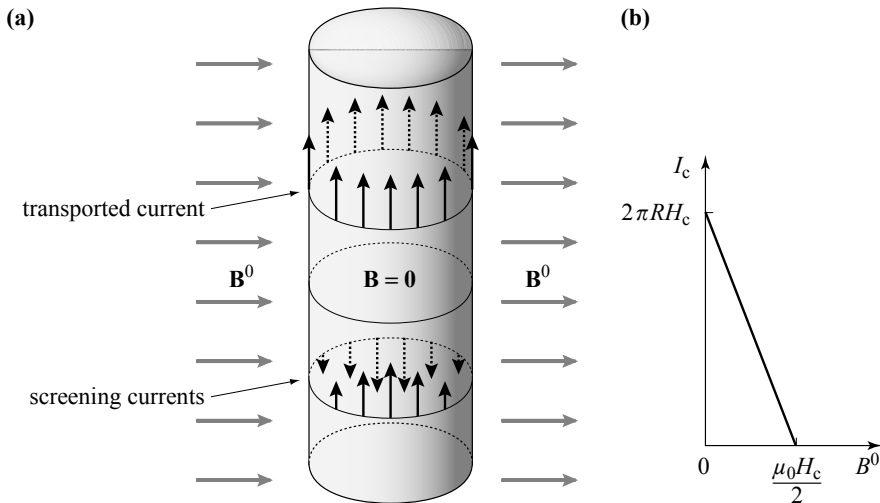


**Figure 5.15 - Distribution of transported current and screening current in a superconducting wire carrying a current  $I$  and subject to a field  $B^0$  that is perpendicular to the wire's axis**

(a) The screening currents  $j^{\text{screen}}$  flow within the penetration depth from the surface and in the opposite senses on the two sides of the plane of symmetry: those that are to the front flow up, and those that are to the rear flow down. The transported  $j^{\text{trans}}$  is localized within the penetration depth from the surface and always flows from down to up. The current densities to the front add, while those to the rear partially cancel. (b) Variation of the critical current intensity as a function of  $B^0$ .

# Chapter 6

## TYPE II SUPERCONDUCTORS

The distinction between type I and type II superconductors is a key element in superconductivity. It results from the relative values of two characteristic lengths:

- » the penetration depth  $\lambda$ , the distance over which the magnetic field decreases from the surface towards zero or, more generally, the distance over which the magnetic field can vary;
- » the coherence length  $\xi$ , the distance necessary for restoring “complete” superconductivity starting from an interface with a region that is in the normal state.

The ratio  $\kappa = \lambda/\xi$ , called the “GINZBURG-LANDAU parameter,” determines the nature of a given superconducting material. Whether the value of  $\kappa$  is below or above a critical value  $\kappa_c$  close to 1, the superconductor is of type I or II. In this chapter, a simple thermodynamic approach is preferred to the phenomenological GINZBURG-LANDAU model. That model introduces in a natural and very powerful way these two length scales, but is still difficult because it is formulated from a non-trivial starting point and has equations that are non-linear. In this chapter, we introduce the different key elements step by step, including the vortices that fulfil a vital role in type II superconductivity.

### 6.1 - Two types of magnetic behavior

#### 6.1.1 - The emergence of type II superconductors

The existence of two types of superconductors came to light slowly. The first signs of type II superconductivity date from the 1930's when anomalies were detected in the magnetic behavior of superconducting alloys. The group at Oxford lead by MENDELSSOHN demonstrated an incomplete MEISSNER effect characterized by an average magnetization  $\langle -M \rangle$  less than 1. Meanwhile DE HAAS and VOOGD in Leiden measured critical fields that were abnormally high, for example 2 teslas in the alloy Sn-Bi instead of the few tenths of a tesla found in pure metals. At first these effects were attributed to impurities that might be perturbing the standard superconducting behavior. For recognition of a second type of superconductivity we must await ABRIKOSOV in 1957. Starting from the GINZBURG-LANDAU equations that had been published in 1950, he showed that two different forms of superconducting

behavior were possible. In 1959 it was GORKOV who proved the equivalence between the GINZBURG-LANDAU equations and the microscopic BCS theory.

### 6.1.2 - Magnetic behavior of type II superconductors

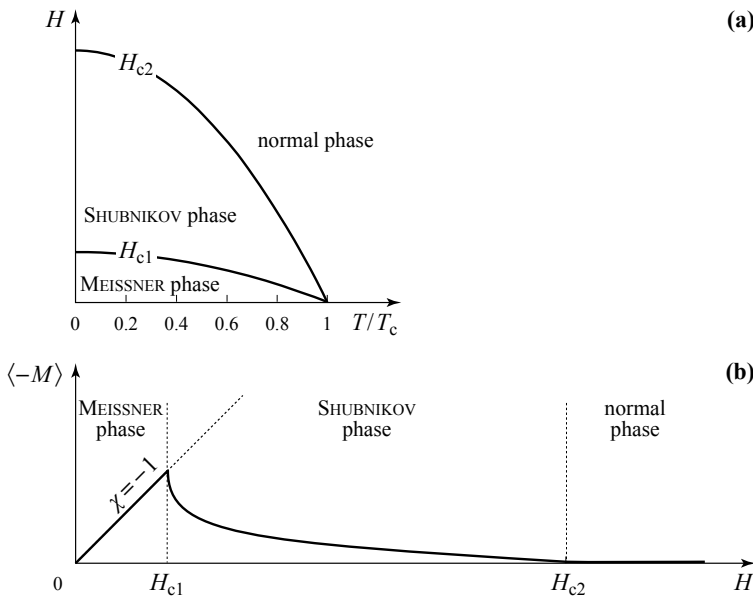


**Figure 6.1 - Type II superconductors**

(a) Phase diagram of a type II superconductor

(b) Dependence of the average magnetization on field  $H$  in a type II superconductor

### Type I superconductors

We have already described in Chapter 4 the magnetic behavior of type I superconductors (see Fig. 4.1): in the phase diagram represented in the  $(H,T)$  plane, the normal and superconducting states are separated by a single line  $H_c(T)$ . In the superconducting phase the material behaves as a perfect diamagnet within which  $\mathbf{M} = -\mathbf{H}$  ( $\chi = -1$ ).

### Type II superconductors

In contrast to type I superconductors, the phase diagram of type II superconductors is characterized by two transition lines  $H_{c1}(T)$  and  $H_{c2}(T)$  terminating at the same transition temperature  $T_c$  in zero field. These lines divide the superconducting state into two regions, corresponding to two distinct phases called the “MEISSNER phase” and the “SHUBNIKOV phase” (called also “mixed state”).

In the MEISSNER phase ( $H < H_{c1}$ ) the magnetization  $\mathbf{M}$  equals  $-\mathbf{H}$ , as in a type I superconductor. The material behaves as a perfect diamagnet: the susceptibility

$\chi = -1$  and there is total exclusion of the magnetic field from the bulk ( $\mathbf{B} = \mathbf{0}$ ) except within a penetration depth of the surface.

In the SHUBNIKOV phase ( $H_{c1} < H < H_{c2}$ ), the superconductor remains diamagnetic ( $\chi < 0$ ) but is no longer perfectly so  $|\chi| < 1$ . The average magnetization of the sample  $\langle -M \rangle$  decreases with  $H$ , the MEISSNER effect is incomplete and the magnetic field averaged over the whole sample differs from zero ( $\langle B \rangle \neq 0$ ).

*Surface superconductivity:* It turns out that if the bulk of the material returns to the normal state at the field  $H_{c2}$ , the same is not true of its surface, which continues to exhibit signs of superconductivity up to a field value  $H_{c3} > H_{c2}$ . This aspect will not be discussed in this book.

### 6.1.3 - Classification of superconducting materials

All known type I superconductors<sup>1</sup> are pure metals, and pure metals that superconduct are almost all of type I, with the few exceptions including niobium and tantalum, that are of type II. Their critical fields at 0 K,  $B_c = \mu_0 H_c$ , are all less than a tenth of a tesla (see Table 4.4).

The other superconducting materials (alloys, organic compounds, cuprates, heavy fermions, iron-based superconductors...) are of type II. While the values of lower critical fields  $B_{c1} = \mu_0 H_{c1}$  are on the whole lower than the critical fields  $H_c$  of type I superconductor (Table 6.1), the upper critical field  $B_{c2} = \mu_0 H_{c2}$  can be very high: 13 T for NbTi, 23T for Nb<sub>3</sub>Sn.

**Table 6.1 - Critical fields of type II superconductors representative of the principal families of materials<sup>2</sup>**

We note the low values of  $H_{c1}$  and the high values of  $H_{c2}$ .  $T_c$  is the critical temperature under 0 field.

Materials	$T_c$ [K]	$\mu_0 H_{c1}(0)$ [T]	$\mu_0 H_{c2}(0)$ [T]
Nb (wire)	9.3	0.18	2
NbTi	9.5		13
Nb <sub>3</sub> Sn	18.2	0.44	23
NbN	16	0.0093	15
LaMo <sub>6</sub> S <sub>8</sub>	11		44.5
UBe <sub>13</sub>	0.9		6
K <sub>3</sub> C <sub>60</sub>	19	0.013	32
Rb <sub>3</sub> C <sub>60</sub>	29.6	0.012	57

1 From measurements on ScGa<sub>3</sub> and LuGa<sub>3</sub>, SVANIDZE and MOROSAN claim nonetheless that a very rare class of compounds can show type I behavior (E. SVANIDZE & E. MOROSAN (2012) *Phys. Rev. B* **85**, 174514).

2 Numerical values collected by C. POOLE, H. FARACH & R. CRESWICK in *Superconductivity* (1995) Academic Press, New York, Chap. 9.

A certain number of very anisotropic materials, including the organic compounds, the cuprates and iron-based superconductors, show different critical fields depending on the direction of the applied field. Among the selection of values given in Table 6.2, we can see the particularly high values of the field  $H_{c2}$  in the cuprates and iron-based superconductors.

**Table 6.2 - Critical fields of some anisotropic materials<sup>2</sup>**

These materials show a 2D character and are almost isotropic in the (*ab*) plane. The figures given here are typical values of individual samples. There is a very large spread of values, notably because of the doping.

Materials	$T_c$ [K]	$\mu_0 H_{c1}^{ab}(0)$ [T]	$\mu_0 H_{c2}^{ab}(0)$ [T]	$\mu_0 H_{c1}^c(0)$ [T]	$\mu_0 H_{c2}^c(0)$ [T]
$\beta$ -(ET) <sub>2</sub> I <sub>3</sub>	1.5	0.007	1.74	0.036	0.02
MgB <sub>2</sub> <sup>3</sup>	39	0.11	14-19	0.11	3-4
YBaCuO	92	0.005	140	0.5	29
HgBa <sub>2</sub> Cu <sub>3</sub> O <sub>8+x</sub>	131			0.045	190
Ba(Fe <sub>0.9</sub> Co <sub>0.1</sub> )As <sub>2</sub> <sup>4</sup>	22.5		70		50

## 6.2 - Surface magnetic free enthalpy

As shown in section 4.5.1, the difference in free enthalpy density between superconducting and normal phases of a material can be expressed as (relation 4.27)

$$g_s - g_n = -\mu_0 \left( \frac{H_c^2}{2} - \frac{H^2}{2} \right). \quad (6.1)$$

It is the sum of a negative “condensation” term  $g_s^{\text{cond}} = -\mu_0 H_c^2/2$  and a positive magnetic term  $g_s^{\text{mag}} = \mu_0 H^2/2$ . The material passes from the superconducting state to the normal when  $g_s^{\text{mag}}$ , which is zero in the superconductor for  $H = 0$ , increases sufficiently to compensate  $g_s^{\text{cond}}$ , thus making the density of total free enthalpy in the superconductor equal to that of the normal metal (Fig. 6.2).

### 6.2.1 - Surface magnetic free enthalpy density

Now the expression for the magnetic free enthalpy density  $g_s^{\text{mag}}$  relies on the equation of state  $\mathbf{M} = -\mathbf{H}$  (relation 4.17) valid only when  $\mathbf{B} = \mathbf{0}$ , that is beyond the penetration depth  $\lambda$ . It turns out then, that to realize a more realistic description, we must re-evaluate  $g_s^{\text{mag}}$  in the vicinity of an interface with a normal metal or the vacuum.

3 T. MURANAKA *et al.* (2005) Superconductivity in MgB<sub>2</sub>, in *Frontiers in Superconducting Materials*, A.V. NARLIKAR Ed., Springer, 937.

4 A. YAMAMOTO *et al.* (2009) *Applied physics Letters* **94**, 062511.

Since the magnetic field no longer vanishes everywhere in the superconductor but decreases from its surfaces as

$$B(u) = B^0 e^{-\frac{u}{\lambda}} \quad (6.2)$$

where  $u$  is the distance from the interface, and the magnetization develops from the same surfaces as

$$M(u, H) = \frac{B(u)}{\mu_0} - H = H \left( e^{-\frac{u}{\lambda}} - 1 \right). \quad (6.3)$$

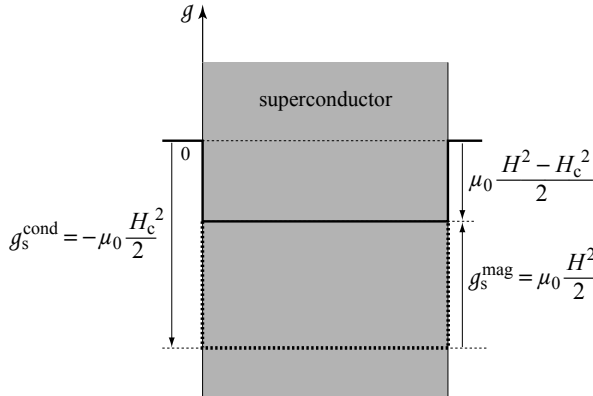


**Figure 6.2 - Bulk free enthalpy density in the superconducting phase**

Compared to the normal state, the bulk free enthalpy density is:

- lowered by the free enthalpy density of condensation  $g_s^{\text{cond}} = -\mu_0 H_c^2 / 2$
- raised by the magnetic free enthalpy density  $g_s^{\text{mag}} = \mu_0 H^2 / 2$

With this new local equation of state, the magnetic free enthalpy density at distance  $u$  from the interface becomes (see relation 4.23)

$$g_s^{\text{mag}}(u) = -\mu_0 \int_0^H M(u, H') dH' \quad (6.4)$$

or, after replacing  $M(u, H')$  by its form (6.3) and integrating,

$$g_s^{\text{mag}}(u) = \mu_0 \frac{H^2}{2} \left( 1 - e^{-\frac{u}{\lambda}} \right). \quad (6.5)$$

Therefore the contribution to the magnetic free enthalpy density, so far considered as equal everywhere to  $g_s^{\text{mag}} = \mu_0 H^2 / 2$ , is diminished from this value near each interface (Fig. 6.3) by an amount

$$\delta g_s^{\text{mag}}(u) = -\mu_0 \frac{H^2}{2} e^{-\frac{u}{\lambda}} \quad (6.6)$$

that is greatest at the surface and decreases exponentially over the penetration depth  $\lambda$  as we move into the bulk.

We define then a “surface magnetic free enthalpy density” (per unit area of the sample surface), as the difference between the actual magnetic free enthalpy density and the free enthalpy density we would have found for a uniform density of magnetization  $M = -H$

$$G_s^{\text{mag,surface}} = - \int_0^\infty \mu_0 \frac{H^2}{2} e^{-\frac{u}{\lambda}} du = -\mu_0 \lambda \frac{H^2}{2}. \quad (6.7)$$

The surface magnetic free enthalpy is **negative**.

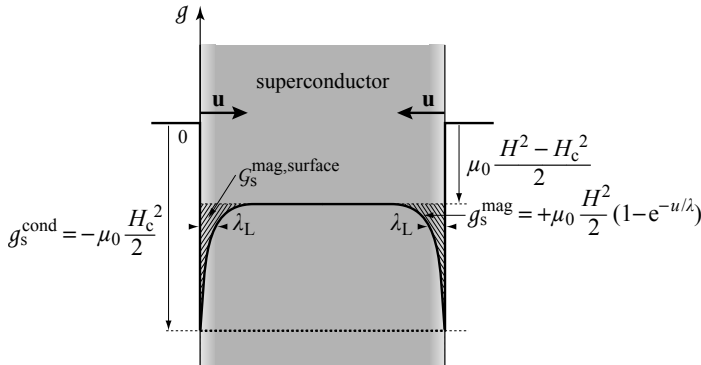


**Figure 6.3 - Magnetic free enthalpy density close to the surface**

Because of the reduction in the magnetization in the LONDON region, the magnetic free enthalpy density is reduced close to the surface (compare with Fig. 6.2).  $G_s^{\text{mag,surface}}$  represents the lowering of free enthalpy per unit area of (flat) surface of the sample.

### 6.2.2 - A first step toward vortices

Let us see what happens if we consider only this free surface enthalpy density. As the equilibrium state of a superconductor subject to a field  $H$  minimizes the total free enthalpy, the system will try to form the maximum possible number of LONDON regions that bring negative contributions to the total free enthalpy. Obviously it cannot do so by changing shape, but it can achieve this by generating a number of filaments of normal phase inside, around each of which there are LONDON regions (Fig. 6.4a).

The multiplication of such filaments where  $M = 0$  and of their LONDON regions in which  $-H < M < 0$ , leads to a deficit of magnetization (incomplete MEISSNER effect) such as is seen in the SHUBNIKOV phase (see Fig. 6.1b). The profile of free enthalpy density represented in Figure 6.4 shows that creation of a cylindrical normal filament of radius  $a$ , surrounded by a LONDON region of extent  $\lambda$ , modifies the total free enthalpy in two ways:

- » inside the normal filament, the free enthalpy per unity of filament length increases by an amount represented in Figure 6.4b by the area marked ①, i.e.

$$\mu_0 \pi a^2 \frac{H_c^2 - H^2}{2}; \quad (6.8a)$$

» in the LONDON region that surrounds it ( $r > a$ ) the free enthalpy is, by applying relation (6.6), lowered by an amount represented by the area marked ②, namely

$$-\int_a^\infty \mu_0 \frac{H^2}{2} e^{-\frac{r}{\lambda}} 2\pi r dr = -2\pi \mu_0 \frac{H^2}{2} \lambda(a + \lambda) e^{-\frac{a}{\lambda}}. \quad (6.8b)$$

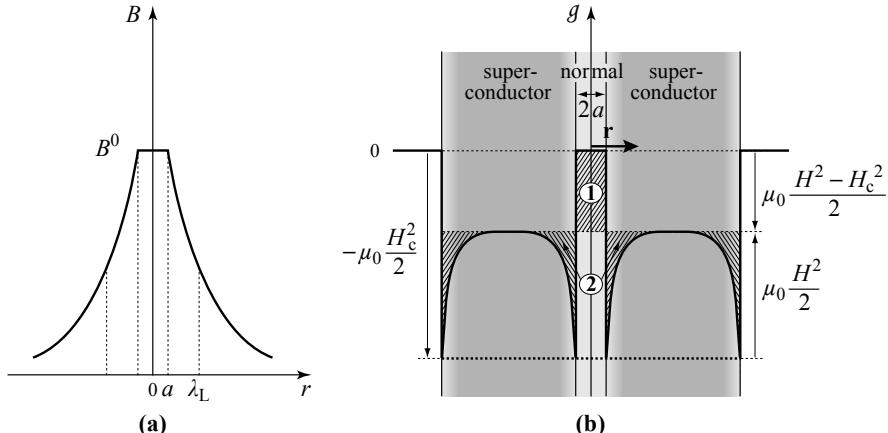


**Figure 6.4 - Normal filament within a superconductor**

(a) Profile of the magnetic field in and around a normal cylindrical filament created in a superconductor. (b) Profile of the free enthalpy density in, and around, the normal filament. ① represents the increase of free enthalpy in the normal filament and ② the decrease in free enthalpy in the LONDON region.

The difference in total free enthalpy between the superconductor with or without the normal filament accompanied by its LONDON region is therefore, per unit length,

$$\Delta G = \mu_0 \left[ \pi a^2 \frac{H_c^2 - H^2}{2} - 2\pi \frac{H^2}{2} \lambda(a + \lambda) e^{-\frac{a}{\lambda}} \right]. \quad (6.8c)$$

Finally, this normal filament surrounded by its London region is thermodynamically stable if  $\Delta G < 0$ , i.e. from Equation (6.8c), if the field  $H$  exceeds the value  $H^\#$  given by

$$H^\# = \sqrt{\frac{a^2}{a^2 + 2\lambda(a + \lambda)e^{-\frac{a}{\lambda}}} H_c}. \quad (6.9)$$

Therefore, the surface magnetic free enthalpy favors an incomplete MEISSNER effect in agreement with experiment. However, this term has to be balanced, since, whatever the values of  $a$  and  $\lambda$ , the field  $H^\#$  determined by the relation (6.9) is found to be less than the critical field  $H_c$ . This means that if we restrict ourselves to

this surface contribution alone, there would always be a field  $H^\#$ , less than  $H_c$ , beyond which filaments of normal phase would become stable within the superconducting phase. Such a result would imply that all materials would show a SHUBNIKOV phase and be of type II, which is contrary to experiment.

The original question must therefore be inverted. We no longer need to know the origin of type II superconductors, instead we ask why do type I superconductors exist?

## 6.3 - Surface free enthalpy of condensation

### 6.3.1 - Coherence length

When we write that the density of free enthalpy of condensation (relation 6.1) is equal to  $-\mu_0 H_c^2/2$  everywhere in the superconductor, we are actually assuming that there can be an infinitesimally thin transitional region that separates the normal regions, where no electrons are superconducting, from the superconducting regions, where the density of superconducting electrons becomes uniform. In other words, this assumes that the density of superconducting electrons can jump in a single step, from zero to its bulk value  $n_{s\infty}$ <sup>5</sup> as soon as the interface is crossed.

In fact this is not true: the density of superconducting charges can only pass from 0 to  $n_{s\infty}$  over a finite distance of order the coherence length  $\xi$  which is interpreted as the average distance between two electrons in the same COOPER pair.

In a simple model, we suppose that the density  $n_s$  of superconducting electrons increases within the superconductor starting from the interface with the normal phase or vacuum according to the formula

$$n_s(u) = n_{s\infty} \left( 1 - e^{-\frac{u}{\xi}} \right). \quad (6.10)$$

This means that when there is an external magnetic field, as we move into the sample there is simultaneously a decrease of the magnetic field  $B$  over the penetration depth  $\lambda$  and an increase of the density  $n_s(u)$  of superconducting electrons over the characteristic scale  $\xi$  (Fig. 6.5).

### 6.3.2 - Geometric interpretation of the coherence length

The PIPPARD coherence length was introduced in Chapter 3 as the distance over which the potential vector  $\mathbf{A}$  should be averaged in order to determine the current density  $\mathbf{j}$  at a point. It was interpreted as the average distance ( $\xi_0$  in clean superconductors or  $\xi_p$  in dirty superconductors) that separates two electrons of a COOPER pair at 0 K.

---

5 If we do not specify further,  $n_s$  is the density of superconducting electrons in the bulk. It will be denoted  $n_{s\infty}$  in special contexts where the density varies in space. The notations  $n_s(u)$  and  $n_s(r)$  are reserved for local densities.

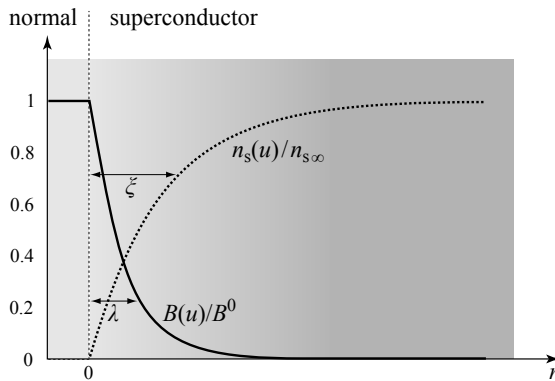


**Figure 6.5 - Magnetic field and density of superconducting electrons near a Normal/Superconducting interface**

Close to an interface the magnetic field  $B$  decreases exponentially over the characteristic length  $\lambda$ . Simultaneously the density of superconducting electrons increases with another characteristic length  $\xi$ .

This picture also allows us to provide a qualitative justification for the density profile of the centers of gravity of COOPER pairs. We can consider it to be the quantity  $n_s(u)/2$  introduced in the previous section (each COOPER pair is made up of two superconducting electrons). Figure 6.6 shows different situations and the qualitative result that we obtain as we move away from the interface.

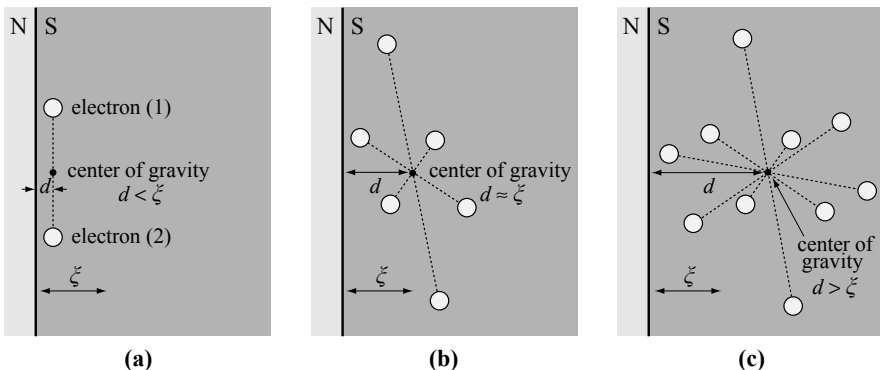


**Figure 6.6 - Illustration of possible configurations of COOPER pairs**

as a function of the distance of their centers of gravity with respect to the surface

- (a) For the center of gravity of a pair to be in the immediate neighborhood of the surface, the constituent electrons must themselves be in close proximity to the surface. This condition leaves few favorable geometric configurations and the density of centers of gravity of the pairs is extremely reduced near the surface.
- (b) At a point further from the surface, the number of configurations increases as now the COOPER pairs whose electrons are close can be oriented in any direction in space. This is not yet the case for COOPER pairs whose electrons are further apart.
- (c) At a distance  $\xi$  from the interface and beyond, the geometric restrictions on the orientation of COOPER pairs vanish. The density of centers of gravity of the pairs reaches its bulk value  $n_{s\infty}/2$ .

We should be careful, however, since the coherence length  $\xi$  only coincides with the size of COOPER pairs at 0 K, as we shall see later. What remains true is the central rôle played by the non-local character of superconductivity that we have already seen with the PIPPARD equations in Chapter 3, section 3.2, that discussed the finite extent of COOPER pairs.

### 6.3.3 - Surface free enthalpy density of condensation

If the density of superconducting electrons is reduced close to the surface, so too must be the density of the free enthalpy of condensation, interpreted as the free enthalpy of formation of COOPER pairs, to which it should be proportional.

From its value  $-\mu_0 H_c^2/2$  in the bulk, where the density of superconducting electrons is  $n_{s\infty}$ , it follows that at a distance  $u$  from the interface where the density of superconducting electrons is  $n_s(u)$  it should equal

$$g_s^{\text{cond}}(u) = -\mu_0 \frac{H_c^2}{2} \frac{n_s(u)}{n_{s\infty}} = -\mu_0 \frac{H_c^2}{2} \left(1 - e^{-\frac{u}{\xi}}\right) \quad (6.11)$$

which in comparison to the situation where the density of carriers would be uniformly  $n_{s\infty}$ , constitutes a change in the free enthalpy density of condensation of

$$\delta g_s^{\text{cond}}(u) = +\mu_0 \frac{H_c^2}{2} e^{-\frac{u}{\xi}}. \quad (6.12)$$

As for the magnetic term (section 6.2), we define the surface free enthalpy density of condensation (per unit area of the sample surface), as the difference between the actual free enthalpy density of condensation and what would be found for the free enthalpy density with uniform condensation

$$G_s^{\text{cond,surface}} = \int_0^\infty \mu_0 \frac{H_c^2}{2} e^{-\frac{u}{\xi}} du = \mu_0 \xi \frac{H_c^2}{2}. \quad (6.13)$$

*The surface free enthalpy of condensation is positive.*

## 6.4 - Total surface free enthalpy

The sum of magnetic terms (6.7) and condensation terms (6.13) constitute the total free enthalpy per unit surface area of creation of a planar Normal/Superconducting interface,

$$G_s^{\text{surface}} = -\mu_0 \left( \lambda \frac{H^2}{2} - \xi \frac{H_c^2}{2} \right). \quad (6.14)$$

Its sign depends on the applied field and on the GINZBURG-LANDAU parameter  $\kappa = \frac{\lambda}{\xi}$ .

$$\begin{aligned}
 G_s^{\text{surface}} < 0 & \quad \text{if} \quad H > \frac{H_c}{\sqrt{\kappa}} \\
 G_s^{\text{surface}} > 0 & \quad \text{if} \quad H < \frac{H_c}{\sqrt{\kappa}}
 \end{aligned}
 \quad (\text{for a planar surface}). \quad (6.15)$$

Profiles for the densities of surface free enthalpies are represented on Figure 6.7 for  $H/H_c = 0.8$ ;  $\lambda = 80 \text{ nm}$  and several values  $\xi$ .

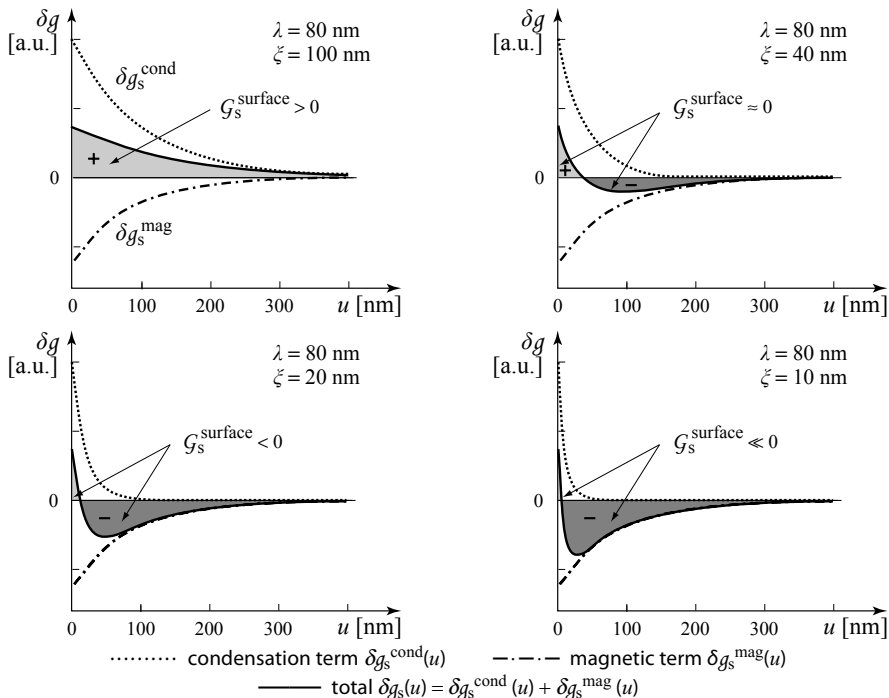


**Figure 6.7 - Density of surface free enthalpy**  $H/H_c = 0.8 ; \lambda = 80 \text{ nm} ; 10 < \xi < 100 \text{ nm}$

Representation of the differences between the densities of free enthalpy close to a surface and in the bulk. The integrated area between  $\delta g_s(u)$  and the horizontal axis (with signs as indicated by + or -) represents surface free enthalpy. For a field  $H/H_c = 0.8$  and a penetration depth  $\lambda = 80 \text{ nm}$ , it is positive when  $\xi > 40 \text{ nm}$  and negative for smaller values.

## 6.5 - Vortices and type II superconductors

### 6.5.1 - Description of a vortex

Once we have introduced a coherence length  $\xi$ , the model of a geometrically well-defined normal filament in the superconductor, surrounded by a LONDON region of decreasing magnetic field, has been made obsolete.

The normal filament must be replaced by a vortex which is described as a physical “object” of cylindrical symmetry (Fig. 6.8) within which, starting from a central axis, the density of superconducting electrons increases from zero to  $n_{s\infty}$  over a characteristic distance  $\xi$  and from which the magnetic field decreases from a maximum  $B_{\text{center}}$  towards zero over the characteristic distance  $\lambda$ . According to the laws of electromagnetism and the second LONDON equation, emergence of the magnetic field  $\mathbf{B}$  requires vortex currents of the LONDON type. These are most commonly considered as screening currents, but here we visualize them more as currents generating an islet of magnetic field within the superconductor.

The name “vortex” is an archaic form of the Latin word “*vertex*” that means “whirlpool.”

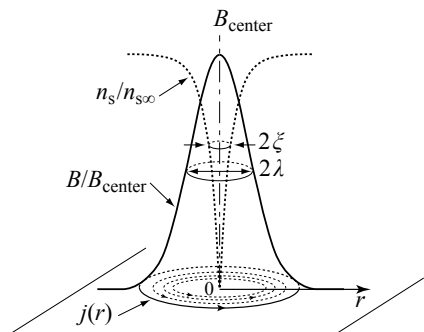


**Figure 6.8 - A vortex**

Starting from a central axis, the magnetic field  $B$  taking a maximum value of  $B_{\text{center}}$  accompanied with whirling superconducting currents, decreases over the characteristic distance  $\lambda$  while the density of superconducting electrons increases from zero to its bulk value  $n_{s\infty}$  over the coherence length  $\xi$ . The magnetic field varies little around the vortex center because of the low density of LONDON currents in the core region.

Rigorous determination of the conditions for stability of a vortex requires a precise knowledge of the real profiles of the magnetic field  $B(r)$  and the density of superconducting electrons  $n_s(r)$ . This problem can be treated starting from the GINZBURG-LANDAU equations and leads to a magnetic field which has the form drawn in Figure 6.8. At this stage we make the simple approximation that  $n_s(r)$  and  $B(r)$  vary exponentially from the central axis<sup>6</sup>, each with its characteristic length ( $\xi$  and  $\lambda$  respectively) as they would from a planar surface, *i.e.*

$$n_s(r) = n_{s\infty} \left(1 - e^{-\frac{r}{\xi}}\right) ; \quad B(r) = B_{\text{center}} e^{-\frac{r}{\lambda}}. \quad (6.16)$$

We should not forget that the penetration depth  $\lambda$  is not independent of  $\xi$  as the depletion of superconducting carriers reduces the density of LONDON currents that must then spread out more to maintain the magnetic field. In fact this has already been taken into account in going from the LONDON length  $\lambda_L$  to the penetration length  $\lambda$  in the relation (3.6).

6 A more realistic profile has been proposed within the framework of the GINZBURG-LANDAU model.

### 6.5.2 - Stability of vortices

#### Stability condition

Without vortices the free enthalpy density of the superconductor is uniform and given by the relation (6.1).

With one vortex centered at  $r = 0$ , it becomes (by relations 6.6 and 6.12),

$$g_s(H, r) = g_n - \mu_0 \left[ \frac{H_c^2}{2} \left( 1 - e^{-\frac{r}{\xi}} \right) - \frac{H^2}{2} \left( 1 - e^{-\frac{r}{\lambda}} \right) \right] \quad (6.17)$$

which leads to the free enthalpy per unit length for the creation of a vortex, defined as the difference between the free enthalpy of a sample with and without a vortex,

$$\mathcal{G}^{\text{vortex}} = + \mu_0 \frac{H_c^2}{2} \left( \int_0^\infty 2\pi r e^{-\frac{r}{\xi}} dr \right) - \mu_0 \frac{H^2}{2} \left( \int_0^\infty 2\pi r e^{-\frac{r}{\lambda}} dr \right) \quad (6.18)$$

cost in "condensation"
gain in "magnetic"

free enthalpy
free enthalpy

that after integrating is per unit length

$$\mathcal{G}^{\text{vortex}} = 2\pi \mu_0 (\xi^2 H_c^2 - \lambda^2 H^2). \quad (6.19)$$

The free enthalpy of formation of a vortex is positive in zero field, decreases as the field increases and turns negative when  $H$  is larger than  $(\xi/\lambda)H_c$ . This result makes appear the two categories of superconducting materials depending on the relative values of  $\xi$  and  $\lambda$ :

- » superconductors of type I,  $\xi > \lambda$ : the critical field  $H_c$  is reached before  $\mathcal{G}^{\text{vortex}}$  becomes negative and therefore before a vortex is stable; the superconducting state disappears uniformly at  $H_c$  before any vortex can appear;
- » superconductors of type II,  $\xi < \lambda$ :  $\mathcal{G}^{\text{vortex}}$  becomes negative for a field  $H_{c1}$  less than the critical field  $H_c$ ; the vortices become stable starting from the field

$$H_{c1} = \frac{\xi}{\lambda} H_c = \frac{H_c}{\kappa}. \quad (6.20)$$

Here the critical value  $\kappa_c$  of the GINZBURG-LANDAU parameter that separates type I and II superconductors is equal to one. A more thorough analysis starting from the

GINZBURG-LANDAU equations changes it to  $\kappa_c = \frac{1}{\sqrt{2}}$

with  $\kappa < \kappa_c$  the superconductor is of type I  
 $\kappa > \kappa_c$  the superconductor is of type II (6.21)

The characteristic lengths  $\lambda$ ,  $\xi$  and the values of  $\kappa$  listed in Table 6.3 are in agreement with the fact that the majority of pure metallic superconductors are of type I, while alloys and compounds are of type II. We also see that while the penetration depths  $\lambda$  are relatively close to one another (the different materials differ by

relative factors no larger than 7), the coherence lengths are very widely distributed (factors greater than 200), which means that the nature, type I or type II, of the superconductor depends above all on the coherence length  $\xi$ . The ratio between extreme values of  $\kappa$  is more than 5000.

**Table 6.3 - Experimental values of the GINZBURG-LANDAU parameter  $\kappa = \lambda/\xi$**

Note that its value is much less than 1 for pure metals, the majority of which are of type I, and much greater than 1 for alloys and compounds that are all of type II. This broad spectrum of  $\kappa$  is essentially due to the range of values for the coherence length  $\xi$ .

Material	$T_c$ [K]	$\xi$ [nm]	$\lambda$ [nm]	$\kappa = \lambda/\xi$
Al	1.175	550	40	0.03
In	3.41	360	40	0.11
Ta	4.47	93	35	0.38
Pb	7.20	82	39	0.48
Nb	9.25	39	50	1.28
Pb-In	7	30	150	5
Nb-Ti	9.50	4	300	75
$\text{Nb}_3\text{Sn}$ (A15)	18,1	3	65	22
$\text{PbMo}_6\text{S}_8$ (CHEVREL)	15	2	200	100
$\text{Rb}_3\text{C}_{60}$	29.60	2	247	124

Very anisotropic materials present penetration and coherence lengths that are anisotropic, just like their critical fields (Table 6.4).

**Table 6.4 - Penetration and coherence lengths at 0 K for some anisotropic materials**

These materials have a 2D character and are quasi-isotropic in the  $(ab)$  plane.

Material	$T_c$ [K]	$\lambda_{ab}$ [nm]	$\lambda_c$ [nm]	$\xi_{ab}$ [nm]	$\xi_c$ [nm]
$\text{MgB}_2$ <sup>7</sup>	39	1000	1000	11.8	2.8
$\text{YBaCuO}$	91	$\approx 130$	$\approx 450$	$\approx 1.3$	$\approx 0.2$
$\text{HgBaCuO}$	133	$\approx 130$	$\approx 3500$	$\approx 1.3$	

### Temperature dependence

Like the thermodynamic critical field  $H_c$ , the fields  $H_{c1}$  and  $H_{c2}$  decrease when the temperature is raised, going from their maximum values  $H_{c1}(0)$  and  $H_{c2}(0)$  at zero temperature, to zero when the temperature reaches  $T_c$  (see Fig. 6.1a). Note that the penetration  $\lambda$  and coherence lengths  $\xi$  vary with temperature in much the same way

<sup>7</sup> A.V. SOLOGUBENKO (2002) *Phys. Rev. B* **65**, 180505; J.D. FLETCHER (2005) *Phys. Rev. Lett.* **95**, 097005.

which means that their ratio  $\kappa$  depends weakly on temperature and makes the nature of the superconductor, of type I or II, an intrinsic property (Table 6.5).

**Table 6.5 - Behavior of the penetration depth  $\lambda$  and the coherence length  $\xi$  near  $T_c$  as a function of the characteristic parameters<sup>8</sup>**

$\lambda(0)$  is the penetration depth at 0 K in the pure materials,  $\xi_0$  the BCS coherence length at 0 K,  $\ell$  the mean free path in the normal metal

	Pure superconductor	Dirty superconductor
Coherence length $\xi(T)$	$0.74\xi_0\left(1-\frac{T}{T_c}\right)^{-\frac{1}{2}}$	$0.85\sqrt{\ell\xi_0}\left(1-\frac{T}{T_c}\right)^{-\frac{1}{2}}$
Penetration depth $\lambda(T)$	$\frac{1}{\sqrt{2}}\lambda(0)\left(1-\frac{T}{T_c}\right)^{-\frac{1}{2}}$	$\frac{1}{\sqrt{2}}\lambda(0)\sqrt{\frac{\xi_0}{\ell}}\left(1-\frac{T}{T_c}\right)^{-\frac{1}{2}}$
$\kappa(T) = \frac{\lambda(T)}{\xi(T)}$	$\approx 0.96 \frac{\lambda(0)}{\xi_0}$	$\approx 0.715 \frac{\lambda(0)}{\ell}$

### Impurity effects

The presence of impurities in metals reduces the mean free path of electrons, which has the effect of decreasing the mean distance between electrons in the COOPER pairs. This has two consequences (Table 6.5):

- » a reduction in the coherence length by a factor  $\sqrt{\ell/\xi_0}$ ,
- » an increase in the penetration depth  $\lambda$  by a factor  $\sqrt{\xi_0/\ell}$ .

These two effects act in the same sense of an increase in the GINZBURG-LANDAU parameter  $\kappa = \lambda/\xi$ . For this reason, once the concentration of impurities is sufficient a material originally of type I ( $\kappa < \kappa_c$ ) becomes of type II ( $\kappa > \kappa_c$ ).

### 6.5.3 - Quantization of the flux carried by a vortex

While the thermodynamic approach is satisfactory in that it provides the stability conditions for the vortex, it completely misses the quantization of the flux of the magnetic field it carries, a fundamental property of the vortex. Indeed it will be seen in Chapter 9 that the quantum coherent state of the superconducting condensate<sup>9</sup> constrains the total magnetic field flux associated with a vortex to be equal to a fixed quantity  $\phi_0$  called the “quantum of flux” or “fluxon”

$$\phi_0 = \frac{h}{2e} = 2.07 \times 10^{-15} \text{ Wb.} \quad (6.22)$$

<sup>8</sup> See for example, M. TINKHAM (1996) *Introduction to Superconductivity*, 2<sup>nd</sup> ed., Dover, New York, section 4.2, 118.

<sup>9</sup> This property will be discussed in detail in section 9.3.1.

As the profile of the magnetic field and its spatial extent are determined by the penetration depth  $\lambda$ , the only adjustable parameter allowing this condition to be satisfied is the value of the magnetic field at the center of the vortex  $B_{\text{center}}$ , which acts as a normalization factor. Within the approximation of an exponential decrease of the magnetic field (Eq. 6.16),

$$\phi_0 = \int_0^\infty B(r) 2\pi r dr = \int_0^\infty B_{\text{center}} e^{-\frac{r}{\lambda}} 2\pi r dr = 2\pi \lambda^2 B_{\text{center}} \quad (6.23)$$

or  $B_{\text{center}} = \frac{\phi_0}{2\pi \lambda^2}.$  (6.24)

So we see that, whatever the magnetic field created by the external solenoid, the magnetic field at the center of the vortex is not equal to  $B^0$  but maintains the value  $B_{\text{center}}$  given by relation (6.24), determined by the penetration depth  $\lambda$ . As we shall see further on, this discussion makes sense only if the vortex is isolated.

This value of  $B_{\text{center}}$  forces us to question the magnetization profile introduced in the relation (6.2) where we have implicitly assumed that  $B_{\text{center}} = \mu_0 H^0$ . Nonetheless, it turns out that while this constraint on the magnetic field modifies the magnetization profile and the change in free enthalpy during formation of a vortex, the competition between the surface magnetic and condensation enthalpies certainly remains the driving force behind the formation of vortices.

#### 6.5.4 - Results of "GLAG" theory

Starting from a form of free energy that had been proposed by GINZBURG and LANDAU, and by including the thermodynamic parameters, the electromagnetic parameters and the coherence constraints, ABRIKOSOV and GORKOV made a more precise calculation of the critical fields  $H_c$ ,  $H_{c1}$ ,  $H_{c2}$ , the energy  $\varepsilon_1$  of formation of a vortex and the magnetic field at the center. The relations between the critical fields and the penetration and coherence lengths in this GINZBURG- LANDAU- ABRIKOSOV-GORKOV model (or GLAG, to recall the names of the four Russian physicists)<sup>10</sup> take, for  $\kappa \gg 1$  and at temperature  $T$ , the forms given below

$$H_c(T) = \frac{\phi_0}{2\pi\sqrt{2}\mu_0\lambda(T)\xi(T)} \quad (6.25)$$

$$H_{c1}(T) \approx \frac{H_c}{\sqrt{2}} \frac{\ln \kappa}{\kappa} = \frac{\phi_0}{4\pi\mu_0\lambda^2(T)} \ln \kappa \quad (6.26)$$

$$\varepsilon_1 = \frac{\phi_0^2}{4\pi\mu_0\lambda^2} \ln \kappa \quad B_{\text{center}} \approx \frac{\phi_0}{2\pi\lambda^2} \ln \kappa = 2\mu_0 H_{c1} \quad (6.27)$$

---

<sup>10</sup> D. SAINT JAMES & G. SARMA (1969) *Type II superconductivity*, Pergamon Press, Oxford-New York.

$$H_{c2}(T) = \frac{\phi_0}{2\pi\mu_0\xi^2(T)} = \sqrt{2}\kappa H_c \quad (6.28)$$

$$\frac{H_{c2}}{H_{c1}} = \frac{2\kappa^2}{\ln\kappa} \quad H_{c1}H_{c2} = H_c^2 \ln\kappa. \quad (6.29)$$

Since the value of  $\ln\kappa$  is between 1 and 5, the expression for  $H_{c1}$  predicts values not very far from (6.20). The expression (6.28) for the critical field  $H_{c2}$  will be justified in section 6.7 and the relation (6.25) in Chapter 8 (relation 8.96).

## 6.6 - Vortex lattice

### 6.6.1 - ABRIKOSOV lattice

Suppose we take a superconducting bar sufficiently long to avoid any effects of demagnetizing fields, and place it in a uniform magnetic field  $\mathbf{B}^0$  that creates a uniform field  $\mathbf{H}$  equal to  $\mathbf{H}^0 = \mathbf{B}^0/\mu_0$  in the sample.

When  $H$  reaches  $H_{c1}$ , and if nothing prevents either their penetration or their displacement in the material, the vortices will ideally proliferate in such a way that the magnetic field flux  $B^0 S$  that impinges on the base of surface area  $S$  will cross by subdividing into  $N_v$  fluxons (Fig. 6.9) such that

$$B^0 S = \phi_0 N_v. \quad (6.30)$$

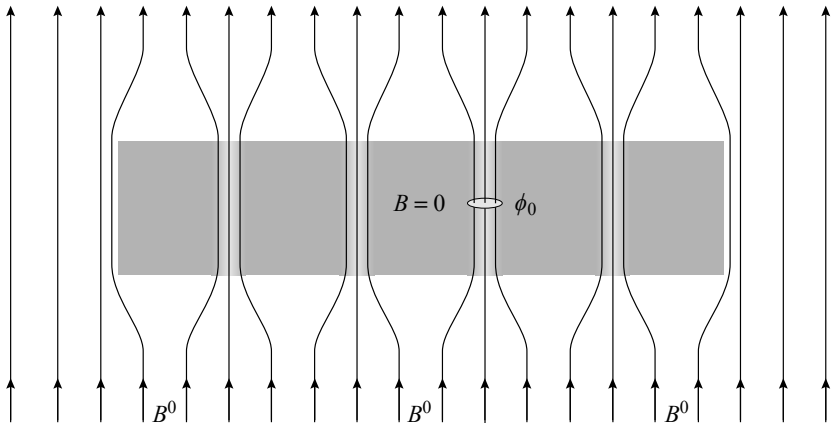


**Figure 6.9 - Idealized soft superconductor**

In an idealized soft superconductor, the magnetic field flux  $B^0$  which "invades" the sample crosses it by fluxons, each carrying a quantum of flux  $\phi_0$ .

The density of vortices per unit surface area of the the base is therefore

$$n_v = \frac{B^0}{\phi_0}. \quad (6.31)$$

Because of repulsion between vortices, they tend to distribute themselves as uniformly as possible. Calculations show that the total free enthalpy is minimal when they organize into an hexagonal lattice in two dimensions, called the “ABRIKOSOV lattice” (Fig. 6.10). The distance  $d_v$  between vortices in this lattice is

$$d_v = \sqrt{\frac{2}{\sqrt{3}}} \sqrt{\frac{1}{n_v}} = \sqrt{\frac{2}{\sqrt{3}}} \sqrt{\frac{\phi_0}{B^0}} \quad (6.32)$$

or,  $d_v \approx \frac{49}{\sqrt{B^0}}$  for  $d_v$  in nm and  $B^0$  in T.

A few numerical values are given in Table 6.6.

**Table 6.6 - Distance between vortices as a function of applied magnetic field**

In an ABRIKOSOV lattice the distances between vortices do not depend on the nature of the material, but just on the applied field.

$B^0$ [T]	$10^{-2}$	$10^{-1}$	1	10	100
$d_v$ [nm]	490	155	49	15.5	4.9

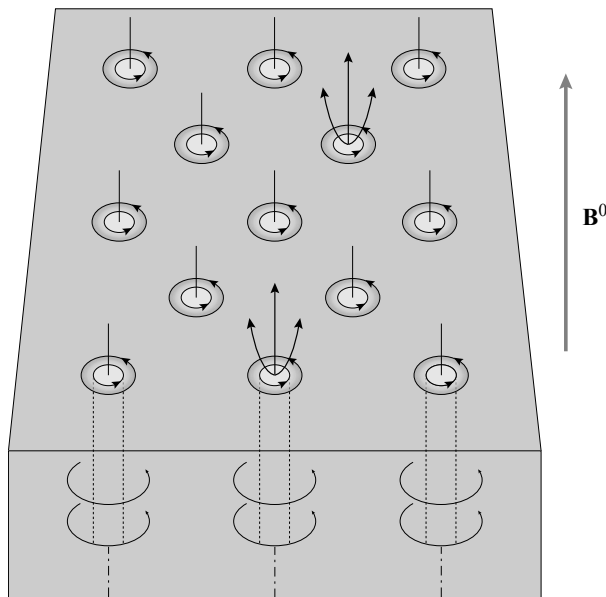


**Figure 6.10 - ABRIKOSOV lattice**

Resembling a crystal lattice, vortices form a two-dimensional lattice that is most commonly hexagonal.

In practice the hypothesis that the external field is totally absorbed by the vortex lattice is not completely correct, since it would imply that  $\langle -M \rangle$  falls abruptly to zero immediately after  $H_{c1}$ . The discrepancy is due to the repulsion between vortices, that makes their penetration more difficult since any new ones are pushed

away by those that are already present. The fraction of flux absorbed by the vortices is represented by the difference between the magnetization of the perfect diamagnet  $\langle -M \rangle = H$  (the continuation of the dotted line in Fig. 6.1b) and the measured magnetization density  $\langle -M \rangle$ . The rapid decrease of  $\langle -M \rangle$  at  $H_{c1}$  shows that a large number of vortices penetrate instantaneously into the sample, but that the external flux is not totally absorbed and that LONDON-type screening remains. With increasing  $H$ , the fraction of the flux transmitted by the vortices becomes very large.

The distance between vortices when  $B^0$  reaches  $B_{c1} = \mu_0 H_{c1}$  is, using expressions (6.26) and (6.32),

$$d_v(H_{c1}) \approx \frac{2}{\ln \kappa} \lambda \quad (6.33)$$

i.e. typically the penetration depth  $\lambda$ . This means that at the phase transition between the MEISSNER and SHUBNIKOV phases, the LONDON regions of the vortices appear to be almost touching. The system is then, (see Fig. 6.14a) at the limit of isolated vortices with profiles as drawn in Figure 6.8.

When the field grows, the vortices approach one another and their LONDON regions interpenetrate.

### 6.6.2 - Imaging vortex lattices

Following ABRIKOSOV's work, great efforts were made experimentally to show the presence of vortices and to reveal the precise details of their organization.

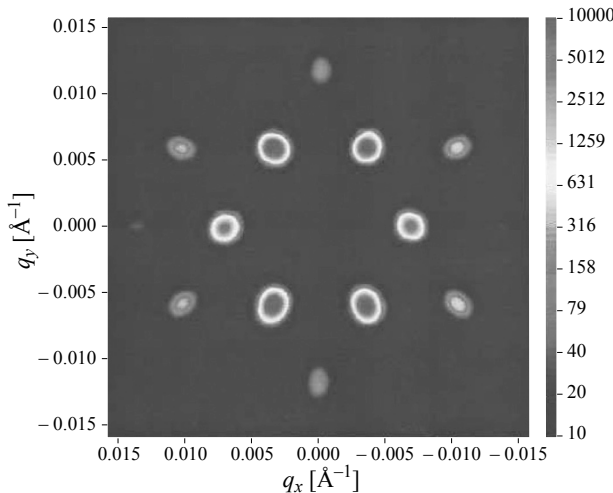
Following a suggestion of P.G. DE GENNES and J. MATRICON, proof of the existence of the vortex lattice in type II superconductors was given by diffraction experiments with thermal neutrons<sup>11</sup> performed by D. CRIBIER and his colleagues.<sup>12</sup>

Figure 6.11 shows a neutron diffraction spectrum from a vortex lattice in a single crystal of niobium (dimensions  $7 \times 9 \text{ mm}^2$ , thickness 2.46 mm) of high purity that had been subject to annealing and surface treatments to eliminate any defect likely to hinder the vortex organization. This figure can be compared to diffraction images of atomic lattices: it is of a single crystal of vortices for which each diffraction point can be indexed according to the conventions of crystallography. We see clearly the symmetry of order 6 characteristic of an hexagonal lattice in two dimensions, and from the position of the diffraction peaks we can directly deduce the distance between vortices. While this technique really brings decisive proof of the organization of the vortices into a regular lattice, it does not give a direct image.

---

11 As they have spin  $\frac{1}{2}$ , neutrons interact with the magnetic field carried by the vortices.

12 D. CRIBIER *et al.* (1964) *Phys. Rev. Lett.* **9**, 106.



**Figure 6.11 - Diffraction pattern of neutrons by a vortex lattice**

When they interact with the magnetic field of the vortices the neutrons are diffracted. This diffraction pattern was obtained on a single crystal niobium sample of  $7 \times 9 \text{ mm}^2$  with surface and thermal treatments aimed to suppress all defects likely to pin vortices. Obtained at 3.2 K under a field of 0.2 T, it reflects the existence, on the scale of the crystal, of a hexagonal single crystal of vortices. [From FORGAN *et al.* 2002, © The American Physical Society, with permission]<sup>13</sup>

The first images were produced by ESSMANN and TRAUBLE<sup>14</sup> in 1965 by a decoration technique: nano-particles of cobalt were deposited by evaporation under vacuum onto a Pb-In sample. They are attracted to wherever on the surface the magnetic field is highest, namely where the vortices come out of the sample. Under a magnetic field of 0.02 T, they obtained the image of Figure 6.12, that clearly shows a lattice, whose lattice parameter is of the order of 350 nm.

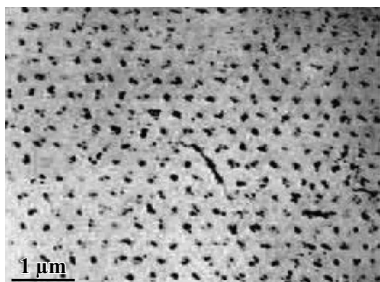


**Figure 6.12**

**Imaging an ABRIKOSOV lattice by decoration**

Pb-In;  $T = 1.1 \text{ K}$ ;  $B^0 = 0.3 \text{ T}$

Attracted by the magnetic fields, nano-particles of cobalt come to the points on the surface where the vortices come out of the sample.

The black points correspond to the vortex cores.

[From ESSMANN & TRAUBLE, 1967,

© Elsevier, with permission]<sup>13</sup>

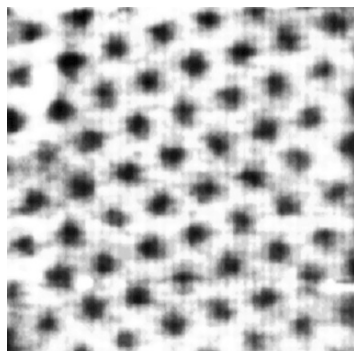
It was only thanks to the development of the tunneling microscope in the 1980's, that the vortices could be imaged precisely and that their cores could be explored.

13 E.M. FORGAN *et al.* (2002) *Phys. Rev. Lett.* **88**, 167003.

14 U. ESSMANN & H. TRAUBLE (1967) *Phys. Lett. A* **24**, 526.

Figure 6.13 (a sample of  $\text{NbSe}_2$  at 4 K under a field of 4 T) shows an image produced by this technique. In this experiment, the distance between vortices follows the relation (6.32) almost perfectly.

**Figure 6.13**  
**Imaging vortices by the tunneling effect<sup>15</sup>**  
 $\text{NbSe}_2$  sample;  $T = 4 \text{ K}$ ;  $H = 4 \text{ T}$ ; size  $630 \times 500 \text{ nm}$   
 Because of their specific densities of states  
 for superconducting quasi-particles  
 (unpaired electrons), the vortices show  
 contrast and can be localized very precisely.  
 The points in black correspond to vortex cores.



Experiments using tunneling spectroscopy have allowed the vortex cores to be localized precisely, since they have the density of states of a normal metal while the regions outside them show a characteristic gap.<sup>16</sup> Scanning measurements allow one to trace the profile of superconducting electrons densities even inside the vortex core.

Vortices can also be visualized by magneto-optics, scanning HALL effect microscopy, micro-SQUID...

## 6.7 - Critical field $H_{c2}$

With the increase of the applied field  $B^0$ , the vortices multiply and become more dense. The LONDON regions of neighboring vortices, which were practically touching at  $B^0 = B_{c1}$ , increasingly overlap one another. Inside the sample,  $B$  oscillates around  $B^0$  with an amplitude that is smaller and smaller as the field is raised. Each period of  $B$  corresponds to one extra fluxon (see the region of Fig. 6.14b shaded in gray).

- » As long as the applied field remains weak, the vortex cores, of dimension  $\xi \ll \lambda$ , stay well separated and the density of superconducting electrons still reaches  $n_{s\infty}$  in the greater part of the sample (Figs 6.14a and 6.14b).
- » When the field  $B^0$  approaches  $B_{c2}$ , the increasing density of the vortices becomes sufficiently high that now the vortex cores start to touch (Fig. 6.14c). The density of superconducting electrons collapses and the superconductivity disappears. The

<sup>15</sup> STM Image: The tunneling spectroscopy image was obtained in the laboratory of D. RODITCHEV, Institute of Nanosciences in Paris, (CNRS & Pierre and Marie CURIE University).

<sup>16</sup> O. FISCHER *et al.* (2007) *Rev. Mod. Phys.* **79**, 353.

amplitude of oscillations of the magnetic field in the sample decreases, and it becomes uniform and equal to  $B_{c2}$ .

Qualitatively, the critical magnetic field  $B_{c2}$  is the field value  $B^0$  for which the distance between two fluxons is of order  $\xi$ . The field  $B_{c2}$  obtained in the GLAG theory by energy arguments is

$$B_{c2} = \frac{\phi_0}{2\pi\xi^2} \quad \text{and} \quad H_{c2} = \frac{\phi_0}{2\pi\mu_0\xi^2} \quad (6.34)$$

for which, by the relation (6.32), the distance between vortices equals  $2\sqrt{\frac{\pi}{\sqrt{3}}}\xi \approx 2.7\xi$ .

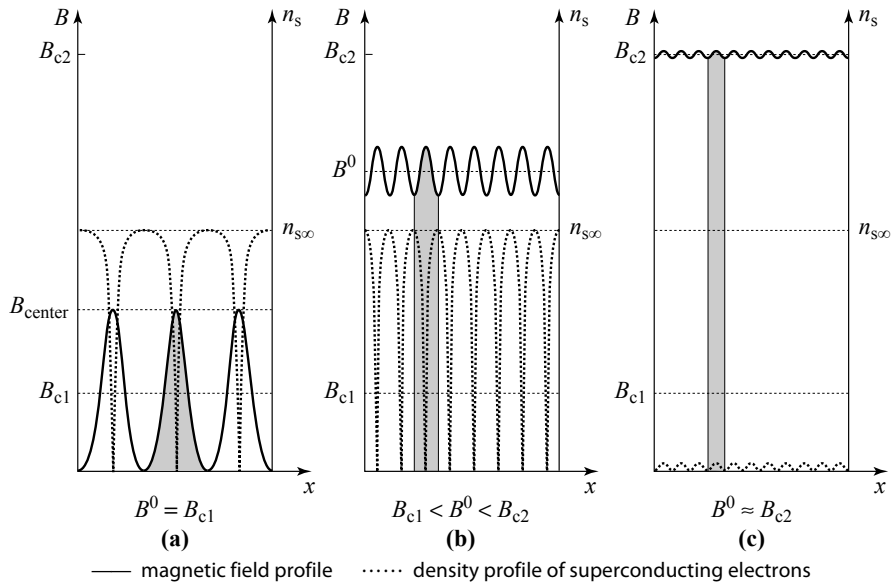


Figure 6.14 - Vortices in the SHUBNIKOV phase

As soon as they form at field  $H_{c1}$ , the LONDON regions of the vortices touch; as the field grows, they overlap. The superconductivity disappears at the field  $H_{c2}$  when the vortex cores of size  $2\xi$  "fill" all of space.

## 6.8 - Elements of the structure and dynamics of vortices

Vortices are also physical objects studied for their own sake – people speak of “vortex matter”<sup>17</sup> – and whole conferences are devoted to them. They are the subject of much study, both theoretical and experimental, notably because of their

<sup>17</sup> G. BLATTER & G.B. GESHKENBEIN (2008) “Vortex Matter” in *Superconductivity Vol. I: Conventional and Unconventional superconductors*, Eds. K.H. Bennemann & J. Ketterson, Springer, 495-637.

implication in electromechanical applications. In particular it is their mobility that plays a crucial role, since this property determines the capacity of a superconducting wire to bear high magnetic fields and to transport high current densities.

The dynamics is introduced here in rather summary fashion, but we will return and develop the subject further in Chapter 7, devoted to the transport of current in type II superconductors in their SHUBNIKOV phase.

*We will say that a superconductor is “soft” if the vortices can move easily, otherwise, when the vortices are strongly pinned, we will describe it as “hard.”*

### 6.8.1 - Penetration of vortices

The question of the penetration of vortices into matter can be addressed by considering two different histories leading to the SHUBNIKOV phase. If we follow the first, the sample is cooled and brought to the superconducting state in an applied field  $B^0$ ; for the second,  $B^0$  is applied only after cooling under zero field.

- » **1<sup>st</sup> History:** when the sample is cooled in a magnetic field  $B^0$  above the critical field  $B_{c1} = \mu_0 H_{c1}$ , it enters the SHUBNIKOV phase directly. The vortices appear spontaneously with the superconducting phase and spread “uniformly” with a density such that they absorb the totality (or at least the greatest part) of the magnetic field flux that crossed the the sample in the normal phase. The average magnetic field in the sample, carried by the vortices as one fluxon each, equals  $\langle B \rangle \approx B^0$ .
- » **2<sup>nd</sup> History:** when the sample is cooled and brought to the superconducting state in zero field, no vortex will form until the magnetic field applied at low temperature equals  $B_{c1}$ . Beyond this field, the creation of vortices is energetically favorable, and we would expect to see a proliferation of vortices until they are sufficiently numerous to absorb the external magnetic flux. To do this, however, they must be able not only to penetrate into the sample but also to move inside.

The penetration mechanism is shown schematically in Figure 6.15: the LONDON currents flowing on the outside surface are distorted to form loops that separate into the form of vortices that can then migrate into the sample.

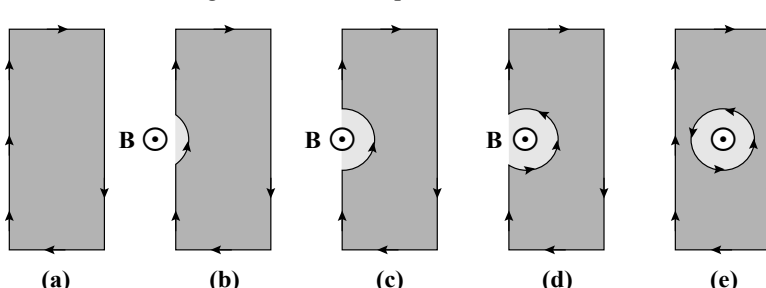
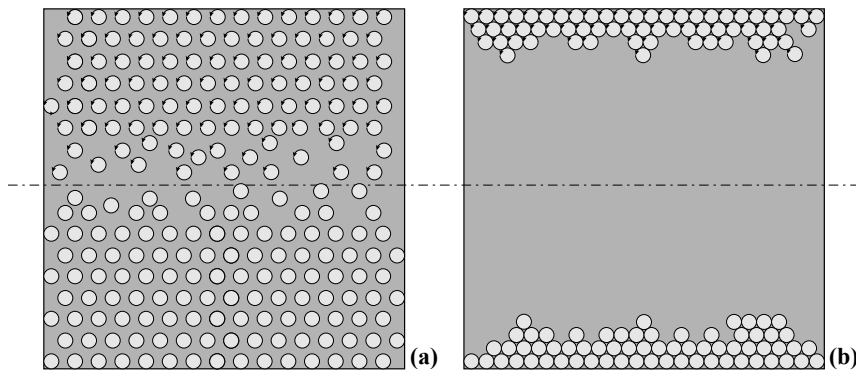


Figure 6.15 - Process of forming a vortex at the surface

The LONDON currents flowing on the outside surface are distorted at some favorable point to gradually form a loop, which then separates to form a vortex.

In a soft superconductor, migration is easy (Fig. 6.16a) and the vortices tend to spread out throughout the sample volume.<sup>18</sup> In a hard superconductor migration is difficult and will be incomplete because of the many defects encountered. The vortices formed will mostly stay close to the surfaces, with the stronger the interaction with defects, the higher the gradient of their concentration (Fig. 6.16b). They can only be moved towards the interior of the sample by application of high fields (see Chap. 7).



**Figure 6.16 - Distribution of vortices in soft and hard superconductors  
after cooling in zero field and then application of a field**

- (a) In a soft superconductor, the vortices infiltrate the whole sample.
- (b) In a hard superconductor they are trapped by defects and tend to stay close to the surfaces.

### 6.8.2 - Phase diagrams of vortices

As the vortices repel one another and their mobility depends on the applied magnetic field, on the temperature and on their interactions with defects, numerous arrangements and dynamical régimes have been observed and/or predicted. Veritable phase diagrams have been drawn. Among the phases most frequently met, we find:

#### *Vortex crystals*

At low temperatures, in a moderate field and in the absence of defects in the material, the distribution of vortices is dominated by the repulsive interactions that lead to lattice formation. In an isotropic material the hexagonal lattice is the most stable but other lattices are also seen. We can speak of vortex crystals with their lattice parameters, their elastic constants and, in certain cases, their defects such as dislocations and other topological defects. By neutron diffraction, very narrow peaks are obtained (“DIRAC peaks” convoluted with the instrumental resolution).

<sup>18</sup> In certain cases, the vortices are repelled by surfaces, and once they have penetrated inside they are propelled to the center of the sample (see section 6.11.3).

### ***BRAGG glass***

In the presence of a number of defects, which constitute as many trapping centers, the vortex lines will distort and, going from vortex to vortex, lose any memory of the position of the vortex at the origin. The vortex-vortex correlation function decreases slowly to zero with distance. The diffraction pattern is no longer constituted of “DIRAC peaks” but at the BRAGG positions there are peaks with diverging intensity and wings decreasing with power laws. As order is lost progressively, in real space the vortex images are little different locally from those of a crystal, with six neighbors and without dislocations. This structure is given the name “BRAGG glass”<sup>19</sup> because of the many configurations that the vortex lines can take, making its ground state highly degenerate. The dynamical properties of this phase resemble those of glasses.

### ***Vortex glass***

When the distortion of the vortices becomes large, only short range remains, as in a glass. The distances between the closest neighbors do not differ very much but the distances between successive neighbors become further and further dispersed, with loss of long-range order. The diffraction pattern reduces to a few broad rings.

### ***Vortex liquid***

When the temperature increases and we approach the limit of stability of the superconducting phase, thermal fluctuations, that have been neglected up to now, increase in amplitude. As long as their amplitudes remain less than the inter-vortex distance, they can be compared to atomic vibrations in a solid, but when they reach or exceed this value, the solid collapses, whether it is crystalline or glassy. We then speak of a vortex liquid, making the analogy to ordinary liquids, where long range order has been lost and in which each vortex can move over the entire sample.

### ***Phase diagram***

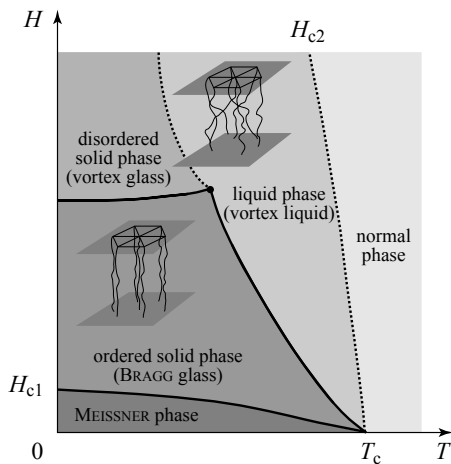
A typical phase diagram is shown in Figure 6.17. Within it we can see the MEISSNER phase below  $H_{c1}(T)$ , the normal phase above  $H_{c2}(T)$  and three vortex phases: the BRAGG phase, the vortex glass and the vortex liquid, originally undifferentiated with the generic name of the SHUBNIKOV phase.

Other phase diagrams, generally more complex, have been published. Debate has been as much about the structure and dynamics of the different phases as the nature of the lines separating them, and of the singular points that appear. It is even more complicated in the cuprates where several types of vortex develop because of the strong anisotropy. The nature of the defects in each phase is of prime importance. The reality of the ABRIKOSOV lattice is not in question, but it is very clear that it is

---

19 T. GIAMARCHI & S. BHATTACHARYA (2001) *Lecture notes in physics*, Springer, 595, 314-360.

an ideal case, that to be observed necessitates special care in the preparation of the material (see the caption of Figure 6.11).



Within the intermediate phase, known as the SHUBNIKOV or mixed phase, vortices form many phases whose diagrams depend strongly on the material and its microstructure. One of the simplest has an ordered solid phase where the vortices are periodically arranged in space, a disordered phase, also called a "vortex glass" and a disordered phase where the vortex are mobile, called a "vortex liquid." More complex phase diagrams have been proposed with, for example, several crystal phases.

Figure 6.17 - Example of a vortex phase diagram<sup>16</sup>

## 6.9 - Electric transport in type II superconductors

### 6.9.1 - The problem of type II superconductors

As they can survive magnetic fields up to 13 T (NbTi), 23 T (Nb<sub>3</sub>Sn) and even up to much higher values (in cuprates or iron-based superconductors) without reverting to the normal phases, type II superconductors appear to be the only potentially interesting candidates for the transport of intense currents and the production of high field superconducting coils. Since they acquire such performances only in the SHUBNIKOV phase, we might question their capacity to transport strong current intensities without losses by JOULE heating. In light of the major technological implications, this problem will be treated in detail in Chapter 7 and here we will introduce only a few general principles concerning the distribution of current density and the notion of critical current densities in the SHUBNIKOV phase.

### 6.9.2 - Distribution of the current density

In the SHUBNIKOV phase the distribution of current density is very different from that in the MEISSNER phase where, as we saw in section 2.6.2, the current is localized near the external surfaces in a layer of thickness equal to the penetration depth  $\lambda$ . In fact in the SHUBNIKOV phase the superconducting electrons carrying the current can "sneak" across the LONDON regions of the vortices avoiding only the cores of radius  $\xi$  ( $\xi \ll \lambda$ ) which are "almost" normal (Fig. 6.18). Therefore since the LONDON regions of the vortices are practically touching at  $H_{c1}$  and above, and that the core radii are much smaller, we can consider that the electric current is

distributed quasi-uniformly through the parts of the sample penetrated by the vortices. This can be the whole volume when the vortices have infiltrated the whole of the sample, or a layer of the sample situated in the neighborhood of the surface if their distribution is as in Figure 6.16b.

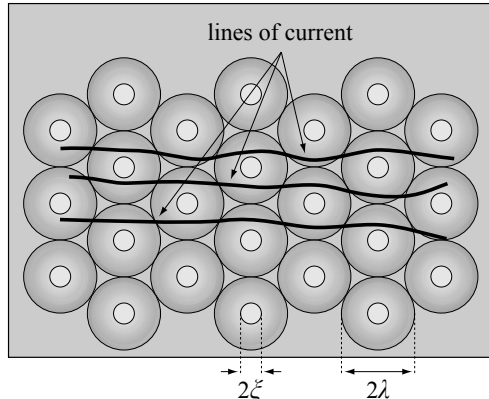


Figure 6.18

#### Transport in type II superconductors

In the SHUBNIKOV phase, superconducting electrons move in the LONDON regions of the vortices avoiding the almost normal cores. The current distribution is then quasi-uniform.

From now on we shall denote by  $\bar{J}$  the locally averaged current density which flows across the LONDON regions of the vortices.

#### 6.9.3 - Critical current density

In this way, in type II superconductors the current density  $\bar{J}$  which can flow without JOULE heating is limited not by the critical value  $j_c$  beyond which there is depairing of the COOPER pairs (see Chap. 8) and a return to the normal state as prescribed by the generalized SILSBEE criterion (see section 5.1), but by a critical current density  $J_c$  due to a quite different mechanism.

Indeed, in the SHUBNIKOV phase the electric current that is transported exerts forces on the vortices that tends to displace them (see section 7.1.1). There are two possible outcomes:

- » **First possibility:** The vortices, that are mobile, start to move. There is then displacement of the point where the forces are applied, production of work and dissipation of energy. To compensate this energy dissipation, it is necessary to provide electromotive work by applying a potential difference at the boundaries of the system. The superconductor no longer appears to be a perfect conductor: it becomes macroscopically resistive.
- » **Second possibility:** The vortices, trapped by defects in the material remain fixed. Without displacement of the points where the forces are applied, there is no work produced and therefore no energy dissipation. In this case the material transports the current without JOULE heating.

The critical current density then becomes the value of  $\bar{J}$  that leads to “unpinning” of the vortices. In the following we will denote this new critical current density  $J_c$ . It decreases when we approach the critical line  $H_{c2}$  or the critical temperature  $T_c$  and depends strongly on the mesoscopic structure and of the metallurgical state of the material. Introduction of impurities, defects and precipitates are parameters strongly influencing the value of this critical current density.

*In a soft superconductor, where vortices are easily displaced, the critical current density  $J_c$  is low; in contrast, it is high in a hard superconductor where vortices are strongly pinned.*

The critical current densities for depinning  $J_c$ , obtained after optimized thermal treatments, are between  $10^3$  and  $10^4 \text{ A mm}^{-2}$ . For comparison, copper wires in domestic appliances transport a few  $\text{A mm}^{-2}$ .

## 6.10 - Levitation in the presence of vortices

Vortex pinning brings a qualitative explanation to the special features of the levitation of type II superconductors that are seen with chips of high temperature superconductors such as YBaCuO. It differs from the levitation of type I superconductors in two respects. Firstly, the superconductor can be just as well in a levitated state above the magnet producing the field as in a suspended state below this magnet. Secondly, it tends to stay in a magnetic field of the same value as it was in when it made its transition into the superconducting state, and therefore this is how it is stabilized laterally.

These new effects appear when the superconductor has been cooled in a magnetic field, and has trapped vortices during the Normal/Superconducting transition. These vortices, behaving like strongly pinned canals by which the quantized flux crosses the sample, exert a restoring force on the superconducting material towards a magnetic field identical in form to the one it was cooled in. This includes the case when we invert the pair of magnet and superconducting chip. As we can convince ourselves by imagining vertical or horizontal displacements of the superconducting chip shown in Figure 6.19b, any departure from this position, while maintaining the tubes of magnetic flux that the vortices constitute, leads to a modification of the field lines outside the sample and leads to an increase in the magnetic energy. The effect of “restoring forces” is all the more efficient in that the cooling has taken place in a spatially varying magnetic field that has created curved vortices (Fig 6.19b). Of course, the stronger the pinning forces, the stronger the restoring force.

A small superconducting train can move in levitation or in suspension above or below a rail along which the magnetic field topology is identical to that in which it was cooled. On the other hand, it is subject to forces of reaction that act laterally or

at the ends of the line, as we can see in Figure 6.19d. As it wishes to conserve the flux carried by the “last vortex”, the sample deforms the external lines of magnetic field. This increases the energy of the system and, in reaction to this, the sample feels a restoring force. The vortices act in a sense like springs that are increasingly rigid as the pinning forces are made stronger.

We can obtain the same sort of behavior after cooling in zero field by forcing the sample into a position immediately adjacent to a magnet. The magnetic field must be sufficiently strong to make the vortices penetrate the sample. When the sample is released, it will find an equilibrium position in a weaker magnetic field within which the vortices become fixed.

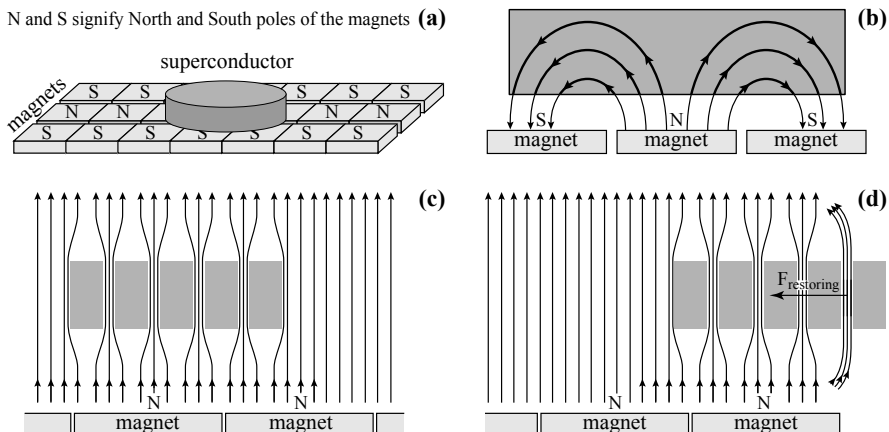


**Figure 6.19 - Displacement and stabilization of a superconducting block on a rail  
(hard superconductor cooled in a magnetic field)**

**(a)** Side view. **(b)** Front view. With a central track with “North pole upwards” and side tracks with “South pole upwards”, we have a rapid return of the field lines and a strong gradient of magnetic field which amplifies the repulsive forces. **(c)** The vortices tend to rest in a magnetic field whose topology is identical to the one they were created in. They can therefore move without friction along the rail. **(d)** When they arrive at the end of the rail, in a magnetic field different from the one that created them, the vortices feel a restoring force. The same type of restoring force guarantees the lateral stability of the superconductor.

## 6.11 - A few illustrations of the diverse behavior of vortices

Vortices depend on a multitude of parameters, such as the nature of the material, the geometry, the thermo-magnetic history of the sample, surface effects and even indirect parameters such as magneto-mechanical constraints. As a result, numerous stable or metastable configurations have been observed. We shall give examples to stimulate the curiosity of the reader, presenting five from a list that could be much longer.

### 6.11.1 - Effect of the demagnetizing field

To avoid further complications, the rôle of the demagnetizing field has been neglected in this chapter up to now. It is not absent, however, and can cause the appearance of phase mixtures similar to those we described in Chapter 5 for type I superconductors. For example, when the external field is close to  $H_{c1}$ , we can often observe a mixture of MEISSNER and SHUBNIKOV phases (Fig. 6.20).

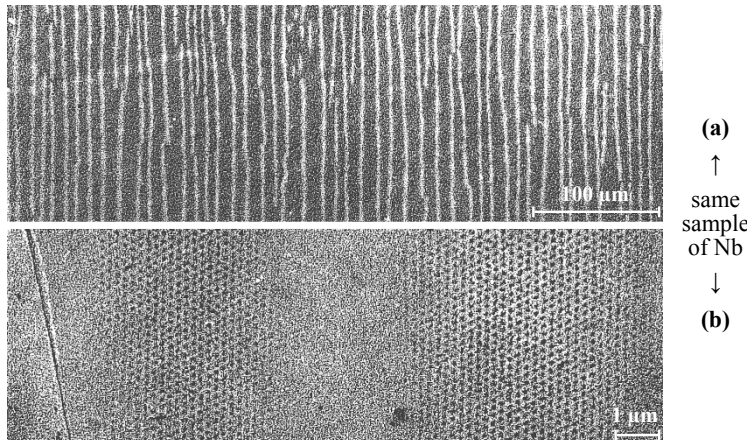


**Figure 6.20 - "Intermediate" state of MEISSNER and SHUBNIKOV phases**

Near  $H_{c1}$  and with demagnetizing fields, we sometimes see, with samples of materials at the type I-type II limit, coarse mixtures of MEISSNER and SHUBNIKOV phases reminiscent of the mixtures of normal and superconducting phases in the intermediate state of type I superconductors (section 5.6). The images were taken of a niobium disk 40 mm in thickness, 4 mm in diameter, at 1.2 K and in a field of 74 mT. (a) Optical image showing the coexistence of two lamellar phases. (b) Image by a scanning electron tunneling microscope showing that the alternating bands are of MEISSNER and SHUBNIKOV phases (note the difference of scale between the two images). [From BRANDT & ESSMANN, 1987, © Wiley-VCH Verlag GmbH & Co. KGaA]<sup>20</sup>

### 6.11.2 - Crystal growth by transported current

Just as for atomic arrangements, the ABRIKOSOV lattice can be a single crystal or poly-crystalline. Neutron diffraction, which averages the order over the whole macroscopic sample, revealed a polycrystalline structure for the vortex lattice in a sample of Pb-In ( $30 \times 5.5 \times 0.5 \text{ mm}^3$ ,  $T = 4 \text{ K}$ ,  $B^0 = 0.2 \text{ T}$ ). This 2D poly-crystal is formed of grains of about  $100 \mu\text{m}^2$ . In other words, taking into account the inter-vortex distance of 110 nm (relation 6.32), each grain contains of the order of  $10^4$  vortices.

The curious feature of this system is that when sufficient current is present to de-pin the vortices, the diffraction pattern develops a texture revealing the gradual

20 E.H. BRANDT & U. ESSMANN (1987) The Flux-Line Lattice in Type-II Superconductors, *Phys. Stat. Sol. B* **144**, 13.

formation of a single crystal (Fig. 6.21). The interpretation of the experimentalists was that numerous dislocations existing in the vortex lattice before the current passed were destabilized when the vortices were made to move. This is another proof of the interaction between the current transported and the vortex lattice.

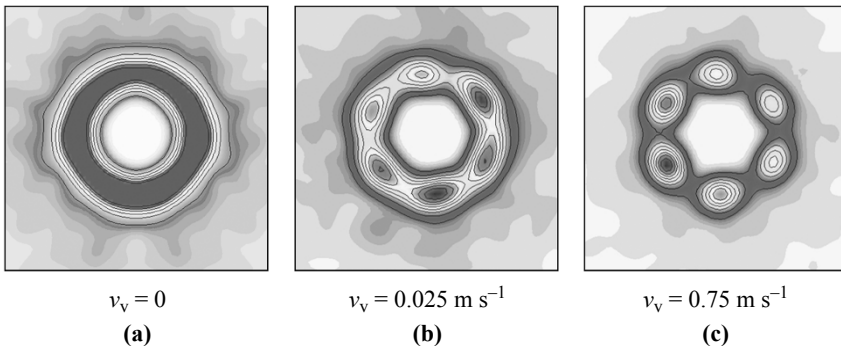


**Figure 6.21 - Poly-crystalline and mono-crystalline ABRIKOSOV lattice**

Neutron diffraction patterns from a plate of Pb-In alloy of dimension  $30 \times 5.5 \times 0.5 \text{ mm}^3$  at 4 K and in a magnetic field of 0.2 T: (a) In the absence of current, (b) and (c) with a current which, as its intensity increases, imparts to the the vortices the translational velocity indicated below each image. On a macroscopic scale the vortex lattice that was initially poly-crystalline ("powder" diffraction pattern) becomes progressively mono-crystalline. [From PAUTRAT *et al.*, 2005, © The American Physical Society]<sup>21</sup>

### 6.11.3 - Repulsion by surfaces

The most frequently found profile of the distribution of vortices is the "V-shaped", also called the "BEAN" profile, where the vortices stay concentrated close to the surface because of pinning by impurities and are pushed inside only when the applied magnetic field leads to the penetration of new vortices. There are situations, nonetheless, where a dome-like profile occurs. This happens in systems where the vortices, once they have overcome the surface barrier, are pushed towards the center of the sample and, because of the inter-vortex repulsion, they develop the profile shown in Figure 6.22a. This is a situation we would expect to find in defect-free samples where the extremely mobile vortices are subject to the repulsive forces from the MEISSNER currents and currents associated with the "corners" of the real samples, whose geometry differs from elliptical forms (geometric barriers). Most of the time, defects prevent the dome-shaped profile from developing, except in a few cases such as the compound MgB<sub>2</sub>.<sup>22</sup>

21 A. PAUTRAT *et al.* (2005), *Phys. Rev. B* **71**, 064517.

22 T. KLEIN, *personal communication* and L. LYARD *et al.* (2004) *Phys. Rev. B* **70**, 180. See also L. LYARD (2005) *MgB<sub>2</sub>, le supraconducteur à deux gaps, (MgB<sub>2</sub>, The Two-Gap Superconductor)* Thesis, University Joseph-Fourier, Grenoble, France.

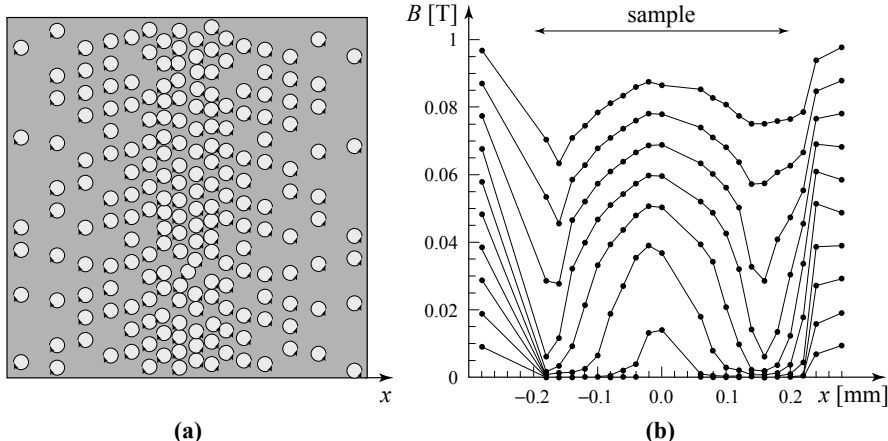


**Figure 6.22 - Distribution of vortices into a dome**

(a) In a certain number of systems of appropriate geometry, vortices that have overcome the surface barrier are pushed towards the center of the sample because of the interaction with surface currents where, owing to repulsive inter-vortex interactions, they assume a dome-like profile. (b) Example of a dome profile in plate-like samples of  $\text{MgB}_2$ . It was determined by measuring the average magnetic field carried by the vortices. [With the kind permission of T. KLEIN, NÉEL Institute, Grenoble, France]<sup>21</sup>

#### 6.11.4 - Trapping vortex lines by depressions in thin films

With the development of nanotechnologies, numerous studies have been made of the effects on superconducting properties and vortex behavior of the size of objects previously engraved on the sample surfaces. Many spectacular vortex configurations have been observed in these experiments.

As an example, in a niobium film of thickness  $d_f$ , circular depressions of depth  $d_b$  were etched (Fig. 6.23a). Above the critical temperature a magnetic field was applied perpendicular to the plane of the film, which was then cooled in the field. In spectacular fashion (Fig. 6.23b), the vortices are trapped around the depressions with, in addition, a vortex in the center if the hole is wide enough.

This experiment stimulates questions concerning the interaction between a vortex and a thick step, as well as the form of repulsion between vortices that can lead to such regular order.

#### 6.11.5 - Effects of confinement

While the effects of confinement had been predicted many years earlier,<sup>23</sup> advances in micro-engraving techniques allowed evidence for them to be given for objects

23 H.J. FINK & A.G. PRESSON (1966) *Phys. Rev.* **151**, 219;  
V.A. SCHWEIGERT, F.M. PEETERS & P.S. DEO (1998) *Phys. Rev. Lett.* **81**, 2783.

of size comparable to the characteristic lengths  $\lambda$  and  $\xi$ . Particularly revealing results in this respect were obtained in a series of experiments at the Institute of Nanosciences in Paris<sup>24</sup> on the visualization of vortices by microscopy and tunneling spectroscopy.

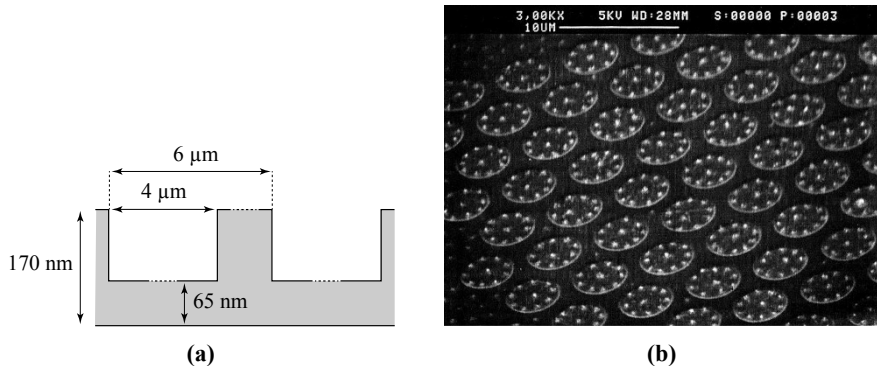


**Figure 6.23 - Vortices trapped in a triangular lattice of open micro-holes<sup>25</sup>**

(a) Open pits of depth  $d_f = 65 \text{ nm}$  and diameter  $\approx 4 \mu\text{m}$  were etched in a triangular lattice of periodicity  $\approx 6 \mu\text{m}$  in a niobium film of thickness  $d_f = 170 \text{ nm}$ . (b) After cooling in a field  $B^0 = 6.37 \cdot 10^{-4} \text{ T}$  the vortices, imaged by decoration, were concentrated along the perimeters, except for one found at the center of each pit. [With the kind permission of B. PANNETIER, NÉEL Institute, Grenoble, France]

A very instructive example is provided by the effects of a magnetic field on a mono-crystalline patch of lead, oriented in the (111) direction, that was fabricated by evaporation under high vacuum. The sample was a right-angled prism with rectangular base of sides  $d = 80 \text{ nm}$  and  $D = 140 \text{ nm}$  and of height  $h = 2.3 \text{ nm}$ , which represents eight single atomic layers.

In the bulk, lead is a type I superconductor ( $\lambda_0 \approx 50 \text{ nm}$ ,  $\xi_0 \approx 80 \text{ nm}$ ). Because of the reduction in the electron mean free path  $\ell$  to 2 or 3 times the height  $h$ , the characteristic lengths of the superconductivity are renormalized (see Table 6.5) to  $\lambda \approx \lambda_0 \sqrt{\xi_0 / \ell}$  and  $\xi \approx \sqrt{\xi_0 \ell}$ , which lead those authors to estimate that after adjustment:  $\xi \approx 27 \text{ nm}$  and  $\kappa = \lambda / \xi \approx 8$  ( $\lambda \approx 200 \text{ nm}$ ). With a GINZBURG-LANDAU parameter  $\kappa > 1/\sqrt{2}$ , the patch of lead then becomes a type II superconductor capable of bearing vortices.

As the width of the patch is within the range  $\xi < d \ll \lambda$ , we can question whether it is possible to place vortices whose size, typically of the order of the penetration depth  $\lambda$ , is much larger than the object and whose core  $\xi$  is not much smaller. A series of situations is encountered (Fig. 6.24):

24 T. CREN *et al.* (2009) *Phys. Rev. Lett.* **102**, 127005;  
T. CREN *et al.* (2011) *Phys. Rev. Lett.* **107**, 097202.

25 A. BEZRYADIN *et al.* (1996) *Phys. Rev. B* **53**, 8553.

- (a)  $B^0 = 0$ : there are neither screening current nor vortices.
- (b)  $B^0 = 0.2$  T: the patch is in the MEISSNER phase. Because its size is much less than the penetration depth, the LONDON currents extend as far as the middle of the sample but, even so, do not manage to screen the external magnetic field completely (see section 2.4.4).
- (c)  $B^0 = 0.6$  T: a vortex has penetrated the sample. Associated with its field are swirling currents that are superimposed on the LONDON currents flowing in the opposite sense. A line of vanishing current appears. The magnetic field flux through the surface bounded by this line is equal to one fluxon  $\phi_0$  (see section 9.5.3).
- (d)  $B^0 = 0.8$  T: a second vortex has penetrated the patch. The inter-vortex distance equals  $1.43 \xi$ , *i.e.* it is less than  $2.7 \xi$  that is the minimal distance predicted at  $H_{c2}$  where a bulk superconductor transits to the normal state (Eq. 6.34).
- (e)  $B^0 = 1$  T: a third vortex has penetrated the sample. The distance between vortices has again diminished and becomes of the order of  $\xi$ , *i.e.* three times smaller than the usual vortex-vortex distance at  $H_{c2}$ . We are in the presence of a super-dense “vortex phase.”
- (f)  $B^0 = 1.4$  T: the entrance of a fourth vortex has lead to a fusion of the cores and appearance of a giant vortex with a single core, at the expense of four individual vortices.

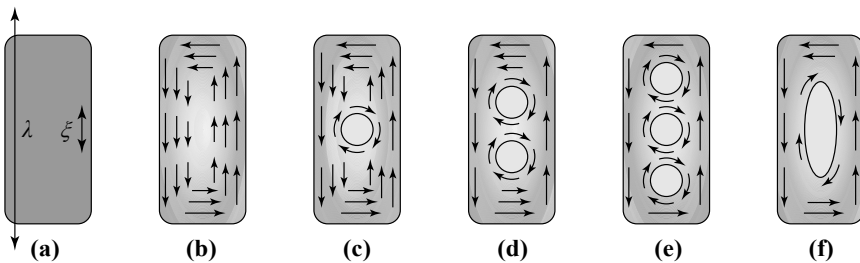


Figure 6.24 - Behavior of vortices in a confined space

The patch has the form of a right-angled prism with a nearly rectangular base (width  $d = 80$  nm, length  $D = 140$  nm) and a very small height (8 atomic layers,  $h = 2.3$  nm). The series of figures (a), (b), (c), (d), (e), (f) shows schematically the six situations described in the text as the magnetic field is raised. We observe the successive entry of vortices that become extremely close and eventually fuse into one giant vortex with a single core. The effective penetration depths and coherence lengths marked in Figure (a) allow us to compare the theoretical sizes of the core (diameter  $2\xi$ ) and the range of the vortex currents (diameter  $2\lambda$ ) of an unconfined vortex.

The restricted space has then caused, in this experiment, three effects:

- » a change in the nature of the superconductivity: in nanometric dimensions Pb becomes a type II superconductor;
- » the first effect of confinement: as soon as the second vortex enters, the inter-vortex distance is already smaller than the minimal distance between vortices in a bulk material;

- » the second effect of confinement: when the density of vortices becomes too great, they fuse and form a giant vortex with a single core and carrying several fluxons (see section 9.5.3).

## Chapter 7

# FIELDS AND CURRENTS IN TYPE II SUPERCONDUCTORS MODELS OF THE CRITICAL STATE

Transport of electric current, without losses by the JOULE effect, and the generation of intense magnetic fields constitute the most important industrial uses of superconducting wires. In order to optimize performance, they must be capable of bearing current densities and magnetic fields as high as possible. Because they have a critical magnetic field  $B_c = \mu_0 H_c$  that is always low, type I superconductors never have the properties needed. The same is true for type II superconductors in the MEISSNER regime since  $B_{c1} = \mu_0 H_{c1}$  is generally less than a few hundredths of a tesla. Industrial electromechanical applications can be imagined only in the SHUBNIKOV phase, with stability limited by the magnetic field  $B_{c2} = \mu_0 H_{c2}$ , which can reach several dozens, or even hundreds, of teslas. It is therefore of prime importance to understand the mechanisms of magnetization and current transport in this phase so we might prevent, or at least slow, energy dissipation, notably in preventing vortex motion (see section 6.9.3).

### 7.1 - Forces acting on vortices

In a type II superconductor with a large GINZBURG-LANDAU parameter  $\kappa = \lambda/\zeta$ , a vortex element of unit length, in the presence of a current density  $\mathbf{J}$  external to the vortex, is subject to a force<sup>1</sup>

$$\mathbf{f}_\phi = \mathbf{J} \times \phi_0 \hat{\mathbf{u}} \quad (7.1)$$

where  $\hat{\mathbf{u}}$  is the unit vector parallel to the vortex axis and pointing in the direction of the magnetic field that this vortex carries.<sup>2</sup> Because of its form,  $\mathbf{f}_\phi$  is often called the “LORENTZ force” or “LORENTZ-like force” even if its origin and interpretation are still the subject of much debate (see App. 7A).

This general result covers several special situations that differ according to the origin of the current density  $\mathbf{J}$ .

---

1 J. FRIEDEL, P.G. DE GENNES & J. MATRICON (1963) *Appl. Phys. Lett.* **2**, 119.

2 Sometimes the vector  $\phi_0$  of norm  $\phi_0$ , oriented in the direction of the magnetic field carried by the vortex is used. The force acting per unit length of the vortex is then  $\mathbf{J} \times \phi_0$ .

### 7.1.1 - Force exerted on a vortex by a transported current

The first situation we consider is when the current density  $\mathbf{J}$ , in the  $y$  direction, carries a continuous current across the LONDON regions of the vortices that are present (see Fig. 6.18).

As seen in Figure 7.1, the force acting on each vortex is transverse and directed perpendicularly to the direction of the current.

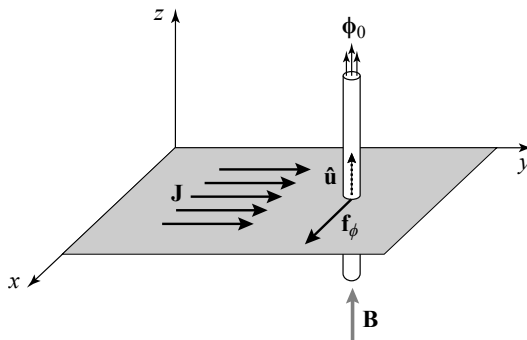


**Figure 7.1**  
**Force acting on a vortex in the presence of a uniform current density  $\mathbf{J}$**   
 In the presence of a uniform superconducting current density  $\mathbf{J}$ , a vortex is subjected to a transverse force given by the relation (7.1).

### 7.1.2 - Interaction forces between vortices

#### Force between two vortices

The second situation is when two vortices V1 and V2 are sufficiently close that each interacts with the vortex current of the other. An element of unit length of the vortex V1, which feels the current density  $\mathbf{j}_2$  associated with the vortex V2 (Fig. 7.2), is subject to a repulsive force from that vortex,

$$\mathbf{f}_{1-2} = \phi_0 \mathbf{j}_2 \times \hat{\mathbf{u}}_1 \quad (7.2)$$

where  $\hat{\mathbf{u}}_1$  is the unit vector along the axis of vortex V1. In return the vortex V2 feels an equal but opposite force from V1.

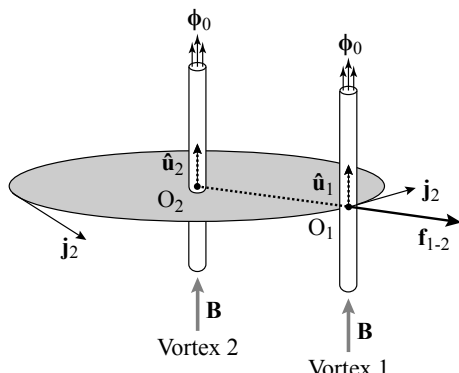


**Figure 7.2**  
**Repulsive force between two vortices**  
 As each vortex feels the vortex current of the other, it experiences a repulsive force given by (7.2).

### Force on a vortex within a group of vortices

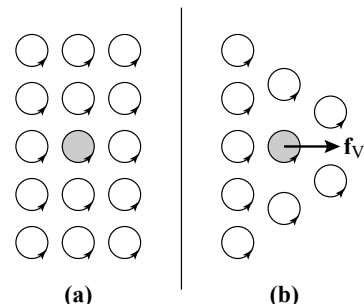
Within a group, each vortex interacts with the current density  $\mathbf{J}$  that results from the superposition of the vortex current densities associated with all the others. Two situations merit particular attention:

- » the vortices are uniformly spaced, in a lattice for example. The forces associated with the current densities of neighboring vortices compensate one another and the resultant force vanishes (Fig. 7.3a);
- » the vortices are not uniformly spaced. There is no longer compensation and each vortex is subject to a net force that pushes it towards regions with relatively few other vortices (Fig. 7.3b).

**Figure 7.3**

#### Force felt by a vortex situated in a mass of vortices

If it is in a mass of uniform density, (a), a vortex is subject to no force because of the compensation of vortex currents associated with neighboring vortices. In a non-uniform mass (b), it feels a force directed towards regions of low vortex concentration.



### Force density

While it is interesting to know the force acting on a particular vortex, in fact it is more relevant to introduce the average force  $\bar{\mathbf{f}}_\phi(\mathbf{r})$ <sup>3</sup> that acts on each of the vortices situated in the vicinity of the point  $\mathbf{r}$  where there is an average magnetic field  $\bar{\mathbf{B}}(\mathbf{r})$ . As it is carried by the vortices themselves,  $\bar{\mathbf{B}}(\mathbf{r})$  is related to their surface density<sup>4</sup>  $n_v(\mathbf{r})$  by the expression

$$\bar{\mathbf{B}}(\mathbf{r}) = n_v(\mathbf{r})\phi_0 \hat{\mathbf{u}}. \quad (7.3)$$

Since the average local current density  $\bar{\mathbf{J}}(\mathbf{r})$  that interacts with the vortices is related to  $\bar{\mathbf{B}}$  by the fourth MAXWELL's equation, the average force acting on each vortex, per unit length is

$$\bar{\mathbf{f}}_\phi = \bar{\mathbf{J}} \times \phi_0 \hat{\mathbf{u}} \quad (7.4)$$

with

$$\mu_0 \bar{\mathbf{J}} = \nabla \times \bar{\mathbf{B}}. \quad (7.5)$$

<sup>3</sup> We recall that a bar over a physical quantity represents a *local* average, while brackets indicate an average *over the whole sample*.

<sup>4</sup> The surface density of vortices is the number of vortices that cross a unit surface area perpendicular to their common axis.

To make sense, the averages need to be made over volumes containing a sufficient number of vortices and are restricted to distributions where  $n_v$  varies slowly in space.

Finally, in this context of averaging, we introduce the bulk force density  $\mathbf{F}_\phi(\mathbf{r})$ , the net force acting on all of the vortices situated in a unit element of volume around the point  $\mathbf{r}$ . This force per unit of volume equals the average force per unit length of the vortex, multiplied by the vortex density, or

$$\mathbf{F}_\phi = n_v \bar{\mathbf{f}}_\phi = \bar{\mathbf{J}} \times n_v \phi_0 \hat{\mathbf{u}} = \bar{\mathbf{J}} \times \bar{\mathbf{B}}. \quad (7.6)$$

## 7.2 - Energy dissipation by vortex displacement

### 7.2.1 - Model of vortex flow

Under the effects of the driving force  $\bar{f}_\phi$  that is written, when the current density is perpendicular to the direction of the vortices,

$$\bar{f}_\phi = \bar{J}\phi_0 \quad (7.7)$$

each vortex can move. At the speed  $v_v$ , it feels a drag force with the damping coefficient  $\eta$

$$f_\eta = -\eta v_v \quad (7.8)$$

leading to the equation of motion,

$$\bar{f}_\phi = m_v \frac{dv_v}{dt} + \eta v_v \quad (7.9)$$

where  $m_v$  represents an “effective mass” per unit length of a vortex. In the steady state, reached when  $dv_v/dt = 0$ , the vortices move with a velocity

$$v_v = \frac{\bar{f}_\phi}{\eta} = \frac{\bar{J}\phi_0}{\eta} \quad (7.10)$$

which implies dissipation  $p$  per unit vortex length of

$$p = \bar{f}_\phi v_v = \frac{\bar{J}^2 \phi_0^2}{\eta} \quad (7.11)$$

and a power  $\mathcal{P}$  dissipated per unit volume of the material,

$$\mathcal{P} = \frac{n_v \phi_0^2}{\eta} \bar{J}^2 = n_v \eta v_v^2. \quad (7.12)$$

By analogy with the dissipative regime of a conductor of resistivity  $\rho$  that dissipates power per unit volume of  $\rho j^2$ , we define the flux-flow resistivity  $\rho_{ff}$  by

$$\mathcal{P} = \rho_{ff} \bar{J}^2 \quad i.e. \quad \rho_{ff} = \frac{n_v \phi_0^2}{\eta}. \quad (7.13)$$

This dissipated power can only be compensated by a generator, the only external element connected to the superconductor. To drive the current  $I$ , it must maintain its terminals at a potential difference  $V$  such  $\mathcal{P} = VI$ .

### 7.2.2 - Induced electric field

According to FARADAY's law of induction the voltage induced across the ends of a filament equals

$$V = + \frac{\delta\phi_{\text{cut}}}{\delta t} \quad (7.14)$$

where  $\phi_{\text{cut}}$  is the magnetic flux cut by the filament in its relative movement. We consider a sample in the form of a plate (Fig. 7.4) of length  $b$  in the  $y$  direction and of width  $a$  in the  $x$  direction and we specify, in the  $x$  direction a slice of dimension  $\delta a$  sufficiently small that it can be considered as a "filament" of length  $b$ . As the current is flowing in the  $y$  direction the vortices oriented in the  $z$  direction move transversely, in the  $x$  direction.

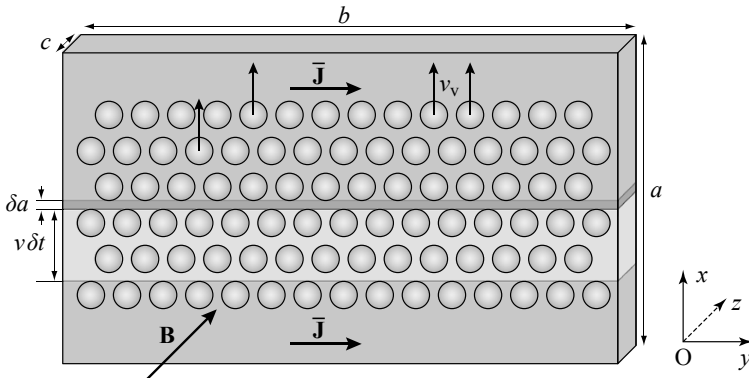


**Figure 7.4 - Electromotive force induced by the displacement of vortices**

The potential difference (electromotive force) between the ends of a filament equals  $V = + \delta\phi_{\text{cut}} / \delta t$  where  $\delta\phi_{\text{cut}}$  is the flux cut by the wire during the time  $\delta t$ .

The vortices that cross the line defined by the "filament" between  $t$  and  $t + \delta t$  are located, at the instant  $t$ , within a surface element  $dS_{\text{cut}} = bv_v \delta t$ , leading to the flux change

$$\delta\phi_{\text{cut}} = \bar{B} dS_{\text{cut}} = (n_v \phi_0)(bv_v \delta t) \quad (7.15)$$

and to a potential difference between the extremities of the "filament", and therefore of the plate that is constituted of parallel "filament",

$$V = \frac{\delta\phi_{\text{cut}}}{\delta t} = n_v \phi_0 b v_v. \quad (7.16)$$

Using expression (7.10) for the speed of displacement of the vortices, the electric field in the plate can be written as

$$E = \frac{V}{b} = \frac{n_v \phi_0^2}{\eta} \bar{J} = \rho_{ff} \bar{J} \quad (7.17)$$

where again the flux-flow resistivity appears, this time through the usual relation between the electric field  $E$  and the current density  $\bar{J}$ .

### 7.2.3 - The BARDEEN-STEPHEN model

The microscopic mechanism at the origin of energy dissipation is rather complex. The model developed by BARDEEN and STEPHEN,<sup>5</sup> reproduced in Appendix 7B, shows that movement of a vortex induces in its core an electric field. Subjected to this field, the *normal electrons* found in the core move and dissipate energy by JOULE heating.

According to this model the damping coefficient can be written

$$\eta = \frac{\phi_0}{\rho_n} \mu_0 H_{c2} \quad (7.18)$$

and the flux-flow resistivity  $\rho_{ff}$ , related to the damping coefficient by the relation (7.13) becomes

$$\rho_{ff} = \frac{n_v \phi_0^2}{\eta} = \rho_n \frac{n_v \phi_0}{\mu_0 H_{c2}} = \rho_n \frac{\bar{B}}{\mu_0 H_{c2}}, \quad (7.19)$$

an expression that is to be compared to the empirical relation proposed by KIM and STEPHEN starting from an analysis of experimental results<sup>6</sup> (Fig. 7.5)

$$\rho_{ff} = \rho_n \frac{B^0}{\mu_0 H_{c2}} f\left(\frac{T}{T_c}\right). \quad (7.20)$$

## 7.3 - Critical current density in type II superconductors

### 7.3.1 - Pinning force

So far we have not taken into account defects such as micro-cavities, impurities, precipitates, dislocations, and so forth, all of which can act to trap vortices and hinder their motion.

The vortices, which interact strongly among one another and respond collectively, are only freed by application of a bulk force density  $F_\phi$  greater than a “bulk pinning force” density  $F_p$ <sup>7</sup> that depends on the nature of the defects (chemical composition, size, concentration, distribution), but is also a function of the rigidity of the vortex lattice, the applied field and the temperature.

5 J. BARDEEN & M.J. STEPHEN (1965) *Phys. Rev.* **140**, A1197.

6 Y.B. KIM & M. J. STEPHEN (1969) in *Superconductivity*, R.D. PARKS ed., Marcel Dekker, N.Y.

7 We recall the definition: the bulk force is the force applied to the whole set of vortices contained in a unit volume.

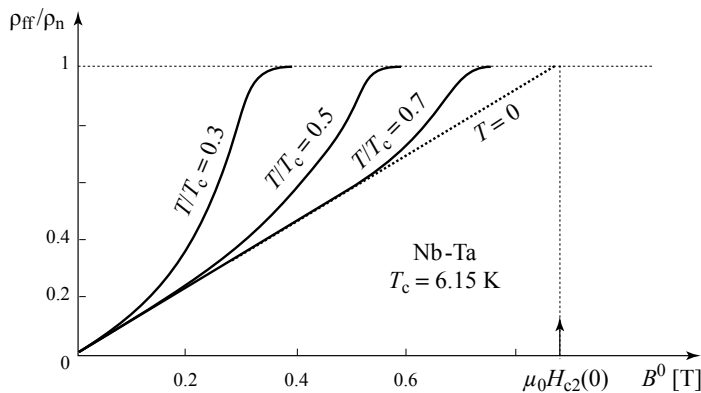


**Figure 7.5 - Flux-flow resistivity**

Flux-flow resistivity of a niobium-tantalum tape at different temperatures as a function of the applied magnetic field. The dotted line is the extrapolation to  $T = 0$  K; its intersection with  $\rho_{ff}/\rho_n = 1$  gives to  $\mu_0 H_{c2}(0) = 0.86$  T. [From Kim et al., 1964, © The American Physical Society, with permission]<sup>8</sup>

### 7.3.2 - Critical current density

Subject to bulk force densities  $F_\phi$  from the interaction with the current density, the vortices do not move (collectively) as long as  $F_\phi < F_p$ . De-pinning occurs when  $F_\phi$  becomes at least equal to  $F_p$ , that is, when the current density  $\bar{J}$  attains a critical density  $J_c$  that, taking (7.6) into account, is related to  $F_p$  and the average field  $\bar{B}$  by

$$J_c = \frac{F_p}{\bar{B}} = \frac{F_p}{n_v \phi_0} \quad (7.21)$$

which leads us to specify that the regime becomes dissipative when  $\bar{J} > J_c$  or, because of (7.5), when  $|\nabla \times \mathbf{B}| > \mu_0 J_c$ .

It is therefore equivalent to say that the vortices only start to move locally and that energy dissipation appears when any (and therefore all) of the following hold

$$F_\phi > F_p \Leftrightarrow \bar{J} > J_c \Leftrightarrow |\nabla \times \mathbf{B}| > \mu_0 J_c. \quad (7.22)$$

In general,  $F_p$  and therefore  $J_c$  depend on the temperature  $T$  and on the field  $\bar{B}$ .

### 7.3.3 - Return to the flux-flow resistivity

In a dynamical regime, the driving force exerted on each vortex becomes equal to the difference between the force  $\bar{f}_\phi = F_\phi / n_v$  of interaction with the current and the pinning force  $\bar{f}_p = F_p / n_v$  that resists the movement. Including the damping force  $f_\eta = -\eta v_v$  that must be added, the equation of motion becomes

<sup>8</sup> Y.B. Kim et al. (1964) *Phys. Rev. Lett.* **13**, 794.

$$\bar{f}_\phi - \bar{f}_P = m_v \frac{dv_v}{dt} + \eta v_v \quad (7.23)$$

or, using (7.1) and (7.21),  $\bar{f}_\phi - \bar{f}_P = \phi_0 (\bar{J} - J_c)$  (7.24)

which leads to a speed of displacement in the steady state

$$v_v = \frac{(\bar{J} - J_c)\phi_0}{\eta} \quad (7.25)$$

and to a voltage between the ends of the ribbon

$$V = \frac{\delta\phi_{cut}}{\delta t} = n_v \phi_0 b v_v = n_v \phi_0 b \frac{(\bar{J} - J_c)\phi_0}{\eta} \quad (7.26)$$

which, with the expression for  $\rho_{ff}$  (7.13), can be written

$$V = \rho_{ff} b (\bar{J} - J_c). \quad (7.27)$$

Such a relation of proportionality between an increment of current density  $\delta\bar{J}$  and the resulting increment of voltage  $\delta V$ ,

$$\frac{\delta V}{\delta \bar{J}} = \rho_{ff} b \quad (7.28)$$

means that the flux-flow resistivity, the dynamical resistivity introduced in section 7.2.1, has only a weak dependence on  $J_c$  and, to a certain extent, on the metallurgical state of the sample.

Even if the transition between resistive and non-resistive states is not as clearly defined as this model predicts, the proportionality between  $\delta V$  and  $\delta\bar{J}$  is verified by experiment, as we can see in Figure 7.6, where two samples of Nb-Ta, after different thermal treatments, show identical voltage/current slopes above  $J_c$ .

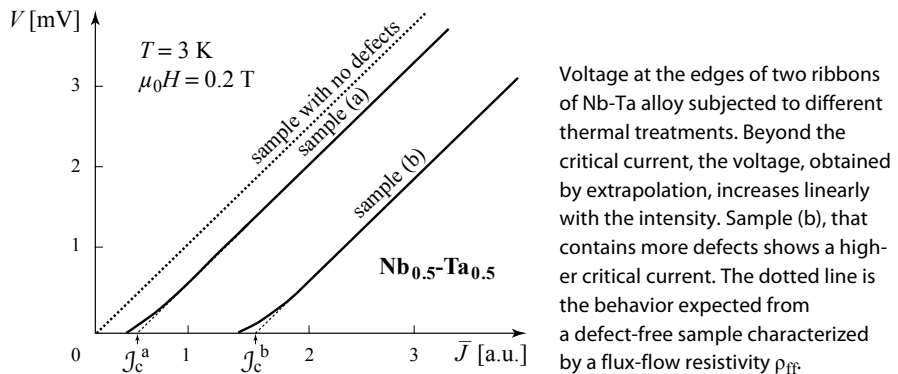


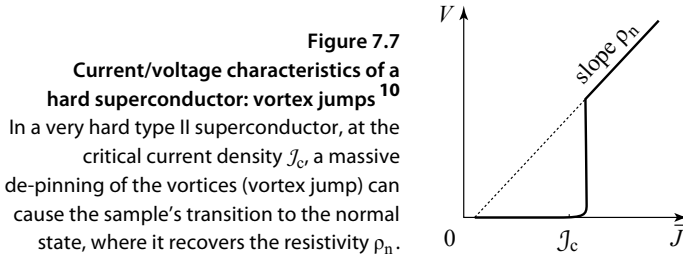
**Figure 7.6 - Current/voltage characteristics of a soft Nb-Ta alloy: flux flow**  
[From STRAND *et al.*, 1964, ©The American Physical Society, with permission]<sup>9</sup>

9 A. STRAND *et al.* (1964) *Phys. Rev. Lett.* **13**, 794.

This result confirms the idea that unlike the pinning force density and the critical current densities,  $\eta$  depends weakly on the metallurgical state of the sample and hence on the structure of its defects.

#### 7.3.4 - Vortex jumps

When superconductors are very hard, the critical current density becomes very large and in addition to flux flow, we can see vortex jumps due to the de-pinning of packets of vortices that were under great stress. The massive displacement of vortices is accompanied by a high production of heat, that can provoke the transition of the superconductor to its normal state. The resistivity then changes directly to that of the normal metal (Fig. 7.7).



Vortex jumps also exist in the case of temperature fluctuations. By reducing the pinning force density  $F_p$ , which can become less than  $F_\phi$ , a local heat fluctuation may be capable of producing a sudden vortex movement that dissipates heat, and thus an amplification of the thermal fluctuation, and finally an avalanche effect that can transform the material from the superconducting to the normal state. Vortex jumps are feared in superconducting coils that can, by this stochastic process, suddenly transit towards the normal state. An example of this will be given in Figure 7.18.

#### 7.3.5 - Vortex flux creep

To distinguish it from “flux flow”, which describes the displacement of vortices under the effect of the force density  $F_\phi - F_p$ , the term *flux creep* is used to denote the effects of de-pinning and mobility of vortices by thermal activation when  $F_\phi < F_p$ .

In superconductors with low critical temperatures, the effect is relatively limited because of the collective behavior of the vortices due to the rigidity of their lattice. This means that the height of the barrier to surmount is not the pinning energy of the individual vortex, but the much higher energy for a group of strongly bound

---

10 E.W. COLLINGS (1986) Applied Superconductivity, *The International Cryogenics Monograph Series*, volume 2, section 18, Plenum Press, New York.

vortices. In general the phenomenon of flux creep remains slow and is significant only when the difference between  $F_p$  and  $F_\phi$  becomes small.

In High critical Temperature Superconductors (HTS), the effect is more pronounced because of the weakness of pinning forces, which reduces the height of the barrier, of the effects of anisotropy, and of the higher temperatures at which they can be used, which increase exponentially the probability of crossing the barrier.

### 7.3.6 - Other behavior

If the current-voltage curves of Figures 7.6 and 7.7 are the most standard, they are far from universal, and specific behavior for the different vortex phases (see Fig. 6.17) has been predicted and observed.<sup>11</sup> Among these, we find those of Figure 7.8 that concern vortex liquids with pinning centers and vortex glasses. In particular, the vortex liquid with pinning centers shows “Thermally Assisted Flux-Flow” (TAFF) before it recovers to the ideal flux-flow regime, for which the curve of constant resistance passes through the origin.

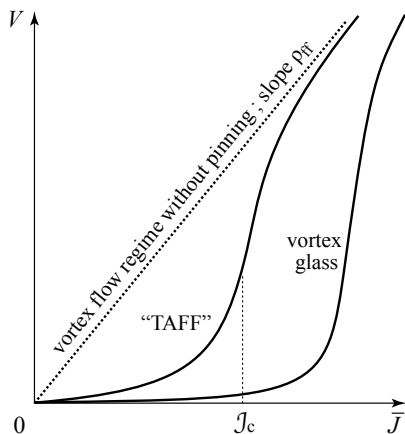


**Figure 7.8**  
**Current/voltage**  
**characteristics of selected phases**  
 The vortex liquid with pinning shows a Thermally Assisted Flux-Flow (TAFF) regime which joins the flux-flow regime (the curve with constant resistance passing through the origin). [From BLATTER *et al.*,<sup>11</sup> © Review of Modern Physics]

## 7.4 - Models of the critical state

### 7.4.1 - Critical state

During current transport, or in response to an external magnetic field, the superconductor in the SHUBNIKOV phase carries a local average current density  $\bar{J}(\mathbf{r})$ . In the non-dissipative regime, in other words in an equilibrium state where the vortices do not move, the distribution of  $\bar{J}$  is very different from what is seen in type I superconductors, and it can be described well by critical state models.

11 G. BLATTER *et al.* (1994) *Rev. Mod. Phys.* **66**, 1125.

*Critical state models require that at equilibrium, at each point of the superconductor, the current density  $\bar{J}$  must either be equal to the critical current density  $J_c$ , or be zero.*

The justification is provided by the following argument, considering first the points where there are vortices and then those without vortices:

- » at a point where vortices are present and are static (equilibrium situation),  $\bar{J}$  cannot exceed  $J_c$ , since otherwise the vortices would begin to move. Neither can  $\bar{J}$  be less than  $J_c$  since at some previous time the current density must have been greater than  $J_c$  in order to have moved the vortices to this point. Subsequently, when  $\bar{J}$  has returned to the value  $J_c$  because of their reorganization, the vortices can no longer move and  $\bar{J}$ , which depends on their distribution (relations 7.3 and 7.5), cannot decrease any further;
- » in the opposite situation, at a point where there are no vortices, by the same argument none could ever have been there in the past.  $\bar{B}$ , which is related to the vortex density by (7.3) must always have vanished, and  $\bar{J}$ , which is related to  $\bar{B}$  by (7.5), equals zero.

Following the relations (7.22), we therefore have the equivalent statements valid wherever there are vortices

$$\text{Critical state} \Leftrightarrow F_\phi = F_p \Leftrightarrow \bar{J} = J_c \Leftrightarrow |\nabla \times \bar{\mathbf{B}}| = \mu_0 J_c. \quad (7.29)$$

#### 7.4.2 - Laws of behavior

As a precise determination of the pinning forces and their dependence on field and temperature turns out to be complex, engineers mostly use phenomenological laws for critical currents that are easier to handle. The simplest formulation was proposed by BEAN<sup>12</sup> with a model requiring that critical current density  $J_c^{\text{Bean}}$  to be independent of  $\bar{B}$  and to be a function only of the temperature

$$J_c^{\text{Bean}} = \alpha(T) \quad (\text{critical BEAN equation}). \quad (7.30)$$

This model is easy to use and allows us to give a rough idea, often sufficient, of the distribution of the vortices, magnetic fields and current densities in a sample subject to an applied magnetic field and/or carrying a current, notably as a function of its magnetic history.

The price to pay for this simplicity is that it cannot cope with certain situations, and most importantly, cannot include the response of the superconductor subjected to high magnetic fields. To mitigate this, other more complicated laws have been proposed with additional adjustable parameters, ( $B_K$  and  $\beta$ ):

---

12 C.P. BEAN (1962) *Phys. Rev. Lett.* **8**, 250.

» the critical equation of KIM-JI <sup>13</sup>       $\mathcal{J}_c^{KJ} = \frac{\alpha(T)}{\bar{B}/B_K},$       (7.31a)

» the critical equation of KIM <sup>14</sup>       $\mathcal{J}_c^{Kim} = \frac{\alpha(T)}{1 + \bar{B}/B_K},$       (7.31b)

» the generalized critical equation <sup>15</sup>       $\mathcal{J}_c^G = \frac{\alpha(T)}{(1 + \bar{B}/B_K)^\beta}.$       (7.31c)

Essentially these laws incorporate the way in which  $\mathcal{J}_c$  decreases as a function of  $\bar{B}$  when the magnetic field approaches  $B_{c2}$ .

## 7.5 - The BEAN model

### 7.5.1 - Increasing field: vortex penetration

Consider now a semi-infinite superconducting medium bounded by the  $yz$  plane through the origin (the other surface is very far away) and subject to a uniform field  $\mathbf{B}_1^0$  oriented in the  $z$  direction. Anticipating the final results, we assume that inside the sample the magnetic field  $\bar{B}_z(x)$  decreases linearly, from its value  $B_1^0$  at the surface, where  $x = 0$ , with a slope equal to  $-\mu_0 \mathcal{J}_c^{\text{Bean}}$  (Fig. 7.9a). Let  $x_1$  be the  $x$ -coordinate of the point for which  $\bar{B}(x_1) = 0$  (the position of the “vortex front”).

$$0 < x < x_1 \quad \bar{J}_y(x) = -\frac{1}{\mu_0} \frac{\partial \bar{B}_z}{\partial x} = -\frac{1}{\mu_0} \phi_0 \frac{\partial \bar{n}_v(x)}{\partial x} = \mathcal{J}_c^{\text{Bean}} \quad (7.32)$$

$$x > x_1 \quad \bar{J}_y, \bar{B}_z \text{ and } n_v \text{ are zero.}$$

Suppose we now change the field at the surface to a new value  $B_2^0 > B_1^0$  (Fig. 7.9a). The redistribution of vortices is not instantaneous, so that initially  $\bar{B}_z(x)$  stays unchanged, except close to the surface where by continuity of the magnetic field,  $-\partial \bar{B}_z / \partial x$ , which is the only non-zero component of  $\nabla \times \mathbf{B}$ , becomes greater than  $\mu_0 \mathcal{J}_c^{\text{Bean}}$ . This local magnetic field gradient (see 7.22) generates a force density  $F_\phi$  acting on vortices near the surface that is greater than the pinning force density  $F_p$ , pushing them towards the interior of the sample, and in this way stimulates the entry of new vortices.

The penetration of the vortices and their displacements towards the interior of the material continues as long as there is some point where  $F_\phi$  is greater than  $F_p$ , that is where  $\bar{J}_y$  exceeds  $\mathcal{J}_c^{\text{Bean}}$ . The process of entry and migration of vortices comes to an end only when the condition (7.29)  $|\nabla \times \mathbf{B}| = \mu_0 \mathcal{J}_c$  is again satisfied,

13 L. JI *et al.* (1989) *Phys. Rev. B* **40**, 1936.

14 Y.B. KIM, C.F. HEMPSTEAD & A.R. STRNAD (1962) *Phys. Rev. Lett.* **9**, 306.

15 Q.H. LAM, Y. KIM & C.D. JEFFRIES (1990) *Phys. Rev. B* **42**, 4846;  
M. XU, D. SHI & R. FOX (1990) *Phys. Rev. B* **42**, 1773.

i.e. when we again find  $\bar{J}_y(x) = -\frac{1}{\mu_0} \frac{\partial \bar{B}_z}{\partial x} = J_c^{\text{Bean}}$ .

In this new equilibrium state, the average magnetic field decreases linearly with slope  $-\mu_0 J_c^{\text{Bean}}$  from the value  $B_2^0$  at  $x = 0$ , until  $\bar{B}_z = 0$  at  $x_2$ . Beyond this, it stays at zero (Fig. 7.9b).

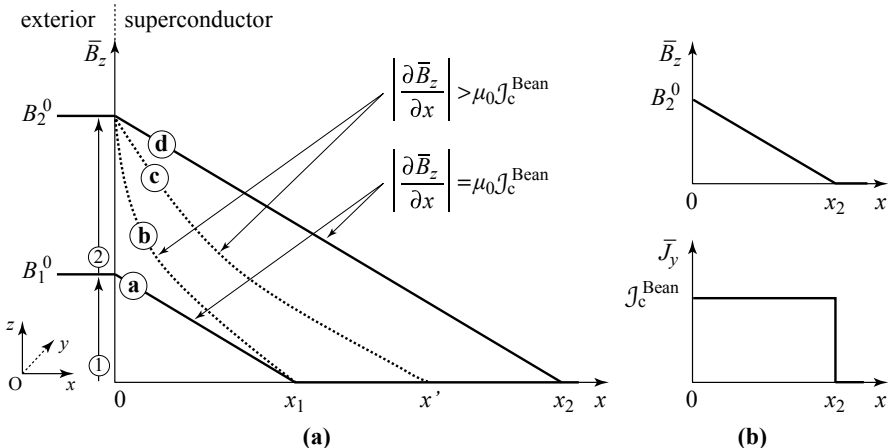


**Figure 7.9 - Model for the penetration of vortices in increasing field: advance of a vortex front**

(a) As the field at the surface increases from  $B_1^0$  to  $B_2^0$ , the field distribution in the interior of the superconductor evolves progressively from  $\bar{B}_{1z}(x)$  (curve a) to  $\bar{B}_{2z}(x)$  (curve d). Hypothetical intermediate stages (curves b and c) where  $\bar{J}_y(x) = -\frac{1}{\mu_0} \frac{\partial \bar{B}}{\partial x} > J_c^{\text{Bean}}$  are dotted.

The equilibrium profile decreases linearly with slope  $\bar{J}_y(x) = -\frac{1}{\mu_0} \frac{\partial \bar{B}}{\partial x} = J_c^{\text{Bean}}$ . Hypothetical intermediate stages (curves b and c) where  $\bar{J}_y(x) = -\frac{1}{\mu_0} \frac{\partial \bar{B}}{\partial x} > J_c^{\text{Bean}}$  are dotted.

(b) Profile of the average magnetic field  $\bar{B}_{2z}(x)$  and the average current density  $\bar{J}_y(x)$  in equilibrium after application of the magnetic field  $B_2^0$ .

A further increase of the external field would induce a new displacement of the vortex front and a new linear profile of the magnetic field satisfying  $\bar{J}_y = J_c^{\text{Bean}}$  which justifies, *a posteriori*, the profile of  $\bar{B}_{1z}(x)$  we initially assumed, at least if we are discussing the history the first time the field is raised.

The current density  $J_c^{\text{Bean}}$  that flows between  $x = 0$  and the vortex front plays the role of a screening current which maintains a vanishing magnetic field beyond the vortex front.

It differs, however, in nature from the screening current encountered in type I superconductors or type II superconductors in the MEISSNER phase, where the current density decreases exponentially over the penetration depth  $\lambda$ , independently of the applied field.

In the BEAN model the current density is uniformly equal to  $J_c^{\text{Bean}}$  between the surface and the vortex front, whose position is a function of the field at the surface and the critical current density (Fig. 7.9b).

We note, however, that by assuming continuity between  $B^0$  and  $\bar{B}$ , we did not take into account the LONDON currents flowing near the external surfaces.

### 7.5.2 - Decreasing field: field profile and the vortex distribution

Starting from the highest previous value  $B_2^0$ , we now decrease the applied field down to a value  $B_3^0 < B_2^0$  (Fig. 7.10).

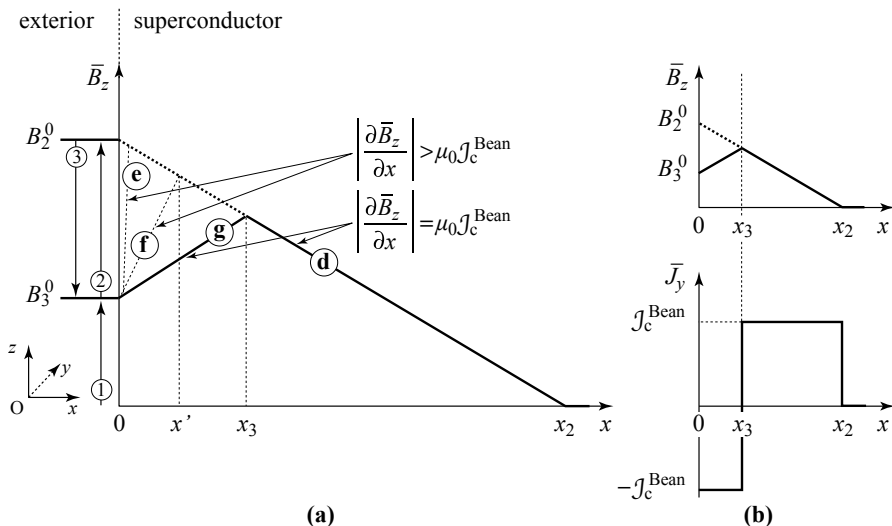


**Figure 7.10 - Evolution of the profile of the magnetic field for decreasing magnetic field**

(a) With the field at the surface decreased from  $B_2^0$  to  $B_3^0$ ,  $\bar{B}_z(x)$  now follows the dashed line (d, g) where everywhere  $\left| \frac{\partial \bar{B}_z(x)}{\partial x} \right| = \mu_0 J_c^{\text{Bean}}$ . The dotted lines (e, f) represent hypothetical intermediate states in which  $\left| \frac{\partial \bar{B}_z(x)}{\partial x} \right| > \mu_0 J_c^{\text{Bean}}$ . (b) Profile of the average magnetic field  $\bar{B}_{3z}(x)$  and of the average current density  $\bar{J}_y(x)$  at equilibrium after application  $B_3^0$ , following the previous value  $B_2^0$ .

As in the preceding section, a steep field gradient  $\partial \bar{B}_z(x) / \partial x$ , this time positive, immediately appears close to the surface and, it is accompanied by a current density  $\bar{J}_y$  greater than the critical current density flowing in the  $-y$  direction. This current density imparts to the vortices involved a force density  $F_\phi > F_F$  which now moves them towards the surface, until they are ejected from the material. The process continues until  $\bar{J}_y$  nowhere exceeds  $J_c^{\text{Bean}}$ , leading to a field profile with

$$0 < x < x_3 \quad \frac{\partial \bar{B}_z(x)}{\partial x} = \mu_0 J_c^{\text{Bean}}$$

$$\begin{aligned} x_3 < x < x_2 \quad \frac{\partial \bar{B}_z(x)}{\partial x} &= -\mu_0 J_c^{\text{Bean}} \\ x > x_2 \quad \bar{B}_z(x) &= 0 \end{aligned} \quad (7.33)$$

where  $x_3$  is the  $x$ -coordinate of the plane where the current  $\bar{J}_y$  changes sign.

When subsequently the magnetic field at the surface takes values  $B_4^0$ , and then  $B_5^0$ , we obtain profiles of the average fields and current densities as shown in Figure 7.11.

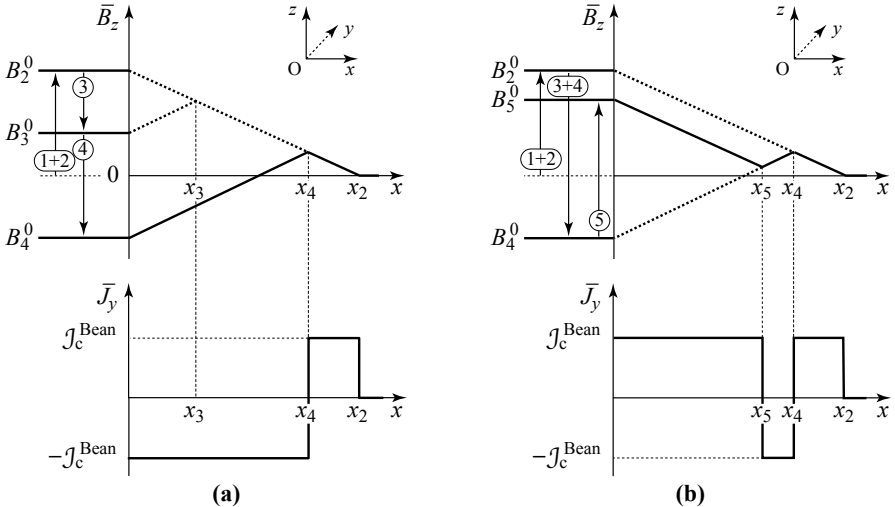


**Figure 7.11 - Equilibrium states  $\bar{B}_{4z}(x)$  and  $\bar{B}_{5z}(x)$  after successive application of  $B_4^0$  and  $B_5^0$ , following fields  $B_2^0$  and then  $B_3^0$ , and the corresponding profiles of current density  $\bar{J}_{4y}(x)$  and  $\bar{J}_{5y}(x)$ .**

The straight-line segments of the average magnetic field profiles have slopes  $\pm \mu_0 J_c^{\text{Bean}}$ .

### 7.5.3 - Rules for the profile of magnetic field and current density (in planar geometry)

We shall now consider the case of a plate-like sample with  $\tilde{\mathbf{B}}$ , the magnetic field parallel to the surfaces.  $\tilde{\mathbf{B}}$  may be  $\mathbf{B}^0$  alone, as in the preceding example, but more generally it is the total magnetic field on the surface, including the self-induced field  $\mathbf{B}^1$  created by the transported current. In the BEAN model, the curves of  $\bar{B}$  and  $\bar{J}$  obey a few simple rules:

- 1 -  $\bar{B}$  is a broken line, composed of straight segments of slope  $\pm \mu_0 J_c^{\text{Bean}}$ . Its origin is situated at  $B(x = 0) = \tilde{B}$  and it extends up to the vortex front beyond which  $\bar{B}$  vanishes.
- 2 - The sections of negative slope  $\partial \bar{B}_z(x)/\partial x$  carry a uniform current density  $+J_c^{\text{Bean}}$  in the  $y$  direction, while those of positive slope carry a current density  $-J_c^{\text{Bean}}$ .

- 3** - After each change in the surface magnetic field  $\tilde{B}_i \rightarrow \tilde{B}_{i+1}$ , the new profile is obtained by drawing from the point  $(x = 0, \tilde{B}_{i+1})$  a straight line of slope  $\pm \partial \bar{B}_z(x) / \partial x$  which will cut the preceding profile at an  $x$ -coordinate  $x_{i+1}$ . This new straight section will replace the previous broken line over the interval  $[0, x_{i+1}]$ . Beyond  $x_{i+1}$ , the profile of  $\bar{B}$  is unaltered.
- 4** - The vortex front never moves backwards. It advances into the sample a little more each time that the intensity of the surface field exceeds (independently of its orientation) any previous surface field. The position of the vortex front is at the  $x$ -coordinate  $x_f = \tilde{B}_f / \mu_0 J_c^{\text{Bean}}$  where  $\tilde{B}_f$  is the highest surface field since it went superconducting.  
If the vortex fronts coming from opposite sides of the sample meet, then rule **3** applies.

## 7.6 - Magnetization of a type II superconducting plate

### 7.6.1 - Geometry and magnetization

Following Appendix 4 (Eq. 4.52), the average magnetization over the entire sample is

$$\langle \mathbf{M} \rangle = \frac{1}{V} \iiint_V \mathbf{M}(\mathbf{r}) d^3r = \frac{1}{V} \iiint_V \left[ \frac{\mathbf{B}(\mathbf{r})}{\mu_0} - \mathbf{H}(\mathbf{r}) \right] d^3r. \quad (7.34)$$

For a sample with the form of a parallelepiped of sides  $c > b \gg a$  (Fig. 7.12) inserted in a magnetic field  $\mathbf{B}^0$  parallel to the largest dimension and therefore with zero demagnetizing field, which gives a constant  $\mathbf{H}$  equal to  $\mathbf{B}^0/\mu_0$ , we have simply

$$\langle M \rangle = \frac{1}{\mu_0} (\langle \bar{B} \rangle - B^0). \quad (7.35)$$

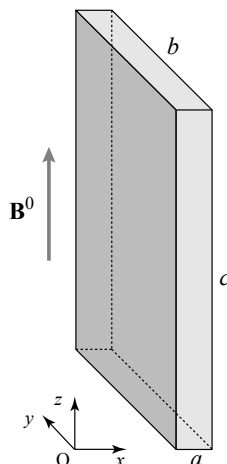


**Figure 7.12**

**Sample geometry**

Sample in the form of a parallelepiped with dimensions  $a \ll b < c$  and external field //z axis

Geometrically  $\langle M \rangle$  is proportional to the area, including signs, between the broken line representing  $\bar{B}(x)$  and the horizontal line with ordinate  $B^0$ .

### 7.6.2 - Initial magnetization curve (BEAN model)

We shall now examine the different magnetic states that the plate acquires when we increase the field  $\mathbf{B}^0 = \mu_0 \mathbf{H}^0$ , starting from zero. The effects of decreasing and then reversing the field will be discussed in the next section.

»  $B^0 < \mu_0 H_{c1}$  (Fig. 7.13a): this is the MEISSNER regime. Neglecting the LONDON region, which affects only a tiny part of the sample, gives us

$$\bar{B}_z(x) = 0 \quad ; \quad \langle M \rangle = -\frac{B^0}{\mu_0}. \quad (7.36)$$

»  $\mu_0 H_{c1} < B^0 < B^*$  (Fig. 7.13b) where, by definition,  $B^*$  is the value of  $B^0$  for which the vortex fronts meet at the medial plane of the sample. The vortices penetrate into the material starting from both surfaces. The fronts of the vortices reach the points  $-x_f$  and  $+x_f$  distant of  $u_f = B^0 / \mu_0 J_c^{\text{Bean}}$  from the surfaces. The average field in the sample and the average magnetization take the respective values:

$$\langle \bar{B} \rangle = B^0 \frac{u_f}{a} = \frac{1}{a} \frac{(B^0)^2}{\mu_0 J_c^{\text{Bean}}} \quad ; \quad \langle M \rangle = -\frac{B^0}{\mu_0} \left( 1 - \frac{B^0}{a \mu_0 J_c^{\text{Bean}}} \right). \quad (7.37)$$

»  $B^0 = B^*$  (Fig. 7.13c). The magnetic field profile becomes V-shaped and the average magnetization corresponds to the basin formed by this V:

$$B^* = \frac{a}{2} \mu_0 J_c^{\text{Bean}} \quad ; \quad \langle \bar{B} \rangle = \frac{1}{2} B^* \quad ; \quad \langle M \rangle = -\frac{B^0}{2\mu_0}. \quad (7.38)$$

»  $B^0 > B^*$  (Fig. 7.13d). The density of vortices increases, without modifying their gradient. The V-shaped profile of  $\bar{B}_z(x)$  is simply translated up by a constant value.

The area included between  $\bar{B}_z(x)$  and  $B^0$  remains independent of  $B^0$ , which means that the magnetization has reached saturation,

$$\langle \bar{B} \rangle = B^0 + \frac{1}{2} B^* \quad ; \quad \langle M \rangle = -\frac{B^*}{2\mu_0}. \quad (7.39)$$

The curve of initial magnetization predicted by this model is represented in Figure 7.14. On the same figure we show typical forms of the measured mean magnetizations in:

- » an ideal soft superconductor, where there is a decrease of total magnetization starting from  $H_{c1}$  (see Chap. 6, section 6.8);
- » a hard superconductor, where the decrease of magnetization begins at a field close to  $H^*$  and tends to zero at  $H_{c2}$ .

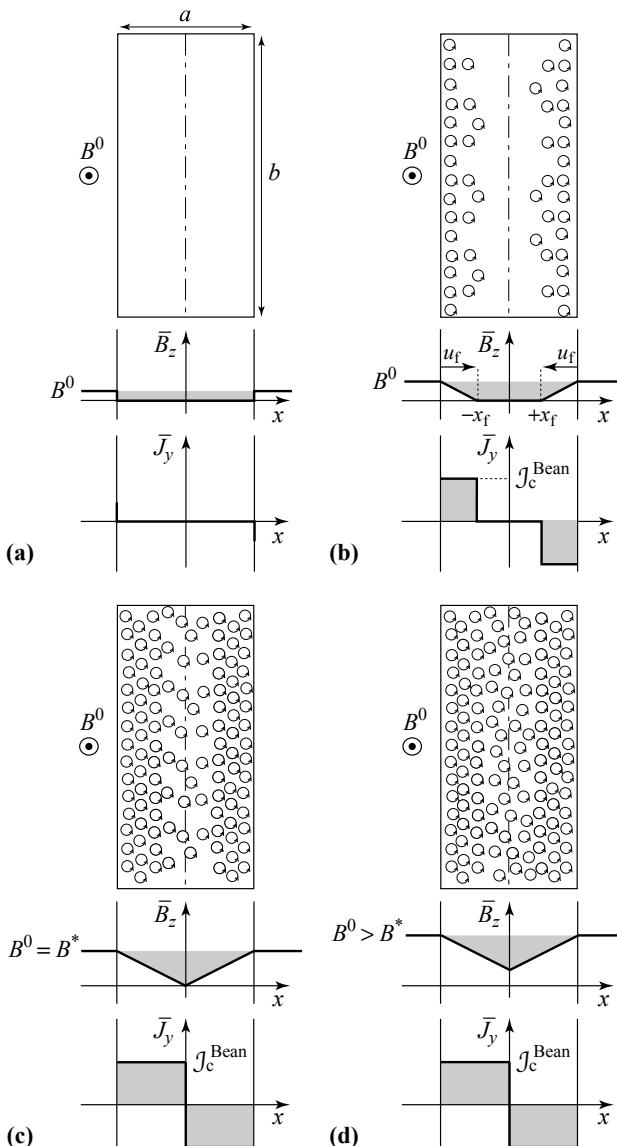


**Figure 7.13 - Initial magnetization of a plate (the BEAN model)**

The magnetic field is directed in the  $z$  direction. (a)  $B^0 < B_{c1}$ ; (b)  $B_{c1} < B^0 < B^*$ ; (c)  $B^0 = B^*$ ; (d)  $B^* < B^0 < B_{c2}$ .  $B^*$  is the value of  $B^0$  for which the vortex fronts join at the medial plane of the sample. In each figure we find from top to bottom: at the top, a schematic representation of the vortices crossing the  $xy$  plane; in the middle, the average local field  $\bar{B}_z(x)$  whose slope is either zero or  $\pm \mu_0 \mathcal{J}_c^{\text{Bean}}$ ; at the bottom, the superconducting current density  $\bar{J}_y$ . The average magnetization is directly proportional to the grey area included between  $B^0$  and  $\bar{B}_z(x)$ .

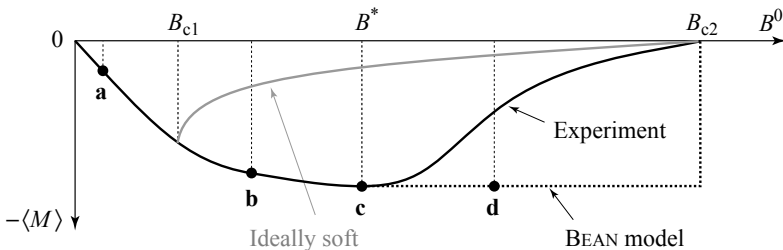


Figure 7.14 - Initial magnetization curve in the BEAN model

Points **a** to **d** correspond to the situations referred to by the same letters as in Figure 7.13. Typical curves of initial magnetization of samples of soft and hard superconductors have been added for comparison (with the value of  $B_{c1}$  exaggerated to make the different regimes apparent).

### 7.6.3 - Hysteresis loop in the BEAN model

Starting again from the magnetized state given by Figure 7.13d that corresponds to the maximum applied field  $B^0 = B_{\max}^0$ , we shall now decrease the field to zero, and then inverse it down to  $-B_{\max}^0$ . Different intermediate stages, as obtained by the rules defined in section 7.5.3 are represented in Figure 7.15.

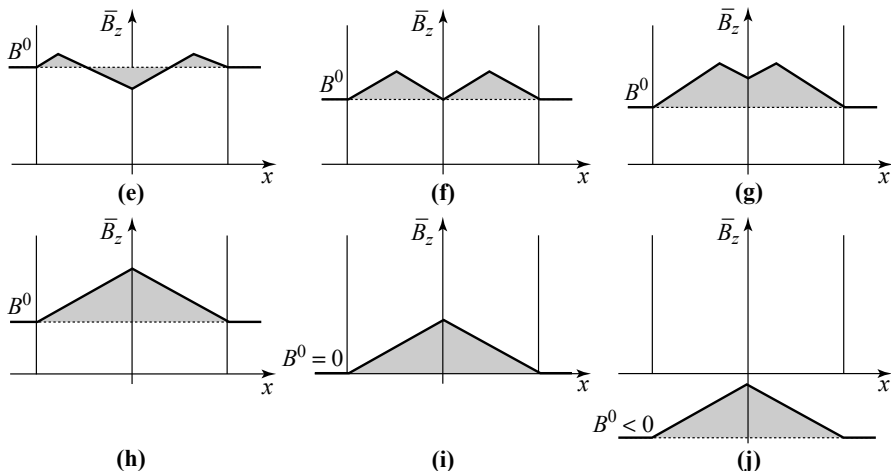


Figure 7.15 - Magnetization of a plate. Evolution of the average local field  $\bar{B}_z(x)$  during the decrease, then the reversal of the field

The history follows that of Figure 7.13. The average magnetizations, proportional to the signed area between  $B^0$  and  $\bar{B}_z(x)$ , are marked on the curve of Figure 7.16 (points e to k).  
**(e)**  $B_{\max}^0 > B^0 > B_{\max}^0 - B^*$ ; **(f)**  $B^0 = B_{\max}^0 - B^*$ ; **(g)** and **(h)**  $B_{\max}^0 - B^* > B^0 > B_{\max}^0 - 2B^*$ ; **(i)** and **(j)**  $B_{\max}^0 - 2B^* > B^0 > -B_{\max}^0$ .

»  $B_{\max}^0 \geq B^0 > B_{\max}^0 - 2B^*$  (section between **d** and **h** Fig. 7.16 - (e) (f) (g) Fig. 7.15)

The magnetization has the form of a line bent into four segments, leading to

$$\langle M \rangle = \frac{1}{\mu_0} \left[ -\frac{1}{2} B^* + (B_{\max}^0 - B^0) - \frac{1}{4} \frac{(B_{\max}^0 - B^0)^2}{B^*} \right]. \quad (7.40a)$$

The coercive field  $B_{\text{coer}}^0$ , where the magnetization vanishes, (**e**) and the saturation field  $B_{\text{sat}}^0$  where the magnetization saturates (**h**) are

$$B_{\text{coer}}^0 = B_{\max}^0 - (2 - \sqrt{2}) B^* \quad \text{and} \quad B_{\text{sat}}^0 = B_{\max}^0 - 2 B^*. \quad (7.40b)$$

$\gg B_{\max}^0 - 2 B^* > B^0 \geq -B_{\max}^0$  (section between **h** and **k** Fig. 7.16 - (**h**) (**i**) (**j**) Fig. 7.15)

$\bar{B}_z(x)$  recovers its V-shape, but is inverted with respect to (7.13d). Inverse saturation is reached with

$$\langle \bar{B} \rangle = B^0 + \frac{1}{2} B^* \quad ; \quad \langle M \rangle = \frac{B^*}{2\mu_0}. \quad (7.41)$$

Figure 7.16 shows that the BEAN model predicts the same general form as the experimental hysteresis loop, at least as long as the field  $B_{\max}^0$  is not much greater than  $B^*$ .

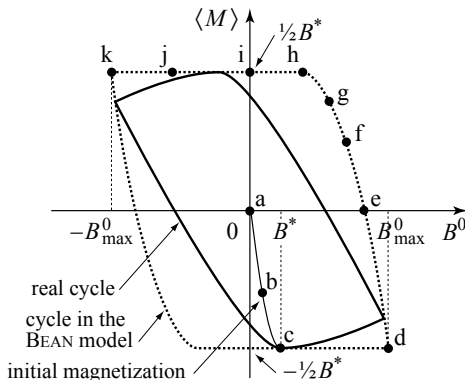


**Figure 7.16**  
Typical hysteresis loop of a type II superconductor for the case of a maximum field greater than  $B^*$ , but well below  $H_{c2}$ . Points **a** to **d** and **e** to **j** correspond to the situations referred to by the same letters as in Figures 7.13 and 7.15.

#### 7.6.4 - Hysteresis loop in the KIM-JI model

The phenomenon of saturation of the magnetization given by the BEAN model comes from the fact that, as the critical current density does not depend on the field, the rigid V-shaped profile of  $\bar{B}$  is simply translated when  $B^0$  increases. In order to have a reduction in the magnetization for high values of  $B^0$  we would need this V to flatten, *i.e.* that in the critical state the gradient  $\partial \bar{B}_z / \partial x$  should decrease, and that the corresponding critical current density  $J_c$  should diminish as the field  $\bar{B}$  grows.

The expressions (7.31) clearly go in this direction and, as an example, we will consider the KIM-JI model whose behavior is given by the expression (7.31a). Applied to the plate geometry in Figure 7.12 it predicts, as we move into the sample ( $u$  is the distance from the closer surface),

$$\frac{d\bar{B}_z}{du} = -\mu_0 \frac{\mathcal{J}_c^{KJ}}{\bar{B}_z/B_K} \quad \text{or} \quad \bar{B}_z = \sqrt{(B^0)^2 - 2\mu_0 B_K \mathcal{J}_c^{KJ} u} \quad (7.42)$$

which leads to the profiles of Figure 7.17. It is seen that the areas between  $B^0$  and  $\bar{B}$  (shaded in grey in the figure), fade away in high fields.

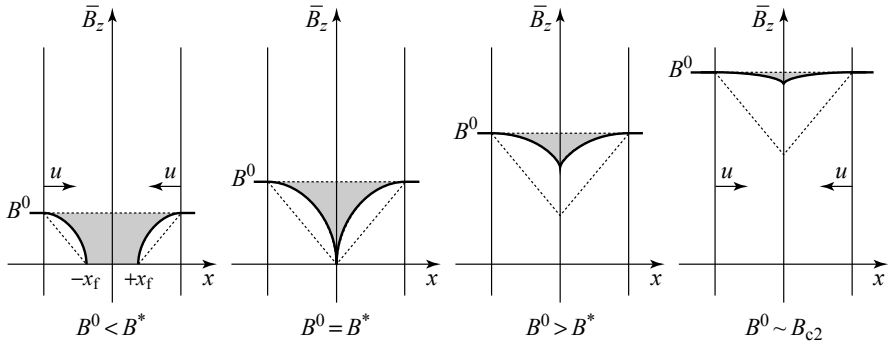


**Figure 7.17 - Magnetic field  $\bar{B}$  within a plate in the Kim-Ji model**

A curved profile replaces the straight V-shape (the dotted line) of the BEAN model. The grey areas that represent the average magnetization are less than predicted by the BEAN model and tend to zero when  $B^0$  becomes high.

A typical form of the hysteresis loop is shown in Figure 7.18. The different expressions for the initial magnetization curve determined starting from (7.42) are indicated in Table 7.1. This model and its variants (7.31) reproduce experimental hysteresis loops satisfactorily, both for complete cycles and for secondary loops (cycles between two values of  $B^0$ ). In the figure we have added some effects of flux jumps, as described in section 7.3.4.

**Table 7.1 - Average magnetization of a plate as predicted by the Kim-Ji model**

$B^0 < \mu_0 H_{c1}$	$M = -\frac{B^0}{\mu_0}$ (very weak)	
$\mu_0 H_{c1} < B^0 < B^*$	$\langle M \rangle = \frac{B^0}{\mu_0} \left[ \frac{2}{3} \left( \frac{B^0}{B^*} \right)^2 - 1 \right]$	$u_f = \frac{a}{2} \left( \frac{B^0}{B^*} \right)^2$
$B^0 = B^* = \sqrt{\mu_0 B_K \mathcal{J}_c^{KJ} a}$	$\langle M \rangle = M^* = -\frac{B^*}{3\mu_0}$	$u_f = \frac{a}{2} \quad (x_f = 0)$
$B^0 > B^*$	$\langle M \rangle = -\frac{B^0}{\mu_0} + \frac{2}{3} \frac{B^0}{\mu_0} \left( \frac{B^0}{B^*} \right)^2 \left\{ 1 - \left[ 1 - \left( \frac{B^*}{B^0} \right)^2 \right]^{3/2} \right\}$	

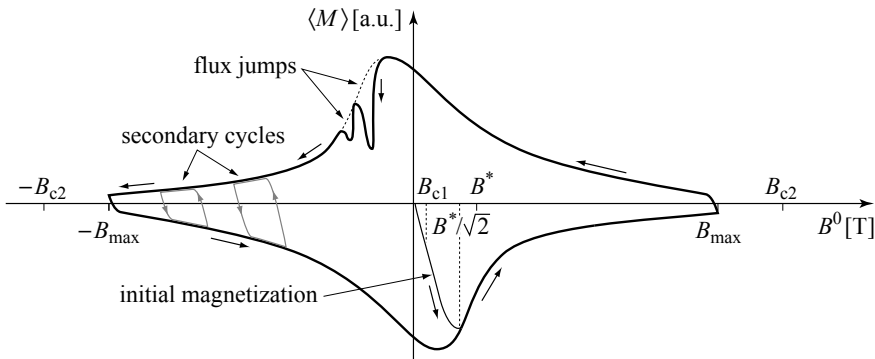


**Figure 7.18 - Form of the hysteresis loops of type II superconductors** <sup>16</sup>

As well as a complete cycle of hysteresis between extreme values  $B_{\max}^0$  close to  $B_{c2}$ , we indicate the initial curve of magnetization and secondary cycles between intermediate values of  $B^0$ . These loops are reasonably reproduced by the Kim-Ji model or its variants, as defined by the relations (7.31). In this figure we have added effects of "flux jump" which can occur randomly when there is a very high local magnetization.

Note finally that the hysteresis curves may be significantly modified by the superposition of flux-creep effects. Their forms therefore depend on the speed with which the fields are swept.

## 7.7 - Magnetization in cylindrical geometry (BEAN model)

While the parallelepiped is the simplest to treat, cylindrical geometry is more relevant to superconducting wires of Nb-Ti and Nb<sub>3</sub>-Sn, that are widely used in the construction of high field coils. We will consider here only the situation where the magnetic field  $\mathbf{B}^0$  is applied along the cylinder axis, as the calculations for perpendicular field are much more burdensome.

### 7.7.1 - Magnetization of a solid cylinder

In the usual cylindrical coordinate system, where the magnetic field is oriented along the  $z$  axis, the relation (7.29) can be reduced, whenever  $\bar{B}$  is non-zero, to

$$\frac{\partial \bar{B}_z}{\partial r} = \pm \mu_0 J_c^{\text{Bean}}. \quad (7.43)$$

With the boundary conditions including the condition that at the surface of a cylinder of radius surface  $R$ ,  $\bar{B}_z(R) = B^0$ , integration of (7.43) leads to

$$\bar{B}_z(r) = B^0 - \mu_0 J_c^{\text{Bean}} R \left( 1 - \frac{r}{R} \right) \quad (7.44)$$

<sup>16</sup> Cycle adapted from measurements by A.M. CAMPBELL, J.E. EVETTS & DEW-HUGHES (1966) *Phil. Mag.* **10**, 333;  
J.E. EVETTS, A.M. CAMPBELL & DEW-HUGHES (1966) *Phil. Mag.* **10**, 339.

which places the vortex front on a cylinder of radius  $r_f$  given by

$$r_f = R - \frac{B^0}{\mu_0 J_c^{\text{Bean}}}. \quad (7.45)$$

Exactly as for the plate, the field  $B^*$  is defined as being the value of field  $B^0$  for which the vortex fronts join, or  $r_f = 0$  (Fig. 7.19a),

$$B^* = \mu_0 J_c^{\text{Bean}} R. \quad (7.46)$$

**Table 7.2 - Average magnetization of a cylinder predicted by the BEAN model**

Initial magnetization	$B^0 < B^*$	$\langle M \rangle = -\frac{B^0}{\mu_0} \left[ 1 - \frac{B^0}{B^*} + \frac{1}{3} \left( \frac{B^0}{B^*} \right)^2 \right]$
	$B^0 \geq B^*$	$\langle M \rangle = -\frac{B^*}{3\mu_0}$
Decrease, then inversion of the field	$B_{\max}^0 - 2B^* < B^0 < B_{\max}^0$	$\langle M \rangle = -\frac{B^*}{12\mu_0} \left[ 4 - 12 \frac{U}{B^*} + 6 \left( \frac{U}{B^*} \right)^2 - \left( \frac{U}{B^*} \right)^3 \right]$ $U = B_{\max}^0 - B^0$
	$-B_{\max}^0 < B^0 < B^*$	$\langle M \rangle = \frac{B^*}{3\mu_0}$

Calculated starting from expressions (7.44) and (7.34), the average magnetization in the cylinder is given in Table 7.2.

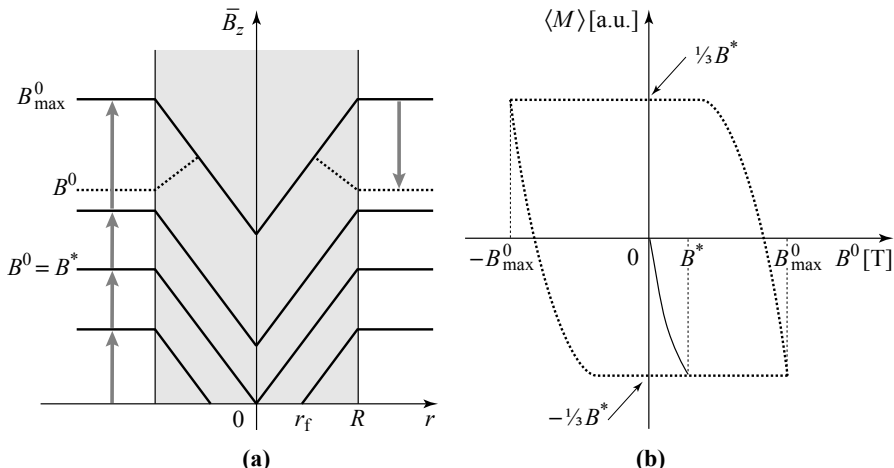


**Figure 7.19 - Magnetic field and magnetization of a cylindrical sample**

(a) Distribution of the average local field predicted by the BEAN model across a diameter during the first application of the field up to the field  $B_{\max}^0$ , then at the beginning of the decrease in field (dotted curve). (b) Hysteresis loop predicted by the BEAN model.

The current density  $\bar{J}_\theta = \frac{1}{\mu_0} \frac{\partial \bar{B}_z}{\partial r}$  associated with the field  $\bar{B}$  is normal to the radial direction (Fig. 7.20). The screening effect clearly makes sense only for  $B_0 < B^*$ , and only for the first time the field is increased.

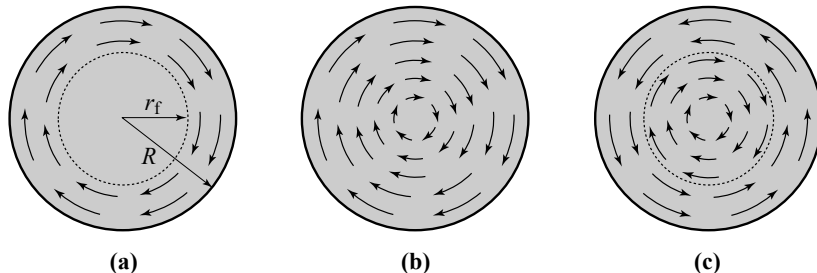


**Figure 7.20 - Current density in the superconducting cylinder subject to an axial field (Bean model)**

The current density, equal to the critical current density  $J_c^{\text{Bean}}$  when non-zero, is circular. (a)  $B^0 < B^*$ : the current flows between  $r_f$  and  $R$  (see Fig. 7.19a). It acts like a screening current for the part inside the radius  $r_f$  for which the field  $\bar{B}$  stays at zero. (b)  $B^0 > B^*$ : the circular current has invested the whole sample. (c) In decreasing field the current is inverted in an external sheath which grows gradually to include the whole sample.

### 7.7.2 - Magnetization of a thick-walled tube

Let us now consider a cylindrical tube with a thick wall, of external and internal radii,  $R_e$  and  $R_i$  respectively, cooled in zero field and then subjected to a magnetic field  $B^0$  parallel to its axis and external to the tube (Fig. 7.21).

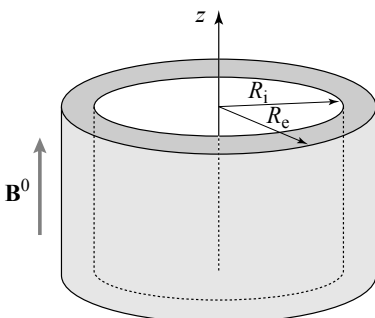


**Figure 7.21**  
**Magnetic field in a tubular geometry**  
The experiment consists of applying a magnetic field outside the tube and measuring the magnetic field in the empty central part.

As long as  $r_f$  is greater than the internal radius  $R_i$ , the evolution of the profile of  $\bar{B}$  is exactly like that seen for the solid cylinder, with the magnetic field staying at zero inside the cylinder of radius  $r_f$ . This is true both in the material and in the empty central core. The external field is shielded by the current density  $\bar{J}_\theta = J_c^{\text{Bean}}$  that flows between  $r_f$  and  $R_e$ .

Beyond the magnetic field  $B^0 = B^{**}$  for which  $r_f = R_i$ , the vortex front can no longer progress. To maintain a gradient  $\partial \bar{B}_z / \partial r$  equal to  $\mu_0 J_c^{\text{Bean}}$  between  $R_i$  and  $R_e$ , there is no other solution than allowing a magnetic field  $B_i$  to penetration into the central part with value,

$$B_i = B^0 - \mu_0 J_c^{\text{Bean}}(R_e - R_i). \quad (7.47)$$

Physically the magnetic field  $B_i$  increases by transferring fluxons from the outside to the inside: each increase in  $B^0$  temporarily enhances the gradient of  $\bar{B}$  between  $R_e$  and  $R_i$ . This has the effect of displacing the vortices towards the central part and “emptying” them there by increasing  $B_i$  until the critical gradient is re-established. The evolutions of the profiles of  $\bar{B}$  and of  $B_i$  in equilibrium are represented in Figure 7.22.

The average magnetization (7.34) formally includes two contributions: the first due to the difference between  $\bar{B}$  and  $B^0$  in the material, the second coming from the central cavity because of the equivalence between screening currents which act as AMPÈRE CURRENTS, and magnetization, the interior vacuum appear as “magnetized” (see Fig. 4.2).

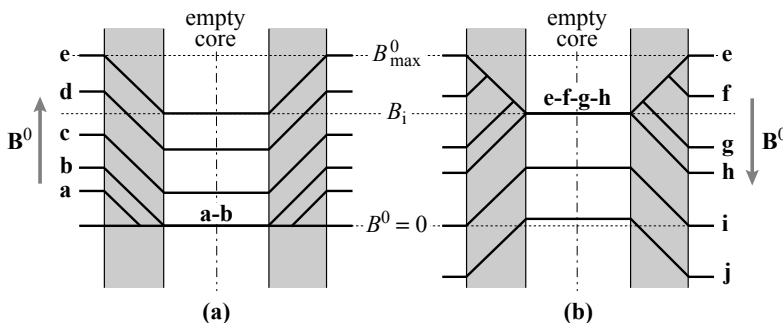


Figure 7.22 - Magnetic field in a tubular cylinder with a thick wall and in the empty central core (BEAN model)

The magnetization is represented by the difference between  $\bar{B}$  and  $B^0$ . Starting with profile e, two contributions appear: one in the material and one in the empty core (from the difference between  $B_i$  and  $B^0$ ).

## 7.8 - Experimental evidence for critical states

By inserting a HALL probe in a hole drilled perpendicularly to the axis of a sample of Nb-Ti in the form of a solid cylinder, COFFEY measured the magnetic field profile  $\bar{B}$  in an increasing field  $B^0$ . The result of this experiment is shown in Figure 7.23.

The first observations in the study were a series of profiles characteristic of critical states, reminiscent of the BEAN model, but closer to those of Figure 7.17 deduced from the KIM-JI model (relation 7.31a). This behavior constitutes an undeniable experimental proof of the critical state model.

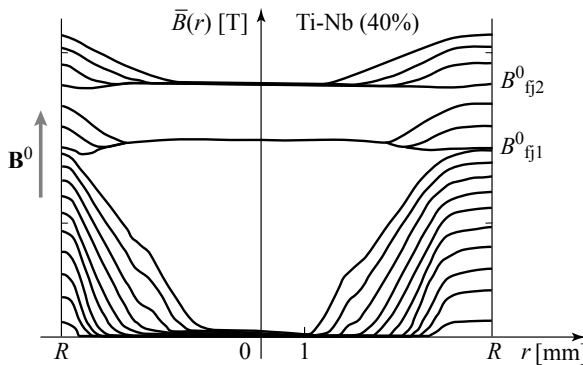


**Figure 7.23 - Evidence for the critical state.  
Measurement of the magnetic field in a solid cylinder**

Variation of the average magnetic field measured with a HALL probe of dimension  $5 \times 10 \mu\text{m}$  along a diameter drilled across the sample. The measurements were made in increasing field starting from zero field. Two “flux jumps” were observed at fields  $B_{fj1}^0$  and  $B_{fj2}^0$ . [From COFFEY, 1967, © Elsevier, with permission]<sup>17</sup>

However even before the vortex fronts reached the center of the sample, COFFEY observed the phenomenon of “flux jump,” that we discussed in section 7.6.4 (Fig. 7.18). When the magnetic field reaches  $B_{fj1}^0$ , an avalanche of flux jumps increases the temperature and transforms the material to the normal phase, allowing the magnetic field to penetrate the sample uniformly. When cooling in field  $B_{fj1}^0$  and recovering the superconducting state, the vortices form spontaneously and distribute themselves quasi-uniformly in the sample giving  $\bar{B} \approx B_{fj1}^0$  and  $\langle M \rangle \approx 0$ . With a further increase in  $B^0$ , new vortices enter by the surfaces, in agreement with the critical state models, until the appearance of new accidental flux jumps at a field  $B_{fj2}^0$ .

Another way to test the critical field model consists of measuring the internal magnetic field of a hollow cylinder inserted in an external field  $B^0$ . Admittedly this method does not lead to determination of the profile of  $\bar{B}$ , but it is less aggressive and allows us to collect some valuable information.

The results shown in Figure 7.24 are, once again, in agreement with critical state models:

- »  $B_i$  stays zero as long as  $B^0$  has not reached  $B^{**}$ ;
- » Beyond  $B^{**}$  the difference  $(B^0 - B_i)$  is, however, not constant as it would be in the BEAN model, but decreases as predicted by the KIM-JI model and its variants.

<sup>17</sup> H.T. COFFEY (1968) Distribution of magnetic fields and currents in type II superconductors, *Cryogenics* 7, 73.

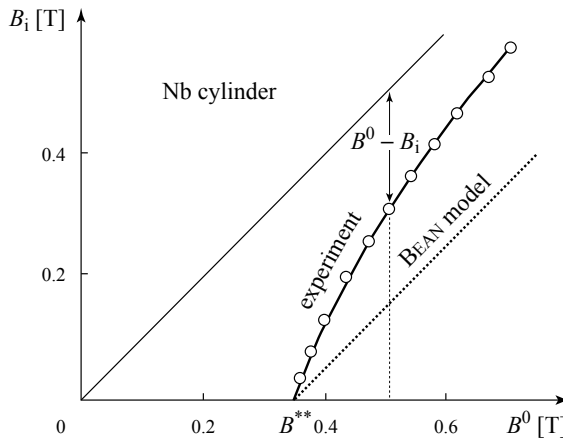


**Figure 7.24 - Magnetic field inside a hollow cylinder subject to a field  $B^0$**

In agreement with critical state models, the magnetic field in the tube is zero as long as  $B^0$  is less than a field  $B^{**}$ . The difference between the external field  $B^0$  and the internal field  $B_i$ , indicated by a double arrow, decreases when  $B^0$  grows as predicted by the Kim-Ji model and variants. [From HEMPSTEAD, KIM & STRNAD, 1963, © American Institute of Physics, with permission] <sup>18</sup>

## 7.9 - Current transport in the SHUBNIKOV phase

### 7.9.1 - Current transport in the absence of applied magnetic field

In the absence of an applied field, the only magnetic field present in a linear conductor is the self-generated magnetic field  $\mathbf{B}^I$  created by the transported current. A field due to a winding of the wire (or ribbon) would be included here as an applied field.

Let us then consider a straight ribbon (Fig. 7.25a) of a type II superconductor in the SHUBNIKOV phase, centered at  $x = 0$ , of thickness  $a$  and width  $c$ , that carries a current of intensity  $I$  flowing in the positive  $y$  direction. The current generates a magnetic field  $\mathbf{B}^I$  oriented in the  $z$  direction with absolute value depending only on  $x$ .

By application of AMPÈRE's theorem, we have

$$\tilde{\mathbf{B}}\left(-\frac{a}{2}\right) - \tilde{\mathbf{B}}\left(\frac{a}{2}\right) = \mu_0 \frac{I}{c} \hat{\mathbf{z}} \quad (7.48)$$

which, in the absence of applied field this leads to

$$\tilde{\mathbf{B}}\left(-\frac{a}{2}\right) = \mu_0 \frac{I}{2c} \hat{\mathbf{z}} \quad ; \quad \tilde{\mathbf{B}}\left(\frac{a}{2}\right) = -\mu_0 \frac{I}{2c} \hat{\mathbf{z}}. \quad (7.49)$$

<sup>18</sup> C.F. HEMPSTEAD, Y.B. KIM & A.R. STRNAD (1963)  
Inductive Behavior of Superconducting Magnets, *J. Appl. Phys.* **34**, 3226.

Applying the rules of the BEAN model, and imposing these boundary conditions we find

$$-\frac{a}{2} < x < -x_f \Rightarrow \bar{B}_z(x) = \mu_0 \frac{I}{2c} - \mu_0 J_c^{\text{Bean}} \left( x + \frac{a}{2} \right) \quad (7.50\text{a})$$

$$x_f < x < \frac{a}{2} \Rightarrow \bar{B}_z(x) = -\mu_0 \frac{I}{2c} + \mu_0 J_c^{\text{Bean}} \left( \frac{a}{2} - x \right) \quad (7.50\text{b})$$

$$-x_f < x < +x_f \Rightarrow \bar{B}_z(x) = 0 \quad (7.50\text{c})$$

where  $x_f$ , the position of the vortex front in the positive region, is given by

$$x_f = \frac{1}{2} \left( a - \frac{I}{c J_c^{\text{Bean}}} \right). \quad (7.51)$$

The profile of current density  $\bar{J}_y(x) = -\frac{1}{\mu_0} \frac{\partial \bar{B}_z}{\partial x}$  ( $\mu_0 \bar{\mathbf{J}} = \nabla \times \bar{\mathbf{B}}$ ) associated with the

relations (7.50), (Fig. 7.25b), shows that the current flows near the surfaces in a layer of thickness

$$u_f = \frac{I}{2c J_c^{\text{Bean}}} \quad (7.52)$$

with a uniform density  $J_c^{\text{Bean}}$ .

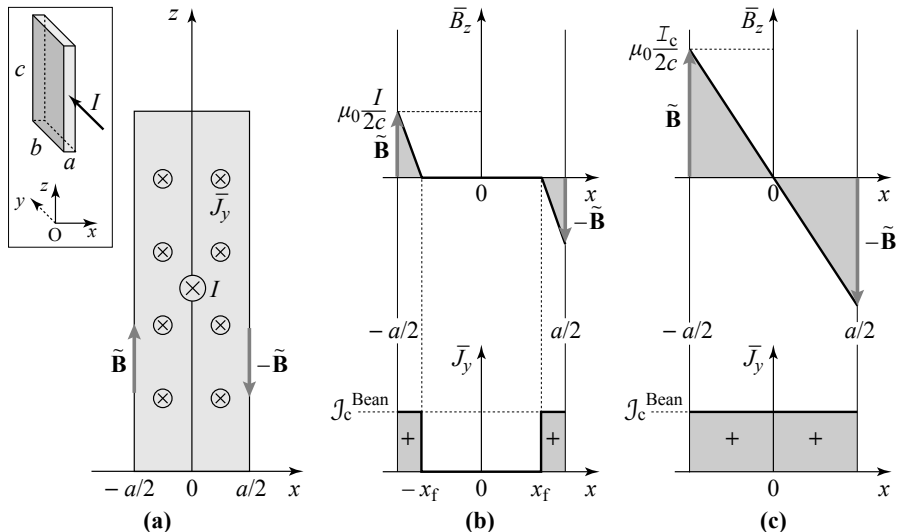


**Figure 7.25 - Critical states of a superconductor transporting a current of intensity  $I$  in the absence of an external magnetic field (BEAN model)**

**(a)** Geometry of the system. The current crosses the section from the front to the back. **(b)** Critical state with current  $I < I_c$ : average field  $\bar{B}_z(x)$  and current density  $\bar{J}_y(x)$ . **(c)** Critical state at the critical current  $I_c$ .

An increase in the intensity leads to a greater value of  $\tilde{B}$  which produces a displacement of the vortex front towards the median plane. When the two vortex fronts meet ( $x_f = 0$ ), the current density  $\bar{J}$  becomes uniformly equal to  $J_c^{\text{Bean}}$  and the current intensity then takes the value

$$I_c = ac J_c^{\text{Bean}}. \quad (7.53)$$

Beyond this intensity  $I_c$ , a magnetic field gradient exceeding  $\mu_0 J_c^{\text{Bean}}$  is created within the superconductor. Once again, this pushes the vortices from the surfaces towards the center of the plate, where they meet. Since those coming from the right and those from the left carry opposite magnetic fields and whirlwind currents flowing in opposite senses, these vortices annihilate without restoring the field gradients of the critical state. There results a permanent flux of vortices penetrating by each surface and annihilating at the center, without reaching any state of equilibrium.

The intensity  $I_c$  appears as a critical intensity beyond which there is no current transport without dissipation of heat because of the constant movement of the vortices.

If we decrease the intensity of transported current and bring it to zero,  $\tilde{B}$  diminishes but  $\bar{J}$  never comes back to be uniformly zero (Fig. 7.26). There remain trapped fields and currents flowing in opposing senses.

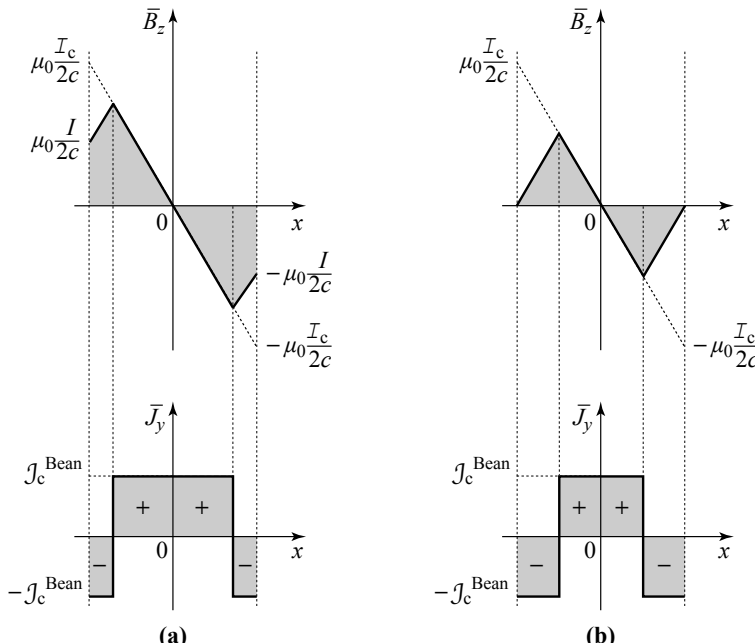


**Figure 7.26 - Critical states of a superconductor carrying a current intensity that decreases, starting from  $I_c$ .** (a)  $0 < I < I_c$ ; (b)  $I = 0$

At zero current, the current density alternates in sign with amplitude  $J_c^{\text{Bean}}$ .

### 7.9.2 - Current transport in an applied magnetic field

The same plate, carrying a current of intensity  $I$  in the  $y$  direction is now inserted into a magnetic field  $\mathbf{B}^0$  parallel to the  $z$  axis. As the self-generated field  $\mathbf{B}^I$  and the applied  $\mathbf{B}^0$  are oriented in the same direction, they add on the surface of coordinate  $x = -a/2$  and subtract on the surface  $x = +a/2$ , leading to

$$\tilde{B}_z\left(-\frac{a}{2}\right) = \mu_0 \frac{I}{2c} + B^0 \quad ; \quad \tilde{B}_z\left(\frac{a}{2}\right) = -\mu_0 \frac{I}{2c} + B^0. \quad (7.54)$$

Supposing that the intensity  $I$  increases at constant  $B^0$ , we obtain successive critical states, as those presented in Figure 7.27:

»  $I = 0$  (Fig. 7.27a): the situation is identical to that of Figure 7.13b. Currents of intensities equal to  $J_c^{\text{Bean}}$  flow in opposite directions within layers of the same thickness near each of the two surfaces.

»  $I < acJ_c^{\text{Bean}}$  (Figs. 7.27b and 7.27c):

- › On the side  $x < 0$ :  $\tilde{B}(-a/2)$  increases. Vortices penetrate by the face situated at  $-a/2$  and the vortex front moves towards the opposite side.
- › On the side  $x > 0$ :  $\tilde{B}(a/2)$  decreases. The profile of  $\bar{B}$  is transformed into a broken line, consistent with the rules of section 7.5.3.

The current density takes the forms of Figures 7.27b and then 7.27c. There remain layers where the current density is oriented opposite to the direction of the transported current.

»  $I = I_c = acJ_c^{\text{Bean}}$  (Figs. 7.27d and 7.27e):

$\bar{J}$  becomes uniform and equal to  $J_c^{\text{Bean}}$ , and  $\bar{B}$  reduces to a straight line of slope  $-\mu_0 J_c^{\text{Bean}}$ . Figures 7.25d and 7.25e correspond to  $B^0 < \mu_0 \frac{I_c}{2c}$  and

$B^0 > \mu_0 \frac{I_c}{2c}$  respectively.

»  $I > I_c$ : Following situations (d) and (e), there are the two possibilities:

›  $B^0 < \mu_0 \frac{I_c}{2c}$ :  $\bar{B}$  passes through zero. The vortices enter each of the two faces with opposite signs and are driven towards the vortex front where they annihilate in pairs.

›  $B^0 > \mu_0 \frac{I_c}{2c}$ :  $\bar{B}$  is always positive. The vortices enter by the face  $x = -a/2$ , cross the sample, and exit by the opposite face at  $x = +a/2$ .

In either of the two cases just described, the movement of the vortices produces dissipation of energy and the ribbon is no longer a perfect conductor.

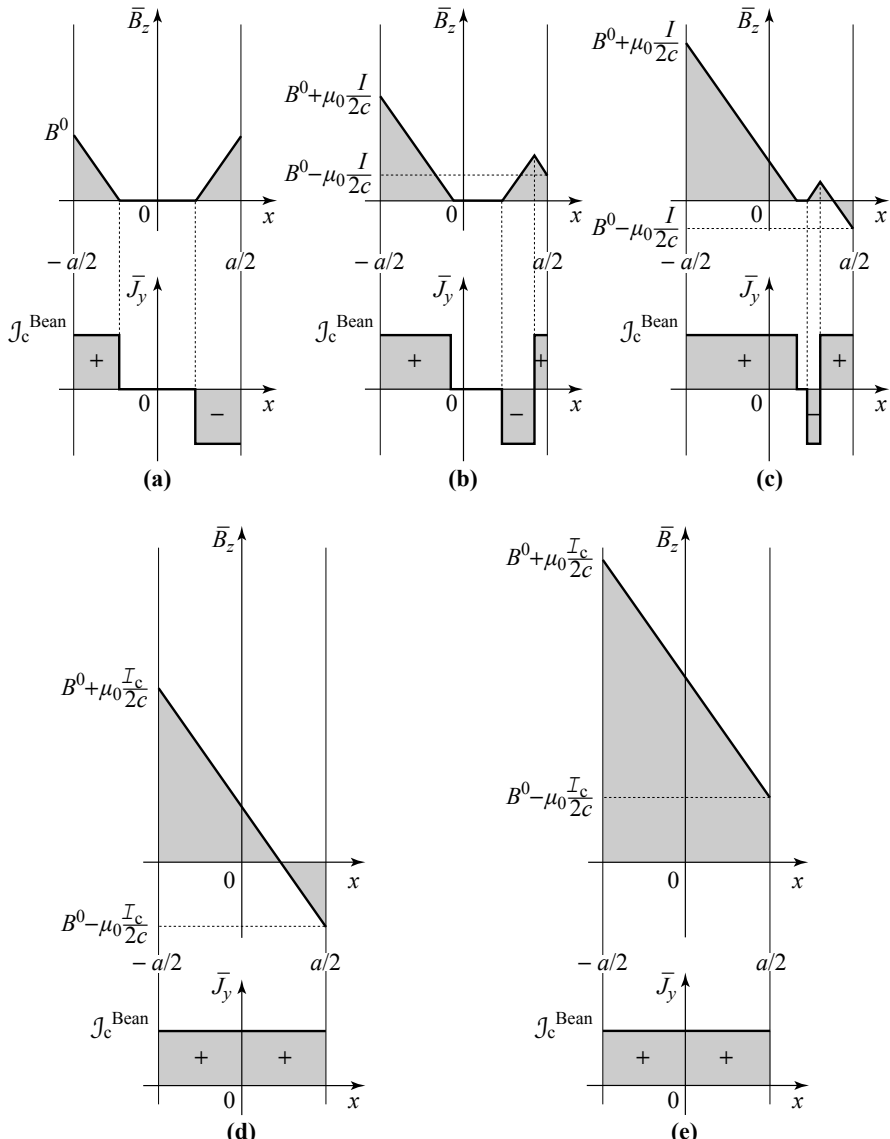


**Figure 7.27 - Critical states of a superconductor carrying a current of intensity  $I$  in the presence of an external magnetic field  $B^0$  (BEAN model)**

**(a)**  $I = 0$ ; **(b)-(c)**  $I < I_c$ ; **(d)**  $I = I_c$  and  $B^0 < (\mu_0 I_c) / (2c)$ ; **(e)**  $I = I_c$  and  $B^0 > (\mu_0 I_c) / (2c)$

At the surfaces,  $x = \pm a/2$  the current creates a self-generated field  $B^I = (\mu_0 I) / (2c)$  that, depending on which face it is, is added to or subtracted from  $B^0$ . We take the case where  $B^0 < B^*$ . The current density is  $I_c = ac J_c^{\text{Bean}}$ .

## Appendix 7A

### Different aspects of the “LORENTZ force”

#### A7A.1 - Introduction

The expression for the force per unit length  $\mathbf{f}_\phi$  acting on a vortex immersed in a current density  $\mathbf{J}$ ,

$$\mathbf{f}_\phi = \mathbf{J} \times \phi_0 \hat{\mathbf{u}} \quad (7.55)$$

where  $\hat{\mathbf{u}}$  is the unit vector parallel to the axis of the vortex oriented in the sense of the magnetic field, even today continues to be the object of discussion and debate. This is despite the fact that it was accepted long ago and has been analyzed by many authors.<sup>19, 20, 21</sup> Three different origins, presented as being in competition or complementary, are most often invoked:

- » the LORENTZ force between the magnetic field attached to the vortex and the current density  $\mathbf{J}$ ;
- » the LONDON force, which is derived from the energy of interaction between vortices, and whose form depends directly on the second LONDON equation and its extension to the interaction between an external current and a vortex;
- » the MAGNUS force, of hydro-dynamical origin, which applies to a rotating body immersed in a moving fluid.

The aim of this appendix is limited to introduce these forces, while referring the reader to more specialized articles for a more thorough discussion.

We shall keep to the case of a superconductor with a very large GINZBURG-LANDAU parameter  $\kappa$ , and thus with vortices of small core radius  $\xi$ . The lines of current  $\mathbf{J}$  cross the magnetic field region associated with the vortices, that is they are tangled with the vortex currents that extend over a distance  $\lambda$  very much larger than  $\xi$  (Fig. 7.28). Only the case of a fixed vortex will be considered.

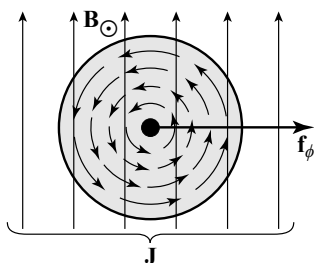


**Figure 7.28**  
Vortex immersed in a current of density  $\mathbf{J}$   
The current  $\mathbf{J}$  crosses the LONDON region of the vortex with its magnetic field and vortex currents (the central part is the vortex core).

19 J. FRIEDEL, P.G. DE GENNES & J. MATRICON (1963) *Appl. Phys. Lett.* **2**, 119;  
P.G. DE GENNES & J. MATRICON (1964) *Rev. Mod. Phys.* **36**, 45.

20 P. NOZIÈRES & W.F. VINEN (1966) *Phil. Mag.* **14**, 667.

21 J. BARDEEN & M.J. STEPHEN (1965) *Phys. Rev.* **140**, A1197.

### A7A.2 - LORENTZ force

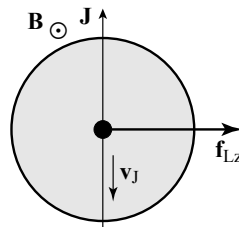


Figure 7.29

#### LORENTZ force

The current density  $\mathbf{J}$  and the electrons that carry it are subject to a LORENTZ force  $\mathbf{f}_{Lz}$  towards the right, identical to the force  $\mathbf{f}_\phi$  acting on the vortex.

When it crosses the magnetic field of the vortex, each of the electrons carrying the current density  $\mathbf{J}$ , as it moves with velocity  $\mathbf{v}_J$ , feels at the point  $\mathbf{r}$  a force

$$\mathbf{f}_{Lz}^{(e)} = (-e)\mathbf{v}_J \times \mathbf{B}(\mathbf{r}) \quad (7.56)$$

where  $\mathbf{B}(\mathbf{r})$  is the magnetic field associated with the vortex centered at the origin.

Denoting by  $n_s$  the number of superconducting electrons per unit volume that carry the current density  $\mathbf{J}$ ,

$$\mathbf{J} = n_s(-e)\mathbf{v}_J \quad (7.57)$$

the total LORENTZ force  $\mathbf{f}_{Lz}$  per unit length of the vortex can be written, by integrating over the surface through which there is non-zero magnetic field associated with the vortex, as

$$\mathbf{f}_{Lz} = \iint_S n_s(-e)(\mathbf{v}_J \times \mathbf{B})d\mathbf{S} = \mathbf{J} \times \phi_0 \hat{\mathbf{u}} \quad (7.58)$$

which is seen to be equal to  $\mathbf{f}_\phi$ .

This model is, however, rejected by many authors<sup>22</sup> since if the magnetic field associated with the vortex imparts a force  $\mathbf{f}_{Lz}$  on the current density  $\mathbf{J}$ , the vortex should experience the equal and opposite force of reaction, which would then be  $-\mathbf{f}_\phi$ .

### A7A.3 - LONDON force

This force is a generalization of the repulsive force between two vortices (see section 7.1.2).

#### Field and kinetic energies

As we showed in Chapter 2, the free energy of a superconducting sample of volume  $\mathcal{V}$  is the sum of the kinetic energy of the electrons and of the magnetic energy integrated over the whole volume  $\mathcal{V}$  (relation 2.59),

$$E = \frac{1}{2\mu_0} \iiint_{\mathcal{V}} [\mathbf{B}^2 + \lambda^2(\nabla \times \mathbf{B})^2] d^3r. \quad (7.59)$$

<sup>22</sup> O. NARAYAN (2003) *Journal of Physics A* **36**, L373.

Using the relation  $\nabla \cdot (\mathbf{u} \times \mathbf{w}) = \mathbf{w} \cdot (\nabla \times \mathbf{u}) - \mathbf{u} \cdot (\nabla \times \mathbf{w})$  (7.60)

with  $\mathbf{w} = \mathbf{B}$  and  $\mathbf{u} = \nabla \times \mathbf{B}$ , this energy can be written

$$E = \frac{1}{2\mu_0} \iiint_V [\mathbf{B}^2 + \lambda^2 \mathbf{B} \cdot \nabla \times (\nabla \times \mathbf{B})] d^3r - \frac{1}{2\mu_0} \iiint_V [\nabla \cdot ((\nabla \times \mathbf{B}) \times \mathbf{B})] d^3r \quad (7.61)$$

or, applying STOKES theorem, and thereby transforming the second term into an integral on the surface  $\Sigma$  enclosing the volume,

$$E = \frac{1}{2\mu_0} \iiint_V [\mathbf{B} + \lambda^2 \nabla \times (\nabla \times \mathbf{B})] \cdot \mathbf{B} d^3r - \frac{1}{2\mu_0} \iint_{\Sigma} ((\nabla \times \mathbf{B}) \times \mathbf{B}) \cdot d\Sigma. \quad (7.62)$$

When the magnetic field and the current density are associated with one or several parallel vortices, and because the vector product  $(\nabla \times \mathbf{B}) \times \mathbf{B}$  decreases faster than the integration surface around the vortex lines grows, only the bulk term remains. The sum of the magnetic energy and of the kinetic energy of the electrons is then, per unit of length of the vortices

$$\varepsilon = \frac{1}{2\mu_0} \iint_S (\mathbf{B} + \mu_0 \lambda^2 \nabla \times \mathbf{j}) \cdot \mathbf{B} dS \quad (7.63)$$

where  $\mathbf{j}$  is the current density related to  $\mathbf{B}$  by  $\nabla \times \mathbf{B} = \mu_0 \mathbf{j}$  and  $dS$  the surface elements perpendicular to the vortex lines.

#### **Evaluation of the energy of an isolated vortex**

By using the generalized LONDON equation developed in section 9.6 (relation 9.32), we have

$$\mathbf{B}(\mathbf{r}) + \mu_0 \lambda^2 \nabla \times \mathbf{j}(\mathbf{r}) = \phi_0 \delta_2(\mathbf{r} - \mathbf{r}_0) \hat{\mathbf{u}}_0 \quad (7.64)$$

where  $\delta_2(\mathbf{r} - \mathbf{r}_0)$  is the two-dimensional DIRAC delta function and  $\mathbf{r}_0$  is the position of the axis situated on the plane containing  $\mathbf{r}$  and perpendicular to the unit vector  $\hat{\mathbf{u}}_0$  along the vortex axis. Then the energy  $\varepsilon_1$  of a single vortex, neglecting the energy of its very small core, is obtained by substituting (7.64) into (7.63),<sup>23</sup>

$$\varepsilon_1 = \frac{1}{2\mu_0} \iiint_V \phi_0 \delta_2(\mathbf{r} - \mathbf{r}_0) \hat{\mathbf{z}} \cdot \mathbf{B} dr^3 = \frac{\phi_0}{2\mu_0} B(\mathbf{r}_0) \quad (7.65)$$

which is simply the relation (6.27), with  $B(\mathbf{r}_0)$  being precisely the magnetic field at the center of the vortex.

#### **Interaction energy between vortices**

In the presence of two vortices,  $V_1$  centered at  $\mathbf{r}_1$  and  $V_2$  centered at  $\mathbf{r}_2$ , the second generalized LONDON equation (7.64) becomes

$$\mathbf{B}(\mathbf{r}) + \mu_0 \lambda_L^2 \nabla \times \mathbf{j}(\mathbf{r}) = \phi_0 \delta_2(\mathbf{r} - \mathbf{r}_1) \hat{\mathbf{u}}_1 + \phi_0 \delta_2(\mathbf{r} - \mathbf{r}_2) \hat{\mathbf{u}}_2 \quad (7.66)$$

<sup>23</sup> There are more accurate calculations than shown here, including corrections that have, however, no incidence on the force between vortices.

where  $\mathbf{B}(\mathbf{r}) = \mathbf{B}_1(\mathbf{r}) + \mathbf{B}_2(\mathbf{r})$  is the sum of the magnetic fields associated with the two vortices.

If we insert this expression into (7.63) we have the energy  $\varepsilon_2$

$$\varepsilon_2 = \frac{\phi_0}{2\mu_0} [B_1(\mathbf{r}_1) + B_2(\mathbf{r}_2) + B_1(\mathbf{r}_2) + B_2(\mathbf{r}_1)]. \quad (7.67)$$

The first two terms represent the energy of formation of the two isolated vortices,

$$\frac{\phi_0}{2\mu_0} [B_1(\mathbf{r}_1) + B_2(\mathbf{r}_1)] = 2\varepsilon_1 \quad (7.68)$$

and the cross-terms a supplementary energy  $W_{1-2}$  of interaction between the vortices.

$$\frac{\phi_0}{2\mu_0} [B_1(\mathbf{r}_2) + B_2(\mathbf{r}_1)] = W_{1-2}. \quad (7.69)$$

Since the vortices are identical, the field  $\mathbf{B}_1(\mathbf{r}_2)$  created at  $\mathbf{r}_2$  by the vortex centered at  $\mathbf{r}_1$  and the field  $\mathbf{B}_2(\mathbf{r}_1)$  created at  $\mathbf{r}_1$  by the field centered at  $\mathbf{r}_2$  depend only on the distance  $r = |\mathbf{r}_2 - \mathbf{r}_1|$  that separates them, and we have

$$B_1(\mathbf{r}_2) = B_2(\mathbf{r}_1) = B(r). \quad (7.70)$$

### **Force between vortices**

The force between the vortices, that tends to minimize the interaction energy, is repulsive. The force on the vortex  $V_1$  due to the presence of  $V_2$  is (see Fig. 7.30a),

$$f_{1-2} = -\frac{\partial W_{1-2}}{\partial r} = -\frac{\phi_0}{\mu_0} \frac{\partial B_2}{\partial r} \Big|_{\mathbf{r}_1} = \phi_0 j_2(\mathbf{r}_1) \quad (7.71)$$

where  $j_2(\mathbf{r}_1)$  is the current density associated with the vortex  $V_2$  at the core of  $V_1$ . This expression is identical to (7.55) in both direction and magnitude.

### **Force acting on a vortex immersed in a uniform current density**

If we make the hypothesis that the force on the vortex  $V_1$  immersed in the current density  $\mathbf{j}_2(\mathbf{r}_1)$  of the vortex  $V_2$  (7.71) would be the same if the current density were from any other source, then a vortex  $V$  immersed in a current density  $\mathbf{J}$  feels the force expressed by (7.55). This force, intimately linked to the generalized LONDON equation (7.64), is called  $\mathbf{f}_{Ln}$ , the “LONDON force” (Fig. 7.30b).

In fact this assertion is not easily proved, as the current density density  $\mathbf{J}$  in which the vortex is immersed is not of the same nature as that associated with another vortex. Its source is external and if we wish to calculate the force acting on  $V$  by applying the theorem of virtual work, we must include the potential difference that appears and the work that must be provided to maintain it.<sup>24</sup>

---

24 D.X. CHEN, E. PARDO & A. SANCHEZ (2010) *Physica C* **470**, 444.

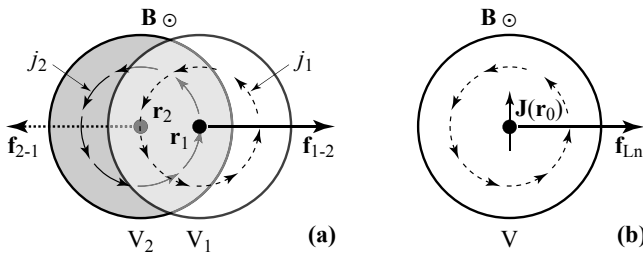


**Figure 7.30 - Forces acting on the vortices**

(a) The repulsive force between vortices:  $\mathbf{f}_{1-2}$  is the repulsive force acting on the vortex  $V_1$  (in white) with center at  $\mathbf{r}_1$  coming from the vortex  $V_2$  centered at  $\mathbf{r}_2$  (in grey). The force  $\mathbf{f}_{1-2}$  can be expressed as a function of the current density  $j_2(\mathbf{r}_1)$  that the vortex  $V_2$  produces at  $\mathbf{r}_1$ . (b) Force on a vortex immersed in a current density  $\mathbf{J}$ : the expression for the force  $\mathbf{f}_{1-2}$  in figure (a) generalizes to any current density, whether it is created by another vortex or whether it comes from a transport current of density  $\mathbf{J}$ .

#### A7A.4 - MAGNUS force

The most spectacular demonstration of a MAGNUS force is when a soccer player produces a curved trajectory by giving spin to the ball, making it rotate with respect to the mass of air it is moving through.

The ball is here the core of the vortex, its rotation is that of the whirlwind current that surrounds it, and the fluid through which it is moving is the current density  $\mathbf{J}$ . The transverse force is the subject of this appendix.

#### Fixed cylinder in a moving fluid

We consider a fluid, here electrons in uniform translation moving at a speed  $v_J$ , in which we place a cylinder with its axis perpendicular to the velocity of the fluid's displacement (Fig. 7.31a).

The lines of current surround the fixed cylinder and are squeezed above and below. Fluid mechanics teaches us that when the fluid is irrotational, its velocity tangential to the cylinder surface is<sup>25</sup>

$$2v_J |\sin \theta|. \quad (7.71)$$

In Figure 7.31a the vector of current density is directed to the left and the electrons move to the right.

#### Velocity of the electrons around the core of an isolated vortex

The vortex core is considered as a rigid cylinder of radius  $\xi$ . The tangential velocity  $v_t$  (Fig. 7.31) of the electrons that carry the whirlwind current  $\mathbf{j}_t$  at the surface of the cylinder equals (see relation 9.30)

<sup>25</sup> E. GUYON, J-P. HULIN & L. PETIT (2015) *Physical Hydrodynamics*, 2<sup>nd</sup> English Edition, OUP, Oxford.

$$v_t = \frac{\phi_0}{2\pi m \xi} e. \quad (7.72)$$

The electrons are represented in Figure 7.31b. For a magnetic field pointing out of the page, the electrons turn clockwise.

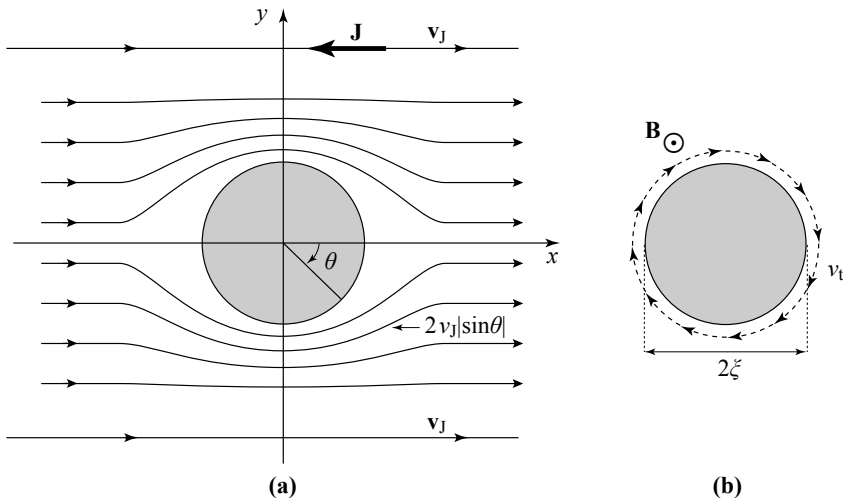


Figure 7.31

(a) Cylinder in a fluid in uniform translation: the fluid with speed  $v_J$  flows around the cylinder. The tangential speed at the cylinder is  $2v_J|\sin\theta|$ . (b) The trajectory of the electrons associated with the vortex current around a vortex core.

### MAGNUS force

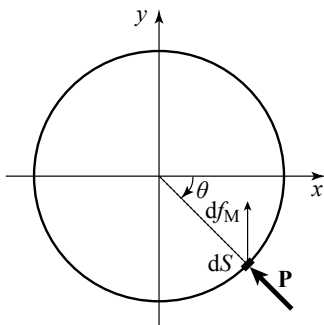
The total velocity of the electrons just around a vortex core immersed in a current density  $J$  is the sum of the tangential currents (7.71) and (7.72) which add in the upper part and subtract in the lower part. In so far as  $v_t \gg v_J$

$$v^2 = v_t^2 + 4v_t v_J \sin\theta. \quad (7.73)$$

Since we are in the steady state, we can apply the BERNOULLI equation.

$$P + \frac{1}{2}nmv^2 = \text{Constant}. \quad (7.74)$$

This signifies that the sum of the pressure on an object and the density of kinetic energy of the fluid in its immediate vicinity is the same at any point of its surface ( $n$  is the density of particles and  $m$  their mass). Without even making a calculation, it is apparent that as the velocity of the electrons above is greater than it is below, the vortex core feels a force directed upwards, *i.e.* the direction of  $\mathbf{f}_\phi$  predicted by the relation (7.55).

**Figure 7.32****MAGNUS force**

The pressure on each surface element of the cylinder, is a function of the local fluid velocity as given by the BERNOULLI equation.  $df_M$  is the contribution of the surface element  $dS$  to the MAGNUS force.

More precisely, the pressure at a point of the surface is a constant to which is added the term,

$$\delta P = 2 v_t v_J \sin \theta \quad (7.75)$$

and, in consequence, an element of surface  $dS = \zeta d\theta$  experiences, per unit length of the vortex, a net force with vertical component

$$df_M = \delta P dS \sin \theta = \frac{1}{2} nm \left( 4 \frac{\phi_0}{2\pi m \xi} e v_J \sin^2 \theta \right) \xi d\theta \quad (7.76)$$

or, integrating from 0 to  $2\pi$ ,  $f_M = J \phi_0$ . (7.77)

This is the MAGNUS force, which is found to be equal to  $\mathbf{f}_\phi$  in direction and in magnitude. More refined analyses have been developed.<sup>26</sup>

#### A7A.5 - Conclusions

We are confronted, therefore, with three types of force that have been invoked to justify the relation (7.55):

- » the LORENTZ force, where there is serious uncertainty as to its direction;
- » the LONDON force that results from the interaction energy between pairs of vortices but whose extension to the interaction between a vortex and an external current has not been established definitively;
- » the MAGNUS force of hydrodynamic origin. It is the subject of numerous discussions to include the distribution of superconducting electrons close to the core, the effects of quasi-particles or simply the vortex displacements.

We can find very thorough discussions of these different contributions in the articles cited in this appendix, without definitive conclusions having been drawn to this day.

---

<sup>26</sup> E.B. SONIN (1997) *Phys. Rev. B* **55**, 485; B. PLAÇAIS *et al.* (1997) *Phys. Rev. B* **54**, 13083.

## Appendix 7B

### Energy dissipated by a moving vortex

#### The BARDEEN-STEPHEN model

##### A7B.1 - Construction of the argument

The reasoning behind the BARDEEN-STEPHEN model can be constructed schematically from six premises:

1. The vortex is modelled by a normal core of radius  $\xi$  and resistivity  $\rho_n$ , surrounded by a whirlwind of superconducting electrons of current density  $\mathbf{j}$ .
2. Displacement of the vortex implies displacement of the whirlwind current of superconducting electrons.
3. To displace the whirlwind current, an electric field  $\mathbf{E}^{\text{ext}}$  must be present outside the core, and this field must be related to  $\mathbf{j}$  by the first LONDON equation.
4. To create the electric field  $\mathbf{E}^{\text{ext}}$  outside the core, it is necessary to make a charge surface density  $\sigma_{\text{surf}}$  appear at the surface of the core.
5. These surface charges create a field  $\mathbf{E}^{\text{int}}$  within the core.
6. Subject to the field  $\mathbf{E}^{\text{int}}$ , the normal electrons of the core move and dissipate energy by the JOULE effect, leading to the flux-flow resistivity.

##### A7B.2 - Current density

In the region  $\xi < r \ll \lambda$  of the vortex that is considered here, the whirlwind current density can be written in cylindrical coordinates,<sup>27</sup>

$$j_\theta(r) \approx \frac{\phi_0}{2\pi\mu_0\lambda^2} \frac{1}{r} \quad (7.78)$$

and in Cartesian coordinates,

$$j_x(r) \approx -\frac{\phi_0}{2\pi\mu_0\lambda^2} \frac{y}{x^2 + y^2} \quad ; \quad j_y(r) \approx \frac{\phi_0}{2\pi\mu_0\lambda^2} \frac{x}{x^2 + y^2}. \quad (7.79)$$

##### A7B.3 - Exterior electric field

In order to calculate the electric field  $\mathbf{E}^{\text{ext}}$  necessary for the displacement of the whirlwind current of a vortex at velocity  $\mathbf{v}$ , we consider two points situated at  $\mathbf{r}$  and  $\mathbf{r} - \mathbf{v}\delta t$  where at time  $t$  the instantaneous current densities are  $\mathbf{j}(\mathbf{r})$  and  $\mathbf{j}(\mathbf{r} - \mathbf{v}\delta t)$ . Because of the global translation of the vortex, the current density at the point  $\mathbf{r}$  at time  $t + \delta t$  is equal to what it was at time  $t$  at the point  $\mathbf{r} - \mathbf{v}\delta t$ . Hence the change in the current at point  $\mathbf{r}$  between times  $t$  and  $t + \delta t$  is

$$\delta \mathbf{j}(\mathbf{r})|_{\text{between } t \text{ and } t+\delta t} = \mathbf{j}(\mathbf{r} - \mathbf{v}\delta t) - \mathbf{j}(\mathbf{r})|_{\text{at time } t}. \quad (7.80)$$

---

<sup>27</sup> This relation will be demonstrated in section 9.5.4 (relation 9.31).

Close to a vortex oriented along the  $z$  axis and moving along the  $x$  axis with velocity  $v_x$ , the changes in the components  $j_x^v$  and  $j_y^v$  at the point  $\mathbf{r}$  between  $t$  and  $t + \delta t$  are then

$$\delta j_x^v = -\frac{\partial j_x}{\partial x} v_x \delta t \quad \text{and} \quad \delta j_y^v = -\frac{\partial j_y}{\partial x} v_x \delta t \quad (7.81)$$

which, from the first LONDON equation

$$\mathbf{E}^{\text{ext}} = -\mu_0 \lambda^2 \frac{\partial \mathbf{j}}{\partial t} \quad (7.82)$$

requires that components of  $\mathbf{E}^{\text{ext}}$  satisfy

$$E_x^{\text{ext}} = -\mu_0 \lambda^2 \frac{\partial j_x^v}{\partial x} v_x \quad \text{and} \quad E_y^{\text{ext}} = -\mu_0 \lambda^2 \frac{\partial j_y^v}{\partial x} v_x. \quad (7.83)$$

From the expression (7.78), this can be rewritten

$$E_x^{\text{ext}} = -v_x \frac{\phi_0}{2\pi} \frac{2xy}{(x^2 + y^2)^2} \quad \text{and} \quad E_y^{\text{ext}} = -v_x \frac{\phi_0}{2\pi} \frac{y^2 - x^2}{(x^2 + y^2)^2} \quad (7.84)$$

or, in vector notation, for a point  $M$  situated at  $\mathbf{r}$ ,

$$\mathbf{E}^{\text{ext}} = -v_x \frac{\phi_0}{2\pi} \frac{2(\hat{\mathbf{y}} \cdot \mathbf{u}_r) \mathbf{u}_r - \hat{\mathbf{y}}}{r^2} \quad (7.85)$$

where  $\hat{\mathbf{y}}$  is the unit vector in the  $y$  direction, and  $\mathbf{u}_r$  the unit vector in the direction from the origin to  $M$ .

#### A7B.4 - Charge density at the core surface

It so happens that the expression (7.85) is formally identical to that of an electric field

$$\mathbf{E}^{\text{ext}} = R^2 \frac{\sigma_0}{2\epsilon_0} \frac{2(\hat{\mathbf{y}} \cdot \mathbf{u}_r) \mathbf{u}_r - \hat{\mathbf{y}}}{r^2} \quad (7.86)$$

created outside an infinite cylinder along the  $z$  axis and of radius  $R$ , with surface charge<sup>28</sup>

$$\sigma_{\text{surf}} = \sigma_0 \cos \theta \quad (7.87)$$

where  $\theta$  is the azimuthal angle (with respect to the  $y$  axis). This leads us to consider the vortex core as a cylinder of radius  $R = \xi$  with surface charge  $\sigma_{\text{surf}} = \sigma_0 \cos \theta$  where

$$\sigma_0 = -2\epsilon_0 v_x \frac{\phi_0}{2\pi \xi^2} \quad (7.88)$$

---

<sup>28</sup> C. GARING (1995) *Milieux diélectriques*, Ellipse, p. 34,  
[http://faculty.uml.edu/cbaIRD/all\\_homework\\_solutions/Jackson\\_4\\_8\\_Homework\\_Solution.pdf](http://faculty.uml.edu/cbaIRD/all_homework_solutions/Jackson_4_8_Homework_Solution.pdf)

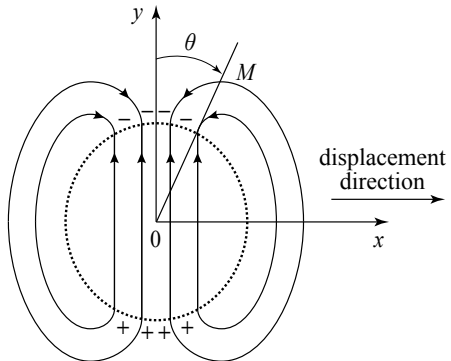


Figure 7.33

**Electric field lines created by a cylindrical bar of radius  $R$  and carrying surface charges  $\sigma_{\text{surf}} = \sigma_0 \cos \theta$**   
The external electric field distribution is similar to that created nearby a moving vortex.  
The electric field is uniform in the interior of the cylinder with value  $E^{\text{int}} = -\sigma_0 / 2\epsilon_0$ .  
Note that the electric field is perpendicular to the displacement velocity.

### A7B.5 - Internal field

Since the electric field created in the interior of a cylinder carrying a surface charge density  $\sigma_{\text{surf}} = \sigma_0 \cos \theta$  is uniform,

$$E^{\text{int}} = -\frac{\sigma_0}{2\epsilon_0}. \quad (7.89)$$

BARDEEN and STEPHEN wrote, by simple transposition, that the electric field inside the vortex core was

$$E^{\text{int}} = v_x \frac{\phi_0}{2\pi\xi^2}. \quad (7.90)$$

### A7B.6 - Dissipated power and flux-flow resistivity

Since the power dissipated per unit volume of the vortex core of resistivity  $\rho_n$  (the core is in the normal state), where there is the electric field  $E^{\text{int}}$ , is  $(E^{\text{int}})^2 / \rho_n$ , the power dissipated per unit length of the vortex can be written as

$$p = \pi \xi^2 \frac{(E^{\text{int}})^2}{\rho_n} = \pi \xi^2 \frac{1}{\rho_n} \left( v_x \frac{\phi_0}{2\pi\xi^2} \right)^2 = \frac{v_x^2}{\rho_n} \frac{\phi_0^2}{4\pi\xi^2} \quad (7.91)$$

or, per unit volume of the superconductor containing  $n_v$  vortices per unit area

$$\mathcal{P} = n_v p = n_v \frac{v_x^2}{\rho_n} \frac{\phi_0^2}{4\pi\xi^2}. \quad (7.92)$$

Identifying this result to the relation (7.12) derived in a model of viscous friction we find

$$\eta = \frac{2\mathcal{P}}{n_v v_x^2} = \frac{1}{\rho_n} \frac{\phi_0^2}{2\pi\xi^2} \quad (7.93)$$

where we have introduced an extra factor of 2 that BARDEEN and STEPHEN justified by showing that some of the electrons, whose trajectories are modified by the vortex motion, come very close to the core without actually penetrating and then they too become resistive.<sup>4</sup> Using the relation (6.28) between  $H_{c2}$  and  $\xi$ , we obtain the expression (7.18) for the resistive coefficient  $\eta$ .

$$\eta = \frac{\phi_0}{\rho_n} \mu_0 H_{c2}. \quad (7.94)$$

## Chapter 8

# COOPER PAIRS PRINCIPAL RESULTS OF BCS THEORY

The microscopic mechanism at the origin of the superconductivity emerged in two stages. The first was the proof, by Leon COOPER, that two electrons at the FERMI level with an attractive interaction form a bound state and constitute a pair, now called the “COOPER pair.” The second stage was the application by BARDEEN, COOPER and SCHRIEFFER of the techniques of the many-body problem to treat the system consisting of  $N$  electrons which form COOPER pairs condensed in a boson-like coherent state. This theory, called “BCS” to recall the names of its authors, was published in an historic article<sup>1</sup> whose results are in agreement with the principal properties of superconductors such as the MEISSNER effect, the critical field, the critical current density, electromagnetic absorption, the nature of the coherence length introduced by the non-local PIPPARD equations... Exploitation of this theory, where superconductivity appears as a BOSE-like condensation of COOPER pairs, later lead to the discovery of the JOSEPHSON effects and justified the phenomenological theory of GINZBURG and LANDAU.

After giving a detailed treatment of the formation of a COOPER pair, the elements of BCS theory will be presented in a qualitative way.

### 8.1 - Free electron gas

#### 8.1.1 - Free electron gas at 0 K

The metallic state is characterized by the presence in the material of mobile electrons called “conduction electrons.” To a first approximation we consider that each of them moves freely in the uniform average potential created by the ions and the other electrons of the metal. They are treated as a gas of  $N$  independent electrons inside a rectangular box of volume  $\mathcal{V}$ (of dimensions  $L_1, L_2, L_3$ ) that obey FERMI-DIRAC statistics.

---

<sup>1</sup> J. BARDEEN, L.N. COOPER & J.R. SCHRIEFFER (1957) *Phys. Rev.* **108**, 1175.

Without interactions, their energy is purely kinetic and the Hamiltonian of each electron is

$$\hat{H}_0 = -\frac{\hbar^2}{2m} \nabla^2. \quad (8.1)$$

The energy levels  $\varepsilon_{\mathbf{k}}$  are solutions of the eigenvalue equation

$$\hat{H}_0 \phi_{\mathbf{k}} = \varepsilon_{\mathbf{k}} \phi_{\mathbf{k}} \quad (8.2)$$

where, adopting the periodic boundary conditions of BORN-VON KARMAN<sup>2</sup>

$$\varepsilon_{\mathbf{k}} = \frac{\hbar^2}{2m} (k_1^2 + k_2^2 + k_3^2) \quad \text{with } k_i = \frac{2\pi}{L_i} n_i. \quad (8.3)$$

The  $n_i$  are positive or negative integers and the  $k_i$  ( $i = 1, 2, 3$ ) appear as the components of a wave vector  $\mathbf{k}$ . The corresponding wave functions  $\phi_{\mathbf{k}}$  are plane waves,

$$\phi_{\mathbf{k}}(\mathbf{r}) = \frac{1}{\sqrt{\mathcal{V}}} e^{i\mathbf{k} \cdot \mathbf{r}} \quad \text{with } \varepsilon_{\mathbf{k}} = \frac{\hbar^2}{2m} \mathbf{k}^2. \quad (8.4)$$

The normalization factor  $1/\sqrt{\mathcal{V}}$  is chosen so that the integral of the probability density  $\phi_{\mathbf{k}}^*(\mathbf{r}) \phi_{\mathbf{k}}(\mathbf{r})$  over the volume  $\mathcal{V}$  of the box equals unity.

To define the quantum state of the electron completely, we must add its spin. Each quantum state of a particle is then represented by a point of coordinates  $k_1, k_2, k_3$  in the wave vector space (reciprocal space), to which is associated a component of spin,  $\uparrow$  or  $\downarrow$ .

**Note** - when such precision is needed, the wave function of an electron of spin  $\uparrow$  occupying the quantum state  $\mathbf{k}$  will be denoted by  $\phi_{\mathbf{k}\uparrow}(\mathbf{r})$ .

### Density of states

As the separation of two adjacent nodes is very small ( $2\pi/L_i$  along each axis), the quantum states can be considered as forming a continuum both in  $k$  and in energy  $\varepsilon$ . Every state “occupies” in  $\mathbf{k}$ -space a volume  $8\pi^3/\mathcal{V}$  so that the number  $dN_{\text{state}}$  of quantum states per spin component whose wave vector has a magnitude between  $k$  and  $k + dk$  is

$$dN_{\text{state}} = \frac{\mathcal{V}}{8\pi^3} 4\pi k^2 dk = \mathcal{V} G(k) dk \quad \text{with } G(k) = \frac{1}{2\pi^2} k^2 \quad (8.5)$$

where  $G(k)$  is the density of states in  $k$  per unit volume and per spin state. The density of states in energy  $G(\varepsilon)$ , always per unit volume and per spin state, is such that the number of quantum states between  $\varepsilon$  and  $(\varepsilon + d\varepsilon)$  is

$$dN_{\text{state}} = \mathcal{V} G(\varepsilon) d\varepsilon. \quad (8.6)$$

---

2  $\phi(x + n_1 L_1, y + n_2 L_2, z + n_3 L_3) = \phi(x, y, z); n_1, n_2, n_3$  are arbitrary integers.

Using the dispersion relation  $\varepsilon_{\mathbf{k}} = \frac{\hbar^2 k^2}{2m}$  and conservation of the number of states,

$$dN_{\text{state}} = \mathcal{V} G(\varepsilon) d\varepsilon = \mathcal{V} G(k) dk \quad (8.7)$$

giving

$$G(\varepsilon) = \frac{1}{4\pi^2} \left( \frac{2m}{\hbar^2} \right)^{3/2} \sqrt{\varepsilon}. \quad (8.8)$$

**Remark** - Note that we have defined  $G(k)$  and  $G(\varepsilon)$  as the electronic density of states *per spin state* and *per unit volume*. They must be distinguished from  $g(k)$  and  $g(\varepsilon)$ , which are densities of states of electrons of the two spin states. Obviously we have

$$g(k) = 2G(k) \quad \text{and} \quad g(\varepsilon) = 2G(\varepsilon). \quad (8.9)$$

### FERMI level

At 0 K, the  $N$  electrons populate the lowest energy levels. The occupied states of  $\mathbf{k}$  space lie inside a sphere, called the “FERMI sphere” (Fig. 8.1) of radius  $k_F$ , the “FERMI wave vector”. The FERMI energy  $\varepsilon_F$ , the highest occupied energy at 0 K (also called the “FERMI level”) is related to  $k_F$  by

$$\varepsilon_F = \frac{\hbar^2}{2m} k_F^2 \quad (8.10)$$

and since the  $N$  electrons fill all the levels up to  $k_F$ , we have

$$N = 2\mathcal{V} \int_0^{k_F} G(k) dk = \frac{\mathcal{V}}{\pi^2} \frac{k_F^3}{3}. \quad (8.11)$$

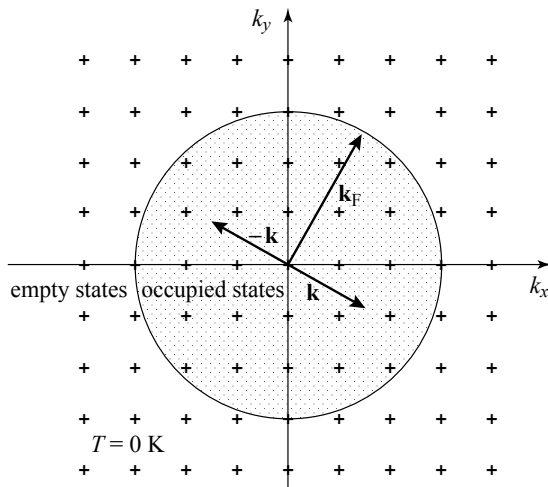


Figure 8.1 - FERMI sphere

The energy levels are attached to points of reciprocal space that form a lattice with parameters  $2\pi/L_i$ . Each point accommodates two opposite spins. The FERMI sphere bounds the volume occupied by the electrons at zero temperature. It is of radius  $k_F$ .

The wave vector, the energy and the speed of electrons at the FERMI level are therefore given by

$$k_F = \left( \frac{3\pi^2 N}{\mathcal{V}} \right)^{1/3} ; \quad \varepsilon_F = \frac{\hbar^2}{2m} \left( \frac{3\pi^2 N}{\mathcal{V}} \right)^{2/3} ; \quad v_F = \frac{\hbar k_F}{m}. \quad (8.12)$$

These parameters depend only on the density of free electrons  $n = N / \mathcal{V}$ . In metals we have typically  $\varepsilon_F \sim 5\text{-}10 \text{ eV}$ ,  $k_F \sim 1.25 \cdot 10^{10} \text{ m}^{-1}$  and  $v_F \sim 10^6 \text{ m s}^{-1}$ .

Expressions (8.8) and (8.12) lead to a density of states at the FERMI level per unit volume and for one spin state

$$G(\varepsilon_F) = \frac{3n}{4\varepsilon_F}. \quad (8.13)$$

### **Effects of temperature**

Qualitatively, the temperature has the effect of exciting particles by giving them an energy of order  $k_B T$ , where  $k_B = 0.86 \cdot 10^{-4} \text{ eV K}^{-1}$  is the BOLTZMANN constant; this represents an energy of 25 meV at 300 K or 2.5 meV at 30 K. As these energies are considerably less than the FERMI energy and because of the PAULI principle, only electrons located in a slice of energy  $k_B T$  wide below the FERMI level can be excited (Fig. 8.2b) and promoted to an empty level. Each of the  $2G(\varepsilon_F) k_B T$  electrons in this layer (the factor 2 taking into account the spin) acquires an average energy of order  $k_B T$ , leading to an increase in the energy per unit volume

$$\delta u \approx 2G(\varepsilon_F) k_B^2 T^2 \quad (8.14)$$

and an electronic specific heat per unit volume (of the normal state),

$$C_n^{\text{el}} = \frac{\partial(\delta u)}{\partial T} \approx 4G(\varepsilon_F) k_B^2 T \quad (8.15)$$

linear in  $T$ , as already mentioned in section 4.4.2, and proportional to the density of states at the FERMI level. More rigorously, the energy distribution of the electrons at temperature  $T$  is the product of the density of states  $2G(\varepsilon)$  with the FERMI function,

$$f(T, \varepsilon) = \frac{1}{1 + e^{\frac{\varepsilon - \varepsilon_F}{k_B T}}}. \quad (8.16)$$

The number of electrons (of the two spin states and per unit volume) of energy between  $\varepsilon$  and  $\varepsilon + d\varepsilon$  is written

$$dN(\varepsilon) = 2f(\varepsilon)G(\varepsilon)d\varepsilon. \quad (8.17)$$

The total energy of the free electron gas per unit volume is

$$u = \int_0^\infty 2\varepsilon f(\varepsilon)G(\varepsilon)d\varepsilon. \quad (8.18)$$

Differentiating with respect to  $T$ , the expression for the electronic specific heat becomes

$$C_n^{\text{el}} = \frac{2\pi^2}{3} G(\varepsilon_F) k_B^2 T \quad (8.19)$$

that differs little from (8.15).

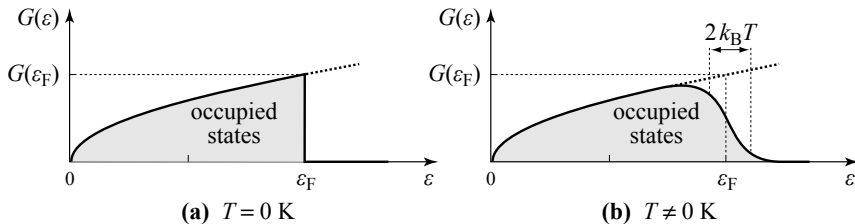


**Figure 8.2 - The electronic distribution at zero (a) and non-zero (b) temperatures**

The electronic density is the product of the density of states  $2G(\varepsilon)$  and the FERMI function  $f(T, \varepsilon)$ . At zero temperature, all states of energy less than the FERMI energy  $\varepsilon_F$  are occupied by electrons and the higher energy states are empty. At non-zero temperatures,  $f(T, \varepsilon)$  varies around the FERMI level from 1 to 0 over an energy interval of a few  $k_B T$ , leading to the electronic distribution shaded in grey.

## 8.2 - Interacting electron gas

### 8.2.1 - Wave functions of two independent particles

The kinetic energy of a system of two independent particles is the sum of the kinetic energy of each particle. In the absence of an interaction, its Hamiltonian is written

$$\hat{H}_0(\mathbf{r}_1, \mathbf{r}_2) = -\frac{\hbar^2}{2m} \nabla_1^2 - \frac{\hbar^2}{2m} \nabla_2^2 \quad (8.20)$$

where  $\nabla_1^2$  and  $\nabla_2^2$  are the Laplacians with respect to the variables  $\mathbf{r}_1$  and  $\mathbf{r}_2$  respectively. The eigenvalue equation can be resolved by separation of variables and the eigenfunctions  $\phi(\mathbf{r}_1, \mathbf{r}_2)$  of two independent particles are products of the eigenfunctions (8.4) of the single particle system

$$\phi_{\mathbf{k}_m \mathbf{k}_n}(\mathbf{r}_1, \mathbf{r}_2) = \phi_{\mathbf{k}_m}(\mathbf{r}_1) \phi_{\mathbf{k}_n}(\mathbf{r}_2) = \frac{1}{V} e^{i\mathbf{k}_m \cdot \mathbf{r}_1} e^{i\mathbf{k}_n \cdot \mathbf{r}_2}. \quad (8.21)$$

This wave function represents the probability amplitude of finding particle 1 at  $\mathbf{r}_1$  in the state  $\mathbf{k}_m$  and particle 2 at  $\mathbf{r}_2$  in the state  $\mathbf{k}_n$ . Because the electrons are indistinguishable and they are fermions, the wave function must be anti-symmetric, i.e. it must change sign if we permute the electrons

$$\phi_{\mathbf{k}_m \mathbf{k}_n}^{\text{AS}}(\mathbf{r}_1, \mathbf{r}_2) = -\phi_{\mathbf{k}_m \mathbf{k}_n}^{\text{AS}}(\mathbf{r}_2, \mathbf{r}_1). \quad (8.22)$$

This can be satisfied by writing the wave function as a SLATER determinant

$$\phi_{\mathbf{k}_m \mathbf{k}_n}^{\text{AS}}(\mathbf{r}_1, \mathbf{r}_2) = \frac{1}{\sqrt{2}} \begin{vmatrix} \varphi_{\mathbf{k}_m}(\mathbf{r}_1) & \varphi_{\mathbf{k}_m}(\mathbf{r}_2) \\ \varphi_{\mathbf{k}_n}(\mathbf{r}_1) & \varphi_{\mathbf{k}_n}(\mathbf{r}_2) \end{vmatrix} \quad (8.23)$$

which is interpreted as the probability amplitude of finding one electron at  $\mathbf{r}_1$  and the other at  $\mathbf{r}_2$ , one in the state  $\mathbf{k}_m$  and the other in the state  $\mathbf{k}_n$ , without any other precision (implicitly, the states  $\mathbf{k}_n$  and  $\mathbf{k}_m$  contain the spin indices). This way of writing the wave function appears a little clumsy and will mostly be unnecessary here. The anti-symmetrized function (8.23) showing explicitly the orbital and spin variables will be reintroduced only when strictly necessary.

The eigenvalues associated with the eigenfunctions  $\phi_{\mathbf{k}_m \mathbf{k}_n}(\mathbf{r}_1, \mathbf{r}_2)$  are the sums of the kinetic energies of the individual independent particles, or

$$\varepsilon_{\mathbf{k}_m \mathbf{k}_n} = \frac{\hbar^2 \mathbf{k}_m^2}{2m} + \frac{\hbar^2 \mathbf{k}_n^2}{2m} = \varepsilon_{\mathbf{k}_m} + \varepsilon_{\mathbf{k}_n}. \quad (8.24)$$

In the basis of functions  $\phi_{\mathbf{k}_m \mathbf{k}_n}(\mathbf{r}_1, \mathbf{r}_2)$ , the Hamiltonian (8.20) is diagonal and the diagonal elements are the eigenvalues  $\varepsilon_{\mathbf{k}_m \mathbf{k}_n}$ .

### 8.2.2 - Interaction potential

When the particles interact with each other, we must add an interaction term  $\hat{V}(\mathbf{r}_1, \mathbf{r}_2)$  to the two-particle Hamiltonian which becomes

$$\hat{H}_0(\mathbf{r}_1, \mathbf{r}_2) = -\frac{\hbar^2}{2m} \nabla_1^2 - \frac{\hbar^2}{2m} \nabla_2^2 + \hat{V}(\mathbf{r}_1, \mathbf{r}_2). \quad (8.25)$$

In this case it is no longer possible to proceed by separating variables. The search for new energy levels requires diagonalization of the matrix  $\hat{H}$  that, in the basis  $\phi_{\mathbf{k}_m \mathbf{k}_n}(\mathbf{r}_1, \mathbf{r}_2)$  of eigenvectors of the non-interacting system of two particles, has in addition to the diagonal terms we have just seen, non-diagonal terms that are the matrix elements

$$\langle \mathbf{p}, \mathbf{s} | \hat{V} | \mathbf{m}, \mathbf{n} \rangle = \frac{1}{V^2} \iiint e^{-i\mathbf{k}_p \cdot \mathbf{r}_1} e^{-i\mathbf{k}_s \cdot \mathbf{r}_2} V(|\mathbf{r}_2 - \mathbf{r}_1|) e^{i\mathbf{k}_m \cdot \mathbf{r}_1} e^{i\mathbf{k}_n \cdot \mathbf{r}_2} d^3 r_1 d^3 r_2. \quad (8.26)$$

Integration over  $\mathbf{r}_1$  and  $\mathbf{r}_2$  extends over the volume of the box. This matrix element takes the value, in a *unit* volume (see Ap. 8),

$$\langle \mathbf{p}, \mathbf{s} | \hat{V} | \mathbf{m}, \mathbf{n} \rangle = \begin{cases} V(\mathbf{q}) & \text{if } \mathbf{q} = \mathbf{k}_s - \mathbf{k}_n = \mathbf{k}_m - \mathbf{k}_p \\ 0 & \text{otherwise} \end{cases} \quad (8.27)$$

with

$$V(\mathbf{q}) = \iiint V(\mathbf{r}) e^{-i\mathbf{q} \cdot \mathbf{r}} d^3 r. \quad (8.28)$$

The process of interaction can be interpreted as follows (Fig. 8.3):

- » two electrons are initially in states  $|\mathbf{m}\rangle$  and  $|\mathbf{n}\rangle$  (momenta  $\hbar\mathbf{k}_m$  and  $\hbar\mathbf{k}_n$ );
- » during the interaction they exchange a momentum  $\hbar\mathbf{q}$  with probability amplitude  $V(\mathbf{q})$ ;

- » after this exchange, the electrons are to be found in states  $|\mathbf{p}\rangle = |\mathbf{m} - \mathbf{q}\rangle$  and  $|\mathbf{s}\rangle = |\mathbf{n} + \mathbf{q}\rangle$  with momenta  $\hbar(\mathbf{k}_m - \mathbf{q})$  and  $\hbar(\mathbf{k}_n + \mathbf{q})$ .

Because this exchange must be without any change in total momentum, only terms satisfying the condition

$$\hbar\mathbf{k}_m + \hbar\mathbf{k}_n = \hbar\mathbf{k}_p + \hbar\mathbf{k}_s \quad (8.29)$$

are non-zero.

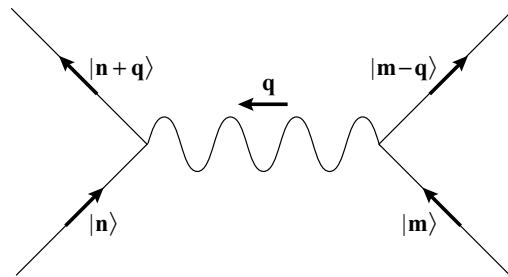


**Figure 8.3 - Diagrammatic presentation of the interaction between two particles**

In the initial state, the particles are in states  $|\mathbf{m}\rangle$  and  $|\mathbf{n}\rangle$ . By exchanging momentum  $\hbar\mathbf{q}$ , they are scattered into the states  $|\mathbf{m} - \mathbf{q}\rangle$  and  $|\mathbf{n} + \mathbf{q}\rangle$ .

### 8.2.3 - Interaction mediated by phonons

Starting with experiments that had shown (although this is not verified in every system) that two isotopes of the same element do not exhibit the same critical temperature  $T_c$  for the transition between the normal and superconducting phases, but follow an empirical law

$$T_c^{\text{iso}} = \frac{\text{Constant}}{\sqrt{M^{\text{iso}}}} \quad (8.30)$$

where  $M^{\text{iso}}$  is the isotope mass, FRÖHLICH<sup>3</sup> proposed the idea that the lattice vibrations (phonons), whose frequency is inversely proportional to the square root of  $M^{\text{iso}}$ , play a dominant role in the mechanism of superconductivity. Following this line of thought, BARDEEN, COOPER and SCHRIEFFER (BCS) considered that the attractive electron-electron interaction, responsible for superconductivity, is due to the exchange of phonons. The process is as follows:

- » an electron of initial momentum  $\hbar\mathbf{k}_m$  “excites” a phonon of wave vector  $\mathbf{q}$  transferring a momentum  $\hbar\mathbf{q}$ ; its final momentum is  $\hbar(\mathbf{k}_m - \mathbf{q})$ ;
- » the created phonon interacts with an electron of momentum  $\hbar\mathbf{k}_n$  that “absorbs” it, acquiring a momentum  $\hbar(\mathbf{k}_n + \mathbf{q})$ .

The excitation and absorption of the phonon are caused by the electrostatic interaction between electrons and crystal ions. During its motion, the first electron (of

3 H. FRÖHLICH (1936) *Elektronentheorie der Metalle*, Springer.

negative charge) displaces crystal ions (of positive charge) and generates the phonon. The moving ions will interact with the second electron by giving up their own movement to it. A detailed analysis reveals that to be non-vanishing, the non-diagonal elements of the interaction matrix should satisfy two conditions:

» The initial and final states must be states of *opposite wave vectors and opposite spins*. They are therefore of the form

$$V_{\mathbf{k}'\mathbf{k}} = \langle \mathbf{k}'_\uparrow, -\mathbf{k}'_\downarrow | \hat{V} | \mathbf{k}_\uparrow, -\mathbf{k}_\downarrow \rangle. \quad (8.31)$$

Such states  $|\mathbf{k}_\uparrow, -\mathbf{k}_\downarrow\rangle$  are called "pair states."

» As the particles exchanged during the interaction process are phonons, the only transitions possible are between pair states involving energy transfers less than the maximum phonon energy, which is order  $\hbar\omega_D$  (the DEBYE energy  $\approx 10$  to  $20$  meV). As a consequence the only "pair states" that can be involved in the transitions are those constructed out of wave vectors of wavelength  $\mathbf{k}$  whose energies  $\epsilon_{\mathbf{k}}$  lie in a band of energies of order  $\hbar\omega_D$  around the FERMI energy  $\epsilon_F$ .

The simple BCS approximation then considers that the non-zero matrix elements that describe the interaction are all equal with

$$V_{\mathbf{k}'\mathbf{k}} = \begin{cases} -V & \text{if } \epsilon_F - \hbar\omega_D < (\epsilon_{\mathbf{k}} \text{ and } \epsilon_{\mathbf{k}'}) < \epsilon_F + \hbar\omega_D \\ 0 & \text{otherwise} \end{cases} \quad (8.32)$$

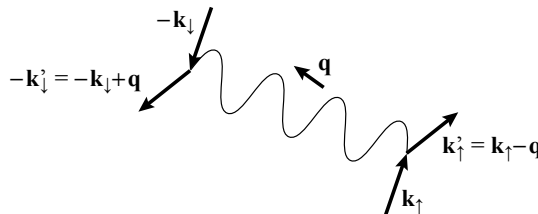


**Figure 8.4 - Graph of the interaction at the origin of BCS superconductivity**

Initially, two electrons occupy the pair state  $|\mathbf{k}_\uparrow, -\mathbf{k}_\downarrow\rangle$ . At time  $t$ , the electron of wave vector  $\mathbf{k}_\uparrow$  creates a phonon of wave vector  $\mathbf{q}$  and acquires the wave vector  $\mathbf{k}'_\uparrow = \mathbf{k}_\uparrow - \mathbf{q}$ . At a later time, the electron of wave vector  $-\mathbf{k}_\downarrow$  absorbs the phonon and its wave vector becomes  $-\mathbf{k}'_\downarrow = -\mathbf{k}_\downarrow + \mathbf{q}$ . The net effect is that the electron pair has been scattered from the state  $|\mathbf{k}_\uparrow, -\mathbf{k}_\downarrow\rangle$  into the state  $|\mathbf{k}'_\uparrow, -\mathbf{k}'_\downarrow\rangle$ .

To these conditions related to the nature and the form of the interaction potential we must add a condition to respect the PAULI principle: a transition from an initial state  $|\mathbf{k}_\uparrow, -\mathbf{k}_\downarrow\rangle$  towards a final state  $|\mathbf{k}'_\uparrow, -\mathbf{k}'_\downarrow\rangle$  can only occur if the initial state is occupied (electrons present in *both*  $|\mathbf{k}_\uparrow\rangle$  and  $|\mathbf{-k}_\downarrow\rangle$ ) and the final state is empty (electrons in *neither*  $|\mathbf{k}'_\uparrow\rangle$  nor  $|\mathbf{-k}'_\downarrow\rangle$ ).

## 8.3 - The reference system

Before beginning a general discussion of the stability of COOPER pairs, we will examine the effect of a negative potential on a system of a single particle. In the rest of this chapter we will often refer to the results of this “reference system”.

### 8.3.1 - One particle system

#### System of degenerate states

Consider a system of four states  $|1\rangle, |2\rangle, |3\rangle, |4\rangle$  forming a basis in which the Hamiltonian  $\hat{H}_0$  is diagonal, with four identical eigenvalues  $\varepsilon$ . We then add an interaction potential  $\hat{V}$  that has matrix elements in this basis that are all identical and negative, with value  $-V$ .

$$\langle \mathbf{j} | \hat{V} | \mathbf{i} \rangle = V_{ji} = -V. \quad (8.33)$$

Finding the new energy levels, *i.e.* the new eigenvalues of the Hamiltonian, involves solving the system of equations

$$\begin{pmatrix} \varepsilon - V - E & -V & -V & -V \\ -V & \varepsilon - V - E & -V & -V \\ -V & -V & \varepsilon - V - E & -V \\ -V & -V & -V & \varepsilon - V - E \end{pmatrix} \begin{pmatrix} c_1 \\ c_2 \\ c_3 \\ c_4 \end{pmatrix} = \begin{pmatrix} 0 \\ 0 \\ 0 \\ 0 \end{pmatrix}. \quad (8.34)$$

The solutions are the values of  $E$  making the determinant vanish or,

$$(E - \varepsilon)^3 [4V - (\varepsilon - E)] = 0 \quad (8.35)$$

which leads to three levels of energy equal to the initial energy and to a fourth energy level  $E_\alpha$  that is lower,

$$E_\beta = E_\gamma = E_\delta = \varepsilon ; \quad E_\alpha = \varepsilon - 4V. \quad (8.36)$$

The eigenvector  $|\alpha\rangle$  associated with this last level is the symmetric linear combination of the states  $|1\rangle, |2\rangle, |3\rangle$  and  $|4\rangle$ ,

$$|\alpha\rangle = \frac{1}{\sqrt{4}}(|1\rangle + |2\rangle + |3\rangle + |4\rangle). \quad (8.37)$$

In the language of quantum mechanics  $|\alpha\rangle$  is a stationary state, which means that:

» if the particle is in this state at time  $t = 0$  it will stay in this state indefinitely, with

quantum phase factor  $e^{-\frac{iE_\alpha}{\hbar}t}$ ;

» if at time  $t = 0$ , the particle is, for example, in the state  $|1\rangle$  which is not an eigenvector of the complete Hamiltonian, at later times it will be found with non-zero probabilities in the other states  $|2\rangle, |3\rangle$  and  $|4\rangle$ . The evolution of the system is given by the time-dependent equation

$$i\hbar \frac{dc_i(t)}{dt} = \sum_j V_{ij} c_j(t) \quad (8.38)$$

where  $c_i$  is the probability amplitude of finding the particle in the state  $|i\rangle$ .

We say that a particle in the state  $|a\rangle$  is delocalized over the states  $|1\rangle, |2\rangle, |3\rangle$  and  $|4\rangle$ . In addition to corresponding to the probability of finding the particle in each of the states  $|i\rangle$ , this delocalization has a dynamic character since it can be seen as a repeated jumping between the states  $|1\rangle, |2\rangle, |3\rangle$  and  $|4\rangle$  with a frequency of order  $V/\hbar$ .

This “dynamical” delocalization is a generalization from the two-state system (the molecule  $\text{NH}_3$ , for example) where in the bound state there is an oscillation between two configurations (the nitrogen above or below the plane of the hydrogens) by the effect of a non-diagonal matrix element.<sup>4</sup> This kind of “generalized oscillation” is among all four states  $|i\rangle$  here.

#### **Generalization to $N$ degenerate states**

The result obtained for the system with 4 states can be generalized to  $N$  states: the Hamiltonian matrix formed by  $N$  diagonal terms equal to  $(\varepsilon - V)$  and non-diagonal terms all equal to  $-V$ , has *one* bound state  $|a\rangle$  of energy

$$E_a = \varepsilon - NV \quad (8.39)$$

while the energy of all the other states stays as  $\varepsilon$ ,

$$E_\beta = E_\gamma = \dots = E_{v_+} = \varepsilon. \quad (8.40)$$

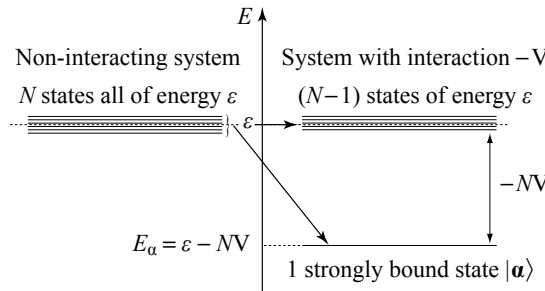


**Figure 8.5 - Bound state in an initially degenerate system**

An interaction that adds a term  $-V$  to each element of the Hamiltonian matrix leads to the emergence of a strongly bound state. The binding energy is proportional to the dimension  $N$  of the matrix.

<sup>4</sup> R. FEYNMAN, R. B. LEIGHTON, M. SANDS (1966) *The Feynman Lectures in Physics, Vol. III: Quantum Mechanics*, Addison-Wesley, New York. The new Millennium edition is available on-line at <http://www.feynmanlectures.caltech.edu>.

The decrease in energy  $-NV$ , also called the “binding energy,” becomes larger and larger as the number of states  $N$  increases. This means that in a system with a very large number of states, even a very weak attractive potential can lead to a state with energy significantly lower than in the non-interacting system.

As in four dimensions (the expression 8.37), the eigenvector associated with the state of lowest energy is the symmetric combination of all the states  $|i\rangle$ ,

$$|\alpha\rangle = \frac{1}{\sqrt{N}}(|1\rangle + |2\rangle + \dots + |i\rangle + \dots + |N\rangle). \quad (8.41)$$

Thus the more states over which the bound state is delocalized, the lower is its energy and the stronger the binding.

#### **System with non-degenerate states**

We now consider the case where eigenvectors of the non-interacting system  $|1\rangle$ ,  $|2\rangle$ ,  $|3\rangle$  and  $|4\rangle$  correspond to different energies  $\varepsilon_1$ ,  $\varepsilon_2$ ,  $\varepsilon_3$  and  $\varepsilon_4$ . Introduction of the potential  $\hat{V}$  leads to the eigenvalue equation

$$\begin{pmatrix} \varepsilon_1 - V - E & -V & -V & -V \\ -V & \varepsilon_2 - V - E & -V & -V \\ -V & -V & \varepsilon_3 - V - E & -V \\ -V & -V & -V & \varepsilon_4 - V - E \end{pmatrix} \begin{pmatrix} c_1 \\ c_2 \\ c_3 \\ c_4 \end{pmatrix} = \begin{pmatrix} 0 \\ 0 \\ 0 \\ 0 \end{pmatrix} \quad (8.42)$$

i.e., to four equations with four unknowns

$$V(c_1 + c_2 + c_3 + c_4) = c_i(\varepsilon_i - E) \quad ; \quad i \in [1,4] \quad (8.43)$$

or, equivalently, to the four relations

$$\frac{c_i}{V} = \frac{c_1 + c_2 + c_3 + c_4}{\varepsilon_i - E} \quad ; \quad i \in [1,4]. \quad (8.44)$$

Summing each of the two sides of (8.44) over the index “ $i$ ” we then obtain a general relation,

$$\frac{1}{V} = \sum_{i=1}^4 \frac{1}{\varepsilon_i - E}. \quad (8.45)$$

If  $\varepsilon_1 = \varepsilon_2 = \varepsilon_3 = \varepsilon_4 = \varepsilon$  we recover the solution (8.39)  $E_\alpha = \varepsilon - NV$ .

When the energies  $\varepsilon_i$  differ ( $\varepsilon_1 < \varepsilon_2 < \varepsilon_3 < \varepsilon_4$ ), the equation (8.42) always has one, and only one, energy lower than the lowest of the original energies as appears clearly by examination of the drawing in Figure 8.6. It is the only solution for which all the  $c_i$  are positive.

The eigenvector  $|\alpha\rangle$  associated with the eigenvalue  $E_\alpha$  can be written in the basis of non-perturbed eigenvector as

$$|\alpha\rangle = c_1|1\rangle + c_2|2\rangle + c_3|3\rangle + c_4|4\rangle \quad (8.46)$$

with

$$c_i = \frac{V \sum_{j=1}^4 c_j}{\epsilon_i - E_a}. \quad (8.47)$$

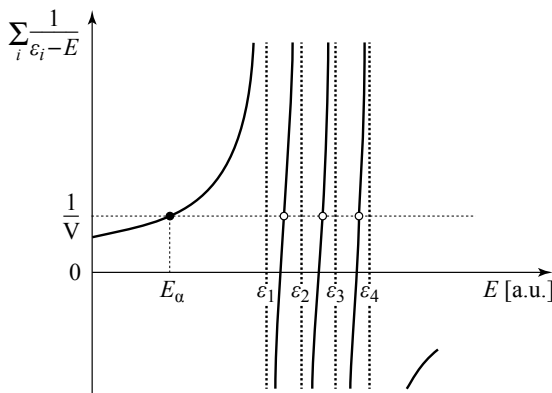


**Figure 8.6 - Bound state in an initially non-degenerate state**

An interaction that adds a term  $-V$  to each element of an initially non-degenerate Hamiltonian matrix leads to the emergence of one, and only one, energy level  $E_a$  below the lowest non-perturbed level.

The  $c_i$ , components of the “bound” state  $|\alpha\rangle$  of the eigenvectors of the non-interacting Hamiltonian, satisfy the relations  $c_1 > c_2 > c_3 > c_4$  (Fig. 8.7). The states of lowest energy therefore appear with a greater weight in the projection of  $|\alpha\rangle$ . This means that in the dynamic picture described previously, according to which the electron jumps between the stationary states of the non-perturbed system with occupation probabilities  $c_j^2$ , the particle has a higher probability to be found in the states of lowest energy.

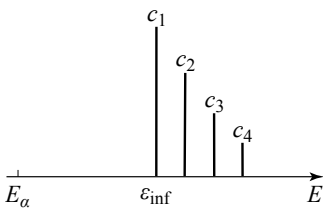


**Figure 8.7**  
**Weight of the initial states in the bound state**  
The respective weights of coefficients  $c_i$  of the bound state  $|\alpha\rangle$  projected on the basis of unperturbed states  $|i\rangle$ , when the initial state is non-degenerate.

### Generalization to N non-degenerate states

The result found in the previous paragraph for a four-state system can be generalized to  $N$  states that initially form a quasi-continuum of energy levels. The interaction  $-V$  causes the appearance of one state  $|\alpha\rangle$  at an energy below the lowest value of the quasi-continuum (Fig. 8.8).

In the dynamic picture, exploration of the states by the system privileges those that are lowest in the quasi-continuum of non-interacting states (Fig. 8.8).

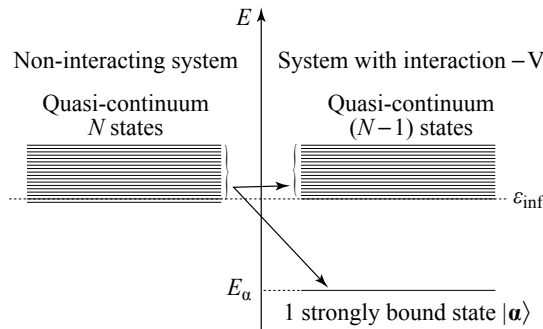


**Figure 8.8 - System of  $N$  levels forming a quasi-continuum**  
With the interaction  $-V$ , one, and only one, state emerges  
with energy below the lowest value of the continuum.

### 8.3.2 - Systems of pairs

We now turn to a system consisting of two electrons that, without interactions, can occupy, taking into account the exclusion principle, four one-particle states, two of energy  $\varepsilon$  and two of energy  $\varepsilon'$  with  $\varepsilon < \varepsilon'$  (the energy of each state is shown in brackets):

$$|1\rangle = |\mathbf{k}\uparrow\rangle (\varepsilon) ; |2\rangle = |-\mathbf{k}\downarrow\rangle (\varepsilon) ; |3\rangle = |\mathbf{k}'\uparrow\rangle (\varepsilon') ; |4\rangle = |-\mathbf{k}'\downarrow\rangle (\varepsilon') \quad (8.48)$$

The two-electron states of this system consist of (Fig. 8.9):

- » two pair states which satisfy the conditions of opposite wave vectors and opposite spins

$$|1,2\rangle = |\mathbf{k}\uparrow, -\mathbf{k}\downarrow\rangle (2\varepsilon) \quad \text{and} \quad |3,4\rangle = |\mathbf{k}'\uparrow, -\mathbf{k}'\downarrow\rangle (2\varepsilon'); \quad (8.49)$$

- » four states that are not pair states, as they do not satisfy these conditions

$$\begin{aligned} |1,3\rangle &= |\mathbf{k}\uparrow, \mathbf{k}'\uparrow\rangle (\varepsilon + \varepsilon') ; & |1,4\rangle &= |\mathbf{k}\uparrow, -\mathbf{k}'\downarrow\rangle (\varepsilon + \varepsilon') \\ |2,3\rangle &= |-\mathbf{k}\downarrow, \mathbf{k}'\uparrow\rangle (\varepsilon + \varepsilon') ; & |2,4\rangle &= |-\mathbf{k}\downarrow, -\mathbf{k}'\downarrow\rangle (\varepsilon + \varepsilon') \end{aligned} \quad (8.50)$$

(Pair states with two identical single particle states are excluded as they are incompatible with the PAULI principle).

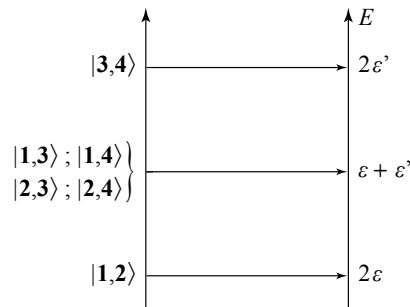


**Figure 8.9**  
**Energies of pair states of**  
**non-interacting electrons**

The energy of a pair state is the sum  
of the energies of the one-electron  
states constituting the pair.

We now introduce an interaction potential  $\hat{V}$  whose only non-zero matrix elements (which are all equal) are those coupling two pair states of type  $|\mathbf{k}_\uparrow, -\mathbf{k}_\downarrow\rangle$

$$\langle \mathbf{1}, \mathbf{2} | \hat{V} | \mathbf{1}, \mathbf{2} \rangle = \langle \mathbf{1}, \mathbf{2} | \hat{V} | \mathbf{3}, \mathbf{4} \rangle = \langle \mathbf{3}, \mathbf{4} | \hat{V} | \mathbf{1}, \mathbf{2} \rangle = \langle \mathbf{3}, \mathbf{4} | \hat{V} | \mathbf{3}, \mathbf{4} \rangle = -V. \quad (8.51)$$

In the basis ( $|\mathbf{1}, \mathbf{3}\rangle; |\mathbf{1}, \mathbf{4}\rangle; |\mathbf{2}, \mathbf{3}\rangle; |\mathbf{2}, \mathbf{4}\rangle; |\mathbf{1}, \mathbf{2}\rangle; |\mathbf{3}, \mathbf{4}\rangle$ ) (note the order of the vectors) the Hamiltonian matrix becomes

$$\hat{H} = \begin{pmatrix} \varepsilon + \varepsilon' & 0 & 0 & 0 & 0 & 0 \\ 0 & \varepsilon + \varepsilon' & 0 & 0 & 0 & 0 \\ 0 & 0 & \varepsilon + \varepsilon' & 0 & 0 & 0 \\ 0 & 0 & 0 & \varepsilon + \varepsilon' & 0 & 0 \\ 0 & 0 & 0 & 0 & 2\varepsilon - V & -V \\ 0 & 0 & 0 & 0 & -V & 2\varepsilon' - V \end{pmatrix}. \quad (8.52)$$

When we diagonalize it in order to find the energy levels of the two-particle system, the first block diagonal (of size  $4 \times 4$ ) which corresponds to two-electron states that are not pair states is unchanged. The second block is the  $(2 \times 2)$  subspace of pair states with eigenvalues

$$E_{\alpha\beta} = [(\varepsilon + \varepsilon') - V] \pm \sqrt{(\varepsilon - \varepsilon')^2 + V^2}. \quad (8.53)$$

The associated eigenvectors are linear combinations of the states  $|\mathbf{1}, \mathbf{2}\rangle$  and  $|\mathbf{3}, \mathbf{4}\rangle$ . The minus sign (-) corresponds to the bonding state of lower energy and the plus sign (+) to an anti-bonding state of higher energy.

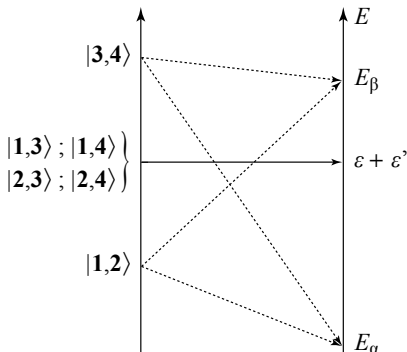


**Figure 8.10**  
**Interacting system containing two pair states**  
 From the pair states emerge a bonding state  
 of energy  $E_\alpha$  and an anti-bonding state  $E_\beta$ .  
 The states that are not pair states are unchanged.

The generalization to an increasing number of initial one-electron states is immediate. For instance, if we begin with 12 individual states of type  $|\mathbf{k}\rangle, |\mathbf{k}'\rangle, |\mathbf{k}''\rangle$  we can construct 66 two-particle states of which only 6 are pair states.

$$|\mathbf{k}_\uparrow, -\mathbf{k}_\downarrow\rangle; |\mathbf{k}'_\uparrow, -\mathbf{k}'_\downarrow\rangle; |\mathbf{k}''_\uparrow, -\mathbf{k}''_\downarrow\rangle; |\mathbf{k}_\downarrow, -\mathbf{k}_\uparrow\rangle; |\mathbf{k}'_\downarrow, -\mathbf{k}'_\uparrow\rangle; |\mathbf{k}''_\downarrow, -\mathbf{k}''_\uparrow\rangle.$$

If we add an interaction with non-diagonal elements  $-V$  only between pair states, the Hamiltonian becomes the direct sum of a  $(60 \times 60)$  diagonal block and a  $(6 \times 6)$  block in the subspace of pair states

$$\hat{H} = \begin{pmatrix} 2\varepsilon & 0 & * & 0 & 0 & 0 & 0 & 0 & 0 \\ 0 & 2\varepsilon & * & 0 & 0 & 0 & 0 & 0 & 0 \\ * & * & * & * & * & * & * & * & * \\ 0 & 0 & * & 2\varepsilon & 0 & 0 & 0 & 0 & 0 \\ 0 & 0 & * & 0 & 2\varepsilon - V & -V & -V & -V & -V \\ 0 & 0 & * & 0 & -V & 2\varepsilon - V & -V & -V & -V \\ 0 & 0 & * & 0 & -V & -V & 2\varepsilon' - V & -V & -V \\ 0 & 0 & * & 0 & -V & -V & -V & 2\varepsilon'' - V & -V \\ 0 & 0 & * & 0 & -V & -V & -V & -V & 2\varepsilon''' - V \end{pmatrix}. \quad (8.54)$$

This subspace of pair states, whose Hamiltonian matrix resembles exactly that of (8.42), returns to the results of the previous section. By simple transposition of the expression (8.45), we deduce the relation

$$\frac{1}{V} = \sum_i \frac{1}{2\varepsilon_i - E} \quad (8.55)$$

that makes appear a bound state  $|\alpha\rangle$  of energy  $E_\alpha$  as a linear combination of the pair states

$$|\alpha\rangle = \frac{1}{\sqrt{6}} \left\{ c_1 |\mathbf{k}_\uparrow, -\mathbf{k}_\downarrow\rangle + c_2 |\mathbf{k}_\downarrow, -\mathbf{k}_\uparrow\rangle + c_3 |\mathbf{k}'_\uparrow, -\mathbf{k}'_\downarrow\rangle \right. \\ \left. + c_4 |\mathbf{k}'_\downarrow, -\mathbf{k}'_\uparrow\rangle + c_5 |\mathbf{k}''_\uparrow, -\mathbf{k}''_\downarrow\rangle + c_6 |\mathbf{k}''_\downarrow, -\mathbf{k}''_\uparrow\rangle \right\} \quad (8.56)$$

whose coefficients satisfy  $c_i = \frac{V}{2\varepsilon_i - E_\alpha} \sum_j c_j$ . (8.57)

As in the previous example, a pair of electrons placed in the state  $|\alpha\rangle$  is delocalized over the six available pair states of type  $|\mathbf{k}_\uparrow, -\mathbf{k}_\downarrow\rangle$  with occupation probabilities  $|c_i|^2$ .

## 8.4 - COOPER pairs

### 8.4.1 - The accessible pair states

In a metal at 0 K, the conduction electrons are distributed on the lowest energy states, up to the FERMI level of energy  $\varepsilon_F$ . Above  $\varepsilon_F$  all the levels are empty, below all are filled. In this ideal situation, let us consider two electrons at the FERMI level, coupled by the BCS interaction (relation 8.32). Available to them are pair states of the form  $|\mathbf{k}_\uparrow, -\mathbf{k}_\downarrow\rangle$  that are unoccupied, *i.e.* situated above the FERMI level. Since, as indicated in section 8.2.3, scattering of a COOPER pair from one pair state  $|\mathbf{k}_\uparrow, -\mathbf{k}_\downarrow\rangle$  to another  $|\mathbf{k}'_\uparrow, -\mathbf{k}'_\downarrow\rangle$  cannot be accompanied by an energy transfer greater than the DEBYE energy, the only pair states accessible to the COOPER pair are those whose one-particle energy states satisfy  $\varepsilon_F < \varepsilon_k < \varepsilon_F + \hbar\omega_D$ , leading us to keep only pair states whose wave vectors  $\mathbf{k}$  are in the range

$$\frac{\hbar^2 k_F^2}{2m} < \frac{\hbar^2 k^2}{2m} < \frac{\hbar^2 k_F^2}{2m} + \hbar\omega_D \quad (8.58)$$

i.e. those in the band such that

$$k_F < k < k_c \quad \text{with} \quad \frac{\hbar^2 k_c^2}{2m} = \frac{\hbar^2 k_F^2}{2m} + \hbar\omega_D \quad (8.59)$$

or, since  $\hbar\omega_D \ll \frac{\hbar^2 k_F^2}{2m}$ ,

$$\hbar\omega_D \approx \frac{\hbar^2 k_F}{m} (k_c - k_F). \quad (8.60)$$

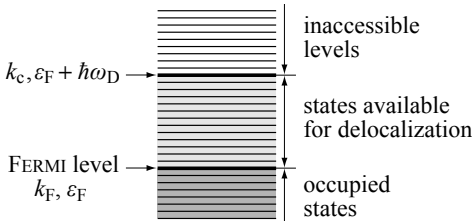


**Figure 8.11**

**Pair states accessible to delocalization of a COOPER pair**

Measuring the initial energy  $\xi_k$  from the FERMI level ( $\xi_k = \epsilon_k - \epsilon_F$ ), the accessible pair states are those whose single particle energy levels lie in the interval:  $0 < \xi_k < \hbar\omega_D \Leftrightarrow k_F < k < k_c$  with  $\hbar\omega_D = (\hbar^2 k_F/m) (k_c - k_F)$ .

#### 8.4.2 - Redefinition of the zero of energy

As the physics of superconductivity is concentrated around the immediate vicinity of the FERMI level, it turns out to be much more practical to take the FERMI energy as the zero of energies and to rename  $\xi_k$  the kinetic energy of a free electron in the state  $|\mathbf{k}\rangle$ . We have therefore<sup>5</sup>

$$\xi_k = \epsilon_k - \epsilon_F = \frac{\hbar^2}{2m} (k^2 - k_F^2) \quad (8.61)$$

and, in so far as  $k$  is very close to  $k_F$

$$\xi_k \equiv \frac{\hbar^2 k_F}{m} (k - k_F). \quad (8.62)$$

#### 8.4.3 - Bound state of the COOPER pair at 0 K

The problem can be treated by simple transposition of the “reference system” example. The expression (8.55) relating the energy  $E_\alpha$  of the bound state and the matrix element –  $V$  becomes

$$\frac{1}{V} = \sum_{k_F}^{k_c} \frac{1}{2\xi_k - E_\alpha} \quad (8.63)$$

and as there is a continuum of available pair states, it can be transformed into the integral

<sup>5</sup>  $\xi$  (regular font) = energy measured from the FERMI level.  
 $\xi$  (italics) = correlation length (see Chap. 3).

$$\frac{1}{V} = \int_{k_F}^{k_c} G(k) \frac{dk}{2\xi(k) - E_\alpha} \quad (8.64)$$

where  $G(k)$  is the density of states per unit volume ( $-V$  is the matrix element corresponding to a unit volume).  $E_\alpha$  is the energy of the bound state measured from the FERMI level taken as zero.  $E_\alpha$  is therefore negative.

By a change of variables  $k \rightarrow \varepsilon$  (see relation 8.7) and using the fact that the integration is over a very small region near the FERMI level, within which the density of states is almost constant with the value  $G(\varepsilon_F)$ ,

$$\frac{1}{V} = G(\varepsilon_F) \int_0^{\hbar\omega_D} \frac{d\xi}{2\xi - E_\alpha} \quad (8.65)$$

or, after integration,

$$\frac{1}{V} = \frac{1}{2} G(\varepsilon_F) \left[ \ln(2\xi - E_\alpha) \right]_0^{\hbar\omega_D} = \frac{1}{2} G(\varepsilon_F) \ln \left( 1 - \frac{2\hbar\omega_D}{E_\alpha} \right). \quad (8.66)$$

As experiments show that superconductivity of BCS type disappears beyond a few kelvins, the energy  $E_\alpha$  stays very small compared to the DEBYE energy that is several hundreds of degrees. We can then neglect the constant 1 compared to  $2\hbar\omega_D/E_\alpha$  and the expression (8.66) reduces to

$$\frac{1}{V} \approx \frac{1}{2} G(\varepsilon_F) \ln \left( -\frac{2\hbar\omega_D}{E_\alpha} \right) \quad (8.67)$$

and finally we have

$$E_\alpha \approx -2\hbar\omega_D e^{-\frac{2}{VG(\varepsilon_F)}}. \quad (8.68)$$

The binding energy  $E_b$  defined as

$$E_b = -E_\alpha. \quad (8.69)$$

is the lowering of the two electron energy by their association to form a COOPER pair delocalized over the available pair states. To have a definite idea of scales, typical values of the energies involved are:  $\varepsilon_F \approx 5$  eV;  $\hbar\omega_D \approx 20$  meV;  $G(\varepsilon_F)V \approx 0.25$ ;  $E_b \approx 0.013$  meV.

We can check that, as was assumed to find (8.68),

$$E_b \ll \hbar\omega_D \ll \varepsilon_F. \quad (8.70)$$

**Remark** -  $V$  and  $G(\varepsilon_F)$  have been defined per unit volume. As shown in Appendix 8, any other choice would have lead to the same result since for a volume  $\mathcal{V}$ ,  $V$  and  $G(\varepsilon_F)$  would be replaced by  $V/\mathcal{V}$  and  $\mathcal{V}G(\varepsilon_F)$  respectively, leaving the binding energy  $E_b$  of the COOPER pair unchanged.

#### 8.4.4 - Wave function, occupation probability

Similarly to (8.46), the quantum state of lowest energy can be projected onto the basis of pair states according to

$$|\alpha\rangle = \sum_{\mathbf{k}_i} c_{\mathbf{k}_i} |\mathbf{k}_i\uparrow, -\mathbf{k}_i\downarrow\rangle \quad (8.71)$$

and, exactly as in relation (8.57) this gives,

$$c_{\mathbf{k}_i} = \frac{1}{2\xi_i + E_b} \left[ V \sum_{\mathbf{k}_F}^{\mathbf{k}_c} c_{\mathbf{k}_j} \right] = \frac{K}{2\xi_i + E_b} \quad (8.72)$$

where  $K$  is a normalization constant such that

$$\sum_{\mathbf{k}_F}^{\mathbf{k}_c} c_{\mathbf{k}_j}^2 = 1. \quad (8.73)$$

In the state  $|\alpha\rangle$ , the occupation probability of an electron pair in the pair state  $|\mathbf{k}_m\uparrow, -\mathbf{k}_m\downarrow\rangle$  is equal to  $c_{\mathbf{k}_m}^2$ . Its variation as a function of energy  $\xi$  and wave vector  $k$  is shown in Figure 8.12.

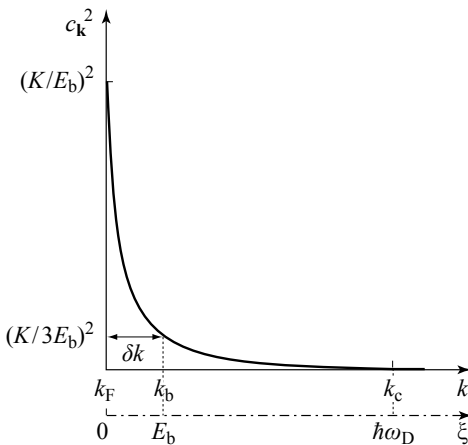


**Figure 8.12**  
**Profile of occupation probabilities of a COOPER pair over the pair states  $|\mathbf{k}_\uparrow, -\mathbf{k}_\downarrow\rangle$**   
 It takes a maximum at the FERMI level and decreases rapidly to 1/9 of its initial value at  $k_b$ .  
 The total probability for a COOPER pair to be in one of the pair states in the range  $k_F < k < k_b$  is 2/3.

This occupation probability decreases rapidly starting from  $k_F$  where it takes the value  $(K/E_b)^2$ . At the wave vector  $k_b$  defined by analogy to  $k_c$  by

$$\frac{\hbar^2 k_F^2}{2m} + E_b = \frac{\hbar^2 k_b^2}{2m} \quad (8.74)$$

it has decreased to 1/9 of this value. Integration of  $c_{\mathbf{k}}^2$  between 0 and  $E_b$  shows that the occupation probability of the COOPER pair over pair states in the band  $\delta k$  between  $k_F$  and  $k_b$  is equal to  $\frac{2}{3}$  and, as a consequence, the pair states situated between  $k_b$  and  $k_c$ , while available, are infrequently “visited”.

This result comes from a compromise between two terms with opposite effects:

- » the gain in the delocalization energy; the higher the number of pair states visited, the stronger this gain will be;
- » the energy cost in exploring levels that by their large values of  $k$  make a greater contribution to the kinetic energy.

It turns out to be energetically favorable to explore fewer states, avoiding those that are most costly in kinetic energy.

#### 8.4.5 - Spatial extent of a COOPER pair

It is well known in quantum mechanics (the uncertainty principle) that when a particle is described by a wave packet (a superposition of plane waves  $(1/\sqrt{\mathcal{V}})e^{ikr}$  whose wave vectors extend over a width  $\delta k$ ) the occupation probability of the particle extends over a distance  $\delta r$  such that

$$\delta r \approx \frac{1}{\delta k}. \quad (8.75)$$

In the same way, when a COOPER pair is described as a superposition of pair states  $|\mathbf{k}_\uparrow, -\mathbf{k}_\downarrow\rangle$ , i.e. by a superposition of plane waves  $(1/\mathcal{V})e^{i\mathbf{k}(\mathbf{r}_1-\mathbf{r}_2)}$  whose wave vectors extend over a width  $\delta k$ , the mean distance  $\delta r$  between the two particles forming the pair is given by the relation (8.75). As  $\delta k$  is close to  $(k_b - k_F)$ , we can relate  $\delta r$  to  $E_b$  by the following steps (see the approximation giving (8.62) from (8.61)): first

$$E_b \approx \frac{\hbar^2 k_F}{m} (k_b - k_F). \quad (8.76)$$

Introducing the FERMI velocity  $v_F$ , this then gives

$$\delta k = \frac{m}{\hbar^2 k_F} E_b = \frac{E_b}{\hbar v_F} \quad (8.77)$$

and finally the average distance between electrons in a COOPER pair

$$\delta r = \frac{1}{\delta k} \approx \frac{\hbar v_F}{E_b}. \quad (8.78)$$

### 8.5 - Elements of BCS theory

*From now on we give the results of the BCS calculation without explicit derivation, but referring to the formation of COOPER pairs at a qualitative level.*

#### 8.5.1 - Collection of COOPER pairs

In the previous section, it was shown that at 0 K, two electrons initially situated at the FERMI level see their energy lowered by joining to form a COOPER pair which is delocalized over, and jumps among, the pair states  $|\mathbf{k}_\uparrow, -\mathbf{k}_\downarrow\rangle$  available between  $k_F$  and  $k_c$ , with an occupation probability dominated by those between  $k_F$  and  $k_b$ .

By extension, there is no reason to stop at two electrons, and the energy of the system will be further diminished if we take two other electrons at the FERMI level to form a second COOPER pair, then two more to form a third...

We see then, with the successive formation of COOPER pairs, three phenomena would appear:

- » the energy of the system is lowered as each new COOPER pair “emerges”;
- » the pair states  $|\mathbf{k}_\uparrow, -\mathbf{k}_\downarrow\rangle$  situated at the FERMI level or slightly below, whose electrons are taken out in pairs to form COOPER pairs which explore higher levels, are now partially empty. They can therefore be added to the pair states available for the delocalization of the COOPER pairs, that now will have access to states of energy less than the FERMI level;
- » the COOPER pairs, as they are more and more numerous, start to “disturb” one another. The pair states are more and more filled and therefore less and less available as final states in the scattering from one pair state  $|\mathbf{k}_\uparrow, -\mathbf{k}_\downarrow\rangle$  to another  $|\mathbf{k}'_\uparrow, -\mathbf{k}'_\downarrow\rangle$ . In the language of the reference system, this reduces the dimension of the matrix and as a consequence, the binding energy. There are more COOPER pairs but each pair can find fewer states to jump between, leading to a phenomenon of saturation.

### 8.5.2 - Ground state

This qualitative reasoning shows that we cannot consider COOPER pairs separately, but must treat all the electrons globally. The progressive addition of COOPER pairs is artificial, because they appear simultaneously, forming a BOSE-like coherent state in which all of them are described by a unique wave function with a unique phase  $\theta$ . BCS formalized this aspect using many-body techniques. We summarize their results:

- » The lowering of the energy of the system is due to the attractive potential between electrons of reversed wave vector and opposite spin. It leads to a “delocalization” of the COOPER pairs over the pair states  $|\mathbf{k}_\uparrow, -\mathbf{k}_\downarrow\rangle$  situated near the FERMI level.
- » The occupation probabilities of a state  $|\mathbf{k}_\uparrow, -\mathbf{k}_\downarrow\rangle$  by a COOPER pair at 0 K is given by a function  $v_{\mathbf{k}}^2$  and its complement, the probability of non-occupation, by  $u_{\mathbf{k}}^2 = 1 - v_{\mathbf{k}}^2$ , as shown in Figure 8.13.
- » At 0 K the energy of the system is lowered, with respect to the normal state by

$$(u_s - u_n)(T = 0) = - \frac{G(\epsilon_F)}{2} \Delta^2(0) \quad (8.79)$$

where  $\Delta$ , called the “gap,” is substituted for  $E_b$  and is written

$$\Delta(0) = 2\hbar\omega_D e^{-\frac{1}{VG(\epsilon_F)}}. \quad (8.80)$$

Note however the numerically significant difference between (8.68) and (8.80) introduced by the replacement in the numerator of 2 by 1 in the argument of the exponential, since with the same numerical values we obtain

$$\varepsilon_F \approx 5 \text{ eV} ; \hbar\omega_D \approx 20 \text{ meV} ; G(\varepsilon_F)V \approx 0.25 ; \Delta(0) \approx 0.75 \text{ meV}$$

(0.75 meV is equivalent to a temperature of  $T = 8.5 \text{ K}$  that is of the order of magnitude of critical temperatures in metals and superconducting alloys).

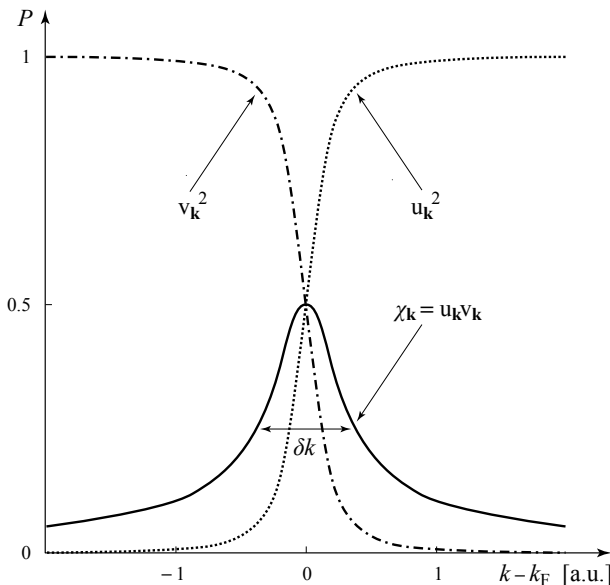


**Figure 8.13 - Probability of occupation  $v_k^2$  and of non-occupation  $u_k^2$  of a pair state  $|k_1, -k_1\rangle$  by a COOPER pair**

$\chi_k = u_k v_k$  is the condensation amplitude. It translates the "involvement" of the pair state  $|k_1, -k_1\rangle$  in lowering the energy of the system.

» Scattering of pairs of electrons between states  $|k_1, -k_1\rangle$  by the effects of interaction is central. A pair state  $|k_1, -k_1\rangle$  contributes all the more to the lowering of the energy of the system if it can be both an initial state with a large probability of being occupied and a final state with a significant probability of being empty. The relevant quantity, which weights these two contradictory aspects, is the condensation amplitude

$$\chi_k = u_k v_k \quad (8.81)$$

the product of the probability amplitude of occupation  $v_k$  by the probability amplitude of non-occupation  $u_k$  in this state. BCS theory shows that the gap  $\Delta$  is also the product of the potential  $V$  and of the sum of condensation amplitudes over all the pair states

$$\Delta = V \sum_k \chi_k . \quad (8.82)$$

It is clearly seen (in Fig. 8.13) that the unavailable pair states ( $k \gg k_F$ ;  $v_k = 0$ ) or those occupied by electrons that are blocked ( $k \ll k_F$ ;  $u_k = 0$ ) do not contribute to the gap. Those that do participate are situated in the vicinity of the FERMI level where the product  $u_k v_k$  is highest.

Similarly to (8.77), the range of delocalization, which is the width of the function  $\chi_k$ , is extended over an interval  $\delta k$  related to  $\Delta$  by

$$\delta k \approx \frac{\pi \Delta}{\hbar v_F}. \quad (8.83)$$

- › The form of the internal energy of the superconductor (8.79) can be understood by writing that the number of pair states situated in the band  $\delta k$  is of order  $G(\varepsilon_F)\Delta$  and each contributes to a lowering of the energy of order  $\Delta/2$ .
- › In view of the expression (8.13) for  $G(\varepsilon_F)$ , the number of electrons that contribute effectively to the lowering of energy by delocalization amount typically to a fraction  $\Delta/\varepsilon_F \approx 2 \cdot 10^{-4}$  of the conduction electrons. Expressed per conduction electron of the metal, the energy gain is of order  $\Delta^2/\varepsilon_F \approx 0.2 \text{ } \mu\text{eV}$  (equivalent to a temperature  $\approx 2 \cdot 10^{-3} \text{ K}$ ).

### 8.5.3 - Quasiparticles

» **In the normal metal** at 0 K, the levels  $k_<$  (of negative energy  $\xi_{k_<}^6$ ) situated below the FERMI level are occupied while the levels  $k_>$  (of positive energy  $\xi_{k_>}$ ) situated above are empty. An electron (quasiparticle) placed in a state  $k_>$  ( $k_> > k_F$ ) increases the energy of the system by an amount  $E_k^n = \xi_{k_>}$ . A hole (quasiparticle) created on a level  $k_<$  ( $k_< < k_F$ ) increases the energy of the system by (a positive)  $E_k^n = -\xi_{k_<}$  since it was necessary to take away an electron of (negative) energy  $\xi_{k_<}$  in order to create it. Close to the FERMI level the energies of the quasiparticles of the normal metal is

$$E_k^n = |\xi_k| = \frac{\hbar^2}{2m} |k^2 - k_F^2| \approx \frac{\hbar^2 k_F}{m} |k - k_F| \quad (8.84a)$$

with two distinct linear branches: one branch  $k_>$  of “electron” quasiparticles and one branch  $k_<$  of “hole” quasiparticles (Fig. 8.14a).

» **In the superconductor** the notion of quasiparticle becomes more subtle since near the FERMI level the pair states, over which the COOPER pairs are delocalized, are occupied with probability  $v_k^2$  and unoccupied with probability  $u_k^2$  and one can no longer draw a clear distinction between the electron and hole quasiparticles. We emphasize three major points:

- › unlike COOPER pairs which are delocalized over pair states, the quasiparticles of the superconductor occupy *individual* states  $|k_\uparrow\rangle$  and/or states  $|-\mathbf{k}_\downarrow\rangle$  “stably”;

---

6 We recall that  $\xi$  is the energy measured from the FERMI level.

- › each quasiparticle has both electron and hole character. A quasiparticle occupying a state  $|\mathbf{k}\uparrow\rangle$  or  $|- \mathbf{k}\downarrow\rangle$  appears with probability  $v_k^2$  in the form of a hole and with probability  $u_k^2$  in the form of an electron;<sup>7</sup>
- › the creation of quasiparticles in the states  $|\mathbf{k}\uparrow\rangle$  and/or  $|- \mathbf{k}\downarrow\rangle$  is necessarily accompanied by the elimination of the pair state  $|\mathbf{k}\uparrow, -\mathbf{k}\downarrow\rangle$  from the set of the states over which the COOPER pairs can be delocalized, which has a significant cost in energy. From the perspective of single COOPER pairs this is clear since the fewer the states over which a COOPER pair is delocalized, the less is its binding energy. This translates in BCS into the result that the calculated gap diminishes because the sum in equation (8.82) is over fewer values of  $\mathbf{k}$ . Taking into account the contribution of the kinetic energy, we can show that the total energy necessary for the creation of such quasiparticles is

$$E_{\mathbf{k}} = \sqrt{\Delta^2 + \xi_{\mathbf{k}}^2} = \sqrt{\Delta^2 + \left(\frac{\hbar^2 k^2}{2m} - \varepsilon_F\right)^2}. \quad (8.84b)$$

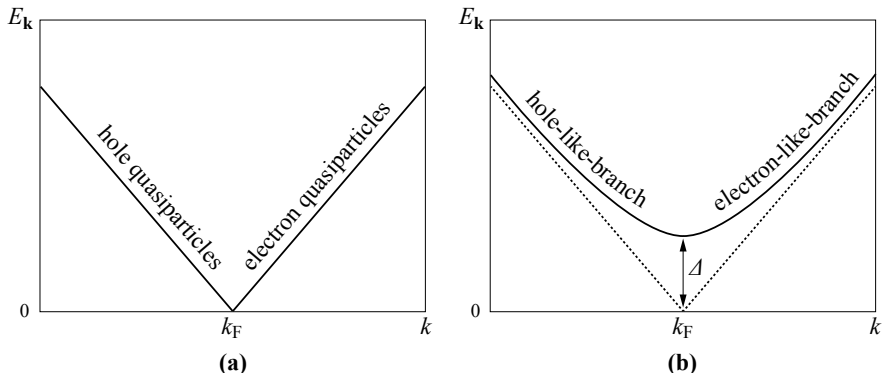


Figure 8.14 - Quasiparticle dispersion near the FERMI level

In a normal metal (a)  $k_F$  perfectly separates the electron quasiparticles from the hole quasiparticles. Near the FERMI level, the dispersion is linear. In a BCS superconductor (b) there is no definite limit between the two types of quasiparticles. While far from  $k_F$ , the quasiparticles can be identified as being electrons or holes, it is not the same near  $k_F$  where the quasiparticles combine the two aspects.

It then follows that their dispersion relation has a hyperbolic form (Fig. 8.14b) with a branch  $k_>$  said to be “electron-like”, on which the probability for a quasiparticle to appear in the form of an electron is higher ( $u_k^2 > v_k^2$ ), and a “hole-like” branch ( $u_k^2 < v_k^2$ ) on which it is now the probability to appear in the form of a hole that is higher. When  $|\xi_{\mathbf{k}}|$  increases and becomes larger than  $\Delta$ , these branches tend asymptotically towards those with the same names in the normal state, corresponding to ( $u_k = 1, v_k = 0$ ) and ( $u_k = 0, v_k = 1$ ) respectively. The minimum energy required for

7 N.N. BOGOLIUBOV (1958) *Nuovo Cimento* 7, 794;  
J.G. VALATIN (1958) *Nuovo Cimento* 7, 843.

the creation of a quasiparticle is the quantity  $\Delta$  which then takes it full sense of a “gap”. In the simplest description we only retain the notion that a fraction of the electrons have left the superconducting condensate in order to behave as “normal electrons”.

Since each individual state  $|\mathbf{k}\rangle$  corresponds to a possible quasiparticle state, the density of quasiparticle states  $D(E)$  is related to  $G(k)$  by

$$D(E) dE = G(k) dk \quad (8.85)$$

or, with the dispersion relation (8.84)

$$D(E) = G(\varepsilon_F) \frac{E}{\sqrt{E^2 - \Delta^2}}. \quad (8.86)$$

As a consequence of the conservation of the total number of states, those in the normal metal that were between  $\varepsilon_F$  and  $\varepsilon_F + \Delta$  are mainly “transferred” to the divergent part of  $D(E)$  (Fig. 8.15).

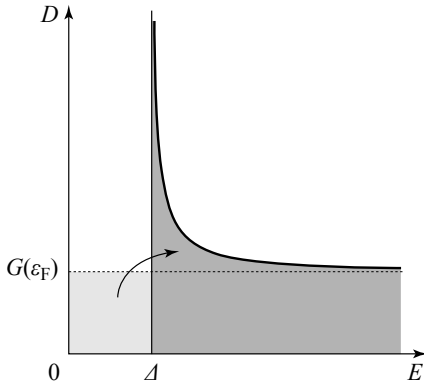


**Figure 8.15**  
**Quasiparticle density of states**  
The density of states  $D(E)$  of the quasiparticles has an energy gap  $\Delta$ .  $D(E)$  diverges at  $\Delta$  and then decreases towards the free electron density of states  $G(\varepsilon_F)$ . The free-electron states of the non-superconducting material that had been between 0 and  $\Delta$ , are “transferred” to energies above  $\Delta$ .

## 8.6 - Consequences of the energy structure

### 8.6.1 - Critical temperature

At a non-zero temperature  $T$ , some COOPER pairs are disassociated by thermal activation to give quasiparticles that eliminate pair states from those available for the delocalization of the remaining COOPER pairs (Fig. 8.16), and thus reduce the gap.

The gap at temperature  $T$  can be determined by showing that each pair state  $|\mathbf{k}_\uparrow, -\mathbf{k}_\downarrow\rangle$  has a probability  $2f(T, E_\mathbf{k})$  of being eliminated from the states available to the COOPER pairs for delocalization, where  $f(T, E_\mathbf{k})$  is the FERMI function for the occupation of a state  $|\mathbf{k}\rangle$ , and that the condensation amplitude (8.82) is reduced by the factor  $1 - 2f(T, E_\mathbf{k})$ , leading to

$$\Delta(T) = V \sum_{\mathbf{k}} \chi_{\mathbf{k}} [1 - 2f(T, E_{\mathbf{k}})]. \quad (8.87)$$

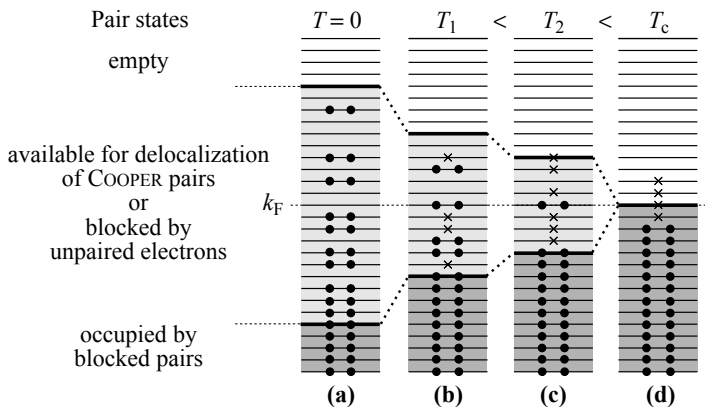


Figure 8.16 - COOPER pairs and quasiparticles

**(a)** at 0 K the COOPER pairs (•) are delocalized between the pair states situated essentially in the layer  $\delta k$  contained between  $k_F - k_A$  and  $k_F + k_A$ . The higher states are empty and the lower states are occupied by blocked pairs. **(b) (c)** At non-zero temperatures, quasiparticles (x) occupy some of the individual states of the layer  $\delta k$  and eliminate pair states constructed from these single-particle states from the states over which COOPER pairs can be delocalized. This results in a decrease of the gap and a reduction of  $\delta k$  which eventually leads to disappearance of the superconductivity at  $T_c$ . **(d)** At  $T_c$  and above, we find the usual schema with quasiparticles (normal electrons) on an interval of order  $k_B T$  around the FERMI level.

After a slow decrease of the gap as long as  $k_B T \ll \Delta(0)$ , we see a phenomenon of collapse when  $k_B T$  approaches  $\Delta(0)$ . There is then a rapid multiplication in the number of quasiparticles that eliminate more and more pair states from possible delocalization and cause a reduction in the gap which facilitates the generation of new quasiparticles that in turn reduce the gap, and so on... By an avalanche effect, the gap decreases very rapidly from about 0.75  $T_c$  to disappear at  $T_c$  (Fig. 8.17).

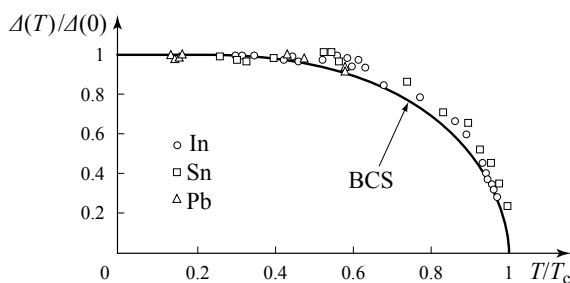


Figure 8.17 - Temperature dependence of the gap

The gap decreases with temperature, at first very slowly between 0 K and  $T_c/2$  then with a rapid collapse above  $0.75 T_c$ . The experimental points are results of measurements on indium, tin and lead. The full line represents the prediction of BCS theory. [From GIAEVER & MERGELE, 1961, © The American Physical Society]<sup>8</sup>

8 I. GIAEVER & K. MEGERLE (1961) *Phys. Rev.* **122**, 1101.

The superconductivity disappears by the multiplication of quasiparticles that become normal holes and electrons and by a reduction of the density of COOPER pairs that find fewer and fewer states over which they can be delocalized.

The BCS calculation leads to the relation between the critical temperature  $T_c$  and the energy gap at 0 K

$$\Delta(0) = 1.76 k_B T_c \quad (8.88)$$

and shows that close to  $T_c$ , the gap varies as

$$\Delta(T) = 1.55\Delta(0)\left(1 - \frac{T}{T_c}\right)^{1/2}. \quad (8.89)$$

**Table 8.1 - Values of characteristic physical variables in some “classical” superconductors**

The values of  $2\Delta(0)/k_B T_c$  should be compared to the value 3.52 of the BCS model. When it is significantly larger we speak of strong coupling.

	$T_c$ [K]	$\hbar\omega_D$ [meV]	$2\Delta(0)$ [meV]	$2\Delta(0)/k_B T_c$
Al	1.175	35.76	0.34	3.40
Pb	7.196	8.67	2.70	4.41
Nb	9.250	22.79	3.00	3.81
Sn (white tin)	3.720	16.45	1.40	4.43
Hg	4.150	5.95	1.70	4.82

**Remark** - The blocking effects of pair states by quasiparticles is also seen when, without changing the temperature  $T$ , new quasiparticles are introduced by tunneling processes, by breaking COOPER pairs via irradiation, or by injection of quasiparticles. By blocking new pair states  $|\mathbf{k}_\uparrow, -\mathbf{k}_\downarrow\rangle$  the excess quasiparticles produce a reduction in the gap.<sup>9</sup>

In the inverse effect, the extraction of quasiparticles by techniques of tunneling frees up pair states and leads to an increase in  $T_c$ .<sup>10</sup> More subtly, a microwave of energy less than  $2\Delta$ , that cannot destroy COOPER pairs, increases the gap and  $T_c$  by ejecting quasiparticles from the region  $\delta k$  where they were blocking the heavily weighted pair states towards higher energy states rarely visited by COOPER pairs.<sup>11</sup>

As this process occurs out of equilibrium, the amplitude of the effect is intrinsically tied to the time necessary for recombination of quasiparticles into COOPER pairs.

9 C.S. OWEN & D.J. SCALAPINO (1972) *Phys. Rev. Lett.* **28**, 1559 ; J. FUCHS *et al.* (1977) *Phys. Rev. Lett.* **38**, 919.

10 C.C. CHI & J. CLARKE (1979) *Phys. Rev. B* **20**, 4465.

11 T. KOMMER & J. CLARKE (1977) *Phys. Rev. Lett.* **38**, 1091.

### 8.6.2 - Nature of the superconducting gap

The superconducting gap is of a nature very different from that of a semiconductor which is due to the periodic potential of the lattice ions. In that case the structure of the energy levels is essentially independent of temperature and the electrons occupy the levels individually with a probability given by the FERMI function. The electron interactions bring only minor corrections.

In superconductors, the gap has its origin in the interactions between electrons. At low temperatures it varies little, but after the quasiparticles occupy the pair states it collapses and falls to zero, which marks the disappearance of superconductivity.

There exists an operational semiconductor representation of the “density of states” of superconductors. In that representation the two bands equivalent to the conduction and valence bands of semiconductors are, for the first, the density of states  $D(E)$  of the quasiparticles and for the second  $D^*(E) = D(-E)$  (Fig. 8.18). They are separated by  $2\Delta$  (the gap in the semiconductor sense).

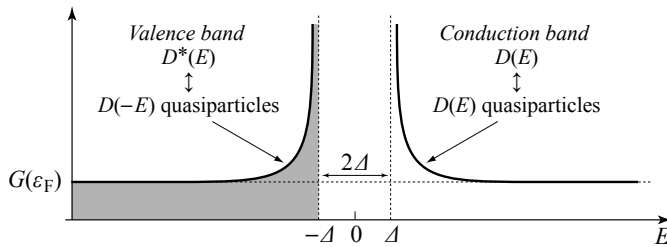


**Figure 8.18 - Semiconductor representation**

The equivalents of the “conduction band” and the “valence band” are the density of states of quasiparticles and its reflection, respectively. This representation is particularly convenient if we wish to take into account tunneling effects of quasiparticles.

This operational representation is particularly useful to describe the tunneling effects of quasiparticles (to be distinguished from JOSEPHSON effects that are the tunneling of COOPER pairs) and must be restricted to such effects.

### 8.6.3 - Coherence length<sup>12</sup>

Similarly to the result of section 8.4.5, the average distance between two electrons in a pair is related, by the uncertainty principle, to the spread  $\delta k$  over pair states  $|\mathbf{k}_\uparrow, -\mathbf{k}_\downarrow\rangle$  visited by the COOPER pairs. The calculation, like that giving the relation (8.78), leads to the result

$$\xi_{\text{BCS}}(0) = \frac{\hbar v_F}{\pi \Delta(0)} \quad (8.90)$$

<sup>12</sup> We remind the reader: the energy measured from the FERMI level  $\xi$  (in regular type) and the coherence length  $\xi$  (in italics).

that is to be identified, in clean superconductors, with the length  $\xi_0$  defined in Chapter 3 (section 3.2). As was mentioned in the same section, for rather subtle reasons the spatial extension of COOPER pairs is  $\xi_0 \equiv \xi_{\text{BCS}}(0)$ , not only at 0 K, but at all temperatures.

The BCS coherence length  $\xi_{\text{BCS}}(T)$  is given by a generalization to non-zero temperature of (8.90)

$$\xi_{\text{BCS}}(T) = \frac{\hbar v_F}{\pi \Delta(T)}. \quad (8.91)$$

In clean superconductors,  $\xi_{\text{BCS}}(T)$  is also the coherence length  $\xi(T)$ , introduced in Chapter 6 (section 6.4.1) as the distance necessary for a density of superconducting electrons  $n_s$  to pass from a value of zero at a surface to its bulk value  $n_{\infty}$ .  $\xi_{\text{BCS}}(T)$  varies as the inverse of the gap  $\Delta(T)$  represented in Figure 8.17 and, in view of the relation (8.89), diverges at  $T_c$  as follows

$$\xi_{\text{BCS}}(T) \approx (T_c - T)^{-\frac{1}{2}} \quad T \approx T_c. \quad (8.92)$$

In dirty superconductors (with electron mean free path  $\ell$  less than  $\xi_0$ ), we must distinguish between the coherence length  $\xi_{\text{BCS}}(T)$  related to the gap and defined by (8.90), the coherence length  $\xi(T)$  that is the distance over which the superconducting electron density changes from 0 at a surface to its bulk value  $n_{\infty}$ , the PIPPARD length  $\xi_p$  entering into the relation (3.25) for the vector potential, and the distance between two electrons in a COOPER pair, close to the coherence length  $\xi_0$ .

#### 8.6.4 - Critical field - Free enthalpy of condensation

The free enthalpy of condensation introduced in Chapter 4

$$g_s^{\text{cond}} = -\mu_0 \frac{H_c^2}{2} \quad (8.93)$$

was interpreted as the free enthalpy of the formation of COOPER pairs per unit volume.

At zero temperature and zero field, where the density of free enthalpy  $g = u - \mu_0 M H - T s$  coincides with the internal energy, expression (8.79) gives us

$$G(\varepsilon_F) \frac{\Delta^2(0)}{2} = \mu_0 \frac{H_c^2(0)}{2} \quad (8.94)$$

which relates the superconducting gap and the thermodynamic critical field,

$$H_c(0) = \sqrt{\frac{G(\varepsilon_F)}{\mu_0}} \Delta(0). \quad (8.95)$$

Expressing the gap  $\Delta$  as a function of  $\xi_{\text{BCS}}$  (8.90), and relating the LONDON penetration depth  $\lambda_L$  (2.24) to the density of states  $G(\varepsilon_F)$  (8.13), to the FERMI velocity

$v_F = \hbar k_F / m$  where  $k_F$  is the FERMI wave vector (8.12) and to the flux quantum (6.22 and 9.16), we obtain the expression for  $H_c(0)$ ,

$$H_c(0) = \frac{\sqrt{3}}{2\pi} \frac{\phi_0}{\mu_0 \lambda_L(0) \xi_{BCS}(0)} \quad (8.96)$$

close to the relation of GINZBURG-LANDAU theory (6.25).

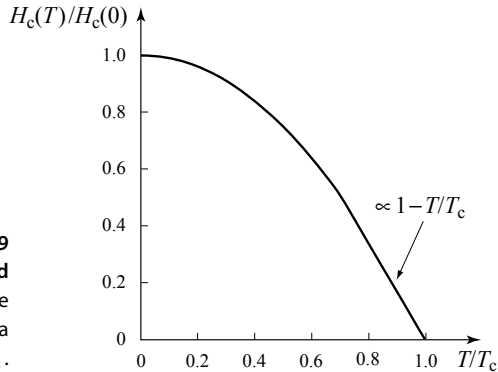


**Figure 8.19**  
**The critical field**

BCS theory predicts variation of the critical field close to TUYN's law with a behavior  $H_c(T) \propto H_c(0) [1 - T/T_c]$  near  $T_c$ .

### 8.6.5 - Electronic specific heat

At low temperatures, typically below  $T_c/2$ , the gap is to a first approximation constant and equal to  $\Delta(0)$ . Because of the divergence of the density of states  $D(E)$  at the gap edge (Fig. 8.15) we can consider, in a slightly simplistic "two-state" model, that all the levels that in the normal state had been between  $\varepsilon_F$  and  $\varepsilon_F + \Delta$  are pushed to the gap edge, which produces  $2G(\varepsilon_F)\Delta(0)$  states of quasiparticles squeezed together at  $\Delta(0)$ . With an occupation probability of each of these states of  $e^{-\Delta(0)/k_B T}$ , ( $k_B T$  being smaller than  $\Delta(0)$ , the excited states are in the tail of the FERMI function) we obtain at temperature  $T$ ,

$$\delta U = [2G(\varepsilon_F)\Delta(0)]\Delta(0) e^{-\frac{\Delta(0)}{k_B T}} \quad (8.97)$$

and hence a specific heat

$$C_s^{\text{el}} = \frac{d(\delta U)}{dT} \approx \frac{2G(\varepsilon_F)[\Delta(0)]^3}{k_B T^2} e^{-\frac{\Delta(0)}{k_B T}} \quad (8.98)$$

dominated at low temperatures by the exponential term, or

$$C_s^{\text{el}} \sim A e^{-\frac{\Delta(0)}{k_B T}} \quad (8.99)$$

that corresponds precisely to the experimental results shown in Figure 4.5.

A more exact expression but similar to this<sup>13</sup> was obtained by BCS. The exponential term is due to the fact that quasiparticle creation requires a minimal non-zero energy. This is the signature of a gap for all the quasiparticle states.

Close to  $T_c$ , we must include the strong temperature dependence of the gap and the two-state model is no longer valid. By rigorous analysis, the BCS theory predicts a discontinuity (Fig. 8.20)

$$\frac{C_s^{\text{el}} - C_n^{\text{el}}}{C_n^{\text{el}}} = 1.43 \quad (8.100)$$

consistent with experimental results.

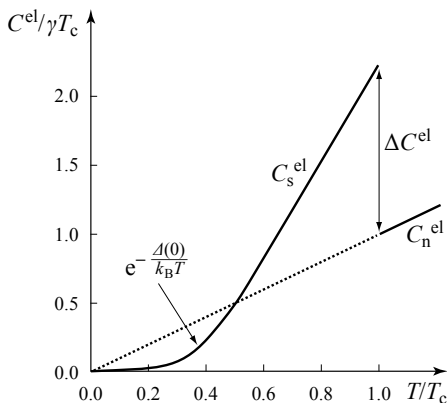


**Figure 8.20 - Electronic specific heat**  
At low temperatures the electronic specific heat of the normal state is linear in  $T$ , while in the superconductor it varies exponentially because of the gap. A discontinuity appears at  $T_c$ .

### 8.6.6 - Critical current density

We shall now see how the existence of a gap leads to a critical velocity  $v_c$  for the electrons (and therefore to a critical current density) beyond which the energy of a COOPER pair becomes greater than that of two unpaired electrons, leading to pair-breaking.

#### Normal metal

At 0 K, the electrons of the normal metal occupy the states  $k < k_F$ , inside the FERMI sphere (see section 8.1.1).

» In the absence of an electric field, the distribution of momenta  $\mathbf{p} = \hbar\mathbf{k}$  of the electrons is isotropic, as is that of the velocities. The mean velocity  $\langle \mathbf{v} \rangle$  of all the electrons is zero. In  $\mathbf{k}$  space (Fig. 8.21a), the FERMI sphere is at rest.

13 The expression given by BCS at low temperatures ( $T \ll \Delta(0)/k_B$ )

$$\text{is } C_s^{\text{el}}(T) = \frac{2k_B}{(k_B T)^{3/2}} G(\epsilon_F) [\Delta(0)]^{5/2} e^{-\frac{\Delta(0)}{k_B T}}.$$

» Under the effect of an electric field  $\mathbf{E}$  applied in the  $-x$  direction (Fig. 8.21b), each electron experiences a force

$$\mathbf{F} = q_e \mathbf{E} = m \frac{d\mathbf{v}}{dt} = \hbar \frac{d\mathbf{k}}{dt} \quad (8.101)$$

that translates into a uniform displacement of the FERMI sphere by an amount

$$\langle k_x \rangle = \frac{eE}{\hbar} t \quad (8.102)$$

and, in real space, by an increasing average velocity of the whole set of electrons in the  $x$  direction,

$$\langle v \rangle = \frac{eE}{m} t \quad (8.103)$$

which corresponds to an increasing current density in the  $\mathbf{E}$  direction

$$j = ne\langle v \rangle = \frac{ne^2 E}{m} t. \quad (8.104)$$

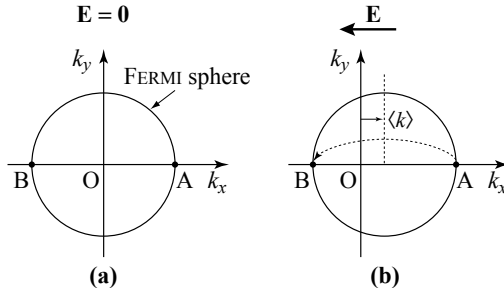


**Figure 8.21 - Representation, in the space of wave vectors, of the behavior of the electrons of a “normal” metal in an electric field**

- (a) Without the electric field, the FERMI sphere is centered at the origin.
- (b) With the electric field, the FERMI sphere is shifted by  $\langle k_{x\infty} \rangle$ .

The “frictional” term that leads to a limiting average velocity  $\langle v_\infty \rangle$  of the electrons (see section 2.2.1) includes the existence of collisions with defects and phonons by which the electrons located in the front of the displaced FERMI sphere (Fig. 8.21b, point A) are scattered to the rear (point B) thereby losing a momentum  $2\hbar k_F$ . When a balance is reached between the displacement in velocity (8.103) of the FERMI sphere due to the electric field and the constant transfer of electrons from the front to the rear, the sphere appears to be immobile and shifted by  $\langle k_{x\infty} \rangle$ . The electrons then have an average velocity

$$\langle v_\infty \rangle = \frac{\hbar \langle k_{x\infty} \rangle}{m} \quad (8.105)$$

and transport a steady current density

$$j_\infty = ne\langle v_\infty \rangle. \quad (8.106)$$

### Metal in the superconducting phase

#### Possible scattering processes

In the superconducting phase and in a zero field, the electrons that form COOPER pairs are scattered from pair states  $|\mathbf{k}_\uparrow, -\mathbf{k}_\downarrow\rangle$  towards pair states  $|\mathbf{k}'_\uparrow, -\mathbf{k}'_\downarrow\rangle$ , which means that the scattering of an electron from a state  $|\mathbf{k}_\uparrow\rangle$  into a state  $|\mathbf{k}'_\uparrow\rangle$  entails, by solidarity, the scattering of its partner in the state  $|\mathbf{-k}_\downarrow\rangle$  into the state  $|\mathbf{-k}'_\downarrow\rangle$ . This is in particular the case of electrons occupying pair states whose single-particle states are located one in the front and the other to the rear of the FERMI sphere: a COOPER pair occupying the state  $|\mathbf{k}_\uparrow, -\mathbf{k}_\downarrow\rangle$  (Fig. 8.22a, black dots) will occupy after scattering the state  $|\mathbf{k}'_\uparrow, -\mathbf{k}'_\downarrow\rangle$  (white dots). Let us focus on these front to rear scatterings, which in fact are those that are the most efficient for depairing.

If, as in a normal metal, we turn on an electric field  $\mathbf{E}$  in the  $x$  direction, the FERMI sphere is displaced. The pair state  $|\mathbf{k}_\uparrow, -\mathbf{k}_\downarrow\rangle$  becomes  $|(\mathbf{k} + \langle k_x \rangle)_\uparrow, (-\mathbf{k} + \langle k_x \rangle)_\downarrow\rangle$  and the pair state  $|\mathbf{k}'_\uparrow, -\mathbf{k}'_\downarrow\rangle$  becomes  $|(\mathbf{k}' + \langle k_x \rangle)_\uparrow, (-\mathbf{k}' + \langle k_x \rangle)_\downarrow\rangle$ . During a collision, there are two possible processes:

- » first process (Fig. 8.22b): the COOPER pair is scattered from the pair state  $|(\mathbf{k} + \langle k_x \rangle)_\uparrow, (-\mathbf{k} + \langle k_x \rangle)_\downarrow\rangle$  into the pair state  $|(\mathbf{k}' + \langle k_x \rangle)_\uparrow, (-\mathbf{k}' + \langle k_x \rangle)_\downarrow\rangle$ . Scattering of an electron from the front towards the back is compensated by scattering of an electron from the back towards the front. The mechanism stabilizing the apparent displacement of the FERMI sphere has disappeared. As in a perfect conductor, the effect of an electric field is to increase the displacement of the FERMI sphere in  $\mathbf{k}$  space according to the relation (8.102). If we turn off the electric field ( $E = 0$ ), the FERMI sphere keeps the shift it has acquired, and the current density remains constant: the superconductor appears a perfect conductor, with resistivity null;
- » second process (Fig. 8.22c): the pair breaks into independent single electrons. The electron  $|(\mathbf{k} + \langle k_x \rangle)_\uparrow\rangle$  that was to the front, is back-scattered into the state  $|(-\mathbf{k} + \langle k_x \rangle)_\uparrow\rangle$  without the second electron of wave vector  $|(-\mathbf{k}' + \langle k_x \rangle)_\downarrow\rangle$  being forward scattered. This is the process encountered in normal resistive metals.

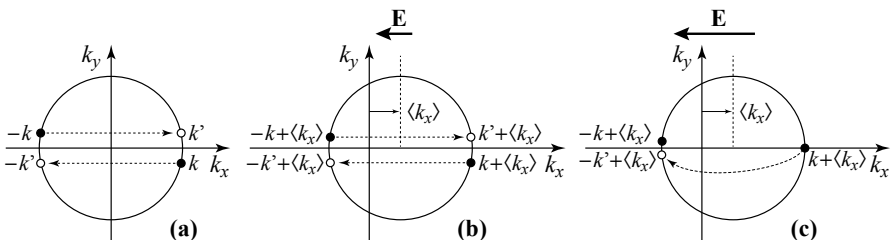


**Figure 8.22 - FERMI sphere and scattering processes in an electric field**

(a)  $E = 0$ : FERMI sphere at rest. Example of a scattering process,  $|\mathbf{k}_\uparrow, -\mathbf{k}_\downarrow\rangle \rightarrow |\mathbf{k}'_\uparrow, -\mathbf{k}'_\downarrow\rangle$ ,  
 (b)  $E \neq 0$ : FERMI sphere shifted by  $\langle k \rangle$ . Examples of scattering processes: (b) without pair breaking, below the critical current, (c) with pair breaking, beyond the critical current.

### Energy balance

The process that actually occurs will be whichever has lower energy. The net initial energy  $E_{\text{initial}}$  of the two electrons before scattering is equal to the sum of the kinetic energies of the electrons, diminished by the binding energy  $2\Delta$  of the pair,

$$E_{\text{initial}} = \frac{\hbar^2}{2m} |k_F + \langle k_x \rangle|^2 + \frac{\hbar^2}{2m} |-k_F + \langle k_x \rangle|^2 - 2\Delta. \quad (8.107)$$

During scattering without pair-breaking (Fig. 8.22b), the net energy of the two electrons is not modified. The final energy of the scenario represented in Figure 8.22b is therefore

$$E_{\text{final}}^{(b)} = E_{\text{initial}}. \quad (8.108)$$

When there is scattering with pair-breaking (Fig. 8.22c), on one hand the kinetic energy of the electron that passes from the front to the back diminishes, without any modification of the kinetic energy of the other electron; and on the other hand the binding energy disappears. The final energy in the scenario of Figure 8.22c becomes

$$E_{\text{final}}^{(c)} = \frac{\hbar^2}{2m} |-k_F + \langle k_x \rangle|^2 + \frac{\hbar^2}{2m} |-k_F + \langle k_x \rangle|^2 \quad (8.109)$$

or, using the fact that  $\langle k \rangle \ll k_F$ ,

$$E_{\text{final}}^{(c)} - E_{\text{initial}} = 2\Delta - 4 \frac{\hbar^2 k_F}{2m} \langle k \rangle. \quad (8.110)$$

As a consequence, the superconducting state will be destroyed if  $E_{\text{final}}^{(c)} < E_{\text{final}}^{(b)}$ , i.e. if

$$2\Delta - 4 \frac{\hbar^2 k_F}{2m} \langle k_x \rangle < 0 \quad \text{or equivalently} \quad \langle k_x \rangle > \frac{m\Delta}{\hbar^2 k_F} \quad (8.111)$$

which shows that there is a critical velocity  $v_c$  for the displacement of a COOPER pair. Beyond the velocity  $v_c$ , breaking up the COOPER pair into two normal electrons is energetically more favorable, leading to depairing.

$$v_c = \frac{\hbar}{m} \frac{m\Delta}{\hbar^2 k_F}. \quad (8.112)$$

There is therefore a critical current  $j_c$  beyond which the material reverts to the normal state, given by

$$j_c = nev_c = \frac{ne\Delta}{\hbar k_F} \quad (8.113)$$

which, from the relations (8.95), (8.13) and (8.10), namely

$$H_c = \sqrt{\frac{G(\varepsilon_F)}{\mu_0}} \Delta \quad ; \quad G(\varepsilon_F) = \frac{3n}{4\varepsilon_F} \quad ; \quad \varepsilon_F = \frac{\hbar^2 k_F^2}{2m} \quad (8.114)$$

can be rewritten as

$$j_c = \sqrt{\frac{2}{3}} \sqrt{\frac{\mu_0 n e^2}{m}} = \sqrt{\frac{2}{3}} \frac{H_c}{\lambda_L}. \quad (8.115)$$

Up to a coefficient  $\sqrt{\frac{2}{3}}$ , this is the generalized SILSBE criterion formulated in Chapter 5 (section 5.1), *i.e.* when the current density reaches the critical current  $j_c$  at some place, the superconductor passes to the normal state there.

A model that is more exact numerically should take into account the distribution of transitions from the whole of the front to the rear.

## 8.7 - Superconducting electrons and the LONDON penetration depth

The microscopic approach to superconductivity also allows us to clarify the notion of the “density of superconducting electrons”  $n_s$  that appears in the expression for the LONDON penetration depth and the statement (see section 2.4.1) that at 0 K, it involves all the free electrons.

$$\lambda_L = \sqrt{\frac{m}{\mu_0 n_s e^2}} \quad (8.116)$$

Up to now, we have distinguished somewhat artificially three categories of electrons:

- » the blocked electrons sufficiently far below the FERMI level; they are the majority of the electronic population;
- » the electrons in COOPER pairs that are delocalized and jump between pair states  $|\mathbf{k}_\uparrow, -\mathbf{k}_\downarrow\rangle$  within an interval  $\delta k$  centered on the FERMI surface;
- » the single electrons (quasiparticles) that occupy some of the states  $\mathbf{k}$  in the layer  $\delta k$ .

In order to count the number of electrons that intervene in the expression for the LONDON penetration depth, and before considering the superconductor at finite temperatures, we must return to the scattering processes leading to the resistivities of the normal metal and the superconductor at 0 K.

In the normal metal, the shift of the FERMI sphere under the influence of an electric field stabilizes at  $\langle k_{x\infty} \rangle$  by the process of scattering of electrons from the front of the sphere to those at the rear (Fig. 8.21b). This scattering process *concerns only* the electrons situated in the vicinity of the FERMI level, while the shift in  $\mathbf{k}$ , or the frictional velocity, involves *all* the conduction electrons, as is apparent in the relation (8.104). Likewise in the superconducting state at zero temperatures, *only* the COOPER pairs around the FERMI level are scattered without being disassociated while *all* the electrons of the metal (relation 8.102) are uniformly accelerated.

To sum up the situation, in both the normal metal and in the superconductor, only the electrons at the FERMI level enter into the scattering process and they bring underlying electrons in their wake.

In the superconductor at a non-zero temperatures there is, close to the FERMI level a coexistence of electrons bound in COOPER pairs and of single electrons (quasiparticles). In the above image, and by a pure counting argument, we can consider that each of these electron populations situated near the FERMI level brings along “its” own group of underlying electrons:

- » the underlying electrons of the quasiparticles appear as normal electrons (in the resistive sense). We denote their density by  $n_n(T)$ ;
- » the underlying electrons of the COOPER pairs are the superconducting electrons. Their density is  $n_s(T) = n - n_n(T)$  ( $n$  is the total density of electrons).

Very qualitatively, we can make the hypothesis that the ratio  $n_s(T)/n_n(T)$  is the ratio of the populations of electrons involved in COOPER pairs to quasiparticles at the FERMI level. With this we return to a two-fluid model, like that proposed by GORTER and CASIMIR.<sup>14</sup> The decrease in the number of COOPER pairs in favor of quasiparticles near the FERMI level is then accompanied by the decrease in the density of superconducting electrons  $n_s$  in favor of the normal electrons  $n_n$ .

The BCS calculation allows us to determine the number of normal electrons and, by subtraction, the number of superconducting electrons. The  $n_s(T)$  that enters into the expression for  $\lambda_L(T)$  (relation 2.24) is sometimes referred to as the “operational” density of superconducting electrons.

---

14 C.J. GORTER & H.B.G. CASIMIR (1934) *Physik. Z.* **35**, 963.

## Appendix 8

### Matrix elements for the interaction potential between particles

The non-diagonal terms are the matrix elements

$$\langle \mathbf{p}, \mathbf{s} | \hat{V} | \mathbf{m}, \mathbf{n} \rangle = \frac{1}{\mathcal{V}^2} \iiint_{\mathcal{V}} \iiint_{\mathcal{V}} e^{-i\mathbf{k}_p \cdot \mathbf{r}_1} e^{-i\mathbf{k}_s \cdot \mathbf{r}_2} V(|\mathbf{r}_2 - \mathbf{r}_1|) e^{i\mathbf{k}_m \cdot \mathbf{r}_1} e^{i\mathbf{k}_n \cdot \mathbf{r}_2} d^3 r_1 d^3 r_2. \quad (8.117)$$

The integration on  $\mathbf{r}_1$  and  $\mathbf{r}_2$  is over the volume  $\mathcal{V}$  of the box. Defining

$$\mathbf{r}_1 - \mathbf{r}_2 = \mathbf{r}$$

we can write, if the volume tends to *infinity*,

$$\langle \mathbf{p}, \mathbf{s} | \hat{V} | \mathbf{m}, \mathbf{n} \rangle = \frac{1}{\mathcal{V}^2} \iiint_{\mathcal{V}} V(\mathbf{r}) e^{-i(\mathbf{k}_s - \mathbf{k}_n) \cdot \mathbf{r}} d^3 r \iiint_{\mathcal{V}} e^{-i[(\mathbf{k}_s - \mathbf{k}_n) - (\mathbf{k}_m - \mathbf{k}_p)] \cdot \mathbf{r}_1} d^3 r_1. \quad (8.118)$$

This remains a good approximation if for  $\mathbf{r}_1$  in the box, so too is  $\mathbf{r}_2 = \mathbf{r}_1 + \mathbf{r}$  for all  $\mathbf{r}$  less than the range of the potential, *i.e.* if the size of the box is much larger than the range of the potential (to avoid boundary effects). Under these conditions, we can also make the approximation

$$\iiint_{\mathcal{V}} V(\mathbf{r}) e^{-i(\mathbf{k}_s - \mathbf{k}_n) \cdot \mathbf{r}} d^3 r \approx \iiint_{\text{all space}} V(\mathbf{r}) e^{-i(\mathbf{k}_s - \mathbf{k}_n) \cdot \mathbf{r}} d^3 r = \mathcal{V} V(\mathbf{q}) \quad (8.119)$$

$$\mathbf{q} = \mathbf{k}_s - \mathbf{k}_n$$

where here the combination  $\mathcal{V} V(\mathbf{q})$  (and not just  $V(\mathbf{q})$ ) is the FOURIER transformation of  $V(\mathbf{r})$  (whose range is limited to be within a unit volume  $\mathcal{V}$ ).

When  $\mathcal{V} \rightarrow \infty$ ,  $\frac{1}{\mathcal{V}} \iiint_{\mathcal{V}} e^{-i[(\mathbf{k}_s - \mathbf{k}_n) - (\mathbf{k}_m - \mathbf{k}_p)] \cdot \mathbf{r}_1} d^3 r_1 \rightarrow 1$  for  $\mathbf{k}_m - \mathbf{k}_p = \mathbf{k}_s - \mathbf{k}_n$  and  $\rightarrow 0$

for  $\mathbf{k}_m - \mathbf{k}_p \neq \mathbf{k}_s - \mathbf{k}_n$ .

So, if  $\mathbf{q} = \mathbf{k}_s - \mathbf{k}_n = \mathbf{k}_m - \mathbf{k}_p$ ,  $\langle \mathbf{p}, \mathbf{s} | \hat{V} | \mathbf{m}, \mathbf{n} \rangle = V(\mathbf{q})$  (8.120)

and otherwise,  $\langle \mathbf{p}, \mathbf{s} | \hat{V} | \mathbf{m}, \mathbf{n} \rangle = 0$ .

## Chapter 9

# COHERENCE AND THE FLUX QUANTUM

As described by BCS theory, that we have introduced qualitatively in Chapter 8, the superconducting state results from the formation of a “coherent” state of COOPER pairs formed by the association of two electrons. Although this association is dynamic and non-local, the COOPER pairs will be considered in this chapter as “particles” of mass  $m_p$  and charge  $q_p$  double those of an electron, and whose density  $n_p$  is half that of superconducting electrons

$$m_p = 2m \quad ; \quad q_p = -2e \quad ; \quad n_p = \frac{n_s}{2}. \quad (9.1)$$

In the language of Chapter 8 (section 8.7), they are operational COOPER pairs, relevant only when discussing transport phenomena.

The totality of the particles in the BOSE-EINSTEIN condensate is described by a *single wave function*<sup>1</sup>  $\phi_p(\mathbf{r}, t)$ ,

$$\phi_p(\mathbf{r}, t) = \sqrt{n_p(\mathbf{r}, t)} e^{i\theta(\mathbf{r}, t)} \quad (9.2)$$

where  $\theta(\mathbf{r}, t)$  is the phase of the wave associated with the “particles” that are COOPER pairs and  $n_p(\mathbf{r}, t)$  is their density at the point  $\mathbf{r}$  at time  $t$ .

$$n_p(\mathbf{r}, t) = \phi_p^*(\mathbf{r}, t) \phi_p(\mathbf{r}, t). \quad (9.3)$$

### 9.1 - Current density and the LONDON equation

In the presence of a vector potential  $\mathbf{A}$  and an electric potential  $V$ :

» the (generalized) momentum of the “particle” (the COOPER pair) can be written as for any charged particle<sup>2</sup> (see App.9.1)

$$\mathbf{p} = m_p \mathbf{v} + q_p \mathbf{A} \quad (9.4)$$

where  $\mathbf{v}$  is the velocity of the center of gravity of the COOPER pair;

---

1  $\phi$  in “regular type” denotes a two-particle wave function, while the “italic”  $\phi$  is reserved for the notation of magnetic field fluxes.

2 C. COHEN-TANNOUDJI, B. DIU & F. LALOE (1986)  
*Quantum Mechanics Vol. II*, 1491-94.

» the Hamiltonian takes the form (see App. 9.2)

$$\hat{H} = \frac{1}{2m_p} \left( \frac{\hbar}{i} \nabla - q_p \mathbf{A} \right) \left( \frac{\hbar}{i} \nabla - q_p \mathbf{A} \right) + q_p V; \quad (9.5)$$

» the density of electric current  $\mathbf{j}(\mathbf{r}, t)$  is defined by

$$\mathbf{j}(\mathbf{r}, t) = q_p \operatorname{Re} \left[ \phi_p^* \frac{1}{m_p} \left( \frac{\hbar}{i} \nabla - q_p \mathbf{A} \right) \phi_p \right]. \quad (9.6)$$

Substituting the expression for the wave function (9.2) into (9.6), in a situation where the density of COOPER pairs  $n_p$  is uniform throughout the sample, the current density becomes

$$\mathbf{j}(\mathbf{r}, t) = n_p q_p \frac{\hbar}{m_p} \left[ \nabla \theta(\mathbf{r}, t) - \frac{q_p}{\hbar} \mathbf{A}(\mathbf{r}, t) \right] \quad (9.7)$$

or, after taking the **curl** (the vector product of the gradient operator  $\nabla$ ) of the two sides, and using the general relations  $\mathbf{B} = \nabla \times \mathbf{A}$  and  $\nabla \times \nabla = 0$ ,

$$\nabla \times \mathbf{j} = - \frac{n_p q_p^2}{m_p} \mathbf{B} \quad (9.8)$$

which, from the definitions (9.1), is nothing other than the second LONDON equation. In the expression (9.7), the phase  $\theta(\mathbf{r}, t)$  can be connected to the integration constant  $\chi(\mathbf{r}, t)$  in the relation (2.89) of Chapter 2, section 2.12.2 (see App. 9.3) with  $\nabla \theta(\mathbf{r}, t) = \frac{q_p}{\hbar} \nabla \chi(\mathbf{r}, t)$ .

## 9.2 - Phase of the wave function

As in optics, the change of the phase  $\delta\theta$  along a line ( $\Gamma$ ) is equal to the circulation of the wave vector  $\mathbf{k} = \mathbf{p}/\hbar$  (Fig. 9.1)

$$\delta\theta|_{\Gamma} = \int_{\Gamma} \mathbf{k} \cdot d\mathbf{l} = \int_{\Gamma} \frac{\mathbf{p}}{\hbar} \cdot d\mathbf{l} \quad (9.9)$$

or, using the expression  $\mathbf{p} = m_p \mathbf{v} + q_p \mathbf{A}$  for the momentum,

$$\delta\theta|_{\Gamma} = \frac{m_p}{\hbar} \int_{\Gamma} \mathbf{v} \cdot d\mathbf{l} + \frac{q_p}{\hbar} \int_{\Gamma} \mathbf{A} \cdot d\mathbf{l} \quad (9.10)$$

phase change along a line ( $\Gamma$ )	contribution due to the velocity $\delta\theta _{\Gamma}^{\text{velocity}}$	magnetic contribution $\delta\theta _{\Gamma}^{\text{mag}}$
---	--	--

and if we make the additional hypothesis that the density of COOPER pairs is uniform on the path followed and  $\mathbf{j} = n_p q_p \mathbf{v}$

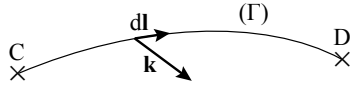
$$\delta\theta|_{\Gamma} = \frac{m_p}{n_p q_p \hbar} \int_{\Gamma} \mathbf{j} \cdot d\mathbf{l} + \frac{q_p}{\hbar} \int_{\Gamma} \mathbf{A} \cdot d\mathbf{l}$$

phase change contribution due to the magnetic contribution  
along a line ( $\Gamma$ ) current density  $\delta\theta|_{\Gamma}^{\text{current}}$   $\delta\theta|_{\Gamma}^{\text{mag}}$

(9.11)

**Figure 9.1 - Phase of the wave function**

The variation of the phase of the wave function of the condensate along a circuit equals the circulation of the wave vector along this circuit.



*The phase change of a wave function of the superconducting condensate during a displacement along a line ( $\Gamma$ ) between two points C and D equals the sum of the circulations of the current density  $\mathbf{j}$  (weighted with the coefficient  $[m_p / n_p q_p \hbar]$ ) and of the vector potential  $\mathbf{A}$  (weighted with the coefficient  $q_p / \hbar$ ) on the path used to join the two points, provided there is a uniform density of COOPER pairs along this path.*

## 9.3 - Flux quantization

### 9.3.1 - The fluxon

If we follow a closed path, the acquired phase can only be a multiple of  $2\pi$ , so that

$$\oint_{\Gamma} \delta\theta = \frac{m_p}{\hbar} \oint_{\Gamma} \mathbf{v} \cdot d\mathbf{l} + \frac{q_p}{\hbar} \oint_{\Gamma} \mathbf{A} \cdot d\mathbf{l} = -2s\pi \quad (s \text{ integer}) \quad (9.12)$$

and if the pair density  $n_p$  is uniform,

$$\oint_{\Gamma} \delta\theta = \frac{m_p}{n_p q_p \hbar} \oint_{\Gamma} \mathbf{j} \cdot d\mathbf{l} + \frac{q_p}{\hbar} \oint_{\Gamma} \mathbf{A} \cdot d\mathbf{l} = -2s\pi. \quad (9.13)$$

As the integer  $s$  can be positive or negative, the minus sign before  $2s\pi$  is introduced for convenience, essentially because of the negative charge  $q_p$  of the COOPER pairs.

Since the circulation of  $\mathbf{A}$  around a closed path is the flux of  $\mathbf{B} = \nabla \times \mathbf{A}$  across any surface limited by this path, for the orientation of Figure 9.2 we have

$$\frac{m_p}{q_p} \oint_{\Gamma} \mathbf{v} \cdot d\mathbf{l} + \iint_S \mathbf{B} \cdot d\mathbf{S} = -\frac{h}{q_p} s = s\phi_0 \quad (9.14)$$

and if the density of COOPER pairs  $n_p$  is uniform along the path,

$$\frac{m_p}{n_p q_p^2} \oint_{\Gamma} \mathbf{j} \cdot d\mathbf{l} + \iint_S \mathbf{B} \cdot d\mathbf{S} = s\phi_0. \quad (9.15)$$

$\phi_0$ , which has the dimension of a flux,

$$\phi_0 = -\frac{h}{q_p} = \frac{h}{2e} = 2.068 \cdot 10^{-15} \text{ Wb} \quad (9.16)$$

and depends only on the universal constants of PLANCK and the electron charge, is called the “magnetic flux quantum” or also the “fluxon”. We note that its value is particularly tiny, since it is the flux of a magnetic field of  $2.07 \cdot 10^{-9}$  T across a surface of  $1 \text{ mm}^2$ , or of  $2.07 \cdot 10^{-3}$  T across  $1 \mu\text{m}^2$ .

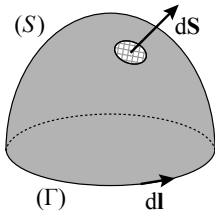


**Figure 9.2**

**Relative orientations of a closed loop and the surface it delimits**

Note the relative orientations of the element of length  $dl$  and of a surface element  $dS$ .

### 9.3.2 - Simply connected superconductor

We shall now consider an initial closed loop ( $\Gamma$ ) in a simply connected<sup>3</sup> superconductor. Since the solid has no hole that “crosses it”, this loop can be progressively reduced to a single point by a succession of loops ( $\Gamma_i$ ) infinitesimally close to one another (Fig. 9.3a). The change in phase is obviously zero ( $s = 0$ ) when the loop shrinks to a point, and provided there is no reason for the value of  $s$  to change during an infinitesimal modification of the loop, we conclude that  $s = 0$  for all internal loops of the superconductor, whether they are large or small. Therefore, by virtue of (9.15),

$$\oint_{\Gamma} \delta\theta = \frac{m_p}{n_p q_p \hbar} \oint_{\Gamma} \mathbf{j} \cdot d\mathbf{l} + \frac{q_p}{\hbar} \iint_S \mathbf{B} \cdot d\mathbf{S} = 0. \quad (9.17a)$$

This is particularly obvious if the closed path is well inside the superconductor, where both the magnetic field and the current density vanish. It remains true if the path crosses the LONDON region for the contributions of the current and the magnetic field there are equal and opposite. If we split a loop such as  $\Gamma_1$  into two parts: first a path  $\Gamma_{1\alpha}$  from C to some other point D on  $\Gamma_1$  and a second  $\Gamma_{1\beta}$  from D to C, we have

$$\int_{C(\Gamma_{1\alpha})}^D \delta\theta + \int_{D(\Gamma_{1\beta})}^C \delta\theta = 0 \Rightarrow \int_{C(\Gamma_{1\alpha})}^D \delta\theta = \int_{C(\Gamma_{1\beta})}^D \delta\theta. \quad (9.17b)$$

3 In other words the superconductor has no hole that comes out at two distinct parts of the surface. For more details, see note 11 of Chapter 2.

Therefore in a simply connected superconductor, the phase change between any two points C and D does not depend on the path followed, and consequently at each point we can define a unique phase  $\theta(\mathbf{r}, t)$ .

### 9.3.3 - Multiply connected superconductor

The situation is different in a multiply connected superconductor, i.e. one that has at least one hole coming out at two distinct parts of the surface. An example is a plate with a hole (Fig. 9.3b). In this case, it is no longer possible to shrink a loop that passes through the hole and reduce it to a point while remaining inside the superconductor, and there is no longer any reason for  $s$  to vanish.

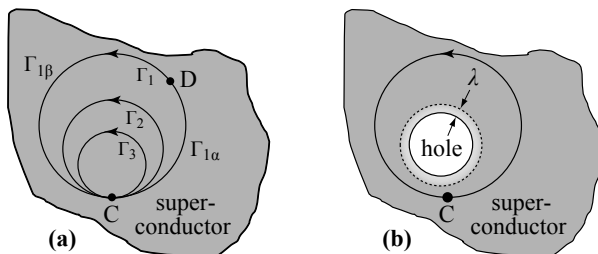


Figure 9.3 - Closed paths in simply connected and non-simply connected superconductors

- (a) In a simply connected superconductor any closed loop can be continuously deformed until it reduces to a single point without singularity.
- (b) In a multiply connected body the loop surrounding a hole can no longer be shrunk to a point. The loop represented here avoids the LONDON region and any screening currents associated with it.

When the closed loop ( $\Gamma$ ) is wide enough never to pass inside the LONDON region around the hole crossed by a magnetic field  $\mathbf{B}$ , and therefore never crosses a non-zero current density, the relation (9.15) reduces to

$$\iint_S \mathbf{B} \cdot d\mathbf{S} = s\phi_0. \quad (9.18)$$

In a multiply connected superconductor, the flux  $\phi$  of the magnetic field through a surface bounded by a closed loop that avoids all LONDON regions (Fig. 9.4), is equal to an integer number of fluxons.

### 9.3.4 - Experimental proof of the existence of COOPER pairs

In their original article V. GINZBURG and L. LANDAU<sup>4</sup> wrote that the electric charge carried by superconductivity has no reason to be different from that of the electron. This means that still at that time no-one had imagined the existence of COOPER pairs, even if we can suspect that this remark betrayed some uncertainty about the issue.

4 V. GINZBURG & L. LANDAU (1950) *Zh. Eksp. Teor. Fiz.* **20**, 1064.

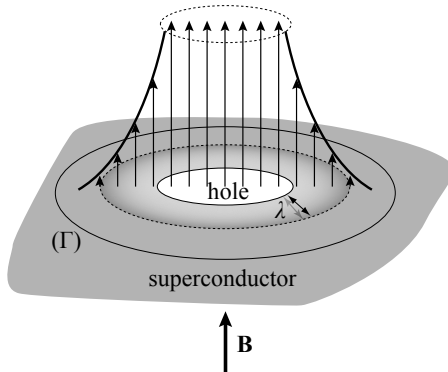


**Figure 9.4 - Flux of magnetic field “through” a “superconducting hole”**

The magnetic field present in the hole fades away in the superconductor with the penetration depth  $\lambda$ . The surface across which the flux is quantized encompasses not only the hole, but also the region of decreasing field in the superconductor. The large circle  $(\Gamma)$  that limits the surface through which the flux is determined avoids the LONDON region.

The possibility of determining the charge of the carriers of superconductivity, and thereby reveal the existence of the COOPER pairs, appears only with a measurement of the flux quantum. In fact, even though it involves the particle charge, the LONDON penetration depth does not allow us to determine its value. This is because in the formula for  $\lambda_L$  (Table 9.1), if the charge and mass are doubled, the carrier density must also be halved, which leaves the final result unchanged.

**Table 9.1 - Confirmation of the COOPER pairs by the flux quantum**

The combination of measurements of the LONDON penetration depth and the flux quantum show that the particles at the origin of superconductivity have a mass and a charge double those of the electron.

LONDON penetration depth	Flux quantum
$\lambda_L^2 = \frac{m}{\mu_0 n_s e^2} = \frac{m_p}{\mu_0 n_p q_p^2}$ The expression for $\lambda_L$ is insensitive to a grouping of the electrons into pairs, to the extent that the mass and charge are multiplied by two but the density is divided by two.	$\phi_0 = \frac{2\pi\hbar}{-q_p} = \frac{h}{2e}$ Measurements of $\phi_0$ show that the particles involved in the flux quantization carry a charge double that of the electron.

Experimental proof of the existence of COOPER pairs was provided by the measurement of the flux trapped in a hollow cylinder<sup>5</sup> (Fig. 9.5). The results show unambiguously that the flux is quantized and the charge to include in the expression for the flux quantum is double the electronic charge  $q_p = -2e$ .

5 W. GOODMAN & B.S. DEAVER (1970) *Phys. Rev. Letters* **24**, 870.

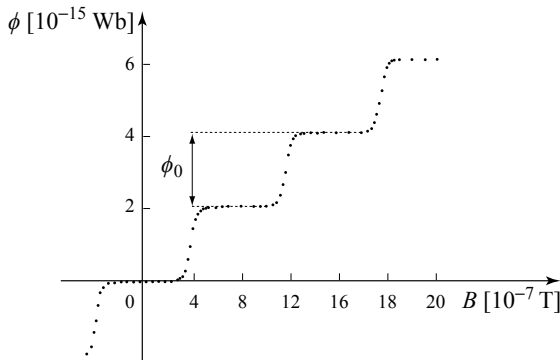


Figure 9.5 - Demonstration of flux quantization

The flux trapped in a hollow tin cylinder (of diameter 56  $\mu\text{m}$ , thickness 0.5  $\mu\text{m}$ ) as a function of the field in which it has been cooled. The flux increments are equal to the flux quantum  $\phi_0$  given in the expression (9.16). [From GOODMAN & DEAVER, 1970, © The American Physical Society, with permission]<sup>5</sup>

## 9.4 - Back to gauges

### 9.4.1 - The second LONDON equation

Independently of any choice of gauge, the equation

$$\nabla \times \mathbf{p} = \mathbf{0} \quad (9.19)$$

leads to the second LONDON equation (9.8). In reality this equation is more powerful, since it remains valid even if the charge density is not uniform. Indeed, if we replace the momentum  $\mathbf{p}$  by its definition (9.4), it becomes

$$\nabla \times \mathbf{v} = -\frac{q_p}{m_p} \mathbf{B} \quad (9.20)$$

called the “root equation” (see 2.70), from which the LONDON equation can be derived when the charge density is uniform.

### 9.4.2 - Simply connected superconductor

We saw in section 2.12 that in a simply connected superconductor, the choice of the LONDON gauge, which constrains the vector potential  $\mathbf{A}$  (a non-physical variable) by the conditions  $\nabla \cdot \mathbf{A} = 0$  (in the bulk) and  $\mathbf{A} \cdot \mathbf{n} = 0$  (on the surface) modelled on the properties of  $\mathbf{j}$  (a physical variable), leaves the integration constant  $\chi(\mathbf{r}, t)$  uniform, and leads to the second LONDON equation in the form

$$\mathbf{j}(\mathbf{r}, t) = -\frac{1}{\mu_0 \lambda_L} \mathbf{A}(\mathbf{r}, t) \quad \text{in the LONDON gauge} \quad (9.21)$$

which is equivalent to taking the momentum  $\mathbf{p}$  to be zero

$$\mathbf{p} = \mathbf{0} \quad \text{in the LONDON gauge} \quad (9.22)$$

and since the wave vector  $\mathbf{k}$  is related to this generalized momentum  $\mathbf{p}$ ,

$$\mathbf{k} = \frac{\mathbf{p}}{\hbar} = \mathbf{0} \quad \text{in the LONDON gauge (9.23)}$$

the phase difference between any two points vanishes and the phase is uniform in the sample (see relation 9.9)

$$\theta(\mathbf{r}, t) = \text{constant} \quad \text{in the LONDON gauge (9.24)}$$

This gauge is said to be “rigid.” In this gauge,  $\theta(\mathbf{r}, t)$ , the phase of the wave function, and  $\chi(\mathbf{r}, t)$ , which appeared as the constant of integration in (2.89) represent the same quantity up to a multiplicative constant

$$\theta(\mathbf{r}, t) = \frac{q_p}{\hbar} \chi(\mathbf{r}, t). \quad (9.25)$$

#### 9.4.3 - Multiply connected superconductor

When the superconductor is not simply connected (see Fig. 9.4), a magnetic field can pass through the superconductor via the hole and the surrounding superconducting material within the penetration depth  $\lambda$ . The flux  $\phi$  across a surface bounded by a closed path ( $\Gamma$ ), that is far enough from the edge of the hole that the current density  $\mathbf{j}$  vanishes everywhere, is equal to

$$\phi = \iint_S \mathbf{B} \cdot d\mathbf{S} = \oint_{\Gamma} \mathbf{A} \cdot d\mathbf{l} = s\phi_0 \quad (9.26)$$

a result incompatible with the relation (9.21) since, if  $\mathbf{A}$  were proportional to  $\mathbf{j}$ , the integral along ( $\Gamma$ ) would vanish.

In a multiply connected body, the conditions  $\nabla \cdot \mathbf{A} = 0$  (in the bulk) and  $\mathbf{A} \cdot \mathbf{n} = 0$  (on the surface) become insufficient to define a gauge, and we must define for each hole the value of  $s$  such that  $\int_{\Gamma} \mathbf{A} \cdot d\mathbf{l} = s\phi_0$ .

## 9.5 - Flux quantization: application to vortices

### 9.5.1 - Fluxon carried by a single vortex

The arguments of section 9.3.3 for a hole can be repeated for a single, isolated, vortex which has a central non-superconducting singularity that prevents a closed loop surrounding it from being deformed to a single point. Applying the relation (9.18), the flux of the magnetic field across a surface bounded by a path which is sufficiently wide to avoid the vortex super-currents, and therefore includes all the magnetic fields associated with the vortex, is an integer number of fluxons (Fig. 9.6). In fact, although flux quantization allows one vortex to carry several fluxons, energy considerations show that except for exceptional cases (see Chap. 6, section 6.11.5) it is more favorable to create two vortices, each carrying one fluxon, rather than a single vortex bearing two fluxons.

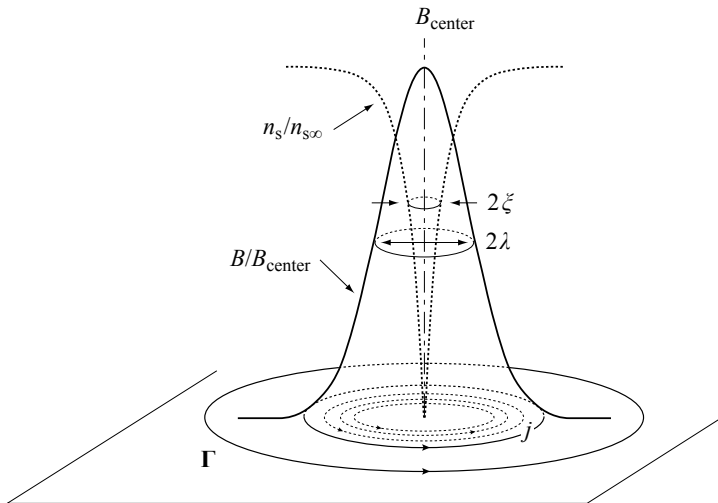


**Figure 9.6 - Flux quantum carried by a vortex**

The total flux of all magnetic fields around the vortex is quantified and equals one quantum of flux  $\phi_0$ . The large circle that delimits the area through which the flux is measured avoids any regions of current or field.

### 9.5.2 - Fluxon in the ABRIKOSOV lattice

When organized into an ABRIKOSOV lattice (see Chap. 6, section 6.6), the vortices become denser with increasing magnetic field, the LONDON zones of neighboring vortices overlap and the magnetic field no longer vanishes between the vortex cores (see Fig. 6.14). How then, can we associate a fluxon with each vortex?

A geometrical argument, illustrated in Figure 9.7 provides the answer.

Suppose we take two vortices  $V_1$  and  $V_2$  and a point  $M$  on the perpendicular bisector of their centers which passes through the centers of vortices  $V_3$  and  $V_4$  (Fig. 9.7a). If from  $M$  we draw the radial currents supposed to be “associated” with each vortex (the number of each generating vortex is given in brackets, Fig. 9.7b), it is clear by symmetry that the current (3) and the vector sum of currents (1) and (2) are normal to the perpendicular bisector of  $V_1$  and  $V_2$ .

Furthermore, as we follow the polygonal path (here hexagonal) formed by the bisectors of a central vortex and its neighbors (the WIGNER cell) we see only current densities normal to the path. It follows that the circulation of the current density around the path vanishes and the magnetic flux across the WIGNER cell is equal to one fluxon (see Fig. 9.6).

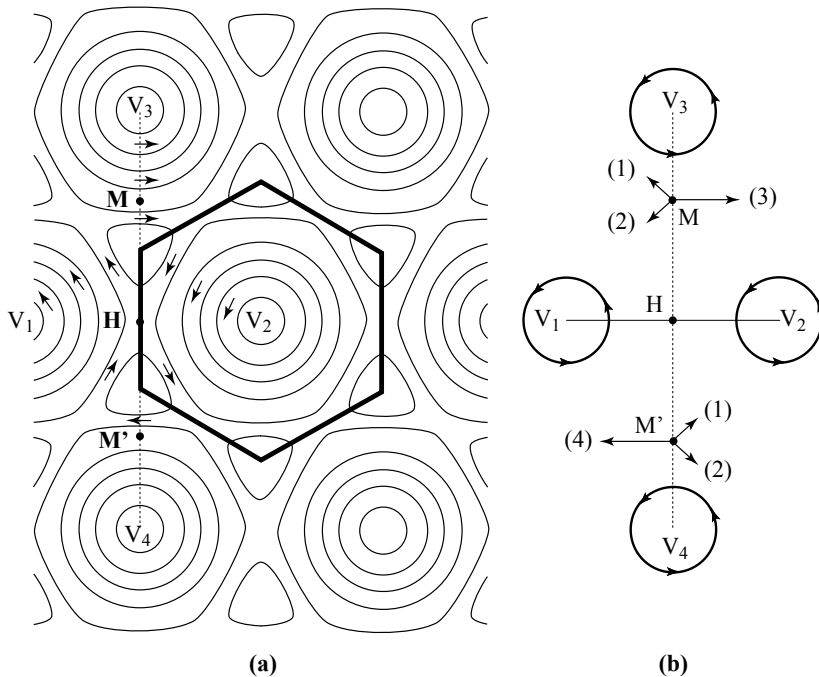


**Figure 9.7 - Fluxons in an ABRIKOSOV lattice**

(a) Lines of equal density of superconducting electrons and currents in a dense hexagonal ABRIKOSOV lattice<sup>6</sup>. The LONDON currents of two neighboring vortices cancel at the middle of the line separating them. (b) The current densities at M and M', imagined as hypothetical superpositions of the currents “associated” with each vortex are normal to the perpendicular bisector of  $V_1V_2$ . The circulation of the current density vanishes around the polygon formed by the bisectors between a central vortex and its neighbors (the WIGNER-SEITZ cell). The flux crossing such a cell is equal to the fluxon  $\phi_0$ .

### 9.5.3 - A confined vortex

In the experiment described in Chapter 6 (section 6.11.5, fig. 6.24), where a vortex is confined to a sample of nanometric scale, the LONDON currents near the surface and the vortex currents turn in opposite directions and are therefore separated by a neutral line where the current density vanishes. Once again, by applying (9.18), the path following this closed line can only be crossed by an integer number of fluxons: one if it is a simple vortex, or several if it is a super-vortex.

The sample itself is subject to a higher flux since we must add the contribution of the decreasing magnetic field in the LONDON zone.

---

6 W.H. KLEINER, L.M. ROTH & S.H. AUTLER (1964) *Phys. Rev.* **133**, A1226.

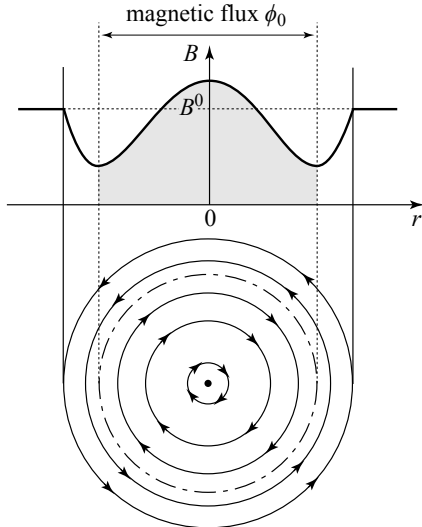


Figure 9.8

**Flux through a region with a confined vortex**

**Above:** the magnetic field that decreases from the surface (LONDON) and increases as the vortex centre is approached.

**Below:** Lines of current density dominated by the vortex current near the center and by screening currents towards the outside. The currents, which turn in opposite directions, are separated by a line of vanishing current. The magnetic flux across the area enclosed by this line is equal to one flux quantum  $\phi_0$ .

#### 9.5.4 - Current density around a vortex core

When we calculated the flux-flow resistivity (see App. 7-B.2, expression 7.78), we proposed that in a type II superconductor with a high value of  $\kappa$ , in other words with a small core radius  $\xi$ , the current density can be approximated in the region  $\xi < r \ll \lambda$  by

$$j_\theta(r) \approx \frac{\phi_0}{2\pi\mu_0\lambda^2} \frac{1}{r}. \quad (9.27)$$

This expression, which can be derived from the fourth MAXWELL's equation using a realistic form for the field  $\mathbf{B}$ , also follows as a consequence of the phase coherence of COOPER pairs.

In fact, since the total change of the phase  $\theta$  around a closed path of radius greater than  $\lambda$  is  $2\pi$ , it must be the same for any path differing by continuous modification of the initial one which does not cross a singularity. This is the case for a path of radius  $r$  slightly greater than that of the core ( $\xi < r \ll \lambda$ ). The phase variation going once around such a path is given, by the relation (9.13), as

$$\frac{m_p}{q_p} \oint \mathbf{v} \cdot d\mathbf{l} + \oint \mathbf{A} \cdot d\mathbf{l} = -2\pi \frac{\hbar}{q_p} = \phi_0 \quad (9.28)$$

or, with  $\phi$  denoting the flux through the path of radius  $r$ ,

$$\frac{m_p}{q_p} (2\pi r v) + \phi = \phi_0. \quad (9.29)$$

In so far as the radius  $r$  is very small compared to the penetration depth, the flux  $\phi$  remains much smaller than  $\phi_0$  and, to a first approximation,

$$v \approx \phi_0 \frac{q_p}{2\pi m_p r}. \quad (9.30)$$

When the density of pairs is uniform,

$$j \approx \phi_0 \frac{n_p q_p^2}{2\pi m_p r} \quad (9.31)$$

thereby proving the formula (9.27).

## 9.6 - Generalized LONDON equation in the presence of vortices

In the presence of a vortex the LONDON equation takes the generalized form

$$\mathbf{B}(\mathbf{r}) + \mu_0 \lambda^2 \nabla \times \mathbf{j}(\mathbf{r}) = \phi_0 \delta_2(\mathbf{r} - \mathbf{r}_0) \hat{\mathbf{u}}_0 \quad (9.32)$$

where  $\delta_2(\mathbf{r} - \mathbf{r}_0)$  is the DIRAC function in two dimensions and  $\mathbf{r}_0$  is the point on the axis of the vortex located in the plane that is perpendicular to the unit vector  $\hat{\mathbf{u}}_0$  along the vortex axis and that contains the point  $\mathbf{r}$ . In fact this equation (9.32), equivalent to the usual LONDON equation at any point other than  $\mathbf{r} = \mathbf{r}_0$  (only the vortex axis is completely in the normal state), also includes the quantization of the flux. Indeed by taking the flux of the left and right sides of this equation across the surface limited by a contour ( $\Gamma$ ) surrounding the vortex axis, we find (see equation 9.15)<sup>7</sup>

$$\iint_S \mathbf{B}(\mathbf{r}) \cdot d\mathbf{S} + \mu_0 \lambda^2 \oint_{\Gamma} \mathbf{j}(\mathbf{r}) \cdot d\mathbf{l} = \phi_0. \quad (9.33)$$

When the contour is drawn well beyond the penetration depth,

$$\iint_S \mathbf{B}(\mathbf{r}) \cdot d\mathbf{S} = \phi_0. \quad (9.34)$$

In the presence of several vortices, (9.32) generalizes to

$$\mathbf{B}(\mathbf{r}) + \mu_0 \lambda^2 \nabla \times \mathbf{j}(\mathbf{r}) = \phi_0 \sum_i \delta_2(\mathbf{r} - \mathbf{r}_i) \cdot \hat{\mathbf{u}}_i. \quad (9.35)$$

With these generalized forms, it is easy to calculate the energy of formation of a vortex and the repulsive force between two vortices (see App. 7A.3).

## 9.7 - Return to the LONDON moment

In Chapter 2 (section 2.11), it was shown that the second LONDON equation (2.26) was inapplicable when the superconducting electron density is not uniform or when the current density is determined by more than just the velocity of the electrons, as

---

<sup>7</sup>  $\iint \delta_2(\mathbf{r} - \mathbf{r}_0) \hat{\mathbf{u}}_0 d\mathbf{S} = 1$

is the case for a rotating sphere (LONDON moment). To treat this class of problems, we must start from the root equation (9.20).

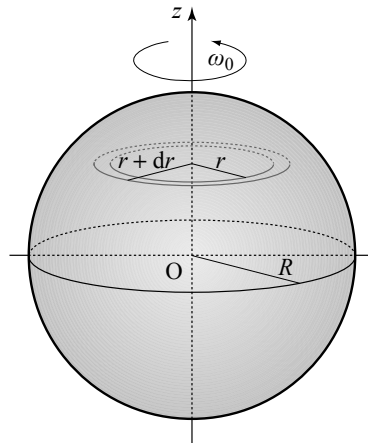


**Figure 9.9**  
Superconducting sphere  
and the LONDON moment

The superconducting sphere of radius  $R \gg \lambda$  is rotating and paths of radius  $r$  and  $r + dr$  are centered on the axis of rotation. Inside the rotating sphere, the magnetic field is uniform for distances to the surface great compared to the penetration depth  $\lambda$ .

Consider, therefore a superconducting sphere rotating around an axis  $z$  with constant angular momentum  $\omega_0$ , and take a circular loop of radius  $r$  around the central axis, deep enough in the sphere to avoid the LONDON region bordering the surface. Following the arguments developed in section 2.11.1, we suppose that the COOPER pairs of this internal region are driven by the ions and turn at the speed of the positive charges  $v = \omega_0 r$ .

Considering that by symmetry, the field  $\mathbf{B}(r)$  is oriented along the axis of rotation of the sphere and that the loop can, by continuity and without crossing any singularities, be collapsed to a point, which requires  $s = 0$ , it follows (from 9.14)

$$m_p(\omega_0 r)(2\pi r) + q_p \phi = 0 \quad (9.36)$$

where  $\phi$  is the magnetic flux through the loop.

Now we take a second concentric circle of radius  $(r + dr)$  that, compared to the first, has a perimeter enlarged by  $2\pi dr$  and the flux through it increased by  $B(r) 2\pi r dr$ . As the second loop satisfies the same condition as (9.36),

$$m_p[\omega_0(r + dr)][2\pi(r + dr)] + q_p \phi + q_p B(r) 2\pi r dr = 0. \quad (9.37)$$

Subtracting the two equations and working to first order in  $dr$

$$B(r) = -\frac{2m_p}{q_p} \omega_0 = \frac{2m}{e} \omega_0 \quad (9.38)$$

which is the relation (2.81). It appears naturally that the magnetic field does not depend on  $r$  and that is therefore uniform inside the rotating sphere at points whose distance from the surface is further than the penetration depth.

## Appendix 9

### Generalized momentum

#### A9.1 - Lagrangian and Hamiltonian mechanics

##### Notation

It is usual in Lagrangian mechanics to denote a particle's velocity  $\mathbf{v}$  and acceleration  $\mathbf{a}$  and their components by

$$\mathbf{v} = \dot{\mathbf{r}} = \frac{d\mathbf{r}}{dt} \quad v_x = \dot{x} = \frac{dx}{dt} \quad \mathbf{a} = \ddot{\mathbf{r}} = \frac{d^2\mathbf{r}}{dt^2} \quad a_x = \ddot{x} = \frac{d^2x}{dt^2}. \quad (9.39)$$

As Lagrangian mechanics is very general and is used for systems with a large number of degrees of liberty, we usually find the equations written with generalized coordinates and associated velocities denoted  $q$  (instead of  $x$ ) and  $\dot{q}$  (instead of  $\dot{x}$ ).

##### The Lagrangian and the LAGRANGE equations

The Lagrangian of a particle subject to various potentials is a function  $\mathcal{L}(\mathbf{r}, \dot{\mathbf{r}}, t)$  of the variables of position, velocity and time, taken as being independent. The equation of motion can be derived from the LAGRANGE equations written for each component  $x$

$$\frac{d}{dt} \left( \frac{\partial \mathcal{L}}{\partial \dot{x}} \right) - \frac{\partial \mathcal{L}}{\partial x} = 0. \quad (9.40)$$

##### Lagrangian of a charged particle

We can easily verify that the Lagrangian of a charged particle in an electromagnetic field

$$\mathcal{L}(\mathbf{r}, \dot{\mathbf{r}}, t) = \frac{1}{2} m \dot{\mathbf{r}}^2 + q \dot{\mathbf{r}} \cdot \mathbf{A}(\mathbf{r}, t) - q V(\mathbf{r}, t) \quad (9.41)$$

implies, by the LAGRANGE equations, the equation of motion of a charge in an electromagnetic field,

$$m \ddot{\mathbf{r}} = q [ \mathbf{E}(\mathbf{r}, t) + \mathbf{v} \times \mathbf{B}(\mathbf{r}, t) ] \quad (9.42)$$

with  $\mathbf{B}(\mathbf{r}, t) = \nabla \times \mathbf{A}(\mathbf{r}, t)$      $\mathbf{E}(\mathbf{r}, t) = -\nabla V(\mathbf{r}, t) - \frac{\partial \mathbf{A}(\mathbf{r}, t)}{\partial t}$ .    (9.43)

##### Momentum of a charged particle

The momentum component of a particle in the  $x$  direction is defined from the Lagrangian by

$$p_x = - \frac{\partial \mathcal{L}}{\partial \dot{x}}. \quad (9.44)$$

We say that  $p_x$  is the variable conjugate to  $x$ .

For a charged particle in an electromagnetic field it becomes

$$p_x = m\dot{x} + qA_x(\mathbf{r}, t) \quad \text{or} \quad \mathbf{p} = m\mathbf{v} + q\mathbf{A}(\mathbf{r}, t). \quad (9.45)$$

### The HAMILTON function

The HAMILTON function is defined by the LEGENDRE transformation of the LAGRANGE equation

$$\mathcal{H}(\mathbf{r}, \mathbf{p}, t) = \mathbf{p}\dot{\mathbf{r}} - \mathcal{L}(\mathbf{r}, \dot{\mathbf{r}}, t) \quad (9.46)$$

where  $\mathcal{H}$  is now a function of the independent variables: position  $\mathbf{r}$ , momentum  $\mathbf{p}$  and time  $t$ . Replacing the LAGRANGE equations there are the HAMILTON-JACOBI equations

$$\frac{d\mathbf{x}}{dt} = \frac{\partial \mathcal{H}}{\partial p_x} \quad ; \quad \frac{dp_x}{dt} = -\frac{\partial \mathcal{H}}{\partial x}. \quad (9.47)$$

We can easily check that the HAMILTON function of a particle in an electromagnetic field is

$$\mathcal{H}(\mathbf{r}, \dot{\mathbf{r}}, t) = \frac{[\mathbf{p} - q\mathbf{A}(\mathbf{r}, t)]^2}{2m} + qV(\mathbf{r}, t) \quad (9.48)$$

where the first term is the kinetic energy and the second the potential energy

$$\begin{aligned} E_{\text{kin}} &= \frac{1}{2}m\mathbf{v}^2 = \frac{1}{2m}(\mathbf{p} - q\mathbf{A})^2 \\ E_{\text{pot}} &= qV(\mathbf{r}, t). \end{aligned} \quad (9.49)$$

The HAMILTON function thus coincides with the total energy function.

### A9.2 - The passage to quantum mechanics

#### A few principles

Quantum mechanics teaches us that *to each physical variable corresponds an operator*, and that *the result of a measurement can only be one of the eigenvalues of the operator*.

The correspondence principle associates the momentum component  $p_x$  with the operator  $\hat{p}_x = \frac{\hbar}{i} \frac{\partial}{\partial x}$ , and including the other components:

$$\text{momentum } \mathbf{p} \Rightarrow \text{operator } \hat{\mathbf{p}} = \frac{\hbar}{i} \nabla. \quad (9.50)$$

#### Momentum and wave vector

$$\text{The plane wave} \quad \varphi(\mathbf{r}) = e^{i\mathbf{k}\cdot\mathbf{r}} \quad (9.51)$$

is an eigenfunction of the momentum operator with eigenvalue  $\hbar\mathbf{k}$

$$\hat{\mathbf{p}} e^{i\mathbf{k}\cdot\mathbf{r}} = \frac{\hbar}{i} \nabla e^{i\mathbf{k}\cdot\mathbf{r}} = \hbar \mathbf{k} e^{i\mathbf{k}\cdot\mathbf{r}} \quad (9.52)$$

leading to the usual vector relation between the momentum of the particle and the wave vector of the associated plane wave

$$\mathbf{p} = \hbar \mathbf{k}. \quad (9.53)$$

### ***Hamiltonian of a particle in an electromagnetic field***

Application of the correspondence principle to the HAMILTON function (9.48) leads to<sup>8</sup>

$$\hat{H} = \frac{1}{2m} \left[ \frac{\hbar}{i} \nabla - q \mathbf{A}(\mathbf{r}, t) \right] \left[ \frac{\hbar}{i} \nabla - q \mathbf{A}(\mathbf{r}, t) \right] + qV(\mathbf{r}, t). \quad (9.54)$$

### ***Current density***

By definition, the current density is the quantity  $\mathbf{j}$  satisfying

$$\nabla \cdot \mathbf{j} + \frac{\partial \rho_{\text{vol}}}{\partial t} = 0 \quad (9.55)$$

where  $\rho_{\text{vol}}$ , the bulk charge density, is related to the density  $n$  of particles and to the wave function by

$$\rho_{\text{vol}} = q n(\mathbf{r}, t) = q \varphi^*(\mathbf{r}, t) \varphi(\mathbf{r}, t). \quad (9.56)$$

Determining  $\partial \rho_{\text{vol}} / \partial t$  by the SCHRÖDINGER equation,

$$\hat{H} \varphi = i\hbar \frac{\partial \varphi}{\partial t} \quad \text{and} \quad \hat{H} \varphi^* = -i\hbar \frac{\partial \varphi^*}{\partial t} \quad (9.57)$$

we obtain 
$$\mathbf{j} = q \operatorname{Re} \left[ \varphi^* \frac{1}{m} \left( \frac{\hbar}{i} \nabla - q \mathbf{A}(\mathbf{r}, t) \right) \varphi \right]. \quad (9.58)$$

### ***A9.3 - Gauges***

The momentum  $\mathbf{p}$  is an unphysical variable since it is the sum of a physical variable  $m\mathbf{v}$  and of the vector potential  $\mathbf{A}$ , an unphysical variable that depends on the choice of gauge. To keep  $m\mathbf{v}$  invariant, a change of gauge which modifies the vector potential must be accompanied by a modification in the momentum such that

$$\mathbf{A}' = \mathbf{A} + \nabla \chi(\mathbf{r}, t) \iff \mathbf{p}' = \mathbf{p} + q \nabla \chi(\mathbf{r}, t) \quad (9.59)$$

and therefore of the wave vector

$$\mathbf{k}' = \frac{\mathbf{p}'}{\hbar} = \mathbf{k} + \frac{q}{\hbar} \nabla \chi(\mathbf{r}, t). \quad (9.60)$$

---

<sup>8</sup> Since the operators  $\nabla$  and  $\mathbf{A}$  do not commute, the Hamiltonian is written in the form of a product.

The plane wave function, for which  $\hbar \mathbf{k}'$  must be the eigenvalue associated with the new form of the momentum operator, becomes

$$\varphi'(\mathbf{r}) = e^{i\mathbf{k}' \cdot \mathbf{r}} = e^{i\mathbf{k} \cdot \mathbf{r}} e^{\frac{iq}{\hbar} \chi} \quad (9.61)$$

which does indeed satisfy

$$\frac{\hbar}{i} \nabla \left( e^{i\mathbf{k} \cdot \mathbf{r}} e^{\frac{iq}{\hbar} \chi(\mathbf{r}, t)} \right) = \left( \mathbf{k} + \frac{q}{\hbar} \nabla \chi(\mathbf{r}, t) \right) \left( e^{i\mathbf{k} \cdot \mathbf{r}} e^{\frac{iq}{\hbar} \chi(\mathbf{r}, t)} \right). \quad (9.62)$$

The phase  $\theta = \mathbf{k} \cdot \mathbf{r}$  changes to  $\theta' = \left[ \mathbf{k} + \frac{q}{\hbar} \nabla \chi(\mathbf{r}, t) \right] \mathbf{r}$ .

*In this way, making a gauge transformation leads us to replace simultaneously  $\mathbf{A}$ ,  $\mathbf{p}$  and  $\theta$  according to the rules imposed by the relations*

$$\begin{aligned} \mathbf{A}' &= \mathbf{A} + \nabla \chi(\mathbf{r}, t) \\ \mathbf{p}' &= \mathbf{p} + q \nabla \chi(\mathbf{r}, t) \end{aligned} \quad (9.63)$$

$$\theta' = \theta + \frac{q}{\hbar} \chi(\mathbf{r}, t).$$

# Chapter 10

## THE JOSEPHSON EFFECT

The JOSEPHSON effect results from the passage of “particles” COOPER pairs, and not of individual electrons, between two superconductors separated by an insulating barrier (SIS), by a normal metal (SNS), by a simple constriction in the superconductor (SCS or “weak link”) or by a ferromagnetic layer (SFS). Each of the superconductors, ( $S_1$ ) or ( $S_2$ ), hosts a superconducting condensate whose wave function (expression 9.2) possesses its own characteristics: a number of COOPER pairs  $n_1(\mathbf{r},t)$  or  $n_2(\mathbf{r},t)$  and a phase  $\theta_1(\mathbf{r},t)$  or  $\theta_2(\mathbf{r},t)$ . In the first sections of this chapter we will discuss in detail the “standard” case of the SIS junction, where the COOPER pairs pass from one of the superconductors to the other by tunneling.

The more complex SNS junctions will be introduced in section 10.7. The SFS junction will be the subject of section 10.8. All these junctions are known as “JOSEPHSON junctions.”

### 10.1 - JOSEPHSON equations in an SIS junction

As the thickness of the insulating layer is of order of a nanometer, the wave function of the COOPER pairs of the superconductor ( $S_1$ ) extends into the superconductor ( $S_2$ ) and inversely, which leads to a non-zero probability of transfer of COOPER pairs from one to the other by the tunnel effect (Fig. 10.1b).

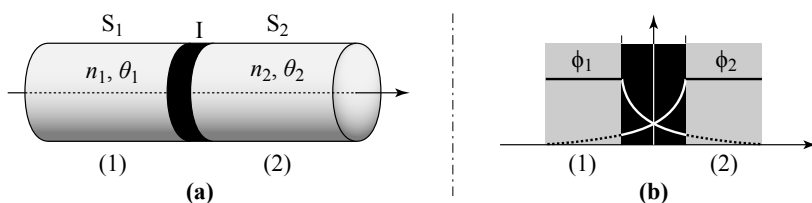


Figure 10.1 - SIS JOSEPHSON Junction

(a) An SIS JOSEPHSON junction is composed of two superconducting blocks (1) and (2) separated by an insulating barrier. Each block is characterized by its number of Cooper pairs  $n_1$  or  $n_2$  and by the phase of its wave function  $\theta_1$  or  $\theta_2$ . (b) The overlap of the evanescent parts of the wave functions of the COOPER pairs of each side allows the barrier to be crossed by tunneling.

Even though this is a many-body problem (see section 10.9 further on), as a first step we will follow the method of FEYNMAN<sup>1</sup> that takes the total wave function  $|\Psi(t)\rangle$  as a linear combination of the wave functions of each condensate.

### 10.1.1 - The ionized hydrogen molecule

Such an approach is classic for a two-state system such as the ionized hydrogen molecule  $\text{H}_2^+$ , where we are interested in a single particle, the electron, that can be “close” to one or other of the two protons. Depending on whether the electron is in the neighborhood of proton (1) or of proton (2), the system is to be considered to be in the state  $|1\rangle$  or  $|2\rangle$ , the most general state being a linear combination of these two states,

$$|\Psi(t)\rangle = c_1(t)|1\rangle + c_2(t)|2\rangle. \quad (10.1)$$

The coefficients  $c_1(t)$  and  $c_2(t)$  are the probability amplitudes for the presence of the electron near protons (1) and (2) respectively (the probabilities are  $|c_1(t)|^2$  and  $|c_2(t)|^2$ ). Their time evolution obeys the matrix SCHRÖDINGER equation,

$$\begin{pmatrix} E_1 & -K \\ -K & E_2 \end{pmatrix} \begin{pmatrix} c_1(t) \\ c_2(t) \end{pmatrix} = i\hbar \frac{d}{dt} \begin{pmatrix} c_1(t) \\ c_2(t) \end{pmatrix} \quad (10.2)$$

where  $E_1$  is the energy of the electron when it is bound to the isolated proton (1),  $E_2$  its energy when it is bound to proton (2) and  $K$  the coupling constant between the two states that expresses the probability amplitude  $-iK/\hbar$  for the electron to pass from one site to the other per unit time. When the molecule is symmetric, as is the case for  $\text{H}_2^+$ , we obviously have  $E_1 = E_2$ .

### 10.1.2 - Transfer between superconducting blocks

As the relevant quantity is no longer the probability of presence of the electron near the proton  $\text{H}^+$  (1) or (2), but the number of COOPER pairs in the blocks (1) or (2), we define, by extension,

$$c_1(t) = \sqrt{n_1(t)} e^{i\theta_1(t)} \quad \text{and} \quad c_2(t) = \sqrt{n_2(t)} e^{i\theta_2(t)} \quad (10.3)$$

where  $|c_1(t)|^2 = n_1(t)$  and  $|c_2(t)|^2 = n_2(t)$  represent the number of COOPER pairs in each block. The wave function is then written

$$|\Psi(t)\rangle = \sqrt{n_1(t)} e^{i\theta_1(t)} |1\rangle + \sqrt{n_2(t)} e^{i\theta_2(t)} |2\rangle \quad (10.4)$$

and the SCHRÖDINGER equation becomes

$$\begin{pmatrix} E_1 & -K \\ -K & E_2 \end{pmatrix} \begin{pmatrix} \sqrt{n_1(t)} e^{i\theta_1(t)} \\ \sqrt{n_2(t)} e^{i\theta_2(t)} \end{pmatrix} = i\hbar \frac{d}{dt} \begin{pmatrix} \sqrt{n_1(t)} e^{i\theta_1(t)} \\ \sqrt{n_2(t)} e^{i\theta_2(t)} \end{pmatrix}. \quad (10.5)$$

<sup>1</sup> R. FEYNMAN, R. B. LEIGHTON, M. SANDS (1966) *The Feynman Lectures in Physics, Vol. III: Quantum Mechanics*, Addison-Wesley, Chap. 21. The new Millennium edition is available on-line at <http://www.feynmanlectures.caltech.edu>.

In the special case where the superconductors  $S_1$  and  $S_2$  are identical and connected to electric potentials  $+V/2$  and  $-V/2$  respectively, the energy of the COOPER pairs in the two isolated block becomes

$$E_1 = E_0 + \frac{q_p V}{2} ; \quad E_2 = E_0 - \frac{q_p V}{2} \quad (10.6)$$

or, by choosing the zero of energy such that  $E_0 = 0$

$$E_1 = +\frac{q_p V}{2} ; \quad E_2 = -\frac{q_p V}{2}. \quad (10.7)$$

Substituting these expressions in (10.5) and separating the real and imaginary parts, we derive (see App. 10A) the four relations

$$\frac{dn_1}{dt} = -\frac{dn_2}{dt} = \frac{2}{\hbar} K \sqrt{n_1 n_2} \sin(\theta_1 - \theta_2) \quad (10.8)$$

$$\frac{d\theta_1}{dt} = \frac{K}{\hbar} \sqrt{\frac{n_2}{n_1}} \cos(\theta_1 - \theta_2) - \frac{q_p V}{2\hbar} \quad (10.9a)$$

$$\frac{d\theta_2}{dt} = \frac{K}{\hbar} \sqrt{\frac{n_1}{n_2}} \cos(\theta_1 - \theta_2) + \frac{q_p V}{2\hbar} \quad (10.9b)$$

that lead to a series of remarkable effects:

- » the d.c. JOSEPHSON effect when the voltage  $V$  is zero,
- » the a.c. JOSEPHSON effect when the voltage  $V$  is constant and non-zero,
- » the resonant JOSEPHSON effect when, on a constant voltage  $V$ , is superposed a weak a.c. component  $v$ .

We note that the choice of the zero of energy and that of the symmetric distribution of the potential  $V$  between the two blocks has no reason other than to simplify the calculations. Any other choice would lead to a shift in the global phase, which would change none of the final results.

From now on, the phase difference between the two superconducting blocks will be denoted

$$\Theta_{1,2} = \theta_1 - \theta_2 \quad (10.10)$$

(or just  $\Theta$  when there is no ambiguity).

## 10.2 - The d.c. JOSEPHSON effect

### 10.2.1 - The JOSEPHSON current

The first equality of the equation (10.8), where  $dn_1/dt$  and  $dn_2/dt$  represent the variations in the number of particles in blocks (1) and (2), maintains the conservation

of the total number of COOPER pairs. The current intensity  $I$  that flows between the superconducting blocks, considered positive when it is from  $S_1$  to  $S_2$ , is given by

$$I = I_{1 \rightarrow 2} = q_p \frac{dn_2}{dt} = -q_p \frac{dn_1}{dt} = -\frac{2q_p}{\hbar} K \sqrt{n_1(t)n_2(t)} \sin \Theta_{1,2} \quad (10.11)$$

or, if the superconductors are identical and using the fact that the number of COOPER pairs transferred is always negligible compared to the total number in each solid block, *i.e.* that  $\sqrt{n_1(t)n_2(t)} \approx \text{constant} = n_p$

$$I = -\frac{2q_p}{\hbar} K n_p \sin \Theta_{1,2}. \quad (10.12)$$

*Even in the absence of a potential difference between the superconducting blocks, an electric current called the “JOSEPHSON current” appears with intensity  $I$  proportional to the sine of the phase difference between the wave functions of the two condensates. When  $\Theta_{1,2}$  is constant, this current is continuous.*

In contrast to a junction between two normal metals, it is no longer the difference of potentials that directly controls the tunnel current, but the difference of phases!

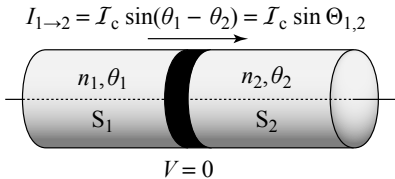


**Figure 10.2**

**The d.c. JOSEPHSON effect**

In the absence of a potential difference ( $V = 0$ ) but with a constant phase difference, a continuous current proportional to the sine of the phase difference flows between the superconducting blocks.

Because the sine function has a maximum value of one, the relation (10.12) implies a maximum value  $I_c$  of the JOSEPHSON current intensity called the “critical current intensity”<sup>2</sup>

$$I_c = -\frac{2q_p}{\hbar} K n_p = \frac{2e}{\hbar} K n_s. \quad (10.13)$$

The current intensity through the barrier is then given then by JOSEPHSON’s first equation,

$$I_{1 \rightarrow 2} = I_c \sin \Theta_{1,2} = I_c \sin(\theta_1 - \theta_2) \quad (10.14)$$

that is most often likely to be read in the inverse form

$$\Theta_{1,2} = \sin^{-1} \left( \frac{I_{1 \rightarrow 2}}{I_c} \right). \quad (10.15)$$

2  $n_p$  = number of operational COOPER pairs;  $q_p$  = charge of a pair =  $-2e$ ,  $n_s$  = number of superconducting electrons =  $2n_p$ .

If we inject a current of intensity  $I < I_c$  across a JOSEPHSON junction, a phase difference  $\Theta$  develops between the condensates on each side of the junction without the appearance of any voltage.

When the injected current exceeds  $I_c$ , a voltage difference appears between the leads of the junction. Continuity of the superconductivity is broken.

### 10.2.2 - Critical intensity of the JOSEPHSON current

The maximum intensity  $I_c$  that can pass a JOSEPHSON junction without generating a potential difference is a physical characteristic of the device.

#### *The AMBEGAOKAR and BARATOFF relation (SIS junction)*

BCS theory provides a relation between  $I_c$  and the resistance  $R_n$  of the SIS junction when the two superconductors are in the normal state. AMBEGAOKAR and BARATOFF<sup>3</sup> showed that, when the two superconductors of an SIS junction are identical with gap  $\Delta$ , at temperature  $T$  there is the relation

$$R_n I_c(T) = \frac{\pi \Delta(T)}{2e} \tanh \frac{\Delta(T)}{2k_B T} \quad (10.16)$$

and at 0 K,

$$I_c(0) = \frac{\pi \Delta(0)}{2e R_n}. \quad (10.17)$$

The experimental results of Figure 10.3 show that in agreement with equation (10.16),  $I_c$  decreases with  $T$  and vanishes at the critical temperature  $T_c$ .

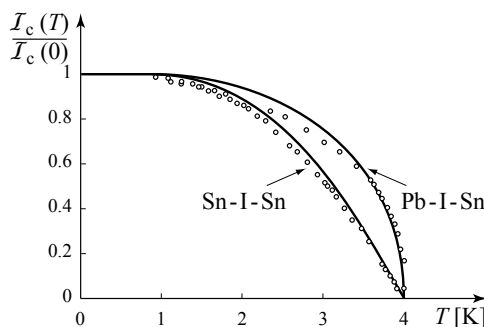


Figure 10.3 - Temperature dependence of the critical current intensity  $I_c$  of an SIS JOSEPHSON junction

The intensity of the critical JOSEPHSON current decreases with temperature and goes to zero at  $T_c$ . To the experimental points are added the theoretical curves of AMBEGAOKAR and BARATOFF when the superconductors are identical (relation 10.16) or, by generalisation of the formula, when they have different gaps. [From AMBEGAOKAR and BARATOFF, 1963, © The American Physical Society, with permission].<sup>3</sup>

3 V. AMBEGAOKAR & A. BARATOFF (1963) *Phys. Rev. Lett.* **10**, 486 & erratum **11**, 104.

## 10.3 - The a.c. JOSEPHSON effect

### 10.3.1 - The JOSEPHSON frequency

We now apply a constant potential difference between the two superconductors. By subtracting the relation (10.9b) from (10.9a) and taking  $n_1(t) \approx n_2(t)$ , we obtain the second JOSEPHSON equation, which defines the time evolution of the phase difference, that determines the JOSEPHSON current, as a function of the potential  $V$  at the terminals of the junction,

$$\frac{d\Theta}{dt} = -\frac{q_p V}{\hbar} = \frac{2e}{\hbar} V = 2\pi \frac{V}{\phi_0}. \quad (10.18)$$

By integration this leads to  $\Theta(t) = \Theta(0) + \frac{2eV}{\hbar} t$  (10.19)

and, using the relation (10.12), to an alternating current of intensity  $I$  and angular velocity  $\omega_J$  given by,

$$I(t) = I_c \sin \Theta(t) = I_c \sin \left[ \frac{2eV}{\hbar} t + \Theta(0) \right] \quad (10.20)$$

with  $\omega_J = \frac{2eV}{\hbar}$  ;  $f_J = \frac{2eV}{h}$  (10.21)

called the JOSEPHSON angular velocity and the JOSEPHSON frequency. Their values are close to  $3.04 \cdot 10^9 \text{ s}^{-1}$  and 483 MHz per  $\mu\text{V}$  of applied voltage respectively.

We note that the associated quantum of energy  $\hbar\omega_J$  is none other than the change in potential energy  $2eV$  of a COOPER pair as it passes from the superconductor of one side of the junction to the other.

*Application of a voltage  $V$  to the terminals of a JOSEPHSON junction produces an alternating current of frequency  $f_J = 2eV/h$ . This is the a.c. JOSEPHSON effect.*

### 10.3.2 - Application: definition of the standard volt

A JOSEPHSON junction therefore functions as a frequency-voltage converter, which is all the more relevant since frequencies are among the physical quantities that we know how to measure with the greatest precision.

This was why, following the international conference on weights and measures (the 18<sup>th</sup> meeting in 1987, resolution 6), the international committee of weights and measures recommended:<sup>4</sup> *that 483 597.9 GHz/V exactly be adopted as a conventional value, denoted by  $K_{J-90}$ , for the JOSEPHSON constant  $K_J = 2e/h$ , ... that this new value be used from this same date (1<sup>st</sup> January 1990) by all laboratories which base their measurements of electromotive force on the JOSEPHSON effect...*

---

<sup>4</sup> <http://www.bipm.org/en/CIPM/db/1988/1/>

## 10.4 - “Current-voltage” characteristics of an SIS JOSEPHSON junction

As the first JOSEPHSON equation is non-linear, it is not equivalent to fix the voltage and follow the current intensity or to inject current across the JOSEPHSON junction and to follow the voltage. Besides, as we shall see later, since the JOSEPHSON junction cannot be reduced to the single “JOSEPHSON channel,” hysteretic effects can occur in a real current-driven JOSEPHSON junction.

### 10.4.1 - Voltage-biased JOSEPHSON junction

Putting aside the technical difficulties that this may involve, biasing a JOSEPHSON with voltage leads first to the two effects we have just seen:

- » d.c. JOSEPHSON effect: at zero voltage, a current  $I$  lying between  $-\mathcal{I}_c$  and  $+\mathcal{I}_c$  that depends on the phase difference between the two bulk superconductors;
- » a.c. JOSEPHSON effect: at non-zero voltage, an alternating current of very high frequency that for a large number of measuring devices averages over time to  $\langle I \rangle = 0$ .

In fact, this description is only accurate at 0 K and only if the voltage  $V$  is less than a voltage  $V_g(0) = 2\Delta(0)/e$  called the “gap voltage.”<sup>5</sup> If these conditions are not satisfied it is necessary to add to the JOSEPHSON channel (the components of current introduced above) two other channels of current transfer:

- » a tunnel current  $I_{P \rightarrow Q}$  resulting from a transfer of quasi-particles (Q) (see section 8.5.3) coming from COOPER pairs (P) which break up at the interface between the superconductors if  $V > V_g(T)$ . This current appears for any temperature, and in particular at 0 K. With increasing voltage, its intensity very quickly approaches the value expected for the tunneling current when the electrodes are in their normal state ( $I = V/\mathcal{R}_n$ );

We note that at 0 K the critical current  $\mathcal{I}_c(0)$ , which was determined by AMBEGAOKAR and BARATOFF for an SIS junction (relation 10.17) to be equal to  $[\pi/4] [V_g(0)/\mathcal{R}_n]$ , is therefore very close to the normal current (above  $T_c$ ) when the applied voltage equals  $V_g(0)$ .

- » a tunnel current  $I_{Q \rightarrow Q}$  that occurs at non-zero temperature because of thermally induced break-up of a proportion of the COOPER pairs into quasiparticles. These quasiparticles then coexist within each superconductor with the remaining pairs and carry a current parallel to that of the pairs.

These two currents can be clearly identified close to 0 K (Fig. 10.4) where the contribution  $I_{Q \rightarrow Q}$  remains weak and grows as  $G_n e^{-\Delta/k_B T}$  while the contribution  $I_{P \rightarrow Q}$  increases abruptly at  $V_g$ .

---

<sup>5</sup> When the two superconductors are different,  $V_g = (\Delta_1 + \Delta_2)/e$ .

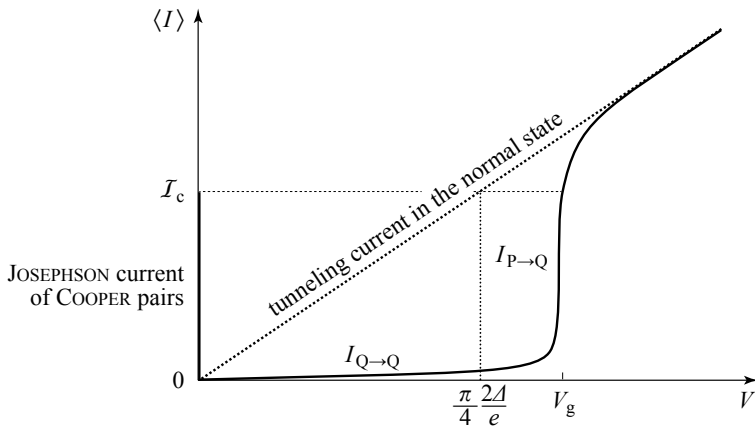


**Figure 10.4 - Characteristics of an SIS junction linked to a voltage generator at low temperatures**

The time-averaged intensity  $\langle I \rangle$  across the junction is the superposition of three components:

- › the d.c. JOSEPHSON effect, that provides an intensity between  $+I_c$  and  $-I_c$  for  $V=0$ ,
- ›  $I_{P \rightarrow Q}$ : the tunneling current of quasiparticles created by the disassociation of COOPER pairs at the junction when the potential exceeds  $V_g = 2\Delta/e$ ,
- ›  $I_{Q \rightarrow Q}$ : the tunnel current of quasiparticles created by the thermal break-up of COOPER pairs inside each superconducting block.

The a.c. JOSEPHSON effect is unobservable because the measuring instrument cannot respond to the very high frequencies.

The distinction between the different contributions becomes, nonetheless, less and less clear as the temperature grows, producing a multiplication of quasiparticles and a decrease of the gap (Fig. 10.5).

*We should be careful to remember that in most observations, such as in Figures 10.4 and 10.5, the alternating components are unobservable and the intensity shown is  $\langle I \rangle$  averaged over time. This is typically how measured results appear in instruments that are unable to resolve the very high frequencies and therefore yield time-averaged values.*

#### 10.4.2 - The RCSJ model

In practice, JOSEPHSON junctions are simultaneously capacitive, since they have two superconducting surfaces opposite each other, and resistive, as the quasiparticles provide a “normal” current superimposed on the JOSEPHSON current. The real junction then appears as a device with, in parallel, a JOSEPHSON channel  $J$  (an idealized JOSEPHSON junction), a capacitor  $C$  and a conductance  $G$ . This is the RCSJ model, an acronym of “*Resistively and Capacitively Shunted Junction*.”

In this model, the value chosen for the conductance  $G$  must be considered carefully, as near 0 K the natural conductance is weak when  $V < V_g$  and it becomes higher, very close to  $1/\mathcal{R}_n$ , for  $V > V_g$  (see Fig. 10.4). It is then most accurate to choose for

the conductance  $G$  a value appropriate to the range of voltages considered. When we approach  $T_c$  the difficulty lessens since the conductance is close to  $1/R_n$ . It is also possible, and sometimes necessary for specific applications, to include an external shunt of high conductance (low resistance) that dominates the natural conductance of the junction.

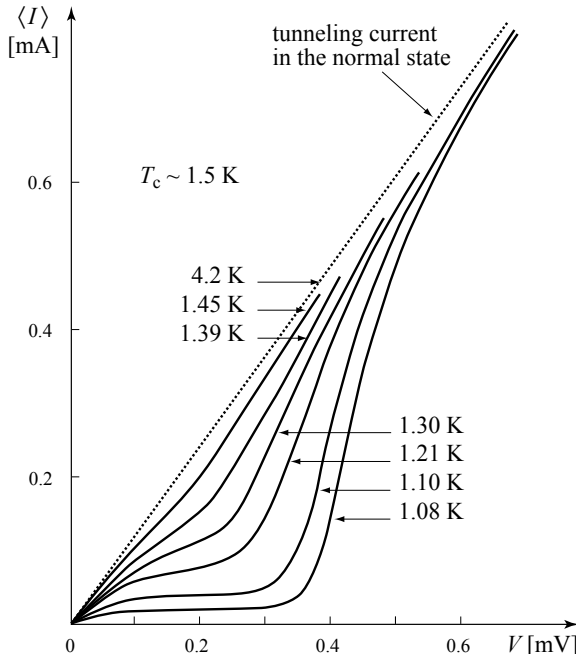


**Figure 10.5 - Tunneling current across an Al/Al<sub>2</sub>O<sub>3</sub>/Al junction as a function of temperature**<sup>6</sup>

When the temperature increases, the density of quasiparticles grows and the gap voltage decreases. The two contributions  $I_{Q \rightarrow Q}$  and  $I_{P \rightarrow Q}$  are no longer independent, and are more and more difficult to identify separately. For any voltage  $V$ , the conductance tends towards that of the junction for the normal state. During these measurements, the transition temperature of the Al/Al<sub>2</sub>O<sub>3</sub>/Al junction has been estimated as  $T_c = 1.5$  K and the gap voltage at zero temperature  $V_g(0) = 0.42$  mV.

#### 10.4.3 - Equations for the current-biased RCSJ system

Let  $I$  be the total current intensity that is fixed by the generator (Fig. 10.6). It can be divided into the superconducting current  $I_J$  carried by the COOPER pairs,  $I_G$  the current across the conductance  $G$ , and  $I_K$  the charge current of the capacitor.

$$I = I_J + I_G + I_K. \quad (10.22)$$

6 I. GIAEVER & K. MEGERLE (1961) *Phys. Rev.* **122**, 1101.

These current intensities are related to the potential and phase differences between the electrodes by the expressions

$$I_J = I_c \sin \Theta(t) ; \quad I_G = GV(t) ; \quad I_K = C \frac{dV(t)}{dt} ; \quad V = \frac{\hbar}{2e} \frac{d\Theta(t)}{dt} \quad (10.23)$$

Substituted into (10.22), they lead to the master equation

$$I(t) = \frac{\hbar C}{2e} \frac{d^2\Theta(t)}{dt^2} + \frac{\hbar G}{2e} \frac{d\Theta(t)}{dt} + I_c \sin \Theta(t) \quad (10.24)$$

which is a non-linear second-order differential equation.

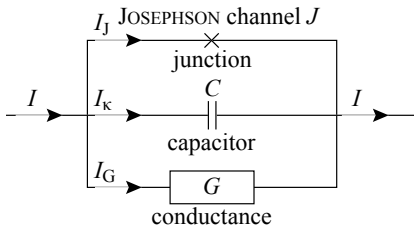


**Figure 10.6**  
**The RCSJ model of the JOSEPHSON junction**  
The JOSEPHSON junction is equivalent to three parallel elements: the JOSEPHSON channel  $J$ , the capacitor  $C$ , and a conductance  $G$ .

#### 10.4.4 - Mechanical analogy to the RCSJ model

Although in the general case, the equation (10.24) has no analytical solution, the behavior of the junction can be understood quite intuitively thanks to an analogy with a rigid pendulum of length  $L$ , mass  $M$  and moment of inertia  $J_{in}$ , immersed in a viscous medium so that with angular velocity  $\omega$ , it experiences a frictional torque  $-\eta\omega$  where  $\eta$  is called the “damping coefficient” (Fig. 10.7).

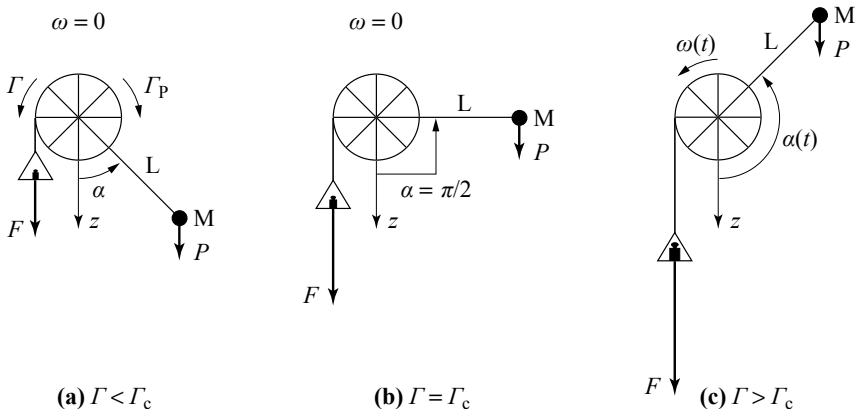


**Figure 10.7 - Mechanical analogy to a JOSEPHSON junction**

The master equation of the RCSJ model is formally identical to the equation of angular motion of a rigid pendulum with the correspondences given in Table 10.1. The pulley and the bar of length  $L$  are rigidly attached.  $\Gamma$  is the torque applied through the force  $F$  and  $\Gamma_p$  is that exerted by the weight of the mass  $M$ . For convenience,  $\Gamma_p$  is taken positive when applied clockwise and then the total torque is  $\Gamma - \Gamma_p$ .

When subject to a torque  $\Gamma(t)$  (for example by a force  $F(t)$  applied to a rope that passes around an attached pulley) the angular position of the pendulum  $\alpha(t)$  obeys

$$\Gamma(t) = J_{\text{in}} \frac{d^2\alpha(t)}{dt^2} + \eta \frac{d\alpha(t)}{dt} + \Gamma_c \sin \alpha(t) \quad (10.25)$$

a relation that with the correspondences written out in detail in Table 10.1, is formally identical to equation (10.24).

**Table 10.1 - Correspondence between the parameters of the JOSEPHSON junction and of the equivalent mechanical system**

Mechanical System	JOSEPHSON junction
Applied Torque $\Gamma(t)$	Imposed Current $I(t)$
Angular coordinate $\alpha(t)$	Phase difference $\Theta(t)$
Angular velocity $\omega(t) = \frac{d\alpha(t)}{dt}$	Time derivative $= \frac{d\Theta(t)}{dt}$ Voltage $V(t) = \frac{\phi_0}{2\pi} \frac{d\Theta(t)}{dt}$
Damping coefficient $\eta$	Reduced conductance $\frac{\hbar G}{2e}$
Moment of inertia $J_{\text{in}} = ML^2$	Reduced capacitance $\frac{\hbar C}{2e}$
Critical torque $\Gamma_c = MgL$	Critical current $I_c$
Pendulum torque exerted by the weight of the mass $M$ as shown in Fig. 10.7 $\Gamma_p(t) = \Gamma_c \sin \alpha(t)$ The total torque is $\Gamma(t) - \Gamma_p(t)$	JOSEPHSON current $I_J(t) = I_c \sin \Theta$
Frequency of small displacements $\Omega = \sqrt{\frac{\Gamma_c}{J_{\text{in}}}} = \sqrt{\frac{g}{L}}$	Plasma frequency $\omega_p = \sqrt{\frac{2eI_c}{\hbar C}}$
Inertial parameter $\mu_c = \frac{J_{\text{in}}}{\eta^2} \Gamma_c$	STEWART-MCCUMBER parameter $\beta_c = \frac{2e}{\hbar} \frac{C}{G^2} I_c$
Quality factor of the pendulum $Q_p = \Omega \frac{J_{\text{in}}}{\eta} = (\mu_c)^{1/2}$	Quality factor $Q = \omega_p \frac{C}{G} = (\beta_c)^{1/2}$
Potential energy $E(\alpha) = \Gamma_c(1 - \cos \alpha)$	Energy of the junction $E(\Theta) = \frac{I_c \phi_0}{2\pi} (1 - \cos \Theta)$

According to Table 10.1, the behavior of the voltage at the leads of the RCSJ circuit connected to a generator injecting a current  $I$ , is similar to the angular velocity of a pendulum of moment of inertia  $J_{\text{in}}$ , immersed in a medium producing by viscosity a damping coefficient  $\eta$ , under applied torque  $\Gamma$ . We note in particular that

the “pendulum torque”  $\Gamma_p = \Gamma_c \sin \alpha(t)$  exerted by the weight of the mass M, as shown in figure 10.7, is equivalent to the intensity of the JOSEPHSON current. With this sign convention  $\Gamma_p$  positive when applied clockwise, the total torque is  $\Gamma(t) - \Gamma_p(t)$ .

In the same way that the pendulum’s movement depends on a reduced damping coefficient  $\mu_c$ , the behavior of the junction depends on a reduced parameter called the “STEWART-MCCUMBER parameter”

$$\beta_c = \frac{2e}{\hbar} \frac{C}{G^2} I_c. \quad (10.26)$$

#### 10.4.5 - Characteristic frequencies

##### *Of oscillation of the free pendulum*

When both  $G$  is very small and  $I$  close to 0, i.e.  $\alpha(t)$  is small ( $\sin x \sim x$ ), the master equation of the pendulum becomes

$$0 = J_{in} \frac{d^2 \alpha(t)}{dt^2} + \Gamma_c \alpha(t) \quad (10.27a)$$

which is the differential equation of the normal mode of oscillation for very weak amplitude at frequency  $\Omega$  where

$$\Omega = \sqrt{\frac{\Gamma_c}{J_{in}}} = \sqrt{\frac{g}{L}}. \quad (10.28a)$$

##### *Of oscillation of the phase difference between the leads of a junction*

Similarly, when  $\eta$  is very weak and  $I$  close to 0, i.e.  $\Theta(t)$  small, the master equation of the junction becomes

$$0 = \frac{\hbar C}{2e} \frac{d^2 \Theta(t)}{dt^2} + I_c \Theta(t) \quad (10.27b)$$

which is exactly the same differential equation as (10.27a), but now for the oscillation of the phase difference between the leads of the JOSEPHSON junction. The characteristic frequency  $\omega_p$  of this oscillation is called the “plasma frequency” of the junction,

$$\omega_p = \sqrt{\frac{2e I_c}{\hbar C}}. \quad (10.28b)$$

#### 10.4.6 - Comparison of the response of the mechanical systems and RCSJ “biased” by a torque $\Gamma$ or an intensity $I$

Let us look at the comparative responses of the each system when we increase progressively the applied torque  $\Gamma$  (for the pendulum) or the injected current  $I$  (for the junction):

**Initial state**

$$\text{Zero torque, } \Gamma = 0 \Leftrightarrow \text{Zero current, } I = 0$$

Mechanical system	JOSEPHSON junction
Zero angle from the vertical $\alpha = 0$	Phase difference $\Theta = 0$
Zero angular velocity $\omega = 0$	Voltage $V = 0$

**JOSEPHSON regime** (Fig. 10.7a)

$$0 < \Gamma < \Gamma_c \Leftrightarrow 0 < I < I_c$$

Mechanical system	JOSEPHSON junction
Fixed angle $0 < \alpha < \pi/2$	Fixed phase difference $0 < \Theta < \pi/2$
Pendulum torque $\Gamma = \Gamma_c \sin \alpha$	Current intensity $I = I_c \sin \Theta$
Zero angular velocity $\omega = 0$	Voltage $V = 0$

**Critical threshold** (Fig. 10.7b)

$$\Gamma = \Gamma_c \Leftrightarrow I = I_c$$

Mechanical system	JOSEPHSON junction
Angle $\alpha = \pi/2$	Phase difference $\Theta = \pi/2$
Critical pendulum torque $\Gamma_c$	Critical current $I_c$
Angular velocity $\omega = 0$	Voltage $V = 0$

**Beyond the critical threshold** (Fig. 10.7c)

$$\Gamma > \Gamma_c \Leftrightarrow I > I_c$$

Mechanical system	JOSEPHSON junction
When $\Gamma > \Gamma_c$ , the pendulum starts to rotate like a sling.	Injecting $I > I_c$ , the phase $\Theta(t)$ increases indefinitely.
After each increment of $\Gamma$ , following a transitory period, the system will reach a stable regime of rotation where on average the damping torque compensates $\Gamma$ .	After each increment of $I$ , following a transitory period, the system will reach a stable regime where on average the current though the conductance reaches $I$ .
The transitional regime (drag) that is seen during the rise as well as the descent of $\Gamma$ leads to phenomena of hysteresis. They are inexistent for $\mu_c = 0$ and become increasingly important when the inertia is large and the damping coefficient is small; in other words when the value of $\mu_c$ is high.	The transitional regime (drag) that is seen during the rise as well as the descent leads to phenomena of hysteresis. They are inexistent for $\beta_c = 0$ and become increasingly important when the capacitance is large and the conductance is small; in other words when the value of $\beta_c$ is high.

**Return to below the critical threshold - Hysteresis**

$$\Gamma \rightarrow [0, \Gamma_c] \Leftrightarrow I \rightarrow [0, I_c]$$

Mechanical system	JOSEPHSON junction
<p>The torque <math>\Gamma</math> is brought back to a value less than <math>\Gamma_c</math>. The pendulum continues its rotation by inertia. The greater the moment of inertia <math>J_{in}</math> and the smaller the coefficient of resistance, the longer this lasts.<sup>7</sup></p> <p>It will stop rotating and rejoin a point of equilibrium for a “retrapping” torque <math>\Gamma_r</math> that decreases for increasing values of <math>\mu_c</math>.</p>	<p>When the current is returned to a value less than <math>I_c</math>, a voltage persists across the junction leads. The larger the capacitance <math>C</math> and the smaller the conductance <math>G</math>, the slower the voltage decreases.</p> <p>The voltage returns to zero for a value of <math>I</math> that equals a “retrapping” current <math>I_r</math> that decreases for increasing values of the parameter <math>\beta_c</math>.</p>

#### 10.4.7 - Over-damped regime

In the limit of  $\mu_c = 0$  ( $\eta$  large,  $J_{in}$  small), equation (10.25) becomes,

$$\omega(t) = \frac{\Gamma - \Gamma_c \sin \alpha(t)}{\eta} \quad (10.29a)$$

with a direct relation between  $\alpha(t)$  and  $\omega(t)$ .

Similarly, in the limit of  $\beta_c = 0$  ( $G$  large,  $C$  small), equation (10.24) becomes,

$$V(t) = \frac{I - I_c \sin \Theta(t)}{G} \quad (10.29b)$$

with a direct relation between  $\Theta(t)$  and  $V(t)$ .

In each case the effects of hysteresis are smeared; we say that the system is over-damped. The behavior of the over-damped JOSEPHSON junction can be understood qualitatively from the pendulum, in particular beyond the JOSEPHSON regime ( $I > I_c$ ;  $\Gamma > \Gamma_c$ ).

Mechanical system	JOSEPHSON junction
<p>From equation (10.29a), the angular velocity <math>\omega</math> is controlled by the difference between the applied torque <math>\Gamma</math> and the torque of the pendulum <math>\Gamma_c \sin \alpha</math>.</p> <p>It varies periodically between a minimum value <math>\omega_{\min} = \frac{\Gamma - \Gamma_c}{\eta}</math> when <math>\alpha = \frac{\pi}{2}</math> (pendulum</p>	<p>From equation (10.29b), the voltage <math>V</math> is controlled by the difference between the injected current <math>I</math> and the JOSEPHSON current <math>I_c \sin \Theta</math>.</p> <p>It varies periodically between a minimum value <math>V_{\min} = \frac{I - I_c}{G}</math> when <math>\Theta = \frac{\pi}{2}</math> and a</p>

<sup>7</sup> In the limit when there is no friction at all, (neither viscous nor solid), movement will continue indefinitely.

winding up)<sup>8</sup> and a maximum value  $\omega_{\max} = \frac{\Gamma + \Gamma_c}{\eta}$  when  $\alpha = \frac{3\pi}{2}$  (pendulum winding down).

It is the sum of a constant component  $\omega_{\text{norm}} = \frac{\Gamma}{\eta}$  and a periodic (but non-sinusoidal)  $\omega_{\text{per}}(t)$  that varies between  $+\frac{\Gamma_c}{\eta}$  and  $-\frac{\Gamma_c}{\eta}$ .

maximum value  $V_{\max} = \frac{I + I_c}{G}$  when  $\Theta = \frac{3\pi}{2}$ .

It is the sum of a constant component  $V_{\text{norm}} = \frac{I}{G}$  and a periodic (but non-sinusoidal)  $V_{\text{per}}(t)$  that varies between  $+\frac{I_c}{G}$  and  $-\frac{I_c}{G}$ .

$V_{\text{norm}}$  is the voltage that would appear at the leads of the device if the junction were normal and characterized only by its conductance  $G$ .

Mechanical system	Pendulum period $\Leftrightarrow$ JOSEPHSON period	JOSEPHSON junction
<p>The pendulum spends more time with a lower angular velocity when it is being wound up, than when it is winding down, with higher angular velocity.</p> <p>The period is the time taken for a change (this is called a “slip”) of the angle <math>\alpha</math> by <math>2\pi</math>.</p> <p><math>T = \frac{2\pi}{\langle \omega \rangle}</math> where <math>\langle \omega \rangle</math> is the time-averaged angular velocity.</p> <p>It can be shown that</p> $\langle \omega \rangle = \frac{1}{\eta} \sqrt{\Gamma^2 - \Gamma_c^2} \quad (10.30a)$ <p>When <math>\Gamma</math> is slightly larger than <math>\Gamma_c</math>, <math>\omega_{\min}</math> is very small compared to <math>\omega_{\max}</math> and the system spends much more time in winding up than in winding down, which makes the curve <math>\omega(t)</math> appear as periodic peaks of height <math>2 \frac{\Gamma_c}{\eta}</math> superimposed on <math>\omega_{\min}</math>.</p>	<p>The system spends more time in the interval <math>0 &lt; \Theta &lt; \pi</math> (where the voltage is weaker) than in the interval <math>\pi &lt; \Theta &lt; 2\pi</math> (where the voltage is stronger).</p> <p>The period is the time taken for a “slip” in the phase difference <math>\Theta</math> by <math>2\pi</math>.</p> <p><math>T_J = \frac{h}{2e\langle V \rangle}</math> is the JOSEPHSON period corresponding to the time-averaged voltage <math>\langle V \rangle</math>.</p> <p>We will show that</p> $\langle V \rangle = \frac{1}{G} \sqrt{I^2 - I_c^2} \quad (10.30b)$ <p>(see the derivation in App. 10B)</p> <p>When <math>I</math> is slightly more than <math>I_c</math> the system spends much longer between <math>0 &lt; \Theta &lt; \pi</math> than between <math>\pi &lt; \Theta &lt; 2\pi</math>, which makes the curve <math>V(t)</math> appear as periodic peaks of height <math>2 \frac{I_c}{G}</math> superimposed on <math>V_{\min}</math>.</p>	

8 Note that all the indicated angles are defined modulo  $2\pi$ , which is not explicitly mentioned in order to simplify the text.

Pendulum torque	$\Leftrightarrow$	JOSEPHSON current
Mechanical system		JOSEPHSON junction
<p>The pendulum torque <math>\Gamma_p(t)</math> varies periodically between <math>\pm \Gamma_c</math>. It is positive (clockwise according to the convention of fig. 10.7) in winding up, where the pendulum spends more time, than in winding down.</p> <p>Its time variation is a periodic series of inverted peaks. Its average value <math>\langle \Gamma_p \rangle</math> is positive.</p> <p>When <math>\Gamma</math> becomes much greater than <math>\Gamma_c</math>, the motion approaches a uniform rotation. The period shortens and the relative difference between <math>\omega_{\min}</math> and <math>\omega_{\max}</math> is reduced (although <math>(\omega_{\max} - \omega_{\min})</math> stays the same) and becomes sinusoidal. The average angular velocity tends to</p> $\langle \omega \rangle = \Gamma / \eta$		<p>The JOSEPHSON current <math>I_J(t)</math> varies periodically between <math>\pm I_c</math>. It is positive for <math>0 &lt; \Theta &lt; \pi</math>, where the system spends more time, and negative when <math>\pi &lt; \Theta &lt; 2\pi</math>.</p> <p>Its time variation is a periodic series of inverted peaks. Its average value <math>\langle I_J \rangle</math> is positive.</p> <p>When <math>I</math> becomes much greater than <math>I_c</math>, the relative difference between <math>V_{\min}</math> and <math>V_{\max}</math> is reduced (although <math>(V_{\max} - V_{\min})</math> stays the same). The period shortens and the periodic component of the voltage tends to sinusoidal. The average voltage tends to</p> $\langle V \rangle = I / G$

#### 10.4.8 - Graphical representations<sup>9</sup>

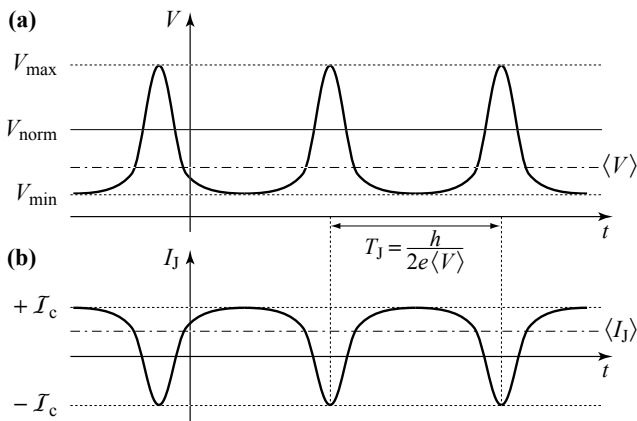
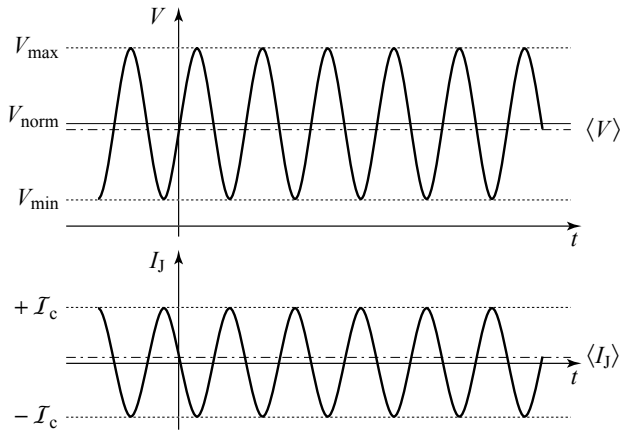


Figure 10.8 - JOSEPHSON current and voltage at the leads of the over-damped RCSJ circuit ( $\beta_c = 0$ ) biased by a current  $I > I_c$

**(a)** The voltage varies periodically. It appears in the form of peaks that are more and more marked as the intensity approaches  $I_c$  (from above).  $V_{\text{norm}}$  is the voltage that would appear at the leads of the device if the junction were normal. **(b)** The JOSEPHSON current shows inverted peaks and varies with the same period between the values  $+I_c$  and  $-I_c$ . Its average value  $\langle I_J \rangle$  is always positive.

9 K.K. LIKHAREV (1986) *Dynamics of Josephson Junctions and Circuits*, Gordon and Breach, Philadelphia, Chap. 4.



**Figure 10.9 - JOSEPHSON current and voltage at the leads of the over-damped RCSJ circuit ( $\beta_c = 0$ ) driven by a current  $I \gg I_c$**

The curves of Figure 10.8 have the asymptotic form of a sine wave with increasing frequency. The time-averaged value  $\langle I_J \rangle$  of the JOSEPHSON current tends to 0.

As well as the time variations shown in Figures 10.8 and 10.9, it is instructive to consider the dependence of the mean values of intensities  $I_J$  and  $I_G$  and of the potential  $V$  on the intensity  $I$  of the injected current (Fig. 10.10):

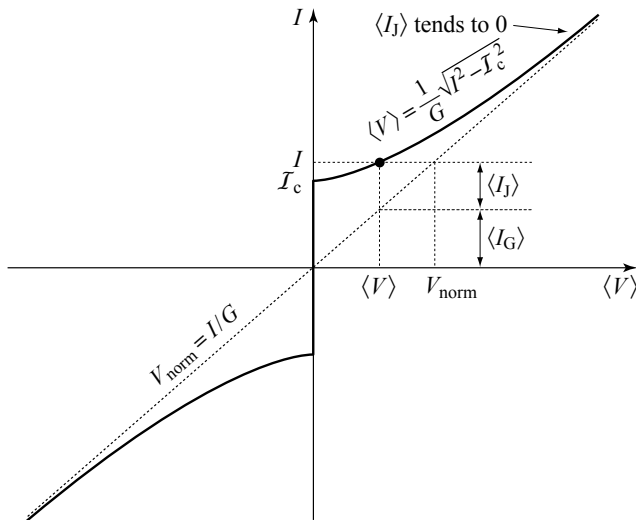


**Figure 10.10 - Current-voltage characteristics of the current-biased RCSJ circuit in the over-damped regime ( $\beta_c = 0$ )**

$\langle V \rangle$  is the time-averaged value of the voltage at the leads of the superconducting junction with injected current  $I$ .  $V_{\text{norm}}$  is the voltage at the junction leads in the normal state with the same current,  $\langle I_J \rangle$  the time-averaged JOSEPHSON intensity and  $\langle I_G \rangle$  the time-averaged current intensity across the conductance  $G$ .

- » for  $I \gg I_c$ , the JOSEPHSON current becomes quasi-sinusoidal, with an average value  $\langle I_J \rangle$  which tends to zero.  $\langle V \rangle$  rejoins asymptotically the voltage  $V_{\text{norm}}$  that it would have with the conductance  $G$  alone;
- » when  $I$  approaches  $I_c$ , the shift between  $\langle I_J \rangle$  and  $I$  diminishes. The period becomes large and the JOSEPHSON current spends an increasing part of its time near  $+I_c$ . Simultaneously, the voltage spends increasingly long times close to  $V_{\text{min}}$ . The average voltage  $\langle V \rangle$  develops as a function of the intensity according to the relation (10.30b) derived in Appendix 10B;
- » when  $I = I_c$ , the period diverges. The intensity spends an infinite time at  $+I_c$  and the voltage stays indefinitely at  $V_{\text{min}}$ , that goes to zero. The d.c. JOSEPHSON effect is recovered.

#### 10.4.9 - Weak and intermediate damping

When the system is no longer over-damped ( $\beta_c \neq 0$ ), only numerical solution of the equation (10.24) provides the variation of average voltage at the leads of the junction as a function of the current intensity (Fig. 10.11). The analogy with the pendulum allows us, nonetheless, to have a feeling for the behavior of the junction, at least in the limit when  $\beta_c$  is large.

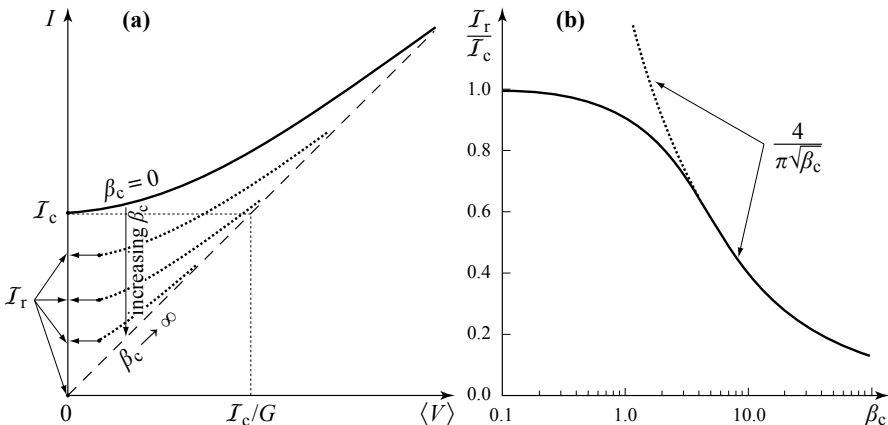


**Figure 10.11 - Voltage of return and re-trapping current in an under-damped JOSEPHSON junction**

(a) During the decrease of the biasing current the average voltage decreases, following curves that depend on the STEWART-MCCUMBER parameter  $\beta_c$ . The voltage reaches zero for an intensity  $I_r$  called the re-trapping current. (b) Relative value of the re-trapping current as a function of the parameter  $\beta_c$ . The continuous line corresponds to the exact calculation. The dotted line is the result of the calculation made in section 10.4.9, valid when  $\beta_c$  is sufficiently large.

Starting with zero applied torque and as long as  $\Gamma$  is less than  $\Gamma_c$ , the pendulum adopts an equilibrium position independent of  $\beta_c$  maintaining  $\omega = 0$ . When  $\Gamma$  becomes larger than  $\Gamma_c$  it moves like a sling and accelerates until the average frictional torque becomes equal to  $\Gamma$ .

When the torque decreases, the pendulum carried by its momentum, continues to swing, even when  $\Gamma$  becomes smaller than  $\Gamma_c$ . It stops rotating only when  $\Gamma$  attains a value  $\Gamma_r < \Gamma_c$  such that over one period the work of the torque  $\Gamma_r$  equals the work of the frictional torque  $\eta(d\alpha/dt) = \eta\omega$ . This limiting value  $\Gamma_r$  is such that the pendulum passes the vertical position with vanishing angular velocity. Between two passages by this position, the work of the torque  $\Gamma_r$  is  $2\pi\Gamma_r$  and that of the frictional torque is  $\int_0^{2\pi} \eta\omega d\alpha$ . Since in this particular case the sum of the kinetic and potential energies is  $MgL = \Gamma_c$  we have

$$\frac{1}{2}J_{in}\omega^2 = \Gamma_c(1 - \cos\alpha) \quad i.e. \quad \omega = \sqrt{\frac{2\Gamma_c}{J_{in}}}\sqrt{1 - \cos\alpha}. \quad (10.31)$$

Equating the work by torque  $\Gamma_r$  to the frictional torque over one period, leads us to

$$2\pi\Gamma_r = \eta\sqrt{\frac{2\Gamma_c}{J_{in}}}\int_0^{2\pi} \sqrt{1 - \cos\alpha} d\alpha = 8\eta\sqrt{\frac{\Gamma_c}{J_{in}}} \quad (10.32a)$$

or, using the definition of the quality factor of the pendulum  $Q_p$  (Table 10.1),

$$\Gamma_r = \frac{4}{\pi Q_p} \Gamma_c. \quad (10.32b)$$

By direct transposition, the d.c. JOSEPHSON current or “re-trapping current” that the junction takes at zero voltage during the decrease of injected current can be written

$$I_r = \frac{4}{\pi Q} I_c \quad \text{or} \quad \frac{I_r}{I_c} = \frac{4}{\pi} \beta_c^{-\frac{1}{2}}. \quad (10.33)$$

#### 10.4.10 - Some examples of SIS junctions

Figure 10.12 presents schematically a typical JOSEPHSON junction used as a voltage standard.<sup>10</sup>

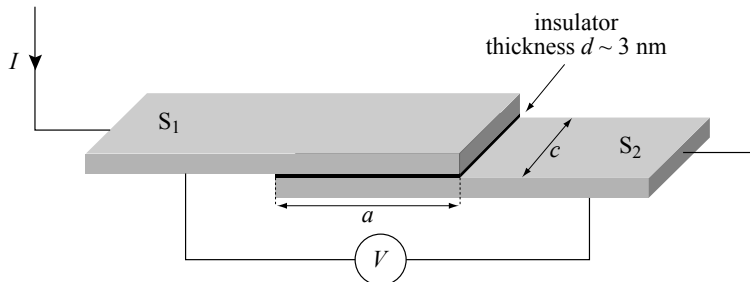


**Figure 10.12 - Schematic image of a typical SIS junction**

It is formed by two superconducting films of width  $c$ , that are superimposed for a length  $a$  over which they are separated by an insulator of thickness  $d \sim 3$  nm.

A few examples of the orders of magnitude involved, taken for the most typical junctions:

» Nb/Al<sub>2</sub>O<sub>3</sub>/Nb<sup>10</sup> (niobium gap:  $\Delta = 1.5$  meV)  $c = 30 \mu\text{m}$  and  $a = 18 \mu\text{m}$

This junction displays a critical intensity  $I_c \approx 110 \mu\text{A}$ , or a critical current density  $j_c = I_c/ca \approx 20 \text{ A cm}^{-2}$  and a resistance  $R_n$  of order  $20 \Omega$ ;

» Al/Al<sub>2</sub>O<sub>3</sub>/Al<sup>11</sup> (aluminum gap:  $\Delta = 0.175$  meV)  $d \sim 2 \text{ nm}$

For a cross-section  $\approx 2 \mu\text{m}^2$ ,  $R_n \approx 100 \Omega$  and  $I_c \approx 2 \mu\text{A}$ .

For a cross-section  $\approx 0.02 \mu\text{m}^2$ ,  $R_n \approx 10 \text{ k}\Omega$  and  $I_c \approx 20 \text{ nA}$ .

So for this type of junction a critical current density  $j_c \approx 200 \text{ A cm}^{-2}$ ;

» Nb/AlO<sub>x</sub>/Nb

These junctions can attain critical current densities of the order of  $j_c \approx 1$  to  $10 \text{ kA cm}^{-2}$  for cross-sections of a few  $\mu\text{m}^2$ .

SIS junctions are commonly fabricated by deposition of thin films with critical current densities  $j_c$  that range from  $10 \text{ A cm}^{-2}$  to  $10 \text{ kA cm}^{-2}$ . The usual required critical current densities are typically<sup>12</sup>  $j_c \approx 1 \text{ kA cm}^{-2}$  for applications in electronics,  $j_c \approx 100 \text{ A cm}^{-2}$  for SQUIDs (see Chap. 11) and  $j_c \approx 10 \text{ A cm}^{-2}$  for devices in metrology.

## 10.5 - Energy stocked in a JOSEPHSON junction (SIS)

Using the relations (10.14) and (10.18), the work  $W$  that a generator connected to the leads of a JOSEPHSON junction must provide so that the junction can pass a current  $I = I_c \sin \Theta$  after a time  $\Delta t$ , starting from zero intensity, is

$$W = \int_0^{\Delta t} V(t)I(t) dt = \frac{I_c \hbar}{2e} \int_0^\Theta \sin \Theta' d\Theta' = \frac{I_c \hbar}{2e} (1 - \cos \Theta). \quad (10.34)$$

By definition, this work represents the potential energy  $E(\Theta)$  stored in the junction. From the expression for the quantum of flux  $\phi_0$

$$E(\Theta) = E_J(1 - \cos \Theta) \quad (10.35)$$

where  $E_J$ , called the “JOSEPHSON energy”, is defined as

$$E_J = \frac{I_c \phi_0}{2\pi}. \quad (10.36)$$

This expression inspires several remarks:

» the lowest energy state of the JOSEPHSON junction is that for which the phase difference  $\Theta$  between its leads is zero ( $\Theta = 0, I = 0$ );

---

<sup>11</sup> H. COURTOIS, personal communication.

<sup>12</sup> S. ANDERS *et al.* (2010) European roadmap on superconductive electronics. Status and Perspectives, *Physica C* **470**, 2079.

- » as the same current injected into the junction can, according to (10.14), give rise just as well to the phase difference  $\Theta = \theta_1 - \theta_2$  as to the difference  $\Theta = \pi - (\theta_1 - \theta_2)$  [each being defined modulo  $2\pi$ ], the phase difference taken will be whichever one minimizes the potential energy, *i.e.*, according to (10.35), that which lies between  $-\pi/2$  and  $+\pi/2$ ;
- » as the potential energy minima for  $\Theta = 2n\pi$  are separated by barriers of height  $E_J$ , the junction will be severely perturbed by any energy fluctuation of this order of magnitude. Therefore to function correctly at a temperature  $T$ , the junction should have a current  $I_c$  such that  $E_J \gg k_B T$ ; in reality that means a current more intense than  $0.04 \mu\text{A K}^{-1}$ . In certain JOSEPHSON diode arrays of high- $T_c$  superconductors that function at relatively high temperatures, this criterion makes it necessary to have available large currents  $I_c$ .

## 10.6 - JOSEPHSON junction subject to an electromagnetic wave

### 10.6.1 - Resonance effects

We come back to an elementary junction reduced to the JOSEPHSON channel and superimpose on the constant potential  $V$  applied between the two superconductor blocks a small alternating component  $v \cos(\omega_0 t + \varphi)$  carried, for example, by high-frequency electromagnetic wave.

Following (10.18), the equation for the evolution of the phase difference between the two superconductors becomes

$$\frac{d\Theta}{dt} = \frac{2e}{\hbar} V + \frac{2e}{\hbar} v \cos(\omega_0 t + \varphi) \quad (10.37)$$

or, after integration over time

$$\Theta(t) = \frac{2e}{\hbar} V t + \frac{2e}{\hbar \omega_0} v \sin(\omega_0 t + \varphi) + \Theta(0). \quad (10.38)$$

The current intensity through the junction  $I = I_c \sin \Theta$  becomes after applying the formula of SCHLÖMILCH<sup>13</sup>

$$I = I_c \sum_{n=0}^{n=\infty} (-1)^n J_n \left( \frac{2e}{\hbar \omega_0} v \right) \sin \left[ \left( \frac{2e}{\hbar} V \pm n \omega_0 \right) t + \delta_n \right] \quad (10.39)$$

where  $J_n$  is the integer BESSEL function of order  $n$ . Note that the  $\pm$  written in the arguments of the sine function indicate that there are in fact two terms for each non-zero value of  $n$  in the summation (see below, Eq. (10.100) and (10.101), for more explicit forms).

This expression makes it apparent that, for an applied voltage  $V$ , the current intensity is a superposition of sinusoidal components of high frequencies unless

---

<sup>13</sup> See Appendix 10C at the end of this chapter.

$\frac{2e}{\hbar}V \pm n\omega_0 = 0$ , i.e. unless the voltage  $V$  takes one of the values  $V_n$  where

$$V_n = n\frac{\hbar\omega_0}{2e} \quad (n \text{ integer}). \quad (10.40)$$

When this condition is satisfied, the frequency of the component  $n$  vanishes, which means that it carries a constant current that is superimposed on the alternating currents coming from the other components which, because of their high frequencies, are smeared out and averaged to zero in most measurements. As the phase  $\delta_n$  is adjustable, the intensity of this d.c. component can be written

$$I_n = I_c \mathcal{J}_n \left( \frac{2e}{\hbar\omega_0} v \right) \sin \delta_n \quad (10.41)$$

that can take any value lying between

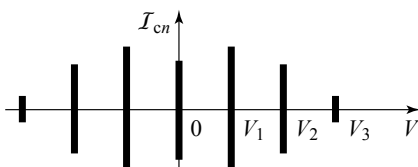
$$-I_{cn} = -I_c \mathcal{J}_n \left( \frac{2e}{\hbar\omega_0} v \right) \quad \text{and} \quad +I_{cn} = I_c \mathcal{J}_n \left( \frac{2e}{\hbar\omega_0} v \right). \quad (10.42)$$

This is, then, an extension of the continuous JOSEPHSON current that is no longer seen only at voltage zero, but for a series of characteristic voltages  $V_n$ , each with its own critical intensity  $I_{cn}$ .

The “ordinary” JOSEPHSON current tension, at  $V = 0$  and  $v = 0$ , appears as the special case  $n = 0$ . As  $\mathcal{J}_0(0)$  equals 1, we obviously recover  $I_{c0} = I_c$ .

### 10.6.2 - SHAPIRO steps

The continuous components can be demonstrated as well in the under-damped regime (Fig. 10.13) as in the over-damped regime. In that latter case, a sequence of increments called “SHAPIRO steps” appear within a current/voltage curve similar to that of Figure 10.10.



Under the effect of a component of alternating voltage of amplitude  $v$  that is superimposed on the voltage  $V$ , JOSEPHSON currents appear at voltages  $V_n = n\hbar\omega_0/2e$  with amplitudes given by the relation (10.42).

Figure 10.13 - JOSEPHSON currents and SHAPIRO components in the under-damped regime

Quantitative confirmation of the results of the preceding calculation was provided by GRIMES and SHAPIRO<sup>14</sup> in an experiment that allowed them to measure the amplitudes of the steps and to compare them with those of the critical currents  $I_{cn}$  predicted by the relation (10.41). To do this, they placed a JOSEPHSON junction in a

14 CC. GRIMES & S. SHAPIRO (1968) *Phys. Rev.* **169**, 397.

waveguide oscillating at a frequency of 72 GHz and follow the behavior of the average voltage at the leads as a function of the injected intensity for different rates of attenuation of the wave (Fig. 10.14a). At maximum attenuation, *i.e.* without any high frequency component ( $v = 0$ ), they recover, as expected, a figure like Figure 10.10. This fits into the general case, since the values of the BESSEL function at the origin  $\mathcal{J}_0(0) = 1$  and  $\mathcal{J}_{n \geq 1}(0) = 0$ , meaning that the limiting JOSEPHSON currents are  $I_{c0} = I_c$  and  $I_{cn \geq 1}(0) = 0$ . With decreasing attenuation and consequently increasing  $v$ , “SHAPIRO steps” appear at voltages  $V_n$  independent of the amplitude  $v$  and in exact agreement with the values predicted by the relation (10.40). Looking at the heights of the steps (Fig. 10.14a) it is apparent that:

- »  $I_{c0}$ , which has its maximum at  $v = 0$ , decreases to 0 at around –34 db, then grows to a maximum close to –31 db and vanishes again towards –28 db;
- »  $I_{c1}$ , which vanishes for maximum attenuation ( $v = 0$ ), has a maximum near –37 db, returns to 0 close to –29 db after which it increases again;
- »  $I_{c2}$ , which vanishes for maximum attenuation has a maximum at –34 db and then vanishes again near –29 db.

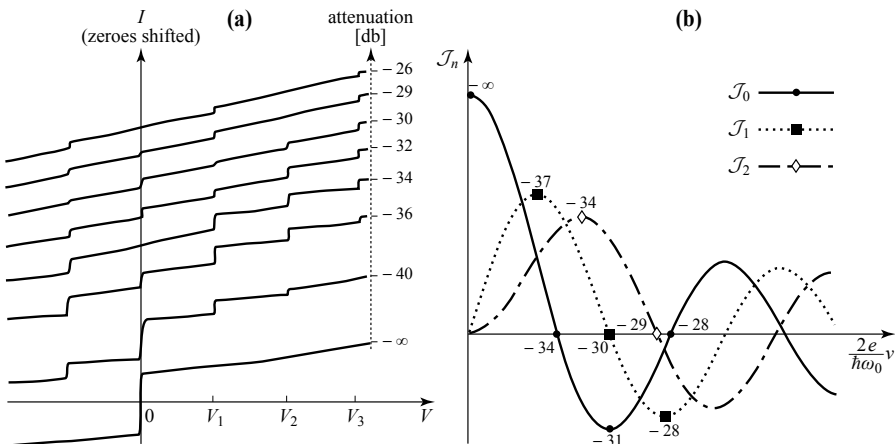


**Figure 10.14 - SHAPIRO steps measured on a point contact Nb-Nb JOSEPHSON junction in the over-damped regime**

**(a)** Voltage-current curves obtained at 4.2 K on a junction exposed to an electromagnetic wave of frequency 72 GHz for different degrees of attenuation. The curves have been shifted vertically for clarity. [Curves adapted from Reference 14]

**(b)** BESSEL functions  $\mathcal{J}_0$ ,  $\mathcal{J}_1$  and  $\mathcal{J}_2$  for which we note the attenuations corresponding to maxima and minima of the steps situated at  $V_0$ ,  $V_1$ ,  $V_2$  of part (a) of the figure.

On Figure 10.14b showing the dependence of the first three BESSEL functions as a function of  $v$ , we have marked the rates of attenuation where the  $\mathcal{J}_n\left(\frac{2e}{\hbar\omega_0}v\right)$  are extremal or vanishing. Examination of the figure shows that the changes in the  $I_{cn}$

are in agreement, at least qualitatively, with the relation (10.41). A more detailed analysis of the step heights is presented in the article of GRIMES and SHAPIRO.

## 10.7 - SNS junctions

The mechanisms by which currents pass with the direct or indirect transfer of COOPER pairs from one superconducting electrode to the other across a normal metal or a constriction constitute a problem that has been, and continues to be, the object of numerous studies.<sup>15</sup> There are many parameters: the length and width of the junction, the mean free path of electrons in the normal metal, the coherence length in each of the superconductors...

After presenting two models among the many that have been imagined to evaluate the JOSEPHSON current, a few other types of junction will be examined. The general characteristics and the signature of the JOSEPHSON effect will be pointed out from these examples.

### 10.7.1 - Proximity effect, the ASLAMAZOV-LARKIN model

In the first model, that was proposed by DE GENNES,<sup>16</sup> it was assumed that, by a proximity effect, the COOPER pairs diffuse into the normal metal over a distance of order of  $\xi_N \approx \frac{\hbar v_F}{kT_c}$  that can reach 10 to 1000 nm. When the thickness of the layer

separating the superconductors is less than this distance (see Fig. 10.1), there is continuity of the superconductivity across the normal layer between  $S_1$  and  $S_2$  each characterized by its own wave function  $\phi_1 = \sqrt{n_1} e^{i\theta_1}$  and  $\phi_2 = \sqrt{n_2} e^{i\theta_2}$ . The ASLAMAZOV-LARKIN model<sup>17</sup> relying on arguments founded on GINZBURG-LANDAU theory, leads us to express the wave function in the normal layer N in the form,

$$\phi(x) = F(x) \sqrt{n_1} e^{i\theta_1} + [1 - F(x)] \sqrt{n_2} e^{i\theta_2} \quad (10.43)$$

where  $F(x)$  is a weighting function between  $\phi_1$  and  $\phi_2$  taking values 1 and 0 at the interfaces  $S_1/N$  and  $N/S_2$  respectively. The current density can be deduced from the relation (9.6), that in the absence of a magnetic field ( $\mathbf{A} = \mathbf{0}$ ) and in one dimension becomes

$$j = -\frac{\hbar q_p}{m_p} \text{Im} \left( \phi^* \frac{\partial \phi}{\partial x} \right) \quad (10.44)$$

15 K.K. LIKHAREV (1979) *Reviews of Modern Physics* **51**, 101;  
A.A. GOBULOV, M. Yu. KUPIRIYANOV & E. LL'ICHEV (1964)  
*Reviews of Modern Physics* **76**, 411.

16 P.G. DE GENNES (1964) *Superconductivity of Metal and Alloys*,  
Benjamin, New York, 234.

17 L.G. ASLAMAZOV & A.I. LARKIN (1969) *Zh. Eksp. Teor. Fiz. Pis'Red.* **9**, 150;  
(1969) *JETP Lett.* **9**, 87.

or, using the expression for  $\phi$  in (10.43),

$$j = \frac{\hbar}{\mu_0 \lambda_L q_p} \sin(\theta_1 - \theta_2) \quad (10.45)$$

which is precisely the first JOSEPHSON equation.

In this model, when  $T$  is close to  $T_c$ , we obtain

$$I_c R_n = \frac{\pi}{4} \frac{\Delta^2}{ek_B T} \quad (10.46)$$

which is the limit for  $\Delta \rightarrow 0$  of the relation (10.16) relating the superconducting current to the gap in the model of AMBEGAOKAR and BARATOFF<sup>18</sup> (see section 10.2.2).

As this model recovers the JOSEPHSON equation and the results of AMBEGAOKAR and BARATOFF we might think that the mechanism is general. The following section shows that this is *not* the case.

### 10.7.2 - JOSEPHSON current via the ANDREEV levels

#### Quasiparticles

When the layer separating the two superconducting electrodes itself contains charge carriers (*i.e.* is a normal metal) we can imagine a quite different mechanism of transferring COOPER pairs involving quasiparticles. To introduce this mechanism, we first re-examine what the quasiparticles are in each material:

» **In the normal metal:** as we discussed in section 8.5.3, the quasiparticles of the normal metal are of electron or hole character. In the immediate neighborhood of the FERMI level the quasiparticles that are “symmetric” with respect to the FERMI level  $k_> - k_F = k_F - k_<$  ( $k_> > k_F$  and  $k_< < k_F$ ) have the same energy in the expansion of the relation 8.84a

$$E_{\mathbf{k}}^n = \frac{\hbar v_F}{2} (k_> - k_<). \quad (10.47)$$

As the normal metal possesses a continuum of energy levels and there is no gap,  $E_{\mathbf{k}}^n$  can be arbitrarily small.

» **In the superconducting state:** the quasiparticles of the superconductors are electron- or hole-like and appear as electrons with probability  $u_{\mathbf{k}}^2$  and as holes with probability  $v_{\mathbf{k}}^2$  (see section 8.5.3). In contrast to the normal metal, their minimum energy is that of the gap, which means that the superconductor has no quasiparticle energies less than  $\Delta$ .

---

<sup>18</sup> The ASLAMAZOV-LARKIN model was actually constructed by supposing a transition between the gaps  $\Delta(x) = F(x)\Delta e^{i\theta_1} + [1 - F(x)]\Delta e^{i\theta_2}$  and in applying a relation for the current density with a form analogous to (9.6), where  $\phi$  is replaced by  $\Delta$ . It can be shown that these two procedures are equivalent.

### ANDREEV-SAINT JAMES reflections

We consider, in the normal metal layer, an electron (quasiparticle) of wave vector  $k_>$  and of energy  $E_{\mathbf{k}}^n$  less than the gap  $\Delta$  of the neighboring bulk superconductors, that moves towards  $S_2$ . When it has arrived at the  $N/S_2$  interface, it cannot find available states in the superconductor to occupy since the quasiparticle states all have energies greater than  $\Delta$ .

If it were an ordinary potential barrier, the electron would be simply reflected but, as the barrier is a superconductor, it is partly reflected as an electron and partly as a hole. With non-zero probability it is reflected in the form of hole quasiparticle, of wave vector  $k_< < k_F$  and of the same energy, that moves towards the  $N/S_1$ . By charge conservation this reflection is accompanied by the creation of a COOPER pair in  $S_2$ . This is what is called an “ANDREEV-SAINT JAMES reflection” (Fig. 10.15a).<sup>19</sup>

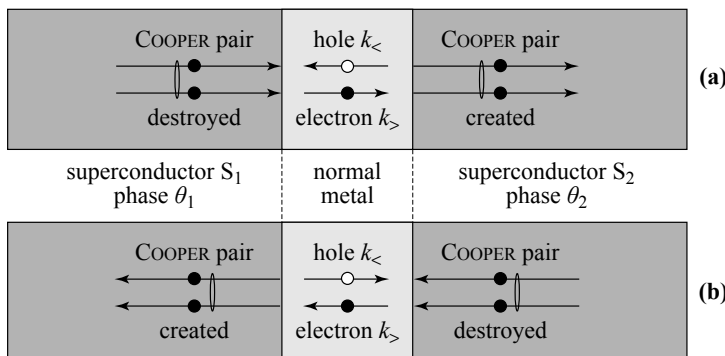


Figure 10.15 - ANDREEV reflections in an SNS junction

The reflection of an electron in the form of a hole at the  $N/S$  interface is accompanied by the creation of a COOPER pair in the superconductor, while the reflection of a hole in the form of an electron is accompanied by the destruction of a COOPER pair. It follows that there is a net transfer of COOPER pairs between the superconducting electrodes that can be from  $S_1$  to  $S_2$  (a) or from  $S_2$  to  $S_1$  (b) according the direction of movement of the electrons and holes in the normal region.

When this hole arrives at the  $N/S_1$  interface, by the same reasoning that its energy is less than the gap in  $S_1$ , there is a non-zero probability for it to be reflected in the form of an electron of wave vector  $k_>$  which returns towards the  $N/S_2$  interface. Charge conservation is maintained by the annihilation of a COOPER pair in  $S_1$ . In this way the net result of a roundtrip in N of a quasiparticle, which is an electron in the direction  $S_1 \rightarrow S_2$  then a hole in the direction  $S_2 \rightarrow S_1$ , is a transfer of a COOPER pair from  $S_1$  to  $S_2$  (Fig. 10.15a). In the inverse process, a round trip in N of a quasiparticle which is an electron in the direction  $S_2 \rightarrow S_1$ , then a hole in the

19 A.F. ANDREEV (1964), *Zh. Eksp. Teor. Fiz.* **46**, 1823 [(1964) Sov. Phys. JETP **19**, 1228]; D. SAINT JAMES (1964), *Le Journal de Physique* **25**, 899.

direction  $S_1 \rightarrow S_2$ , translates into the transfer of a COOPER pair from  $S_2$  to  $S_1$  (Fig. 10.15b).

### ANDREEV levels

In such a device the normal layer also behaves like a resonant cavity of length  $d_N$  in which a wave of wave vector  $k_>$  (associated with an electron) reflects into a wave of wave vector  $-k_<$  (associated with a hole, giving the sign change of the wave vector) which is once again reflected into a wave (an electron) of wave vector  $k_>\dots$ . The dephasing accumulated during this round trip is  $d_N[k_> + (-k_<)]$ . To this dephasing we must add two others:

» the first is produced at any reflection, irrespective of the nature of the incident particle. For a reflection it equals

$$\eta_k = \cos^{-1}\left(\frac{E_k^n}{\Delta}\right); \quad (10.48)$$

» the second is special to the reflection at an N/S interface: reflection of an electron in the form of a hole, at the interface with a superconductor of condensate phase  $\theta$ , is accompanied by a dephasing of  $-\theta$  while reflection of a hole in the form of an electron, at the interface of a superconductor of condensate phase  $\theta$ , is accompanied by a dephasing of  $+\theta$ .

These constant motions back and forth, that lead to transfers of COOPER pairs between  $S_1$  and  $S_2$ , will only be effective if there is constructive interference in the normal layer, *i.e.* if one round trip gives a net dephasing of  $2\ell\pi$ , which will only happen for special pairs of wave vectors ( $k_>$ ,  $k_<$ ) and thus special energy levels that are called the ANDREEV levels.

The levels  $\ell$  that provide the transfer of COOPER pairs from  $S_1$  to  $S_2$  (Fig. 10.15a) satisfy the phase relation:

$$Dephasing \quad (k_> - k_<) d_N - 2\eta_\ell - \theta_2 + \theta_1 = 2\ell\pi \quad (10.49a)$$

$$Origin of the dephasing \quad 1 \quad 2 \quad 3 \quad 4 \quad 5$$

1: path taken, 2: ordinary reflection, 3: electron-hole reflection at the N/ $S_2$  interface, 4: hole-electron reflection at the N/ $S_1$  interface, 5: interference condition.

According to the relation (10.47), their energies are

$$E_\ell^+ = \frac{\hbar v_F}{2d_N} (2\ell\pi + 2\eta_\ell - \Theta). \quad (10.49b)$$

Those that lead to a transfer of COOPER pairs from  $S_2$  towards  $S_1$  (Fig. 10.15b), differ from the previous by reversal of the direction of movement of the holes and electrons, and by the nature of the reflections on each of the superconductors. They satisfy the phase relation:

$$Dephasing \quad (k_> - k_<) d_N - 2\eta_\ell - \theta_1 + \theta_2 = 2\ell\pi \quad (10.50a)$$

$$Origin of the dephasing \quad 1 \quad 2 \quad 3 \quad 4 \quad 5$$

This gives ANDREEV levels at energies

$$E_\ell^- = \frac{\hbar v_F}{2d_N} (2\ell\pi + 2\eta_\ell + \Theta). \quad (10.50b)$$

Thus the levels providing the transfer of COOPER pairs from S<sub>1</sub> to S<sub>2</sub> are separated in energy from those providing transfer from S<sub>2</sub> to S<sub>1</sub>.

### JOSEPHSON current

The current intensity transported by each level then depends on its occupation probability, given by the FERMI function, that in turn depends on the temperature. The JOSEPHSON current will be the sum of the currents (with appropriate signs) carried by each level:

- » if  $\Theta = 0$ , the levels  $E_\ell^+$  and  $E_\ell^-$  are degenerate and equally occupied; there is a cancellation of the transfer of COOPER pairs from S<sub>1</sub> to S<sub>2</sub> and from S<sub>2</sub> to S<sub>1</sub>. No net current crosses the junction;
- » if  $0 < \Theta < \pi$ , the degeneracy is lifted and  $E_\ell^+ < E_\ell^-$ ; the levels  $E_\ell^+$  are systematically more occupied than the levels  $E_\ell^-$  and a net current flows from S<sub>1</sub> to S<sub>2</sub>;
- » if  $-\pi < \Theta < 0$ ,  $E_\ell^- < E_\ell^+$ ; the rates of occupation are reversed and the JOSEPHSON current flows in the opposite direction, *i.e.* from S<sub>2</sub> to S<sub>1</sub>.

A full expression for the JOSEPHSON current requires calculations such as those of GUNSENHEIMER *et al.*,<sup>20</sup> who found the curves of Figure 10.16. There we see that  $I(\Theta)$  oscillates around zero (with period  $2\pi$ ) but is not sinusoidal, although it becomes so when we approach  $T_c$ .

The decrease of  $I_c(T)$  with temperature (Fig. 10.17) is relatively far from the prediction of the model of AMBEGAOKAR and BARATOFF.

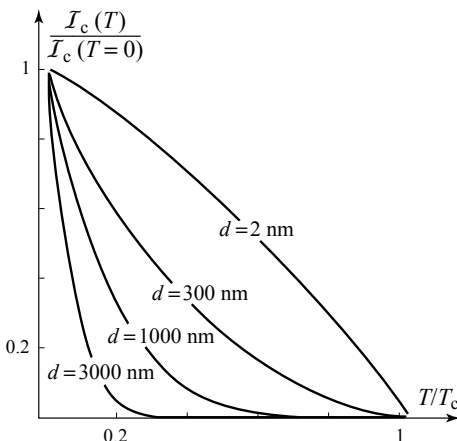


**Figure 10.17**  
**Maximum JOSEPHSON current densities**  
*via the ANDREEV levels of an SNS junction*  
The calculations were made on models for Nb/N/Nb junctions of different lengths. The critical current densities are normalized to their values at 0 K, and range from  $4.69 \cdot 10^7 \text{ A cm}^{-2}$  for the shortest, to  $4.01 \cdot 10^8 \text{ A cm}^{-2}$  for the longest. The curves  $I_c(T)$  show very different behavior from those observed for SIS junctions, except for the thinnest, where they are similar. [From GUNSENHEIMER, SCHÜSSLER & KÜMMEL, 1994, © The American Physical Society, with permission]<sup>20</sup>

20 U. GUNSENHEIMER, U. SCHÜSSLER & R. KÜMMEL (1994) *Phys. Rev. B* **49**, 6111.

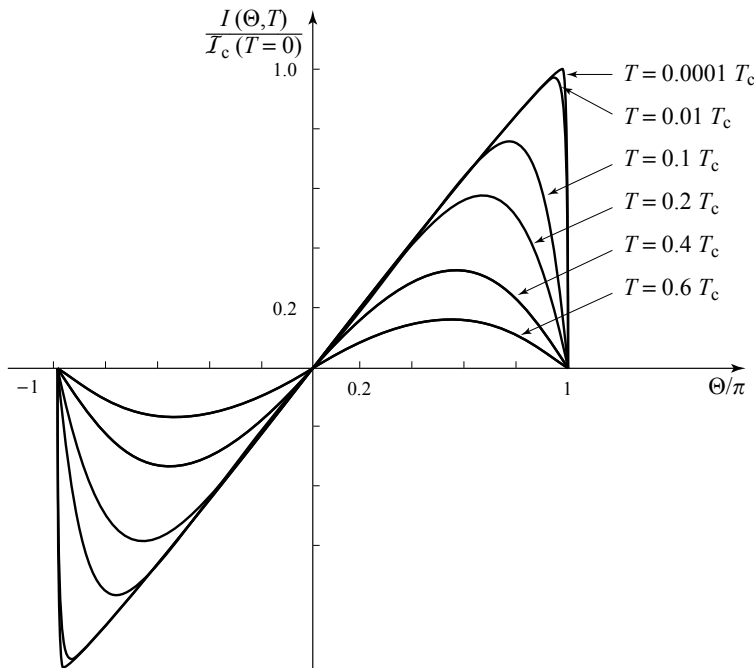


**Figure 10.16 - JOSEPHSON current  $I(\Theta)$  via the ANDREEV levels in an SNS junction**

The calculation was made on a model Nb/N/Nb junction of length  $d_N = 150$  nm. The current intensity  $I_c$  has been normalized to its highest value at 0 K.  $I(\Theta)$  evolves from a sawtooth curve at 0 K towards a sinusoidal form at higher temperatures. [From GUNSENHEIMER, SCHÜSSLER & KÜMMEL, 1994, © The American Physical Society, with permission]<sup>20</sup>

### 10.7.3 - Examples of SNS junctions

An analysis of the properties of many types of SNS junctions can be found in several review articles.<sup>21,22</sup> They differ from SIS junctions, where the thickness of the insulator is a few nm, in that the distance separating the superconducting electrodes is generally from 0.1 to 10  $\mu\text{m}$ .

The behavior of junctions depends not only on their dimensions, but also on parameters such as the mean free path of the electrons, that can be greater or less than the distance between the superconducting electrodes. The resistance  $R_h$  is generally of the order of an ohm or a milliohm and in so far as the superconducting films are not opposite each other, the capacitance of the junction remains insignificant, which makes us expect over-damped junctions.<sup>23</sup>

21 K. LIKHAREV(1979) *Rev of Mod. Phys.* **51**,101.

22 A.A. GOLUBOV, M. YU. KUPIRIYANOV & E. LL'ICHEV (2004) *Rev. of Mod. Phys.* **76**, 411.

23 In spite of this, retrapping currents different from  $I_c$  are still observed in certain systems; see H. COURTOIS *et al.* (2008) *Phys. Rev. Lett.* **101**, 067002.

Methods of fabrication have evolved with micro-etching techniques; as an example Figure 10.18 shows an SNS junction obtained by a method of “shadow deposition.”<sup>24</sup>

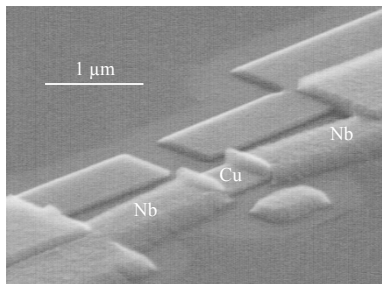


**Figure 10.18**  
**Nb/Cu/Nb junction**

Junction obtained by deposition at different incident angles with a suspended mask. The technique inherently produces some replicas as well as the Nb/Cu/Nb junction, but being disconnected from the sample they are of no consequence. [From DUBOS *et al.*, 2001, © The American Physical Society, with permission]<sup>25</sup>

To obtain this structure, DUBOS *et al.*<sup>25</sup> constructed a silicon mask suspended at a distance of  $0.57 \mu\text{m}$  from the substrate (Fig. 10.19a), then deposited, at appropriate angles (Figs. 10.19b and 10.19c), 100 nm of copper, and then 200 nm of niobium. The widths of the bands of copper and niobium were 600 nm and 800 nm respectively.

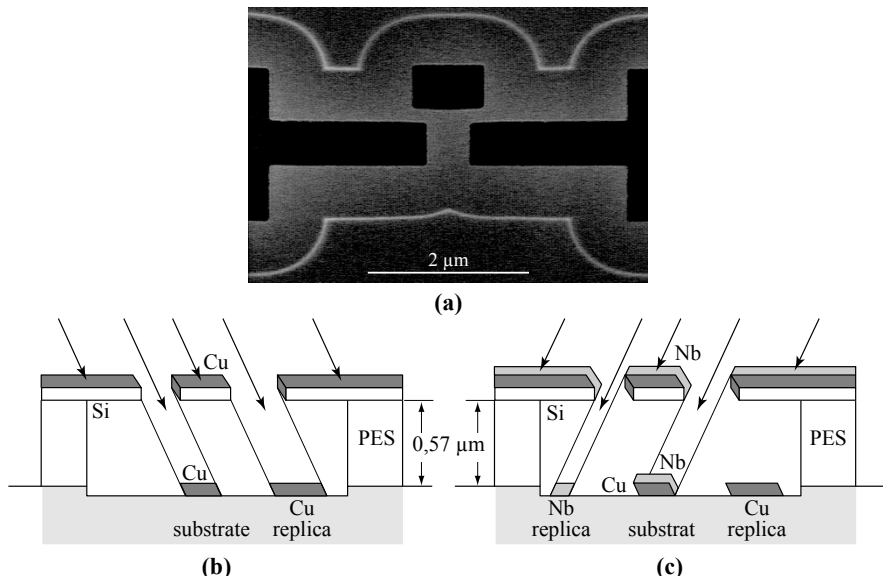


**Figure 10.19 - Shadow deposition**

(a) The mask used;  $h = 850 \text{ nm}$  (b) Deposition of copper (c) Deposition of niobium. The silicon mask is maintained at  $0.57 \mu\text{m}$  from the substrate by an etched layer of PES. [From DUBOS *et al.*, 2001, © The American Physical Society, with permission]<sup>25</sup>

24 P. DUBOS (2000) *Transport électronique dans des nanojonctions supraconducteur - métal normal - supraconducteur*, (Electronic transport in superconductor-normal-superconductor junctions) Thesis, in French, Université Joseph Fourier, Grenoble.

To ensure the contact between metals, the niobium covered the copper at each of its extremities over a distance of 150 nm. Typically, when the distance between the niobium electrodes was 500 nm, a resistance  $R_n \approx 0.20 \Omega$  and a critical current  $I_c \approx 1.2 \text{ mA}$  were found.<sup>25</sup>

#### 10.7.4 - Signature of the JOSEPHSON effect

As well as the two model SNS junctions presented, very many others, sometimes with complex geometries, have been, and continue to be, developed and compared to experiment. The behavior varies from model to model and the following question arises: what is the signature of a JOSEPHSON current? LIKHAREV,<sup>21</sup> followed by GOLUBOV,<sup>22</sup> proposed that the current that flows between two bulk superconductors should be considered to be of JOSEPHSON type if:

- › it flows between two electrodes only because of a phase difference  $\Theta$ ,
- › it is periodic:  $I(\Theta) = I(\Theta + 2\pi)$ ,
- › it is antisymmetric:  $I(-\Theta) = -I(\Theta)$ ; although this condition may not be fulfilled in certain cases of coupling between superconductors where the pairing is of unconventional symmetry,
- › it is zero for  $\Theta = \ell\pi$ ,
- › as a consequence of the previous conditions, it can be written as a series<sup>26</sup>

$$I(\Theta) = \sum_{n \geq 1} I_n \sin(n\Theta) \quad (10.51)$$

- › the phase is related to the potential difference at the leads of the junction by

$$\frac{d\Theta}{dt} = 2 \frac{e}{\hbar} V \quad (10.52)$$

that is insensitive to the details of the model as it involves only universal constants.

**Remark** - We note that when the relation (10.14) is no longer satisfied, the current-voltage characteristics of the RCSJ model in the over-damped regime depart from the relation (10.30b),  $\langle V \rangle = \frac{1}{G} \sqrt{I^2 - I_c^2}$ , as the example of Figure 10.20 shows.

### 10.8 - $\pi$ -type JOSEPHSON junctions

#### 10.8.1 - Definition and energy

A  $\pi$  (“pi”) junction is one for which the intensity of the JOSEPHSON current is related to the phase difference between the two superconductors by

$$I_{1 \rightarrow 2} = -I_c \sin(\theta_1 - \theta_2) = I_c \sin(\Theta + \pi). \quad (10.53)$$

---

25 P. DUBOS *et al.* (2001) *Phys. Rev. B* **63**, 064502 and **87**, 206801.

26 In this sense the  $\sin \Theta$  relation for SIS junctions, or for the limiting cases of SNS or SCS junctions, is only a particular case of a JOSEPHSON junction.

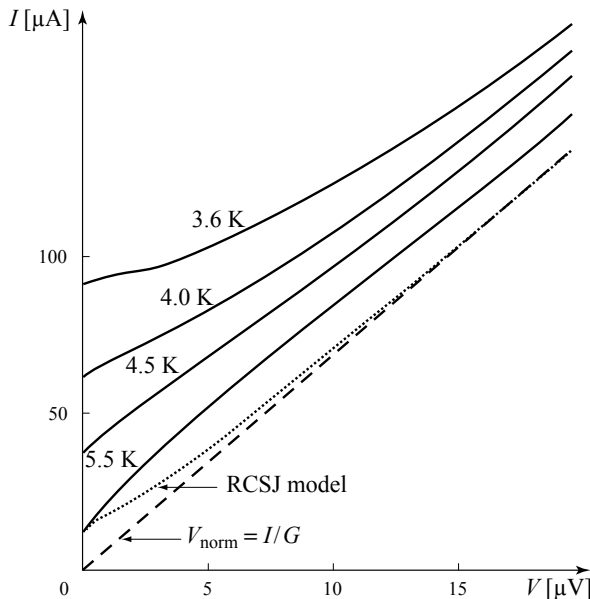


**Figure 10.20 - Example of current-voltage characteristics of an SNS junction<sup>27</sup>**

Curves derived from measurements on a Nb/Cu/Nb sample of length 710 nm, width 580 nm and thickness 100 nm. The junction is diffusive with a diffusion coefficient of the electrons in the normal metal of  $250 \text{ cm}^2 \text{ s}^{-1}$ . The dashed curve is the resistance of the junction in the normal state and, in dots, the predicted characteristics at 5 K by the RCSJ model in the over-damped regime.

It is so named because of the term  $\pi$  that is added to the difference  $\Theta$  between the phases of the two superconductors in the expression for the JOSEPHSON current. In contrast, and when it will be useful, we will describe as being “of type zero” the junctions described in section 10.2. If it is not made precise, a junction is implicitly of type zero.

Proceeding as in section 10.5, we easily calculate that the energy stocked in the  $\pi$  junction is

$$E^\pi(\Theta) = E_J [1 - \cos(\Theta + \pi)] = E_J [1 + \cos \Theta]. \quad (10.54)$$

In contrast to the zero junction whose energy is a minimum for  $\Theta = 0$ , the energy minima of the  $\pi$  junction are situated at  $\Theta = \pm \pi$  and are separated by a potential barrier of height  $2E_J$  whose summit corresponds to an unstable equilibrium at  $\Theta = 0$  (Fig. 10.21).

<sup>27</sup> P. DUBOS, H. COURTOIS, O. BUISSON & B. PANNETIER (2001)  
*Phys. Rev. Lett.* **87**, 206801.

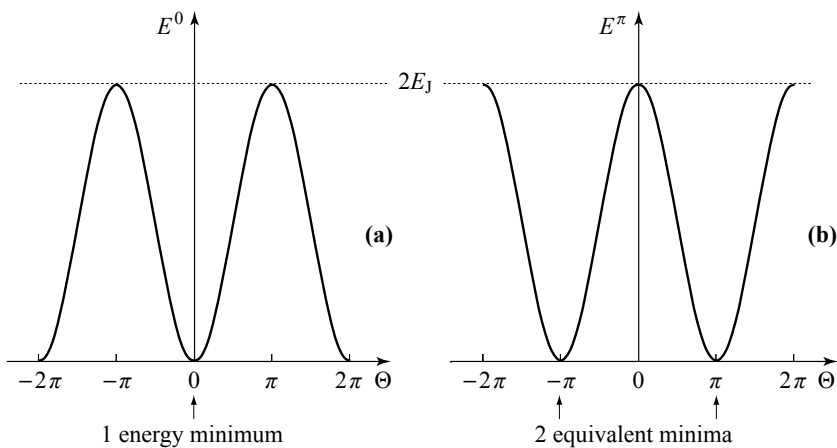


**Figure 10.21 - Energy stored in junctions of type zero (a) and  $\pi$  (b) as a function of the phase difference  $\Theta$  between their leads**

As a result the  $\pi$  junction is bi-stable: at zero current it can be equally be in one or other of the two minima. For an injected current  $I$ , the junction chooses the phase difference closest to  $\pm\pi$ .

### 10.8.2 - Families of JOSEPHSON $\pi$ junctions

The type of a JOSEPHSON junction, zero or  $\pi$ , is an intrinsic property of the combination of materials that form the junction. We now know several families of  $\pi$  junctions:

- » junctions between two superconducting grains of a cuprate (HTS superconductor) oriented in a particular way. Since the superconductivity of the cuprates is carried by  $d_{x_2-y_2}$  orbitals, a junction that places the positive lobes of one superconductor directly opposite the negative lobes of the other, is of  $\pi$  type;
- » certain junctions made of carbon nanotubes connecting two superconductors;<sup>28</sup>
- » some junctions where a layer, or one of several layers, separating the superconductors is ferromagnetic:

Superconductor / Ferromagnet / Superconductor (SFS)

Superconductor / Insulator / Ferromagnet / Superconductor (SIFS)

Superconductor / Insulator / Ferromagnet / Insulator / Superconductor (SIFIS)

28 J.-P. CLEUZIOU, W. WERNSDORFER, V. BOUCHIAT, T. ONDARCUHU & M. MONTHIOUX (2006) *Nature Nanotech.* **1**, 53-59.

### 10.8.3 - SFS junctions: mechanisms of $\pi$ junctions

We consider separately from all others, two electrons of a COOPER pair within the first superconductor  $S_1$  that occupy the two states  $|\mathbf{k}\uparrow\rangle$  ( $+k_F$ ) and  $|-k\downarrow\rangle$  ( $-k_F$ ) situated at the front and rear of the FERMI surface, respectively (Fig. 10.22a).

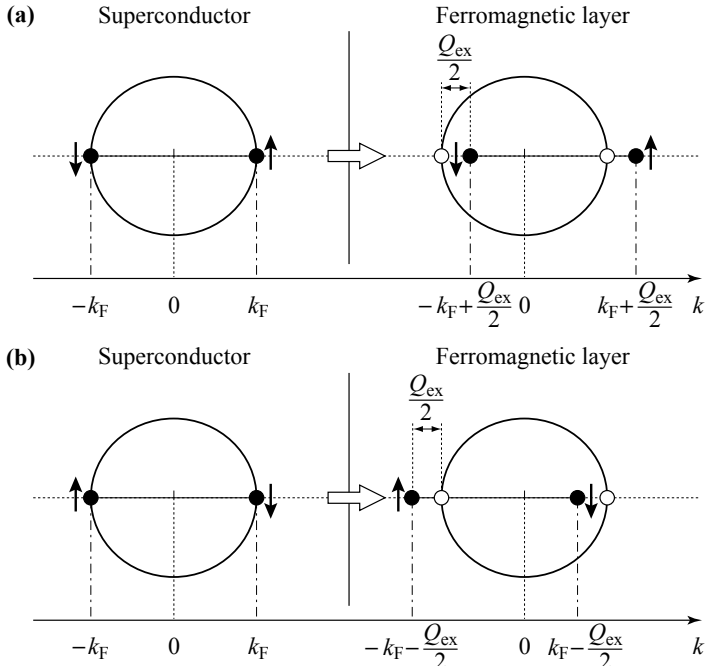


Figure 10.22 - COOPER pair crossing a ferromagnetic material <sup>29</sup>

(a) When the electron in state  $|\mathbf{k}\uparrow\rangle$  is at the front of the FERMI sphere ( $+k_F$ ) and the electron in state  $|\mathbf{k}\downarrow\rangle$  at the back, each of them sees its wave vector increase by  $Q_{ex}/2$  when entering the ferromagnetic material. (b) In the inverse situation their wave vectors decrease by the same amount.

When penetrating the ferromagnetic material, where there is an internal magnetic field  $B_i$  present, the electron in state  $|\mathbf{k}\uparrow\rangle$  acquires, because of its spin  $\uparrow$ , a potential energy  $-\mu_B B_i$  ( $\mu_B$  is the BOHR magneton) while the electron in state  $|\mathbf{k}\downarrow\rangle$  see its potential energy become  $+\mu_B B_i$ . To respect the conservation of its total energy, each electron modifies its kinetic energy by changing its wave vector by an amount  $Q_1$  for the first electron and  $Q_2$  for the second, with respectively:

$$\begin{aligned} \frac{1}{2m} \hbar^2 (k_F + Q_1)^2 - \mu_B B_i &= \frac{\hbar^2}{2m} k_F^2 \\ \frac{1}{2m} \hbar^2 (-k_F + Q_2)^2 + \mu_B B_i &= \frac{\hbar^2}{2m} (-k_F)^2 \end{aligned} \quad (10.55)$$

29 E.A. DEMLER, G.B. ARNOLD & M.R. BEASLEY (1997) *Phys. Rev. B* **55**, 15174.

with, given that  $Q_1$  and  $Q_2 \ll k_F$ ,

$$2Q_1 = 2Q_2 = Q_{\text{ex}} = \frac{2\mu_B B_i}{\hbar v_F} = \frac{2E_{\text{ex}}}{\hbar v_F} \quad (10.56)$$

where  $2E_{\text{ex}}$  is the exchange energy, *i.e.* the change in magnetic energy when the spin is reversed.

As each electron has its momentum increase by  $\hbar(Q_{\text{ex}}/2)$ , the COOPER pair, whose initial momentum is zero, gains momentum  $\hbar Q_{\text{ex}}$  and its wave function acquires a wave vector  $Q_{\text{ex}}$ , which, when it travels a distance  $d$  in the ferromagnetic layer modifies its phase by an amount  $Q_{\text{ex}}d$ . Starting from  $\theta_1$  at the  $S_1/F$  interface, the phase of the COOPER pairs coming from  $S_1$  becomes  $\theta_1 + Q_{\text{ex}}d$  at the  $F/S_2$  interface. If we imagine (Fig. 10.23) introducing a very fine insulating layer between  $F$  and  $S_2$ , the first JOSEPHSON equation across this virtual layer is written  $I = I_c \sin(\theta_1 + Q_{\text{ex}}d - \theta_2)$ . In the special case of  $Q_{\text{ex}}d = \pi$ , or  $d = h\nu_F/4E_{\text{ex}}$ , this leads to  $I = I_c \sin(\Theta_{1,2} + \pi)$ , *i.e.* the form of the JOSEPHSON effect of a  $\pi$  junction.

To be more precise, the wave function associated with the COOPER pair coming from  $S_1$  is the product of wave function of the two electrons, or

$$e^{i\frac{Q_{\text{ex}}}{2}x_1} e^{i\frac{Q_{\text{ex}}}{2}x_2} \otimes |\uparrow\downarrow\rangle = e^{iQ_{\text{ex}}x} \otimes |\uparrow\downarrow\rangle$$

where  $x = (x_1 + x_2)/2$  is the position of the center of gravity of the pair,  $x_1$  is that of the electron whose wave vector  $\mathbf{k}_\uparrow$  is in the front of the Fermi sphere and  $x_2$  the electron of wave vector  $-\mathbf{k}_\downarrow$  situated at the back (Fig. 10.22a).

Now as it includes two electrons, the wave function of the COOPER pair must change sign under exchange of particles and, since it is a spin singlet, it must be the direct product of the antisymmetric spin wave function  $|Y^{AS}\rangle$  and a symmetric orbital function  $\phi^S$ .

Exchange of the particles leads to the configuration of Figure 10.22b and places the electron in state  $|\neg k_\downarrow\rangle$  to the front of the FERMI sphere and those in state  $|k_\uparrow\rangle$  to the back.<sup>29</sup> In this new situation and following the preceding reasoning, we find that each electron sees its wave vector change by  $-Q_{\text{ex}}$  since:

$$\begin{aligned} \frac{1}{2m} \hbar^2 \left( k_F - \frac{Q_{\text{ex}}}{2} \right)^2 + \mu_B B_i &= \frac{\hbar^2}{2m} k_F^2 \\ \frac{1}{2m} \hbar^2 \left( -k_F - \frac{Q_{\text{ex}}}{2} \right)^2 - \mu_B B_i &= \frac{\hbar^2}{2m} (-k_F)^2 \end{aligned} \quad (10.57)$$

which means that the wave function associated with this new configuration is  $e^{-iQ_{\text{ex}}x} \otimes |\downarrow\uparrow\rangle$ . The total wave function, antisymmetric in spin and symmetric in orbital coordinates is then

$$\Phi = \phi^S \otimes |Y^{AS}\rangle = (e^{iQ_{\text{ex}}x} + e^{-iQ_{\text{ex}}x}) \otimes \left( \frac{|\uparrow\downarrow\rangle - |\downarrow\uparrow\rangle}{\sqrt{2}} \right). \quad (10.58)$$

This means that in the ferromagnetic layer the wave function  $\phi_f$  is  $\phi_1$  multiplied by a factor  $\cos(Q_{\text{ex}}x)$ , to which it is natural to add a damping term  $e^{-x/\xi_f}$  that has no effect on the phase. Therefore by following a simple argument, the insulating layer I of an SFIS junction situated at a distance  $d$  from the S<sub>1</sub>/F interface has on its two sides wave functions  $\phi_f(d) = \sqrt{n_1} \cos(Q_{\text{ex}}d) e^{i\theta_1} e^{-d/\xi_f}$  and  $\phi_2 = \sqrt{n_2} e^{i\theta_2}$ , leading to a JOSEPHSON current of intensity

$$I \approx \mathcal{I}_c(d=0) e^{-\frac{d}{\xi_f}} \cos(Q_{\text{ex}}d) \sin(\theta_1 - \theta_2) = \mathcal{I}_c(d) \sin(\theta_1 - \theta_2). \quad (10.59)$$

This predicts that with varying  $d$ , depending on the sign of  $\cos(Q_{\text{ex}}d)$ , there will be alternating zero and  $\pi$  junctions. The fact that  $\mathcal{I}_c$  passes by zero and local maxima was one of the first clues to this alternation. Confirmation will come from SQUID with  $\pi$  junctions (see section 11.4).

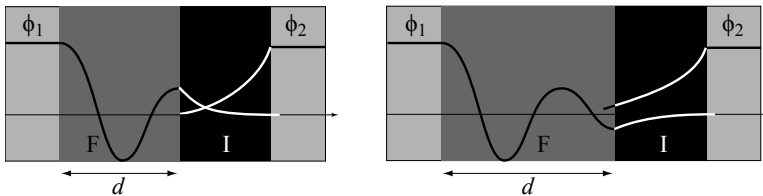


**Figure 10.23 - SFIS model of of JOSEPHSON junctions of types 0 and  $\pi$**

The wave function  $\phi_1$  of the condensate of S<sub>1</sub> extends into the ferromagnetic layer F as an oscillating function  $\phi_f(x) = \phi_1 e^{-x/\xi_f} \cos(Q_{\text{ex}}x)$ . At the F/I interface and depending on the value of  $d$ ,  $\phi_f(d)$  has either the same sign as  $\phi_1$  (**a**) or the opposite sign (**b**). The dephasing between the decaying waves that overlap in I is either the same as that between  $\phi_1$  and  $\phi_2$  (**a**), and the junction is 0 type, or it is of the opposite sign, (**b**), and the junction is  $\pi$  type.

Numerous experiments have provided evidence for this phenomenon. For example Figure 10.24a shows the results of measurements of the critical currents  $\mathcal{I}_c$  for Nb/Al/Al<sub>2</sub>O<sub>3</sub>/PdNi/Nb junctions as a function of the thickness  $d$  of the ferromagnetic PdNi layer. The change in the nature of the junction (0 to  $\pi$ ) is signaled by the fall to zero of  $\mathcal{I}_c$  for  $d \approx 6.5$  nm. Figure 10.24b shows for the system Nb/Cu<sub>52</sub>Ni<sub>48</sub>/Nb that the temperature – by acting on the internal field  $B_i$ , the exchange energy  $E_{\text{ex}}$  and, ultimately, on the periodicity of the oscillating factor  $\cos(Qx)$  – can change the nature of the junction.

An equivalent, and certainly more physical result, can be found by considering that the current is not directly carried across the ferromagnetic layer by COOPER pairs, whose electrons move in opposite directions ( $+k_F$  et  $-k_F$ ) and with opposite spins, but, as in Figure 10.15, by electrons and ANDREEV holes that also move in opposite directions with opposite spins. We no longer need to consider a fictitious insulating layer, the factor  $\cos(Q_{\text{ex}}d)$  representing simply the standing wave associated with electron-hole reflections in the ferromagnetic layer.

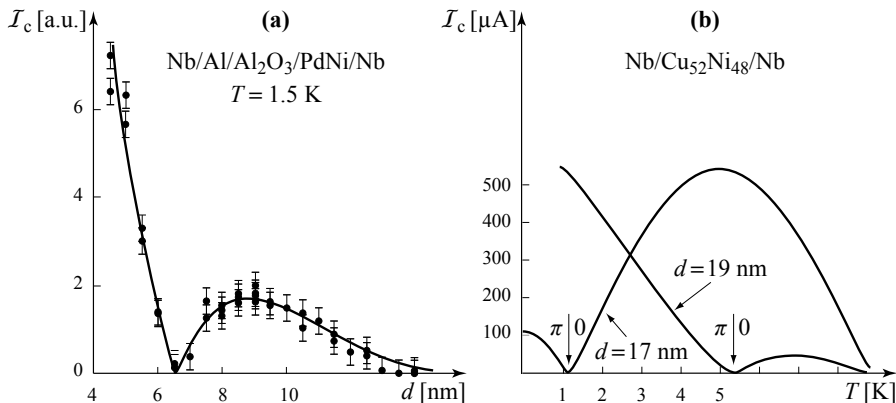


**Figure 10.24 - Junction with a ferromagnetic barrier  
Evidence for change between a junction of 0 type and of  $\pi$  type**

(a) In a Nb/Al/Al<sub>2</sub>O<sub>3</sub>/PdNi/Nb junction as a function of the thickness  $d$  of the PdNi layer. The fall to zero of the maximum current around  $d = 6.5$  nm is the signature of the change in type from 0 to  $\pi$ . [From KONTOS *et al.*, 2002, © The American Physical Society, with permission].<sup>30</sup>

(b) In a Nb/Cu<sub>52</sub>Ni<sub>48</sub>/Nb junction as a function of the temperature  $T$  for two thicknesses of the ferromagnetic layer: the effect of the temperature is to modify the internal magnetic field and thus the wave vector  $Q_{\text{ex}}$ . [From SELLIER *et al.*, 2004, © The American Physical Society, with permission]<sup>31</sup>

The mechanism is nonetheless different depending on whether the exchange energy  $E_{\text{ex}}$  is larger or smaller than the superconducting gap  $\Delta$ .

When  $E_{\text{ex}} \gg \Delta$  the ANDREEV levels are “eliminated” and the simple model presented above is justified.

The case  $E_{\text{ex}} \ll \Delta$  can be treated as a simple perturbation to the ANDREEV levels described in section 10.7.2. If we include the exchange energy of the spins, these levels are not doubled, but quadrupled since the electron quasiparticles can move to the left or the right with either spin  $\uparrow$  or spin  $\downarrow$ , giving four stationary waves. The dominant stationary wave depends on the value of  $d$ . It determines the direction of transport of the COOPER pairs: from S<sub>1</sub> to S<sub>2</sub> or from S<sub>2</sub> to S<sub>1</sub>.

## 10.9 - JOSEPHSON junction: a system with many states

### 10.9.1 - Electron on a chain of atoms

The aim of this section is to show that the JOSEPHSON effect, that was treated artificially in section 10.1 starting from a two-state system, actually involves a large number of states, and can be compared to an electron that moves on a linear chain of atoms.

30 T. KONTOS *et al.* (2002) *Phys. Rev. Lett.* **89**, 137007.

31 H. SELLIER *et al.* (2004) *Phys. Rev. Lett.* **92**, 257005.

We consider, then, a linear chain of atoms with lattice parameter  $b$  and an electron that can be on any atom of the chain. We call  $|n\rangle$  the state of the system when the electron is on the atom at  $x_n = nb$ . In the general case, the state  $|\psi\rangle$  of the system is a linear superposition of states  $|n\rangle$ ,

$$|\psi\rangle = \sum_n c_n |n\rangle \quad (10.60)$$

where  $c_n$  is the probability amplitude of finding the electron on atom  $n$ . The dynamics of an electron on an atomic chain is a classic problem in quantum mechanics that has been analyzed in detail in many texts.<sup>32</sup> We recall that the coefficients  $c_n$  obey the SCHRÖDINGER equation:

$$i\hbar \frac{dc_n}{dt} = E_0 c_n - A c_{n+1} - A c_{n-1} \quad (10.61)$$

where  $E_0$  is the energy of an electron on an isolated atom and  $iA/\hbar$  is the probability amplitude that the electron jumps onto a neighboring site during a unit interval of time, *i.e.* the probability amplitude for the system to pass from the state  $|n\rangle$  to states  $|n+1\rangle$  or  $|n-1\rangle$  (Fig. 10.25).

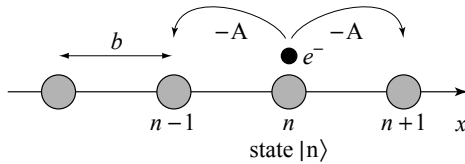


**Figure 10.25 - One-electron system on chain of atoms in the state  $|n\rangle$**

The system is in the state  $|n\rangle$  if the electron is localized near the atom  $n$ . The coefficient  $A$  represents the probability amplitude for the system in state  $|n\rangle$  to pass to one of the “neighboring” states  $|n+1\rangle$  or  $|n-1\rangle$ , *i.e.* for the electron to jump from the atom to one of its nearest neighbors.

The solutions of (10.61) are

$$c_n(k, t) = a_n(k) e^{-i\frac{E_k}{\hbar}t} \quad \text{with} \quad \begin{cases} a_n(k) = e^{ikx_n} \\ E_k = E_0 - 2A \cos(kb) \end{cases} \quad (10.62)$$

giving the time dependence

$$|\psi(t)\rangle = \sum_k c_k(0) e^{-i\frac{E_k}{\hbar}t} |k\rangle \quad (10.63)$$

where the states  $|k\rangle$  and  $|n\rangle$  are related by the FOURIER relations:

$$|k\rangle = \sum_n e^{ikx_n} |n\rangle \quad \text{and} \quad |n\rangle = \sum_k e^{-ikx_n} |k\rangle. \quad (10.64)$$

<sup>32</sup> For example, R. FEYNMAN, R. B. LEIGHTON, M. SANDS (1966) *The Feynman Lectures in Physics, Vol. III: Quantum Mechanics*, Addison-Wesley, New York, Chap. 13. The new Millennium edition is available on-line at <http://www.feynmanlectures.caltech.edu>.

A state  $|k\rangle$  is a coherent superposition of states  $|n\rangle$  with coefficients  $e^{ikx_n}$  of unit modulus, whose phase increases by  $kb$  when we pass from state  $|n\rangle$  to state  $|n+1\rangle$ .

Passing to the continuous limit in the relation (10.63),  $|\Psi(t)\rangle$  appears as a wave packet making the variables  $p = \hbar k$  and  $x = nb$  *canonically conjugate variables*. The electron is described by a wave packet with

$$\delta p \delta x \approx \hbar \quad \text{or} \quad \delta k \delta x \approx 1 \quad (10.65)$$

$\delta k$  and  $\delta x$  are the widths of the spread of the wave vector and position around their mean values  $\langle k \rangle$  and  $\langle x \rangle$ .

In a semi-classical approach, the velocity of motion of the particle is given by the group velocity,

$$v_G = \frac{dx}{dt} = \frac{1}{\hbar} \frac{\partial E}{\partial k} \quad (10.66)$$

and a force  $F = -\partial E / \partial x$ , due to a change of the energy with the position of the particle, for example in presence of an electric field, induces a change in momentum  $F = dp/dt$ , implying

$$\frac{dp}{dt} = \hbar \frac{dk}{dt} = -\frac{\partial E}{\partial x}. \quad (10.67)$$

These equalities constitute the HAMILTON-JACOBI equations.

### 10.9.2 - Generalization

We can rewrite the relations (10.66) by substituting for the variables  $x$  and  $k$ , the variables  $n = x/b$  and  $\Theta = kb$ . The states  $|\Theta\rangle$  replace the states  $|k\rangle$  and we have:

$$a_n = e^{in\Theta} \quad \text{and} \quad E(\Theta) = E_0 - 2A \cos \Theta. \quad (10.68)$$

The HEISENBERG uncertainty relation takes the form

$$\delta \Theta \delta n \approx 1 \quad (10.69)$$

and the HAMILTON-JACOBI relations are written

$$\frac{dn}{dt} = \frac{1}{\hbar} \frac{\partial E}{\partial \Theta} \quad \frac{d\Theta}{dt} = -\frac{1}{\hbar} \frac{\partial E}{\partial n}. \quad (10.70)$$

If, in addition, we consider that the states  $|\Theta\rangle$  form a quasi-continuum, the FOURIER relations (10.64) become

$$|\Theta\rangle = \sum_n e^{in\Theta} |n\rangle \quad ; \quad |n\rangle = \frac{1}{2\pi} \int_0^{2\pi} d\Theta e^{-in\Theta} |\Theta\rangle. \quad (10.71)$$

### 10.9.3 - Application to the JOSEPHSON effect

We consider  $N$  COOPER pairs shared between the two bulk superconducting blocks (1) and (2) separated by a potential barrier. At a given time, they number  $n_1$

on block (1) and  $n_2$  on block (2). The state  $|n\rangle$  is characterized by the single variable  $n$  defined such that

$$n_1 = (N/2) + n \quad \text{and} \quad n_2 = (N/2) - n \quad (10.72)$$

The most general state of the BOSE-EINSTEIN condensate can be written as a coherent superposition of these states

$$|\Psi\rangle = \sum_n c_n |n\rangle \quad (10.73)$$

where  $c_n$  is the probability amplitude of finding the system in state  $|n\rangle$ . In the limit where  $n$  is tiny compared to the statistical fluctuations in the number of COOPER pairs in each block ( $n \ll \sqrt{N} \ll N$ ), one COOPER pair can pass from one block to the other without changing the total energy of the system.

Transfer of a COOPER pair from block (1) to block (2) corresponds to the passage of the system from state  $|n\rangle$  to  $|n+1\rangle$  while transfer from block (2) to block (1) corresponds to passage of the system from state  $|n\rangle$  to  $|n-1\rangle$  (Fig. 10.26). As the probability amplitudes for transfer of the COOPER pair from (1) to (2) or from (2) to (1) are identical, we find ourselves with a similar problem to that of an electron on a linear chain that can jump on one or other of its neighboring sites with equal probability amplitudes. The  $c_n(t)$  satisfy the same SCHRÖDINGER equation

$$i\hbar \frac{dc_n}{dt} = E_0 c_n - A c_{n+1} - A c_{n-1}. \quad (10.74)$$

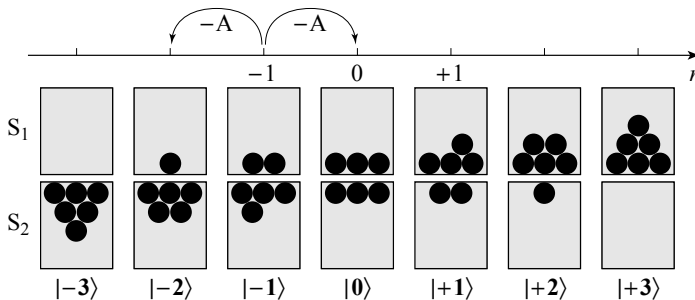


**Figure 10.26 - Representation of the states  $|n\rangle$  of two coupled superconductors**

The system is in state  $|n\rangle$  if the superconducting block (1) contains  $(N/2 + n)$  COOPER pairs and the block (2) contains  $(N/2 - n)$ . The term  $A$  is the probability amplitude for the system in state  $|n\rangle$  to pass to one of its "neighboring" states  $|n+1\rangle$  or  $|n-1\rangle$ , i.e. for a COOPER pair to tunnel from  $S_2$  to  $S_1$  or from  $S_1$  to  $S_2$ .

The stationary solutions are given by the relations (10.68) where  $\Theta$  is the phase difference between the coefficients  $c_n$  and  $c_{n+1}$  that multiply  $|n\rangle$  and  $|n+1\rangle$  to construct a state  $|\Theta\rangle$ . The problem is now formally identical to that of an electron on a linear chain since  $\Theta$  and  $n$  are conjugate variables obeying the uncertainty relations (10.69), the HAMILTON-JACOBI equations (10.70) and the FOURIER relations (10.71).

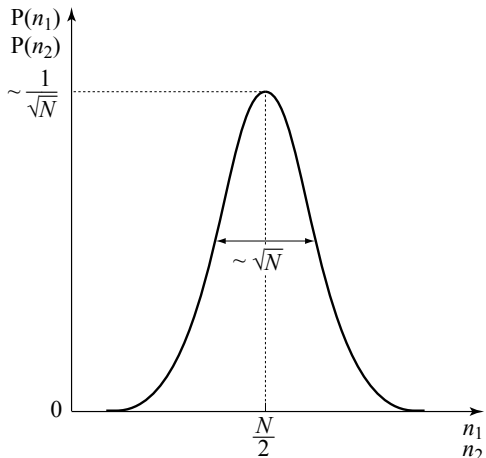


**Figure 10.27**  
**Statistical partition of**  
 **$N$  objects into two boxes**

The probability distribution of finding  $n_1$  objects in the box (1) and  $n_2$  objects in box (2) is, in the limit of large numbers, a Gaussian centered on  $N/2$  with width  $\sqrt{N}$ .

### First JOSEPHSON equation

The variation in  $n$  translates into a flux of COOPER pairs from the superconducting component (1) to the superconducting component (2), and therefore into a current  $I$ . As a direct consequence of the first HAMILTON-JACOBI equation this gives

$$I_{1 \rightarrow 2} = -q_p \frac{dn}{dt} = -\frac{q_p}{\hbar} \frac{\partial E}{\partial \Theta} = I_c \sin \Theta \quad ; \quad I_c = -\frac{2q_p}{\hbar} A = \frac{4\pi}{\phi_0} A \quad (10.75)$$

which is the first JOSEPHSON equation (relation 10.14).

### Stored energy in a junction

Using the expression (10.68) and the relation (10.75) between  $I_c$  and  $A$ , the energy of the system in state  $|\Theta\rangle$  can be written

$$E(\Theta) = E_0 - E_J \cos \Theta \quad \text{with } E_J = \frac{I_c \phi_0}{2\pi} \quad (10.76)$$

that, up to a constant, represents the energy stored in the JOSEPHSON junction as was expressed in relation (10.35).

### Second JOSEPHSON equation

If we apply a potential difference  $V = V_1 - V_2$  between the two superconducting parts, the energy of the system in the  $|n\rangle$  state increases by an amount  $nq_pV$ . By the second HAMILTON-JACOBI relation (10.70) this leads to

$$\frac{d\Theta}{dt} = -\frac{1}{\hbar} \frac{\partial E}{\partial n} = -\frac{q_p V}{\hbar} = \frac{2eV}{\hbar} \quad (10.77)$$

that is none other than the second JOSEPHSON equation (10.18).

**10.9.4 - A general property of BOSE-EINSTEIN condensates**

The “uncertainty relation” (10.69),  $\delta\Theta \delta n \approx 1$ , indicates that we cannot know exactly and simultaneously the phase difference between the blocks and the number of particles that each contains. If we fix the particle number, the phase is indeterminate and if the phase is fixed, it is the particle number that becomes fluctuating. This is a general property of BOSE-EINSTEIN condensates that will re-appear in the BCS treatment of COOPER pairs.

## Appendix 10A

### Solution of the coupling equations

The matrix equation (10.5) couples the superconducting condensates (1) and (2) separated by a thin insulator. When we apply a potential difference  $V$  between the two blocks, the energies  $E_1$  and  $E_2$  of COOPER pairs are given by the expressions (10.7). The equation for the coupling between the condensates of the two superconducting blocks can then be written

$$\begin{pmatrix} \frac{q_p V}{2} & -K \\ -K & \frac{-q_p V}{2} \end{pmatrix} \begin{pmatrix} \sqrt{n_1(t)} e^{i\theta_1(t)} \\ \sqrt{n_2(t)} e^{i\theta_2(t)} \end{pmatrix} = i\hbar \frac{d}{dt} \begin{pmatrix} \sqrt{n_1(t)} e^{i\theta_1(t)} \\ \sqrt{n_2(t)} e^{i\theta_2(t)} \end{pmatrix}. \quad (10.78)$$

We have two differential equations of first order. To pass from one to the other we permute the indices 1 and 2 and simultaneously change  $V$  to  $-V$ . It is therefore enough to resolve the first

$$i\hbar \frac{d}{dt} \left[ \sqrt{n_1} e^{i\theta_1} \right] = \frac{q_p V}{2} \sqrt{n_1} e^{i\theta_1} - K \sqrt{n_2} e^{i\theta_2}. \quad (10.79)$$

By expanding the derivative of the quantity in brackets this gives

$$i\hbar \left[ \frac{\frac{dn_1}{dt}}{2\sqrt{n_1}} e^{i\theta_1} + i\sqrt{n_1} \frac{d\theta_1}{dt} e^{i\theta_1} \right] = \frac{q_p V}{2} \sqrt{n_1} e^{i\theta_1} - K \sqrt{n_2} e^{i\theta_2} \quad (10.80)$$

$$\text{or, } i\hbar \left[ \frac{\frac{dn_1}{dt}}{2\sqrt{n_1}} + i\sqrt{n_1} \frac{d\theta_1}{dt} \right] = \frac{q_p V}{2} \sqrt{n_1} - K \sqrt{n_2} e^{i(\theta_2 - \theta_1)}. \quad (10.81)$$

Equating real and imaginary parts we obtain,

$$\frac{d\theta_1}{dt} = -\frac{q_p V}{2\hbar} + \frac{K}{\hbar} \sqrt{\frac{n_2}{n_1}} \cos(\theta_2 - \theta_1) \quad (10.82a)$$

$$\frac{dn_1}{dt} = \frac{2K}{\hbar} \sqrt{n_1 n_2} \sin(\theta_1 - \theta_2). \quad (10.82b)$$

By making the substitutions mentioned above the solutions of the second equation are

$$\frac{d\theta_2}{dt} = +\frac{q_p V}{2\hbar} + \frac{K}{\hbar} \sqrt{\frac{n_1}{n_2}} \cos(\theta_2 - \theta_1) \quad (10.83a)$$

$$\frac{dn_2}{dt} = -\frac{2K}{\hbar} \sqrt{n_1 n_2} \sin(\theta_1 - \theta_2) = -\frac{dn_1}{dt}. \quad (10.83b)$$

where we recognize the expressions (10.8) and (10.9).

## Appendix 10B

### JOSEPHSON junction in the over-damped regime

#### *Initial equations*

In the over-damped regime, driven by a continuous current of intensity  $I$  above the critical current  $I_c$ , the voltage  $V(t)$  and the phase difference  $\Theta(t)$  are related by (10.29b)

$$V(t) = \frac{I - I_c \sin \Theta(t)}{G} \quad \text{with } I > I_c \quad (10.84)$$

as well as the JOSEPHSON equation (10.23)

$$\frac{d\Theta}{dt} = \frac{2eV}{\hbar}. \quad (10.85)$$

#### *Average voltage $\langle V \rangle$ and the period $T$*

By definition the time-averaged voltage is

$$\langle V \rangle = \frac{1}{T} \int_0^T V(t) dt \quad (10.86)$$

and, since over one period,  $t$  varies from 0 to  $T$  and simultaneously  $\Theta$  varies from 0 to  $2\pi$ , from (10.85),

$$\int_0^{2\pi} d\Theta = 2\pi = \frac{2e}{\hbar} \int_0^T V(t) dt \quad (10.87)$$

so that

$$\frac{1}{T} = \frac{2e}{\hbar} \langle V \rangle. \quad (10.88)$$

The period is identical to the JOSEPHSON period that would be observed for a junction subject to a constant  $V = \langle V \rangle$ .

#### *Average voltage $\langle V \rangle$ as a function of injected current $I$*

Combining relations (10.84) and (10.85) and eliminating  $V$  leads to

$$dt = \frac{\hbar}{2e} \left( \frac{G}{I - I_c \sin \Theta} \right) d\Theta. \quad (10.89a)$$

By integrating over one period and a phase slip in  $\Theta$  of  $2\pi$ , we find

$$\int_0^T dt = T = \frac{\hbar}{2e} \int_0^{2\pi} \frac{G}{I - I_c \sin \Theta} d\Theta \quad (10.89b)$$

and replacing  $T$  by its expression (10.88),

$$\langle V \rangle = \frac{1}{2\pi} \int_0^{2\pi} \frac{G}{I - I_c \sin \Theta} d\Theta. \quad (10.89c)$$

The right hand side of (10.89c) can be evaluated using the indefinite integral <sup>33</sup>

$$\int \frac{1}{I - I_c \sin \Theta} d\Theta = \frac{2}{\sqrt{I^2 - I_c^2}} \tan^{-1} \left( \frac{I \tan\left(\frac{\Theta}{2}\right) - I_c}{\sqrt{I^2 - I_c^2}} \right) \quad (10.90)$$

For the two limits of integration,  $\Theta = 0$  and  $\Theta = 2\pi$ , the argument of the “inverse tangent” function is identical, since in both cases

$$\frac{I \tan\left(\frac{\Theta}{2}\right) - I_c}{\sqrt{I^2 - I_c^2}} = \frac{-I_c}{\sqrt{I^2 - I_c^2}}. \quad (10.91)$$

The  $\tan^{-1}$  function is, however, defined modulo  $\pi$ . This means that if we keep the same value of  $\tan^{-1}$  for  $\Theta = 0$  and  $\Theta = \pi$ , the integral vanishes, while if we choose two different values the integral equals  $\pm \pi$ .

Now if  $I > I_c$ , the term  $I - I_c \sin \Theta$  and the function  $G/(I - I_c \sin \Theta)$  are always positive. The correct choice is then

$$\tan^{-1} \left( \frac{-I_c}{\sqrt{I^2 - I_c^2}} \right)^{\Theta=2\pi} - \tan^{-1} \left( \frac{-I_c}{\sqrt{I^2 - I_c^2}} \right)^{\Theta=0} = \pi. \quad (10.92)$$

Substituted into (10.89) including the constant factors in (10.90), this leads to the result

$$\langle V \rangle = \frac{1}{G} \sqrt{I^2 - I_c^2}. \quad (10.93)$$

33  $\int \frac{dx}{p + q \sin(ax)} = \frac{2}{a\sqrt{p^2 - q^2}} \tan^{-1} \left( \frac{p \tan\left(\frac{ax}{2}\right) + q}{\sqrt{p^2 - q^2}} \right)$

M.R. SPIEGEL (1974) SCHAUM Series, McGraw-Hill Inc, formula (14.36).  
Wolfram Mathematica, On-line integrator : <http://integrals.wolfram.com/index.jsp>

## Appendix 10C

### JOSEPHSON junction subject to an alternating voltage

If to a continuous voltage  $V$ , a small alternating component  $v \cos(\omega_0 t + \varphi)$  is added, the phase difference from one side to the other of the JOSEPHSON junction is given by the integral of the expression (10.18),

$$\begin{aligned} \frac{d\Theta}{dt} &= \frac{2e}{\hbar} [V + v \cos(\omega_0 t + \varphi)] \\ \Rightarrow \quad \Theta(t) &= \frac{2e}{\hbar} \left[ Vt + \frac{v}{\omega_0} \sin(\omega_0 t + \varphi) \right] + \Theta(0). \end{aligned} \quad (10.94)$$

Using the JOSEPHSON equation (10.14), the current intensity across the junction is

$$I = I_c \sin \Theta(t) = I_c \sin \left[ \frac{2e}{\hbar} Vt + \frac{2e}{\omega_0 \hbar} v \sin(\omega_0 t + \varphi) + \Theta(0) \right] \quad (10.95)$$

or, passing from the sine function to the imaginary part of an exponential,

$$I = I_c \operatorname{Im} \left[ e^{i \left( \frac{2e}{\hbar} Vt + \frac{2e}{\omega_0 \hbar} v \sin(\omega_0 t + \varphi) + \Theta(0) \right)} \right] \quad (10.96)$$

where “Im” is the imaginary part of the expression in brackets. This expression can be factorized

$$I = I_c \operatorname{Im} \left[ e^{i \left( \frac{2e}{\hbar} Vt + \Theta(0) \right)} e^{i \left( \frac{2e}{\omega_0 \hbar} v \sin(\omega_0 t + \varphi) \right)} \right]. \quad (10.97)$$

If we expand the exponential according to SCHLÖMILCH’s formula

$$e^{iC \sin x} = \sum_{n=-\infty}^{n=\infty} J_n(C) e^{inx} \quad (10.98)$$

where  $J_n$  is the integer BESSEL function of order  $n$ , we have

$$I = I_c \operatorname{Im} \left[ e^{i \left( \frac{2e}{\hbar} Vt + \Theta(0) \right)} \sum_{n=-\infty}^{n=\infty} J_n \left( \frac{2e}{\hbar \omega_0} \right) v e^{i(n \omega_0 t + n \varphi)} \right] \quad (10.99)$$

that can be reordered as

$$I = I_c \operatorname{Im} \left[ \sum_{n=-\infty}^{n=\infty} J_n \left( \frac{2e}{\hbar \omega_0} \right) v e^{i \left[ \left( \frac{2e}{\hbar} V + n \omega_0 \right) t + n \varphi + \Theta(0) \right]} \right] \quad (10.100)$$

or, using the relation  $J_{-n} = (-1)^n J_n$  and returning to the sine function,

$$I = I_c \sum_{n=0}^{n=\infty} (-1)^n J_n \left( \frac{2e}{\hbar \omega_0} v \right) \sin \left[ \left( \frac{2e}{\hbar} V \pm n \omega_0 \right) t \pm n \varphi + \Theta(0) \right] \quad (10.101)$$

which is just the relation (10.39).

# Chapter 11

## SUPERCONDUCTING QUANTUM INTERFERENCE DEVICE “SQUID”

SQUIDS are closed superconducting circuits containing one or more JOSEPHSON junctions. They may be isolated physically and only interact with the external environment by electromagnetic coupling (rf-SQUID) or they may be inserted into part of electrical devices (DC-SQUID). They are at the heart of the most sensitive instruments for measuring magnetic fields. This chapter will introduce us to how they work and describe some of their most common configurations.

### 11.1 - Nature of the SQUID current

We first consider the simplest SQUID consisting of a superconducting ring interrupted by a single JOSEPHSON junction (Fig. 11.1). A magnetic field flux  $\phi = \iint \mathbf{B} \cdot d\mathbf{S}$  passes through the ring, that carries a current of intensity  $I$ . Positive signs for the orientations of  $\mathbf{B}$  and  $I$  are chosen as indicated in Figure 11.1.

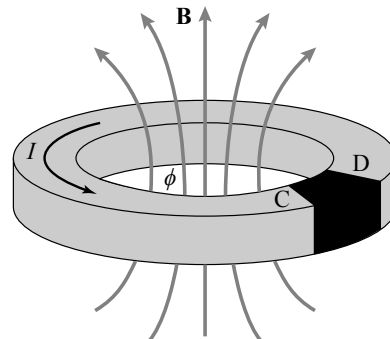


Figure 11.1  
Elementary single junction rf-SQUID

The single junction rf-SQUID is a closed superconducting circuit into which is inserted a JOSEPHSON junction between C and D. A current  $I$  flows in the circuit through which passes a magnetic field flux  $\phi$ .

In such a circuit there are three terms entering the change in phase of the wave function of the superconducting condensate:

- » a phase change due to the circulation of the current density  $\mathbf{j}$  along the path DC (the large arc) followed in the positive direction (expression 9.11);

$$(\theta_C - \theta_D)^{\text{current}} = \frac{m_p}{n_p q_p \hbar} \int_D^C \mathbf{j} \cdot d\mathbf{l}; \quad (11.1)$$

» the phase change due to the circulation of the vector potential  $\mathbf{A}$  along the same path DC (expression 9.11),

$$(\theta_C - \theta_D)^{\text{mag}} = \frac{q_p}{\hbar} \int_D^C \mathbf{A} \cdot d\mathbf{l}; \quad (11.2)$$

» the phase change between points situated on opposite sides of the junction, related to the current that crosses it, (as in equation 10.15)

$$\Theta_{CD} = \theta_C - \theta_D = \sin^{-1} \frac{I}{I_c}. \quad (11.3)$$

If we follow a complete closed circuit the accumulated phase must be a multiple of  $2\pi$ , so these phase changes must satisfy the equation

$$(\theta_C - \theta_D)^{\text{current}} + (\theta_C - \theta_D)^{\text{mag}} + (\theta_D - \theta_C) = -2\pi s \quad (11.4)$$

Phase change from the current circulation      JOSEPHSON phase between  
and the vector potential between D and C      the opposite sides of the junction

where  $s$  is a positive or negative integer, the minus sign being introduced before  $s$  for convenience.

As the points C and D, situated on each side of the JOSEPHSON junction, are very close (of the order of a nanometer), in calculating the phases (11.1) and (11.2) we make a negligible error by considering that the current density  $\mathbf{j}$  and the vector potential  $\mathbf{A}$  make the whole closed circuit. Furthermore, using the fact that the circulation of the vector potential  $\mathbf{A}$  on a closed path equals the magnetic field flux  $\phi$  that crosses any surface bounded by this path, the relation (11.4) becomes

$$\frac{m}{n_p q_p \hbar} \oint \mathbf{j} \cdot d\mathbf{l} + \frac{q_p}{\hbar} \iint \mathbf{B} \cdot d\mathbf{S} + (\theta_D - \theta_C) = -2s\pi \quad (11.5a)$$

$$\text{or } \frac{m}{n_p q_p \hbar} \oint \mathbf{j} \cdot d\mathbf{l} + \frac{q_p}{\hbar} \phi + (\theta_D - \theta_C) = -2s\pi. \quad (11.5b)$$

It is usually the case, and we will assume it for any of the SQUID devices considered in the following, that the critical current of the junction  $I_c$  is sufficiently weak for the current density in the circuit to remain infinitesimal. Therefore, the phase change associated with it is negligible

$$\frac{m}{n_p q_p \hbar} \oint \mathbf{j} \cdot d\mathbf{l} \approx 0. \quad (11.6)$$

Noting the magnetic phase term

$$\Theta^{\text{mag}} = -\frac{q_p}{\hbar} \phi = \frac{2e}{\hbar} \phi = 2\pi \frac{\phi}{\phi_0} \quad (11.7)$$

the phase difference between the opposite sides of the JOSEPHSON junction reduces to

$$\Theta_{CD} = \theta_C - \theta_D = 2\pi s - \Theta^{\text{mag}}. \quad (11.8)$$

The current intensity  $I$  can then be written<sup>1</sup>

$$I = I_c \sin \Theta_{CD} = I_c \sin \left[ 2\pi \left( s - \frac{\phi}{\phi_0} \right) \right] = I_c \sin(2\pi s - \Theta^{\text{mag}}). \quad (11.9)$$

Thus the current  $I$  that crosses the junction adjusts itself so as to satisfy the relation (11.9). The phase deficit  $\Theta_{CD}$  between an integer number times  $2\pi$  and the phase associated with the magnetic field flux  $\Theta^{\text{mag}}$  is “healed” by the JOSEPHSON junction. *This means that the SQUID current appears in order to generate a phase compensating the phase deficit between an integer multiple  $s$  of  $2\pi$  and the phase associated with the magnetic flux  $\Theta^{\text{mag}}$ .*

*In every case, whether the SQUID is isolated or integrated into an electrical device, whether it contains a single or several JOSEPHSON junctions of the same type, ( $0$  or  $\pi$ ), or of two differing types, the role of the JOSEPHSON current is to adjust the phase differences at the edges of the junctions in order to compensate the missing phase  $\tilde{\Theta}$*

$$\tilde{\Theta} = 2\pi \left( s - \frac{\phi}{\phi_0} \right) = 2\pi s - \Theta^{\text{mag}}. \quad (11.10)$$

By applying the relation (11.9), a measurement of  $I$  allows us to obtain information on the magnetic field flux  $\phi$  across the SQUID loop. Knowing the geometry of this loop, we determine the magnetic field itself.

Two important remarks:

- » these relations are only valid if the JOSEPHSON junctions maintain continuity of the superconductivity, *i.e.* if the current intensities across the junctions are less than their critical currents  $I_c$ ;
- » in practice, it is the value of the magnetic field  $B^{\text{ext}}$ , *i.e.* of the field in the absence of the SQUID, that we wish to measure. To do this, we must know how to relate the total flux  $\phi$  across the SQUID circuit to the flux  $\phi^{\text{ext}}$  of the magnetic field  $B^{\text{ext}}$  across the same circuit. In general they are rather different since added to the external flux is the magnetic field flux created by the current  $I$  equal to  $LI$ , where  $L$  is the inductance of the circuit,

$$\phi = \phi^{\text{ext}} + LI. \quad (11.11)$$

In the following we shall first treat, for simplicity, cases of weakly inductive SQUIDS where the contribution of the term  $LI$  is negligible. We shall then discuss several SQUID devices where the inductance brings significant changes of behavior.

---

1 In relation (11.9) we could have suppressed the term  $2\pi s$ , which does not change the value of the sine function. We retain it to clarify the physical mechanism and in order to treat rf-SQUID's with several junctions.

## 11.2 - rf-SQUID with vanishing inductance

### 11.2.1 - Single junction non-inductive rf-SQUID

We shall specify what happens when, after cooling an rf-SQUID in zero magnetic field, an increasing external field  $B^{\text{ext}}$  is applied. If it were a simple closed superconducting circuit, lacking any JOSEPHSON junction, by virtue of the MEISSNER effect and its application to a superconductor with a hole (see section 2.8), a screening current would develop. It would increase with the external field, so that the magnetic flux across the circuit would continue to vanish.

With the addition of the JOSEPHSON junction, the history is no longer the same. As soon as the screening current reaches  $I_c$ , the JOSEPHSON junction shows a loss of continuity in the superconductivity and allows the magnetic field to penetrate into the circuit. The junction only “closes up” when the difference between the external magnetic field flux and the total magnetic field flux becomes less than  $L I_c$ . With  $I_c$  very weak and, as we suppose in this section, a small coefficient of self induction  $L$ , the screening effect is insignificant and, to a first approximation, the total magnetic field flux in the ring remains equal to the external magnetic field flux.

In this very simple case where  $\phi = \phi^{\text{ext}}$ , the magnetic phase change  $\Theta^{\text{mag}}$  represented by a point M on Figure 11.2 varies linearly with the external field flux (relation 11.7).

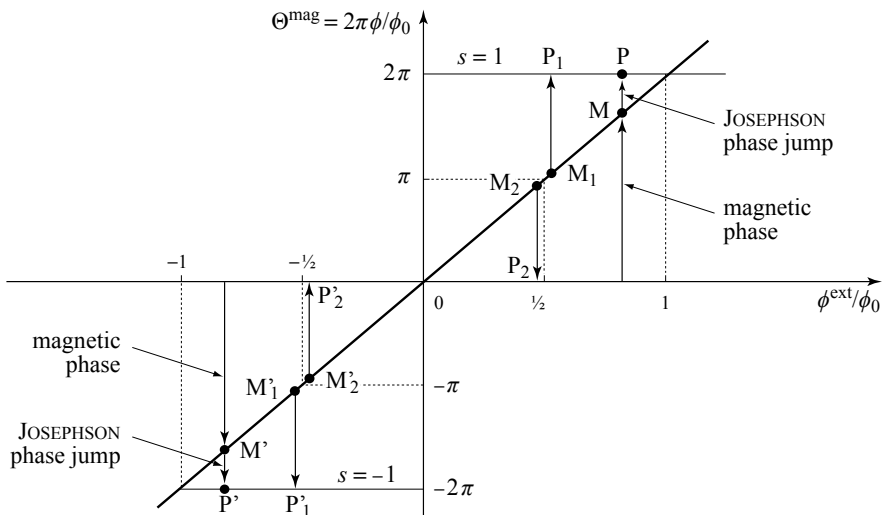


**Figure 11.2 - Magnetic and JOSEPHSON phase changes in a non-inductive rf-SQUID ring with a single junction**

The accumulation of magnetic phase obtained by making a turn of the circuit is represented by a point M located on the line of slope  $2\pi$ . In order that the total change over a turn of the circuit can be multiple of  $2\pi$ , the magnetic phase change must be accompanied by a JOSEPHSON phase jump  $\Theta_{\text{CD}} = (MP)$ . The arrows joining different points  $M_1, M_2\dots$  to points  $P_1, P_2\dots$  represent the JOSEPHSON phase jumps associated with different magnetic phases.

The role of the current  $I$  is to produce between the sides of the JOSEPHSON junction a phase jump  $\tilde{\Theta} = \overline{MP}$  that brings the point M on the line  $\Theta^{\text{mag}} = F(\phi^{\text{ext}}/\phi_0)$ , to the point P situated on the closest horizontal line of ordinate  $2s\pi$  (Fig. 11.2).<sup>2</sup>

Determined in this way, the phase difference  $\tilde{\Theta}$  shows a discontinuity ( $-\pi; +\pi$ ) at half-integer values of  $\phi^{\text{ext}}/\phi_0$  (Fig. 11.3a). The resulting current  $I$  is sinusoidal and varies with the external magnetic flux as shown in Figure 11.3b,

$$I = I_c \sin \tilde{\Theta} = I_c \sin \left( -2\pi \frac{\phi^{\text{ext}}}{\phi_0} \right) \quad (11.12)$$

Because of the very small value of the flux quantum  $\phi_0 = 2.07 \cdot 10^{-15}$  Wb, this device is extremely sensitive to changes in magnetic field. In a SQUID circuit of  $1 \text{ mm}^2$ , each period of current corresponds to a variation in the magnetic field of  $2.07 \cdot 10^{-9}$  T, or of the order of a ten thousandth of the Earth's magnetic field! Since in practice it is possible to detect current variations of about  $10^{-3} I_c$  and therefore fractions of periods of the same order of magnitude, we can measure variations of magnetic fields as weak as  $\sim 10^{-12}$  T. This sensitivity allows for the measurement of tiny magnetic fields such as the biological magnetic fields generated by the electric currents of neurons.

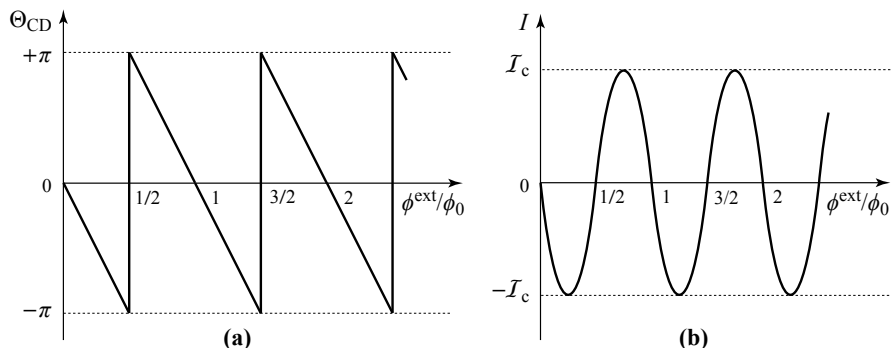


**Figure 11.3 - Phase and current in a single junction, non-inductive rf-SQUID**

(a) The phase difference between the edges of the JOSEPHSON junction varies periodically as a function of the external field flux  $\phi^{\text{ext}}$ . (b) The current intensity is sinusoidal with periodicity  $\phi_0$ .

### 11.2.2 - Non-inductive rf-SQUID with two junctions

When two JOSEPHSON junctions are integrated in an rf-SQUID circuit (Fig. 11.4), the phase  $\tilde{\Theta}$  to be recovered is still given by the relation (11.10) but it is divided between the two junctions, in equal parts if they are identical, with

2 The point P could be positioned on another horizontal line at a multiple of  $2\pi$  without violating the constraints on the phases but the cost in energy would be higher since  $\Theta$  would no longer be between  $-\pi/2$  and  $+\pi/2$ , (see section 10.5).

$$\tilde{\Theta} = \Theta_{\text{EF}} + \Theta_{\text{GH}} \quad ; \quad \Theta_{\text{EF}} = \Theta_{\text{GH}} = \frac{\tilde{\Theta}}{2} \quad ; \quad I = I_c \sin \frac{\tilde{\Theta}}{2}. \quad (11.13)$$

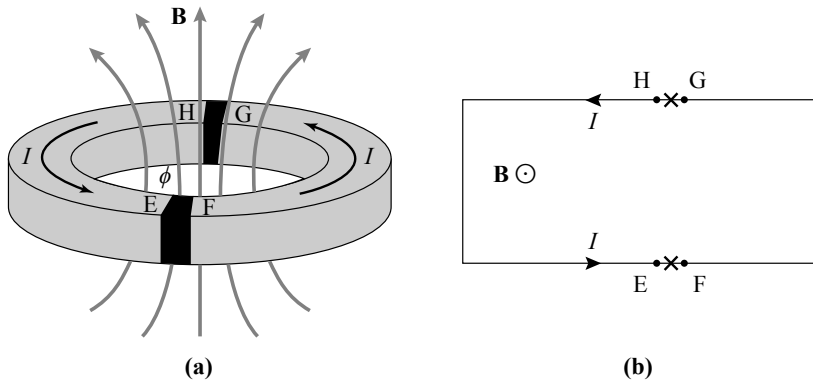


**Figure 11.4 - rf-SQUID ring with two junctions**

Two identical JOSEPHSON junctions are inserted in a closed circuit.

The phase that each JOSEPHSON junction must recover and the current intensity that contributes to it, are drawn in the Figures 11.5a and 11.5b. As for the single junction circuit, the periodicity is  $\phi_0$ , but  $I$  shows discontinuities that are *a priori* easy to detect and treat by signal analysis. Nonetheless, if the JOSEPHSON junctions are slightly different, as is usually the case, the discontinuities are a little smeared out.

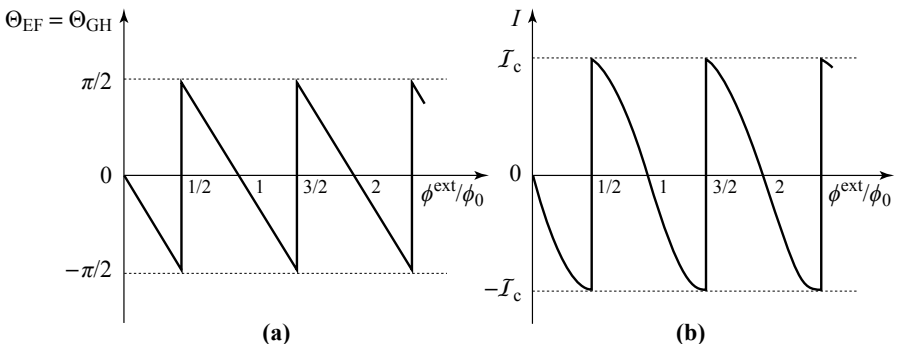


**Figure 11.5 - Current in a non-inductive rf-SQUID ring with two junctions**

(a) The phase difference between the edges of each of the JOSEPHSON junctions is half the phase difference between the edges of the single JOSEPHSON junction of Figure 11.3a. (b) The intensity of the current remains periodic with the appearance of discontinuities when the external field flux is a half-integral number of fluxons.

## 11.3 - Inductive rf-SQUID

### 11.3.1 - Magnetic phase change and the external field flux

In the last paragraphs, it was supposed that the SQUID circuit was non-inductive and that the current  $I$  contributed nothing to the magnetic flux across the circuit, so that we could write  $\phi = \phi^{\text{ext}}$ . When the flux  $LI$  of the magnetic field created by the current  $I$  is taken into account and the flux  $\phi$  across the circuit is given by (11.11), the relation between the external flux and total flux in the circuit becomes, by replacing  $I$  by  $(\phi - \phi^{\text{ext}})/L$  in (11.9)

$$\frac{\phi^{\text{ext}}}{\phi_0} = \frac{\phi}{\phi_0} - \frac{\beta_L}{2\pi} \sin 2\pi \left( s - \frac{\phi}{\phi_0} \right). \quad (11.14)$$

In this expression the inductance of the circuit enters as a reduced parameter  $\beta_L$ , that is called the “screening parameter”,

$$\beta_L = 2\pi \frac{LI_c}{\phi_0}. \quad (11.15)$$

$\beta_L$  represents the maximum magnetic phase change that the circuit inductance can produce. Because of the relation (11.14), the magnetic phase  $\Theta^{\text{mag}} = 2\pi(\phi/\phi_0)$  no longer varies linearly with the reduced external field flux  $(\phi^{\text{ext}}/\phi_0)$  that we may wish to determine from a measurement of  $I$ .

A graphical approach consists of first drawing  $(\phi^{\text{ext}}/\phi_0)$  as a function of  $2\pi(\phi/\phi_0)$  (eq. 11.14) then, by inverting the axes, plotting the curve  $\Theta^{\text{mag}} = F(\phi^{\text{ext}}/\phi_0)$  (Fig. 11.6). We can then place on the curve the points M of coordinates  $(\phi^{\text{ext}}/\phi_0, \Theta^{\text{mag}})$  from which the phases to be added are represented as  $\tilde{\Theta} = \overline{MP}$ , where P are the points situated on the closest horizontal lines of value  $2\pi s$ .

- » The case  $\beta_L = 0$  ( $\phi = \phi^{\text{ext}}$ ) is that of Figure 11.2 where  $\Theta^{\text{mag}}$  varies linearly with  $\phi^{\text{ext}}/\phi_0$ .
- » As  $\beta_L$  increases, the straight line distorts progressively until  $\beta_L = 1$ , at which value vertical tangents appear at half-integer values of  $\phi^{\text{ext}}/\phi_0$ .
- » For values beyond  $\beta_L = 1$ , the function  $\Theta^{\text{mag}} = F(\phi^{\text{ext}}/\phi_0)$  becomes multi-valued and to each value of  $\phi^{\text{ext}}/\phi_0$  within a range of increasing width around  $(n + \frac{1}{2})$  there correspond three possible values for  $\Theta^{\text{mag}}$  (see expression 11.14 and Fig. 11.6).

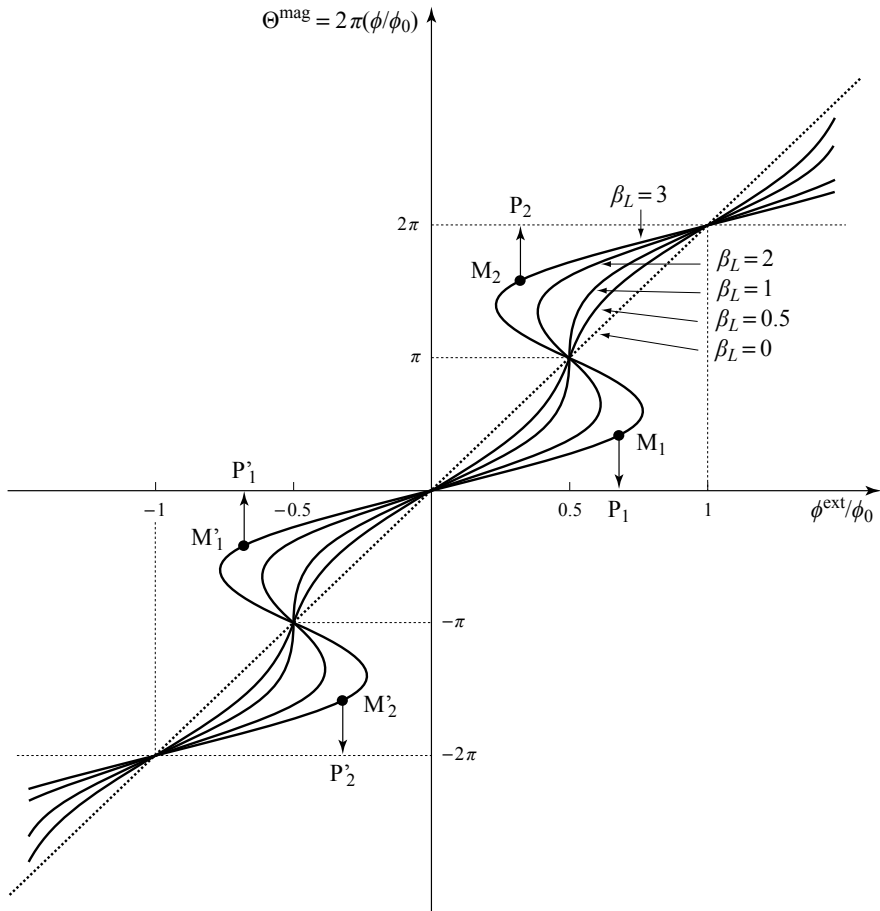


**Figure 11.6 - Inductive rf-SQUID: magnetic phase**

**as a function of the external field flux, for different values of the screening parameter  $\beta_L$**

The magnetic phase difference, that varies linearly with the external magnetic flux in a non-inductive SQUID ( $\beta_L = 0$ ), gradually distorts when  $\beta_L$  increases. For  $\beta_L < 1$ , the relation between the magnetic phase and the external field is single-valued. Beyond  $\beta_L = 1$ , the function is multi-valued with, near half-integer values of  $\phi^{\text{ext}}/\phi_0$ , several phase values possible for the same flux  $\phi^{\text{ext}}$ . Some JOSEPHSON phases are indicated with arrows for the case of  $\beta_L = 3$ .

- » Beyond  $\beta_L \approx 4.61$ , there are three values of  $\Theta^{\text{mag}}$  for each value  $\phi^{\text{ext}}/\phi_0$  and for even higher values of  $\beta_L$  there are ranges near integer values of  $\phi^{\text{ext}}/\phi_0$  where five values of  $\Theta^{\text{mag}}$  are solutions (Fig. 11.7).

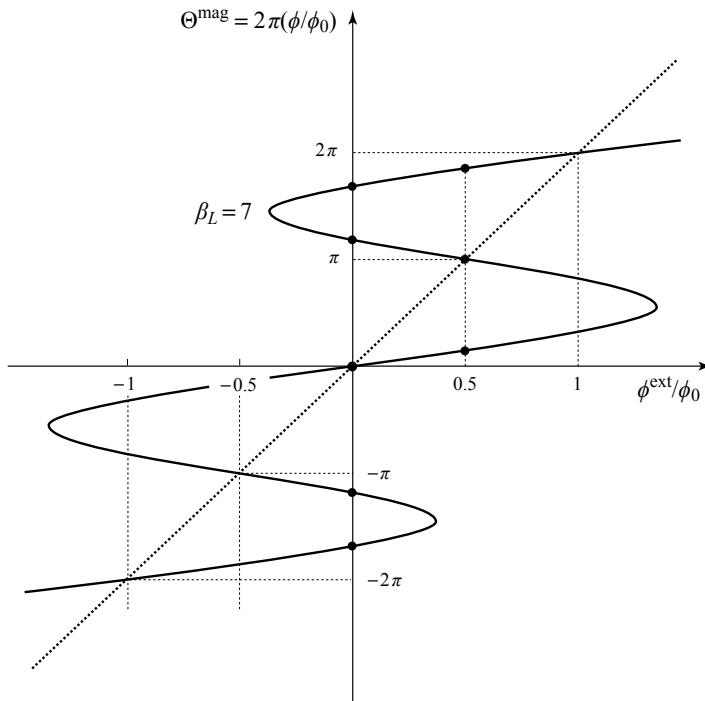


**Figure 11.7 - Magnetic phases at high values of  $\beta_L$**

When  $\beta_L > 4.61$ ,  $\Theta^{\text{mag}}$  is multi-valued for all values of  $\phi^{\text{ext}}$ . On this curve, drawn for  $\beta_L = 7$ , three values of  $\Theta^{\text{mag}}$  satisfy the phase relation (11.14) for half-integer values of  $\phi^{\text{ext}}/\phi_0$  and five for integer values.

### 11.3.2 - Operation of the inductive rf-SQUID

- » As long as  $\beta_L < 1$ , the behavior of the inductive rf-SQUID is qualitatively the same as the non-inductive rf-SQUID, except for a distortion with respect to the sinusoidal regime because of the non-linearity of  $2\pi(\phi/\phi_0) = \Theta^{\text{mag}}$  with  $\phi^{\text{ext}}/\phi_0$ .
  - » For  $\beta_L > 1$  where the function  $\Theta^{\text{mag}} = F(\phi^{\text{ext}}/\phi_0)$  has become multi-valued, the path followed by the point M when changing  $\phi^{\text{ext}}$  becomes hysteretic, as shown in Figure 11.8 for the particular case  $\beta_L = 2.5$ . By construction, the phase correction in the junction  $\tilde{\Theta} = MP$  and therefore of the intensity  $I = I_c \sin \Theta_{CD}$  of the current in the circuit, as represented in Figures 11.9a and 11.9b are also hysteretic.
- The cycles of hysteresis develop around the points  $\Omega_s$  with coordinates  $\{(n + \frac{1}{2}), (2n + 1)\pi\}$ . For each half-integer value of  $\phi^{\text{ext}}/\phi_0$ , in addition to  $\Omega_s$  that corresponds to an unstable situation, two points  $M_1$  and  $M_2$ , positioned symmetrically above and below  $\Omega_s$ , satisfy the conditions required by the phases:  $M_1$  is on the path followed when the magnetic field is raised and  $M_2$  when it descends.

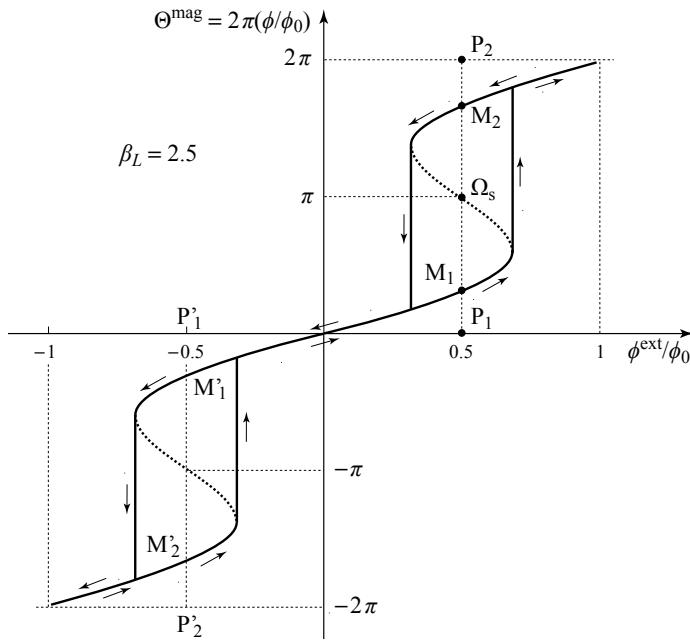


**Figure 11.8 - Phases in an inductive SQUID ring at a junction ( $\beta_L = 2.5$ )**

The total reduced magnetic flux  $\phi/\phi_0$  and the accumulation of magnetic phase that follows are multi-valued functions of  $\phi^{\text{ext}}/\phi_0$ .  $\phi/\phi_0$  follows the different trajectories, as indicated by arrows, for increasing and decreasing  $\phi^{\text{ext}}/\phi_0$ . The JOSEPHSON phase component joins the point that represents the magnetic phase (for example  $M_1$  or  $M_2$ ) to the closest value of  $2s\pi$  ( $P_1$  or  $P_2$  respectively). The dotted line corresponds to unstable situations.

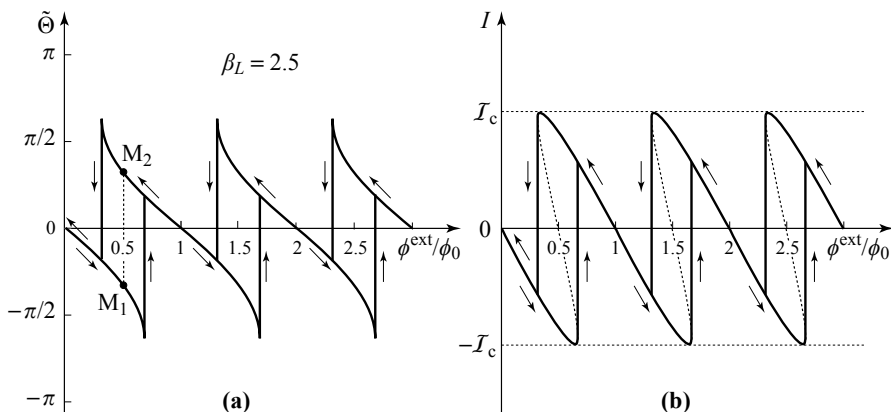


**Figure 11.9 - Phase and current in a single junction, inductive rf-SQUID, ( $\beta_L = 2.5$ )**

**(a)** Phase across the JOSEPHSON junction in a circuit with screening parameter  $\beta_L = 2.5$ . The values associated with the many-valued equation (11.14) but corresponding to unstable situations are shown with dotted lines. The curves followed during the increase, and then the decrease, of the external field are shown with thick lines. **(b)** Variation of the associated JOSEPHSON current.

## 11.4 - rf-SQUID with $\pi$ junction

The equations that govern the behavior of a SQUID ring with a  $\pi$  junction (see section 10.8.1) are formally close to those of a SQUID with a 0 junction. The only modification consists of changing  $\mathcal{I}_c$  to  $-\mathcal{I}_c$  in equation (11.9). This requires a change of sign before  $\beta_L$  in the relation (11.14), which becomes:

$$\frac{\phi^{\text{ext}}}{\phi_0} = \frac{\phi}{\phi_0} + \frac{\beta_L}{2\pi} \sin 2\pi \left( s - \frac{\phi}{\phi_0} \right) \quad (11.16)$$

and, for the same value of  $\beta_L$ , transforms the figure 11.8 into 11.10. The cycles of hysteresis are now centered around the points  $\{\phi^{\text{ext}}/\phi_0 = n, 2\pi\phi/\phi_0 = 2n\pi\}$ . In particular, in the absence of an external field, two points  $M_1$  and  $M_2$ , corresponding to trapped fluxes  $\phi_1$  and  $\phi_2$ , satisfy the imposed phase conditions. They move closer to  $\pm\phi_0/2$  as  $\beta_L$  becomes greater. From the relation  $\phi = \phi^{\text{ext}} + LI$ , they are generated by the spontaneous currents  $\phi_1/L$  for  $M_1$  and  $\phi_2/L$  for  $M_2$  that flow in opposite directions (see Fig. 11.11b).

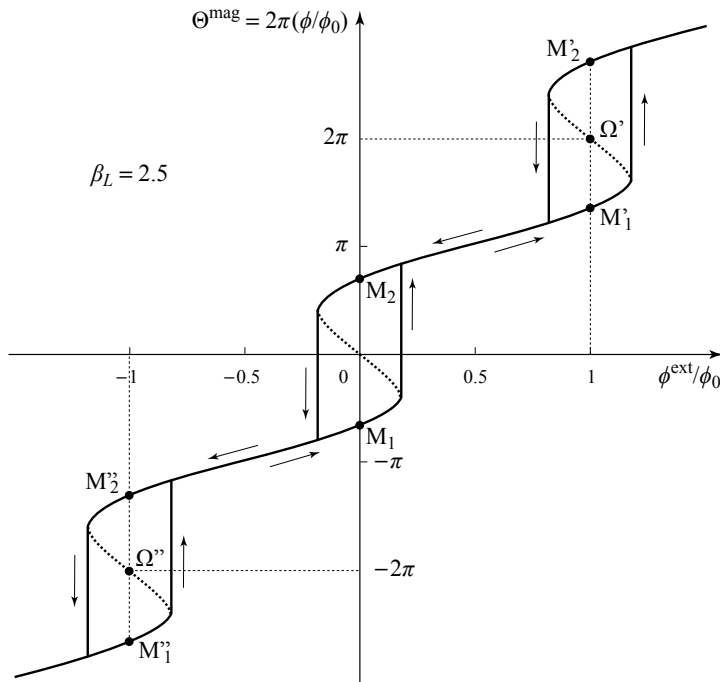


Figure 11.10 – Magnetic phases in an inductive rf-SQUID with a single  $\pi$  junction ( $\beta_L = 2.5$ )

The variation of the magnetic phase as a function of  $\phi^{\text{ext}}/\phi_0$  in the circuit with a  $\pi$  junction ( $\beta_L = 2.5$ ) is to be compared with that produced by a 0 junction as shown in Figure 11.8. The hysteretic cycles are now centered on the points  $(n, 2n\pi)$ . The points  $M_1$  and  $M_2$  indicate the two equivalent states of trapped fluxes in zero external field.

## 11.5 - Inductive single junction SQUID: energetic approach

We now reconsider the single junction SQUID circuit with one JOSEPHSON junction, 0 or  $\pi$ , of inductance  $L$  subject to an external field  $B^{\text{ext}}$ . The flux through the circuit is  $\phi = \phi^{\text{ext}} + LI$ .

The total energy of the system  $E_{\text{tot}}$  is the sum of the magnetic energy of the ring,

$$E_{\text{mag}} = \frac{1}{2}LI^2 = \frac{(\phi - \phi^{\text{ext}})^2}{2L} \quad (11.17)$$

and the energy stored in the 0 or  $\pi$  junction (relations 10.35 and 10.54: the minus sign is for the 0, the plus for the  $\pi$ ),

$$E^{0/\pi} = E_J(1 \mp \cos \tilde{\Theta}) \quad \text{with} \quad E_J = \frac{I_c \phi_0}{2\pi} \quad (11.18)$$

which can be written, using the relation (11.8) relating the phases at the edges of the junction  $\tilde{\Theta}$  to the flux  $\phi$  crossing the circuit,

$$E^{0/\pi} = E_J \left[ 1 \mp \cos \left( 2\pi \frac{\phi}{\phi_0} \right) \right]. \quad (11.19)$$

This leads to, for an rf-SQUID including a junction 0,

$$\frac{E_{\text{tot}}^0}{E_J} = \frac{2\pi^2}{\beta_L} \left( \frac{\phi - \phi^{\text{ext}}}{\phi_0} \right)^2 + 2 \sin^2 \left( \pi \frac{\phi}{\phi_0} \right) \quad (11.20)$$

and for an rf-SQUID with a  $\pi$  junction,

$$\frac{E_{\text{tot}}^\pi}{E_J} = \frac{2\pi^2}{\beta_L} \left( \frac{\phi - \phi^{\text{ext}}}{\phi_0} \right)^2 + 2 \cos^2 \left( \pi \frac{\phi}{\phi_0} \right). \quad (11.21)$$

In zero external field these energies are the sum of a parabolic term  $(2\pi^2/\beta_L)(\phi/\phi_0)^2$  and an oscillatory term whose relative contribution becomes increasingly large as  $\beta_L$  increases.

The variation with  $\phi/\phi_0$  of the total energy of the SQUID with a 0 junction in zero external field is shown in Figure 11.11a. Independently of the circuit parameters, it always has an absolute minimum at  $\phi = 0$ , which is not surprising since both the magnetic energy and the 0 junction are minimized for  $\phi = LI = 0$ .

The case of a SQUID with a  $\pi$  junction is displayed in Figure 11.11b. It shows that for  $\beta_L < 1$ , the minimum energy stays at  $\phi = 0$ , but that when  $\beta_L > 1$ , two equivalent minima appear, at which the flux  $\phi$  through the SQUID approaches  $\pm \phi_0/2$  more and more closely as  $\beta_L$  increases (Fig. 11.12).

With these two energy minima separated by an energy barrier that increases with  $\beta_L$ , the SQUID circuit becomes a bi-stable device. In each of the two energy minima, that incidentally correspond to the points M<sub>2</sub> and M<sub>1</sub> of Figure 11.10, the SQUID carries a spontaneous current  $I$  and traps a flux  $\phi = LI$ .

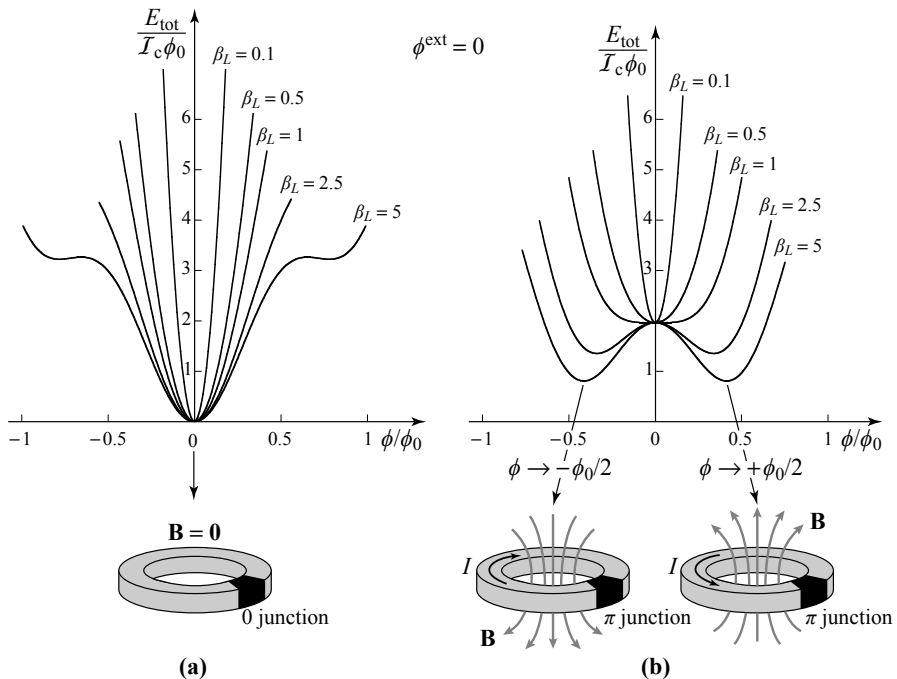
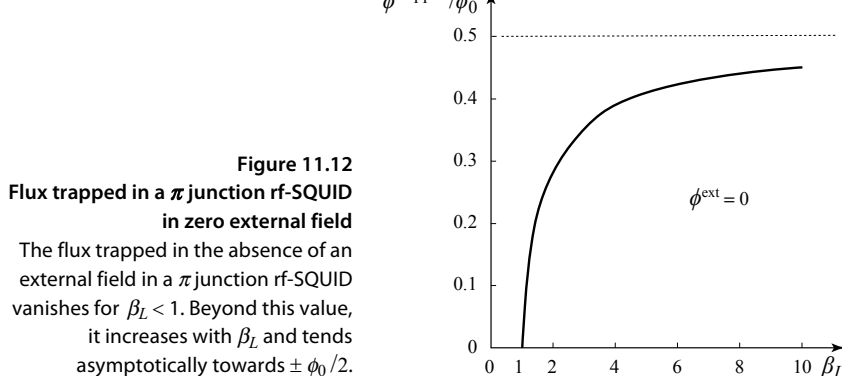


**Figure 11.11 - Energy of a single junction rf-SQUID in zero external field as a function of  $\phi/\phi_0$**

(a) The energy of a rf-SQUID circuit with a single JOSEPHSON junction of type 0 has always a minimum at total flux zero. (b) The energy of a rf-SQUID circuit with a JOSEPHSON junction of type  $\pi$  has two minima when the coefficient  $\beta_L = 2\pi(LI_c/\phi_0)$  exceeds 1. To each minimum there corresponds a trapped flux that comes closer to  $\pm \phi_0/2$  as  $\beta_L$  becomes large.



The flux trapped in the absence of an external field in a  $\pi$  junction rf-SQUID vanishes for  $\beta_L < 1$ . Beyond this value, it increases with  $\beta_L$  and tends asymptotically towards  $\pm \phi_0/2$ .

The emergence of a bi-stable state results from a competition between the minimal magnetic energy for  $\phi = LI = 0$ , and the energy of the isolated junction whose

minima are situated at  $\phi = \pm \phi_0$  (Fig. 10.21b). The term  $\beta_L$ , that represents the relative weight of the junction energy compared to the magnetic energy favors its appearance. The physical reason for trapping a flux close to a half fluxon can be easily understood since if  $L$  is large, a current very small compared to  $I_c$  suffices to generate a flux  $\pm \phi_0/2$  that will minimize the junction energy without producing a significant magnetic energy  $LI^2/2 = \phi^2/2L$ .

The process of reversal of the flux  $\phi$  in a  $\pi$  junction rf-SQUID, under the effect of an external flux  $\phi^{\text{ext}}$ , is visualized in Figure 11.13 for  $\beta_L = 2.5$ . The figure displays both  $\phi/\phi_0$  as a function of  $\phi^{\text{ext}}/\phi_0$  (relation 11.16), and the energy profile  $E_{\text{tot}}^{\pi}$  as a function of  $\phi/\phi_0$  (relation 11.20), for a few values of  $\phi^{\text{ext}}/\phi_0$ .

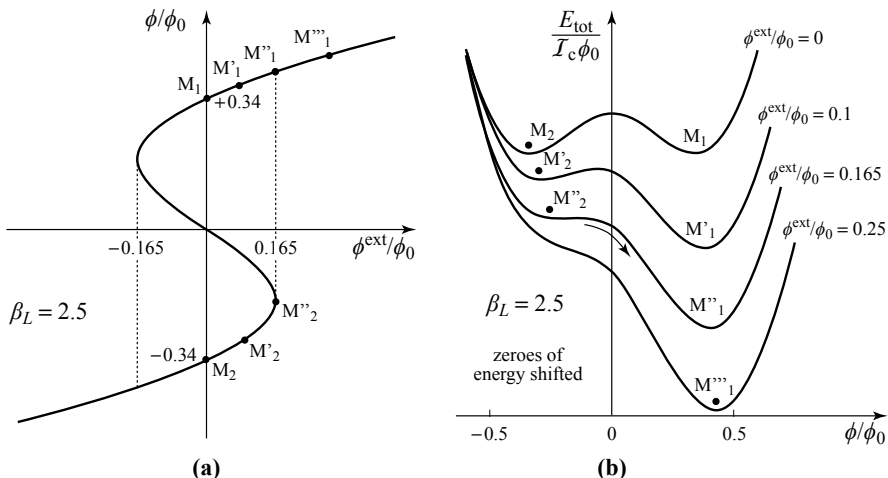


**Figure 11.13 - Process of flux reversal through a  $\pi$ junction rf-SQUID ( $\beta_L = 2.5$ )**

(a) Magnetic flux through a  $\pi$ -junction rf-SQUID ring with  $\beta_L = 2.5$ , as a function of the external field, while satisfying the phase constraints (relation 11.16). The hysteresis represented is simply the central cycle of Figure 11.10. (b) Energy of the rf-SQUID as a function of the magnetic field flux that crosses it for different values of the external field flux. With increasing  $\phi^{\text{ext}}$ , a system that is initially in the state  $M_2$  has its flux reverse when the potential barrier disappears ( $M''_2$ ), and correspondingly  $\phi$  as a function of  $\phi^{\text{ext}}$  no longer has more than a one solution.

At  $\phi^{\text{ext}} = 0$ , after starting from a state with very negative external fields, the system reaches  $M_2$  and the trapped flux is  $\phi_2 \approx -0.34 \phi_0$ . Energetically, it is separated from the state  $M_1$ , of the same energy and of opposite trapped flux  $\phi_1 \approx +0.34 \phi_0$ , by a potential barrier of height  $\approx 0.032 I_c \phi_0$ .

As the external flux increases the system moves to  $M'_2$ . Its energy becomes greater than that of solution  $M'_1$ , but the trapped flux remains negative because of the potential barrier that is certainly lowered, but still remains effective in preventing transitions between the two states.

When the external flux reaches  $\phi^{\text{ext}} \approx 0.165 \phi_0$ , the potential barrier vanishes completely and the solution represented by the point  $M''_2$  becomes energetically unstable. The system then jumps to the state represented by the point  $M''_1$  with positive trapped flux. Consistent with this, the external flux  $\phi^{\text{ext}} \approx 0.165 \phi_0$  constitutes the extreme limit for which the relation (11.8) between phases allows a solution of negative flux. At non-zero temperatures, the barrier may be overcome by thermal excitation and stability of trapped flux is guaranteed only if the barrier height is sufficiently large compared to  $k_B T$ .

## 11.6 - rf-SQUID with two JOSEPHSON junctions of different types

### 11.6.1 - 0- $\pi$ rf-SQUID with zero inductance

The case of an rf-SQUID with two  $\pi$  type junctions is very similar to the rf-SQUID with two 0 type junctions since it suffices to change  $I_c$  into  $-I_c$  in all the expressions derived, which reverses the direction of the current.

The situation is noticeably different (Fig. 11.14) when one of the junctions is of type 0 (EF) and the other of type  $\pi$  (GH) since the phases at the extremities of the JOSEPHSON junctions are related to the current intensity by:

$$I = I_c \sin \Theta_{\text{EF}} \quad I = -I_c \sin \Theta_{\text{GH}} \quad (11.22)$$

which with

$$\tilde{\Theta} = \Theta_{\text{EF}} + \Theta_{\text{GH}} = 2\pi \left( s - \frac{\phi}{\phi_0} \right) \quad (11.23)$$

gives

$$\Theta_{\text{EF}} = \pi \left( s - \frac{\phi}{\phi_0} \right) - \frac{\pi}{2} \quad \text{and} \quad \Theta_{\text{GH}} = \pi \left( s - \frac{\phi}{\phi_0} \right) + \frac{\pi}{2}. \quad (11.24)$$

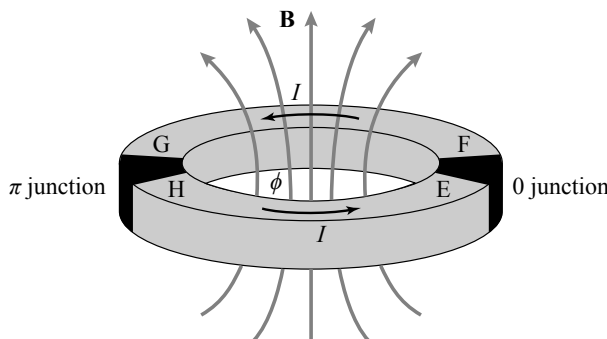
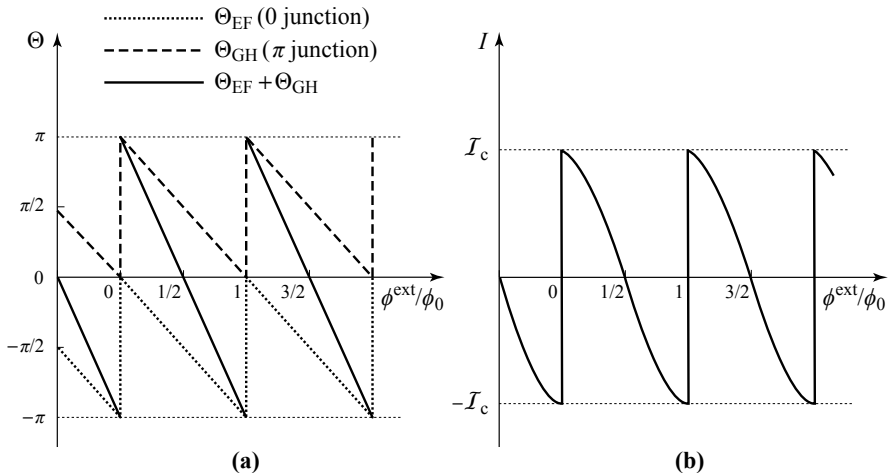


Figure 11.14 - 0- $\pi$  rf-SQUID with 0 and  $\pi$  junctions

Restricting ourselves to the case of zero inductance (field flux created by the current flowing in the ring negligible compared to the flux of the external magnetic field), the phase changes  $\Theta_{\text{EF}}$  and  $\Theta_{\text{GH}}$  are as given by the relation (11.13) shifted

by  $+\pi/2$  for  $\Theta_{\text{GH}}$  and by  $-\pi/2$  for  $\Theta_{\text{EF}}$ . This leads to a “lifting of degeneracy” of the phases (Fig. 11.15a) and a simple shift by a half-fluxon of the JOSEPHSON current (Fig. 11.15b). The discontinuities are then seen at integer values of  $\phi^{\text{ext}}/\phi_0$ .



**Figure 11.15 - Phase changes and JOSEPHSON current in a SQUID loop with two junctions of different type (0 and  $\pi$ )**

- (a) Phase changes  $\Theta_{\text{GH}}$  and  $\Theta_{\text{EF}}$  at the extremities of the  $\pi$  and 0 junctions. (b) Current flowing in the circuit.

### 11.6.2 - 0- $\pi$ rf-SQUID of significant inductance

With the magnetic energy given by the expression (11.17) and the junction energies,

$$E_{\text{EF}} = E_J(1 - \cos\Theta_{\text{EF}}) \quad \text{and} \quad E_{\text{GH}} = E_J(1 + \cos\Theta_{\text{GH}}) \quad (11.25)$$

that, using expressions (11.24), appear to be equal

$$E_{\text{EF}} = E_{\text{GH}} = E_J \left[ 1 - \sin \left( \pi \left( s - \frac{\phi}{\phi_0} \right) \right) \right]. \quad (11.26)$$

The total energy of the SQUID circuit is then

$$\frac{E^{\text{tot}}}{E_J} = \frac{2\pi^2}{\beta_L} \left( \frac{\phi - \phi^{\text{ext}}}{\phi_0} \right)^2 + 4 \sin^2 \left[ \frac{\pi}{4} (2s - 1) - \frac{\pi}{2} \frac{\phi}{\phi_0} \right]. \quad (11.27)$$

In zero external field ( $\phi^{\text{ext}} = 0$ ) the system has, for any value of  $\beta_L \neq 0$ , two minima of the same energy, one for  $s = 0$  and the other for  $s = 1$ . They correspond to spontaneous field fluxes approaching  $-\phi_0/2$  and  $+\phi_0/2$  respectively as  $\beta_L$  becomes large (Figs. 11.16 and 11.17). The system is again bi-stable but, unlike the single  $\pi$ -junction rf-SQUID, it is so for any value of  $\beta_L \neq 0$ .

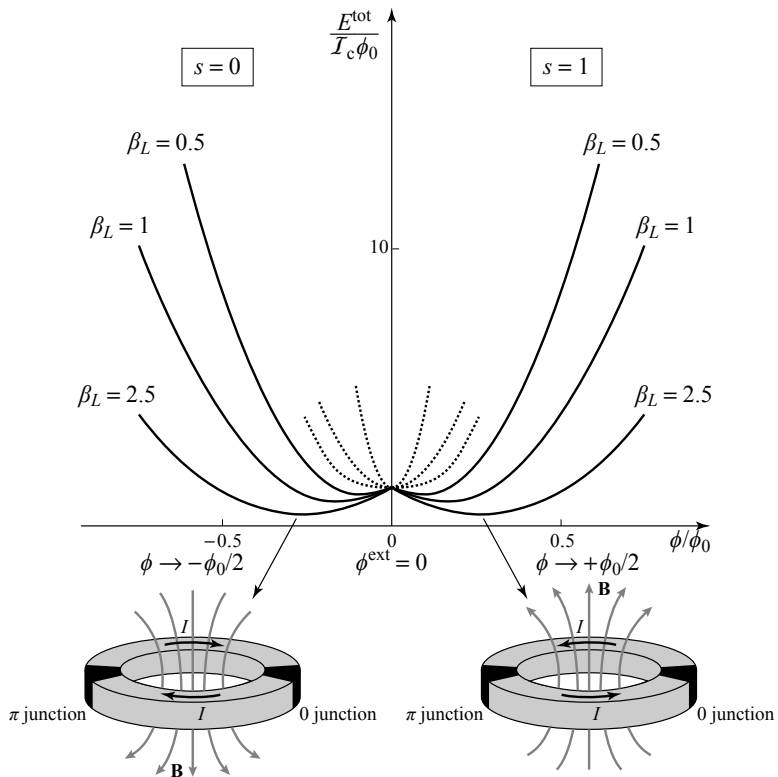


**Figure 11.16 - Energy of an rf-SQUID with two junctions, one of type 0, the other  $\pi$ , at zero field  $B^{\text{ext}}$ , as a function of  $\phi / \phi_0$  and for different values of  $\beta_L$**

For each value of  $\beta_L$ , there are two energy minima corresponding to trapped fluxes of opposite signs. They correspond to the solutions  $s = 0$  and  $s = 1$  of the relation (11.27).

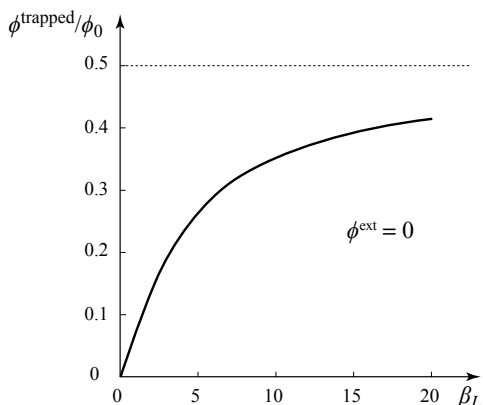


**Figure 11.17**

**Trapped flux in zero external field in an rf-SQUID with two JOSEPHSON junctions, one  $\pi$ , the other 0 type**

In an rf-SQUID with 0 and  $\pi$  type junctions, the trapped flux in the absence of external flux increases from  $\beta_L = 0$  and tends asymptotically towards  $\pm \phi_0 / 2$ .

## 11.7 - Reading an rf-SQUID

As single- or two-junction rf-SQUID loops do not have physical links to external circuits, we have to look for the information they contain without interfering significantly with their operation.

The usual method consists of coupling the rf-SQUID circuit to an RLC circuit (Fig. 11.18), whose period of resonant oscillation is much smaller than the characteristic time for changes in the flux – at the scale of a fluxon – across the rf-SQUID. A detailed analysis shows that the current flowing across the SQUID modifies the resonant frequency of the RLC circuit. Operated at constant voltage and at its natural resonant frequency, the RLC circuit has a current intensity that is directly related to the current flowing in the SQUID circuit and therefore to  $\phi^{\text{ext}}$ .

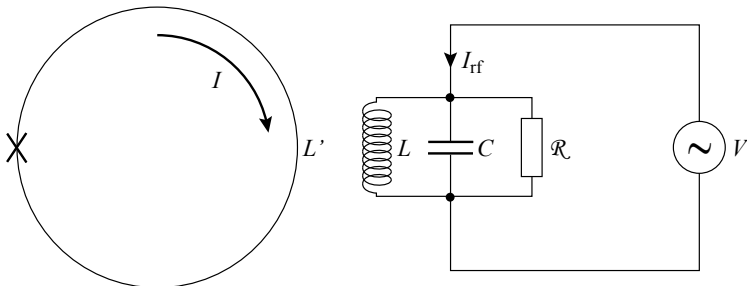


**Figure 11.18 - Reading an rf-SQUID**

The rf-SQUID is a closed circuit in which a JOSEPHSON junction has been inserted. Reading is by measuring the impedance of a resonant circuit to which it is coupled. This impedance is a periodic function, with period  $\phi_0$ , of the flux across the SQUID circuit.

This is the reason why SQUIDs with a closed circuit are also called “SQUIDs with radio-frequency coupling” or “rf-SQUIDs.”

## 11.8 - DC-SQUID (SQUID polarized by Direct Current)

### 11.8.1 - Principle of the DC-SQUID

The DC-SQUID, or SQUID polarized by a Direct Current, is a superconducting loop consisting of two JOSEPHSON junctions inserted into an electrical circuit containing two branches, through which flows a current intensity  $I$  (Fig. 11.19). Compared to an rf-SQUID, it has the advantage of being physically linked to the exterior and therefore adapted for direct readings.

In the device of Figure 11.19, the input current  $I$  separates into two components,  $I_1$  in the lower branch (crossing the junction EF) and  $I_2$  in the upper branch (crossing the junction HG). With complete generality these intensities can be written

$$I_1 = \frac{I}{2} + i \quad ; \quad I_2 = \frac{I}{2} - i \quad (11.28)$$

where  $i$  will adjust itself so that the phase condition (11.10) is satisfied,

$$\tilde{\Theta} = \Theta_{\text{EF}} + \Theta_{\text{GH}} = 2\pi \left( s - \frac{\phi}{\phi_0} \right). \quad (11.29)$$

Furthermore, writing

$$\Theta_{\text{EF}} = \frac{\tilde{\Theta}}{2} + \Theta_0 \quad ; \quad \Theta_{\text{GH}} = \frac{\tilde{\Theta}}{2} - \Theta_0 \quad (11.30)$$

where  $\Theta_0$  is an adjustable phase and using the JOSEPHSON relations

$$I_1 = \mathcal{I}_c \sin \Theta_{\text{EF}} \quad ; \quad I_2 = \mathcal{I}_c \sin \Theta_{\text{HG}} = -\mathcal{I}_c \sin \Theta_{\text{GH}} \quad (11.31)$$

we derive the two equations

$$I_1 = \frac{I}{2} + i = \mathcal{I}_c \sin \left[ \pi \left( s - \frac{\phi}{\phi_0} \right) + \Theta_0 \right] \quad (11.32a)$$

$$I_2 = \frac{I}{2} - i = -\mathcal{I}_c \sin \left[ \pi \left( s - \frac{\phi}{\phi_0} \right) - \Theta_0 \right] \quad (11.32b)$$

from which we find

$$I = I_1 + I_2 = 2\mathcal{I}_c \cos \left[ \pi \left( s - \frac{\phi}{\phi_0} \right) \right] \sin \Theta_0. \quad (11.33)$$

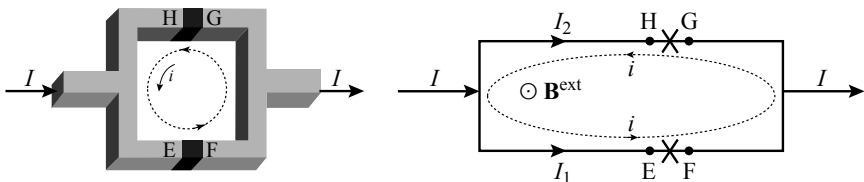


**Figure 11.19 - DC-SQUID**

The DC-SQUID is a superconducting loop with two branches containing JOSEPHSON junctions, inserted into an electric circuit. At the input of the loop, the main current  $I$  divides into two components  $I_1 = I/2 + i$  and  $I_2 = I/2 - i$ .

A non-zero current  $I$  can therefore flow through the device without appearance of a voltage between the leads of the device flow provided its intensity is less than a value  $\mathcal{I}_{\max}(\phi)$

$$\mathcal{I}_{\max}(\phi) = 2\mathcal{I}_c \left| \cos \left[ \pi \left( s - \frac{\phi}{\phi_0} \right) \right] \right|. \quad (11.34)$$

#### DC-SQUID with zero inductance ( $\beta_L = 0$ )

If the inductance of the circuit is negligible,  $\phi = \phi^{\text{ext}}$ , and in so far as the injected current intensity is less than  $\mathcal{I}_{\max}(\phi^{\text{ext}})$ ,  $\Theta_0$  adjusts spontaneously so that the

relation (11.33) is satisfied. As soon as the current exceeds  $\mathcal{I}_{\max}(\phi^{\text{ext}})$ , one at least of the two JOSEPHSON junctions conducts a current exceeding  $\mathcal{I}_c$  and a potential difference appears across the leads of the device.

$\mathcal{I}_{\max}$  oscillates between  $2\mathcal{I}_c$  when  $\phi^{\text{ext}} = n\phi_0$  and 0 when  $\phi^{\text{ext}} = (2n+1)(\phi_0/2)$  (Fig. 11.20). The situation  $\mathcal{I}_{\max} = 2\mathcal{I}_c$  corresponds to  $i = 0$  while  $\mathcal{I}_{\max} = 0$  occurs when  $i = \pm \mathcal{I}_c$ .

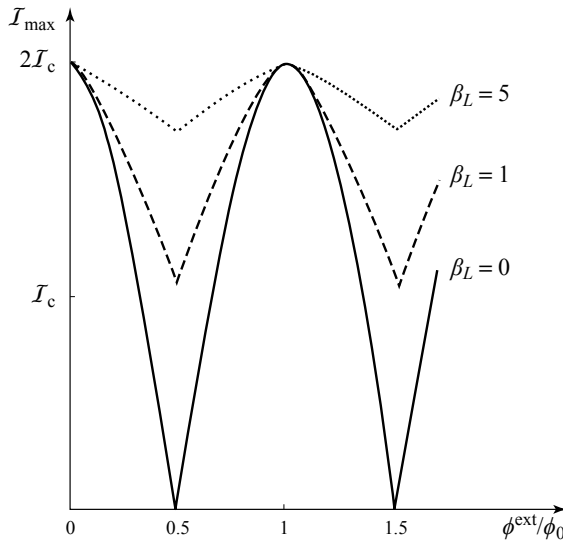


**Figure 11.20 - Maximum current transported by a DC-SQUID**

Theoretical value of the maximum current  $\mathcal{I}_{\max}$  that a DC-SQUID can carry without a potential difference between its leads. It is a periodic function (with period  $\phi_0$ ) of the external flux  $\phi^{\text{ext}}$  that threads it.  $\mathcal{I}_{\max}$  varies between a greatest value of  $2\mathcal{I}_c$  (for  $\phi^{\text{ext}} = n\phi_0$ ) and the smallest value (for  $\phi^{\text{ext}} = (n + \frac{1}{2})\phi_0$ ) that is a function of  $\beta_L$ . The smallest value is 0 for  $\beta_L = 0$  and it approaches  $2\mathcal{I}_c$  when  $\beta_L$  increases.

#### *Inductive DC-SQUID ( $\beta_L \neq 0$ )*

When the DC-SQUID is inductive, the flux  $\phi$  in relations (11.32) becomes

$$\phi = \phi^{\text{ext}} + (L_1 I_1 - L_2 I_2) \quad (11.35a)$$

where  $L_1$  and  $L_2$  are the inductances of each of the SQUID branches, so that when the two are symmetric ( $L_1 = L_2 = L/2$ )

$$(L_1 I_1 - L_2 I_2) = Li \quad (11.35b)$$

$\mathcal{I}_{\max}$  oscillates with the same period  $\phi_0$ , between the greatest value  $2\mathcal{I}_c$ , unchanged since it corresponds to  $i = 0$ , and the smallest value that becomes non-zero and increasingly large as  $\beta_L$  becomes larger (Fig. 11.20).

### 11.8.2 - DC-SQUID in the over-damped regime

In the general case, each of the JOSEPHSON junctions in the DC-SQUID can, according to the RCSJ model (see section 10.4.2), be modelled by a JOSEPHSON channel in parallel with a conductance  $G$  and a capacitance  $C$  (fig. 10.6). The DC-SQUID is then characterized by the screening parameter  $\beta_L$  of the circuit and the STEWART-MCCUMBER parameter  $\beta_c$  of the junctions (defined in Table 10.1).

When we are in the over-damped regime ( $\beta_c = 0$ ) and the injected current exceeds the value of  $I_{\max}(\phi^{\text{ext}})$  for a given flux  $\phi^{\text{ext}}$ , then from the relation (10.30b) the average voltage  $\langle V(\phi^{\text{ext}}) \rangle$  obeys

$$\langle V(\phi^{\text{ext}}) \rangle = \frac{1}{2G} \sqrt{I^2 - [I_{\max}(\phi^{\text{ext}})]^2} \quad (11.36)$$

as represented by the curves in Figure 11.21. They have been drawn for two values of  $\beta_L$  (0 and  $\pi$ ) and for several values of the external flux  $\phi^{\text{ext}} = (n + m)\phi_0$  where  $n$  is an integer and  $m$  is in the ranges  $0 \leq m \leq 0.5$ , with curves corresponding to  $m$  and  $1 - m$  coinciding.

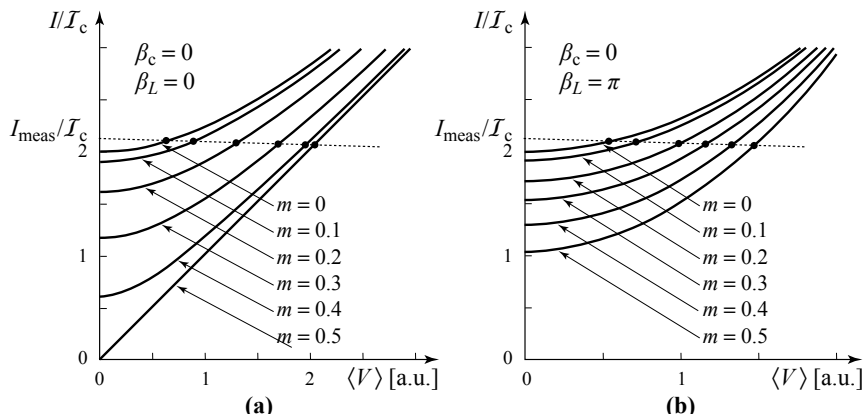


**Figure 11.21 - Average voltage  $\langle V \rangle$  at the leads of a DC SQUID in the over-damped regime as a function of the injected current  $I$**

Each figure presents a collection of curves corresponding to several values of  $m$  defining  $\phi^{\text{ext}} = (n + m)\phi_0$  where  $n$  is an integer and  $0 < m < 0.5$ . The curves with  $m$  replaced by  $(1 - m)$  would be identical. (a)  $\beta_L = 0$ . (b)  $\beta_L = \pi$ . Measurement of the voltage  $\langle V \rangle$  for a fixed value of  $I_{\text{meas}}$  slightly above  $2I_{\max}$  allows  $m$  to be determined, and thereby to count the number of fluxons crossing the SQUID.

### 11.8.3 - Reading a DC-SQUID

One piece of information provided by a DC-SQUID is, from relation (11.34), the maximum intensity  $I_{\max}$  of the current that can pass through the circuit crossed by a magnetic field flux  $\phi^{\text{ext}}$  before a potential difference appears in its leads. The measurement of  $\phi^{\text{ext}}$  can therefore proceed by the determination of  $I_{\max}$ .

In practice this method is difficult, since for each new determination of  $\phi^{\text{ext}}$ , the current intensity  $I$  must be increased from zero up to the value  $\mathcal{I}_{\max}(\phi^{\text{ext}})$  beyond which a voltage is detected in the leads of the DC-SQUID. In particular, if  $\phi^{\text{ext}}$  varies in time it will be necessary to make very rapid scans.

In fact it turns out to be much simpler to make the measurement of  $\phi^{\text{ext}}$  by working in the over-damped (non-hysteretic) mode and keeping the current intensity  $I$  at a value  $I_{\text{meas}}$  slightly above  $2\mathcal{I}_c$ . As can be seen in Figure 11.21a,  $\langle V \rangle$  is at fixed  $I = I_{\text{meas}}$ , different for each value of  $m$ . The measurement of  $\langle V(\phi^{\text{ext}}) \rangle$  for a value just above  $2\mathcal{I}_c$  avoids scanning in  $I$ , as was needed in the previous, more demanding, method that we just described.

#### 11.8.4 - 0- $\pi$ DC-SQUID

If the two junctions are  $\pi$ -type, the relations between intensities and phase changes previously expressed by (11.31) become:

$$I_1 = -\mathcal{I}_c \sin \Theta_{\text{EF}} \quad ; \quad I_2 = -\mathcal{I}_c \sin \Theta_{\text{HG}} \quad (11.37)$$

which, by applying the relations (11.28) to (11.30) leads to a simple change in the sign of  $I$  in (11.33), and therefore to an expression for  $\mathcal{I}_{\max}(\phi^{\text{ext}})$  identical to the relation (11.34).

When one of the junctions is of type 0 (EF) and the other  $\pi$  (HG) the relations between currents and phases become

$$I_1 = \mathcal{I}_c \sin \Theta_{\text{EF}} \quad ; \quad I_2 = -\mathcal{I}_c \sin \Theta_{\text{HG}}. \quad (11.38)$$

The equations (11.32) are transformed as

$$\frac{I}{2} + i = \mathcal{I}_c \sin \left[ \pi \left( s - \frac{\phi^{\text{ext}}}{\phi_0} \right) + \Theta_0 \right] \quad (11.39a)$$

$$\frac{I}{2} - i = +\mathcal{I}_c \sin \left[ \pi \left( s - \frac{\phi^{\text{ext}}}{\phi_0} \right) - \Theta_0 \right] \quad (11.39b)$$

leading to

$$I = 2\mathcal{I}_c \sin \left[ \pi \left( s - \frac{\phi^{\text{ext}}}{\phi_0} \right) \right] \cos \Theta_0 \quad (11.40)$$

and a maximum current

$$I_{\max}(\phi^{\text{ext}}) = 2\mathcal{I}_c \left| \sin \left[ \pi \left( s - \frac{\phi^{\text{ext}}}{\phi_0} \right) \right] \right| \quad (11.41)$$

shifted by a half-fluxon compared to a DC-SQUID with identical junctions.

An excellent demonstration of this behavior was given by W. GUICHARD *et al.*<sup>3</sup> (Fig. 11.22), who showed that the intensities  $\mathcal{I}_{\max}$  of DC-SQUIDs with two

<sup>3</sup> W. GUICHARD *et al.* (2003) *Phys. Rev. Lett.* **90**, 167001.

identical junctions (either 0 or  $\pi$ ) superimpose, while the intensity of a DC-SQUID with two different junctions has the same amplitude but is shifted by a half-fluxon.

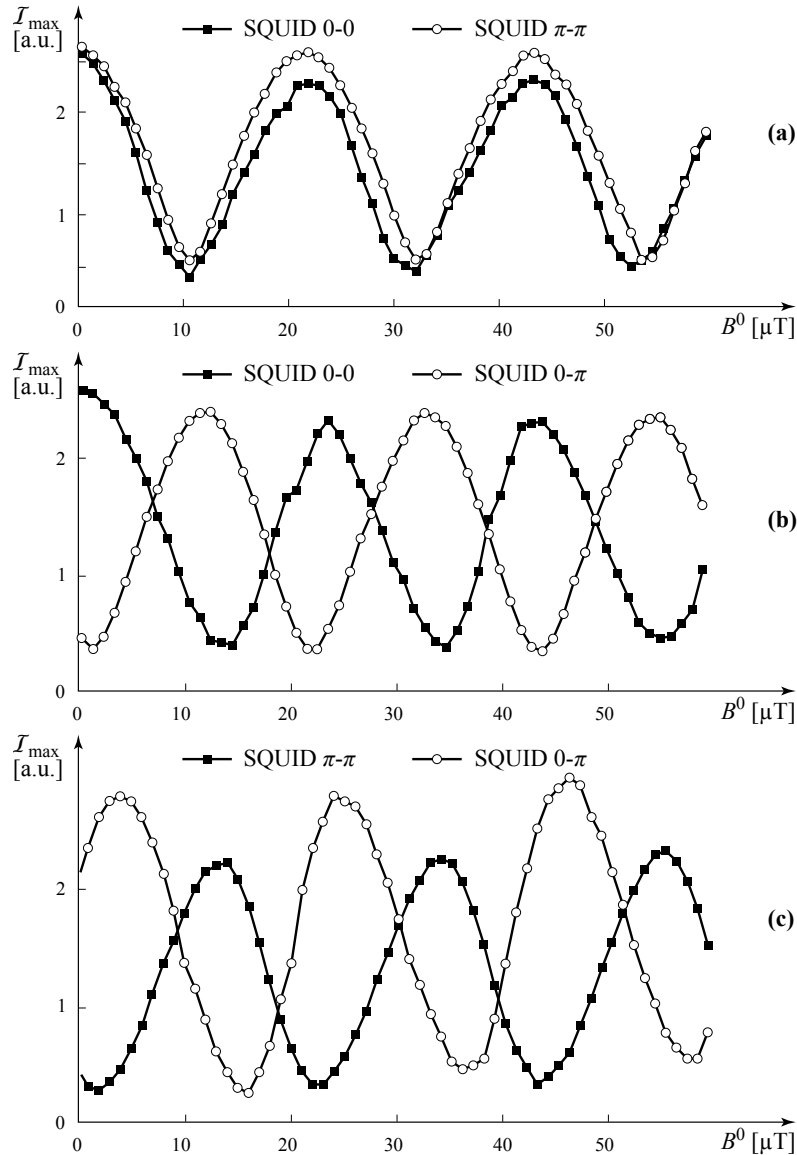


**Figure 11.22 - Maximum currents  $I_{\max}$  in DC-SQUID circuits for homo- and hetero-junctions as a function of applied field**

(a) The currents  $I_{\max}$  of DC-SQUID homo-junctions (0-0) or ( $\pi$ - $\pi$ ) with identical circuits can be superimposed (up to technical difficulties). (b) (c) The currents  $I_{\max}$  of hetero-junctions DC-SQUID (0- $\pi$ ) are opposite in phase compared to those of SQUID homo-junctions with otherwise identical circuits. [From W. GUICHARD *et al.*, 2003, © The American Physical Society, with permission]<sup>3</sup>

## Chapter 12

### JOSEPHSON JUNCTIONS IN A MAGNETIC FIELD

After the introduction to the JOSEPHSON junction (Chap. 10) and the presentation of its role in SQUIDs (Chap. 11), this chapter introduces effects resulting from application of a magnetic field  $\mathbf{B}^{\text{ext}}$  to the junction itself.<sup>1</sup>

In the following, we will consider SIS junctions whose insulating layers are parallelepipeds of length  $a$ , width  $c$  and thickness  $d$ . In all the devices, the current crosses the insulating layer perpendicularly to the  $ac$  plane *i.e.* in the  $d$  direction, and the external field  $\mathbf{B}^{\text{ext}}$  is applied along its width, *i.e.* in the  $c$  direction (Fig. 12.1a). By extension, the parameters  $d$ ,  $c$  and  $a$  of the insulating layers will be referred as the thickness, the width and the length of the JOSEPHSON junctions.

In practice, the insulating layer can be inserted between two superconductors  $S_1$  and  $S_2$ , with different geometry. Among them are the grain boundary geometry (Fig. 12.1b) or the inline geometry (Fig. 12.1c).

The length  $a$  of the junction is the relevant parameter that distinguishes two situations depending on its value compared to the so-called “JOSEPHSON penetration depth  $\Lambda_J$ ” (ranging from 10  $\mu\text{m}$  to 1 mm), which will appear in more precise form in the general analysis.

If  $a$  is much less than  $\Lambda_J$ , the JOSEPHSON junction is said to be “short.” The magnetic field in the insulating layer can be considered as uniformly equal to the external field  $B^{\text{ext}}$  applied on and around the junction, and the JOSEPHSON current as simply superimposed onto the screening currents.

If  $a$  is equal to or larger than  $\Lambda_J$ , the JOSEPHSON junction is said to be “long.” No longer is the magnetic field uniform inside the junction. The screening currents and the JOSEPHSON current now cannot be treated separately.

In the following, we first consider the behavior of a short JOSEPHSON junction before examining the general case, from which the definition of the JOSEPHSON penetration depth  $\Lambda_J$  will emerge naturally. For simplicity, except in section 12.6, we only consider the grain boundary junction of figure 12.1b.

---

<sup>1</sup> A. BARONE and G. PATERNÒ (1982) *Physics and Applications of the JOSEPHSON Effect*, Chapters 4 & 5, John Wiley, New York.

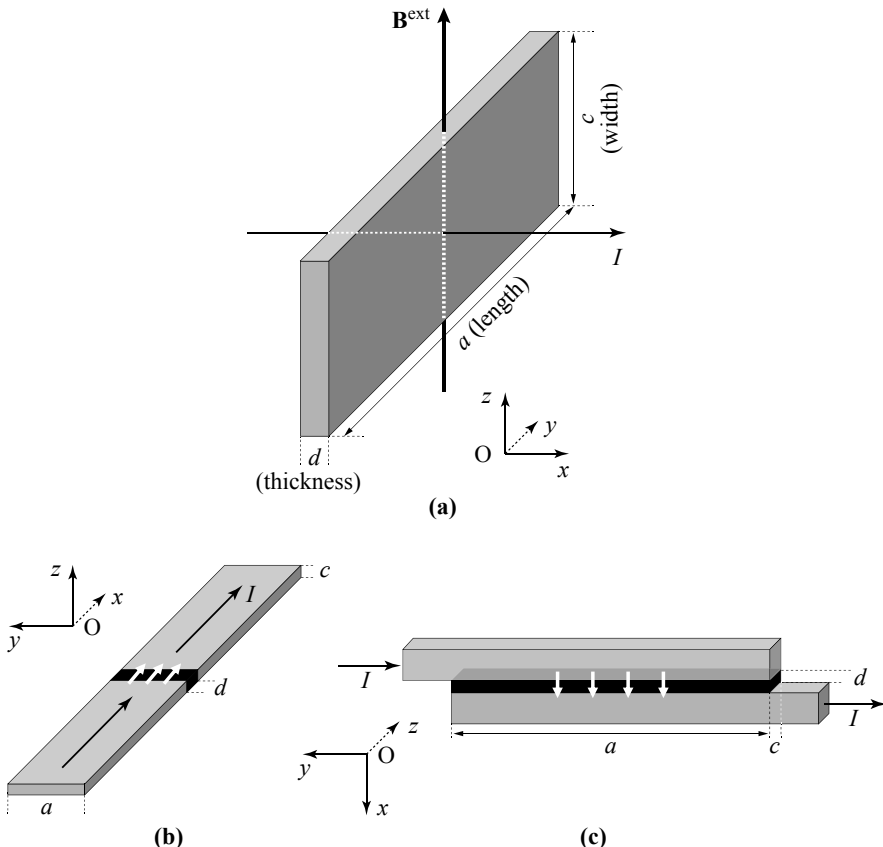


**Figure 12.1 - Various SIS JOSEPHSON junctions**

(a) Geometry of the insulating layer common to all SIS JOSEPHSON junctions. It is a parallelepiped of length  $a$ , width  $c$  and thickness  $d$ . The current flows in the direction of  $d$  and the magnetic field  $\mathbf{B}^{\text{ext}}$  is applied along the width of the layer. (b) Grain boundary JOSEPHSON junction. (c) In-line JOSEPHSON junction.

## 12.1 - Magnetic field on a short JOSEPHSON junction

In such a short junction, the magnetic field inside the insulating layer is simply the field  $\mathbf{B}^{\text{ext}}$  applied on and immediately around the junction. Damped by the screening current, the field decreases exponentially from each side of the insulating layer towards the superconducting parts, with respective penetration depths  $\lambda_1$  and  $\lambda_2$ , (see Figs 12.2 and 12.3a). Provided the length  $a$  of the junction is much greater than the penetration depths of the magnetic field ( $a \gg \lambda_1, \lambda_2$ ) (although still much less than the JOSEPHSON penetration depth), boundary effects near  $y = \pm a/2$  will be negligibly small.

In the coordinate system  $(x,y,z)$  of Figure 12.2, the magnetic field  $\mathbf{B}$  and the screening current density  $\mathbf{j}^{\text{scr}}$  on each side of the insulating layer depend only on  $x$ , and are oriented in the  $z$  (Fig. 12.3b) and  $y$  directions (Fig. 12.3c) respectively.

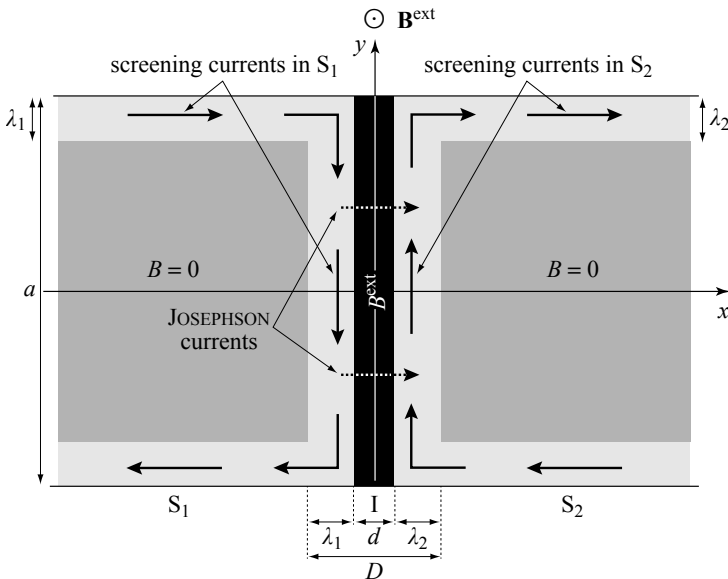


**Figure 12.2 - Magnetic field and screening currents in a short JOSEPHSON junction**

The external field penetrates uniformly into the insulating layer (in black) and, because of screening currents, decreases exponentially in the two superconductors situated at either side, as seen in Fig. 12.3).

For practical reasons, we take the origin of the vector potential  $\mathbf{A}$  at the middle of the insulating layer. Oriented in the  $y$  direction, it is related to the magnetic field by

$$B_z(x) = \frac{\partial A_y(x)}{\partial x} \quad \text{and} \quad A_y(x) = \int_0^x B_z(u) du. \quad (12.1)$$

As shown in figure 12.3d, it varies linearly in the insulating layer. Beyond the LONDON penetration depths ( $|x| \gg \lambda_1, \lambda_2$ ) it tends to the asymptotic values

$$\begin{aligned} A_{y\infty}(S_1) &= -(d/2 + \lambda_1) B^{\text{ext}} \\ A_{y\infty}(S_2) &= (d/2 + \lambda_2) B^{\text{ext}}. \end{aligned} \quad (12.2)$$

## 12.2 - Current in a short JOSEPHSON junction under a magnetic field

In the absence of a magnetic field, the current intensity across the junction obeys the JOSEPHSON equation

$$I = I_c \sin(\theta_1 - \theta_2) \quad (12.3a)$$

where  $\theta_1$  and  $\theta_2$  are the phases of the wave functions of each superconducting block.

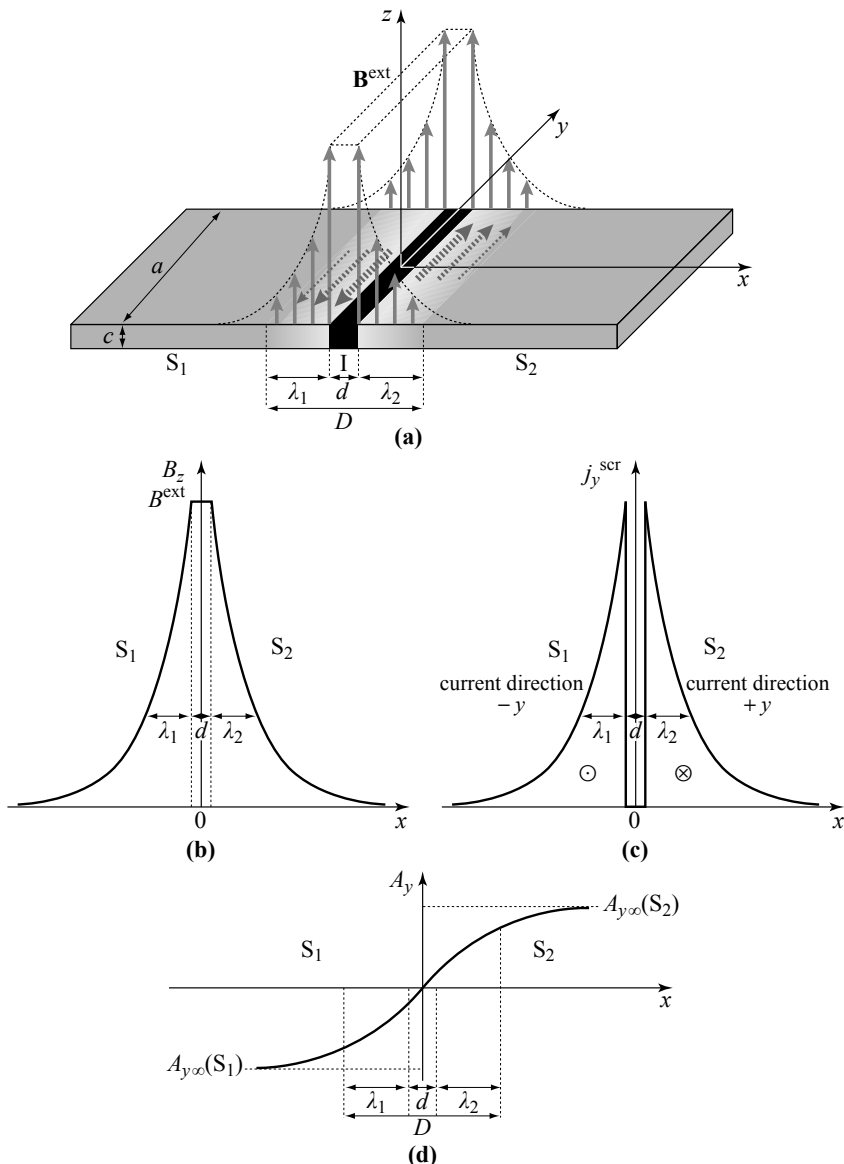


**Figure 12.3 - Magnetic field, vector potential and current density within a short JOSEPHSON junction ( $a \ll A_J$ )**

In the short junction, an external magnetic field oriented in the  $z$  direction penetrates uniformly into the insulator and persists into the superconductor over the LONDON penetration depths. Screening currents flowing in the  $y$  direction, (dotted arrows), accompany the decrease of the magnetic field in the superconductors.  $D$  is the magnetic thickness. (a) Overall view of the magnetic field profile and the screening current. Profiles of (b) the magnetic field, (c) the screening currents and (d) the vector potential.

As far as the phases are uniform in each block, the current density is distributed uniformly across the insulating layer according to

$$j = j_c \sin(\theta_1 - \theta_2) \quad (12.3b)$$

with

$$j_c = \frac{I_c}{ac} \quad (12.4)$$

where  $c$  is the width of the junction (see Fig. 12.1) and  $j_c$  its critical current density.

The aim of the following discussion is to show that when the junction is placed in an uniform magnetic field, the phase difference  $\Theta(y) = \theta_1(y) - \theta_2(y)$  between two points situated on opposite sides of the insulating layer *varies in the y direction* and that as a result, the current density across the junction is no longer uniform. As mentioned in the introduction for this case of a short barrier, we will assume that the JOSEPHSON current density  $\mathbf{j}^J$  flowing across the barrier is weak enough not to modify the screening currents  $\mathbf{j}^{scr}$  that protect the superconducting regions from magnetic field penetration.

We then consider (see Fig. 12.4), points C and D on one side, and E and F on the other side of the insulating layer. The points C and D are on the  $x$  axis ( $y = 0$ ) while E and F have coordinate  $y$ . The points C', D', E', F' have the same  $y$ -coordinates but are sufficiently distant from the insulating layer that the screening current vanishes at each of them, and that the vector potential has reached its asymptotic values  $A_{y\infty}$ .

The JOSEPHSON current densities that cross the insulating layer between points C and D, or between F and E, are determined by the JOSEPHSON equation

$$\int_{C \rightarrow D}^J = j_x(0) = j_c \sin \Theta(0) \quad \text{with } \Theta(0) = \theta_C - \theta_D \quad (12.5a)$$

$$\int_{F \rightarrow E}^J = j_x(y) = j_c \sin \Theta(y) \quad \text{with } \Theta(y) = \theta_F - \theta_E \quad (12.5b)$$

and the phase differences are connected by the relation

$$\theta_F - \theta_E = \begin{cases} (\theta_F - \theta_{F'}) + (\theta_{F'} - \theta_{C'}) + (\theta_{C'} - \theta_C) + (\theta_C - \theta_D) \\ + (\theta_D - \theta_{D'}) + (\theta_{D'} - \theta_{E'}) + (\theta_{E'} - \theta_E) \end{cases} \quad (12.6)$$

where:

» the phase difference between two points situated on the same side of the barrier and with the same  $y$  coordinate, such as DD' (but also CC', EE', and FF') is, according to (9.11),

$$\theta_D - \theta_{D'} = \frac{m_p}{n_p q_p \hbar} \int_{D'}^D \mathbf{j}^{scr} \cdot d\mathbf{l} + \frac{q_p}{\hbar} \int_{D'}^D \mathbf{A} \cdot d\mathbf{l} = 0 \quad (12.7)$$

since both the screening current  $\mathbf{j}^{scr}$  and the vector potential  $\mathbf{A}$  point along the  $y$  direction, *i.e.* are perpendicular to the path D'D;

» the phase differences between points D' and E', or between points F' and C', where the screening currents are zero, reduce the circulation to that of  $\mathbf{A}$  between these points. As we are in a region where the vector potential has reached its asymptotic values, they can be written simply as

$$\theta_{D'} - \theta_{E'} = \frac{q_p}{\hbar} \int_{E'}^D \mathbf{A} \cdot d\mathbf{l} = -\frac{q_p}{\hbar} y A_{y\infty}(S_2) \quad (12.8)$$

$$\theta_{F'} - \theta_{C'} = \frac{q_p}{\hbar} \int_{C'}^{F'} \mathbf{A} \cdot d\mathbf{l} = \frac{q_p}{\hbar} y A_{y\infty}(S_1). \quad (12.9)$$

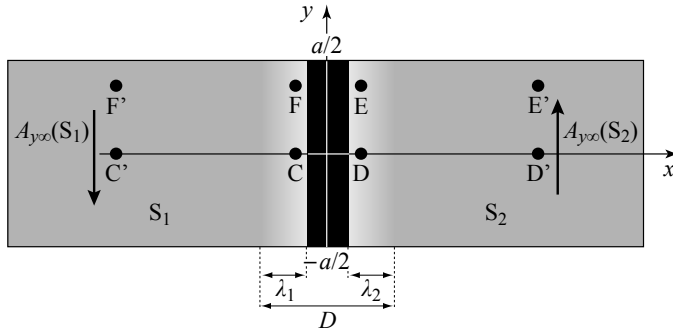


**Figure 12.4 - Points of reference for the junction**

C and D are directly opposite each other across the insulating layer with ordinate 0, as are F and E but with ordinate  $y$ . Each point C', D', E' or F' is located at the same  $y$  coordinate as C, D, E or F, respectively, but is well beyond the LONDON penetration depth, in a region of zero magnetic field and current.

Therefore, since the circulation of the screening current density over the whole circuit C'D'E'F' vanishes, and since from relation (12.2), that of  $\mathbf{A}$  is simply

$$\frac{q_p}{\hbar} \oint \mathbf{A} \cdot d\mathbf{l} = -\frac{q_p}{\hbar} B^{\text{ext}} (\lambda_1 + \lambda_2 + d) y \quad (12.10)$$

the phase difference (12.6) between points situated on each side of the insulator at ordinate  $y$  reduces to

$$\Theta(y) = \Theta(0) + \frac{2\pi}{\phi_0} B^{\text{ext}} D y \quad (12.11)$$

where

$$D = d + \lambda_1 + \lambda_2 \quad (12.12)$$

appears as an effective thickness, in the sense that in the calculation we could have taken  $B^{\text{ext}}$  as a uniform value for the magnetic field across it.  $D$  is called the “magnetic thickness” of the junction.

We call  $\phi_J$  the flux of the magnetic field that crosses the whole of the junction from  $-a/2$  to  $+a/2$ , i.e. the insulating layer plus the LONDON regions that develop on each side (see Fig. 12.4),

$$\phi_J = B^{\text{ext}} Da. \quad (12.13)$$

The expression for the phase difference at ordinate  $y$  then becomes

$$\Theta(y) = \Theta(0) + 2\pi \frac{\phi_J}{\phi_0} \frac{y}{a} \quad (12.14)$$

and the JOSEPHSON current density crossing the barrier at ordinate  $y$  (relation 10.14) can be written

$$j_x^J(y) = j_c \sin \Theta(y) = j_c \sin \left[ \Theta(0) + 2\pi \frac{\phi_J}{\phi_0} \frac{y}{a} \right]. \quad (12.15)$$

The total intensity of the JOSEPHSON current crossing the insulating barrier can be obtained by integrating the current density over the whole cross-section

$$I = c j_c \int_{-a/2}^{a/2} \sin \Theta(y) dy = \left[ I_c \sin \left( \pi \frac{\phi_J}{\phi_0} \right) \right] / \pi \frac{\phi_J}{\phi_0} \sin \Theta(0). \quad (12.16)$$

This means that for a given magnetic flux  $\phi_J$ , the junction can adjust its phase  $\Theta(0)$  in order to transport, in either direction, any value of the current intensity lying between 0 and an upper limit  $I_{\max}$  given by

$$I_{\max}(\phi_J) = I_c \left| \sin \left( \pi \frac{\phi_J}{\phi_0} \right) \right| / \pi \frac{\phi_J}{\phi_0}. \quad (12.17)$$

Except for zero field, where it takes its greatest value, the intensity  $I_{\max}$  reduces to zero for field fluxes  $\phi_J$  equal to an integer number of fluxons. We remark that the profile of  $I_{\max}$  in Figure 12.5 is formally identical to the diffraction figure of light by a slit under the FRAUNHOFER conditions (parallel incident beam and screen infinitely distant).

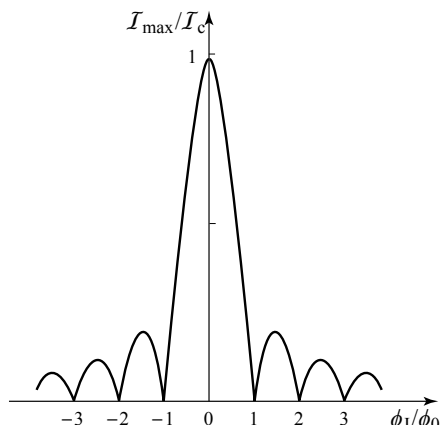


**Figure 12.5**  
Maximum intensity that can be borne  
by a short JOSEPHSON junction  
subject to a magnetic field

The profile of  $I_{\max}$  resembles a diffraction pattern of light by a slit under the FRAUNHOFER conditions. Except at the origin,  $I_{\max}$  is zero for flux values  $\phi_J$  equal to an integer number of fluxons.

Qualitatively, the occurrence of a variation of the maximum intensity as a function of external field in agreement with the FRAUNHOFER diffraction pattern is the signature of the quality of a JOSEPHSON junction, in particular that it is uniform over its entire length.

Current density profiles crossing the barrier and corresponding to different values of  $\phi_j$  are represented in Figure 12.6.

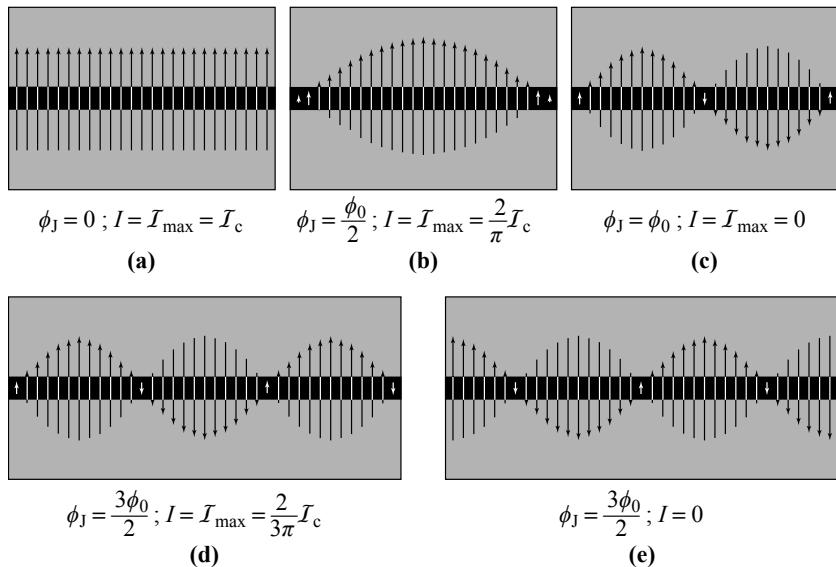


**Figure 12.6 - Profiles of the JOSEPHSON current density across the insulating layer of a short JOSEPHSON junction subject to magnetic field  $B$**   
**(a, b, c, d)** distribution of the JOSEPHSON current across the insulator when the intensity takes its maximum possible value  $I_{\max}$  compatible with four different values for  $\phi_J$ .  
**(d, e)** for the same value of  $\phi_J$  the junction “adjusts” the phase  $\Theta(0)$  to the current intensity  $I$  that is injected: the maximum intensity for **(d)**, or zero for **(e)**.

- » They are sinusoidal (see eq. 12.15) with the number of periods equal to the number of fluxons (whether or not it is integer) that  $\phi_1$  contains. The periodicity is

$$Y = a \frac{\phi_0}{\phi_1} \quad (12.18)$$

- » The magnetic field flux threading a circuit of length  $Y$  (in the  $y$ -direction) and closed beyond the LONDON currents (Fig. 12.7) is one fluxon since by combining (12.13) and (12.18) we find

$$YDB^{\text{ext}} = \phi_0. \quad (12.19)$$

- » Within the limits  $-\mathcal{I}_{\max} < I < \mathcal{I}_{\max}$ , the junction “adjusts”  $\Theta(0)$  to the intensity of the applied current. As illustrated in Figure 12.6 (**d** and **e**), this translates into a

shift of the profile of the JOSEPHSON current density since for the same number of fluxons and therefore of periods, the intensity vanishes in (e) whereas it is a maximum in (d).

- » When  $\phi_J$  is an integer (non-zero) number of fluxons, shifting the current density has no effect and the intensity always vanishes:  $I_{\max}(\phi_J = n\phi_0) = 0$ .

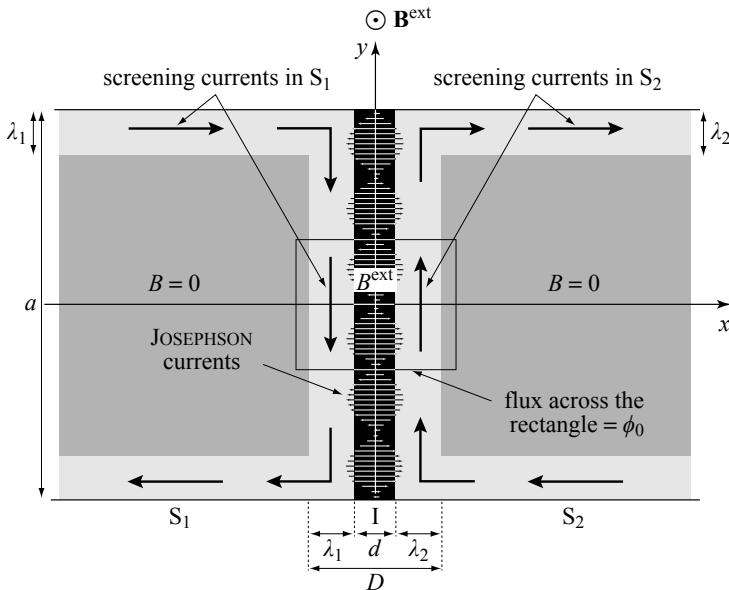


**Figure 12.7 - Screening currents and JOSEPHSON currents in a short junction**

In the treatment of the short junction, the screening currents in the superconducting components are dissociated from the JOSEPHSON currents, that are treated as a first-order perturbation. The magnetic field flux through the rectangle shown, whose length in the  $y$  direction is the periodicity of the current, and which closes far inside the superconducting blocks, equals  $\phi_0$ .

### 12.3 - Short 0- $\pi$ junction in a magnetic field

From the definition (in section 10.8) of a  $\pi$  junction, we can derive the expression for the current intensity that crosses it from the relation (12.16), by simply changing  $I_c$  into  $-I_c$ . Therefore, for a  $\pi$  junction subject to a magnetic field we can write

$$I = \left[ -I_c \sin\left(\pi \frac{\phi_J}{\phi_0}\right) \middle/ \pi \frac{\phi_J}{\phi_0} \right] \sin\Theta(0) \quad (12.20)$$

which means that 0 and  $\pi$  junctions cannot be distinguished experimentally by measuring the maximum current intensity. Indeed the phase  $\Theta(0)$  entering the relations (12.16) and (12.20) can, for each value of  $\phi_J$ , adjust itself to allow any current between the same extrema  $\pm I_{\max}(\phi_J)$  given by the relation (12.17).

More spectacular effects appear with hybrid junctions that are partially 0 and  $\pi$ , as for example a 0- $\pi$  junction, *i.e.* of type 0 over half its length and of type  $\pi$  over the other half (Fig. 12.8). Such a junction can be obtained by inserting as a barrier between the superconducting blocks, ferromagnetic layers with appropriate thicknesses over each section (see section 10.8.2 and Fig. 12.10a).

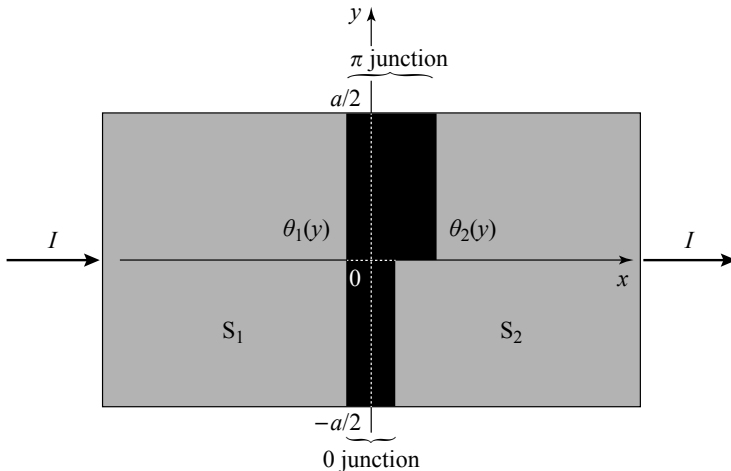


**Figure 12.8 - A 0- $\pi$  hybrid JOSEPHSON junction**

A 0- $\pi$ junction is of type 0 over half its length,  $-a/2 < y < 0$ , and of type  $\pi$  over the other half  $0 < y < a/2$ . Such a junction can be constructed by choosing the appropriate thicknesses of the ferromagnetic layers for each part.

The JOSEPHSON current density across the insulating layer as we move along the  $y$  axis is then:

$$\text{» for } -\frac{a}{2} < y < 0 \quad j_x^J = +j_c \sin[\theta_1(y) - \theta_2(y)], \quad (12.21a)$$

$$\text{» for } 0 < y < \frac{a}{2} \quad j_x^J = -j_c \sin[\theta_1(y) - \theta_2(y)] \quad (12.21b)$$

and the total current across the junction is obtained by integrating the current density over the whole cross-section

$$I^{[0-\pi]} = c \left( \int_{-a/2}^0 j_c \sin \Theta(y) dy - \int_0^{a/2} j_c \sin \Theta(y) dy \right) \quad (12.22)$$

which leads to

$$I^{[0-\pi]} = -I_c \frac{\sin^2 \left( \frac{\pi}{2} \frac{\phi_J}{\phi_0} \right)}{\frac{\pi}{2} \frac{\phi_J}{\phi_0}} \cos \Theta(0) \quad (12.23)$$

and thus a maximum current

$$I_{\max}^{[0-\pi]}(\phi_J) = I_c Z\left(\frac{\pi}{2} \frac{\phi_J}{\phi_0}\right) \quad (12.24a)$$

with

$$Z(w) = \frac{\sin^2 w}{|w|}. \quad (12.24b)$$

The function  $Z(w)$  is zero at the origin and has two principal maxima for arguments  $w \approx \pm 0.73$  where it has the value  $\approx 0.725$ . It then vanishes when  $w = 2n\pi$  and shows secondary local maxima near  $w \approx 2(n+1)\pi$  (Fig. 12.9).

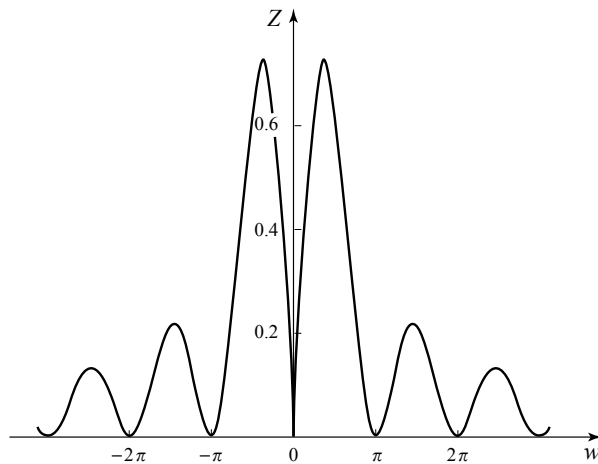


**Figure 12.9 - Graphical representation of the function  $Z(w) = \sin^2 w / |w|$**

The function  $Z(w)$  is zero at  $w = 0$ , has two principal maxima of height  $= 0.725$  near  $\pm 0.73$ , and is zero when  $w = 2n\pi$ .

This behavior has been shown experimentally by WEIDES *et al.*<sup>2</sup> for junctions of Nb/Al/Al<sub>2</sub>O<sub>3</sub>/Ni<sub>60</sub>Cu<sub>40</sub>/Nb where the borderline between 0 and  $\pi$  is situated at the thickness of the ferromagnetic NiCu layer of 5.2 nm and which shows the same values of critical current densities for layer thicknesses of  $d^{(0)} = 5$  nm and  $d^{(\pi)} = 5.5$  nm (Fig. 12.10a). The measured currents  $I_{\max}$  of a 0 junction, a  $\pi$  junction and finally a 0- $\pi$  junction, all with the same geometry (Fig. 12.10b) display behavior consistent with the predictions of relations (12.17) and (12.24). As well as the positions of the maxima and minima, the relative intensities  $I_{\max}$  of the 0 and  $\pi$  junctions on the one hand and the 0- $\pi$  on the other are as expected. In particular the ratio between the intensity of the two principal peaks of the 0- $\pi$  junction and the central peak of the 0 or  $\pi$  junctions is close to 0.725.

2 M. WEIDES *et al.* (2006) *Phys. Rev. Lett.* **97**, 247001.

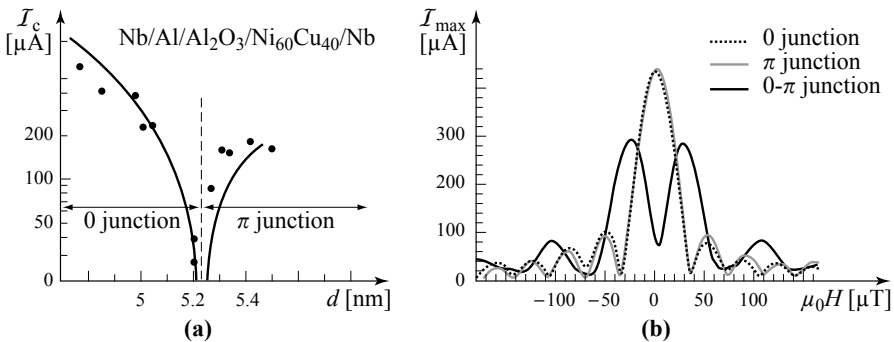


**Figure 12.10 - Critical current  $I_c$  of a  $0-\pi$  junction**

(a) The type and critical current of a  $\text{Nb}/\text{Al}/\text{Al}_2\text{O}_3/\text{Ni}_{60}\text{Cu}_{40}/\text{Nb}$  junction at  $T = 2.65 \text{ K}$  as a function of the thickness  $d$  of the ferromagnetic layer (b) Maximal intensities in JOSEPHSON junctions that are purely of type 0 (5 nm), purely  $\pi$  ( $d = 5.5 \text{ nm}$ ) and  $0-\pi$ . [From WEIDES *et al.*, 2006, © The American Physical Society, with permission].<sup>1</sup>

Measurements made on triple junctions of type  $0/\pi/0$  or periodic junctions  $0/\pi/0/\pi/0/\pi$  confirm this analysis.<sup>3</sup>

## 12.4 - Introduction to the JOSEPHSON penetration depth

In all of the preceding discussion we assumed that the JOSEPHSON current did not perturb the screening currents flowing on each side of the junction. Neither did it modify the magnetic field inside the insulating layer, which remained equal to  $B^{\text{ext}}$ . In fact, when the junction ceases to be short, this is no longer true. The JOSEPHSON current crosses a longer insulating section and the magnetic field it creates is no longer negligible compared to  $B^{\text{ext}}$ . The local magnetic field in the insulating layer deviates from  $B^{\text{ext}}$  and it is no longer valid to treat the screening currents and the JOSEPHSON currents separately.

### 12.4.1 - General equations

Consider now the magnetic field  $B_z(y)$ , the current density  $j_x(y)$  at position  $y$  of the insulating layer, and the phase difference  $\Theta(y)$  between points on each side of the insulator for the same value of  $y$ . These quantities are related to one another by three equations:

» the JOSEPHSON equation

$$j_x(y) = j_c \sin \Theta(y); \quad (12.25)$$

» an equation derived from the relation (12.11), giving the variation of  $\Theta$  as a function of  $y$  when the field in the center of the insulator is  $B(y)$  instead of  $B^{\text{ext}}$

<sup>3</sup> C. GÜRLICH *et al.* (2010) *Phys. Rev. B* **81**, 094502.

$$\frac{\partial \Theta(y)}{\partial y} = \frac{2\pi}{\phi_0} B_z(y) D; \quad (12.26)$$

» the MAXWELL's equation that relates the magnetic field to the current density

$$\frac{\partial B_z(y)}{\partial y} = \mu_0 j_x(y). \quad (12.27)$$

Combining the three leads to the equation of FERRELL and PRANGE<sup>4</sup>

$$\frac{\partial^2 \Theta(y)}{\partial y^2} = \frac{\sin \Theta(y)}{\Lambda_J^2} \quad (12.28)$$

where  $\Lambda_J = \sqrt{\frac{\phi_0}{2\pi \mu_0 D j_c}}$  or  $2\mu_0 \Lambda_J f_c = \frac{\phi_0}{\pi D \Lambda_J}$ . (12.29)

$\Lambda_J$  is on a scale of millimeters, much greater than the LONDON penetration depth since with  $D \approx 50$  nm, it is of order 0.2 mm for  $j_c = 10$  A cm<sup>-2</sup> and 0.02 mm for  $j_c = 1000$  A cm<sup>-2</sup>.

#### 12.4.2 - Behavior in very weak fields

When  $\Theta$  is small,  $\sin \Theta \approx \Theta$  and equation (12.29) becomes

$$\frac{\partial^2 \Theta(y)}{\partial y^2} = \frac{\Theta(y)}{\Lambda_J^2} \quad (12.30)$$

that, using (12.27) and (12.28), leads to

$$\frac{\partial^2 j_x(y)}{\partial y^2} = \frac{j_x(y)}{\Lambda_J^2} \quad (12.31a)$$

$$\frac{\partial^2 B_z(y)}{\partial y^2} = \frac{B_z(y)}{\Lambda_J^2}. \quad (12.31b)$$

These expressions are similar to equations (2.27), the only difference being substitution of the JOSEPHSON penetration depth  $\Lambda_J$  for the LONDON penetration depth  $\lambda_L$ . With the same equations and similar boundary conditions

$$B_z\left(\frac{a}{2}\right) = B_z\left(-\frac{a}{2}\right) = B^{\text{ext}} \quad (12.32)$$

the profiles of magnetic field and the current density within the insulating layer placed in an external field (Fig. 12.11) are identical to those found for a layer subjected to an applied field (section 2.4.4, eq. 2.28) namely,

---

<sup>4</sup> R.A. FERRELL & R.E. PRANGE (1963) *Phys. Rev. Lett.* **10**, 479.

$$B_z(y) = B^{\text{ext}} \frac{\cosh\left(\frac{y}{\Lambda_J}\right)}{\cosh\left(\frac{a}{2\Lambda_J}\right)} ; \quad j_x(y) = \frac{B^{\text{ext}}}{\mu_0 \Lambda_J} \frac{\sinh\left(\frac{y}{\Lambda_J}\right)}{\sinh\left(\frac{a}{2\Lambda_J}\right)}. \quad (12.33)$$

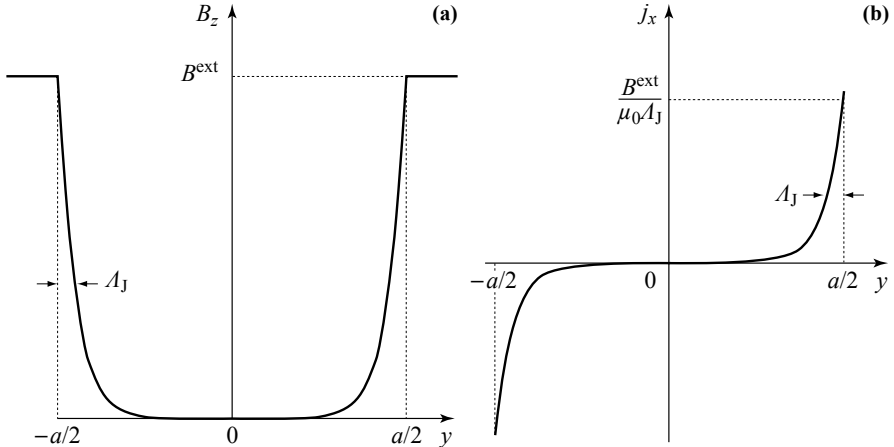


**Figure 12.11 - Magnetic fields and current densities within the insulating layer of a long JOSEPHSON junction subject to a small external field  $B^{\text{ext}}$**

The magnetic field and screening current decrease exponentially over the JOSEPHSON penetration depth  $\Lambda_J$ .

#### Case of a long junction

When  $a \gg \Lambda_J$  (Fig. 12.11a), the magnetic field and the current density in the insulating layer decrease exponentially starting from the lateral surfaces ( $y = \pm a/2$ ) over the characteristic length  $\Lambda_J$ :

$$B_z(u) = B^{\text{ext}} e^{-\frac{u}{\Lambda_J}} ; \quad j_x(u) = \pm \frac{B^{\text{ext}}}{\mu_0 \Lambda_J} e^{-\frac{u}{\Lambda_J}} \quad (12.34)$$

where  $u$  is the distance measured from the edge of junction ( $a/2$  or  $-a/2$ ). The current density  $j_x(u)$  then appears as a screening current for the magnetic field in the insulator.

So in weak fields the LONDON currents that develop laterally, over thicknesses of  $\lambda_1$  and  $\lambda_2$ , to screen the core of the superconducting material extend as JOSEPHSON currents that are localized at the edges of the junction. We then have the configuration of Figure 12.12: the screening currents that are concentrated over a length  $\lambda_1$  in the upper part of the first block spread out over a length  $\Lambda_J$  of the junction before becoming more concentrated within the second block over a length  $\lambda_2$ . The currents flow back in the lower part in the opposite sense.  $\Lambda_J$ , which appears as the

penetration depth of the magnetic field in the insulating layer, is called the “JOSEPHSON penetration depth.”

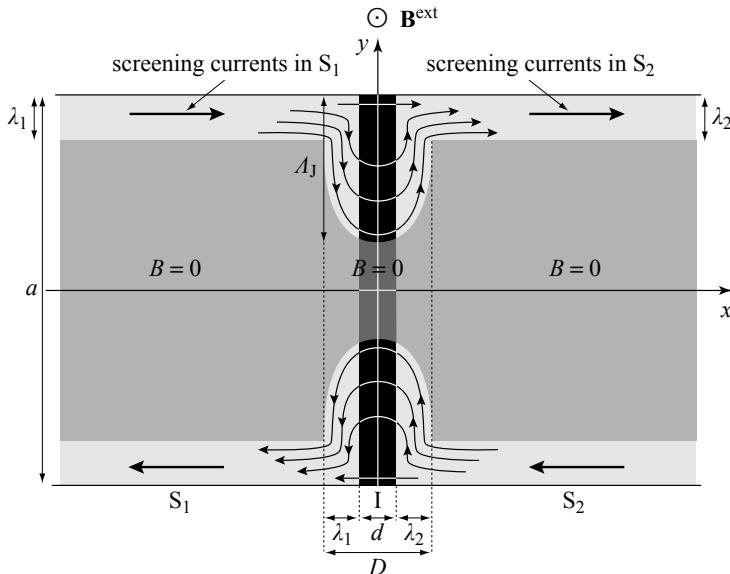


**Figure 12.12 - Penetration of the magnetic field within a long JOSEPHSON junction in the MEISSNER regime**

The screening currents localized over penetration depths  $\lambda_1$  and  $\lambda_2$  in the superconductors spread out in the junction over the JOSEPHSON penetration depth  $A_J$ . This has the effect of screening the magnetic field not only in the superconducting blocks, but also within the insulating layer ( $d \ll \lambda \ll A_J$ ). The magnetic field penetrates laterally into the superconductors over lengths  $\lambda_1$  and  $\lambda_2$ , and in the insulator over a distance  $A_J$ .

### Critical magnetic field

Since the current density is greatest in the immediate proximity of the surface and since it cannot exceed the critical current density  $j_c$  of the junction, the highest external magnetic field that can be screened is

$$B_{cJ}^* = \mu_0 j_c A_J = \frac{\phi_0}{2\pi A_J D}. \quad (12.35)$$

It remains for us to see whether this last relation is compatible with the assumption of small  $\Theta$  that lead to equations (12.31). According to (12.25), the phase difference  $\Theta$  takes its maximum value at  $y = \pm a/2$ , with a value obtained by integrating equation (12.27). As  $B$  vanishes after a few times the JOSEPHSON penetration depth, it can be written

$$\Theta(y = a/2) = \frac{2\pi D}{\phi_0} \int_0^\infty B(u) du = \frac{2\pi D A_J}{\phi_0} B^{\text{ext}}. \quad (12.36)$$

This equals 1 when  $B^{\text{ext}} = B_{\text{cJ}}^*$ , which is beyond the validity of the approximation  $\sin \Theta \approx \Theta$  that allowed equation (12.30) to be derived, so that the exponential profiles of  $B_z(y)$  and  $j_x(y)$  are valid only if  $B^{\text{ext}}$  is a small fraction of  $B_{\text{cJ}}^*$ . We shall return to this issue in section 12.5.

### ***Limiting case of a short junction***

When  $a \ll \Lambda_J$ , we are in a situation formally similar to that of a very thin slab described in Chapter 2: the magnetic field penetrates into the whole junction (Fig. 12.13a, see also Fig. 2.6) and the current density (screening current for the insulating layer) that crosses the junction is insignificant (Fig. 12.13b). This is the hypothesis we formulated initially to treat the short junction.

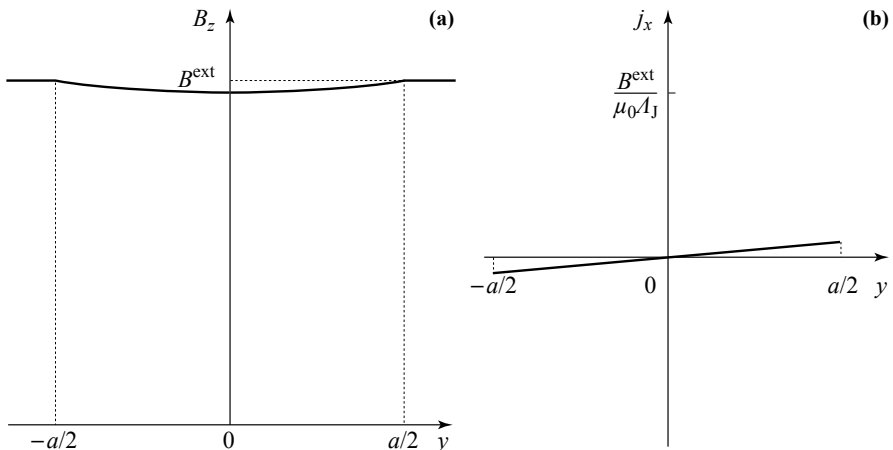


**Figure 12.13 - Magnetic field and current density within a short JOSEPHSON**

**junction ( $a \ll \Lambda_J$ ) subject to a weak external field  $B^{\text{ext}}$  ( $B^{\text{ext}} < \phi_0 / 2\pi D \Lambda_J$ )**

The screening currents are weak and the magnetic field penetrates to the core of the insulating layer.

## **12.5 - Long JOSEPHSON junction in a high magnetic field**

### ***12.5.1 - Mechanical analogy***

When the externally applied field is increased and  $\Theta$  is no longer sufficiently small, we must come back to the FERRELL-PRANGE equation (12.28) whose general solution makes use of complete elliptical integrals.<sup>5</sup> It is, however, possible to understand the behavior of the junction without complex mathematical developments by considering its formal analogy to the movement of a rigid pendulum consisting of a mass  $M$  fixed at the end of a lever of length  $L$ , which can rotate without damping in

<sup>5</sup> C.S. OWEN & J. SCALAPINO (1967) *Phys. Rev.* **164**, 538.

a vertical plane. Its equation of motion is given by the same FERRELL-PRANGE equation

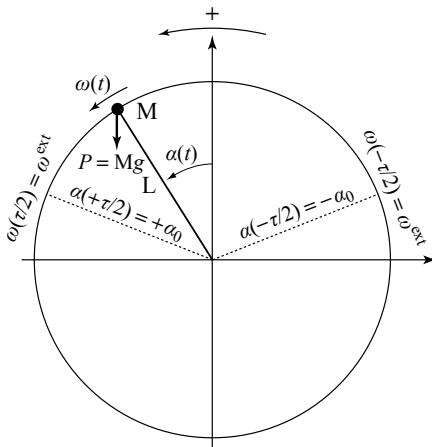
$$\frac{\partial^2 \alpha(t)}{\partial t^2} = \Omega^2 \sin \alpha(t) \quad \text{with } \Omega = \sqrt{\frac{g}{L}} \quad (12.37)$$

where  $\alpha(t)$  is the angle between the stem and the  $z$  axis, that is directed vertically upwards, unlike the mechanical analogy of Chapter 10 where it was directed downwards.

By comparing the equations (12.25) to (12.28) with equation (12.37) and the equations of mechanics, including the dynamical law  $\Gamma_p = ML^2 \frac{d^2\alpha}{dt^2}$ , where  $\Gamma_p$  is the torque exerted by the weight of the pendulum, we have the equivalences of Table 12.1.

**Table 12.1 - Correspondences between quantities related to a JOSEPHSON junction in an external field and the quantities related to the rigid pendulum of Figure 12.14**

Mechanical system	JOSEPHSON junction
Inverse frequency of oscillation of the pendulum $\Omega^{-1} = \sqrt{\frac{L}{g}}$	JOSEPHSON penetration depth $A_J$
Time $t$	$y$ coordinate
Angular displacement $\alpha(t)$	Phase $\Theta(y)$
Angular velocity $\omega(t) = \frac{d\alpha}{dt}$	Magnetic field $B_z(y) = \frac{\phi_0}{2\pi D} \frac{d\Theta}{dy}$
Torque exerted by the pendulum $\Gamma_p(t) = \Gamma_c \sin \alpha(t)$	Current density through the insulator $j_x(y) = j_c \sin \Theta(y)$
Critical torque $\Gamma_c = MgL$	Critical current density $j_c$
Interval in time $\tau$ between $-\tau/2$ and $\tau/2$	Length of the junction $a$ between $-a/2$ and $a/2$
Number of swings during a time $\tau$	Number of fluxons across the junction
$\frac{D}{\phi_0} \int_{-a/2}^{+a/2} B_z(y) dy = \frac{1}{2\pi} \int_{-a/2}^{+a/2} \frac{d\Theta}{dy} dy$ $= \frac{1}{2\pi} \left[ \Theta\left(\frac{a}{2}\right) - \Theta\left(-\frac{a}{2}\right) \right]$	
Constraints on the initial and final angular velocities $\omega(+\tau/2) = \omega(-\tau/2) = \omega^{\text{ext}}$	Boundary conditions determined by the external magnetic field $B_z(+a/2) = B_z(-a/2) = B^{\text{ext}}$

**Figure 12.14****Mechanical analogy:****JOSEPHSON junction / rigid pendulum**

The equation governing the profile of the phase difference  $\Theta(y)$  between points situated on opposite sides of the insulating layer of a JOSEPHSON junction subject to an applied magnetic field  $B^{\text{ext}}$  is analogous to the time-dependent equation of the angular coordinate  $\alpha(t)$  of a rigid pendulum subject to initial and final angular velocities  $\omega^{\text{ext}}$  (see the complete set of correspondences in Table 12.1).

In addition to the equation (12.37), the movement of the pendulum satisfies the condition of conservation of energy,

$$E_{\text{kin}} + E_{\text{pot}} = \text{Constant} \quad (12.38)$$

where  $E_{\text{kin}}$  and  $E_{\text{pot}}$  are the kinetic and potential energies respectively, with zero of the potential taken when the pendulum is horizontal

$$E_{\text{kin}} = \frac{1}{2}ML^2\omega^2 \quad E_{\text{pot}} = MgL\cos\alpha \quad (12.39)$$

The equivalence  $y \leftrightarrow t$  leads us to associate to the length  $a$  of the junction (that extends between  $-a/2$  and  $+a/2$ ), the time interval  $\tau$  during which (between  $-\tau/2$  and  $\tau/2$ ) the pendulum moves. The boundary condition (12.32) corresponds in the pendulum analogy, to the constraint that the initial and final angular velocities be identical:  $\omega(\pm\tau/2) = \omega^{\text{ext}}$ .

Thus for a junction in applied external field  $B^{\text{ext}}$ , the phase variation  $\Theta(y)$  in  $y$  is formally identical to the variation in time of the angle  $\alpha(t)$  of a pendulum to which is given, at time  $t = -\tau/2$  when it is at an initial angle  $\alpha(-\tau/2) = -\alpha_0$ , an angular velocity  $\omega^{\text{ext}}$  such that it passes over the top and continues, so that at time  $t = +\tau/2$  it is at the angle  $\alpha(+\tau/2) = +\alpha_0$  with the same angular velocity  $\omega^{\text{ext}}$ .

### 12.5.2 - Special movements of the pendulum

Among the many types of movement of the pendulum, we shall look at two special scenarios.

#### *First scenario*

By appropriate choices of  $\alpha_0$  and  $\omega^{\text{ext}}$ , the pendulum reaches the top with a very small angular velocity and as a result stays there for a very long time nearby, before

dropping to its final position (without making any complete turns). Taking the kinetic energy to vanish at the top ( $\cos \alpha = 1$ ), energy conservation is expressed as

$$\frac{1}{2}ML^2\omega^2 + MgL\cos\alpha = MgL \quad (12.40)$$

and two limiting cases can be imagined:

» **Case 1:**  $\alpha(t)$  is small,  $\cos \alpha \approx 1 - \alpha^2/2$  and the equation (12.40) becomes, choosing the negative value of the square root that appears,

$$\omega = \frac{d\alpha}{dt} = -\Omega\alpha \quad (12.41)$$

$$\alpha = -\alpha_0 e^{-\Omega(t+\tau/2)}$$

$$\text{whose solutions: } \omega = \omega^{\text{ext}} e^{-\Omega(t+\tau/2)} \quad (12.42a)$$

$$\Gamma_p = -MgLe^{-\Omega(t+\tau/2)}$$

describe the behavior of the pendulum as it swings up. Taking the positive value of the square root provides the equations of motion for the swing down.

$$\begin{aligned} \alpha &= \alpha_0 e^{-\Omega(t-\tau/2)} \\ \omega &= \omega^{\text{ext}} e^{-\Omega(t-\tau/2)} \\ \Gamma_p &= MgLe^{-\Omega(t-\tau/2)}. \end{aligned} \quad (12.42b)$$

» **Case 2:** The initial angle  $-\alpha_0$  is equal to  $-\pi$ , i.e. the pendulum is launched from its lowest position with the angular velocity  $\omega^{\text{ext}} = \omega_c = 2\Omega$  just sufficient for it to arrive at the highest position with zero velocity (relation 12.39). The evolution of the angular velocity  $\omega = d\alpha/dt$  and of the torque  $\Gamma_p$  of the pendulum are intuitively understood in this case, and are qualitatively presented in Table 12.2 and summarized in Figure 12.15.

**Table 12.2 - Time dependence of the angular velocity and the torque acting on a rigid pendulum launched from its lowest position at time  $t = -\tau/2$  with angular velocity  $\omega^{\text{ext}} = 2\Omega$ , such that at time  $t = +\tau/2$  it returns to the same position after having made one complete turn**

Position of the pendulum $\alpha(t)$	Angular velocity $\omega(t)$	Torque acting on the pendulum $\Gamma_p(t)$
Initial position: the lowest point $t = -\frac{\tau}{2}$ $\alpha\left(-\frac{\tau}{2}\right) = -\alpha_0 = -\pi$	$\omega^{\text{ext}} = \omega_c = 2\Omega$	$\Gamma_p = 0$
Sequence (a): $-\pi < \alpha(t) < -\frac{\pi}{2}$	Decreases rapidly	Increases rapidly
Pendulum is horizontal $\alpha = -\frac{\pi}{2}$	$\omega_{\perp} = \sqrt{2}\Omega$	$\Gamma_p = -MgL$

Sequence (b): $-\frac{\pi}{2} < \alpha(t) < 0$	Decreases slowly	Decreases slowly
Top position $t = 0 \quad \alpha = 0$	$\omega \approx 0$ Stays for a long time	$\Gamma_p \approx 0$
Sequence (c): $0 < \alpha(t) < \frac{\pi}{2}$	Increases slowly	Increases slowly
Pendulum is horizontal $\alpha = \frac{\pi}{2}$	$\omega_{\perp} = \sqrt{2}\Omega$	$\Gamma_p = MgL$
Sequence (d): $\frac{\pi}{2} < \alpha(t) < \pi$	Increases rapidly	Decreases rapidly
Final position: at the lowest point		
$t = \frac{\tau}{2} \quad \alpha\left(\frac{\tau}{2}\right) = \alpha_0 = \pi$	$\omega^{\text{ext}} = \omega_c = 2\Omega$	$\Gamma_p = 0$

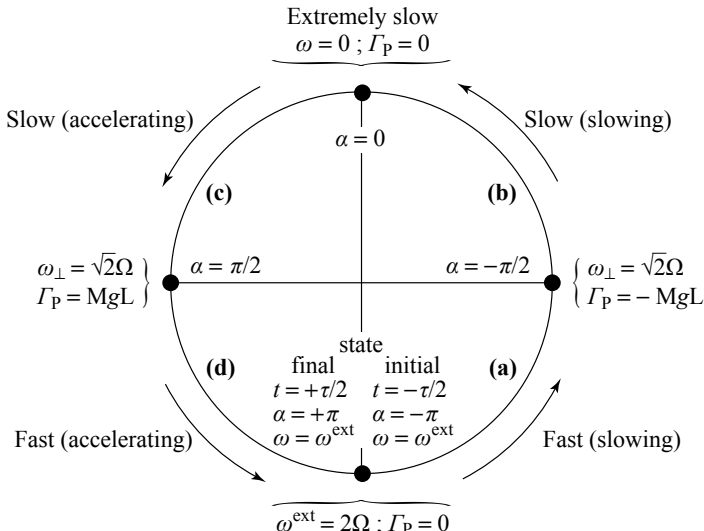


Figure 12.15 - Schematic representation of the time dependence of the angular velocity and the torque acting on a rigid pendulum launched from its lowest position at time  $t = -\tau/2$  with angular velocity  $\omega^{\text{ext}} = 2\Omega$  (Table 12.2)

### Second scenario

The initial angular velocity  $\omega^{\text{ext}}$  exceeds  $2\Omega$  so that the pendulum passes over the highest position with non-zero angular velocity and in addition the time  $\tau$  is sufficient that, like a sling, it can make several turns. In this case we have the following:

- » the angular velocity  $\omega(t)$  is periodic between  $t = -\tau/2$  and  $t = +\tau/2$ ; however its oscillations are asymmetric around a value close to  $\omega^{\text{ext}}$ , since  $\omega(t)$  is smaller near the highest point than it is at the lowest;

- » the torque  $\Gamma_p(t)$  oscillates around 0 asymmetrically with the same period between the extrema  $\pm MgL$  ( $\pm \Gamma_c$ );
- » the angular position always increases, but non-linearly.

In the extreme case where the initial velocity becomes very great, the difference in potential energy between the high and low positions becomes negligible compared to the original kinetic energy. The angular velocity approaches a sine wave with an amplitude that becomes weaker and weaker, and a period that tends towards  $T \approx 2\pi/\omega^{\text{ext}}$ . The torque also becomes sinusoidal with an amplitude that remains equal to  $MgL$ . The variation of the angular position approaches linearity.

### 12.5.3 - Long JOSEPHSON junction in the MEISSNER regime

This is the equivalent of the first scenario of the mechanical system and we find the two limiting cases:

- » **Case 1** is that of very weak fields with solutions (12.34) equivalent to the solutions (12.42) of the linearized FERRELL-PRANGE equations. To verify this it suffices to make the substitutions of Table 12.1 into (12.42).
- » **Case 2** is when the external magnetic field takes the maximum value  $B_{\text{cJ}}$  compatible with the MEISSNER regime. We then find in Table 12.3 the different sequences of Table 12.2.

**Table 12.3 - Limit of the MEISSNER regime**

Profile of the magnetic field and the JOSEPHSON current along the insulating layer of a JOSEPHSON junction subject to an external magnetic field  $B^{\text{ext}} = B_{\text{cJ}}$ . These profiles are to be compared to the time dependence of the angular velocity and the torque for a pendulum given an initial angular velocity  $\omega^{\text{ext}} = 2\Omega$  (Table 12.2).

Phase $\Theta(y)$	Magnetic field across the insulator $B_z(y)$	Current across the insulator $j_x(y)$
Edge of the junction: $y = -\frac{a}{2}$ $\Theta = -\pi$	$B^{\text{ext}} = B_{\text{cJ}} = 2B_{\text{cJ}}^*$	$j = 0$
Sequence (a): $-\pi < \Theta < -\frac{\pi}{2}$	Decreases rapidly	Increases rapidly (in absolute value)
$\Theta = -\frac{\pi}{2}$	$B = \frac{\sqrt{2}}{2} B_{\text{cJ}}$	$j = -j_{\text{c}}$
Sequence (b): $-\frac{\pi}{2} < \Theta < 0$	Decreases slowly	Decreases slowly
Center of the insulator $y = 0$ $\Theta = 0$	$B \approx 0$ , stays small over a large distance	$j = 0$
Sequence (c): $0 < \Theta < \frac{\pi}{2}$	Increases slowly	Increases slowly

$\Theta = +\frac{\pi}{2}$	$B = \frac{\sqrt{2}}{2} B_{cJ}$	$j = +j_c$
Sequence (d): $\frac{\pi}{2} < \Theta < \pi$	Increases rapidly	Decreases rapidly
Extremity of the junction:		

$$y = \frac{a}{2} \quad \Theta = \pi$$

$$B^{\text{ext}} = B_{cJ} = 2 B_{cJ}^*$$

$$j = 0$$

The different sequences of the profiles of  $B_z(y)$  and  $j_x(y)$  obtained by calculations for a junction of length  $10 A_J$  are easily identifiable on Figure 12.16.

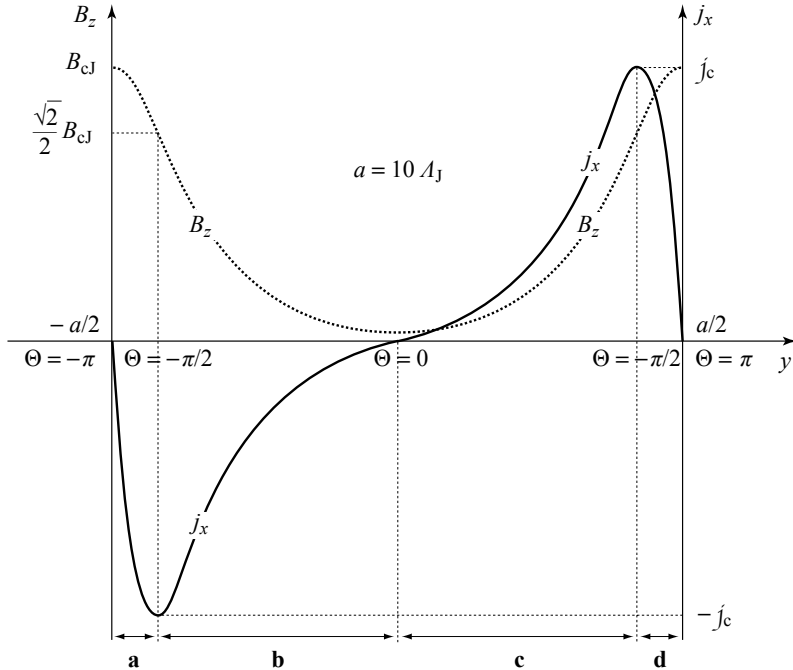


Figure 12.16 - Limit of the MEISSNER regime

Profiles of the magnetic field and of the JOSEPHSON currents, in the limit of the MEISSNER regime ( $B^{\text{ext}} = B_{cJ}$ ), across the insulating layer of a long JOSEPHSON junction described in Table 12.3. The sequences **a**, **b**, **c** and **d** are the equivalents of those shown with the same letters on Figure 12.15. [From OWEN & SCALAPINO, 1967, © The American Physical Society, with permission].<sup>5</sup>

Given the equivalence with the mechanical system, and by taking larger and larger angles  $\alpha_0$  we can easily convince ourselves of the dependence of the MEISSNER regime with field, as presented in Table 12.4.

**Table 12.4 - Long JOSEPHSON junction in the MEISSNER regime**

Dependence on external magnetic field of the profiles of magnetic fields and of the current density along the insulating layer of a long JOSEPHSON junction in the MEISSNER phase

$B^{\text{ext}} \ll \frac{\sqrt{2}}{2} B_{\text{cJ}}$	$B$ and $j$ decrease exponentially starting from the edges of the insulator with the length-scale $\Lambda_J$ .
$B^{\text{ext}} < \frac{\sqrt{2}}{2} B_{\text{cJ}}$	$B$ and $j$ stay with maxima at the extremities but their profiles deviate from decreasing exponential forms.
$B^{\text{ext}} = \frac{\sqrt{2}}{2} B_{\text{cJ}}$	The greatest field for which $j$ has a maximum at the surface with value $j_c$ . The magnetic field flux across the junction is equal to half of a fluxon.
$\frac{\sqrt{2}}{2} B_{\text{cJ}} < B^{\text{ext}} < B_{\text{cJ}}$	The current density at the surface decreases. A bell-shaped curve develops with a maximum that remains at $j_c$ and shifts to within the insulator.
$B^{\text{ext}} = B_{\text{cJ}}$	The maximum external magnetic field compatible with the MEISSNER regime. The current density becomes zero at the surface. The flux across the junction is equal to one fluxon.

The critical JOSEPHSON field beyond which the MEISSNER regime can no longer survive is, according to Table 12.3,

$$B_{\text{cJ}} = 2\mu_0 j_c \Lambda_J = \frac{\phi_0}{\pi \Lambda_J D} \quad (12.43)$$

which is double the value  $B_{\text{cJ}}^*$  (of relation 12.35) derived from linearization of the FERRELL-PRANGE equation, but with very different profiles of  $B_z(y)$  and  $j_x(y)$ . With  $D \approx 50$  nm,  $B_{\text{cJ}}$  is a magnetic field close to  $10^{-4}$  T for  $j_c = 10$  A cm $^{-2}$  and  $10^{-3}$  T for  $j_c = 1$  kA cm $^{-2}$ .

#### 12.5.4 - Long junction in the vortex regime

This corresponds to the second scenario of the mechanical analogy. Translated into the language of the junction, it indicates that when  $B^{\text{ext}} > B_{\text{cJ}}$ , the current density oscillates periodically but asymmetrically around 0 between the extreme values  $\pm j_c$ , and the magnetic field oscillates asymmetrically around a value close to  $B^{\text{ext}}$  and that the phase increases non-monotonically.

In the limit of high external fields, both the oscillations of  $j_x$  around 0, and of  $B_z$  around  $B^{\text{ext}}$ , tend towards sinusoidal functions. The amplitude of oscillation of  $B_z(y)$  decreases, and the variation of  $\Theta(y)$  with  $y$  approaches a straight line. Transposing the relation  $T \approx 2\pi/\Omega_0$ , the period common to both the magnetic field and the current density tends towards

$$Y \approx \frac{\phi_0}{DB^{\text{ext}}} \quad (12.44)$$

The currents that cross the insulating layer close inside the LONDON regions of the superconductors surrounding them, thereby forming a lattice of whirlwind currents in one dimension, that are called the “JOSEPHSON vortices” (Fig. 12.17). The magnetic field  $B_{cJ}$  corresponds for the junction to the critical field  $B_{c1}$  of type II superconductors. The number of fluxons that penetrate the junction then equals the number of periods (integer or fractional) that develop: it increases with more intense  $B^{\text{ext}}$  and larger values of  $a$ .

Some precautions should, however, be taken when using the term “vortices” in this context since they do not have a normal core, even if they surround regions where the density of superconducting electrons is reduced, and we should not expect to see the equivalent of  $B_{c2}$ .

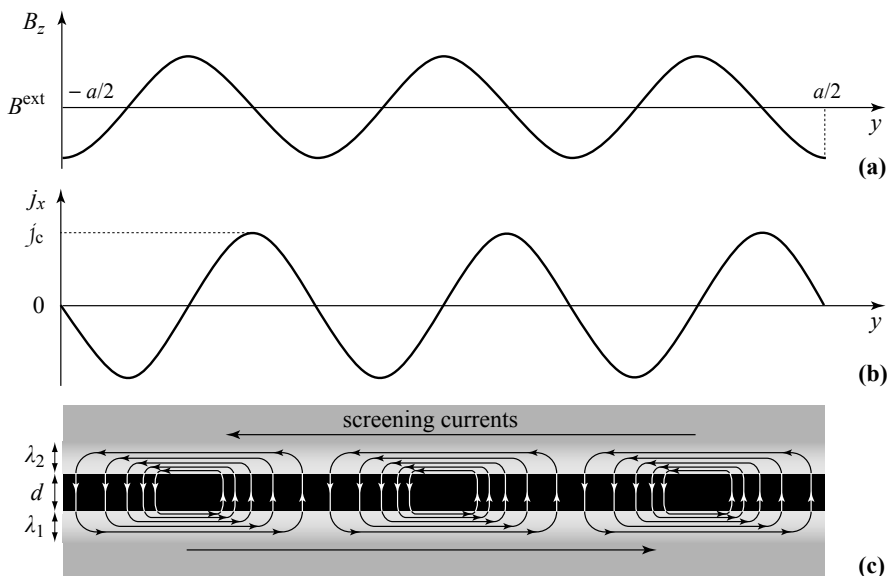


**Figure 12.17 - Magnetic field within the insulating layer  
of a long JOSEPHSON junction in the vortex regime**

(a) The magnetic field oscillates around a value close to  $B^{\text{ext}}$  with an amplitude that decreases as  $B^{\text{ext}}$  increases. (b) The current density oscillates around zero between  $\pm j_c$  with a shift in phase of a quarter period. (c) A schematic view of the currents that cross the junction and close up laterally. They form a one-dimensional lattice of JOSEPHSON vortices.

We note too that while the relation (12.44) resembles (12.19), it refers to a very different situation. In section 12.2 we were discussing the JOSEPHSON currents generated by a current  $I$  injected into a short junction under applied magnetic field, whereas here the vortex currents are created in a long junction subject simply to a magnetic field.

### 12.5.5 - Isolated JOSEPHSON vortex

If in principle the vortex regime only appears when  $B^{\text{ext}} > B_{\text{cJ}}$ , it sometimes happens that vortices can stay in a long junction for  $B^{\text{ext}} < B_{\text{cJ}}$ . In the extreme limit, it is possible to see a single isolated vortex appear in an infinitely long junction, even in the absence of an external field.

The profile of such a vortex centered at  $y = 0$ , in an infinitely long junction, can be calculated analytically without great difficulty. Far from the center of the junction, the current across the insulator vanishes.

In the special case where this phase difference changes by  $2\pi$  between  $y = -\infty$  and  $y = +\infty$  with

$$\Theta(-\infty) = 0 \quad ; \quad \Theta(+\infty) = 2\pi \quad ; \quad \Theta(0) = \pi \quad ; \quad \frac{\partial\Theta}{\partial y}(\pm\infty) = 0 \quad (12.45)$$

equation (12.28) has a solution<sup>6</sup>

$$\Theta(y) = 4 \tan^{-1}\left(e^{\frac{y}{\Lambda_J}}\right) \quad (12.46)$$

and  $\Theta$  passes from 0 to  $2\pi$  over a few JOSEPHSON penetration depths around  $y = 0$  (Fig. 12.18a).

By virtue of the equation (12.27), the profile of the magnetic field along the insulator is found as

$$B_z(y) = \frac{\phi_0}{2\pi D} \frac{\partial\Theta(y)}{\partial y} = \frac{\phi_0}{\pi D \Lambda_J} \frac{1}{\cosh(y/\Lambda_J)} \quad (12.47)$$

and appears as a bell shape (Fig. 12.18b) of width  $\approx 4\Lambda_J$  centered around  $y = 0$  with

$$B_z(0) = \frac{\phi_0}{\pi D \Lambda_J} = B_{\text{cJ}} \quad (12.48)$$

which produces a magnetic field flux across the junction (including both insulating and superconducting materials) equal to one fluxon:

$$\phi = D \int_{-\infty}^{+\infty} B_z(y) dy = \frac{\phi_0}{2\pi} \int_{-\infty}^{+\infty} \frac{\partial\Theta(y)}{\partial y} dy = \frac{\phi_0}{2\pi} [\Theta(+\infty) - \Theta(-\infty)] = \phi_0 \quad (12.49)$$

The current density across the insulator can be found from the equation (12.28) and, using (12.25), is written

$$j_x(y) = \frac{1}{\mu_0} \frac{\partial B_z(y)}{\partial y} = \frac{\phi_0}{\pi \mu_0 D \Lambda_J^2} \frac{\sinh(y/\Lambda_J)}{\cosh^2(y/\Lambda_J)} \quad (12.50a)$$

which is also

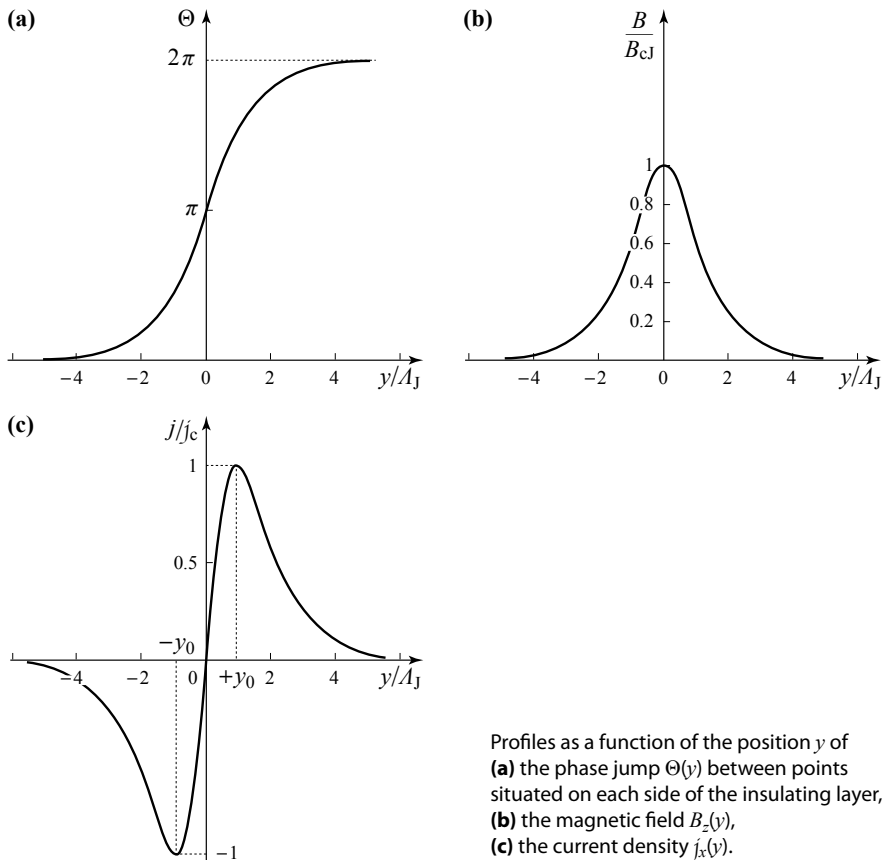
<sup>6</sup> This solution can be found by proceeding as described in Appendix 12, by adapting the boundary conditions to the condition that here the junction is completely of type 0.

$$j_x(y) = 2j_c \frac{\sinh(y/\Lambda_J)}{\cosh^2(y/\Lambda_J)} \equiv j_c \sin\Theta(y). \quad (12.50b)$$

This current density is zero at  $y = 0$ , vanishes asymptotically at infinity, and shows two maxima in absolute value of opposite signs  $\pm j_c$  situated at displacements  $\pm y_0$  from the vortex center, where  $y_0$  satisfies (Fig. 12.18c),

$$\sinh\left(\frac{y_0}{\Lambda_J}\right) = 1 \quad \text{or} \quad y_0 \approx 0.88 \Lambda_J. \quad (12.51)$$

The mechanical analogy of this situation is the pendulum which is released with zero velocity at its highest point at time  $t = -\infty$  ( $\alpha = 0$ ), makes one complete turn so as to come back to the highest point at time  $t = +\infty$  ( $\alpha = 2\pi$ ), after having passed the lowest point with the maximum angular velocity at time  $t = 0$ .



Profiles as a function of the position  $y$  of  
**(a)** the phase jump  $\Theta(y)$  between points  
situated on each side of the insulating layer,  
**(b)** the magnetic field  $B_z(y)$ ,  
**(c)** the current density  $j_x(y)$ .

Figure 12.18 - Isolated vortex at the center of an infinitely long  
JOSEPHSON junction at zero external field

If the pendulum had a long, but not infinitely long, time available it would need to be launched with a minimum angular velocity  $\omega^{\text{ext}} \ll 2\Omega$  in order to complete a swing between  $t = -\tau/2$  and  $t = +\tau/2$ . In the language of the junction, an external magnetic field  $B^{\text{ext}} \ll B_{\text{cJ}}$  would be necessary to allow a JOSEPHSON vortex to stay within a junction that is long, but not infinitely so.

## 12.6 - Current transport in a long JOSEPHSON junction

### 12.6.1 - Long junction carrying a current

At the beginning of section 12.2, we assumed (see relation 12.4) that in zero external field the current density carried was uniformly distributed across the junction. This was, in fact, using the hypothesis of a short junction and we should now return to the problem with the general equations (12.26 to 12.28) or else, if the current is sufficiently small, with their linearized forms (12.30 and 12.31).

In fact, the current distribution will depend on the geometry of the junction. The simplest to analyse is the “in line JOSEPHSON Junction” (Fig. 12.19) where the current circulation in the superconductors electrode creates a magnetic field  $\pm B^{\text{el}}$  along the  $z$  direction<sup>7</sup> at  $y = a/2$  and  $y = -a/2$ . By application of AMPÈRE's law, and taking the thickness  $e$  of the electrode to satisfy  $e \ll c$ ,

$$B^{\text{el}}(+a/2) = \mu_0 \frac{I}{2c} \quad \text{and} \quad B^{\text{el}}(-a/2) = -\mu_0 \frac{I}{2c}. \quad (12.52)$$

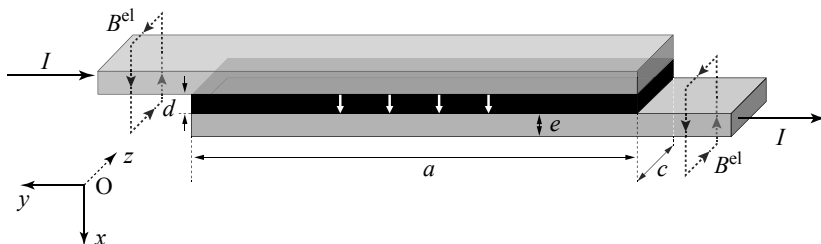


**Figure 12.19 - In-line JOSEPHSON junction**

The current crosses the isolating layer along the  $x$  direction. By application of AMPÈRE's law along the dotted line ( $e \ll c$ ), the magnetic field created by  $I$  circulating in the superconducting electrodes is  $\approx \mu_0 I / 2c$ .

which in the absence of an external field leads to the boundary conditions

$$B_z(+a/2) = \mu_0 \frac{I}{2c} \quad \text{and} \quad B_z(-a/2) = -\mu_0 \frac{I}{2c}. \quad (12.53)$$

<sup>7</sup> R. GROSS and A. MARX

[http://www.wmi.badw.de/teaching/LectureNotes/AS/AS\\_Chapter2.pdf](http://www.wmi.badw.de/teaching/LectureNotes/AS/AS_Chapter2.pdf)

With the linearized form of the equation (12.30), the current density is then distributed according to the relation

$$j_x(y) = \frac{I}{2c\Lambda_J} \frac{\cosh(y/\Lambda_J)}{\cosh(a/2\Lambda_J)} \quad (12.54)$$

This form, for sufficiently large  $a$ , becomes a decreasing exponential of range  $\Lambda_J$  starting from  $y = \pm a/2$  and the critical current intensity is determined by  $j_y(\pm a/2)$  reaching  $j_c$

$$I_{cJ}^* = 2c\Lambda_J j_c. \quad (12.55)$$

As we saw previously (in section 12.4.3) this value of  $I_{cJ}^*$  is just an estimate since it was calculated beyond the range of validity of the approximation  $\sin \Theta \approx \Theta$ . An exact calculation, for  $a = 10\Lambda_J$ , starting from the FERRELL-PRANGE equation and the boundary conditions (12.53), leads, at the limit of the MEISSNER regime, *i.e.* when the current density somewhere approaches  $j_c$ , to the profiles of Figure 12.20.

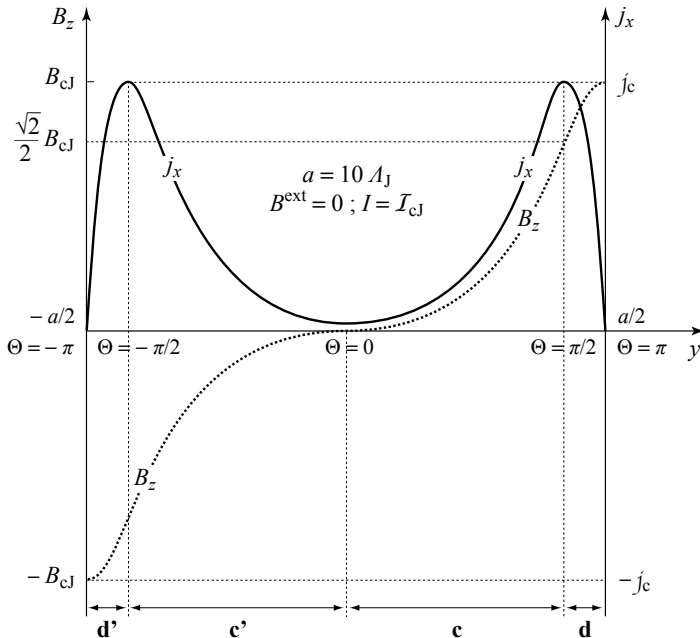


Figure 12.20 - Profile of the critical JOSEPHSON current<sup>5</sup>

The profile of the maximum current density in the MEISSNER regime through a long JOSEPHSON junction has the form of two bell shapes of maximum  $j_c$ , localized at a distance of the order of  $\Lambda_J$  from the edges. The ranges  $\mathbf{d}$  and  $\mathbf{c}$  are equivalent to the sequences of the same name in Figure 12.15. The ranges  $\mathbf{c}'$  and  $\mathbf{d}'$  correspond to the same sequences "followed" in the opposite order.

In it we see that the current density increases from the surfaces, where it is zero, to reach a maximum value equal to  $j_c$  when the induced magnetic field becomes equal to  $\pm\sqrt{2}/2B_{cJ}$ , having decreased in absolute value from the external surfaces where it has its maximum absolute values of  $\pm B_{cJ}$ . In the mechanical analogy of Figure 12.15, the pendulum is launched at the initial time  $t = -\tau/2$  from the lowest position ( $\alpha = \pi$ ) where it is subject to a vanishing torque  $\Gamma_p$  with velocity  $\omega_{-\tau/2}^{\text{ext}} = -2\Omega$  (sequence **d'** equivalent to **d** but followed in the reverse order). It passes the horizontal position with a critical torque  $\Gamma_c$  and then approaches the summit very slowly (sequence **c'** equivalent to **c** followed in the reverse order) close to which it remains for a long time. It then returns by the same path with an increasing angular velocity  $\mathbf{c}$ , passes once again to the horizontal state where it feels the torque  $\Gamma_c$  and comes back to the lowest position **d** with zero torque  $\Gamma_p$  at time  $t = \tau/2$  and with angular velocity  $\omega_{\tau/2}^{\text{ext}} = -2\Omega$ .

The greatest current  $I_{cJ}$  (the critical JOSEPHSON current intensity) that the long junction can withstand corresponds to

$$B_z(+a/2) = \mu_0 \frac{I_{cJ}}{2c} = B_{cJ} \quad \text{and} \quad B_z(-a/2) = -B_{cJ} \quad (12.56)$$

or, when the junction is “infinitely” long,

$$I_{cJ} = 4cA_J j_c. \quad (12.57)$$

Once again, this is double the maximum of current calculated starting from the linearized equation.

### 12.6.2 - Long JOSEPHSON current subject to a magnetic field and carrying a current

#### *MEISSNER regime*

In the presence of an external field, the fields at the edges of the insulator are

$$B_z(+a/2) = B^{\text{ext}} + \mu_0 \frac{I}{2c} \quad \text{and} \quad B_z(-a/2) = B^{\text{ext}} - \mu_0 \frac{I}{2c}. \quad (12.58)$$

The system loses any symmetry it may have had, since in general the magnetic fields at the edges are neither equal nor symmetric. The maximum current,  $I_{\max}(B^{\text{ext}})$ , that the junction can carry is attained when the magnetic field reaches  $B_{cJ}$  on one or other of the surfaces,

$$B^{\text{ext}} + \mu_0 \frac{I_{\max}(B^{\text{ext}})}{2c} = B_{cJ} \quad (12.59)$$

and therefore  $I_{\max}(B^{\text{ext}}) = I_{cJ} - \frac{2cB^{\text{ext}}}{\mu_0} = I_{cJ} \left( 1 - \frac{B^{\text{ext}}}{B_{cJ}} \right)$  (12.60)

which is represented by the straight line labelled [0/1] in Figure 12.21.

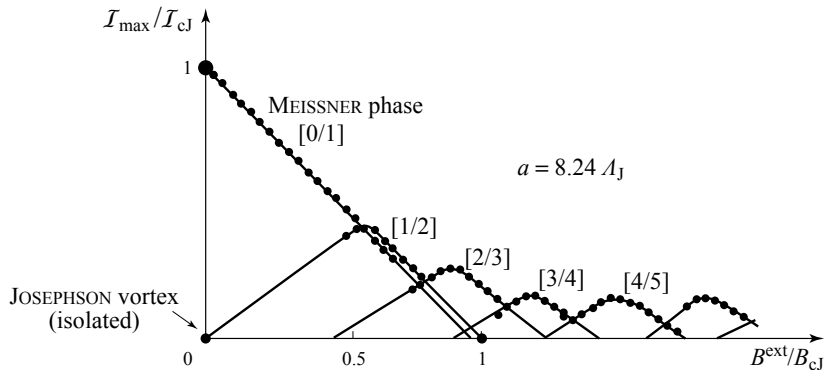


**Figure 12.21 - Maximum current across a long JOSEPHSON junction subject to a magnetic field**

The  $[n/n+1]$  mode is defined to be the solution with flux across the junction lying between  $n$  and  $n+1$  fluxons. Each mode has a maximum possible current. The modes overlap and the highest of the maxima of each of the modes for a given field. The points marked at  $B^{\text{ext}} = 0$  correspond to the isolated JOSEPHSON vortex ( $I_{\max}^{[1/2]} = I_{\text{cJ}}$ , Fig. 12.18b) and to the limit of current transport in the MEISSNER regime ( $I_{\max}^{[0/1]} = I_{\text{cJ}}$ , Fig. 12.20). The profiles of the magnetic field and current density corresponding to the point ( $I_{\max}^{[0/1]} = 0$ ;  $B^{\text{ext}} = B_{\text{cJ}}$ ) of the MEISSNER phase are as shown in Figure 12.16 (in fact, for this point  $B^{\text{ext}}$  is slightly less than  $B_{\text{cJ}}$  because of the finite length of the junction). The continuous lines are from Ref. 5 and the points from Ref. 8.<sup>8</sup>

### Vortex regime

Under an applied external field  $B^{\text{ext}}$ , the FERRELL-PRANGE equation in fact has several solutions, each having a maximum possible current. For example, in zero field there is the solution with the field uniformly zero and also the single vortex solution of Figure 12.18b. Following OWEN and SCALAPINO, the solutions are classified according to the number of fluxons that cross the junction. A solution is of the mode  $[n/n+1]$  if the junction carries between  $n$  and  $n+1$  fluxons, *i.e.* the current has between  $n$  and  $n+1$  periods.

It can be shown that when a current is superimposed on the magnetic field, each mode  $[n/n+1]$  has its own intensity curve with maximum value  $I_{\max}^{[n/n+1]}$  (see Fig. 12.21). However as we see in Figure 12.21, where the length of the junction is  $a = 8.24 A_J$ , the modes can overlap. For example,  $[2/3]$  mode overlaps on the left the  $[0/1]$   $[1/2]$  modes and on its right the  $[3/4]$  and even slightly the  $[4/5]$  mode. As a consequence, the maximum current intensity  $I_{\max}$  that can cross the junction for an applied magnetic field  $B^{\text{ext}}$  is given by the mode giving the highest value of intensity  $I_{\max}^{[n/n+1]}$  for this field (see the points of Figure 12.21).

In fact, when there is a current we need to make a dynamical analysis since as in type II superconductors, a force acts on the vortices, which then move perpendicularly to the current direction.

<sup>8</sup> K. SCHWIDTAL (1970) *Phys. Rev. B* **2**, 2526.

## 12.7 - Half fluxon at the 0- $\pi$ connection of a hybrid JOSEPHSON junction

The phenomenon of trapping of a half fluxon has excited particular interest during the last few years because of its occurrence at certain points of intersection of grain boundaries in YBaCuO.

The calculations developed by XU *et al.*<sup>9</sup> show that such stable pinning is produced at the place where the  $\pi$  and 0 parts of an infinitely long 0- $\pi$  junction meet (*i.e.* at  $y = 0$  for a junction of type 0 between  $y = -\infty$  and  $y = 0$ , and of type  $\pi$  between  $y = 0$  and  $y = +\infty$ ).

As we show in Appendix 12, the phase difference between the two superconducting blocks can be written:

$$\text{» for } y < 0 \quad \Theta(y) = 4 \tan^{-1} \left( e^{\frac{y-y_0}{\Lambda_J}} \right), \quad (12.61a)$$

$$\text{» for } y > 0 \quad \Theta(y) = 4 \tan^{-1} \left( e^{\frac{y+y_0}{\Lambda_J}} \right) - \pi \quad (12.61b)$$

where  $y_0$  is the distance defined by relation (12.51). The magnetic fields, found from  $\Theta(y)$  by the relation (12.26), are of the form:

$$\text{» for } y < 0 \quad B_z(y) = \frac{\phi_0}{\pi D \Lambda_J} \frac{1}{\cosh \left( \frac{y-y_0}{\Lambda_J} \right)}, \quad (12.62a)$$

$$\text{» for } y > 0 \quad B_z(y) = \frac{\phi_0}{\pi D \Lambda_J} \frac{1}{\cosh \left( \frac{y+y_0}{\Lambda_J} \right)}. \quad (12.62b)$$

The field decreases as we go away from either side of the center of the junction, where it takes the value

$$B_z(0) = \frac{\sqrt{2}}{2} \frac{\phi_0}{\pi D \Lambda_J} = \frac{\sqrt{2}}{2} B_{cJ}. \quad (12.63)$$

The total magnetic flux across the junction equals, using the relation (12.49),

$$D \int_{-\infty}^{+\infty} B_z(y) dy = \frac{\phi_0}{2\pi} [\Theta(+\infty) - \Theta(-\infty)] = \frac{\phi_0}{2} \quad (12.64)$$

*i.e.* a half fluxon. The current density across the insulator, as deduced by (12.28) from  $B_z(y)$ , is:

$$\text{» for } y < 0 \quad j_x(y) = 2j_c \frac{\sinh \left( \frac{y-y_0}{\Lambda_J} \right)}{\cosh^2 \left( \frac{y-y_0}{\Lambda_J} \right)}, \quad (12.65a)$$

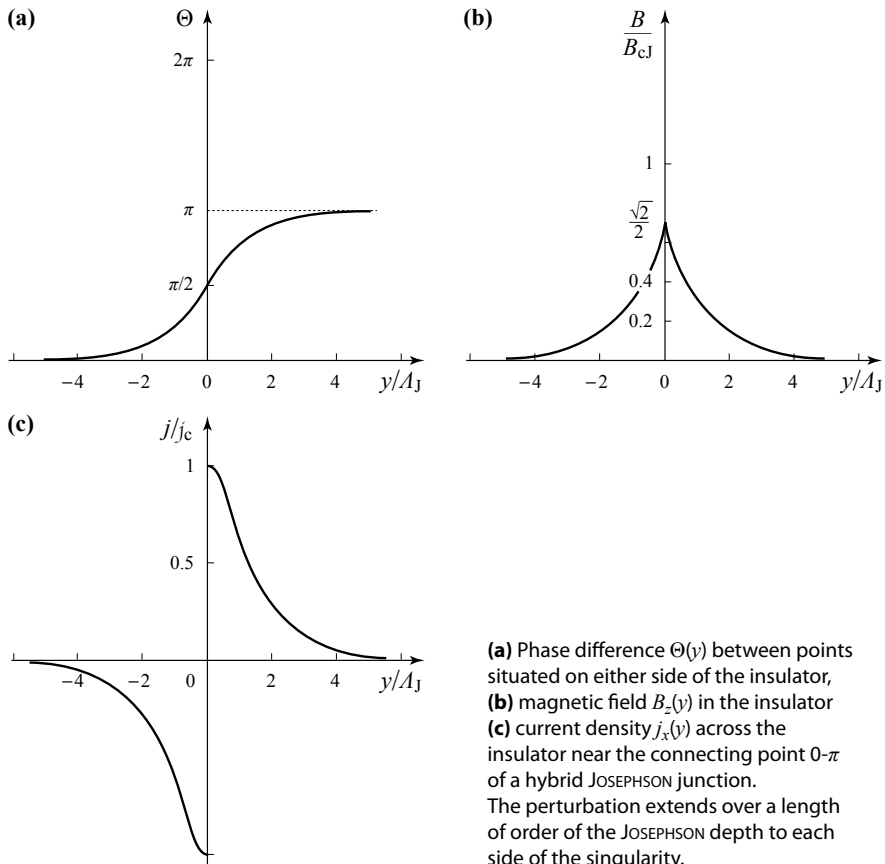
9 J.H. XU *et al.* (1995) *Phys. Rev. B* **51**, 11958.

$$\gg \text{for } y > 0 \quad j_x(y) = 2j_c \frac{\sinh\left(\frac{y+y_0}{\Lambda_J}\right)}{\cosh^2\left(\frac{y+y_0}{\Lambda_J}\right)} \quad (12.65b)$$

making it discontinuous, with limiting values at the origin,

$$j_x(0^\pm) = \pm j_c. \quad (12.66)$$

These different quantities behave as indicated in Figure 12.22 and as we can understand from our previous discussion, the transitional region between the two parts is spread over a few JOSEPHSON depths.



(a) Phase difference  $\Theta(y)$  between points situated on either side of the insulator,  
 (b) magnetic field  $B_z(y)$  in the insulator  
 (c) current density  $j_x(y)$  across the insulator near the connecting point  $0-\pi$  of a hybrid JOSEPHSON junction.  
 The perturbation extends over a length of order of the JOSEPHSON depth to each side of the singularity.

**Figure 12.22 - Half fluxon around the connection between the 0 and  $\pi$  parts of a 0- $\pi$  junction** <sup>10</sup>

This half fluxon is in fact robust since it persists even if a current is driven across the junction. The calculation made by XU *et al.* shows that the profile of the

10 E. GOLDOBIN, D. KOELLE & R. KLEINER (2002) *Phys. Rev. B* **66**, 100508.

maximum current density across the insulator of a 0 or  $\pi$  junction of length  $2\Lambda_J$  is as shown in Figure 12.23a, while that associated with a 0- $\pi$  junction is, for the same conditions, as shown in Figure 12.23b. Since the current transported spreads over a distance  $\Lambda_J$  from the surfaces, and since the current associated with the half-fluxon spreads over a length  $\Lambda_J$  on each side of the point of attachment, there is no interference between the two components, provided the length of the junction is sufficiently large compared to  $\Lambda_J$ .

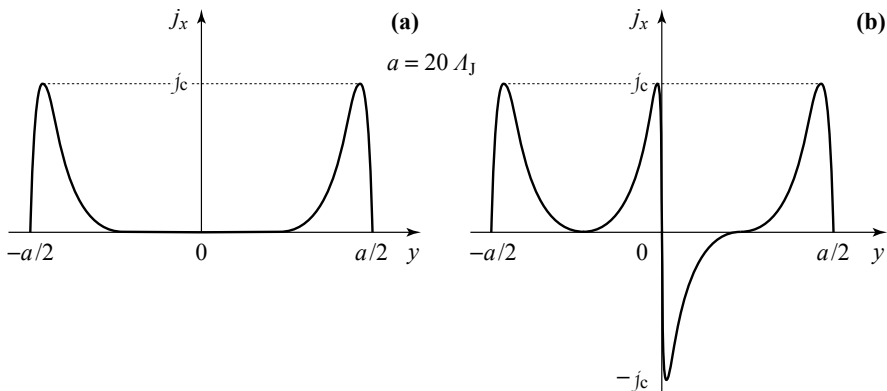


**Figure 12.23 - Density profile of the maximum current transported in the MEISSNER regime<sup>9</sup>**  
**(a) in a 0 (or  $\pi$ ) JOSEPHSON junction (b) in a 0- $\pi$  Josephson junction of length  $20\Lambda_J$**

Very qualitatively, the trapping of a half fluxon at the joining of the two parts of a 0- $\pi$  junction can be understood by gradually enlarging the 0 and  $\pi$  junctions of a SQUID circuit with two junctions of different nature (see section 11.6). The current and the magnetic field extend in the direction of the junctions over a distance that is the order of  $\Lambda_J$  (see relation 12.34 and Fig. 12.24). In contrast, in the perpendicular direction they extend over a distance of order the penetration depths  $\lambda$ .

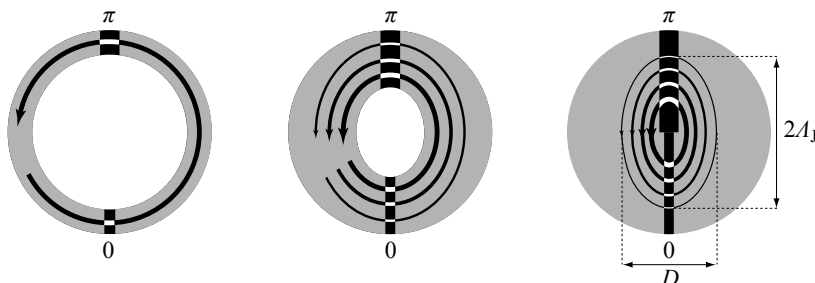


**Figure 12.24 - Intuitive picture of the gradual transition of a current loop trapping a half fluxon in a hetero-junction SQUID circuit into the current distribution around the 0- $\pi$  joint of a hybrid JOSEPHSON junction**

An rf-SQUID ring with two junctions, one of type 0, the other  $\pi$ , spontaneously traps a half fluxon that persists if we “thicken” the circuit, until we finally join the 0 and  $\pi$  junctions to make a 0- $\pi$  junction.

## Appendix 12

### Phase slip between the superconducting blocks within an infinite 0- $\pi$ junction

#### A12.1 - The equations governing the junction

We consider a hybrid JOSEPHSON junction of type 0 for  $y < 0$  and of type  $\pi$  for  $y > 0$  (see Fig. 12.8). Extending over a total length  $a$ , which we will take to its infinite limit, it is subjected to an external magnetic field  $\mathbf{B}^{\text{ext}}$  without imposing any (transported) current.

The equations obeyed by the phase differences  $\Theta(y)$  between the two blocks  $S_1$  and  $S_2$  are written (see expression 12.29):

$$\text{» for } y < 0 \quad \frac{\partial^2 \Theta(y)}{\partial y^2} = + \frac{\sin \Theta(y)}{\Lambda_J^2}, \quad (12.67\text{a})$$

$$\text{» for } y > 0 \quad \frac{\partial^2 \Theta(y)}{\partial y^2} = - \frac{\sin \Theta(y)}{\Lambda_J^2}. \quad (12.67\text{b})$$

The magnetic field  $B_x(y)$  is linked to the variation of the phase difference  $\Theta(y)$  by, (see relations 12.25 and 12.27),

$$B = \frac{\phi_0}{2\pi D} \frac{\partial \Theta(y)}{\partial y} = \mu_0 f_c \Lambda_J^2 \frac{\partial \Theta(y)}{\partial y} \quad (12.68)$$

where the value  $D = d + \lambda_1 + \lambda_2$  (relation 12.12) is essentially determined by  $\lambda_1$  and  $\lambda_2$ , which makes it independent of the nature of the junction, even if  $d$  varies slightly between the parts 0 and  $\pi$ . The same is true for  $\Lambda_J$  that is related to  $D$  by (12.25).

#### A12.2 - Boundary conditions

First of all,  $\Theta(y)$  is continuous since, by the relation (12.68), any discontinuity would imply an unphysical (DIRAC) singularity of the magnetic field.

Furthermore, far from the origin and in the absence of current, the phase of each junction tends asymptotically to the value minimizing the energy it would have if isolated (see sections 10.5 and 10.8.1), leading to the conditions

$$\Theta(-\infty) = 0 \quad \Theta(+\infty) = \pi \quad \text{and} \quad \frac{\partial \Theta}{\partial y}(\pm\infty) = 0. \quad (12.69)$$

Finally, by symmetry,

$$\Theta = \frac{\pi}{2} \quad \text{at } y = 0. \quad (12.70)$$

### A12.3 - Profile of the phase difference

We consider the relation  $\frac{\partial}{\partial y} \left( \frac{\partial \Theta}{\partial y} \right)^2 = 2 \frac{\partial \Theta}{\partial y} \frac{\partial^2 \Theta}{\partial y^2}$ . (12.71)

Using (12.67), this leads to:

» for  $y < 0$   $\frac{\partial}{\partial y} \left( \frac{\partial \Theta}{\partial y} \right)^2 = + 2 \frac{\partial \Theta}{\partial y} \frac{\sin \Theta(y)}{\Lambda_J^2}$ , (12.72a)

» for  $y > 0$   $\frac{\partial}{\partial y} \left( \frac{\partial \Theta}{\partial y} \right)^2 = - 2 \frac{\partial \Theta}{\partial y} \frac{\sin \Theta(y)}{\Lambda_J^2}$ , (12.72b)

or, integrating over  $y$ :

» for  $y < 0$   $\left( \frac{\partial \Theta}{\partial y} \right)^2 = \frac{2}{\Lambda_J^2} (-\cos \Theta(y) + C_-)$ , (12.73a)

» for  $y > 0$   $\left( \frac{\partial \Theta}{\partial y} \right)^2 = \frac{2}{\Lambda_J^2} (+\cos \Theta(y) + C_+)$ . (12.73b)

Since:

» for  $y \rightarrow -\infty$   $\Theta \rightarrow 0$  and  $\cos \Theta \rightarrow +1$ ,

» for  $y \rightarrow +\infty$   $\Theta \rightarrow \pi$  and  $\cos \Theta \rightarrow -1$ ,

we have  $C_+ = C_- = 1$  in (12.73), which leads to:

» for  $y < 0$   $\left( \frac{\partial \Theta}{\partial y} \right)^2 = \frac{4}{\Lambda_J^2} \sin^2 \left( \frac{\Theta}{2} \right)$ , (12.74a)

» for  $y > 0$   $\left( \frac{\partial \Theta}{\partial y} \right)^2 = \frac{4}{\Lambda_J^2} \cos^2 \left( \frac{\Theta}{2} \right)$ . (12.74b)

With the condition  $0 < \Theta < \pi$ , only the positive roots are to be considered, so that:

» for  $y < 0$   $\frac{d \left( \frac{\Theta}{2} \right)}{\sin \left( \frac{\Theta}{2} \right)} = \frac{dy}{\Lambda_J}$ , (12.75a)

» for  $y > 0$   $\frac{d \left( \frac{\Theta}{2} \right)}{\cos \left( \frac{\Theta}{2} \right)} = \frac{dy}{\Lambda_J}$ . (12.75b)

Integrating gives:<sup>11</sup>

$$\text{» for } y < 0 \quad y = \Lambda_J \left[ \ln \left( \tan \left( \frac{\Theta(y)}{4} \right) \right) + D_- \right], \quad (12.76a)$$

$$\text{» for } y > 0 \quad y = \Lambda_J \left[ \ln \left( \tan \left( \frac{\Theta(y)}{4} + \frac{\pi}{4} \right) \right) + D_+ \right], \quad (12.76b)$$

where the constants  $D_-$  and  $D_+$  can be determined by fixing  $\Theta = \pi/2$  for  $y = 0$ , so that

$$D_- = -\ln \left( \tan \frac{\pi}{8} \right) = -\ln(\sqrt{2} - 1) \quad (12.77a)$$

$$D_+ = -\ln \left( \tan \frac{3\pi}{8} \right) = -\ln(\sqrt{2} + 1). \quad (12.77b)$$

Introducing a characteristic length  $y_0$  such that

$$e^{\frac{y_0}{\Lambda_J}} = \sqrt{2} + 1 \quad \text{and} \quad e^{-\frac{y_0}{\Lambda_J}} = \frac{1}{\sqrt{2} + 1} = \sqrt{2} - 1 \quad (12.78)$$

by subtraction of the two expressions, these correspond to

$$\sinh \left( \frac{y_0}{\Lambda_J} \right) = 1$$

$$\text{i.e.} \quad y_0 \approx 0.88 \Lambda_J. \quad (12.79)$$

We finally obtain:

$$\text{» for } y < 0 \quad \Theta(y) = 4 \tan^{-1} \left( e^{\frac{y-y_0}{\Lambda_J}} \right), \quad (12.80a)$$

$$\text{» for } y > 0 \quad \Theta(y) = 4 \tan^{-1} \left( e^{\frac{y-y_0}{\Lambda_J}} \right) - \pi. \quad (12.80b)$$

---

11  $\int \frac{dx}{\sin x} = \ln \left( \tan \left( \frac{x}{2} \right) \right) + \text{Constant}$  and  $\int \frac{dx}{\cos x} = \ln \left[ \tan \left( \frac{x}{2} + \frac{\pi}{4} \right) \right] + \text{Constant}.$

# NOTATION

## General rules

Vectors: **bold Roman characters**; moduli of vectors: *thin italic characters*

Physical variables ( $z$ ):  $\bar{z}$  = local mean value;  $\langle z \rangle$  = macroscopic mean value

Operator A:  $\hat{A}$

### Notation Meaning

<b>A</b>	Vector potential
<b>B</b>	Magnetic field
<b>B</b> <sup>0</sup>	Magnetic field created by currents of a conductor
<b>B</b> <sup>a</sup>	Magnetic field created by AMPÈRE currents
<b>B</b> <sup>ext</sup>	Magnetic field outside the sample
$\tilde{B}$	Magnetic field tangent to the surface
$\bar{\mathbf{B}}$	Local mean magnetic field
$B_c$	Critical magnetic field
$B_{c1}, B_{c2}$	Upper and lower critical magnetic field
$B_{c3}$	Surface critical magnetic field
$C^{\text{vib}}$	Lattice specific heat per unit volume
$C_n^{\text{el}}$	Electronic specific heat in the normal phase
$C_s^{\text{el}}$	Electronic specific heat in the superconducting phase
$D = d + \lambda_1 + \lambda_2$	Magnetic thickness of a JOSEPHSON junction
$D(E)$	Quasiparticle density of states
$d_v$	Nearest-neighbor distance between vortices
<b>E</b>	Electric field
$E$	Energy
$E^0$	Energy stored in a “0” JOSEPHSON junction
$E^\pi$	Energy stored in a “ $\pi$ ” JOSEPHSON junction
$E_J$	JOSEPHSON energy
$E_{\mathbf{k}}$	Energy of a quasiparticle of wave-vector $\mathbf{k}$

---

$e$	Elementary charge ( $1.602 \cdot 10^{-19}$ C)
$F, f$	Free energy (HELMOLTZ function), free energy density
$\mathbf{F}_\phi$	Bulk “LORENTZ” force density on vortices
$\mathbf{f}_\phi$	“LORENTZ” force per unit length of a vortex
$\bar{f}_\phi$	Average “LORENTZ” force per unit length of a vortex
$\mathbf{F}_p$	Bulk pinning force density of vortices
$\bar{\mathbf{f}}_p$	Average pinning force per unit length of a vortex
$f_J, \omega_J$	JOSEPHSON frequency, JOSEPHSON angular frequency
$f(\epsilon)$	FERMI-DIRAC distribution function
$G(k)$	Electronic density of states with respect to wave vector, per spin state
$G(\epsilon)$	Electronic density of states with respect to energy, per spin state
$G(\epsilon_F)$	Density of states at the FERMI level per spin state
$\mathcal{G}, g$	Free enthalpy (GIBBS function), free enthalpy density
$\mathbf{H}$	Field $\mathbf{H}$
$\mathbf{H}^0$	Field $\mathbf{H}$ created by conducting currents
$\mathbf{H}^m$	Demagnetizing field
$H_c$	Critical field
$H_{c1}, H_{c2}$	Lower and upper critical fields
$H_{c3}$	Upper surface critical field $H$
$\mathcal{H}, h$	Enthalpy, enthalpy density
$\hat{H}$	Hamiltonian operator
$h, \hbar$	PLANCK’s constant ( $\hbar = h/2\pi$ )
$I$	Current intensity
$I_c$	Critical intensity in a wire (of a type I superconductor)
$\mathcal{I}_c$	Critical intensity in a JOSEPHSON junction
$\mathcal{I}_c$	Critical intensity in a wire (of a type II superconductor)
$\mathcal{I}_{\max}$	Maximum intensity borned by a JOSEPHSON junction
$\mathcal{I}_r$	Re-trapping current intensity
$\mathcal{J}_n(x)$	Integer BESSEL function of order $n$
$\mathcal{I}_v(x)$	Modified BESSEL function of the first kind of order $v$
$j_v(x)$	Spherical BESSEL function of order $v$
$\bar{\mathbf{J}}$	Average current density

---

<b>j</b>	Current density
<b>j<sup>a</sup></b>	Amperian current density
<b>j<sup>a</sup><sub>surf</sub>, j<sup>a</sup><sub>vol</sub></b>	Surface and bulk Amperian current densities
<i>j<sub>c</sub></i>	Critical current density in a type I superconductor
<i>J<sub>c</sub></i>	Critical current density in a type II superconductor
<i>J<sub>c</sub><sup>Bean</sup></i>	Critical current density in the BEAN model
<i>j<sub>c</sub></i>	Critical current density in a JOSEPHSON junction
<b>k</b>	Wave-vector of a particle in state $ \mathbf{k}\rangle$
$ \mathbf{k}\uparrow\rangle$	State $ \mathbf{k}\rangle$ , with spin up
$ \mathbf{k}\uparrow, -\mathbf{k}\downarrow\rangle$	Pair state
<i>k<sub>B</sub></i>	BOLTZMANN constant
<i>k<sub>c</sub></i>	Cut-off wave-vector (BCS)
<i>k<sub>D</sub></i>	DEBYE wave-vector
<i>k<sub>F</sub></i>	FERMI wave-vector
<i>K<sub>J</sub></i>	JOSEPHSON constant
$\mathcal{K}_v(x)$	Modified BESSEL function of the second kind of order <i>v</i>
<i>L</i>	Length
<i>L</i>	Inductance
<i>L</i>	Latent heat
$\ell$	Mean free path of electrons in the normal state
<b>M</b>	Magnetic moment
<b>M</b>	Magnetization
<i>m</i>	Mass of an electron
<i>m<sub>p</sub></i>	Mass of a COOPER pair ( $2m$ )
<i>m<sub>v</sub></i>	Effective mass of a vortex
<i>N</i>	Demagnetization field factor
<i>N</i>	Total number of electrons
<i>N<sub>A</sub></i>	AVOGADRO number
<i>N<sub>state</sub></i>	Number of quantum states
<i>n</i>	Total electron density
<i>n<sub>n</sub></i>	Density of normal electrons
<i>n<sub>p</sub></i>	Density of COOPER pairs ( $n_s/2$ )

---

$n_s$	Density of superconducting electrons
$n_{s\infty}$	Density of superconducting electrons in the bulk
$n_s(\mathbf{r})$	Local density of superconducting electrons
$n_v$	Vortex density crossing a surface
$\mathbf{n}$	Unit vector normal to the surface
$\mathbf{P}$	Momentum
$\mathcal{P}$	Power
$Q$	Quantity of heat
$\mathbf{q}$	Vector in reciprocal space
$q_e$	Charge of the electron ( $-e$ )
$q_p$	Charge of the COOPER pair ( $-2e$ )
$\mathcal{R}$	Electrical resistance
$R$	Radius
$r$	Length of the vector $\mathbf{r}$
$r, \theta, z$	Cylindrical coordinates
$r, \theta, \varphi$	Spherical coordinates
$S$	Surface
$\mathbf{S}$	Surface vector
$S, s$	Entropy, entropy density
$T$	Temperature
$T_c$	Critical temperature
$t$	Time
$\mathcal{U}, u$	Internal energy, internal energy density
$\mathbf{u}$	Unit vector
$u_{\mathbf{k}}$	Probability amplitude of “non-occupation” of a pair state $ \mathbf{k}\uparrow, -\mathbf{k}\downarrow\rangle$
$\mathcal{V}$	Volume
$V$	Electric potential
$\mathcal{V}$	Electric potential induced by flux change
$V, \hat{V}$	Interaction potential (scalar, operator)
$V_g$	Gap voltage
$V_{\mathbf{k}'\mathbf{k}}$	Matrix element in $\mathbf{k}$ space
$\mathbf{v}$	Velocity

---

$v_F$	FERMI velocity
$v_{\mathbf{k}}$	Probability amplitude of occupation of the pair state $ \mathbf{k}\uparrow, -\mathbf{k}\downarrow\rangle$
$W$	Work
$w$	Work per unit volume
$x, y, z$	Cartesian coordinates
$\beta_c$	STEWART-MCCUMBER parameter of a JOSEPHSON junction
$\beta_L$	Screening factor of a SQUID circuit
$\gamma$	SOMMERFELD constant
$\gamma(q)$	Response function
$\Delta$	Laplacian operator
$\Delta$	Superconducting gap
$\delta$	Increment/uncertainty of a quantity (according to context)
$\delta(x)$	DIRAC function
$\epsilon$	Energy of an electron
$\epsilon_0, \mu_0$	Dielectric constant and permittivity of the vacuum
$\epsilon_1$	Energy of formation of a vortex
$\epsilon_F$	FERMI energy
$\epsilon_{\mathbf{k}}$	Energy of a free electron in the state $ \mathbf{k}\rangle$
$\eta$	Damping coefficient
$\Theta$	Phase difference between two points in a condensate
$\theta_D$	DEBYE temperature
$\theta(\mathbf{r}, t)$	Phase of the wave function of the superconducting condensate
$\kappa = \lambda/\xi$	GINZBURG-LANDAU parameter
$\lambda_J$	JOSEPHSON penetration depth
$\lambda$	Penetration depth of the magnetic field
$\lambda_L$	LONDON penetration depth
$\xi_{\mathbf{k}}$	Energy of a free electron of wave-vector $\mathbf{k}$ with respect to the FERMI energy
$\xi_0$	Coherence length at 0 K
$\xi_p$	PIPPARD length
$\xi_{BCS}$	BCS coherence length
$\rho$	Electrical resistivity
$\rho_{ff}$	Flux-flow resistivity of vortices

---

$\rho_n$	Resistivity in the normal phase
$\rho_{vol}$	Charge density in the bulk
$\rho_{vol}^m$	Bulk density of magnetic charges
$\sigma$	Electrical conductivity
$\sigma_{surf}^m$	Surface density of magnetic charges
$\sigma_{surf}$	Surface charge density
$\phi_p$	Wave function of a condensate of COOPER pairs
$\phi_{k\uparrow}$	Wave function of one electron
$\phi_{k_m k_n}$	Wave function of two electrons
$\phi$	Magnetic field flux
$\phi_0$	Quantum of flux (fluxon)
$\chi$	Magnetic susceptibility
$\chi_k$	Amplitude of condensation in the pair state $ k\uparrow, -k\downarrow\rangle$
$\omega$	Angular velocity
$\omega_D$	DEBYE frequency
$\omega_p$	Plasma frequency of a JOSEPHSON junction

## SOME WORKS OF REFERENCE\*

- BARONE A. & PATERNO G. (1982) *Physics and application of the Josephson Effect*, Wiley-Interscience publication, New York.
- BUCKEL W. & KLEINER R. (2004) *Superconductivity Fundamentals and Applications*, 2<sup>nd</sup> Revised and Enlarged Edition, Wiley-VCH, Weinheim.
- BURGER J.P. (1974) *La supraconductivité des métaux, des alliages et des films minces*, Masson, Paris.
- CLARKE J. & BRAGINSKI A.I. (2004) *The SQUID Handbook: Fundamentals and Technology of SQUIDS and SQUID Systems*, vol. I, Wiley-VCH, Weinheim.
- COLLINGS E.W. (1986) *Applied Superconductivity, Metallurgy, and Physics of Titanium Alloys*, The International cryogenics monograph series, vol. 2, Plenum Press, New York, London.
- CYROT M. & PAVUNA D. (1992) *Introduction to superconductivity and High- $T_c$  materials*, World Scientific, Singapore.
- FONER S. & SCHWARTZ B.B. (1981) *Superconductor Materials Science: Metallurgy Fabrication and Applications* (NATO Advanced Study Institutes Series), Plenum, New York.
- DE GENNES P.G. (1999) *Superconductivity of metals and alloys*, Advaced Books Classics, Westview Press, Boulder.
- KRABBES G., FUCHS G., CANDERS W.R., MAY H. & PALKA R. (2006) *High Temperature Superconductor Bulk Materials*, Wiley-VCH, Weinheim.
- KUPER C.G. (1968) *An introduction to the theory of superconductivity*, Clarendon Press, Oxford.
- LEVY L.P. (1997) *Magnétisme et supraconductivité*, EDP Sciences, Paris.
- LIKHAREV K.K. (1986) *Dynamics of Josephson Junctions and Circuits*, CRC Press, Boca Raton.
- LONDON F. (1961) *Superfluids, Volume I Macroscopic Theory of Superconductivity*, 2<sup>nd</sup> Revised Edition, Dover Publications, New York.
- LYNTON E.A. (1964) *Superconductivity*, Methuen and Company, London.
- MANSKE D. (2004) *Theory of Unconventional Superconductors: Cooper-Pairing Mediated by Spin Excitations*, Springer Tracts in Modern Physics, vol. 202, Springer-Verlag, Berlin and Heidelberg.
- NARLIKAR A.V. (2005) *Frontiers in Superconducting Materials*, Springer-Verlag, Berlin and Heidelberg.

---

\* References to articles treating specific points and to the experimental results shown are included as footnotes within each chapter.

- PARKS R.D. (1969) *Superconductivity*, vol. 1 and 2, Taylor & Francis, London.
- POOLE C. jr, FARACH H., CRESWICK R. & PROROZOV C. (2007) *Superconductivity*, 2<sup>nd</sup> Edition, Academic Press, New York.
- RAVEAU B., MICHEL C., HERVIEU M. & GROULT D. (1991) *Crystal chemistry of high  $T_c$  superconducting copper oxides*, Springer-Verlag, Berlin and Heidelberg.
- ROSE-INNES A.C. & RHODERICK E.H. (1978) *Introduction to Superconductivity*, Revised Edition, Pergamon Press, Oxford.
- SAINT JAMES D., SARMA G. & THOMAS E.J. (1969) *Type II Superconductivity*, Pergamon Press, Oxford.
- SCHRIEFFER J.R. (1983) *Theory of Superconductivity*, Benjamin-Cummings, New York.
- SCHRIEFFER J.R. & BROOK J.S. (2007) *Handbook of High -Temperature Superconductivity: Theory and Experiment*, Springer-Verlag, New York.
- TILLEY D.R. & TILLEY J. (1990) *Superfluidity and superconductivity*, Institute of Physics Publishing, Bristol and Philadelphia.
- TINKHAM M. (2004) *Introduction to Superconductivity*, 2<sup>nd</sup> Edition, Dover Publications, New York.
- TIKADOUR P. (1995) *Les supraconducteurs*, Hermès Science Publications, Paris.
- TIKADOUR P. (2003) *Matériaux Supraconducteurs*, Hermès Science, Lavoisier, Paris.
- VONSOVSKY S.V., IZYUMOV Y.A. & KURMAEV E.Z. (1982) *Superconductivity of transition metals*, Springer Series in Solid-State Sciences, vol. 27, Springer-Verlag, Berlin and Heidelberg.
- WALDRAM J.R. (1996) *Superconductivity of metals and cuprates*, Institute of Physics Publishing, Bristol and Philadelphia.
- WOLF E.L. (2012) *Principles of Electron Tunneling Spectroscopy*, 2<sup>nd</sup> Edition, International Series of Monographs on Physics, vol. 152, Oxford University Press, Oxford.
- ZHOU SHU ANG (1991) *Electrodynamic Theory of Superconductors*, Peter Peregrinus Ltd, London.

# INDEX

## A

- ABRIKOSOV (Alexei) ..... 6, 111  
– vortex lattice ..... 127  
fluxon ..... 232  
AMBEGAOKAR and BARATOFF relation ..... 247  
AMPÈRE  
– currents ..... 61, 77  
– / LONDON currents ..... 61  
ANDERSON (Philip Warren) ..... 1  
ANDREEV (Alexander) ..... 9  
– levels ..... 267  
ANDREEV-SAINT JAMES reflections ..... 268  
anisotropy  
– of critical fields ..... 114  
– of coherence lengths ..... 124  
– of LONDON penetration depths ..... 124  
anomalous skin effect (REUTER and SONDHEIMER) ..... 49  
anti-symmetry of wave functions ..... 194, 277  
applications of superconductors ..... 11  
ASLAMAZOV-LARKIN (model of SNS junction) ..... 266

## B

- BARDEN (John) ..... 8  
BARDEEN-STEPHEN model ..... 152, 185  
BCS  
– approximation ..... 196  
– ground state ..... 208  
– coherence length ..... 51, 118, 125, 215  
– calculation results ..... 207  
condensation amplitude of COOPER pair ..... 209  
critical field  $H_c$  ..... 216  
critical temperature ..... 212  
electronic specific heat ..... 217

---

ground state .....	208
probability amplitude of non-occupation by a COOPER pair $u_k$ .....	209
probability amplitude of occupation by a COOPER pair $v_k$ .....	209
BEAN	
– equation of the critical state .....	157
– model	
– of the critical state .....	156
current transport .....	173
current transport in an applied magnetic field .....	176
hysteresis loop.....	168
magnetization of a cylinder.....	168
magnetization of a plate .....	162
magnetization of a thick walled tube .....	170
rules.....	161
vortex penetration .....	158
BECKER (Richard) .....	38
BEDNORZ (Georg) .....	9
BESSEL functions.....	263
modified – .....	47
spherical – .....	54
BOSE-EINSTEIN condensate.....	225, 284
bound state of a COOPER pair at 0 K .....	204
BRAGG glass (vortex) .....	135

**C**

CASIMIR (Hendrik) .....	6
two fluid model of GORTER and CASIMIR .....	22, 223
charge of the electron .....	14
CHU (Paul).....	10
CLAPEYRON equation.....	74
COFFEY experiment.....	171
coherence length.....	51, 118, 225
BCS expression .....	215
geometric interpretation .....	118
thermal dependence.....	125
condensate (BOSE-EINSTEIN) .....	225, 284
conductor	
normal – .....	14
perfect –.....	15

condensation	
amplitude of – of COOPER pairs .....	209
free enthalpy .....	70, 216
confinement of vortices .....	142, 234
conjugate canonical variables	
phase/number of particles .....	281
position/momentum .....	281
connected	
multiply – superconductor .....	229, 232
simply – superconductor .....	228
constant	
JOSEPHSON – .....	248
SOMMERFELD – .....	68
COOPER (Leon).....	8
– pair.....	189, 203
binding energy.....	205
bound state at 0 K.....	204
charge .....	225
condensation amplitude in BCS .....	209
density .....	225
distance between the electrons .....	207
mass.....	225
phase of the condensate.....	225, 226, 315
proof of existence .....	229
relation with free enthalpy of condensation .....	120
spatial extent .....	118, 207
wave function.....	206
core of a vortex.....	122, 235
CRIBIER (Daniel) .....	7
criteria (SILSBEE).....	88, 222
critical current	
– of a type I superconductor .....	88
– of a type II superconductor .....	157
– of a wire in a parallel magnetic field.....	107
– of a wire in a transverse magnetic field .....	108
– through a JOSEPHSON junction .....	246
AMBEGAOKAR-BARATOFF relation.....	247
JOSEPHSON – .....	341
critical current density	
$-j_c$ (for a type I superconductor) .....	88
$\mathcal{J}_c$ (for a type II superconductor) .....	137, 153

---

– $J_c$ (for a JOSEPHSON junction).....	317
– $J_c^{\text{Bean}}$ (in the BEAN model).....	157
– in SHUBNIKOV phase.....	136
– of depairing .....	218
critical field	
JOSEPHSON – $H_{cJ}$ .....	340
lower – $H_{c1}$ .....	112, 116, 126
surface – $H_{c3}$ .....	113
thermodynamic – $H_c$ .....	59, 69, 88, 126, 132
upper – $H_{c2}$ .....	112, 127, 132
BCS theory .....	217
critical magnetic field $B_c$ .....	88
critical S/N line $H_c(T)$ in type I superconductor .....	69
critical state .....	147
BEAN equation.....	157
experimental evidence.....	171
model.....	147, 156, 158
critical temperature.....	2, 69
BCS .....	214
isotope dependence .....	195
cuprates .....	9
current	
– and equivalent magnetization.....	62
– in a type II superconductor.....	173
– of a long JOSEPHSON junction.....	339
– in a field .....	341
– of a narrow JOSEPHSON junction in a field .....	315
– of conductors.....	61
AMPÈRE – .....	77
JOSEPHSON – .....	4, 246
– in an over-damped RCSJ.....	256
– via ANDREEV levels .....	267
LONDON – .....	20, 61
– / AMPÈRE current .....	61
– / magnetization.....	61
– in a vortex.....	122
re-trapping – in a RCSJ JOSEPHSON junction .....	261
screening – .....	21
SQUID – .....	289
tunnelling – .....	251
transport in the SHUBNIKOV phase.....	173
transport in type II superconductors.....	136

current density	
– around a vortex core .....	235
JOSEPHSON – .....	317
definition in quantum mechanic .....	226, 240
cylinder	
magnetized – .....	79
superconducting/normal transition in a – .....	88
 <b>D</b>	
DC-SQUID .....	306
– in the over-damped regime .....	309
inductive – .....	308
$0/\pi$ – .....	310
reading .....	309
DE GENNES (Pierre-Gilles) .....	7
DEBYE	
– energy .....	196
– temperature $\theta_D$ .....	67
decoration (vortex imaging) .....	130
delocalization of COOPER pairs .....	198
demagnetizing field factor .....	81
DENIS (Jérôme) .....	9
density of states	
– at the FERMI level .....	192
– of free electrons .....	190
– of quasiparticles .....	212
semiconductor representation .....	215
depairing	
critical current density .....	218, 221
critical velocity .....	221
depth	
JOSEPHSON penetration – .....	311, 324
LONDON penetration – .....	22, 25, 49, 51
energetic interpretation .....	34
experimental value .....	26
increase by impurity .....	125
temperature dependence .....	26, 125
penetration – of a magnetic field .....	49, 51, 119
dirty superconductor .....	49, 55
diamagnet (perfect) .....	63, 112
discovery of superconductivity .....	1

**E**

effect	
anomalous skin –	49
incomplete MEISSNER –	111, 116
isotope –	4, 195
JOSEPHSON –	243
a.c. –	248
d.c. –	245
signature	273
MEISSNER –	20
proximity –	266
tunnel –	9
electrical conduction	
normal conductor	14
perfect conductor	15
electromagnetic wave on a JOSEPHSON junction	263
electromagnetism	
first equation of LONDON	22
MAXWELL's equations	13
second equation of LONDON	23
electron	
– charge	14
– gas	
interacting –	193
density of state	190
free – (kinetic energy)	204
normal –	223
superconducting –	22, 26, 222
superconducting – density near a surface	118
mean free path	56, 125
ellipsoid	
field <b>H</b> in an –	81
magnetized –	81
magnetic field <b>B</b> in an –	81
magnetization <b>M</b> in an –	81
superconducting –	91, 92
field <b>H</b> in a –	91
magnetic field <b>B</b> in a –	91
magnetization <b>M</b> in a –	91
energy	
– of a JOSEPHSON junction	262, 283
– of a $\pi$ JOSEPHSON junction	274
– of a SQUID circuit	300

– of an isolated vortex .....	180
– of interaction between vortices .....	180
– of formation of a vortex .....	126
binding – of a COOPER pair.....	205
DEBYE – .....	196
dissipation of – by vortex displacement.....	150, 185
FERMI – .....	191
free – (HELMHOLTZ function) .....	66
kinetic – of free electrons .....	204
N/S interface – (type I superconductor).....	99
quasiparticle – .....	210
equation	
BEAN – of critical state.....	157
CLAPEYRON – (for S/N transition) .....	74
FERRELL-PRANGE – .....	325
HAMILTON JACOBI – .....	239, 281
HELMHOLTZ – (in fluid mechanics) .....	37
KIM-JI – .....	158
LONDON – .....	23
first – .....	22, 38
generalized – .....	180, 236
second –.....	23, 35, 43
MAXWELL’s –.....	13
PIPPARD –.....	49, 52
non-local –.....	49
– in reciprocal space.....	52
FOURIER analysis .....	52
equation of state	
normal state .....	67
superconducting state .....	67
ESSMAN and TRAUBLE (images of vortices) .....	130
exclusion of a magnetic field .....	31
experiment	
COFFEY –.....	171
Gravity-B – .....	41
OCHSENFELD – .....	31
expulsion of a magnetic field .....	21
extent (in space) of a COOPER pair.....	119, 207

**F**

## factor

demagnetizing field –.....	81
quality – of a JOSEPHSON junction (RCSJ) .....	253

FERMI	
– energy .....	191
– function .....	192
– level .....	191
– sphere .....	191
– velocity .....	192
– wave vector .....	192
FERMI-DIRAC statistics.....	189
FERRELL-PRANGE equation.....	325
field	
– $\mathbf{H}$ .....	62, 78
in an ellipsoid .....	81
in a superconducting ellipsoid.....	91
critical –	
thermodynamic – $H_c$ .....	59, 69, 88, 126, 132
lower – $H_{c1}$ .....	112, 116, 126
surface – $H_{c3}$ .....	113
upper – $H_{c2}$ .....	112, 127, 132
demagnetizing – $\mathbf{H}^m$ .....	81
field factor (demagnetizing –).....	81
flux	
– creep (vortex) .....	155
– jump .....	155
– quantization.....	4, 125, 225, 227, 230
– trapped in a hole of superconductor .....	33
– trapped in a non simply-connected superconductor.....	32
flux-flow resistivity .....	150, 153, 187
fluxon (quantum of flux).....	125, 225, 227
– carried by a vortex.....	232
– in an ABRIKOSOV lattice.....	233
half –	
– across an rf-SQUID with a 0 and a $\pi$ junction .....	305
– across an rf-SQUID with a $\pi$ junction.....	301
– at the 0/ $\pi$ connection of a hybrid JOSEPHSON junction .....	343
isolated vortex .....	232
force	
– acting on vortices .....	147
– of interaction between vortices .....	148, 181
LONDON –.....	178, 182
LORENTZ –.....	147, 178, 179
MAGNUS – on a vortex .....	182
force density	
– of vortex pinning .....	152
LORENTZ – on vortices .....	149

FOURIER analysis of PIPPARD equations .....	52
FRAUNHOFER (diffraction figure) .....	319
free enthalpy (GIBBS function)	
– of condensation .....	71, 216
– of surface condensation.....	117
magnetic – .....	71
surface magnetic – .....	114
normal state .....	70
superconducting state .....	70
frequency	
JOSEPHSON – .....	248
plasma – of a JOSEPHSON junction.....	254
FRÖHLICH (Herbert) .....	8
function	
BESSEL –	
modified – .....	47
spherical – .....	54
FERMI – .....	192
GIBBS – (free enthalpy).....	66
HELMOTZ – (free energy).....	66
response –.....	54

## G

gap .....	208, 215
– voltage $V_g$ .....	249
BCS expression .....	209
thermal evolution .....	214
gauge .....	41, 231, 240
– in non simply-connected superconductors .....	44
LONDON –.....	41, 231
transformations.....	240
GIAEVER (Ivar).....	4
GIBBS function (free enthalpy).....	66
GINZBURG (Vitaly).....	6
GINZBURG-LANDAU	
– theory .....	6
– parameter.....	111, 120
critical value .....	123
experimental values.....	124
impurity effects .....	125
GLAG theory (critical field expressions).....	126

## glass

BRAGG vortex –.....	135
vortex – .....	135
GORKOV (Lev).....	7, 111
GORTER (Cornelius Jacobus) .....	6
two fluid model of GORTER and CASIMIR .....	22, 223
ground state in BCS .....	208

**H**

## half fluxon

– across an rf-SQUID with a 0 and a $\pi$ junction .....	305
– across an rf-SQUID with a $\pi$ junction.....	301
– at the 0/ $\pi$ connection of an hybrid JOSEPHSON junction .....	343

HAMILTON-JACOBI equations ..... 239, 281

## Hamiltonian

– of a charged particle in a magnetic field .....	239
– of one particle.....	190
– of two interacting particles.....	194
– of two non-interacting particles .....	193

hard superconductor ..... 134

HEISENBERG (relation between phase and particle number)..... 281

## HELMOLTZ

– equation in fluid mechanics .....	37
– function (free energy).....	66

HOLST (Gilles)..... 2

HTS (High-Temperature Superconductor) ..... 1

## hysteresis

– loop in a type II superconductor .....	165
– loop in the BEAN model .....	165
– loop in the KIM-JI model.....	166

**I**

imaging vortices ..... 129

impurity effects on the coherent length and the penetration depth ..... 125

inductance of a SQUID ..... 295

incomplete MEISSNER effect ..... 111, 113, 116

## intermediate state

– in a current-carrying wire.....	102
– in a plate submitted to a magnetic field .....	97

---

– in a sphere submitted to a magnetic field.....	93
– of a type I superconductor.....	87
interface energy (N/S, of a type I superconductor) .....	99

**J**

JÉROME (Denis).....	9
JOSEPHSON (Brian).....	4
– constant .....	248
– critical field .....	340
– current .....	246
in a over-damped RCSJ.....	256
<i>via ANDREEV levels</i> .....	267
– current density .....	317
– effect.....	243
a.c. – .....	248
d.c. – .....	245
signature .....	273
– energy .....	262
– equation.....	243
first – .....	246, 283
second –.....	248, 283
– frequency.....	248
– junction.....	243
– in a magnetic field .....	313
– subject to an alternating voltage.....	288
– subject to an electromagnetic wave .....	263, 288
0- $\pi$ hybride – .....	273, 276
current driven (RCSJ) in a –, mechanical analogy.....	252
over-damped – .....	256, 286
SCS (simple constriction in the superconductor) – ( <i>weak link</i> ) .....	243
SFS (superconductor/ferromagnetic/superconductor) – .....	243, 276, 279
SIS (superconductor/insulating/superconductor) –.....	243, 249
SNS (superconductor/normal/superconductor) – .....	243, 266, 271
voltage biased – .....	249
current-voltage characteristic .....	249
current-voltage characteristic (in RCSJ) .....	259
magnetic thickness .....	318
order of magnitude of the parameters .....	262
plasma frequency .....	254
STEWART-MCCUMBER parameter .....	254, 309
system with many states.....	279
– penetration depth.....	313, 324
– vortex .....	335-337

---

long – junction	
– carrying a current .....	339
– carrying a current in a magnetic field .....	341
– in a magnetic field.....	328
– in the MEISSNER regime.....	333
– in the vortex regime .....	335
– maximum current density in a magnetic field.....	342
0- $\pi$ -hybrid – .....	346
<b>K</b>	
KIM and STEPHEN relation .....	152
KIM-JI (model of the critical state).....	166
kinetic energy of free electrons .....	204
<b>L</b>	
Lagrangian of a charged particle.....	238
Laminar model of intermediate state of a plate.....	97
LANDAU (Lev).....	6
GINZBURG-LANDAU parameters .....	111, 120
latent heat at the S/N transition .....	74
lattice	
ABRIKOSOV vortices .....	127
JOSEPHSON vortices.....	336
law	
LENZ's –.....	21
RUTGERS' – .....	72
TUYN's – .....	69
length	
coherence – .....	51, 118, 215
PIPPARD – .....	56
LENZ's law .....	21
level	
ANDREEV –.....	267
FERMI – .....	191
levitation	
– in type I superconductor.....	64
– in type II superconductor .....	138
LIKHAREV (Konstantin) .....	273
liquid (vortex –).....	135

---

LONDON (Heinz, Fritz).....	5, 6
– current .....	20, 61
– / AMPÈRE current.....	61
– / magnetization .....	61
– in a vortex.....	122
– equation.....	23
– by fluid mechanics .....	37
– by a variational method.....	35
– from momentum.....	225
first – .....	22, 38
first – with non-linear term .....	38
generalized – .....	180
root of second –.....	38, 43, 231
second –.....	23, 35, 43, 226
second – and momentum.....	43, 231
second – in presence of vortices .....	236
second – in the LONDON gauge.....	43, 231
– force .....	178
– gauge .....	41
– momentum .....	38, 236
– penetration depth $\lambda_L$ .....	22, 25, 118
– / penetration depth $\lambda$ .....	49, 51
energetic interpretation .....	34
experimental measurement .....	25, 26
increase by impurities .....	125
temperature dependence.....	26
– theory .....	13
LORENTZ	
– force .....	147, 178, 179
– on vortices .....	178
bulk – density .....	149

## M

magnetic	
– charges for the calculation of the demagnetizing field factor .....	79
– media.....	77
– moment.....	25
– susceptibility .....	59
magnetic field <b>B</b>	
– at the center of a vortex.....	126
– in an ellipsoid .....	81
– in a superconducting ellipsoid.....	91
– in a perfect conductor.....	16

---

– in a superconductor .....	19
– on the surface $\tilde{B}$ .....	30
critical – $B_c$ .....	88
exclusion of the – .....	31
penetration depth of a –.....	49, 51
self generated – $B^I$ .....	176
magnetization <b>M</b> .....	78
– equivalent to AMPÈRE currents .....	78
– equivalent to LONDON currents.....	62
– of a cylinder in the BEAN model .....	168
– of a superconducting cylinder of type II .....	168
– of a superconducting ellipsoid .....	91
– of a superconducting plate of type II .....	162
– of a thick walled tube in the BEAN model.....	170
– of an ellipsoid.....	81
surface – .....	115
work for the – of matter .....	84
MAGNUS force on a vortex .....	182
materials (superconducting –).....	9, 113
MATTHIAS (Bern).....	1
MAXWELL's equations .....	13
mean free path of electrons .....	49, 56, 125
mechanical analogy	
– of the RCSJ model .....	252
– of a wide JOSEPHSON junction .....	328
MEISSNER (Walther).....	3
– effect.....	20
– in a wide JOSEPHSON junction .....	333
incomplete – .....	111, 113, 116
– phase.....	112
MgB <sub>2</sub> .....	10
mixed state of type II superconductors .....	113
model	
ANDREEV level – .....	267
ASLAMAZOV-LARKIN – .....	266
BARDEEN-STEPHEN – .....	152, 185
BEAN – of the critical state.....	158
critical state – .....	147, 156
KIM-JI – of the critical state .....	166
phenomenological .....	5
RCSJ –.....	250
two fluid – (of GORTER and CASIMIR).....	22, 223

---

moment (LONDON –).....	38, 236
momentum	
generalized – .....	225, 231, 238
second LONDON equation.....	43
MÜLLER (Alex) .....	9

**N**

narrow JOSEPHSON junction	
– in a magnetic field.....	313
0- $\pi$ hybrid – .....	321
Nb <sub>3</sub> -Sn.....	113
Nb-Ti .....	4, 113
neutron diffraction (imaging vortices) .....	129
NOBEL prizes .....	1
non-local PIPPARD equations.....	49
normal	
– conductor.....	14
– electrons .....	223
quasiparticles in – state .....	210

**O**

OCHSENFELD (Robert).....	3
– experiment.....	31
ONNES (Heike Kamerling) .....	2

**P**

pair state	
definition .....	196, 203
occupation probability at 0 K .....	208
parameter	
GINZBURG LANDAU – .....	111, 113, 120
screening – (rf-SQUID) .....	295
STEWART-MCCUMBER – .....	254
penetration depth $\lambda$ .....	119
– / LONDON penetration depth $\lambda_L$ .....	49, 51
impurity effects .....	125
thermal dependence.....	125
penetration depth $\lambda_J$ (of JOSEPHSON) .....	311, 324

---

penetration depth $\lambda_L$ (of LONDON) .....	22, 25, 49, 51
energetic interpretation .....	34
experimental value .....	26
thermal dependence.....	26
perfect conductor.....	14
electrical conduction .....	15
slab .....	17
– / superconductor .....	19
perfect diamagnetism .....	3, 63, 112
phase	
– diagram	
– of a type I superconductor.....	59, 69
– of a type II superconductor .....	112
– of vortices.....	134– transition
first order –.....	75
second order – .....	75
thermodynamic –	
MEISSNER – .....	112
SHUBNIKOV – .....	112
phase of the COOPER pair condensate .....	225, 289, 317
phonon (pairing potential).....	195
pinning of vortices.....	152
PIPPARD (Brian).....	6
– equations .....	49, 52
non-local –.....	49
– in reciprocal space.....	52
FOURIER analysis .....	52
– length.....	56
plasma frequency of a JOSEPHSON junction.....	254
pniotides .....	10
potential of interaction	
– between electrons .....	194
– via phonons .....	195
matrix element of – .....	196
BCS approximation.....	196
principle of correspondence .....	239

## Q

quantum of flux	
fluxon .....	125, 225, 227
half-fluxon.....	302
– across an rf-SQUID with a 0 and a $\pi$ junction .....	305

---

– across an rf-SQUID with a $\pi$ junction.....	301
– at the $0/\pi$ connection of an hybrid JOSEPHSON junction .....	343
quantization (demonstration of –) .....	231
quasiparticle .....	210
density of state .....	212
electron-like – .....	267
hole-like – .....	267
ANDREEV levels .....	269
energy .....	211
normal state .....	210
tunnel current .....	249
semiconductor representation of the density of states .....	215

**R**

RCSJ (Resistively and Capacitively Shunted Junction)	
mechanical equivalence .....	252
model .....	250
re-trapping current .....	261
reference system for bound states	
degenerate .....	197
non degenerate .....	199
reflections (ANDREEV-SAINT JAMES) .....	268
relation	
AMBEGAOKAR and BARATOFF –.....	247
HEISENBERG – (between phase and particle number).....	281
KIM and STEPHEN – .....	152
repulsion of vortices by surfaces .....	141
resistivity (flux-flow –) .....	150, 153, 187
resonance in a JOSEPHSON junction .....	263
retrapping current in a RCSJ .....	261
REUTER and SONDHEIMER (anomalous skin effect) .....	49
rf-SQUID	
– with a $\pi$ junction.....	299
– with a single junction (non-inductive) .....	292
– with two junctions (non-inductive) .....	293
$0-\pi$ – of significant inductance .....	304
$0-\pi$ – with zero inductance .....	303
energetic approach .....	300
inductive –.....	295
operation.....	297
reading.....	306
screening parameter .....	295

ROSSAT-MIGNOT (Jean) .....	11
rotation (superconducting sphere).....	38
RUTGERS' law .....	72

**S**

SAINT-JAMES (Daniel).....	9
SCHLÖMILCH formula .....	263, 288
SCHRIEFFER (Robert).....	8
SCS junction = weak link.....	243
semiconductor representation of the density of state of quasiparticles.....	215
SFS (superconductor/ferromagnetic/superconductor junction) .....	243
examples.....	279
mechanism for a $\pi$ junction .....	276
SHAPIRO steps .....	264
SHUBNIKOV (Lev) .....	12
– phase.....	112, 136
signature of a JOSEPHSON junction.....	273
SILSBEE criteria .....	88, 222
simply connected superconductor .....	228, 231
SIS (superconductor/insulating/superconductor junction).....	243, 249
example of – junction.....	261
slab	
perfectly conducting –.....	17
superconducting – .....	23
thick –.....	23
thin – .....	24
thin – (S/N transition) .....	89
SLATER determinant .....	194
small sample size.....	89
SNS (superconductor/normal metal/superconductor junction) .....	243
ANDREEV model.....	267
ASLAMAZOV-LARKIN model .....	266
example of – fabrication .....	271
S/N transition	
– in a cylinder.....	88
– in a thin slab .....	89
CLAPEYRON equation.....	74
entropy jump .....	74
latent heat .....	74

order of the transition .....	75
specific heat jump .....	73
soft superconductor .....	133
SOMMERFELD constant.....	68
specific heat	
– jump at the S/N transition .....	73
– of the lattice.....	67
electronic – (normal state).....	68, 192
electronic – (superconducting state) .....	68, 217
sphere	
– in an intermediate state .....	93
superconducting – .....	38
SQUID.....	289
inductance of a – .....	291, 295
DC-SQUID.....	289, 306
– in the over-damped regime .....	309
inductive – .....	308
0/ $\pi$ junction – .....	310
reading.....	309
rf-SQUID .....	289
– with a $\pi$ junction.....	299
– with a single junction (non-inductive) .....	292
– with two junctions (non-inductive) .....	293
0- $\pi$ – of significant inductance.....	304
0- $\pi$ – with zero inductance .....	303
energetic approach .....	300
inductive – .....	295
operation.....	297
reading.....	306
screening parameter .....	295
STEWART-MCCUMBER parameter of a JOSEPHSON junction.....	254, 309
superconducting	
– electrons .....	22, 222
– electron density near a surface .....	118
– materials .....	9, 113
– slab .....	23
– sphere .....	38
– thick slab .....	23
– thin slab .....	24
– wire submitted to a field.....	26
– wire carrying a current .....	29
superconductor	
– / normal transition (see S/N transition)	
– / perfect conductor .....	19

anisotropic – .....	124
dirty – .....	49, 55, 125
hard – .....	134
high critical temperature – (HTS) .....	1
iron-based – (pnictide) .....	10
multiply connected – .....	32, 44, 229
non-conventional – .....	10
rotating – .....	39, 237
simply connected – .....	228
soft/hard – .....	133
thermodynamics of a – .....	59, 65
type I – (see type I superconductor)	
type II – (see type II superconductor)	
quasiparticles.....	210
specific heat.....	67
surface	
– free enthalpy.....	114, 117
– free enthalpy density (representation).....	121
superconducting electron density near a – .....	118
magnetization .....	115
superconductivity .....	113

**T**

temperature	
critical – $T_c$ .....	1, 69, 214
DEBYE – $\theta_D$ .....	67
theory	
BCS – .....	8, 189
GINZBURG-LANDAU – .....	6
GLAG – .....	6, 126
LONDON – .....	13
thermodynamic	
– functions of superconductivity .....	65
– of type I superconductors .....	59
– variables .....	60
transport of current (in a type II superconductor) .....	136
trapped flux	
– in a hole inside a superconductor .....	32
– in a perfect conductor .....	20
non simply-connected superconductor .....	32
trapping of vortex lines in nanostructures .....	142

tunneling	
– current across a Al/Al <sub>2</sub> O <sub>3</sub> /Al junction (thermal dependence).....	251
– microscopy (vortex imaging) .....	131
TUYN's law.....	69
two fluid model .....	22, 223
type I and II superconductors .....	3, 111, 123
GINZBURG-LANDAU parameter.....	123
impurity effect.....	125
type I superconductor .....	59, 123
critical current density.....	88
critical field .....	88
critical S/N line $H_c(T)$ .....	59, 69
equation of state .....	67
interface energy N/S.....	99
intermediate state .....	87
– in a current-carrying wire.....	102
– in a plate submitted to a magnetic field .....	97
– in a sphere submitted to a magnetic field.....	93
laminar model of – of a thin plate .....	97
levitation.....	64
phase diagram .....	59, 69
thermodynamics .....	59
type II superconductor.....	111, 123
critical current density.....	152
critical state .....	147
BEAN equation.....	157
experimental proof.....	171
model.....	147, 156, 158
levitation.....	138
magnetization .....	162
mixed state .....	112
phase diagram .....	112
current transport .....	136, 152
SHUBNIKOV phase .....	112

**V**

velocity	
critical –.....	218
FERMI – .....	192
electrons around a vortex core .....	182
volt (standard –) .....	248
voltage (gap –).....	249

vortex.....	7, 121
– confinement.....	142, 234
– core.....	122, 235
– crystal .....	134
– energy.....	126
– imaging.....	129
– by tunnelling effect .....	131
– jumps.....	155
– lattice .....	127
– liquid .....	135
– matter .....	132
– stability.....	123
BRAGG glass –.....	135
current density around a – core .....	235
distribution of magnetic field in –.....	126
flux creep of –.....	155
flux-flow of – .....	150
force acting on –.....	147
giant – carrying several fluxons .....	144
interaction between – .....	148, 181
isolated – .....	232
JOSEPHSON – .....	335-337
lattice of –.....	127
imaging by decoration.....	130
neutron diffraction.....	129
penetration of – .....	133
trapping of a – by depression in thin films.....	142
ABRIKOSOV lattice .....	127, 233
density .....	127
distribution in soft and hard superconductors .....	134
effect of the demagnetizing field .....	140
energy	
– dissipation by displacement .....	150, 185
– of an isolated vortex.....	180
– of formation.....	126
flow model .....	150
flux jump .....	155
flux quantization .....	232
formation mechanism.....	133
glass.....	135
nanostructures .....	142
phase diagram .....	134
representation .....	122
repulsion by surfaces.....	141

**W**

wave function	
– of a free electron .....	190
– of the COOPER pair condensate .....	225
– of two independent electrons .....	194
wave vector (FERMI –) .....	192
weak link (SCS junction) .....	243
wire (superconducting –)	
– carrying a current .....	29
– subject to a magnetic field .....	26
work of magnetization.....	62, 84

**Y**

Y-Ba-Cu-O .....	10, 114
-----------------	---------